NBSIR 83-2742 (R)

Photonuclear Data - Abstract Sheets 1955 - 1982 Volume XIII (Hafnium - Thallium)

U.S. DEPARTMENT OF COMMERCE
National Bureau of Standards
National Measurement Laboratory
Center for Radiation Research
Washington, DC 20234

U.S. DEPARTMENT OF COMMERCE
NATIONAL BUREAU OF STANDARDS

NBSIR 83-2742

PHOTONUCLEAR DATA - ABSTRACT SHEETS
1955 - 1982
VOLUME XIII (HAFNIUM - THALLIUM)

E. G. Fuller, Henry Gerstenberg

U.S. DEPARTMENT OF COMMERCE
National Bureau of Standards
National Measurement Laboratory
Center for Radiation Research
Washington, DC 20234

U.S. DEPARTMENT OF COMMERCE, Malcolm Baldrige, *Secretary*
NATIONAL BUREAU OF STANDARDS, Ernest Ambler, *Director*

TABLE OF CONTENTS

Table of Contents i
Introduction 1
Hafnium (Natural) 3
Hafnium (A=176) 11
Hafnium (A=177) 15
Hafnium (A=178) 21
Hafnium (A=179) 31
Hafnium (A=180) 39
Tantalum (A=181) 45
Tungsten (Natural) 175
Tungsten (A=182) 201
Tungsten (A=183) 211
Tungsten (A=184) 215
Tungsten (A=186) 229
Rhenium (Natural) 245
Rhenium (A=185) 255
Rhenium (A=187) 259
Osmium (Natural) 267
Osmium (A=186) 273
Osmium (A=188) 279
Osmium (A=189) 285
Osmium (A=190) 291
Osmium (A=192) 297
Iridium (Natural) 303
Iridium (A=191) 309
Iridium (A=193) 315

Platinum (Natural) 321
Platinum (A=194) 341
Platinum (A=195) 347
Platinum (A=196) 353
Gold (A=197) 359
Mercury (Natural). 471
Mercury (A=198). 497
Mercury (A=199). 503
Mercury (A=201). 511
Mercury (A=202). 517
Mercury (A=204). 523
Thallium (Natural) 527
Thallium (A=203) 543
Thallium (A=205) 557

Photonuclear Data-Abstract Sheets
1955-1982

I. Introduction

As used in connection with this collection of data-abstract sheets, the term photonuclear data is taken to mean any data leading to information on the electromagnetic matrix element between the ground state and excited states of a given nuclide. The most common types of reactions included in this compilation are: (e,e'), (γ,γ), (γ,γ'), (γ,n), (γ,p), etc. as well as ground-state particle capture reactions, e.g. (α,γ_0). Two reactions which fit the matrix element criterion are not included in the compilation because of their rather special nature. These are heavy particle Coulomb excitation and the thermal neutron capture reaction (n,γ_0). While the energy region of particular interest extends from 0 to 150 MeV, papers are indexed which report measurements in the region from 150 MeV to 4 GeV. Most of the experiments listed are concerned with the excitation energy range from 8 to 30 MeV, the region of the photonuclear giant resonance.

The hierarchical grouping of the photonuclear data-abstract sheets within the file is by: 1. Target Element, 2. Target Isotope, and 3. by the Bibliographic Reference Code assigned to the paper from which the data on the sheet were abstracted. In this file, colored pages are used to mark the beginning and end of the sheets for each chemical element. A brief historical sketch of the element is given on the divider sheet marking the start of each section; the information for this sketch was derived from references such as the Encyclopaedia Britannica. In those cases where the sheets for a given element make up a major part of a volume, colored pages are also used to delineate sections pertaining to the individual isotopes of the element. Each of the sections of the file, as delineated by two colored divider sheets, represents a 27 year history of the study of electromagnetic interactions in either a specific nuclide or a specifc element.

The data-abstract sheets are filed under the element and/or isotope in which the ground-state electromagnetic transition takes place. For example, the abstract sheet for a total neutron yield measurement for a naturally occurring copper sample would appear in the elemental section of the copper file. On the other hand, a measurement of the ^{62}Cu 9.73 minute positron activity produced in the same sample by photons with energies below the three-neutron separation energy for ^{65}Cu (28.68 MeV) would be filed with the sheets for ^{63}Cu. Similarly a measurement of the ground-state neutron capture cross section in ^{12}C would be filed under ^{13}C while the corresponding ground-state alpha-particle capture cross section would be filed under ^{16}O.

At the end of this volume there is a master list of the abbreviations that have been used in the index section of the abstract sheets. The listings are those used in the final published index, Photonuclear Data Index, 1973-1981, NBSIR 82-2543, issued in August 1982 by the U. S. Department of Commerce, National Bureau of Standards, Washington, DC 20234. In some cases two notations are entered for the same quantity. The second entry is the abbreviation that was used in one or more of the earlier published editions of the index.

HAFNIUM
Z=72

Hafnium was discovered by D. Coster and G. C. de Hevesy in 1925. It was named after the Latin word for Copenhagen where the discovery was made. The missing element has always been considered to be a member of the rare-earth group and many early investigators had looked in this group but with no success. Niels Bohr concluded, based on his view of the electronic arrangement in atoms, that the missing element 72 was not a member of the rare-earth group but a member of the zirconium family and should have the properties resembling zirconium. With this information, Coster and de Hevesy searched for and found, in zirconium, clear evidence of the new element.

T. Kaminishi, C. Kojima
Jap. J. Appl. Phys. 2, 399 (1963)

Hf		72

METHOD: Linac; isomer yield; activity

REF. NO.: 63 Ka 2 | NVB

REACTION	RESULT	EXCITATION ENERGY	SOURCE TYPE	SOURCE RANGE	DETECTOR TYPE	DETECTOR RANGE	ANGLE
G,G/	RLY	1	C 5		ACT-I		4PI
		(0.16,).22)					

Table II. The isomers observed

Isomer	Observed value		Referenced value[1)13)]	
	Half-life	Energy (MeV)	Half-life	Energy (MeV)
Se-77m	17.5 sec	0.160	17.5 sec	0.161
Br-79m	4.80 sec	0.209	4.8 sec	0.208
Sr-87m	2.3 hr	0.390	2.8 hr	0.388
Y-89m	15.0 sec	0.920	14 sec	0.915
Rh-103m	58 min	*	57 min	0.040
Ag-107m	42 sec	0.95	44 sec	0.094
Ag-109m			40 sec	0.088
Cd-111m	47 min	0.150,0.255	49 min	0.150,0.247
In-115m	4.5 hr	0.335	4.5 hr	0.335
Sn-117m	17 day	0.160	14 day	0.159,0.161
Ba-137m	2.6 min	0.660	2.6 min	0.662
Er-167m	2.10 sec	0.209	2.5 sec	0.208
Hf-179m	18.5 sec	0.157,0.215	19 sec	0.161,0.217
W-183m	5.4 sec	0.200,0.170,0.115	5.5 sec	0.1025,0.2915 others
Ir-191m	4.90 sac	0.129, <0.07	4.9 sec	0.042-0.129
Pt-195m	4.5 day	0.065**	4.1 day	0.031-0.130
Au-197m	7.0 sec	0.10,0.27,0.40	7.2 sec	0.130,0.270,0.407
Hg-199m	43 min	0.160,0.370	42 min	0.158,0.368

* This isomer was measured with a G-M flow counter.
** This value corresponds to Pt-K X-ray energy.

Table III. Induced activation rate

Element	Beam energy (MeV)	Counting rate (×10000 cpm	Sample form
Se	5	1300	metallic pellet
Br	4	1600	NaBr grain
Sr	6		$SrCO_3$ powder
Y	5		metallic grain
Rh	5	0.2*	$RhCl_3$ grain
Ag	5	130	metallic plate
Cd	6	0.5	$CdCl_2$ grain
In	6	8	metallic plate
Sn	6	0.0005	metallic plate
Ba	5	0.6	BaS powder
Er	4	4900	Er_2O_3 powder
Hf	5	1600	metallic plate
W	5	120	metallic powder
Ir	5	2100	metallic powder
Pt	5	0.3	metallic plate
Au	4	4300	metallic plate
Hg	6	0.09	metallic liquid

* The value measured with a G-M flow counter.

REF.

A. Veres
Acta Phys. Acad. Sci.Hung. 16, 271-73 (1963)

A	Z
Hf	72

METHOD

Radioactive source

REF. NO. 63 Ve 2 NVB

REACTION	RESULT	EXCITATION ENERGY	SOURCE TYPE	SOURCE RANGE	DETECTOR TYPE	DETECTOR RANGE	ANGLE
G,G/	ABX	0-1	D	0-1	NAI-D		

ISOMERS

Таблица II

Измеренные значения после облучения, сравниваемые с другими литературными данными

Элемент	Активность облучения после первого измерения (имп/мин.)	Активн. экстрп. в конце облуч. (имп/мин.)	Литературные данные $T_{1/2}$	Литературные данные E (кэв)	Данные измерений $T_{1/2}$	Данные измерений E (кэв)	σ_m (10^{-28} см^2)	Γ_{ym} (10^{-3} эв)
Se-77m	3842±96	5400	17,5 сек.	160	18,1±1 сек.	160±10	9,5	1,75
Sr-87m	191±5	200	2,8 ч.	390	2,9±0,1 ч.	365±25	0,85	0,2
Y-89m	96±20	170	16 сек.	910	16,7±5 сек.		0,08	0,02
Rh-103m	28±5	31	57 мин.	40	58±2 мин.	20,5±0,5	0,08	0,01
Ag-107m	220±14	250	44 сек.	93	43,8±0,6 сек	91±10	0,8	0,2
Ag-109m			39 сек.	88				
Hf-179m	80±18	155	19 сек.	160; 215	19±2 сек.		1	0,2
Ir-191m	90±20	250	4,9 сек.	42; 130	5±2 сек.		5,6	1
Pt-195m	90±9	100	3,5 д.	31; 100; 130;	3,5±0,2 д.	32±3 67,5±5 96±5 130±10	0,2	0,04
Au-197m	240±16	520	7,2 сек.	130; 277; 407	7,2±1 сек.	68:130: 280±20 390±20	0,07	0,01
Hg-199m	9,6±3,2		42 мин.	160; 370			0,005	0,001

REF. A. V. Mitrofanova, Yu. N. Ranyuk, and P. V. Sorokin
J. Nucl. Phys. (USSR) 6, 703 (1967)
Sov. J. Nucl. Phys. 6, 512 (1968)

ELEM. SYM.	A	Z
Hf		72

METHOD

REF. NO.	
67 Mi 1	HMG

REACTION	RESULT	EXCITATION ENERGY	SOURCE		DETECTOR		ANGLE
			TYPE	RANGE	TYPE	RANGE	
G,F	ABX	300-999		300-999	TRK-I		

Detector: Fission fragment tracks in glass.

999 = 1600 MEV

Angular distribution measured for Pb was found isotropic; for other elements it was assumed isotropic.

Nucleus	Fissionability D	Cross section σ_κ, $\mu\beta$	Nucleus	Fissionability D	Cross section σ_κ, $\mu\beta$
Bi	0.11±0.01	7.8±0.6	Os	0.0058±0.0005	0,37±0.04
Pb	0.050±0.004	3.4±0.3	Re	0.0056±0.0006	0.35±0.04
Tl	0.031±0.003	2,1±0.2	Ta	0.0045±0.0005	0.27±0.03
Au	0.019±0.002	1.25±0.10	Hf	0.0042±0.0004	0.25±0,03
Pt	0.012±0.002	0.80±0.08			

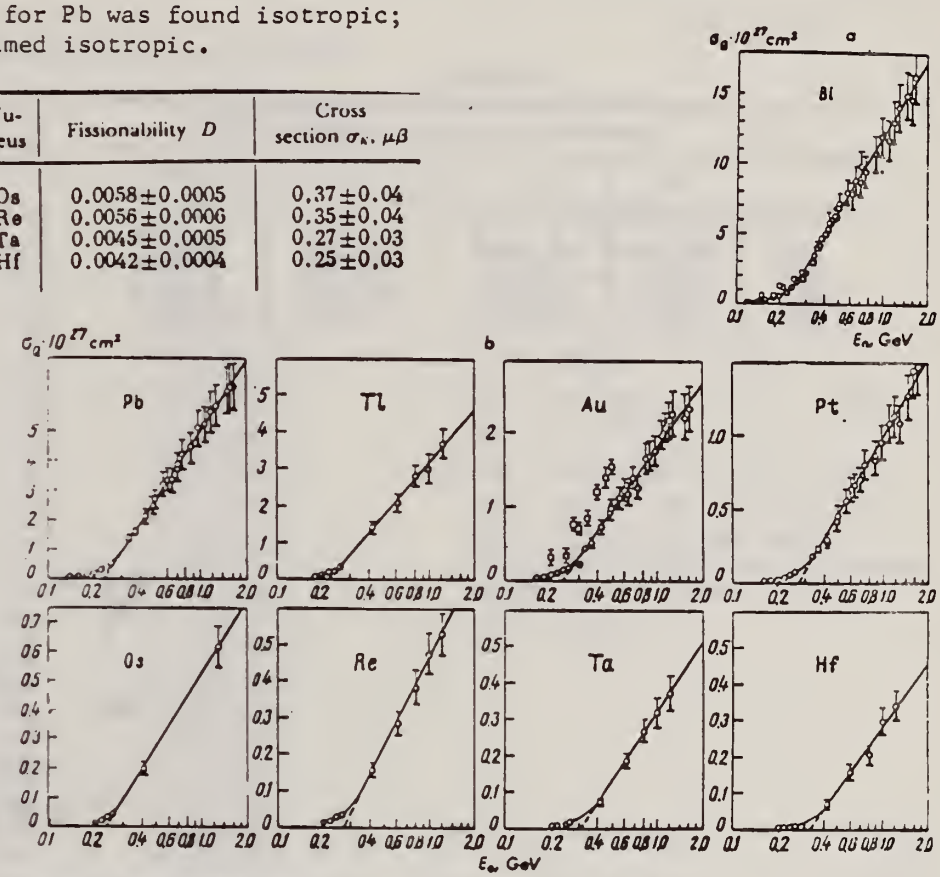

Fig. 1. Photofission fragment yields. ○-present work; □-Jungerman and Steiner.[11] The curves were plotted through the experimental points.

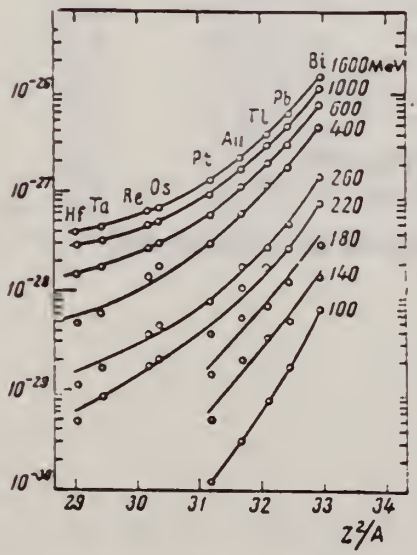

Fig. 2. Photofission fragment yields as a function of Z^2/A. The ordinates are values of σ_0 in units of cm².

REF. Yu. N. Ranyuk and P. V. Sorokin
J. Nucl. Phys. (USSR) 5, 37 (1967)
Sov. J. Nucl. Phys. 5, 26 (1967)

ELEM. SYM.	A	Z
Hf		72

METHOD

REF. NO. 67 Ra 2 HMG

REACTION	RESULT	EXCITATION ENERGY	SOURCE		DETECTOR		ANGLE
			TYPE	RANGE	TYPE	RANGE	
G, F	ABX	THR-260	C	200-260	EMU-I		4PI

TABLE III

$E_{\gamma\,max}$, MeV	Cross section per equivalent γ quantum, 10^{-30} cm²			
	Os	Re	Ta	Hf
200	17±2	11.8±0.8	5.2±0.3	3.2±0.7
220	22±2	17±1	8.6±0.5	4.8±0.3
240	33±3	29±1	13.0±0.6	8.2±0.4
260	45±4	36±2	17.2±0.7	11.2±0.5

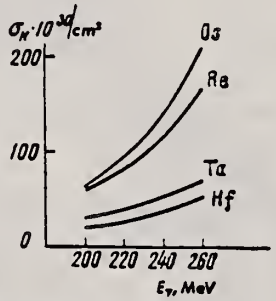

Fig. 4. Photofission cross sections of Os, Re, Ta, and Hf as functions of photon energy.

REF.

V. Emma, S. Lo Nigro, C. Milone
Nucl. Phys. A257, 438 (1976)

EL EM. SYM.	A	Z
Hf		72

METHOD

REF. NO.: 76 Em 2 | egf

REACTION	RESULT	EXCITATION ENERGY	SOURCE TYPE	SOURCE RANGE	DETECTOR TYPE	DETECTOR RANGE	ANGLE
G,F	ABY	THR-999	C	999	TRK-I		4PI

999 = 1 GEV

TABLE 1
Measured values of σ_q at $E = 1000$ MeV and deduced values of σ_t assumed constant from E_0 to 1000 MeV

Element	Z^2/A	σ_q (mb)	E_0 (MeV)	σ_t (mb)
Bi	32.96	12.3 ± 0.6	200	7.6 ± 0.6
Pb	32.45	5.4 ± 0.4	220	3.6 ± 0.3
Tl	32.10	4.1 ± 0.3	230	2.8 ± 0.3
Au	31.68	2.0 ± 0.15	240	1.4 ± 0.2
Pt	31.18	1.1 ± 0.08	255	(8 ± 0.7) × 10^{-1}
Re	30.21	(3.7 ± 0.3) × 10^{-1}	280	(2.9 ± 0.3) × 10^{-1}
W	29.78	(3.5 ± 0.3) × 10^{-1}	290	(2.8 ± 0.3) × 10^{-1}
Ta	29.45	(3.3 ± 0.3) × 10^{-1}	300	(2.7 ± 0.3) × 10^{-1}
Hf	29.04	(1.7 ± 0.2) × 10^{-1}	310	(1.4 ± 0.2) × 10^{-1}
Yb	28.31	(1.3 ± 0.1) × 10^{-1}	330	(1.2 ± 0.1) × 10^{-1}
Tm	28.18	(7.5 ± 0.8) × 10^{-2}	335	(6.8 ± 0.8) × 10^{-2}
Ho	27.21	(3.6 ± 0.4) × 10^{-2}	355	(3.5 ± 0.4) × 10^{-2}
Dy	26.80	(2.6 ± 0.3) × 10^{-2}	360	(2.5 ± 0.3) × 10^{-2}
Tb	26.58	(2.5 ± 0.3) × 10^{-2}	370	(2.5 ± 0.3) × 10^{-2}
Gd	26.04	(1.6 ± 0.2) × 10^{-2}	380	(1.7 ± 0.2) × 10^{-2}
Sm	25.56	(1.3 ± 0.2) × 10^{-2}	390	(1.4 ± 0.2) × 10^{-2}
Nd	24.96	(9.2 ± 0.9) × 10^{-3}	405	(1 ± 0.1) × 10^{-2}
Ce	24.00	(8 ± 0.9) × 10^{-3}	420	(9 ± 1) × 10^{-3}
La	23.39	(8.4 ± 0.9) × 10^{-3}	430	(1 ± 0.1) × 10^{-3}
Sb	21.36	(1.2 ± 0.2) × 10^{-2}	460	(1.5 ± 0.3) × 10^{-2}
Te	21.19	(8.8 ± 1) × 10^{-3}	465	(1.2 ± 0.2) × 10^{-2}
Sn	21.06	(1.3 ± 0.2) × 10^{-2}	465	(1.7 ± 0.3) × 10^{-2}
Cd	20.49	(1.7 ± 0.3) × 10^{-2}	470	(2.2 ± 0.4) × 10^{-2}
Ag	20.47	(2 ± 0.3) × 10^{-2}	470	(2.6 ± 0.4) × 10^{-2}
Zn	13.76	(2 ± 0.4) × 10^{-1}	515	(3 ± 0.6) × 10^{-1}
Cu	13.44	(2.4 ± 0.5) × 10^{-1}	515	(3.6 ± 0.8) × 10^{-1}
Ni	13.35	(2.4 ± 0.5) × 10^{-1}	510	(3.6 ± 0.8) × 10^{-1}
Fe	12.10	(3 ± 0.6) × 10^{-1}	510	(4.4 ± 0.9) × 10^{-1}

[4] A.V. Mitrofanova et al. Sov. J. Nucl. Phys. 6, 512 (1968).

[7] T. Methasiri et al., Nucl. Phys. A167, 97 (1971).

[12] J.R. Nix et al., Nucl. Phys. 81, 61 (1966).

[20] N.A. Perifilov et al., JETP (Sov. Phys.) 14, 623 (1962); Proc. Symp. on the physics & chemistry of fission, Salzburg 1965, vol. 2 (IAEA) Vienna, 1965, p.283.

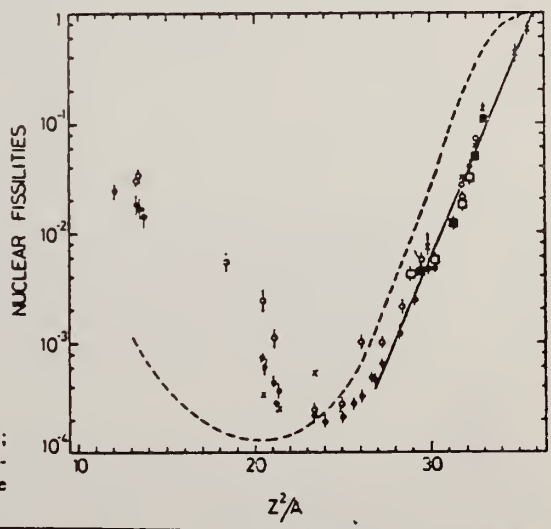

Fig. 2. Nuclear fissilities as a function of Z^2/A. Experimental points: solid circles represent our data; squares, the data from ref. [4]); open circles, the data from ref. [7]); and crosses, the data from (p,f) experiments[20]). The straight line is the best fit calculated from our data for $Z^2/A > 26$. The dashed curve is the curve VI calculated by Nix and Sassi[12]).

HF
A=176

HF
A=176

REF. A.M. Goryachev and G.I. Zalesnyi
Yad. Fiz. 26, 465 (September 1977)
Sov. J. Nucl. Phys. 26, 246 (September 1977)

ELEM. SYM.	A	Z
Hf	176	72

METHOD

REF. NO. 77 Go 4

hmg 11/17/80

REACTION	RESULT	EXCITATION ENERGY	SOURCE		DETECTOR		ANGLE
			TYPE	RANGE	TYPE	RANGE	
G,XN	ABX	8(8.1)-22	C	8-22	BF3-I	---	4PI

Yield curves and photoneutron multiplicities have been measured for the isotopes ^{176,178,180}Hf in a betatron bremsstrahlung beam in the energy range 8–21 MeV with a 0.125-MeV step. The measurements were made on-line with a computer. The cross sections were calculated from the yield curves by the Penfold-Leiss method with a 1.0-MeV step. The multiplicity curves were used to separate the contributions of (γ,n) and $(\gamma,2n)$ reactions. Integrated cross sections calculated from the photoabsorption cross sections are given, and also average energies and deformation parameters. The results are compared with calculations using various versions of the model of coupling of dipole and quadrupole vibrations.

n multiplicity measurement

TABLE V. Average energies.

Nucleus	ε_{M^-}, MeV	ε_{M^+}, MeV	$\varepsilon_M A^{1/3}$	$\varepsilon_M A^{1/3}$	K, MeV
^{176}Hf	14.45	14.51	81.0	34.2	28.3
^{178}Hf	14.41	14.49	81.0	34.2	28.8
^{180}Hf	14.43	14.50	81.5	34.3	29.1

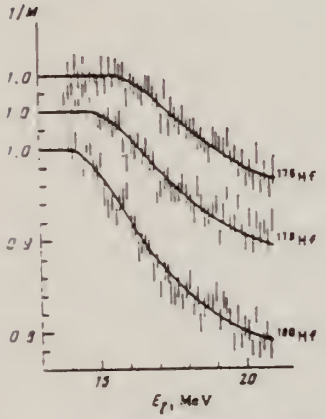

FIG. 1. Multiplicity of photoneutrons for the isotopes ^{176,178,180}Hf. The length of the vertical lines is equal to two standard deviations. The solid curves are the fitted curves $M(E_{\gamma\,max})$ with the parameters given in Table II.

TABLE VI. Deformation β and quadrupole moment Q_0.

Nucleus	Our data		From $B(E2, 2_1^+ \to 0_1^+)$ [a]	
	β	Q_0, b	β	Q_0, b
^{176}Hf	0.30±0.03	7.4±0.6	0.27	7.37±0.17
^{178}Hf	0.30±0.03	7.5±0.5	0.25	6.81±0.07
^{180}Hf	0.30±0.03	7.5±0.7	0.25	6.83±0.06

TABLE VII. Dipole strengths of transverse maximum.

i	γ-vibrational model		Nonaxial rotator model		Davydov–Chaban model	
	λ_i	$(0\|\lambda_i\|)^2$	λ_i	$(0\|\lambda_i\|)^2$	λ_i	$(0\|\lambda_i\|)^2$
1	−0.086	0.923	−0.065	0.94	−0.12	0.86
2	0.992	0.073	1.085	0.06	0.71	0.10
3	1.921	0.003	–	–	1.01	0.04

TABLE II. Parameters of photoneutron multiplicity curves.

Nucleus	a, MeV^{-1}	W	χ^2/f	a, MeV^{-1}	W	χ^2/f
^{176}Hf	7.0±0.5	0	1.07	20.9	0.36±0.03	1.09
^{178}Hf	5.1±0.3	0	0.95	22.6	0.46±0.02	0.91
^{180}Hf	9.3±0.6	0	1.01	23.0	0.24±0.015	0.97

Note. f is the number of degrees of freedom.

TABLE III. Parameters of the Lorentz curves.

Nucleus	E_1, MeV	Γ_1, MeV	σ_1, mb	E_2, MeV	Γ_2, MeV	σ_2, mb	R
^{176}Hf	12.36±0.04	2.96±0.09	272±9	15.71±0.05	5.0±0.02	269±5	0.60±0.07
^{178}Hf	12.41±0.05	3.00±0.1	283±10	15.75±0.06	4.6±0.2	273±5	0.67±0.07
^{180}Hf	12.41±0.04	2.80±0.09	286±8	15.75±0.05	4.4±0.1	261±4	0.65±0.07

TABLE IV. Integrated cross sections

	^{176}Hf	^{178}Hf	^{180}Hf
σ_{int}, MeV-mb	2571 ± 12	2580 ± 15	2535 ± 12
σ_{-1}, mb	184 ± 1	185 ± 1	182 ± 1
σ_{-2}, MeV^{-1} mb	13.65 ± 0.07	13.71 ± 0.08	13.53 ± 0.07
$\sigma_{int}(\gamma, 2n)$, MeV-mb	518 ± 4	683 ± 6	515 ± 5
$\sigma_{int\ L}$, MeV-mb	3370	3318	3188
$\sigma_{int}/60NZ/A$	1.007	1.003	0.978
$\sigma_{-1}A^{-4/3}$	0.186	0.184	0.179
$\sigma_{-2}A^{-5/3}$	0.00247	0.00243	0.00236
$\sigma_{int}(\gamma, 2n)/\sigma_{int}$	0.202	0.265	0.322
$\sigma_{int\ L}/60NZ/A$	1.32	1.29	1.23

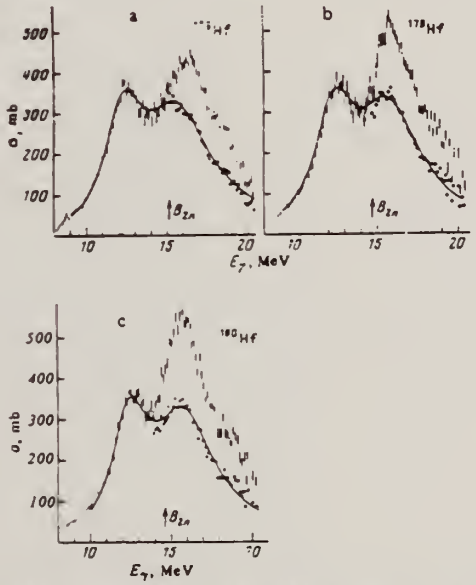

FIG. 2. Photoabsorption cross sections for the isotopes ^{176,178,180}Hf. The vertical lines, whose length is two standard deviations, indicate the cross section $\sigma_{\gamma,abs} = \sigma_{\gamma,n} + 2\sigma_{\gamma,2n} + \sigma_{\gamma,np} + \ldots$ Above the threshold of the $\gamma, 2n$) reaction the photoabsorption cross section is indicated by the solid circles; the smooth curves are fits by Lorentz curves with the parameters given in Table III.

σ_{int} corrected for neutron multiplicity

HF
A=177

HF
A=177

Ref. R. Tobin, J. McElhinney, L. Cohen
Phys. Rev. 110, 1388 (1958)

Elem. Sym.	A	Z
Hf	177	72

Method: 22 MeV betatron; neutron counters

Ref. No.: 58 To 1

Reaction	E or ΔE	E_o	Γ	$\int \sigma dE$	Jπ	Notes
$Hf^{177}(\gamma,n)$	Bremss. 6.3-7					E_{th} = 6.70±0.09

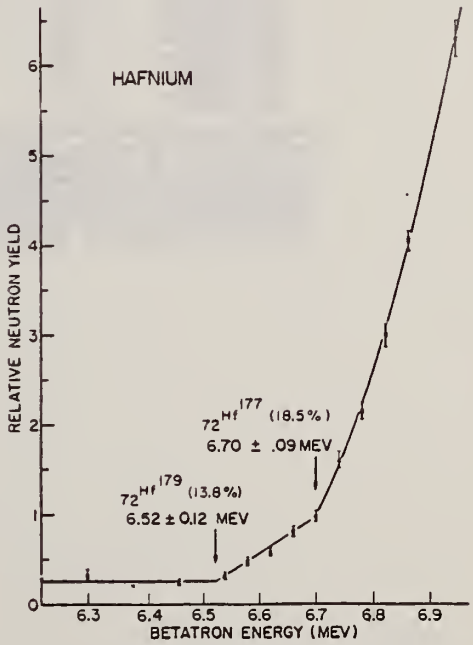

FIG. 7. Photoneutron yield from hafnium as a function of betatron energy.

K. N. Geller, J. Halpern, and E. G. Muirhead
Phys. Rev. 118, 1302-12 (1960)

Hf	177	72

METHOD

Betatron; neutron threshold; ion chamber

REF. NO. 60 Ge 3 | NVB

REACTION	RESULT	EXCITATION ENERGY	SOURCE		DETECTOR		ANGLE
			TYPE	RANGE	TYPE	RANGE	
G,N	NØX	THR	C THR		BF3-I		4 PI

THRESHØLD

TABLE I. Summary and comparison of neutron separation energies inferred from present threshold measurements with values predicted from mass data and reaction energies. All energies are expressed in the center-of-mass system in Mev.

Reaction	No. runs	Present results	Other results	Method	Reference
$Hf^{177}(\gamma,n)Hf^{176}$	1	6.692±0.034(6.606)	6.28 ±0.06 6.70 ±0.09	mass data threshold	q k

[q] W. H. Johnson, Jr., and V. B. Bhanot, Phys. Rev. 107, 6 (1957).

TABLE II. Comparison of measured threshold energies with neutron binding energies predicted by mass data for transitions with $\Delta I \geq 7/2$. All energies in Mev.

Reaction	ΔI[a]	Observed threshold	Mass data Q value	$E_{th}-Q$	Excited state energy
$Cr^{52}(\gamma,n)Cr^{51}$	7/2	12.18±0.14	12.053±0.004[b]	0.13±0.14	...
$Y^{89}(\gamma,n)Y^{88}$	7/2	11.59±0.08	11.53 ±0.40[c]	0.06±0.41	0.387[d]
$In^{116}(\gamma,n)In^{114}$	7/2	9.22±0.03	9.35 ±0.43[e]	−0.13±0.43	0.191[a]
$Ce^{142}(\gamma,n)Ce^{141}$	(7/2)[e]	7.24±0.07	6.97 ±0.07[f]	0.27±0.10	...
$Nd^{146}(\gamma,n)Nd^{144}$	7/2	6.38±0.16	5.97 ±0.19[f]	0.41±0.25	0.690[a]
$Sm^{149}(\gamma,n)Sm^{148}$	7/2	6.45±0.16	5.87 ±0.28[f]	0.58±0.33	0.562[a]
$Er^{167}(\gamma,n)Er^{166}$	7/2	6.65±0.08	6.45 ±0.06[g]	0.20±0.10	0.081[a]
$Hf^{177}(\gamma,n)Hf^{176}$	7/2	6.69±0.03	6.28 ±0.06[g]	0.64±0.07	0.088[a]
$Hf^{179}(\gamma,n)Hf^{178}$	9/2	6.31±0.07	6.17 ±0.06[g]	0.14±0.09	0.093[a]
$Hf^{180}(\gamma,n)Hf^{179}$	9/2	7.85±0.11	7.32 ±0.06[g]	0.53±0.13	0.375[a]

[a] D. Strominger, J. M. Hollander, and G. T. Seaborg, Revs. Modern Phys. 30, 585 (1958).
[b] C. F. Giese and J. L. Benson, Phys. Rev. 110, 712 (1958).
[c] Henry E. Duckworth, *Mass Spectroscopy* (Cambridge University Press, New York, 1958), p. 177.
[d] S. Dzelepov and L. K. Peker, Atomic Energy of Canada Limited Report Tr. AECL-457 (unpublished).
[e] The discrepancy in the case of Ce^{142} predicts a ground-state spin for Ce^{142} of 0, since the spin of Ce^{141} is known to be 7/2.
[f] W. H. Johnson, Jr., and A. O. Nier, Phys. Rev. 105, 1014 (1957).
[g] W. H. Johnson, Jr., and V. B. Bhanot, Phys. Rev. 107, 6 (1957).

W. D. Hamilton and B. S. Sood
Nuclear Phys. 27, 66 (1961)

ELEM. SYM.	A	Z
Hf	177	72

METHOD

REF. NO.	
61 Ha 1	EGF

REACTION	RESULT	EXCITATION ENERGY	SOURCE		DETECTOR		ANGLE
			TYPE	RANGE	TYPE	RANGE	
G,G	LFT	0 - 1	D	0 - 1	NAI-D	0 - 1	110

Used thermal broadening of ^{177}Lu source to supply recoil energy.

Mean lives (113 keV; E2) = 1.5±0.5 nsec

(321 KeV; E1) = 17±5 nsec

REF.

L.M. Dautov, Yu.A. Lysikov, U.M. Makhanov, Yu.K. Shubnyi
Izv. Akad. Nauk SSSR Ser. Fiz. 36, 2544 (1972)
Bull. Acad. Sci. USSR Phys. Ser. 36, 2210 (1972)

ELEM. SYM.	A	Z
Hf	177	72

METHOD

REF. NO. 72 Da 14 hmg

REACTION	RESULT	EXCITATION ENERGY	SOURCE		DETECTOR		ANGLE
			TYPE	RANGE	TYPE	RANGE	
G,G	ABX	250*	D	250*	SCD-D		92

$\sigma = (4.5 \pm .9) \cdot 10^{-27} cm^2 \cdot sr^{-1}$, $\Gamma_{0\gamma} = (2.8 \pm .5) \cdot 10^{-6}$ eV.

* ENERGY IN KEV

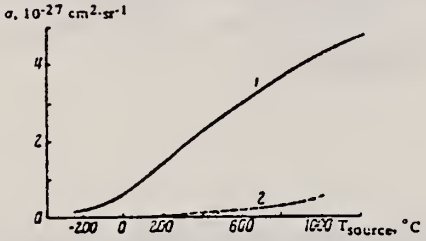

Fig. 1. Resonance scattering cross section as a function of the source temperature: 1) $^{177}Lu \rightarrow \rightarrow {}^{177}Hf$ ($\Gamma_{0\gamma} = 3.4 \cdot 10^{-6}$ eV, $\Gamma_0/\Gamma = 0.5$) 2) $^{159}Gd \rightarrow {}^{159}Tb$ ($\Gamma_{0\gamma} = 2.4 \cdot 10^{-6}$ eV, $\Gamma_0/\Gamma = 0.96$).

HF
A=178

HF
A=178

REF.

B.I. Goryachev, Yu.V. Kuznetsov, V.N. Orlin, N.A. Pozhidaeva, and V.G. Shevchenko
ZhETF Pis. Red. 19, 65 (1974)
JETP Lett. 19, 41 (1974)

ELEM. SYM.	A	Z
Hf	178	72

METHOD

REF. NO.	
74 Go 4	hmg

REACTION	RESULT	EXCITATION ENERGY	SOURCE		DETECTOR		ANGLE
			TYPE	RANGE	TYPE	RANGE	
G,XN	ABX	7- 20	C	7- 20	BF3-I		4PI

$\sigma(\gamma,2n)$ measured but not given.

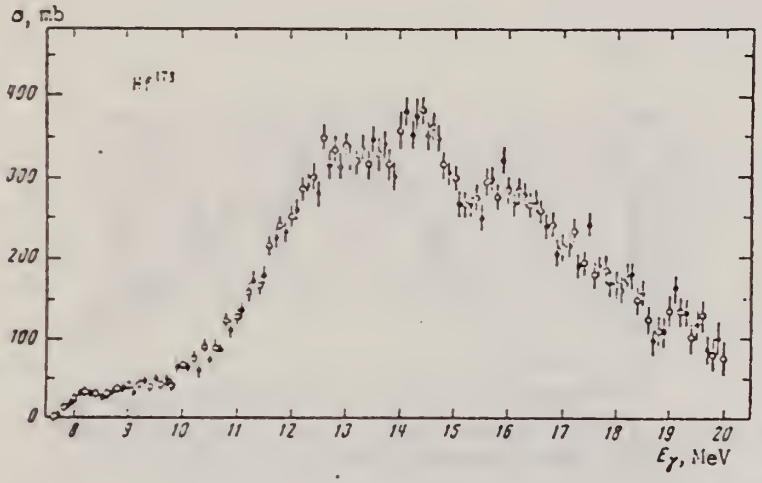

Fig. 2. Cross section σ_γ of Hf^{178}

Note: (γ,sn) cross section determined from $\sigma(\gamma,xn)$ and statistical theory which gives $\sigma(\gamma,2n)$ consistent with measurements.

See Refs. 6&7 for Regularization Method (Least Structure).

[6] A.N. Tikhonov, Dokl.Akad.Nauk SSSR 151, 501 (1963).

[7] B.S. Cook, Nucl.Instr. and Meth. 24, 256 (1963).

Nucleus	σ_{int}, MeV-b	β	Q_0, b
Er^{166}	3.05 ± 0.3	0.33	7.76
Hf^{178}	3.16 ± 0.3	0.26	6.72

The table lists the values of the integral cross sections σ_{int} calculated from σ_γ and the deformation parameters β, as well as the values Q_0 of the intrinsic quadrupole moments of the nuclei, corresponding to the obtained values of β.

REF. B.I. Goryachev, Yu.V. Kuznetsov, V.N. Orlin, N.A. Pzhidaeva, V.G. Shevchenko
Yad. Fiz. 23, 1145 (1976)
Sov. J. Nucl. Phys. 23, 609 (1976)

ELEM. SYM.	A	Z
Hf	178	72

METHOD

REF. NO. 76 Go 4 egf

REACTION	RESULT	EXCITATION ENERGY	SOURCE		DETECTOR		ANGLE
			TYPE	RANGE	TYPE	RANGE	
G,XN	ABX	7- 20	C	UKN	BF3-I		4PI
G,2N	ABX	14- 20	C	UKN	SCI-I		4PI

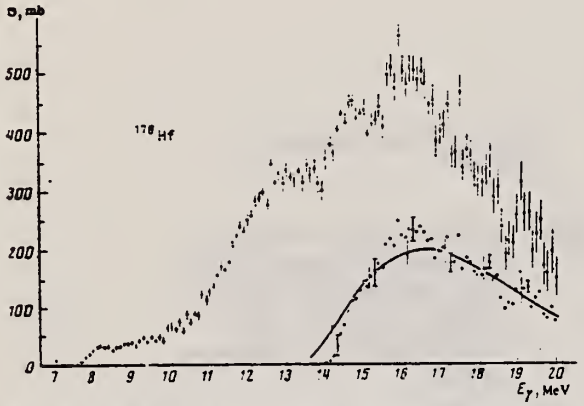

FIG. 2. Cross section σ_n for ^{178}Hf. In the lower part of the figure we have shown the cross section for the reaction ^{178}Hf$(\gamma, 2_n)^{176}$Hf (see the caption for Fig. 1).

FIG. 1. Photoneutron production cross section σ_n obtained for ^{159}Tb (a) and for ^{165}Er (b). The hollow and solid circles correspond to two independent series of data. The solid curves show the $(\gamma, 2n)$ cross sections calculated from the data of a statistical experiment by the regularization method.[12] The circles near the curves give the same cross sections calculated from the formula $\sigma_n(1-f(E,\sigma))$.

TABLE 5. Parameters of curve fitted to the cross section σ_γ in ^{178}Hf.

Number of resonance	E_k, MeV	σ_k, mb	Γ_k, MeV	$\sigma_k\Gamma_k$, $\sigma_0\Gamma_0$
1	12.52	250	2.65	1.09
2	14.30	130	1.07±0.21	0.21±0.06
3	16.07	225	5.21±0.50	1.78±0.29

χ^2=111.4, f=57, E_0=10.6 MeV, σ_0= 20.0 mb

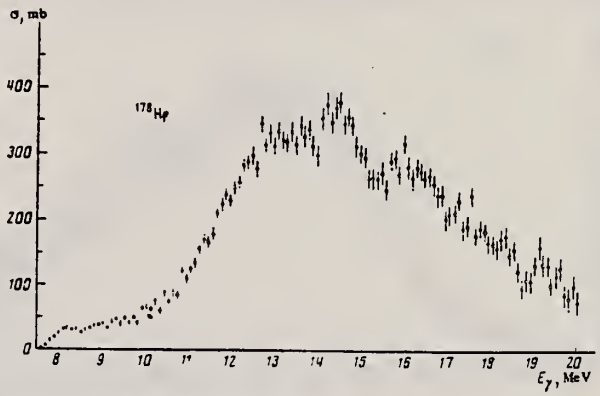

FIG. 7. Cross section σ_γ for ^{178}Hf.

TABLE 3. Static deformation β and intrinsic quadrupole moment Q_0.

Nucleus	Present work		Other photonuclear experiments		Coulomb excitation of nuclei
	β	Q_0, b	β	Q_0, b	Q_0, b
^{159}Tb	0.29	6.53±0.6	0.29 0.32 0.29	6.57 [15] 7.37 [20] 6.6 [21]	7.07 [19]
^{165}Ho	0.32	7.73±0.6	0.29 0.30 0.31	7.01 [15] 7.14 [20] 7.6 [16]	7.80 [19]
^{166}Er	0.30	7.39±0.6	0.28 0.31	6.96 [16] 7.6 [16]	
^{178}Hf	0.26	6.94±0.6			6.79 [22]

TABLE 1. Level-density parameters

Nucleus	a, MeV^{-1}		Nucleus	a, MeV^{-1}	
	Present work	Other studies		Present work	Other studies
^{159}Tb	—	7.7[15]	^{166}Er	6.1±2.5	8[16]
^{165}Ho	4.2±1.5	3.1[15]	^{178}Hf	17.7±7.3	—

(over)

TABLE 2. Parameters of fitted curves $\sigma_\gamma^{(2)}$

Nucleus	E_1, MeV	σ_1, mb	Γ_1 MeV	E_2 MeV	σ_2, mb	Γ_2 MeV	$\sigma_1\Gamma_1/\sigma_2\Gamma_2$	χ^2	f	E_{f_1}, MeV	E_{f_2}, MeV
^{159}Tb	12.28	102	2.91±0.09	15.76	205	5.42±0.18	2.56±0.23	197.3	97	10.4	20.6
	12.41	213	3.31±0.05	15.95	282	5.01±0.07	2	216.8	98	10.4	20.6
^{169}Tlo	12.31	204	2.74±0.11	16.23	306	5.67±0.17	3.11±0.27	176.0	97	10.4	20.6
	12.47	225	3.26±0.06	16.46	293	5.02±0.09	2	200.8	98	10.4	20.6
^{169}Er	12.22	191	2.71±0.14	15.99	306	5.67±0.16	3.38±0.35	138.5	94	10.7	20.6
	12.50	214	3.43±0.08	16.25	284	5.09±0.10	2	161.7	95	10.7	20.6
^{179}Hf	12.08	166	2.35±40	15.05	281	6.04±0.27	4.00±1.76	172.1	89	10.6	20.0
	12.88	216	3.22±0.11	15.48	237	5.37±0.20	2	175.7	90	10.6	20.0

Note. The lower values of the parameters in each column were found with the requirement $\sigma_2\Gamma_2 : \sigma_1\Gamma_1 = 2:1$.

TABLE 6. Integrated cross sections.

Nucleus	σ_0, MeV-b	$\sigma_0 0.0\frac{ZN}{A}$	σ_{-1}, mb	$\sigma_{-1}A^{1/3}$	σ_{-2}, MeV-b	$\sigma_{-2}A^{1/3}$
^{159}Tb	3.79	1.47	210	0.243	15.9	$3.41\cdot10^{-3}$
^{169}Tlo	4.00	1.51	218	0.241	16.1	$3.25\cdot10^{-3}$
^{169}Er	3.56	1.48	206	0.237	16.1	$3.21\cdot10^{-3}$
^{179}Hf	3.03	1.20	196	0.196	14.8	$2.63\cdot10^{-3}$
Average		1.41±0.3		0.23±0.04		$3.1\ 10^{-3}\pm6\cdot10^{-4}$

[12] A.N. Tikhonov, Dokl. Akad. Nauk SSSR 151, 501 (1963), Eng. transl. in Sov. Mathematics-Doklady.

[15] B. L. Berman et al., Phys. Rev. 185, 1576 (1969).

[16] R. Bergere et al., Nucl. Phys. A133, 417 (1969).

[18] E. G. Fuller et al., Nucl. Phys. 30, 613 (1962).

[19] H. Arenhovel et al., Phys. Rev. 157, 1109 (1967).

[20] R. Bergere et al., Nucl. Phys. A121, 463 (1968).

[21] O.V. Bogdankevich et al., Zh. Eksp.Teor.Fiz. 42, 1502 (1962); Sov. Phys. JETP 15, 1044 (1962).

[22] B.S. Dzhelepov in Struktura slozhynkh yader (Structure of Complex Nuclei), Atomizdat, 1966, p. 189.

REF.		ELEM. SYM.	A	Z
	G. M. Gurevich, L. E. Lazareva, V. M. Mazur and G. B. Solodukhov JETP Lett. 23, 370 (1976) Pis'ma Zh. Eksp. Teor. Fiz. 23, 411 (1976)	Hf	178	72

METHOD	REF. NO.	
	76 Gu 5	hmg

REACTION	RESULT	EXCITATION ENERGY	SOURCE		DETECTOR		ANGLE
			TYPE	RANGE	TYPE	RANGE	
G,MU-T	ABX	8- 21	C	35	NAI-D		4PI

We measured the total cross section for the absorption of rays in the region of $E1$ resonance for the nuclei ^{165}Ho, ^{178}Hf, ^{180}Hf, ^{181}Ta, ^{182}W, ^{197}Au, and ^{209}Bi. The singularity in the behavior of the resonance widths, observed in the region $160 < A < 185$, is apparently due to the influence of the neutron subshell $N = 108$.

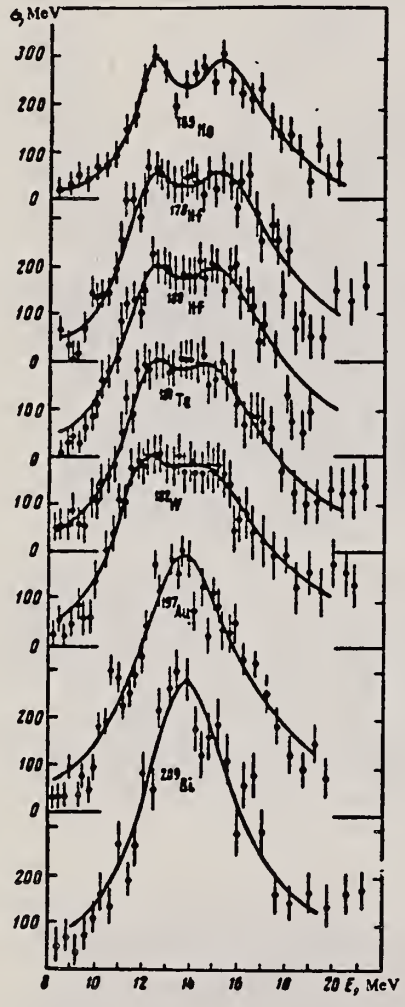

FIG. 1. Total photoabsorption cross sections for the nuclei ^{165}Ho, ^{178}Hf, ^{180}Hf, ^{181}Ta, ^{182}W, ^{197}Au, ^{209}Bi.

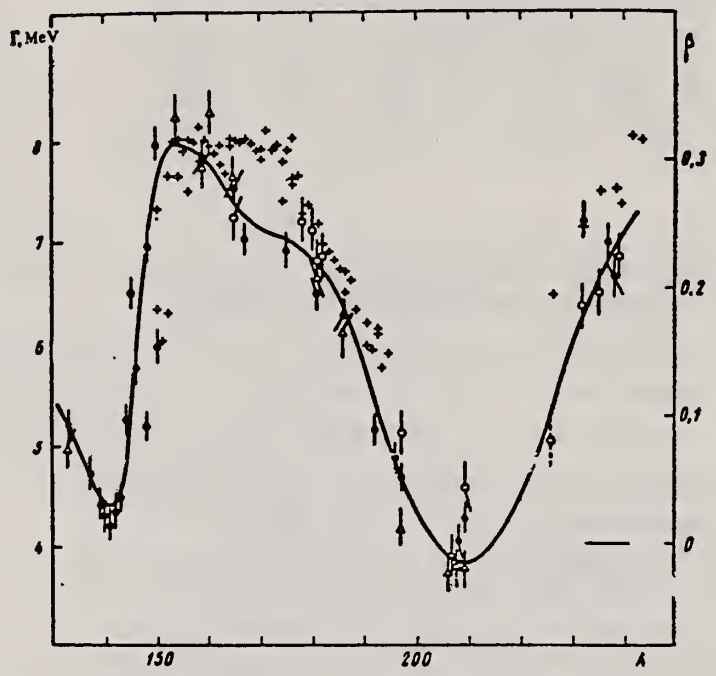

FIG. 2. Widths Γ of $E1$ giant resonance in the region of nuclei with $A > 150$ according to the data of Saclay (●), Livermore (Δ), and the Institute of Nuclear Research of the USSR Academy of Sciences (○). The crosses mark the deformation parameters β.

over

U.S. DEPARTMENT OF COMMERCE
NATIONAL BUREAU OF STANDARDS

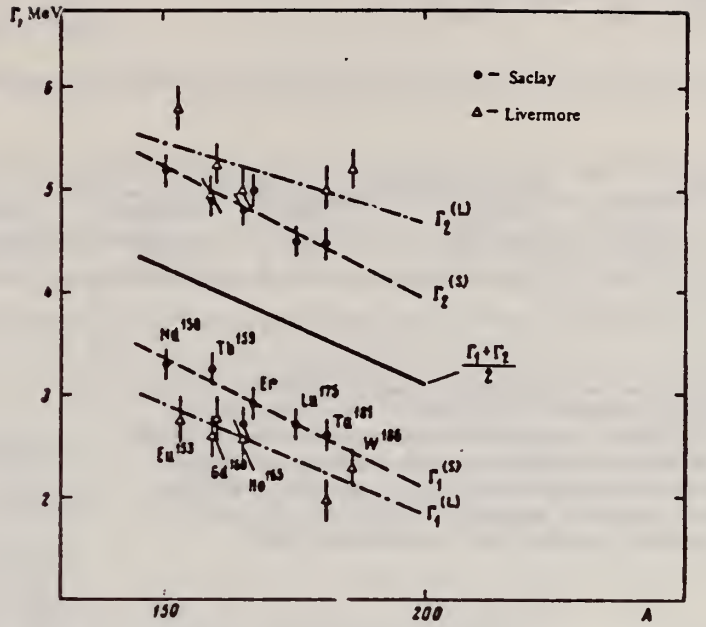

FIG. 3. Width of Lorentz lines approximating the photoabsorption cross sections, for deformed nuclei in the region $150 < A < 185$.

Nucleus	σ_1 mb	Γ_1 MeV	E_1 MeV	σ_2 mb	Γ_2 MeV	E_2 MeV	$\frac{\sigma_2\Gamma_2}{\sigma_1\Gamma_1}$	Q_0 b	β
Ho-165	235	2.0	12.2	272	4.0	15.5	2.3	6.8±0.8	0.29
Hf-178	291	3.1	12.2	334	4.9	15.5	1.8	7.5±0.8	0.28
Hf-180	286	3.2	12.2	324	5.1	15.3	1.8	7.2±0.8	0.27
Ta-181	272	3.0	12.1	316	5.1	15.0	2.0	6.8±0.8	0.26
W-182	267	3.2	11.9	303	5.6	14.8	2.0	7.2±0.8	0.26
Au-197	535	5.2	13.7	...	...	...	...	...	...
Bi-209	600	4.6	13.8	...	...	...	...	...	...

REF. A.M. Goryachev and G.I. Zalesnyi
Yad. Fiz. 26, 465, (September 1977)
Sov. J. Nucl. Phys. 26, 246 (September 1977)

ELEM. SYM.	A	Z
Hf	178	72

METHOD

REF. NO. 77 Go 4

hmg 11/17/80

REACTION	RESULT	EXCITATION ENERGY	SOURCE		DETECTOR		ANGLE
			TYPE	RANGE	TYPE	RANGE	
G,XN	ABX	7(7.6)-22	C	8-22	BF3-I	---	4PI

Yield curves and photoneutron multiplicities have been measured for the isotopes ^{176,178,180}Hf in a betatron bremsstrahlung beam in the energy range 8–21 MeV with a 0.125-MeV step. The measurements were made on-line with a computer. The cross sections were calculated from the yield curves by the Penfold-Leiss method with a 1.0-MeV step. The multiplicity curves were used to separate the contributions of (γ,n) and $(\gamma,2n)$ reactions. Integrated cross sections calculated from the photoabsorption cross sections are given, and also average energies and deformation parameters. The results are compared with calculations using various versions of the model of coupling of dipole and quadrupole vibrations.

n multiplicity measurement

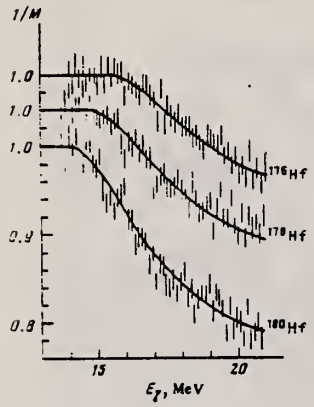

FIG. 1. Multiplicity of photoneutrons for the isotopes ^{176,178,180}Hf. The length of the vertical lines is equal to two standard deviations. The solid curves are the fitted curves $M(E_{\gamma max})$ with the parameters given in Table II.

TABLE II. Parameters of photoneutron multiplicity curves.

Nucleus	a, MeV^{-1}	W	χ^2/f	a, MeV^{-1}	W	χ^2/f
^{176}Hf	7.0±0.5	0	1.07	20.9	0.36±0.03	1.09
^{178}Hf	5.1±0.3	0	0.95	22.6	0.46±0.02	0.91
^{180}Hf	9.3±0.6	0	1.01	23.0	0.24±0.015	0.97

Note. f is the number of degrees of freedom.

TABLE III. Parameters of the Lorentz curves.

Nucleus	E_1, MeV	Γ_1, MeV	σ_1, mb	E_2, MeV	Γ_2, MeV	σ_2, mb	R
^{176}Hf	12.36±0.04	2.96±0.09	272±9	15.71±0.06	5.0±0.2	269±5	0.60±0.07
^{178}Hf	12.41±0.05	3.00±0.1	283±10	15.75±0.06	4.6±0.2	273±5	0.67±0.07
^{180}Hf	12.41±0.04	2.80±0.09	286±8	15.75±0.05	4.4±0.1	281±4	0.65±0.07

TABLE IV. Integrated cross sections

	^{176}Hf	^{178}Hf	^{180}Hf
σ_{int}, MeV-mb	2571 ± 12	2580 ± 15	2535 ± 12
σ_{-1}, mb	184 ± 1	185 ± 1	182 ± 1
σ_{-2}, MeV^{-1} mb	13.65 ± 0.07	13.71 ± 0.08	13.53 ± 0.07
$\sigma_{int}(\gamma, 2n)$, MeV-mb	518 ± 4	683 ± 6	815 ± 5
$\sigma_{int\ L}$, MeV-mb	3370	3318	3188
$\sigma_{int}/60NZ/A$	1.007	1.003	0.978
$\sigma_{-1}A^{-4/3}$	0.186	0.184	0.179
$\sigma_{-2}A^{-5/3}$	0.00247	0.00243	0.00236
$\sigma_{int}(\gamma, 2n)/\sigma_{int}$	0.202	0.265	0.322
$\sigma_{int\ L}/60NZ/A$	1.32	1.29	1.23

TABLE V. Average energies.

Nucleus	E_M, MeV	$E_{M'}$, MeV	$E_M A^{1/3}$	$E_M A^{1/3}$	K, MeV
^{176}Hf	14.45	14.51	81.0	34.2	28.3
^{178}Hf	14.41	14.49	81.0	34.2	28.8
^{180}Hf	14.43	14.50	81.5	34.3	29.1

TABLE VI. Deformation β and quadrupole moment Q_0.

Nucleus	Our data		From $B(E2, 2_1^+ \to 0_1^+)$ [*]	
	β	Q_0, b	β	Q_0, b
^{176}Hf	0.30±0.03	7.4±0.6	0.27	7.37±0.17
^{178}Hf	0.30±0.03	7.5±0.5	0.25	6.81±0.07
^{180}Hf	0.30±0.03	7.5±0.7	0.25	6.83±0.06

TABLE VII. Dipole strengths of transverse maximum.

i	γ-vibrational model		Nonaxial rotator model		Davydov–Chaban model	
	λ_i	$(0\|\lambda_i\|)^2$	λ_i	$(0\|\lambda_i\|)^2$	λ_i	$(0\|\lambda_i\|)^2$
1	−0.066	0.923	−0.085	0.94	−0.12	0.86
2	0.992	0.073	1.085	0.06	0.71	0.10
3	1.921	0.003	–	–	1.01	0.04

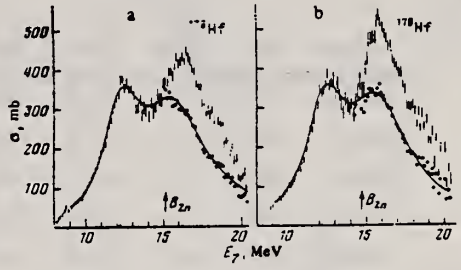

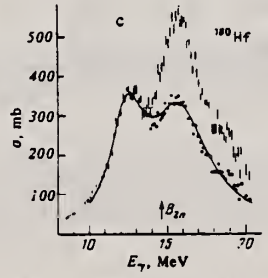

FIG. 2. Photoabsorption cross sections for the isotopes ^{176,178,180}Hf. The vertical lines, whose length is two standard deviations, indicate the cross section $\sigma_{exp} = \sigma_{\gamma,n} + 2\sigma_{\gamma,2n} + \sigma_{\gamma,np} + \ldots$. Above the threshold of the $\gamma, 2n)$ reaction the photoabsorption cross section is indicated by the solid circles; the smooth curves are fits by Lorentz curves with the parameters given in Table III.

σ_{int} corrected for neutron multiplicity

REF. G.M. Gurevich, L.E. Lazareva, V.M. Mazur, S.Yu. Merkulov, G.V. Solodukhov, V.A. Tyutin
Nucl. Phys. A351, 257 (1981)

ELEM. SYM.	A	Z
Hf	178	72

METHOD

REF. NO. 81 Gu 2 hg

REACTION	RESULT	EXCITATION ENERGY	SOURCE		DETECTOR		ANGLE
			TYPE	RANGE	TYPE	RANGE	
G,MU-T	ABX	THR-20	C	27	NAI-D		4PI

Abstract: The curves of the total gamma-absorption cross sections (σ_{tot}) in the E1 giant resonance energy range for the nuclei ^{154}Sm, ^{156}Gd, ^{165}Ho, ^{168}Er, ^{174}Yb, ^{178}Hf, ^{180}Hf, ^{181}Ta, ^{182}W, ^{184}W, ^{186}W and ^{197}Au have been measured using the absorption method. Parameters of the Lorentz curves fitting the measured cross sections σ_{tot} are given. Quadrupole moments (Q_0) and nuclear deformation parameters (β) were obtained.

For deformed nuclei in the $\sim 155 < A < \sim 180$ region a violation of the correlation between giant resonance widths (Γ) and nuclear deformation parameters was found. Γ_1 and Γ_2, the widths of the resonances corresponding to vibrations of nucleons along and across the nuclear deformation axis, were observed to decrease with the increase of A which could be accounted for by the presence of an $N = 108$ subshell.

NUCLEAR REACTIONS ^{154}Sm, ^{156}Gd, ^{165}Ho, ^{168}Er, ^{174}Yb, ^{178,180}Hf, ^{181}Ta, ^{182,184,186}W, ^{197}Au (γ, X), E = 7–20 MeV; measured total $\sigma(E)$; deduced integrated σ, Lorentz line parameters ^{154}Sm, ^{156}Gd, ^{165}Ho, ^{168}Er, ^{174}Yb, ^{178,180}Hf, ^{181}Ta, ^{182,184,186}W, ^{197}Au deduced β, Q_0, Γ; giant resonance evolution. Enriched, natural targets.

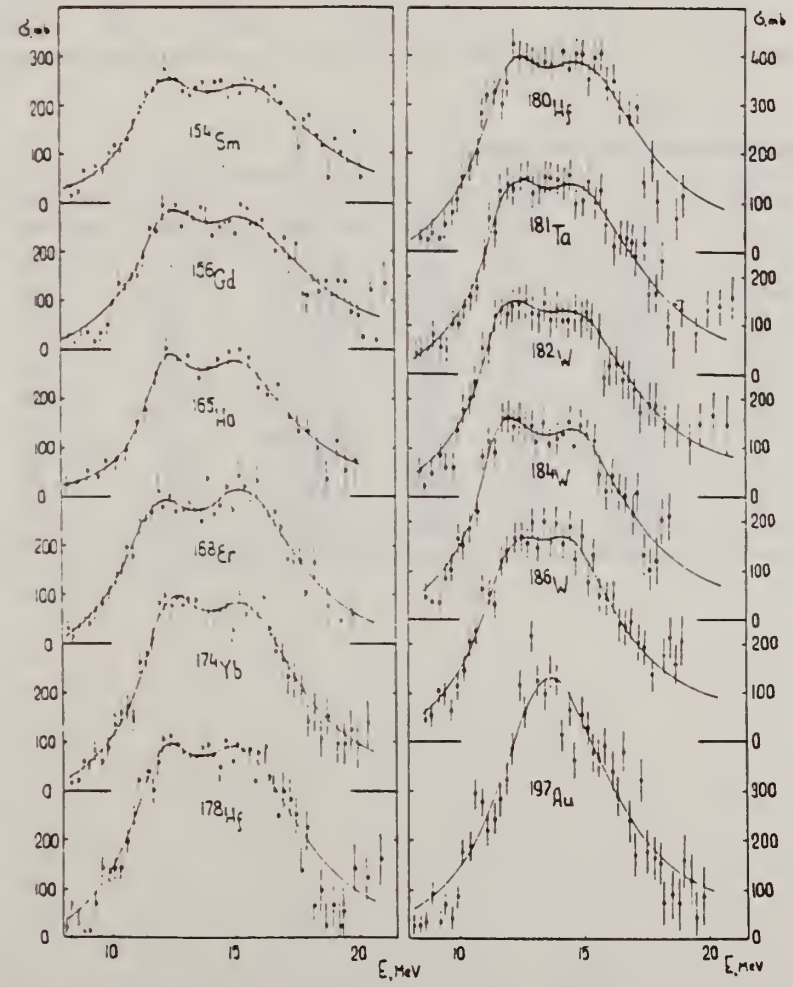

Fig. 2. Total nuclear γ-absorption cross sections (σ_{tot}) measured by the absorption method for ^{154}Sm, ^{156}Gd, ^{165}Ho, ^{168}Er, ^{174}Yb, ^{178}Hf, ^{180}Hf, ^{181}Ta, ^{182}W, ^{184}W, ^{186}W and ^{197}Au. Rms error bars are shown.

(OVER)

TABLE 2

Parameters of Lorentz curves fitting the experimental data on σ_{tot}

Nucleus	E_1 (MeV)	σ_1 (mb)	Γ_1 (MeV)	E_2 (MeV)	σ_2 (mb)	Γ_2 (MeV)	$\frac{\sigma_2\Gamma_2}{\sigma_1\Gamma_1}$	Γ (MeV)
^{154}Sm	12.2	188	3.4	15.7	207	5.7	1.85	8.1
^{156}Gd	12.3	206	3.2	15.7	220	5.5	1.81	7.7
^{165}Ho	12.3	202	2.3	15.2	239	4.8	2.47	7.0
^{168}Er	11.9	222	3.2	15.5	275	4.5	1.73	7.4
^{174}Yb	12.3	297	2.9	15.5	320	4.9	1.80	7.1
^{178}Hf	12.2	291	3.1	15.5	334	4.9	1.80	7.2
^{180}Hf	12.2	286	3.2	15.3	324	5.1	1.81	7.1
^{181}Ta	12.1	272	3.0	15.0	316	5.1	1.97	6.8
^{182}W	11.9	267	3.2	14.8	303	5.6	2.01	6.8
^{184}W	11.9	315	2.9	14.8	321	4.7	1.65	6.8
^{186}W	12.0	246	3.3	14.5	332	5.1	2.07	6.4
^{197}Au	13.7	535	5.2					
Average error	1.4 %	11.2 %	9.3 %	1.5 %	9.7 %	4.6 %	0.22	0.2 MeV

TABLE 3

Ratios of nuclear ellipsoid axes (k), deformation parameters (β) and intrinsic quadrupole moments (Q_0), calculated from E_2, E_1

Nucleus	^{154}Sm	^{156}Gd	^{165}Ho	^{168}Er	^{174}Yb	^{178}Hf	^{180}Hf	^{181}Ta	^{182}W	^{184}W	^{186}W
k	1.320	1.302	1.259	1.327	1.289	1.296	1.281	1.263	1.271	1.268	1.229
β	0.326 ±0.017	0.309 ±0.016	0.266 ±0.036	0.334 ±0.032	0.296 ±0.024	0.303 ±0.032	0.288 ±0.036	0.270 ±0.026	0.278 ±0.030	0.274 ±0.032	0.235 ±0.033
Q_0	6.3 ±0.3	6.2 ±0.3	5.8 ±0.8	7.5 ±0.7	7.0 ±0.6	7.5 ±0.8	7.2 ±0.9	6.9 ±0.7	7.2 ±0.8	7.1 ±0.8	6.2 ±0.9

TABLE 4

Integral characteristics of E1 giant resonance

Nucleus	$\sigma_{0\,exp}$ (MeV · b)	$\sigma_{0\,exp}$ $0.06NZ/A$	σ_{01} (MeV · b)	σ_{01} $0.06NZ/A$	σ_{-1} (mb)	σ_{-1L} (mb)	$\sigma_{-1L}A^{-4/3}$ (mb)	σ_{-2} (mb · MeV^{-1})	σ_{-2L} (mb · MeV^{-1})	$\sigma_{-2L}A^{-5/3}$ (μb · MeV^{-1})
^{154}Sm	1.94 ± 0.06	0.87	2.86	1.29	117 ± 3.5	156	0.189	9.1 ± 0.3	14.3	3.23
^{156}Gd	2.07 ± 0.07	0.91	2.95	1.30	143 ± 4.6	163	0.194	10.5 ± 0.4	14.9	3.30
^{165}Ho	1.86 ± 0.06	0.78	2.53	1.06	155 ± 4.4	160	0.177	10.1 ± 0.3	12.6	2.54
^{168}Er	2.24 ± 0.06	0.92	3.07	1.26	161 ± 4.3	197	0.212	12.0 ± 0.3	16.0	3.13
^{174}Yb	2.69 ± 0.05	1.07	3.82	1.52	195 ± 3.4	240	0.247	14.5 ± 0.3	19.2	3.54
^{178}Hf	2.85 ± 0.07	1.11	3.99	1.55	208 ± 4.9	247	0.247	15.3 ± 0.4	20.2	3.59
^{180}Hf	2.72 ± 0.06	1.05	4.03	1.56	200 ± 4.4	250	0.246	15.1 ± 0.3	20.7	3.61
^{181}Ta	2.84 ± 0.07	1.09	3.81	1.46	210 ± 5.3	245	0.239	16.0 ± 0.4	20.0	3.45
^{182}W	2.86 ± 0.07	1.09	4.01	1.52	211 ± 5.3	256	0.248	16.2 ± 0.4	21.6	3.70
^{184}W	2.78 ± 0.07	1.05	3.80	1.43	207 ± 5.3	251	0.240	15.9 ± 0.4	20.9	3.51
^{186}W	2.90 ± 0.07	1.08	3.95	1.48	214 ± 5.3	256	0.241	16.2 ± 0.4	21.6	3.56
^{197}Au	3.12 ± 0.06	1.10	4.37	1.54	229 ± 4.2	276	0.241	18.6 ± 0.4	23.3	3.49

Hf
A=179

Hf
A=179

Ref. R. Tobin, J. McElhinney, L. Cohen
Phys. Rev. 110, 1388 (1958)

Elem. Sym.	A	Z
Hf	179	72

Method: 22 MeV betatron; neutron counters

Ref. No.: 58 To 1 | EH

Reaction	E or ΔE	E_o	Γ	$\int \sigma dE$	Jπ	Notes
$Hf^{179}(\gamma,n)$	Bremss. 6.3-7					E_{th}=6.52±0.12

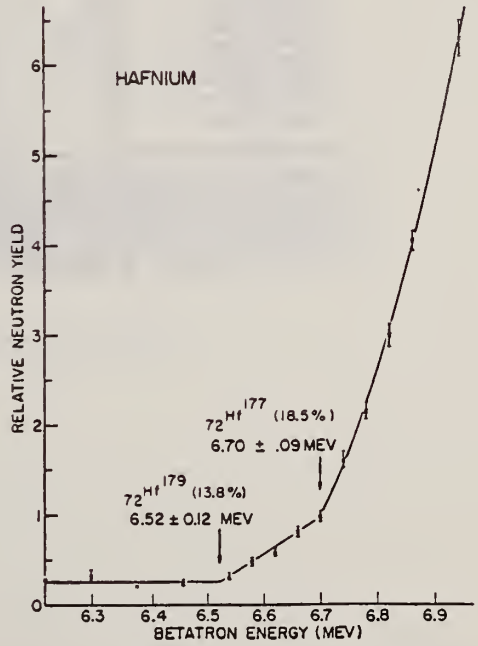

FIG. 7. Photoneutron yield from hafnium as a function of betatron energy.

K. N. Geller, J. Halpern, and L. G. Muirhead
Phys. Rev. 118, 1302-12 (1960)

Hf	179	72

METHOD: Betatron; neutron threshold; ion chamber

REF. NO.: 60 Ge 3 | NVB

REACTION	RESULT	EXCITATION ENERGY	SOURCE TYPE	SOURCE RANGE	DETECTOR TYPE	DETECTOR RANGE	ANGLE
G,N	NØX	THR	C THR		BF3-I		4 PI

THRESHØLD

TABLE I. Summary and comparison of neutron separation energies inferred from present threshold measurements with values predicted from mass data and reaction energies. All energies are expressed in the center-of-mass system in Mev.

Reaction	No. runs	Present results	Other results	Method	Reference
$Hf^{179}(\gamma,n)Hf^{178}$	1	6.31 ±0.07(6.21)	6.17 ±0.06	mass data	q
			6.52 ±0.12	threshold	k

[q] W. H. Johnson, Jr., and V. B. Bhanot, Phys. Rev. 107, 6 (1957).

TABLE II. Comparison of measured threshold energies with neutron binding energies predicted by mass data for transitions with $\Delta I \geq 7/2$. All energies in Mev.

Reaction	ΔI[a]	Observed threshold	Mass data Q value	$E_{th}-Q$	Excited state energy
$Cr^{52}(\gamma,n)Cr^{51}$	7/2	12.18±0.14	12.053±0.004[b]	0.13±0.14	...
$Y^{89}(\gamma,n)Y^{88}$	7/2	11.59±0.08	11.53 ±0.40[c]	0.06±0.41	0.387[d]
$In^{116}(\gamma,n)In^{114}$	7/2	9.22±0.03	9.35 ±0.43[c]	−0.13±0.43	0.191[a]
$Ce^{142}(\gamma,n)Ce^{141}$	(7/2)[e]	7.24±0.07	6.97 ±0.07[f]	0.27±0.10	...
$Nd^{146}(\gamma,n)Nd^{144}$	7/2	6.38±0.16	5.97 ±0.19[f]	0.41±0.25	0.690[a]
$Sm^{149}(\gamma,n)Sm^{148}$	7/2	6.45±0.16	5.87 ±0.28[f]	0.58±0.33	0.562[a]
$Er^{167}(\gamma,n)Er^{166}$	7/2	6.65±0.08	6.45 ±0.06[g]	0.20±0.10	0.081[a]
$Hf^{177}(\gamma,n)Hf^{176}$	7/2	6.69±0.03	6.28 ±0.06[g]	0.64±0.07	0.088[a]
$Hf^{179}(\gamma,n)Hf^{178}$	9/2	6.31±0.07	6.17 ±0.06[g]	0.14±0.09	0.093[a]
$Hf^{180}(\gamma,n)Hf^{179}$	9/2	7.85±0.11	7.32 ±0.06[g]	0.53±0.13	0.375[a]

[a] D. Strominger, J. M. Hollander, and G. T. Seaborg, Revs. Modern Phys. 30, 585 (1958).
[b] C. F. Giese and J. L. Benson, Phys. Rev. 110, 712 (1958).
[c] Henry E. Duckworth, *Mass Spectroscopy* (Cambridge University Press, New York, 1958), p. 177.
[d] S. Dzelepov and L. K. Peker, Atomic Energy of Canada Limited Report Tr. AECL-457 (unpublished).
[e] The discrepancy in the case of Ce^{143} predicts a ground-state spin for Ce^{143} of 0, since the spin of Ce^{141} is known to be 7/2.
[f] W. H. Johnson, Jr., and A. O. Nier, Phys. Rev. 105, 1014 (1957).
[g] W. H. Johnson, Jr., and V. B. Bhanot, Phys. Rev. 107, 6 (1957).

REF.

A. Veres
Acta Phys. Acad. Sci.Hung. 16, 261-73 (1963)

ELEM. SYM.	A	Z
Hf	179	72

METHOD

Radioactive source

REF. NO.

63 Ve 2 NVB

REACTION	RESULT	EXCITATION ENERGY	SOURCE		DETECTOR		ANGLE
			TYPE	RANGE	TYPE	RANGE	
G,G/	ABX	0-1	D	0-1	NAI-D		

ISOMERS

Таблица 11

Измеренные значения после облучения, сравниваемые с другими литературными данными

Элемент	Активность облучения после первого измерения (имп/мин.)	Активн. экстрп. в конце облуч. (имп/мин.)	Литературные данные		Данные измерений		σ_{max} (10^{-28} см^2)	Γ_{ym} (10^{-4} эв)
			$T_{1/2}$	E (кэв)	$T_{1/2}$	E (кэв)		
Se-77m	3842±96	5400	17,5 сек.	160	18,1±1 сек.	160±10	9,5	1,75
Sr-87m	191±5	200	2,8 ч.	390	2,9±0,1 ч.	365±25	0,85	0,2
Y-89m	96±20	170	16 сек.	910	16,7±5 сек.		0,08	0,02
Rh-103m	28±5	31	57 мин.	40	58±2 мин.	20,5±0,5	0,08	0,01
Ag-107m	220±14	250	44 сек.	93	43,8±0,6 сек	91±10	0,8	0,2
Ag-109m			39 сек.	88				
Hf-179m	80±18	155	19 сек.	160; 215	19±2 сек.		1	0,2
Ir-191m	90±20	250	4,9 сек.	42; 130	5±2 сек.		5,6	1
Pt-195m	90±9	100	3,5 д.	31; 100; 130;	3,5±0,2 д.	32±3 67,5±5 96±5 130±10	0,2	0,04
Au-197m	240±16	520	7,2 сек.	130; 277; 407	7,2±1 сек.	68:130: 280±20 390±20	0,07	0,01
Hg-199m	9,6±3,2		42 мин.	160; 370			0,005	0,001

REF.

M. Boivin and V. Zecevic
C.R. Acad. Sc. Paris 270, 1627 (1970)

ELEM. SYM.	A	Z
Hf	179	72

METHOD

REF. NO.: 70 Bo 4 | egf

REACTION	RESULT	EXCITATION ENERGY	SOURCE		DETECTOR		ANGLE
			TYPE	RANGE	TYPE	RANGE	
G,G	ABI	0 - 2	C	0 - 2	ACT-I		4PI

6 LEVELS

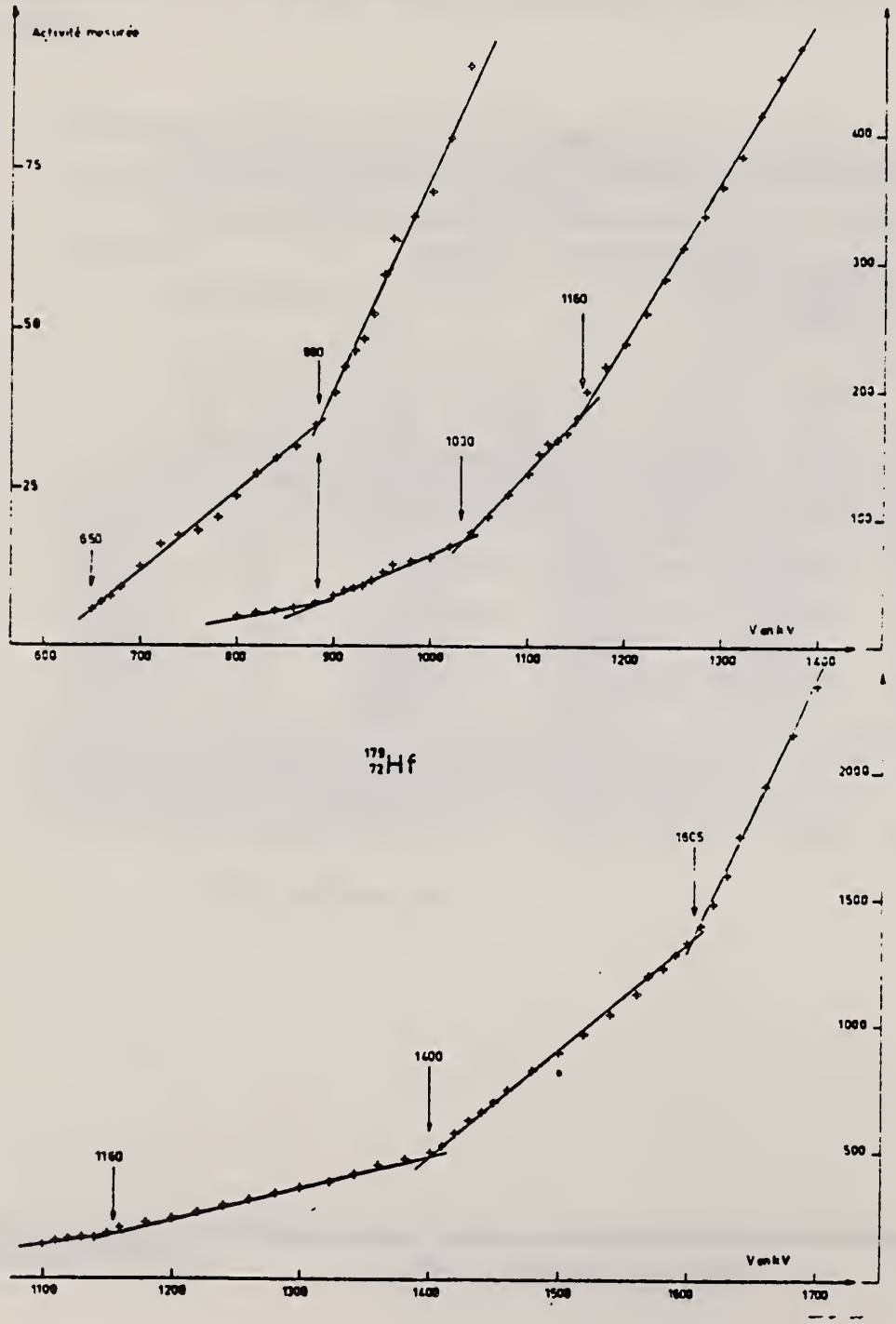

Indirect Activation of 18.6s 378 keV level by .5-2.0 MeV bremsstrahlung.

(over)

TABLEAU.

E (keV).	τ_n (cm^2.MeV).	u (eV).
650 ± 20	$5,7\ ^{+5,9}_{-4,7}.10^{-24}$	$0,7\ ^{+0,7}_{-0,6}.10^{-7}$
880 ± 20	$8,2\ ^{+8,3}_{-6,6}.10^{-24}$	$1,7\ ^{+1,7}_{-1,4}.10^{-7}$
1030 ± 20	$2,5\ ^{+1,7}_{-1,2}.10^{-23}$	$6,8\ ^{+4,6}_{-3,2}.10^{-7}$
1160 ± 20	$2,2\ ^{+1,9}_{-1,5}.10^{-23}$	$7,7\ ^{+6,6}_{-5}.10^{-7}$
$1400\ ^{+10}_{-5}$	$2,0\ ^{+1,1}_{-0,7}.10^{-23}$	$1,0\ ^{+0,6}_{-0,4}.10^{-6}$
$1605\ ^{+10}_{-5}$	$6,3\ ^{+3,1}_{-1,8}.10^{-24}$	$4,2\ ^{+2,1}_{-1,2}.10^{-6}$

Hf
A=180

Hf
A=180

..., J. Halpern, and G. Muirhead
... Rev 118, 1302-12 (1960)

ELEM. SYM.	A	
Hf	180	72

METHOD

Betatron; neutron threshold; ion chamber

REF. NO. 60 Ge 3 | NVB

REACTION	RESULT	EXCITATION ENERGY	SOURCE		DETECTOR		ABLE
			TYPE	RANGE	TYPE	RANGE	
G,N	NØX	THR	C THR		BF3-I		4 PI

THRESHØLD

TABLE I. Summary and comparison of neutron separation energies inferred from present threshold measurements with values predicted from mass data and reaction energies. All energies are expressed in the center-of-mass system in Mev.

Reaction	No. runs	Present results	Other results	Method	Reference
$Hf^{180}(\gamma,n)Hf^{179}$	1	7.85 ±0.11(7.48)	7.32 ±0.06	mass data	q

q W. H. Johnson, Jr., and V. B. Bhanot, Phys. Rev. 107, 6 (1957).

TABLE II. Comparison of measured threshold energies with neutron binding energies predicted by mass data for transitions with $\Delta I \geq 7/2$. All energies in Mev.

Reaction	ΔI[a]	Observed threshold	Mass data Q value	$E_{th}-Q$	Excited state energy
$Cr^{52}(\gamma,n)Cr^{51}$	7/2	12.18±0.14	12.053±0.004[b]	0.13±0.14	...
$Y^{89}(\gamma,n)Y^{88}$	7/2	11.59±0.08	11.53 ±0.40[c]	0.06±0.41	0.387[d]
$In^{115}(\gamma,n)In^{114}$	7/2	9.22±0.03	9.35 ±0.43[e]	−0.13±0.43	0.191[a]
$Ce^{142}(\gamma,n)Ce^{141}$	(7/2)[e]	7.24±0.07	6.97 ±0.07[f]	0.27±0.10	...
$Nd^{144}(\gamma,n)Nd^{143}$	7/2	6.38±0.16	5.97 ±0.19[f]	0.41±0.25	0.690[a]
$Sm^{149}(\gamma,n)Sm^{148}$	7/2	6.45±0.16	5.87 ±0.28[f]	0.58±0.33	0.562[a]
$Er^{167}(\gamma,n)Er^{166}$	7/2	6.65±0.08	6.45 ±0.06[g]	0.20±0.10	0.081[a]
$Hf^{177}(\gamma,n)Hf^{176}$	7/2	6.69±0.03	6.28 ±0.06[g]	0.64±0.07	0.088[a]
$Hf^{179}(\gamma,n)Hf^{178}$	9/2	6.31±0.07	6.17 ±0.06[g]	0.14±0.09	0.093[a]
$Hf^{180}(\gamma,n)Hf^{179}$	9/2	7.85±0.11	7.32 ±0.06[g]	0.53±0.13	0.375[a]

[a] D. Strominger, J. M. Hollander, and G. T. Seaborg, Revs. Modern Phys. 30, 585 (1958).
[b] C. F. Giese and J. L. Benson, Phys. Rev. 110, 712 (1958).
[c] Henry E. Duckworth, *Mass Spectroscopy* (Cambridge University Press, New York, 1958), p. 177.
[d] S. Dzelepov and L. K. Peker, Atomic Energy of Canada Limited Report Tr. AECL-457 (unpublished).
[e] The discrepancy in the case of Ce^{142} predicts a ground-state spin for Ce^{141} of 0, since the spin of Ce^{141} is known to be 7/2.
[f] W. H. Johnson, Jr., and A. O. Nier, Phys. Rev. 105, 1014 (1957).
[g] W. H. Johnson, Jr., and V. B. Bhanot, Phys. Rev. 107, 6 (1957).

REF. A.M. Goryachev and G.I. Zalesnyi
Yad. Fiz. 26, 465 (September 1977)
Sov. J. Nucl. Phys. 26, 246 (September 1977)

ELEM. SYM.	A	Z
Hf	180	72

METHOD

REF. NO. 77 Go 4

hmg 11/17/80

REACTION	RESULT	EXCITATION ENERGY	SOURCE		DETECTOR		ANGLE
			TYPE	RANGE	TYPE	RANGE	
G,XN	ABX	7(7.4)-22	C	8-22	BF3-I	---	4PI

Yield curves and photoneutron multiplicities have been measured for the isotopes ^{176,178,180}Hf in a betatron bremsstrahlung beam in the energy range 8–21 MeV with a 0.125-MeV step. The measurements were made on-line with a computer. The cross sections were calculated from the yield curves by the Penfold-Leiss method with a 1.0-MeV step. The multiplicity curves were used to separate the contributions of (γ,n) and $(\gamma,2n)$ reactions. Integrated cross sections calculated from the photoabsorption cross sections are given, and also average energies and deformation parameters. The results are compared with calculations using various versions of the model of coupling of dipole and quadrupole vibrations.

n multiplicity measurement

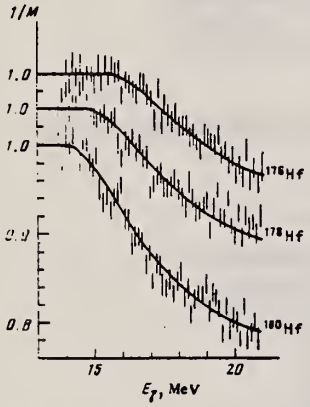

FIG. 1. Multiplicity of photoneutrons for the isotopes ^{176,178,180}Hf. The length of the vertical lines is equal to two standard deviations. The solid curves are the fitted curves $M(E_{\gamma max})$ with the parameters given in Table II.

TABLE II. Parameters of photoneutron multiplicity curves.

Nucleus	a, MeV^{-1}	W	χ^2/f	a, MeV^{-1}	W	χ^2/f
^{176}Hf	7.0±0.5	0	1.07	20.9	0.36±0.03	1.09
^{178}Hf	5.1±0.3	0	0.95	22.6	0.46±0.02	0.91
^{180}Hf	9.3±0.6	0	1.01	23.0	0.24±0.015	0.97

Note. f is the number of degrees of freedom.

TABLE III. Parameters of the Lorentz curves.

Nucleus	E_1, MeV	Γ_1, MeV	σ_1, mb	E_2, MeV	Γ_2, MeV	σ_2, mb	R
^{176}Hf	12.36±0.04	2.96±0.09	272±9	15.71±0.06	5.0±0.02	269±5	0.60±0.07
^{178}Hf	12.41±0.05	3.00±0.1	283±10	15.75±0.06	4.6±0.2	273±5	0.67±0.07
^{180}Hf	12.41±0.04	2.80±0.09	286±8	15.75±0.05	4.4±0.1	281±4	0.65±0.07

TABLE IV. Integrated cross sections

	^{176}Hf	^{178}Hf	^{180}Hf
σ_{int}, MeV-mb	2571 ± 12	2580 ± 15	2535 ± 12
σ_{-1}, mb	184 ± 1	185 ± 1	182 ± 1
σ_{-2}, MeV^{-1} mb	13.65 ± 0.07	13.71 ± 0.08	13.53 ± 0.07
$\sigma_{int}(\gamma, 2n)$, MeV-mb	518 ± 4	683 ± 6	815 ± 5
$\sigma_{int\ L}$, MeV-mb	3370	3318	3188
$\sigma_{int}/60NZ/A$	1.007	1.003	0.978
$\sigma_{-1}A^{-4/3}$	0.186	0.184	0.179
$\sigma_{-2}A^{-5/3}$	0.00247	0.00243	0.00236
$\sigma_{int}(\gamma, 2n)/\sigma_{int}$	0.202	0.265	0.322
$\sigma_{int\ L}/60NZ/A$	1.32	1.29	1.23

TABLE V. Average energies.

Nucleus	E_M, MeV	E_H, MeV	$E_M A^{1/3}$	$E_H A^{1/3}$	K, MeV
^{176}Hf	14.45	14.51	81.0	34.2	28.3
^{178}Hf	14.41	14.49	81.0	34.2	28.8
^{180}Hf	14.43	14.50	81.5	34.3	29.1

TABLE VI. Deformation β and quadrupole moment Q_0.

Nucleus	Our data		From $B(E2, 2_1^+ \to 0_1^+)$ [16]	
	β	Q_0, b	β	Q_0, b
^{176}Hf	0.30±0.03	7.4±0.6	0.27	7.37±0.17
^{178}Hf	0.30±0.03	7.5±0.5	0.25	6.81±0.07
^{180}Hf	0.30±0.03	7.5±0.7	0.25	6.83±0.06

TABLE VII. Dipole strengths of transverse maximum.

i	γ-vibrational model		Nonaxial rotator model		Davydov–Chaban model	
	λ_i	$(0\|\lambda_i)^2$	λ_i	$(0\|\lambda_i)^2$	λ_i	$(0\|\lambda_i)^2$
1	−0.086	0.923	−0.085	0.94	−0.12	0.86
2	0.992	0.073	1.085	0.06	0.71	0.10
3	1.921	0.003	–	–	1.01	0.04

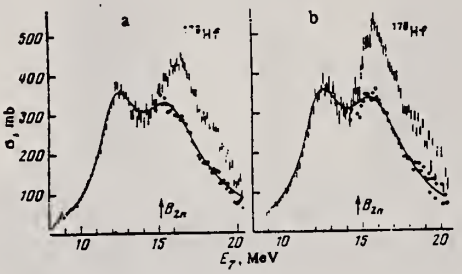

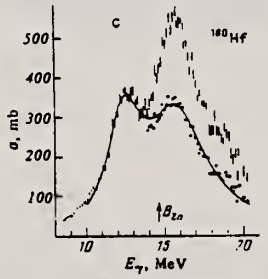

FIG. 2. Photoabsorption cross sections for the isotopes ^{176,178,180}Hf. The vertical lines, whose length is two standard deviations, indicate the cross section $\sigma_{exp} = \sigma_{\gamma,n} + 2\sigma_{\gamma,2n} + \sigma_{\gamma,np} + \ldots$. Above the threshold of the $\gamma, 2n)$ reaction the photoabsorption cross section is indicated by the solid circles; the smooth curves are fits by Lorentz curves with the parameters given in Table III.

σ_{int} corrected for neutron multiplicity

REF. G.M. Gurevich, L.E. Lazareva, V.M. Mazur, S.Yu. Merkulov, G.V. Solodukhov, V.A. Tyutin
Nucl. Phys. A351, 257 (1981)

ELEM. SYM.	A	Z
Hf	180	72

METHOD

REF. NO. 81 Gu 2 hg

REACTION	RESULT	EXCITATION ENERGY	SOURCE		DETECTOR		ANGLE
			TYPE	RANGE	TYPE	RANGE	
G,MU-T	ABX	THR-20	C	27	NAI-D		4PI

Abstract: The curves of the total gamma-absorption cross sections (σ_{tot}) in the E1 giant resonance energy range for the nuclei ^{154}Sm, ^{156}Gd, ^{165}Ho, ^{168}Er, ^{174}Yb, ^{178}Hf, ^{180}Hf, ^{181}Ta, ^{182}W, ^{184}W, ^{186}W and ^{197}Au have been measured using the absorption method. Parameters of the Lorentz curves fitting the measured cross sections σ_{tot} are given. Quadrupole moments (Q_0) and nuclear deformation parameters (β) were obtained.

For deformed nuclei in the $\sim 155 < A < \sim 180$ region a violation of the correlation between giant resonance widths (Γ) and nuclear deformation parameters was found. Γ_1 and Γ_2, the widths of the resonances corresponding to vibrations of nucleons along and across the nuclear deformation axis, were observed to decrease with the increase of A which could be accounted for by the presence of an $N = 108$ subshell.

E

NUCLEAR REACTIONS ^{154}Sm, ^{156}Gd, ^{165}Ho, ^{168}Er, ^{174}Yb, ^{178,180}Hf, ^{181}Ta, ^{182,184,186}W, ^{197}Au (γ, X), E = 7–20 MeV; measured total $\sigma(E)$; deduced integrated σ, Lorentz line parameters. ^{154}Sm, ^{156}Gd, ^{165}Ho, ^{168}Er, ^{174}Yb, ^{178,180}Hf, ^{181}Ta, ^{182,184,186}W, ^{197}Au deduced β, Q_0, Γ, giant resonance evolution. Enriched, natural targets.

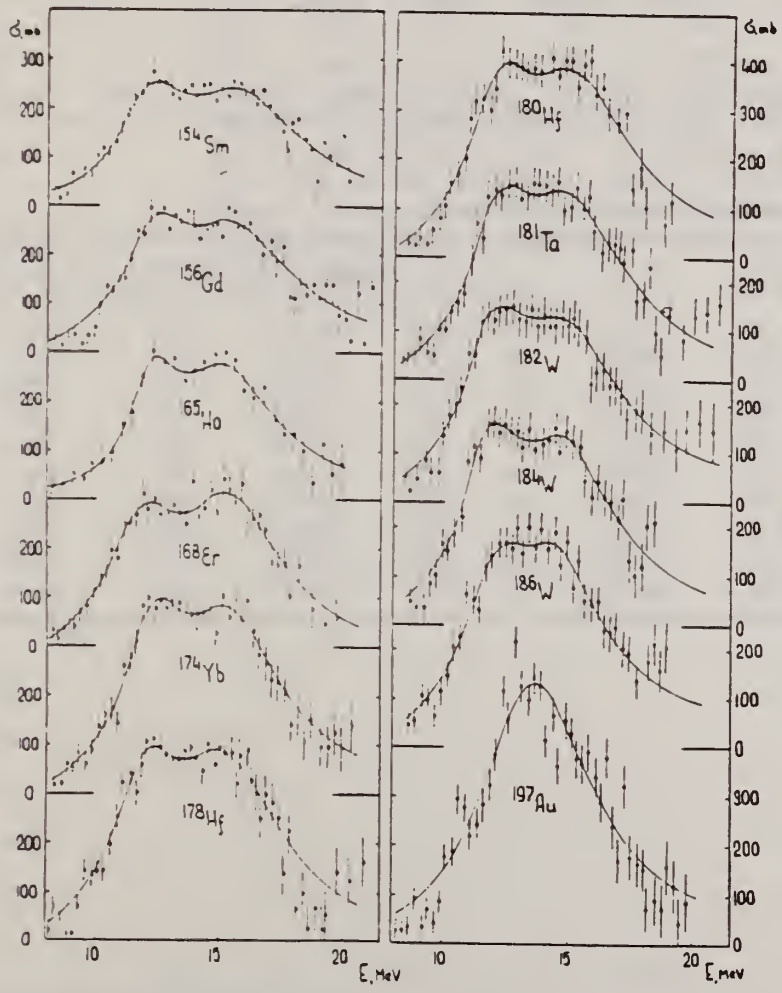

Fig. 2. Total nuclear γ-absorption cross sections (σ_{tot}) measured by the absorption method for ^{154}Sm, ^{156}Gd, ^{165}Ho, ^{168}Er, ^{174}Yb, ^{178}Hf, ^{180}Hf, ^{181}Ta, ^{182}W, ^{184}W, ^{186}W and ^{197}Au. Rms error bars are shown.

(OVER)

TABLE 2

Parameters of Lorentz curves fitting the experimental data on σ_{tot}

Nucleus	E_1 (MeV)	σ_1 (mb)	Γ_1 (MeV)	E_2 (MeV)	σ_2 (mb)	Γ_2 (MeV)	$\frac{\sigma_2\Gamma_2}{\sigma_1\Gamma_1}$	Γ (MeV)
^{154}Sm	12.2	188	3.4	15.7	207	5.7	1.85	8.1
^{156}Gd	12.3	206	3.2	15.7	220	5.5	1.81	7.7
^{165}Ho	12.3	202	2.3	15.2	239	4.8	2.47	7.0
^{168}Er	11.9	222	3.2	15.5	275	4.5	1.73	7.4
^{174}Yb	12.3	297	2.9	15.5	320	4.9	1.80	7.1
^{178}Hf	12.2	291	3.1	15.5	334	4.9	1.80	7.2
^{180}Hf	12.2	286	3.2	15.3	324	5.1	1.81	7.1
^{181}Ta	12.1	272	3.0	15.0	316	5.1	1.97	6.8
^{182}W	11.9	267	3.2	14.8	303	5.6	2.01	6.8
^{184}W	11.9	315	2.9	14.8	321	4.7	1.65	6.8
^{186}W	12.0	246	3.3	14.5	332	5.1	2.07	6.4
^{197}Au	13.7	535	5.2					
Average error	1.4 %	11.2 %	9.3 %	1.5 %	9.7 %	4.6 %	0.22	0.2 MeV

TABLE 3

Ratios of nuclear ellipsoid axes (λ), deformation parameters (β) and intrinsic quadrupole moments (Q_0), calculated from E_2, E_1

Nucleus	^{154}Sm	^{156}Gd	^{165}Ho	^{168}Er	^{174}Yb	^{178}Hf	^{180}Hf	^{181}Ta	^{182}W	^{184}W	^{186}W
λ	1.320	1.302	1.259	1.327	1.289	1.296	1.281	1.263	1.271	1.268	1.229
β	0.326 ±0.017	0.309 ±0.016	0.266 ±0.036	0.334 ±0.032	0.296 ±0.024	0.303 ±0.032	0.288 ±0.036	0.270 ±0.026	0.278 ±0.030	0.274 ±0.032	0.235 ±0.033
Q_0	6.3 ±0.3	6.2 ±0.3	5.8 ±0.8	7.5 ±0.7	7.0 ±0.6	7.5 ±0.8	7.2 ±0.9	6.9 ±0.7	7.2 ±0.8	7.1 ±0.8	6.2 ±0.9

TABLE 4

Integral characteristics of E1 giant resonance

Nucleus	$\sigma_{-1,exp}$ (MeV^{-1}·b)	$\sigma_{0,exp}$ / 0.06NZ/A	σ_{01} (MeV·b)	σ_{01} / 0.06NZ/A	σ_1 (mb)	σ_{1L} (mb)	$\sigma_{1L}A^{-1/3}$ (mb)	σ_2 (mb·MeV^{-1})	σ_{2L} (mb·MeV^{-1})	$\sigma_{2L}A^{-1/3}$ (μb·MeV^{-1})
^{154}Sm	1.94±0.06	0.87	2.86	1.29	117±3.5	156	0.189	9.1±0.3	14.3	3.23
^{156}Gd	2.07±0.07	0.91	2.95	1.30	143±4.6	163	0.194	10.5±0.4	14.9	3.30
^{165}Ho	1.86±0.06	0.78	2.53	1.06	155±4.4	160	0.177	10.1±0.3	12.6	2.54
^{168}Er	2.24±0.06	0.92	3.07	1.26	161±4.3	197	0.212	12.0±0.3	16.0	3.13
^{174}Yb	2.69±0.05	1.07	3.82	1.52	195±3.4	240	0.247	14.5±0.3	19.2	3.54
^{178}Hf	2.85±0.07	1.11	3.99	1.55	208±4.9	247	0.247	15.3±0.4	20.2	3.59
^{180}Hf	2.72±0.06	1.05	4.03	1.56	200±4.4	250	0.246	15.1±0.3	20.7	3.61
^{181}Ta	2.84±0.07	1.09	3.81	1.46	210±5.3	245	0.239	16.0±0.4	20.0	3.45
^{182}W	2.86±0.07	1.09	4.01	1.52	211±5.3	256	0.248	16.2±0.4	21.6	3.70
^{184}W	2.78±0.07	1.05	3.80	1.43	207±5.3	251	0.240	15.9±0.4	20.9	3.51
^{186}W	2.90±0.07	1.08	3.95	1.48	214±5.3	256	0.241	16.2±0.4	21.6	3.56
^{197}Au	3.12±0.06	1.10	4.37	1.54	229±4.2	276	0.241	18.6±0.4	23.3	3.49

# TANTALUM
Z=73

Anders Ekeberg reported the discovery of a metallic nature in some mineral samples taken from Sweden and Finland. Because of the frustrations and problems encountered in defining the properties and chemical nature of the new element, Ekeberg named the substance after Tantalus, a Greek mythological character. Tantalus was a Phrygian king who, for his crimes, was condemned to remain in Tartarus, standing, unable to drink or eat, chin deep in water with fruit-laden branches hanging above his head.

Scrap tantalum is reworked by moderate heating in pressurized hydrogen. The metal increases in volume by a factor of 740 when heated to a dull red, becomes brittle, and is easily pulverized. The powder obtained is washed in acid and further heated in vacuum to a higher temperature to expel the hydrogen. This powder is then used to produce ingots which have properties not quite like those of the primary metal.

Ta
A=181

Ta
A=181

REF.

Sven A. E. Johansson
Phys. Rev. 97, 434-43 (1955)

ELEM. SYM.	A	Z
Ta	181	73

METHOD
Synchrotron; ZnS counter; ion chamber

REF. NO.
55 Jo 1

NVB

REACTION	RESULT	EXCITATION ENERGY	SOURCE		DETECTOR		ANGLE
			TYPE	RANGE	TYPE	RANGE	
G,N	RLY	THR - 65	C 65		SCI-D	5 - +	DST
G,N	RLY	THR - 65	C 65		SCI-D	10 - +	DST

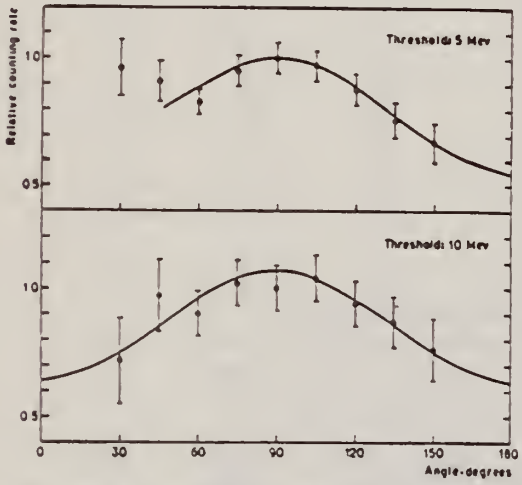

FIG. 8. The angular distributions of the neutrons from tantalum. Counter thresholds at 5 and 10 Mev.

Curves of Form $a + b \sin^2\theta$

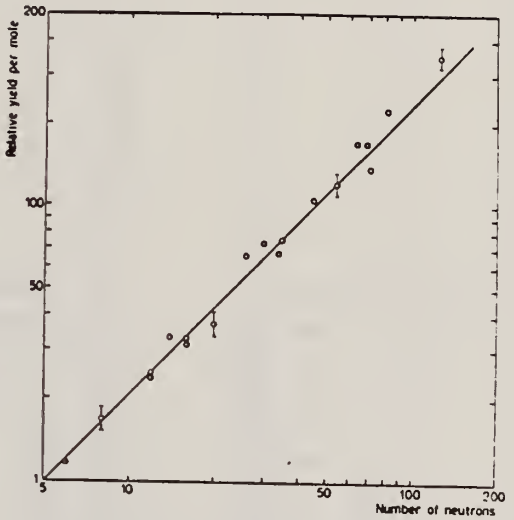

FIG. 11. The relative yield per mole for neutrons above 7.5 Mev as a function of the neutron number.

Ref. M.E. Toms, W.E. Stephens
Phys. Rev. 98, 626 (1955)

Elem. Sym.	A	Z
Ta	181	73

Method Betatron; protron spectrum, yield, angular distribution; nuclear emulsions

Ref. No. 55 To 1 -5 NVB

Reaction	E or ΔE	E_o	Γ	$\int \sigma dE$	Jπ	Notes
$Ta^{181}(\gamma,xp)$	Bremss. 23					

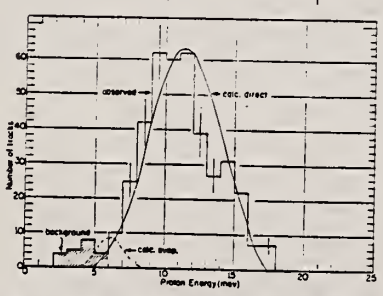

FIG. 1. The histogram gives the energy distribution of the photoprotons from tantalum exposed to 23-Mev bremsstrahlung. The smooth curve is the distribution calculated for the direct process and normalized to the observed protons. The dashed curve is the calculated distribution for the evaporation process fitted to indicate the maximum possible evaporation yield. The shaded groups are background.

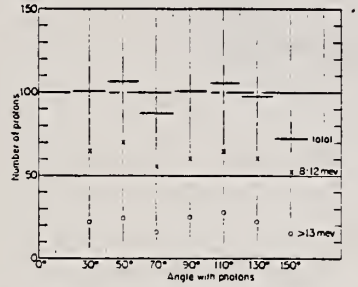

FIG. 3. The numbers of tantalum phntoprotons per unit solid angle in arbitrary units is plotted as a function of their angle from the photon direction. In addition, the crosses show the angular distribution of photoprotons of 8 to 12 Mev energy, the circles photoprotons over 13 Mev.

TABLE II. Calculated and observed photoproton yields.

	Bi	Pb[18]	Ta	Ce	In	Mo[18]	92
Z protons	83	82	73	58	49	42	
B_p (Mev)[a]	3.76	8.02	6.2	8.5	6.8	10.5	8.0
N neutrons	126	126	108	82	66	58	50
B_n (Mev)[a]	7.44	7.38	7.55	7.05	9.05	8.1	13.1
Γ_n (observed) (10[3] protons mole^{-1} roentgen^{-1})	5	2.6	5.6	12 (5 direct)	11.7 (5 direct)	9.2	160
Betatron energy (Mev)	24	23	24	24	24	22.5	22.5
Γ_n(calc. direct) (10[3] protons mole^{-1} roentgen^{-1})	1.5	0.2	0.7	0.7	2		
Γ_n(obs.) − Γ_n(calc. direct)	3.4	13	8	13	4		
Γ_n(calc. evap.) (10[3] protons mole^{-1} roentgen^{-1})	0.3	0.002	0.05	0.07	1.1	0.6 to 0.37	120 to 220
Γ_n(obs.) − Γ_n(calc. evap.)	17	1300	110	170	10	125 to 20	~1
Possible obs. evap.	<0.3	<0.2	<0.2	<3	<3	forward[d]	forward[d]
Angular distr.	far forward[b]	far forward[a]	~isotr.[c]	~isotr.[b]	forward[b]		~isotr.[a]

[a] B_p is the binding energy of the last proton, B_n is the binding energy of the last neutron.
[b] L. Katz and W. E. Stephens, Phys. Rev. 92, 162 (1953).
[c] Present work.
[d] W. N. Butler and G. M. Almy, Phys. Rev. 91, 55 (1953).

B.I. Gavrilov, L.E. Lazareva
Zhur. Eksp. i Teoret. Fiz. 30, 855 (1956);
Soviet Phys. JETP 3, 871 (1957)

Elem. Sym.	A	Z
Ta	181	73

Method: γ-Bremsstrahlung; synchrotron; BF_3 counter

Ref. No.: 56 Ga 1 | EGF

Reaction	E or ΔE	E_0	Γ	$\int \sigma dE$	Jπ	Notes
(γ,xn) 56S	~ 8-27	14.5	6.8	3.87 MeV-b		56Bt
(μ_t)	~ 8-27	13.9	4.5	2.74 MeV-b		

TABLE I. Fundamental characteristics of photoneutron cross sections.

Element	$E_{\sigma_n \max}$ in mev	$\sigma_{n\max}$ in barns	Half width in mev	$\int_{E_n}^{E_0} \sigma_n(E)\,dE$ in mev-barns	$\frac{\int_{E_n}^{E_0} \sigma_n(E)\,dE}{\sigma_{n\max} E_n}$
Copper	17.2	0.125	4.3	0.93	7.4
Zinc	16.3	0.151	6.3	0.96	8.1
Cadmium	15.0	0.250	6.4	2.28	9.4
Iodine	15.5	0.288	6.0	2.35	8.2
Tantalum	13.5	0.452	6.8	3.87	8.6
Gold	14.2	0.571	6.9	4.37	7.6
Thallium	13.6	0.652	5.1	4.99	7.6
Bismuth	13.6	0.507	5.9	3.96	7.4
Thorium	13.5	0.775	5.6	6.20	8.0
Uranium	13.4	1.18	6.8	12.5	10.6

TABLE II. Threshold of photoneutron reactions (mev).

Element	(γ, n)	$(\gamma, 2n)$	$(\gamma, 3n)$	$(\gamma, 4n)$
Cadmium	6.7	14.6	23.0	>30
Iodine	9.4	16.2	26.0	32.0
Tantalum	7.6	13.9	21.6	28.2
Gold	8.1	14.9	23.9	>30
Thallium	7.5	14.0	22	28.8
Bismuth	7.4	14.2	22.5	29.6

TABLE III. Characteristics of the cross section of absorption of γ-quanta by nuclei.

Element	E_{res} in mev	$\sigma_\gamma(E=E_{res})$ in barns	Γ in mev	$\frac{\int_{E_n}^{E_0} \sigma_\gamma dE}{E_n}$ in mev-barns	$\frac{\int_{E_n}^{E_0} \sigma_\gamma dE}{C_n \times (2N/A)}$	$\frac{\int_{E_n}^{E_0} (\sigma_\gamma(E)\,dE}{E_n}$	$\frac{\int_{E_n}^{E_0} (n_\gamma(E)\,dE}{E_n}$	$r_0 \times 10^3$ in cm
Cadmium	15.0	0.263	5.1	1,76	1,04	0,111	0,00715	1,26
Iodine	15.5	0,288	4,5	1,80	1,00	0,117	0,00708	1,16
Tantalum	13.9	0,438	4,5	2,74	1,05	0,190	0,0139	1,15
Gold	14.2	0,571	5,49	3,23	1,23	0,244	0,0182	1,23
Thallium	14.0	0,648	4,6	3,77	1,28	0,296	0,0200	1,25
Bismuth	13.6	0,507	4,5	3,12	1,04	0,220	0,0178	1,16

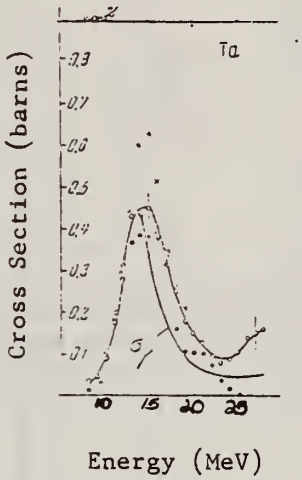

Figure 2: Photoneutron cross section σ_n, computed from the yield curve by the "photon difference method." "x" -- cross section measured in Ref. 10 [E.A. Whalin and A.O. Hanson, Phys. Rev. 89, 324 (1953)] for tantalum. For Cd, I, Ta, Au, Tl and Bi, curves are presented for the cross section of γ-quanta, computed from the statistical theory of nuclei. "•" - cross sections obtained in Ref. 9 [Nathans and Halpern, Phys. Rev. 93, 437 (1954)].

Ref. T.H. Harley, W.E. Stephens, E.J. Winhold
Phys. Rev. 104, 178 (1956)

Elem. Sym.	A	Z
Ta	181	73

Method: Li (p,γ) source, 480 kev protons. BF_3 counters

Ref. No.: 56 Ha 1 | EGF

Reaction	E or ΔE	E_o	Γ	$\int \sigma dE$	Jπ	Notes
$Ta^{181}(\gamma,xn)$						Average Li cross section is 355 mb; cross section with detector response weighted for low energy neutrons, 360 mb. Assumed ratio 17.6/14.8 = 1.7. Calculated cross section at 14.8 and 17.6 MeV assuming cross section curves measured at Pennsylvania and Saskatchewan (refer Table I).

TABLE I. Cross sections for photoneutron emission induced by the lithium gamma rays. The results are compared with previous data

Element	Present cross-section data: Counter Group A	Present cross-section data: Counter Group B	Data of McDaniel et al.[a]	Betatron data: Pennsylvania $\sigma_{14.8}$[b]	Pennsylvania $\sigma_{14.8}/\sigma_{17.6}$	Saskatchewan $\sigma_{14.8}$[b]	Saskatchewan $\sigma_{14.8}/\sigma_{17.6}$	$\sigma_{14.8}$[b]	$\sigma_{17.6}$[b]
Fe	38 mb	33 mb	37 mb						
Co	49	49	47	60[c] mb	0.5	95[f] mb	0.5	23 mb	47 mb
Ni	25	25	23			40[g]	0.7	50	60
Cu	64	61	55±12			95[f]	0.6	22	32
Zn	48	45	48			90[f,h]	0.7	45	75
Ag	175	170	135			240[f]	1.0	38	54
Sn	200	190	180					175	175
Ta	355	360	260	350[d]	1.3	420[a]	2.3	420[i] 550[j]	320[i] 240[j]
W	365	355	325						
Au	330	295		315[e]	1.7	480[f]	1.9	460	255
Hg	365	340	290						
Pb	310	295	250	320[e]	1.6	440[f]	2.5	400[i] 500[j]	250[i] 200[j]
Bi	305	280	250	270[d]	2.6	550[f]	2.4	490	195

[a] See reference 3.
[b] Average of 14.8- and 17.6-Mev cross sections weighted with relative intensities of the lithium gamma-ray lines.
[c] See reference 24.
[d] R. Nathans, Ph.D. thesis, University of Pennsylvania, 1954 (unpublished).
[e] J. Halpern (private communication).
[f] See reference 23.
[g] See reference 32.
[h] Separate cross sections at 14.8 and 17.6 Mev as obtained from Group A data and 14.8/17.6 betatron cross-section ratios.
[i] Obtained using 14.8/17.6 cross-section ratio from Pennsylvania betatron data.
[j] Obtained using 14.8/17.6 cross-section ratio from Saskatchewan betatron data.

Ref. J.H. Carver, R.D. Edge, K.H. Lokan
Proc. Phys. Soc. A 70, 415 (1957)

Elem. Sym.	A	Z
Ta	181	73

Method 31 MeV Canberra electron synchrotron; neutron yield, Szilard-Chalmers detector; $Cu^{63}(\gamma,n)$ monitor

Ref. No. 57 Ca 1 EGF

Reaction	E or ΔE	E_o	Γ	$\int \sigma dE$	Jπ	Notes
$Ta^{181}(\gamma,n)$	Bremss. 8-31					$\int_0^{31} \sigma_1 dE / \int_0^{31} (\sigma_2 + \sigma_3) dE = 2.6 \pm 0.3$
$Ta^{181}(\gamma,2n)$						
$Ta^{181}(\gamma,3n)$						$\int_{17}^{31} \sigma_1 dE / \int_{17}^{31} (\sigma_2 + \sigma_3) dE = 0.86 \pm 0.15$
$Ta^{181}(\gamma,xn)$						

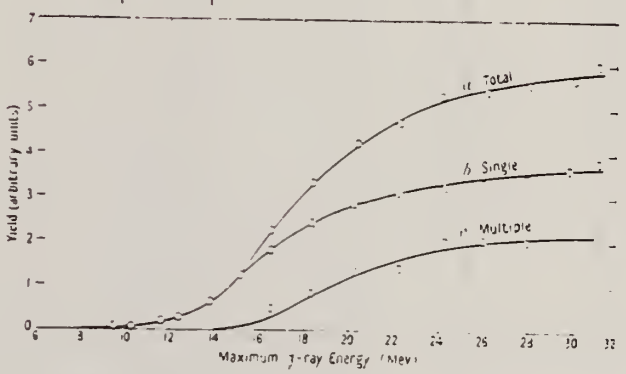

Figure 3. The measured neutron yield curves for tantalum: (*a*) the total yield for all neutron producing reactions obtained from the Szilard-Chalmers measurements; (*b*) the yield for single neutron production obtained from the ^{180}Ta activation measurements; (*c*) the yield for multiple reactions obtained by subtraction.

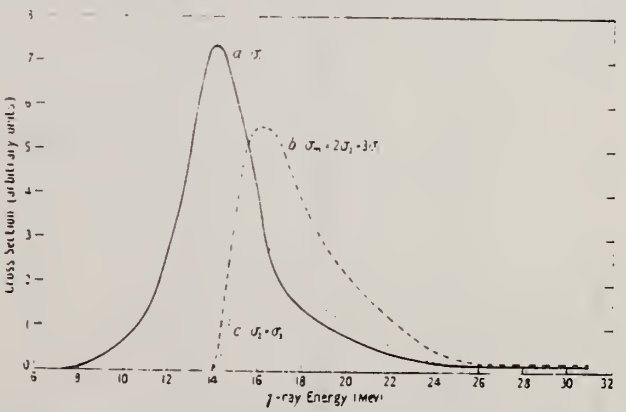

Figure 4.—The measured photoneutron cross sections for tantalum: (*a*) the (γ, n) cross section σ_1; (*b*) the cross section for multiple production $\sigma_m = 2\sigma_2 - 3\sigma_3$; (*c*) the sum of the cross sections for the (γ, 2n) and (γ, 3n) cross sections, $\sigma_2 + \sigma_3$, derived from σ_m assuming the ratio σ_2/σ_3 is as given by the statistical theory.

Ref. P. Erdos, P. Scherrer, P. Stoll
Helva. Phys. Acta 30, 639 (1957)

Elem. Sym.	A	Z
Ta	181	73

Method: Betatron; α yield; radioactivity; $Cu^{65}(\gamma,n)$ reaction.

Ref. No.: 57 Er 1 | EGF

Reaction	E or ΔE	E_o	Γ	$\int \sigma dE$	$J\pi$	Notes
$Ta^{181}(\gamma,\alpha)$	Bremss. 32			0.145±0.03 MeV-mb		Based on yield measurement.

Ref. F. Ferrero, R. Malvano, C. Tribuno
Nuovo Cimento 6, 385 (1957)

Elem. Sym.	A	Z
Ta	181	73

Method: Betatron; neutron yield; threshold detector

Ref. No.: 57 Fe 2 15 NVB

Reaction	E or ΔE	E_o	Γ	$\int \sigma dE$	Jπ	Notes
$Ta^{181}(\gamma,n!)$	Bremss. 14-30					R - ratio between area of second maximum of cross section and first maximum. R = 0.5±0.1 Detector at 90°

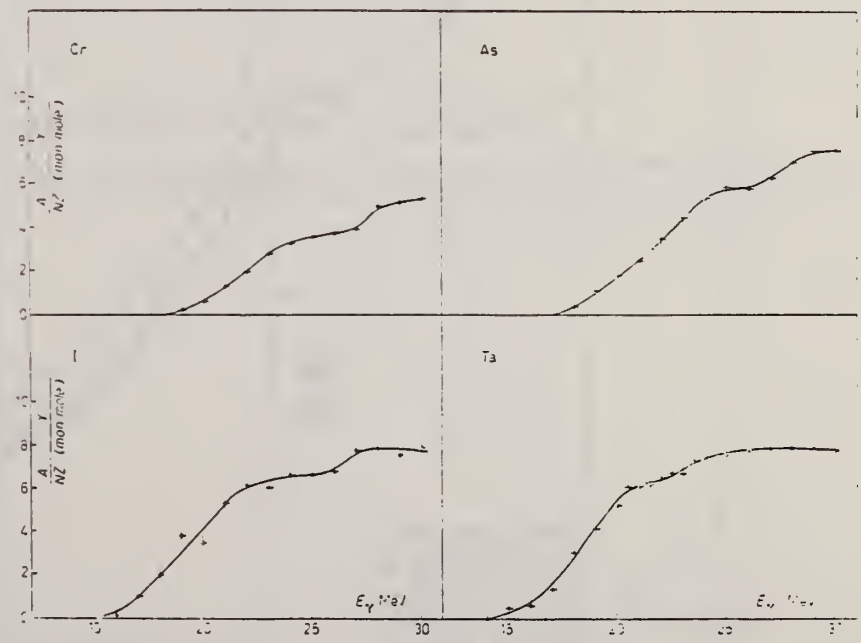

Fig. 1.

Ref. W. Bertozzi, F.R. Paolini, C.P. Sargent
Phys. Rev. 110, 790 (1958)

Elem. Sym.	A	Z
Ta	181	73

Method MIT linear accelerator; time of flight

Ref. No. 58 Be 2 | EH

Reaction	E or ΔE	E_o	Γ	$\int \sigma dE$	Jπ	Notes
Ta (γ,n)	Bremss. ~ 14.3 ~ 15.8					Detector at 120°

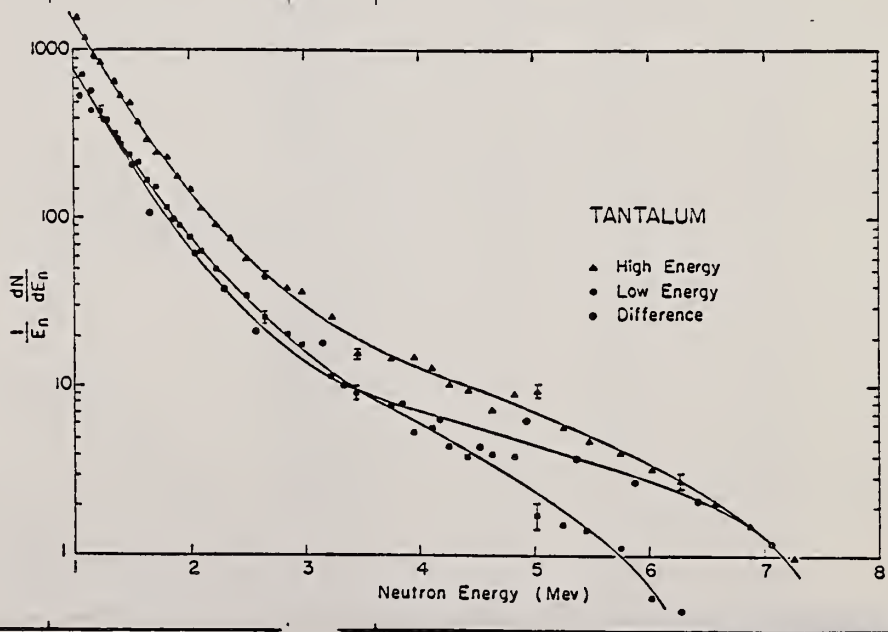

FIG. 3. Energy spectra $(1/E_n)(dN/dE_n)$ of photoneutrons from Ta for bremsstrahlung of maximum energies ~14.3 Mev and ~15.8 Mev, and difference spectrum.

Ref. J.H. Carver, W. Turchinetz
Proc. Phys. Soc. 71, 613 (1958)

Elem. Sym.	A	Z
Ta	181	73

Method Canberra electron synchrotron; neutron yield; radioactivity

Ref. No. 58 Ca 1 EH

Reaction	E or ΔE	E_o	Γ	$\int \sigma dE$	Jπ	Notes
$Ta^{181}(\gamma,n)$	Bremss. 7-32			$\int_{}^{31}$ = 73±3%		E_{th} = 7.6 MeV
$Ta^{181}(\gamma,3n)$				$\int_{}^{31}$ = 3.0±1.2%		E_{th} = 22 MeV
$Ta^{181}(\gamma,2n)$				$\int_{}^{31}$ = 24±3%		E_{th} = 14 MeV
						$\int \sigma_{(tot)} dE$ = 3.3±1.2 MeV-

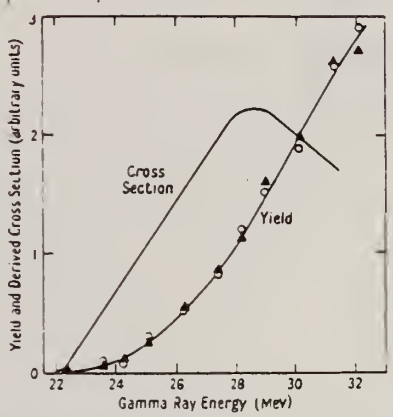

Figure 1. Yield curve and derived cross section for the reaction $^{181}Ta(\gamma, 3n)^{178}Ta$. The circles and triangles refer to the normalized 9·5 min and 150 min observations.

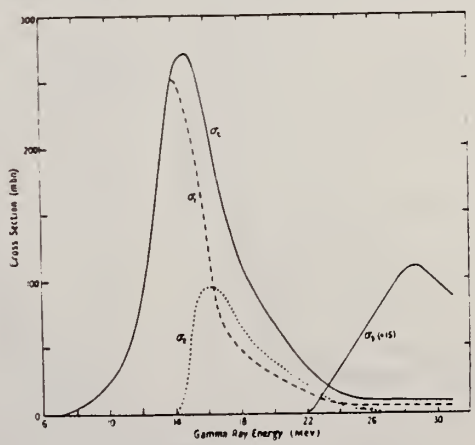

Figure 2. Cross sections σ_1 σ_2 and σ_3 for the reactions $^{181}Ta(\gamma, n)$, $(\gamma, 2n)$ and $(\gamma, 3n)$ and the total cross section σ_t σ_1 σ_2 σ_3.

B.G. Chidley, L. Katz, S. Kowalski
Can. J. Phys. 36, 407 (1958)

ELEM. SYM.	A	Z
Ta	181	73

Betatron

REF. NO.	
58 Ch 2	NVB

REACTION	RESULT	EXCITATION ENERGY	SOURCE		DETECTOR		ANGLE
			TYPE	RANGE	TYPE	RANGE	
G,N	RLY	THR	C	THR	BF3-I		4PI

See 58 Ka 1 for cross sections

THRESHØLD

TABLE I

MEASURED PHOTONEUTRON THRESHOLDS

Reaction	Measured Q value, Mev.	Other Q values, Mev.	Method	Reference
$Ta^{181}(\gamma, n)Ta^{180}$	7.66±0.05			
		7.7 ±0.2	Threshold	McElhinney *et al.* (1949)
		8.0	Threshold	Johns *et al.* (1950)
		7.55 ±0.20	Threshold	Sher *et al.* (1951)

Ref. G. Cortini, C. Milone, A. Rubbino, F. Ferrero
Nuovo Cimento 9, 85 (1958)

Elem. Sym.	A	Z
Ta	181	73

Method
Emulsions; Betatron; ionization chamber

Ref. No. 58 Co 1 EH

Reaction	E or ΔE	E_o	Γ	$\int \sigma dE$	Jπ	Notes
$Ta^{181}(\gamma,n)$	Bremss. 20 30					E_{th} = 7.6 MeV; 90° spectrum. In figure 3, the four theoretical curves (I-IV) are normalized to the experimental yield. Level density: Curve I: $\omega(E_R) = C \exp[2\sqrt{\alpha E_R}]$; $\alpha = \frac{\pi^2 A}{160}$ Curve II: See Weisskopf and Ewing: Phys. Rev. 76, 1550 (49) Curve III: See Price: Phys. Rev. 93, 1279 (1954) Curve IV: See Schiff: Phys. Rev. 73, 1311 (1948)

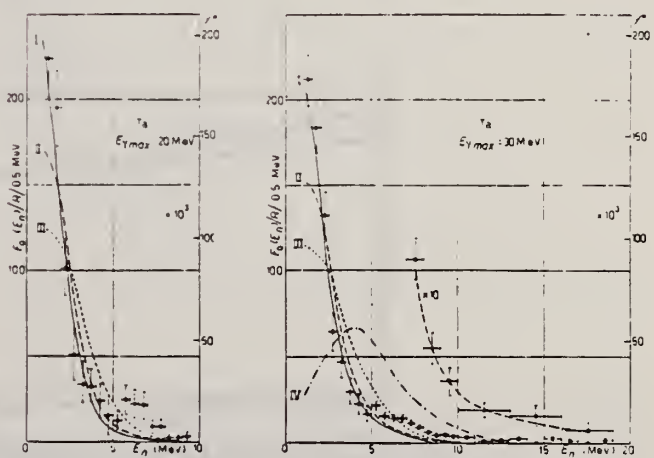

Fig. 3. - Energy spectrum of the photoneutrons from Ta. Experimental figures for the high energy tail are multiplied by 10. The curves I, II, III and IV are the evaporation spectra calculated under different assumptions for the level density (see text).

G. Fuller, B. Petree, M.S. Weiss
ys. Rev. 112, 554 (1958)

ELEM. SYM.	A	Z
Ta	181	73

Betatron; ion chamber

REF. NO.	
58 Fu 1	NVB

REACTION	RESULT	EXCITATION ENERGY	SOURCE		DETECTOR		ANGLE
			TYPE	RANGE	TYPE	RANGE	
G,XN	ABY	7-40	C	7-40	BF3-I		4PI

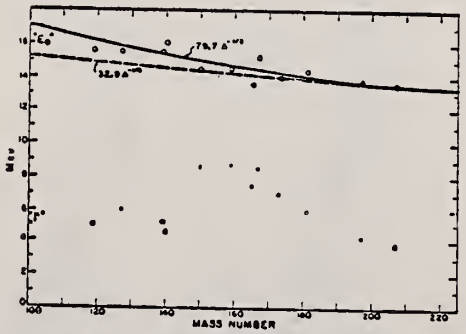

FIG. 6. Mean energy and width of giant resonances. "E_0" and "Γ" are the mean energy for photon absorption and the full width at half maximum of the giant resonance obtained from dashed histograms as in Fig. 5. No attempt was made to fit data with resonance curves to obtain these parameters.

TABLE I. Target properties and results.

Element	Form used	Weight grams	$\sigma^0(\gamma,n)$[a] barns	$\frac{\int\sigma dE^b}{NZ/A}$ Mev-b	"Γ"[a] Mev
Sn	Sn	4.81	0.30	0.064	5.0
I	I	8.55	0.36	0.085	6.0
La	La	10.43	0.34	0.063	5.2
Ce	Ce	4.99	0.45	0.080	4.5
Sm	Sm_2O_3	2.90	0.26	0.073	8.6
Tb	Tb_4O_7	3.04	0.39	0.087	8.7
Ho	Ho_2O_3	1.87	0.41	0.079	7.5
Er	Er_2O_3	5.41	0.50	0.100	8.5
Yb	Yb_2O_3	5.57	0.50	0.090	7.0
Ta	Ta	8.41	0.49	0.077	6.0
Au	Au	3.16	0.68	0.085	4.2
Pb	Pb	8.05	0.75	0.081	3.8

[a] $\sigma^0(\gamma,n)$ is the maximum value and "Γ" the full width at $\sigma^0(\gamma,n)/2$ of the neutron production cross section corrected for multiple neutron emission. Data were not fitted with resonance lines to determine these values.
[b] Integrated neutron production cross sections corrected for multiple neutrons above $(\gamma,2n)$ threshold.

TABLE II. Energies of resonances in deformed nuclei.[a]

Nucleus	E_m Mev	Q_0 barns	Method	E_0 Mev	E_b Mev	$E_{1/2}^-$ Mev	$E_{1/2}^+$ Mev
$_{65}Tb^{159}$	14.7	6.9[b]	CE	11.9	16.2	10.8	19.5
$_{67}Ho^{165}$	14.5	7.8[b]	CE	11.5	16.0	11.0	18.5
$_{68}Er^{167}$	14.5	21[b]	SC	8.5	17.5	11.5	20.0
$_{68}Er^{164}$	14.5	7.8[b]	CE	11.6	15.9	11.5	20.0
$_{73}Ta^{181}$	14.1	12.6[c]	SC	10.5	15.9	11.3	17.3
$_{73}Ta^{181}$	14.1	6.8[b]	CE	11.9	15.2	11.3	17.3
$_{79}Au^{197}$	13.6	3.75[c]	SC	12.5	14.1	11.8	16.2

[a] CE—Coulomb excitation; SC—spectroscopic; $E_{1/2}^-$, $E_{1/2}^+$—energies at which giant resonance drops to half its maximum value.
[b] Adler, Bohr, Huus, Mottelson, and Winther, Revs. Modern Phys. 28, 432 (1956).
[c] M. L. Pool and D. N. Kundu, *Chart of Atomic Nuclei* (Longs College Book Company, Columbus, 1955).

REF.

E.G Fuller, M.S. Weiss
Phys. Rev. 112, 560 (1958)

ELEM. SYM.	A	Z
Ta	181	73

METHOD

Betatron; ion chamber

REF. NO. 58 Fu 2 NVB

REACTION	RESULT	EXCITATION ENERGY	SOURCE		DETECTOR		ANGLE
			TYPE	RANGE	TYPE	RANGE	
G,XN	ABX	8-23	C	THR-25	BF3-I		4PI

CF DANØS THEØRY

TABLE I. Resonance parameters.

	Tb^{159}	Ta^{181}	Au^{197}
B_{1n} (Mev)	5.2	14.0	14.2
E_a (Mev)	12.5	12.45	13.15
σ_a^0 (Mb)	258	308	255
Γ_a (Mev)	2.4	2.3	2.9
E_b (Mev)	16.3	15.45	13.90
σ_b^0 (Mb)	310	348	365
Γ_b (Mev)	4.0	4.4	4.0

TABLE II. Integral cross sections.

	Tb^{159}	Ta^{181}	Au^{197}
$A\int_0^{\infty}\sigma_a dE/0.06NZ$	1.27	1.30	1.29
$\int\sigma_a dE/\int\sigma_a dE$	2.00	2.16	1.97
$A\int_0^{\infty}(\sigma_a+\sigma_b)dE/0.06NZ$	1.27	1.35	1.22

TABLE III. Intrinsic quadrupole moments, in barns.

	Tb^{159}	Ta^{181}	Au^{197}
E_b/E_a	1.30±0.05	1.25±0.01	1.06±0.03
$Q_0(R_0=1.09\times10^{-13}$ cm)	5.6 ±0.6	5.7 ±0.3	1.6 ±0.6
Q_0 (Coulomb excitation)	6.9[a]	6.8[a]	2.6[b]

[a] Adler, Bohr, Huus, Mottelson, and Winter, Revs. Modern Phys. 28, 432 (1956).
[b] P. H. Stelson and F. K. McGowan, Phys. Rev. 99, 112 (1955).

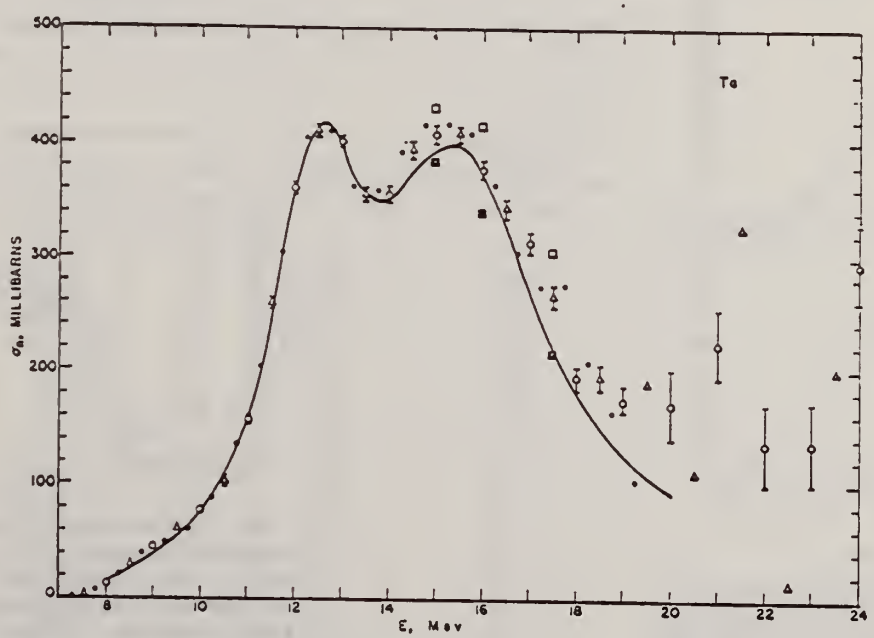

FIG. 6. Neutron cross section for tantalum. See Fig. 5 for description. Circles, triangles, and alternate dots represent four independent determinations of the cross section from the original activation curve. The correction for neutron multiplicity required to bring the experimental points down to the smooth curve in the region from 14 to 16 Mev would probably be within the limits of errors on the cross sections given by Carver and Turchinetz (reference 16). The open squares and closed squares correspond to the limiting positions of the experimental points based on curves *A* and *B* given in Fig. 4.

REF. E.G. Fuller, E. Hayward
Phys. Rev. Letters 1, 465 (1958)

ELEM. SYM.	A	Z
Ta	181	73

METHOD: Betatron

REF. NO.: 58 Fu 3 NVB

REACTION	RESULT	EXCITATION ENERGY	SOURCE		DETECTOR		ANGLE
			TYPE	RANGE	TYPE	RANGE	
G,G	ABX	5-27	C	5-27	NAI-D		120

CF DANØS THEØRY

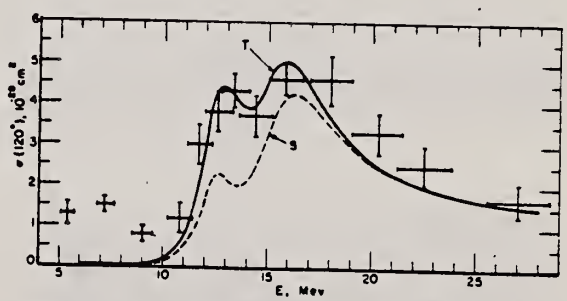

FIG. 1. The differential elastic scattering cross section for tantalum at 120° as a function of photon energy. The smooth curves are calculated using the dispersion relation and the resonance parameters given in reference 1 with the peak cross sections reduced by 10%. The solid curve is the result obtained assuming a tensor electric dipole polarizability [Eq. (5)]; whereas the dashed curve results from assuming a scalar polarizability [Eq. (6)].

L. Katz, G.B. Chidley
Nuclear Reactions at Low and Medium Energies (Academy of Science, USSR: 1958) 371

Ta	181	73

METHOD: Betatron; neutron cross section; BF_3 counters; ion chamber monitor

REF. NO.: 58 Ka 1 | NVB

REACTION	RESULT	EXCITATION ENERGY	SOURCE		DETECTOR		ANGLE
			TYPE	RANGE	TYPE	RANGE	
G,XN	ABX	9-22	C	9-22	BF3-I		4PI

Таблица 2

Пороги испускания фотонейтронов

Изотоп	B_n, *Мэв*	B_{2n}, *Мэв*	Изотоп	B_n, *Мэв*	B_{2n}, *Мэв*
V^{51}	11,16	20,5	La^{139}	8,81	16,1
Mn^{55}	10,14	19,2	Pr^{141}	9,46	17,6
Co^{59}	10,44	18,6	Tb^{159}	8,16	14,8
As^{75}	10,24	18,1	Ho^{165}	8,10	14,6
Y^{89}	11,82	20,7	Tm^{169}	8,00	14,7
Nb^{93}	8,86	17,1	Lu^{175}	7,77	14,2
Rh^{103}	9,46	16,8	Ta^{181}	7,66	13,8
J^{127}	9,14	16,2	Au^{197}	7,96	13,3
Cs^{133}	9,11	16,5	Bi^{209}	7,43	14,5

THRESHOLDS

не приведены, поскольку они превышают 22 *Мэв* во всех случаях, кроме золота, для которого $B_{2n}=21$ *Мэв*. Свойства сечений $\sigma_c(\gamma)$ сведены в табл. 3.

Таблица 1

Изотоп	$E_{макс}$, *Мэв*	$\sigma_n(E_\gamma)$, *барн*	Γ, *Мэв*	$\int\sigma dE$, *Мэв·барн*	Y(22), 10^8 *нейтрон/100 р·моль*
V^{51}	18,4	0,062	5,2	0,33	1,62
Mn^{55}	20,2	0,060	7,0	0,39	2,01
Co^{59}	18,3	0,068	6,3	0,44	2,30
As^{75}	16,4	0,090	9,5	0,74	4,25
Y^{89}	17,1	0,172	5,2	0,93	5,33
Nb^{93}	18,0	0,156	7,5	1,17	6,80
Rh^{103}	17,5	0,160	9,4	1,40	8,28
J^{127}	15,2	0,273	6,8	1,76	11,9
Cs^{133}	16,5	0,238	7,7	1,59	10,7
La^{139}	15,5	0,325	3,8	1,55	11,2
Pr^{141}	15,0	0,320	4,9	1,93	13,1
Tb^{159}	15,6	0,274	9,8	2,49	18,1
Ho^{165}	13,5	0,305	8,9	2,52	18,7
Tm^{169}	16,4	0,250	8,4	1,91	14,9
Lu^{175}	16,0	0,225	8,4	1,90	23,0
Ta^{181}	14,5	0,380	8,5	3,15	22,0
Au^{197}	13,8	0,475	4,7	3,04	22,6
Bi^{209}	13,2	0,455	5,9	2,89	23,2

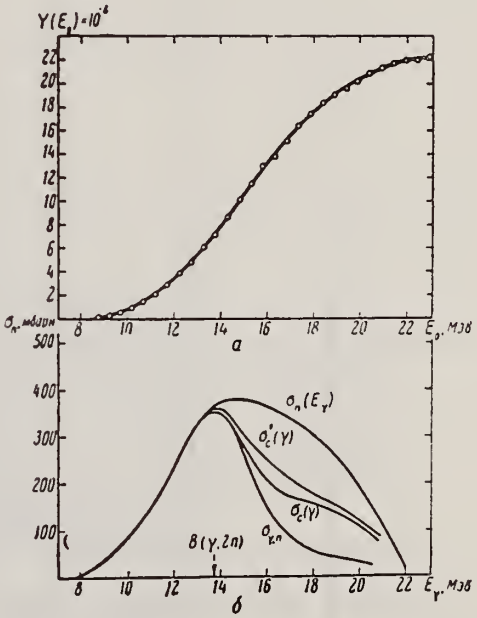

Рис. 15.

а — Выход фотонейтронов для Та; б — $\sigma_n(E_\gamma)$ — сечение испускания фотонейтронов, вычисленное из данных, приведенных на рис. 15, а. $\sigma_{\gamma,n}$ — сечение реакции (γ, n), полученное в работе [20] (нормировка результатов произвольная); $\sigma'_c(\gamma)$ — сечение поглощения γ-квантов, вычисленное по формуле (10); $\sigma_c(\gamma)$ — та же величина, вычисленная по формуле (6)

Ref. B.M. Spicer, H.H. Thies, J.E. Baglin, F.R. Allum
Australian J. Phys. 11, 298 (1958)

Elem. Sym.	A	Z
Ta	181	73

Method 18 MeV electron synchrotron; neutron counters, 25 r Victoreen monitor

Ref. No. 58 Sp 1 | EH

Reaction	E or ΔE	E_o	Γ	$\int \sigma dE$	Jπ	Notes
$Ta^{181}(\gamma,n)$	Bremss. 8-18					

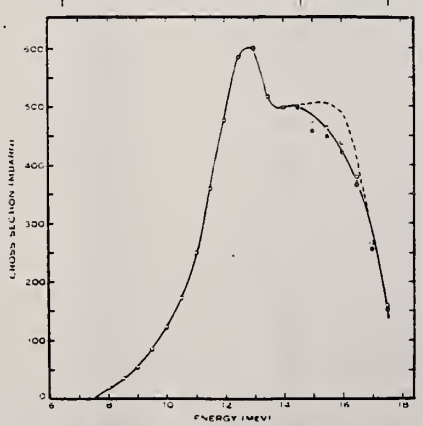

Fig. 4.—The cross section for nuclear absorption of γ-rays in tantalum. The full circles were calculated using curve I of Figure 3, while the open circles were the result of using curve II. Use of curve III led to the dotted cross section.

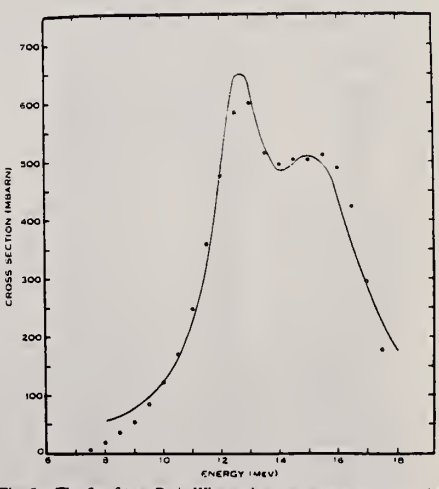

Fig. 5.—The fit of two Breit-Wigner shape resonance curves to the cross section calculated using curve III of Figure 3. Parameters of Breit-Wigner fit to observed σ: $E_1 = 12{\cdot}6$ MeV, $\sigma_{1m} = 500$ mbarn, $\Gamma_1 = 2$ MeV; $E_2 = 15{\cdot}3$ MeV, $\sigma_{2m} = 450$ mbarn, $\Gamma_2 = 4$ MeV.

Ref. L.B. Aull, G.C. Reinhardt, W.D. Whitehead
Nuclear Phys. 13, 292 (1959)

Elem. Sym.	A	Z
Ta	181	73

Method: Si (n,p) radioactivity detector

Ref. No.: 59 Au 1 EGF/EH

Reaction	E or ΔE	E_o	Γ	$\int \sigma dE$	Jπ	Notes
$Ta^{181}(\gamma,n;)$	Bremss. 18-65			$\int^{65} \sim 800$ MeV-mb		Yield measured relative to $Cu^{63}(\gamma,n)$. $E_n \geq 5$ MeV.

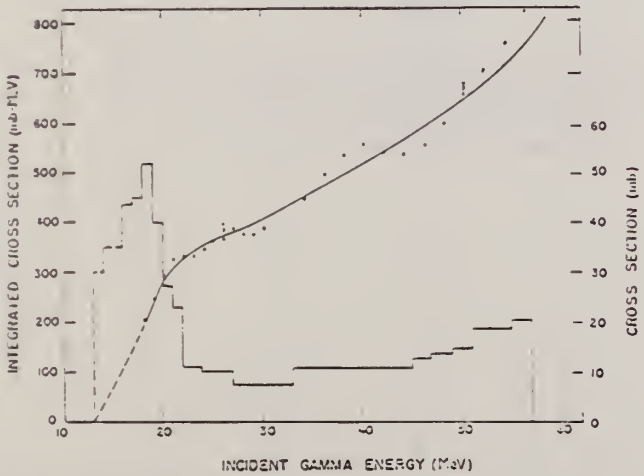

Fig. 3. Tantalum (γ, fast n) smoothed integrated cross section and cross section. The points and the smooth curve represent the smoothed integrated fast neutron cross section (see text) as defined by

$$\int_0^{\infty} \sigma_{\gamma,\,\text{fast n}}\, dE$$

where $\sigma_{\gamma,\text{fast n}}$ is the cross section for photoproduction of neutrons with energies above the 5 MeV, (γ,xn) threshold and E is the incident gamma ray energy. The errors indicated were obtained by propagating the counting uncertainties in the final data through the integral cross section matrix. The histogram represents the first differences of the integrated cross section curve.

TABLE 1

Ratio of fast neutron integrated cross section to total neutron integrated cross section

	24 MeV	30 MeV	60 MeV
Tantalum	10.3 ± 2.4 % [a]	7.3 ± 1.7 % [b]	10.6 ± 2.2 [b]
Gold	10.9 ± 2.7 % [a]		17.4 ± 4.3 [c]

[a]) Compared to (γ, n) cross section of Fuller and Weiss [17]);
[b]) Compared to (γ, xn) of Terwilliger and Jones [18]);
[c]) Compared to (γ, n) of Edwards and McMillan (data taken at 70 MeV) [19]).

Ref 17: Fuller & Weiss - Phys. Rev. 112, 560 (1958)

Ref 18: Jones & Terwillinger - Phys. Rev. 91, 699 (1953)

Ref 19: Edwards & MacMillan - Phys. Rev. 87, 377 (1952)

REF.

W. C. Barber and W. D. George
Phys. Rev. 116, 1551 (1959)

ELEM. SYM.	A	Z
Ta	181	73

METHOD

REF. NO.	
59 Ba 3	EGF

REACTION	RESULT	EXCITATION ENERGY	SOURCE		DETECTOR		ANGLE
			TYPE	RANGE	TYPE	RANGE	
E,N	ABY	THR - 36	D	10 - 36	BF3-I		4PI

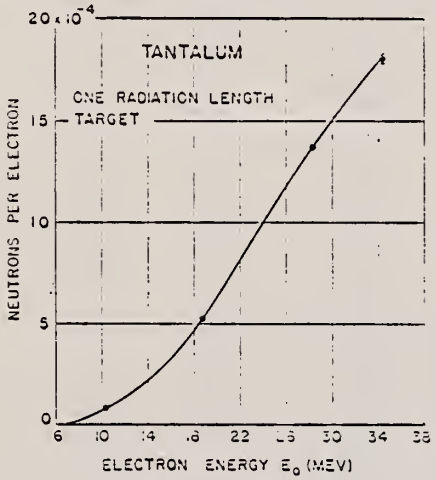

FIG. 7. Yield of neutrons per incident electron as a function of initial electron energy for the Ta target 1 radiation-length thick.

TABLE I. Thicknesses of the targets used in the experiment, with the exception of heavy water, all targets contained isotopes in their naturally-occurring proportions.

Target	Thickness (g/cm²)	Thickness (radiation lengths)
Heavy water	0.698	"thin"
Be	0.559	0.00867
C-I	38.91	0.88
Al-I	24.39	1.60
Cu-A	1.372	0.108
Cu	13.26	1.04
Cu-I	26.56	2.08
Cu-II	39.86	3.13
Cu-IV	53.13	4.17
Ta-I	6.21	0.98
Pb-I	5.88	1.0
Pb-II	11.42	1.97
Pb-III	17.30	2.98
Pb-IV	22.89	3.94
Pb-VI	34.42	5.93
U-I	6.17	1.14
U-II	12.42	2.30
U-III	18.61	3.46
Concrete	28.5	1.19

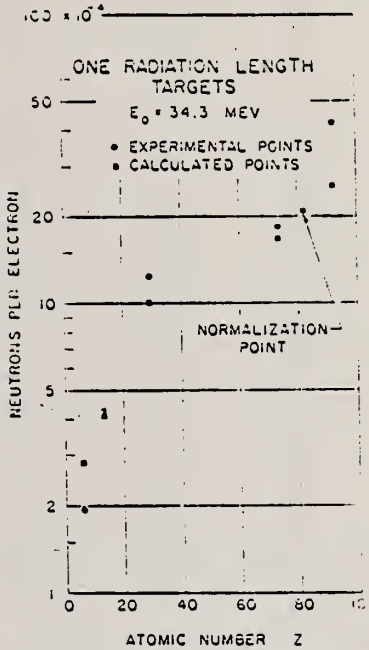

FIG. 14. Experimental and expected yields of neutrons per incident electron for 1-radiation-length targets at 34.3 MeV, as a function of atomic number Z. The experimental yields were obtained by dividing the measured yields from the targets listed in Table I by the actual target thicknesses listed in Table I. The expected yields were calculated from expression (8).

Ref. J.H. Carver, W. Turchinetz
Proc. Phys. Soc. 73, 69 (1959)

Elem. Sym.	A	Z
Ta	181	73

Method 33 MeV synchrotron; radioactivity; NaI spectrometer; r chamber

Ref. No. 59 Ca 3 EH

Reaction	E or ΔE	E_o	Γ	$\int \sigma dE$	Jπ	Notes
$Ta^{181}(\gamma,n)$	Bremss. 8-33	13.5	5.3 MeV	2.4±0.8 MeV-b		

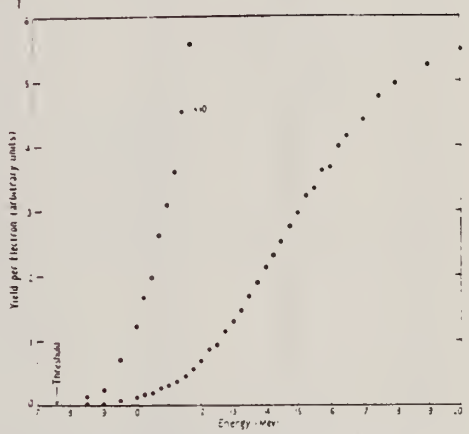

Figure 1. Activation curve for $^{181}Ta(\gamma,n)$ leading to the 8·15 hr level of ^{180}Ta. Statistical errors are smaller than experimental points.

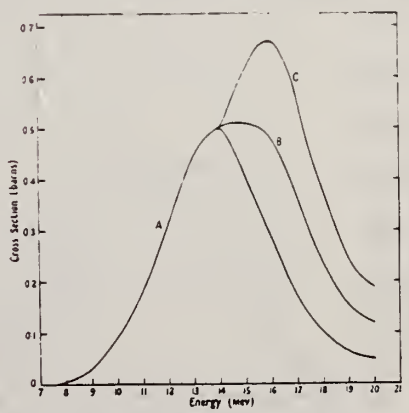

Figure 3. A, derived cross section for $^{181}Ta(\gamma,n)$, σ_1; B, total cross section, $\sigma_1+\sigma_2$ where σ_2 has been taken from the data of Carver and Turchinetz (1958); C, $\sigma_1+2\sigma_2$.

Ref. R.W. Parsons, L. Katz
Can. J. Phys. 37, 809 (1959)

Elem. Sym.	A	Z
Ta	181	73

Method: 22 MeV Saskatchewan Betatron; neutron counting; BF_3 counters; Victoreen ionization chamber

Ref. No.: 59 Pa 1 | EH

Reaction	E or ΔE	E_o	Γ	$\int \sigma dE$	Jπ	Notes
$Ta^{181}(\gamma,n)$	Bremss. 7.6-22	12.75 ± 0.25 15.25 ± 0.25				E_{th} = 7.63 ± 0.05 Mev Yield curve normalized by comparing from Cu (assumed to be 2.71 X 10^8 n/mol/100 r) and Ta at 22 MeV. In Figure 3, neutron multiplicities derived from: "(a)" - Carver and Turchinetz "(b)" - Blatt-Weisskopf formula "0" neutron yield. Solid curve is: $\sigma = \frac{\sigma_1}{1 + (\frac{E-E_1}{\Gamma_1/2})} + \frac{\sigma_2}{1 + (\frac{E-E_2}{\Gamma_2/2})^2}$ where σ_1 = 317 mb σ_2 = 444 mb E_1 = 12.5 E_2 = 15.5 Γ_1 = 2.3 Γ_2 = 3.6 $\frac{\sigma_1\Gamma_1}{\sigma_2\Gamma_2}$ = 0.46

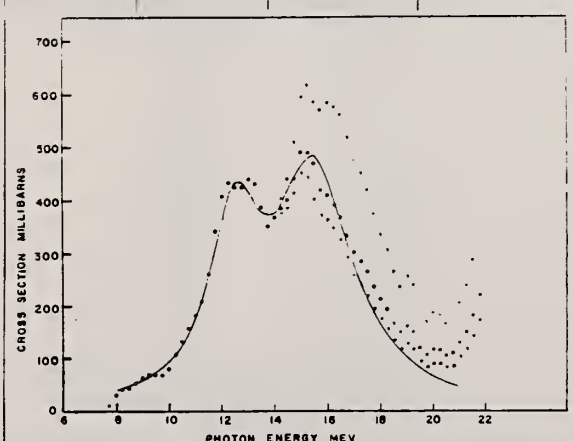

FORM NBS-418 (8-1-63)
USCOMM-DC 18556-P63

U.S. DEPARTMENT OF COMMERCE
NATIONAL BUREAU OF STANDARDS

REF.

W. Sébaoun and H. Gauvin
Compt. Rend. 248, 791 (1959)

ELEM. SYM.	A	Z
Ta	181	73

METHOD

REF. NO.	
59 Se 2	EGF

REACTION	RESULT	EXCITATION ENERGY	SOURCE		DETECTOR		ANGLE
			TYPE	RANGE	TYPE	RANGE	
G,P	ABX	15,18	D	15,18	EMU-I		4PI

14.8 and 17.6 MeV photons

Average $\sigma = 1.6 \pm 1.2 \times 10^{-26}$ cm^2.

Ref. W.C. Barber, T. Wiedling
Nuclear Phys. 18, 575 (1960)

Elem. Sym.	A	Z
Ta	181	73

Method 45 MeV linac; three-foil stack (electrodisintegration target, bremss. radiator, electro- and photodisintegration target); activation

Ref. No. 60 Ba 2 JHH

Reaction	E or ΔE	E_o	Γ	$\int \sigma dE$	Jπ	Notes
(γ,n)						to Ta^{180} (8.1 hours)
(γ,3n)						to Ta^{178} (9.3 min.) (12.1 hours)
(e,e'n) (e,e'3n)						Ratios of electro- to photodisintegration in Figures 5 and 6.

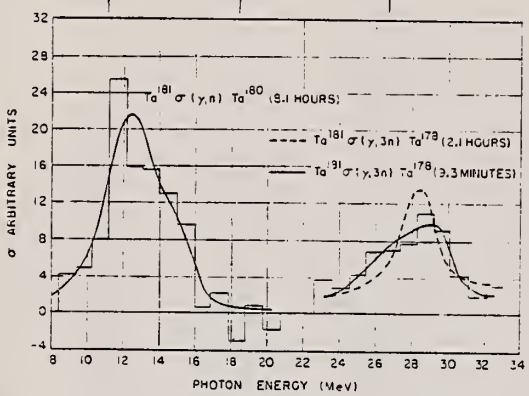

3. Cross sections for Ta derived from the yield curves of fig. 1. The relative magnitudes of the cross section for the different reactions were drawn arbitrarily.

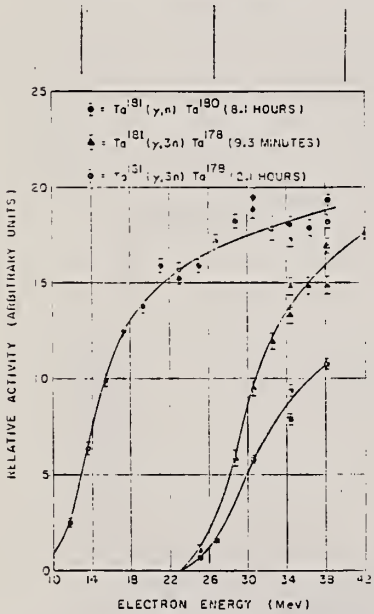

Fig. 1. Yield of Ta radioactivities resulting from the real bremsstrahlung of electrons as a function of the electron energy.

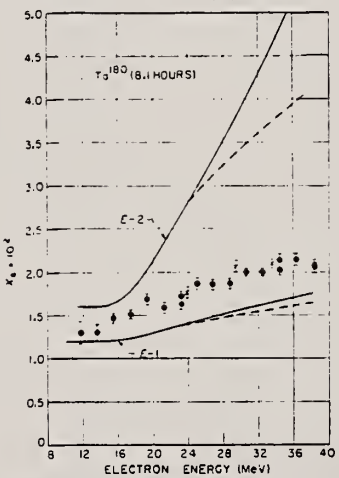

Fig. 5. Ratio of the yields of Ta^{180} from the electrodisintegration of Ta^{181} to those from the photodisintegration as a function of electron energy. The ordinate X_e is the radiation length equivalent of the electrodisintegration. The circles with standard errors indicated are the results of the experiment. The crosses are from the experiment of Brown and Wilson [3]. The theoretical ratios for a point nucleus are shown as solid curves. The dashed curves indicate an approximate correction for the nuclear size.

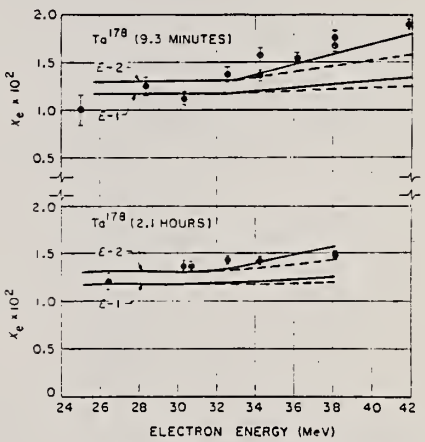

Fig. 6. The radiation length equivalent of the electrodisintegration yields of the two isomers of Ta^{178} produced from Ta^{181} as a function of electron energy. The circles with standard errors indicated are the results of the experiment. The theoretical values of X_e for a point nucleus are shown as solid curves. The dashed curves indicate an approximate correction for the nuclear size.

Ref 3: Phys. Rev. 93, 443 (1954)

Ref.	Elem. Sym.	A	Z
W.C. Barber, V.J. Vanhuyse Nuclear Phys. 16, 381 (1960)	Ta	181	73

Method	Ref No.	
Stanford Mark II accelerator; virtual and real photon spectrum from electrons; magnetic spectrum; KI scintillator crystals.	60 Ba 5	JHH

Reaction	E or ΔE	E_0	Γ	$\int \sigma dE$	Jπ	Notes
$Ta^{181}(\gamma,p)$	E_{e^-} = ≤ 40			$\int_0^{40}$ = 60±25% MeVmb		∫σdE from calculated real and virtual photon spectrum.

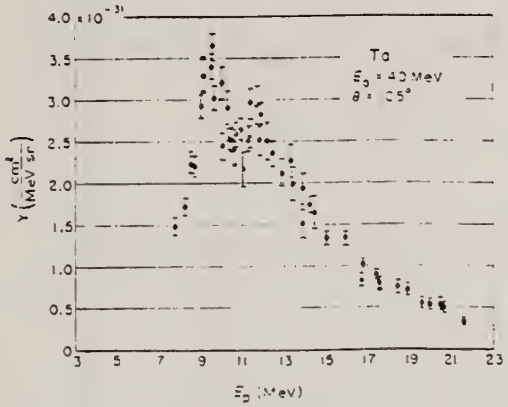

Fig. 6. Energy distribution of protons from Ta at 105°.

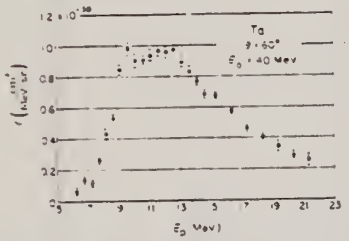

Fig. 7. Energy distribution of protons from Ta at 60°. The scales of abscissae on this figure and fig. 6 are not directly comparable because in the 60° measurements an additional radiator of 5.08×10^{-2} radiation length was in the primary beam upstream from the target.

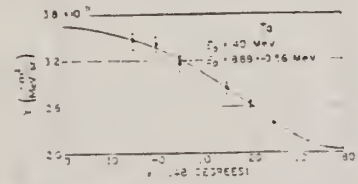

Fig. 11. Angular distribution of those protons in Ta which have energies near the second maximum in the energy distribution. The curve is a plot of $(2.53 - 1.50\cos\theta + 0.21\sin^2\theta - 0.92\cos^2\theta + 0.49\cos^3\theta) \times 10^{-31}$

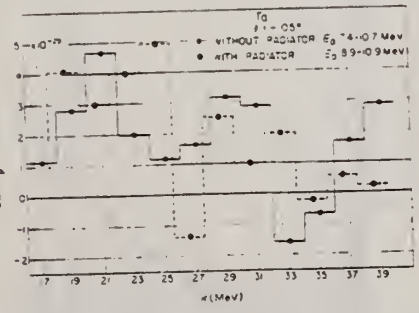

Fig. 20. Differential cross section for producing the lower-energy group of protons from Ta. The two histograms were derived by photon-difference analyses of two excitation functions (not shown) taken with and without the additional Ta radiator of 3.12×10^{-2} radiation length in the primary electron beam. Although the proton energy groups were not exactly the same in the two cases, they are close enough that the cross sections are expected to be nearly the same.

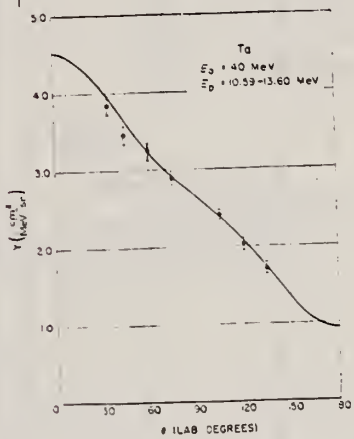

Fig. 12. Angular distribution of protons from Ta having energies near the second maximum in the energy distribution. The curve is a plot of $(2.72 - 1.50\cos\theta - 0.01\sin^2\theta - 0.84\cos\theta\sin^2\theta) \times 10^{-31}$

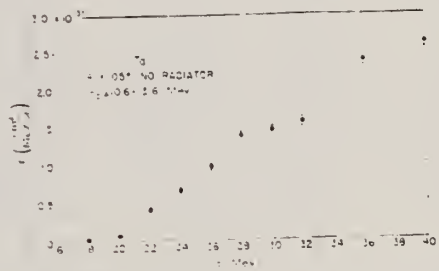

Fig. 16. Excitation of the [illegible] protons from Ta as a function of primary

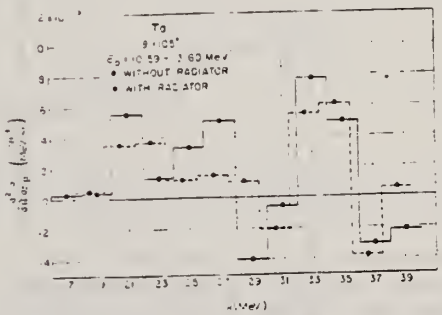

Fig. 19. Differential cross section for producing the higher-energy group of protons from Ta. The solid histogram was derived from a photon-difference analysis of fig. 16. The dashed histogram was similarly derived from an excitation function (not shown) taken with an additional radiator of 3.12×10^{-2} radiation length of Ta in the primary electron beam upstream from the target. The degree of reliability of the results can be judged from the agreement of the two histograms.

Ref. J.H. Carver, R.B. Taylor, W.E. Turchinetz
Australian J. Phys. 13, 617 (1960)

Elem. Sym.	A	Z
Ta	181	73

Method: Electron synchrotron; radioactivity

Ref. No.: 60 Ca 2 EH

Reaction	E or ΔE	E_o	Γ	$\int \sigma dE$	Jπ	Notes
$Ta^{181}(\gamma,p)$	Bremss. 15 ~ 32	28		$\int_{}^{32}$ = 10±2 MeV-mb		E_{th} = 6.7 MeV σ_{max} = 1.0 mb.

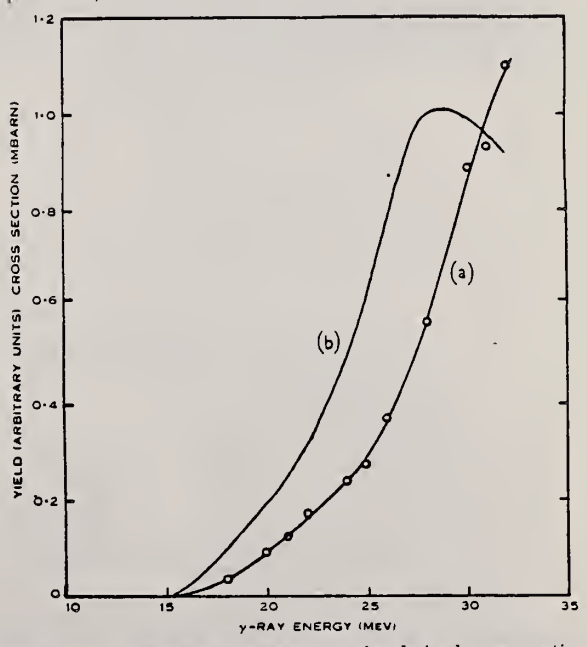

Fig. 3.—(*a*) The yield curve and (*b*) the derived cross section for the $^{181}Ta(\gamma,p)^{180m}Hf$ reaction.

V.P. Chizhov
Zhur. Eksp. i Teoret. Fiz. 38, 809 (1960)
Soviet Phys. JETP 11, 587 (1960)

Elem. Sym.	A	Z
Ta	181	73

Method: 90 MeV Bremsstrahlung; scintillator counter telescope

Ref. No.: 60 Ch 1 JHH

Reaction	E or ΔE	E_o	Γ	$\int \sigma dE$	Jπ	Notes
$Ta^{181}(\gamma,p)$						Energy Range of particles detected:
$Ta^{181}(\gamma,d)$						E_d - 15.5-30 MeV
$Ta^{181}(\gamma,t)$						E_p - 15.5-30 MeV
						E_t - 17-30 MeV
						Ratios:
						$\sigma(\gamma,d)/\sigma(\gamma,p)$, $\sigma(\gamma,t)/\sigma(\gamma,d)$ } at $\theta = 90^\circ$

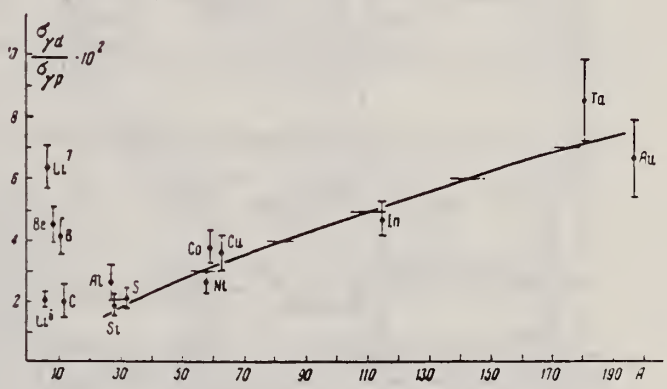

FIG. 3. Ratio of (γ, d) to (γ, p) cross sections for protons and deuterons of energies 15.5–30 Mev as function of atomic weight A. The solid curve shows the dependence given by Eq. (2), arbitrarily normalized.

TABLE I

Element	$100N_t/N_d$	Element	$100N_t/N_d$	Element	$100N_t/N_d$	Element	$100N_t/N_d$
Li^6	30±3	B	39±8	Ni	10±4	In	5±2.5
Li^7	22.5±2.5	Si	10±4	Co	2.5±2	Ta	10±4
Be	13±2.6	S	8±4	Cu	2.2±2	Au	3±3

REF.
K.N. Geller, J. Halpern, E.G. Muirhead
Phys. Rev. 118, 1302 (1960)

ELEM. SYM.	A	Z
Ta	181	73

METHOD
Betatron; neutron threshold; ion chamber

REF. NO.	
60 Ge 3	NVB

REACTION	RESULT	EXCITATION ENERGY	SOURCE		DETECTOR		ANGLE
			TYPE	RANGE	TYPE	RANGE	
G,N	NØX	THR	C	THR	ACT-I		4PI

THRESHØLD

TABLE I. Summary and comparison of neutron separation energies inferred from present threshold measurements with values predicted from mass data and reaction energies. All energies are expressed in the center-of-mass system in Mev.

Reaction	No. runs	Present results	Other results	Method	Reference
$Ta^{181}(\gamma,n)Ta^{180}$	5	7.640±0.025	7.66 ±0.05	threshold	f
$Ta^{181}(\gamma,n)Ta^{180}$ (to 8.1-hr state)	2	7.852±0.025			

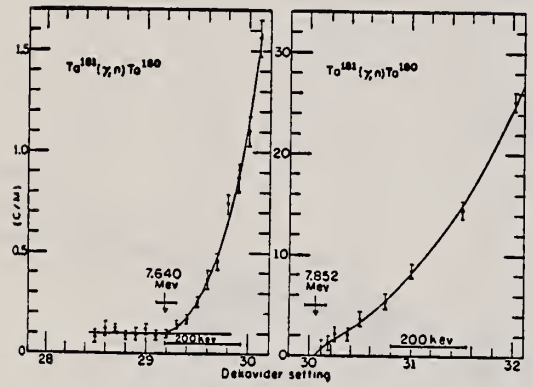

FIG. 8. Photoneutron yield curves for Ta^{181} measured by direct neutron detection and induced radioactivity. The difference in the observed thresholds indicates the 8.1-hr isomer to be 212 kev above the naturally occurring Ta^{180} ground state.

R.G. Baker, K.G. McNeill
Can. J. Phys. 39, 1158(1961)

Ta	181	73

METHOD: betatron; fast neutron yield; angular distribution; Al and Si threshold detectors; ion chamber

REF. NO.: 61 Ba 2 | NVB

REACTION	RESULT	EXCITATION ENERGY	SOURCE TYPE	SOURCE RANGE	DETECTOR TYPE	DETECTOR RANGE*	ANGLE
G,XN	ABY	THR-22	C	22	THR-I	3-+	DST
G,XN	ABY	THR-22	C	22	THR-I	5-+	DST

In Tables 2 and 4:

$\bar{\sigma}$ = average cross section of detector weighted with neutron spectrum

Φ = neutrons/100 roentgen/mole

$$W(\theta) = a_o \sum_{n=1}^{\infty} [1 + A_n P_n (\cos \theta)]$$

* "3-+" is the detector range of Aluminum and "5-+" of Silicon.

TABLE II

Normalized yields for aluminum detectors

Element	Al(n,γ) reaction 30°	90°	150°	a_0	Al(n,p) reactions 30°	60°	90°	a_0	a_1	a_2	$(\bar{\sigma}\Phi)^*\times10^9$
Bismuth	399	567±130	620	541±85	3632	5139±290	3168	4360±185	0.06±0.06	−0.35±0.1	17.76
	478	423±130	641	484±85	2562	5353±290	2955	4144±185	−0.05±0.06	−0.53±0.1	16.87
Lead	426	312±120	725	429±77	3123	5754±260	3154	4591±166	−0.004±0.05	−0.51±0.07	18.68
Tantalum	378	367±190	688	441±122	2757	3024±425	2088	2757±275	0.14±0.14	−0.19±0.17	11.22
Lanthanum	208	222±110	330	243±70	2139	3371±250	1891	2768±160	0.05±0.07	−0.43±0.10	11.27
Arsenic	77	100±50	108	97±32	788	937±115	764	865±74	0.02±0.11	−0.16±0.14	3.52
Copper	13	65±30	70	55±20	710	748±70	569	700±45	0.11±0.08	−0.14±0.11	2.85

*$(\bar{\sigma}\Phi)$ = 4.07×10⁴ a_0 millibarn-neutron.

TABLE IV

Element	II a_0	III a_1	IV a_2	V $(\bar{\sigma}\Phi)\times10^{9*}$	VI Φ_{total}(22 Mev)×10⁹	VII Φ_{fast}/Φ_{total}
Vanadium	245(1±0.06)	0.01±0.08	−0.00±0.10	6.05	0.21	0.12
Chromium	164(1±0.03)	0.04±0.04	−0.05±0.05	4.05	0.17	0.10
Manganese	308(1±0.02)	0.07±0.03	−0.09±0.04	7.61	0.25	0.12
[illegible]	200(1±0.03)	0.05±0.04	−0.17±0.05	4.94	0.18	0.11
[illegible]lt	390(1±0.02)	0.08±0.03	−0.22±0.04	9.63	0.26	0.15
[illegible]	145(1±0.05)	0.07±0.07	−0.23±0.09	3.58	0.12	0.12
[illegible]pper	347(1±0.02)	0.05±0.03	−0.29±0.04	8.57	0.30	0.12
[illegible]c	482(1±0.03)	0.11±0.04	−0.24±0.05	11.91	0.33	0.15
[illegible]dium	638(1±0.05)	0.13±0.06	−0.14±0.08	15.76		
[illegible]ontium	409(1±0.05)	0.10±0.06	−0.17±0.08	10.10		
[illegible]um	290(1±0.10)	0.08±0.12	−0.12±0.15	7.16		
Silver	590(1±0.04)	0.10±0.06	−0.22±0.08	14.57	0.87	0.07
Cadmium	905(1±0.02)	0.02±0.02	−0.26±0.03	22.35		
Iodine	1133(1±0.03)	0.04±0.04	−0.29±0.05	27.99	1.42	0.08
Barium	1048(1±0.04)	0.10±0.06	−0.38±0.08	25.89		
Lanthanum	1595(1±0.02)	0.02±0.03	−0.42±0.04	39.40	1.04	0.15
Cerium	1316(1±0.05)	0.05±0.06	−0.39±0.08	32.50		
Dysprosium	1652(1±0.08)	0.04±0.10	−0.34±0.13	40.80		
Tantalum	1558(1±0.02)	0.04±0.03	−0.22±0.04	38.48	2.50	0.06
Tungsten	1365(1±0.02)	−0.07±0.03	−0.24±0.04	33.71		
Mercury	1345(1±0.02)	0.04±0.03	−0.31±0.04	33.22		
Lead	2274(1±0.01)	0.02±0.02	−0.42±0.03	56.17	2.72	0.08
Bismuth	2162(1±0.02)	0.05±0.03	−0.45±0.04	53.40	3.36	0.06
Thorium	3031(1±0.04)	0.06±0.05	−0.32±0.07	74.87		
Uranium	4630(1±0.02)	0.05±0.03	−0.17±0.04	114.36		

*$(\bar{\sigma}\Phi)$ = 2.47×10⁷ a_0 millibarn-neutron. Errors are standard errors due to counting statistics only.

REF.

A. Bussiere de Nercy
Ann. Phys.(Paris) Third Series 6, 1379 (1961)

ELEM. SYM.	A	Z
Ta	181	73

METHOD

REF. NO.	
61 Bu 4	egf

REACTION	RESULT	EXCITATION ENERGY	SOURCE		DETECTOR		ANGLE
			TYPE	RANGE	TYPE	RANGE	
G,G	ABX	10-25	C	20	NAI-D		DST

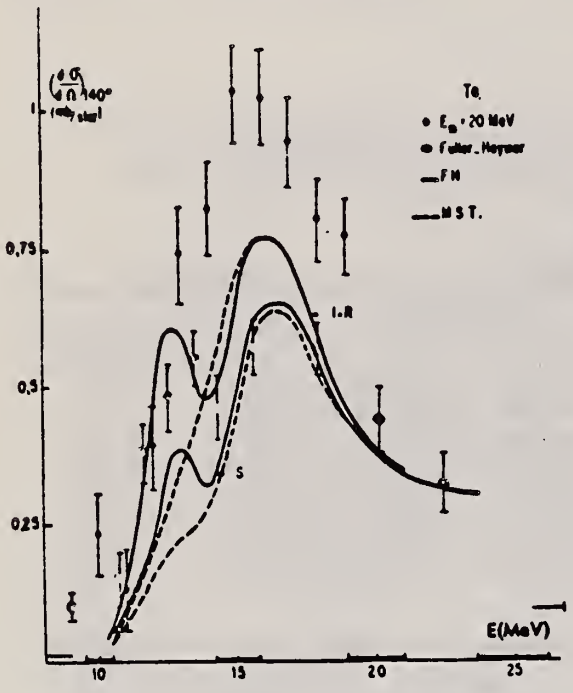

Fig. 24. — Section efficace différentielle de diffusion (γ, γ) à 140° pour le tantale.

=

=

Les courbes en trait plein et en pointillés représentent les sections efficaces prévues par la relation de dispersion.

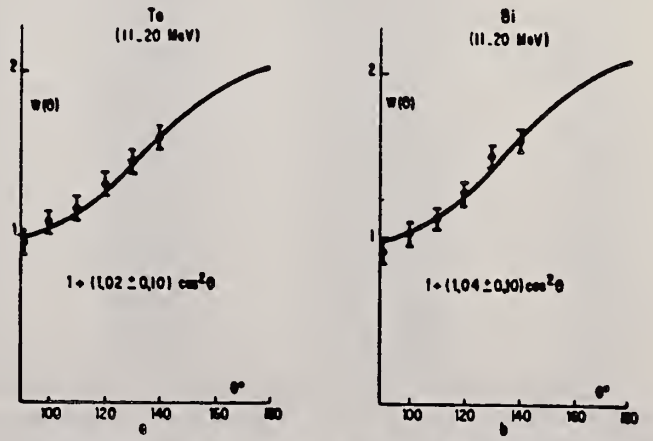

Fig. 27. — Distribution angulaire des photons diffusés par le tantale (*a*) et le bismuth (*b*) (11-20 MeV).

REF.
J. Miller, C. Schuhl, C. Tzara
J. Phys. Radium 22, 529 (1961)

ELEM. SYM.	A	Z
Ta	181	73

METHOD
Positron annihilation; neutron cross section; BF_3 counter; ion chamber

REF. NO.: 61 Mi 1 | NVB

REACTION	RESULT	EXCITATION ENERGY	SOURCE		DETECTOR		ANGLE
			TYPE	RANGE	TYPE	RANGE	
G,XN	ABX	8-22	D	8-22	BF3-I		4PI

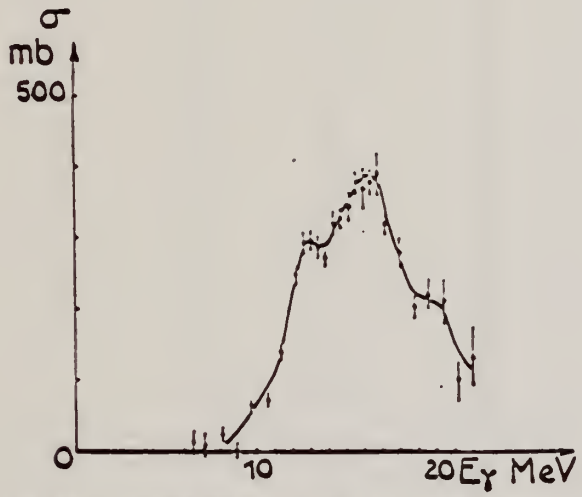

FIG. 36. — Tantalo, $\sigma(\gamma, n) + 2\sigma(\gamma, 2n) + \sigma(\gamma, np) + \ldots$

Ref. R.E. Welsh, D.J. Donahue
Phys. Rev. 121, 880 (1961)

Elem. Sym.	A	Z
Ta	181	73

Method: Monoergic γ's from thermal n-capture; activation

Ref. No.: 61 We 1 JHH

Reaction	E or ΔE	E_o	Γ	$\int \sigma dE$	Jπ	Notes
(γ,n)	7.49-10.83					Measurement of 54-kev K x-ray from K-capture in Ta^{108m}. Data in Table II (millibarns); compares with Fuller and Weiss in Figure 2. $E_{\gamma\ thresh.}$ = 7.60 ± 0.08 MeV

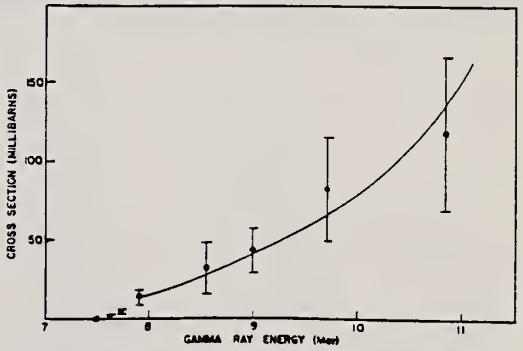

FIG. 2. Cross section vs energy for $Ta^{181}(\gamma,n)Ta^{180m}$(8.15 hr). The smooth curve represents the data of Fuller and Weiss,[8] for the reaction $Ta^{181}(\gamma,n)Ta^{180}$.

TABLE II. Summary of measured cross sections.

γ-ray source / Energy (Mev) / Reaction	Co 7.49	Fe 7.64	Al 7.73	Cu 7.91	Cl 8.56	Ni 8.997	Fe 9.30	Cr 9.72	Fe 10.16	N 10.83
$Ta^{181}(\gamma,n)Ta^{180m}$	0±0.05	0.5±1	4.8±1.6	14±5	32±16	44±15	...	83±33	...	120±48
$Au^{197}(\gamma,n)Au^{196}$	...	...	...	0±2	34±17	44±11	64±30	80±30	...	...
$Ho^{165}(\gamma,n)Ho^{164}$	...	...	...	0±0.1	29±15	30±18	46±21	36±31	...	260±93
$Nb^{93}(\gamma,n)Nb^{92}$	...	...	...	...	...	0.008±0.005	1.0±0.4	2.4±0.7	...	...
$Ag^{107}(\gamma,n)Ag^{106}$	...	...	...	...	...	0±0.1	...	4.4±1.5	22±16	23±7.5

Ref. O.V.Bogdankevich, B.I.Goryachev, V.A.Zapevalov

Zhur.Eksptl. i Teoret.Fiz. 42, 1502 (1962);
Soviet Phys.JETP 15, 1044 (1962)

Elem. Sym.	A	Z
Ta	181	73

Method

30MeV Synchrotron - BF_3

Ref. No. 62Bol BG

Reaction	E or ΔE	E_o	Γ	$\int \sigma dE$	Jπ	Notes 458
(γ,n)	threshold 23 MeV	Fig.5 Data for Lorentz lines given in Table I				fitted with smooth curve which is superposition of 2 Lorentz lines. ($\sigma_{int} = \int_o^\infty \sigma_\gamma dE_\gamma$) $\epsilon = R_1 - R_2/R_0$, R_1 and R_2 are axes of nuclear ellipsoid. R_o radius of sphere with volume equal to nuclear ellipsoid. ϵ_o from other experiments.

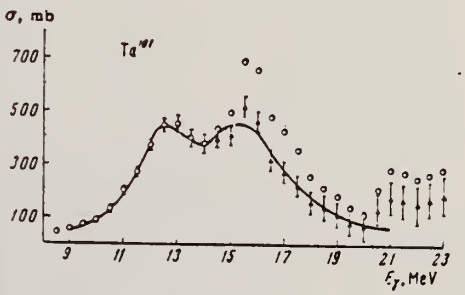

FIG. 5. Photoneutron production cross section of Ta^{181}.

Table I

	Ta^{181}	Rh^{103}	In^{115}		Ta^{181}	Rh^{103}	In^{115}
σ_1^{max}, mb	350	150	166	σ_{int2}, MeV·b	2.38	1.43	1.43
$E_{\sigma 1}$, MeV	12.4	14.25	14	$\sigma_{int2}/\sigma_{int}$	1.8	2.0	1.8
Γ_1, MeV	2.4	3.0	3.0	σ_{int}, MeV·b	3.70	2.13	2.21
σ_{int1}, MeV·b	1.32	0.706	0.78	$\sigma_{int}/(0.058NZ/A)$	1.46	1.44	1.36
σ_2^{max}, mb	400	240	240	a	0.23	0.21	0.15
$E_{\sigma 2}$, MeV	15.5	17.5	16.25	ϵ_0	0.22	0.20	0.14
Γ_2, MeV	3.8	3.8	3.8	Q_0, b	7.1±0.8	2.7±0.3	2.3±0.4

Ref. J. Miller, C. Schuhl, C. Tzara
Nuclear Phys. 32, 236 (1962)

Elem. Sym.	A	Z
Ta	181	73

Method: Linac; monoergic photons by e^+ annihilation in flight; NaI

Ref. No.: 62 Mi 3 JHH

Reaction	E or ΔE	E_o	Γ	$\int \sigma dE$	Jπ	Notes
$Ta^{181}(\gamma,xn)$	7-22	13±0.5 16.5±0.5		$\int_0^{22} = 2.97\pm0.05$ MeV-b		

TABLEAU 5

Résultats expérimentaux

Éléments	Fig. No	E_m (MeV)	σ_{int} (MeV · b) *)	$\frac{\sigma_{int}}{0.06NZA}$	Seuils γ, n	γ, p	γ, 2n	γ, np
Cu	6	17 ±0.5	0.45±0.015	0.47±0.015				
La	7	15.6±0.5	1.91±0.03	0.94±0.015	8.80 [13]		14.25 [13]	14.90 [13]
Ce 140	8	15.6±0.5	1.88±0.03	0.92±0.015	9.05 [14]	8.50 [14]	14.1 [14]	
Ce 142					7.15 [14]	9.50 [14]	14.3 [14]	
Ta 181	9	13 ±0.5 16.5±0.5	2.97±0.05	1.13±0.02	7.55 [13]		13.84 [13]	13.47 [13]
Au 197	10	14.2±0.5	3.00±0.05	1.06±0.02	7.90 [13]		13.71 [13]	12.94 [13]
Pb 206	11	13.8±0.5	4.10±0.06	1.38±0.02	10.6 [13]	7.1 [13]	14.3 [13]	14.5 [13]
Pb 207					7.2 [13]	8.2 [13]	14.3 [13]	17.9 [13]
Pb 208					6.9 [13]	8.4 [13]	15.0 [13]	14.2 [13]
Bi 209	12	14.0±0.5	3.73±0.06	1.24±0.02	7.44 [14]	3.76 [14]	10.4 [14]	

*) L'intégrale $\int_0^E \sigma dE$ est prise jusqu'à E égal à 19.6 MeV pour Cu, à 21.2 MeV pour La et Ce et à 22 MeV pour Ta, Au, Pb et Bi. D'autre part, les erreurs indiquées sont les erreurs statistiques.

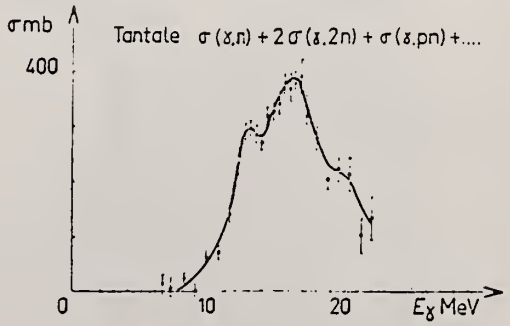

Fig. 9. Section efficace
$\sigma = \sigma(\gamma, n) + \sigma(\gamma, np) + 2\sigma(\gamma, 2n) + \ldots$ pour le tantale.

FORM NBS-418
(6-1-63)
USCOMM-DC 18666-P63

U.S. DEPARTMENT OF COMMERCE
NATIONAL BUREAU OF STANDARDS

Ref.

R.L.Bramblett, J.T.Caldwell, G.F.Auchampaugh, S.C.Fultz

Phys.Rev. 129, 2723 (1963)

Elem. Sym.	A	Z
Ta	181	73

Method

positron annihilation - 4π parafin moderated neutron detector

Ref. No. 63Br1 BG

Reaction	E or ΔE	E_o	Γ	$\int \sigma dE$	Jπ	Notes
544 +(γ,n)	0 - 28	13.5		1.32±0.13) $^{28}_{0}$		(γ,2n) threshold = 13.6±0.2MeV
360 (γ,2n)	0 - 28	16.5		0.93±0.09) $^{28}_{0}$		Intrinsic quadrupole moment = 6.71±.74b
(γ,n) +(γ,2n) +(γ,np)	0 - 28		6.4	2.4±.22) $^{28}_{0}$		Table II data not from this experiment. The two peaks of Fig.1, curve A, are at 12.70 and 15.5 MeV.

359 +

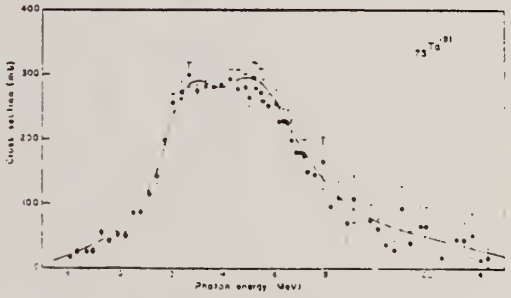

FIG. 3. The formation cross section for the reaction $\sigma(\gamma,n)+\sigma(\gamma,2n)+\sigma(\gamma,np)$ for the compound nucleus Ta^{180}. The solid curve represents the sum of two Lorentz lines with parameters given in Table III.

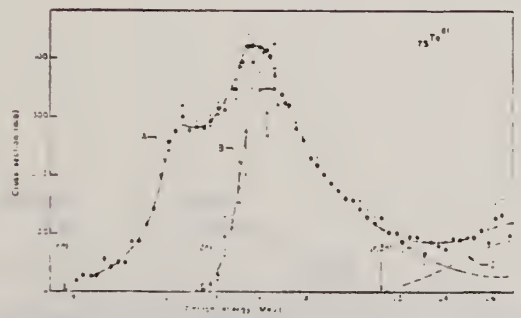

FIG. 1. Cross sections for Ta from neutron yield data. Curve A consists of $\sigma(\gamma,n)+2\sigma(\gamma,2n)+\sigma(\gamma,np)+3\sigma(\gamma,3n)$ and was obtained from single-neutron counting data. Curve B contains $2\sigma(\gamma,2n)$ and was obtained from double-neutron counting data. Curve C contains the estimated contribution of $3\sigma(\gamma,3n)$ to the singles data.

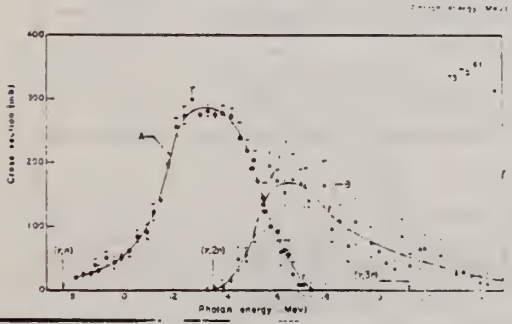

FIG. 2. Partial cross-section curves for Ta. Curve A consists of $\sigma(\gamma,n)+\sigma(\gamma,np)$. Curve B consists of $\sigma(\gamma,2n)+3\sigma(\gamma,3n)$.

TABLE II. Photoneutron data for the Ta and Hu isotopes. The symbols σ_{max}, E_{max}, and E_0 refer to the cross section, the energies at which the maxima in the cross sections occur, and widths at half maximum of the component Lorentz lines used to fit

σ_{max} (mb)	σ_{int} (mb)	E_{max} (MeV)	Γ_{max} (MeV)	E_0 (MeV)	Γ_0 (MeV)	$\int \sigma dE$ (MeV-b)	Ref.
547		14.1		3.3		1.41	11
440		15.0		6.0		4.1	2
450		14.5		6.5		1.52	13
468	114	12.15	15.15	2.9	1.4	1.39	16
515	448	12.5	15.5	2.1	6		17
487	448	12.6	15.5	2.0	6	1.2	18
~500	~395	13	16.5			2.97	19

TABLE III. Lorentz line parameters and intrinsic quadrupole moments for Ta and Hu.

Element	σ_0 (mb)	E_0 (MeV)	Γ_0 (MeV)	σ_{max} (mb)	E_{max} (MeV)	Γ_{max} (MeV)	Q_0 (b)
Ta^{180}	194	1.00	13.75	224	5.0	15.50	6.71 ± 0.74
Hu^{180}	200	2.65	12.10	249	4.4	13.75	7.40 ± 0.90

TABLE IV. Integrated cross sections, level density parameters, and σ_{-1} values.

Element	σ_{-1} mb-MeV	$0.00225(A-2)^2$ mb-MeV	a MeV^{-1}	$\int \sigma dE$ MeV-b	$\int \sigma^2 dE$ MeV-b	$0.06 NZ/A$ MeV-b
Ta^{180}	10.88	13.03	15.7	2.24	2.39	2.61
Hu^{180}	10.93	11.17	22.0	2.37	2.68	2.48

REF.

M. Langevin, J.M. Loiseaux
J. de Physique 24, 1027 (1963)

ELEM. SYM.	A	Z
Ta	181	73

METHOD

Betatron;photon scattering

REF. NO.

63 La 1 NVB

REACTION	RESULT	EXCITATION ENERGY	SOURCE		DETECTOR		ANGLE
			TYPE	RANGE	TYPE	RANGE	
G,G	NΦX	11-22	C	27	NAI-D		DST
		(22)					

In figure 4, $W(\theta) = 1 + a \cos^2\theta$

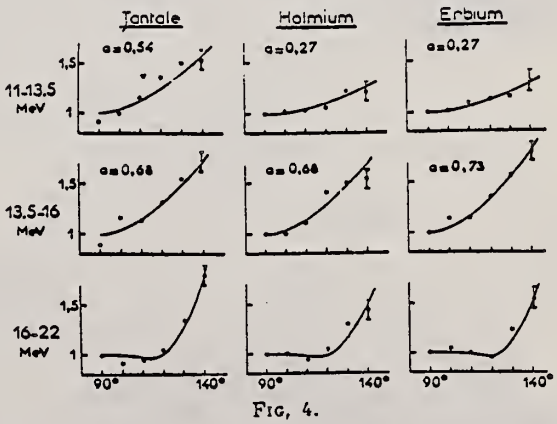

FIG, 4.

Ref. C.S. Young, D.J. Donahue
Phys. Rev. 132, 1724 (1963)

Elem. Sym.	A	Z
Ta	181	73

Method: 200 kW pool reactor; monoergic γ's from (n,γ) in Mn, Fe and Cu; NaI.

Ref. No.: 63 Yo 1 | JHH

Reaction	E or ΔE	E_o	Γ	$\int \sigma dE$	Jπ	Notes
$Ta^{181}(\gamma,\gamma)$	6.0-8.2					Measured σ(elastic scattering) values in Table II; interpolated to 7 MeV in Table V. Detector at 120°

TABLE II. Total elastic scattering cross sections (mb).

Source element	Energy interval (MeV)	Source energy (MeV)	Target (thickness in cm) Ta(1.3)	Hg(3)	Pb(0.6)	Bi(1.3)
Ti	5.0–7.0	6.41 6.75			0.6 ± 0.4	
Mn	6.0–7.5	7.26 7.15 7.05	<0.3	0.5 ±0.3	0.9 ± 0.5	0.8 ±0.4
Fe	6.0–7.6	7.64 7.28	0.7 ±0.4	2.4 ±1.3	125 ±20[a]	2.0 ±1.1
Cu	7.6–8.2	7.91	<0.2	<0.4	<0.2	<0.2

[a] Calculated using the intensity of 7.64-MeV γ rays produced by neutron capture in iron.

TABLE V. Cross sections at about 7 MeV (mb).

	This work	Ref. 2	Ref. 1[a]	Ref. 3	Ref. 4[b]
Ta	<0.3		2		
Hg	0.5±0.3	3.5			
Pb	0.9±0.5	15	17	60	55
Bi	0.8±0.4	17.5	19	35	17

[a] See also E. G. Fuller and Evans Hayward, Phys. Rev. Letters 1, 465 (1958).
[b] Differential cross sections at 135° were multiplied by 11.2.

[1] E. G. Fuller and Evans Hayward, Phys. Rev. 101, 692 (1956); Nucl. Phys. 33, 431 (1962).
[2] K. Riebal and A. K. Mann, Phys. Rev. 118, 701 (1960).
[3] Tsutomu Tohei, Masumi Sugawara, Shigeki Mori, and Motohara Kimara, J. Phys. Soc. Japan 16, 1657 (1961).
[4] P. Axel, K. Min, N. Stein, and D. C. Sutton, Phys. Rev. Letters 10, 299 (1963).

Ref. G.N. Zatsepina, V.V. Igonin, L.E. Lazareva, A.I. Lepestkin
Zhur. Eksp. i Teoret. Fiz. 44, 1787 (1963)
Soviet Phys. JETP 17, 1200 (1963)

Elem. Sym.	A	Z
Ta	181	73

Method: Synchrotron; neutron spectra, angular distribution data; emulsions; ion chamber monitor

Ref. No.: 63 Za 1 JHH

Reaction	E or ΔE	E_0	Γ	$\int \sigma dE$	Jπ	Notes
$Ta^{181}(\gamma,n)$	Bremss.					
	14					
	19					

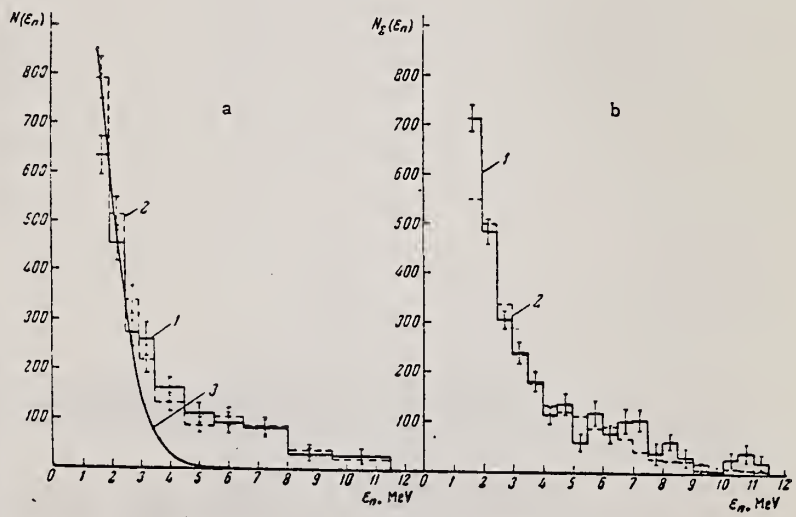

FIG. 9. a – energy distribution of photoneutrons from tantalum at $(h\nu)_{max}$ = 19 MeV; histogram 1 – $N_{90°} + N_{270°}$; 2 – $N_{30°} + N_{150°}$; curve 3 – spectrum of neutrons calculated in accordance with the evaporation model; b – summary neutron spectra for tantalum (1) and bismuth (2) for $(h\nu)_{max}$ = 19 MeV.

FORM NBS-418
(8-1-63)
USCOMM-DC 18556-P63

U.S. DEPARTMENT OF COMMERCE
NATIONAL BUREAU OF STANDARDS

REF.

F.R. Allum, T.W. Quirk, and B.M. Spicer
Nucl. Phys. 53, 545 (1964)

ELEM. SYM.	A	Z
Ta	181	73

METHOD

REF. NO.	
64 Al 5	JOC

REACTION	RESULT	EXCITATION ENERGY	SOURCE		DETECTOR		ANGLE
			TYPE	RANGE	TYPE	RANGE	
G,XN	NØX	THR-34	C	34	THR-I	6-	DST

TABLE 1

Summary of present experimental data at 34 MeV bremsstrahlung

Element		$-\frac{a_2}{a_0}$	$\frac{a_1}{a_0}$
$_{4}$Be		0.43±0.02	0.05±0.01
$_{6}$C		0.61±0.04	0.09±0.02
$_{13}$Al		0.39±0.03	0.05±0.01
$_{22}$Ti		0.34±0.02	0.06±0.01
$_{24}$Cr	34 MeV	0.33±0.02	0.02±0.01
	22 MeV	0.13±0.07	−0.02±0.03
$_{29}$Cu		0.36±0.02	0.10±0.01
$_{50}$Sn		0.38±0.02	0.11±0.01
$_{56}$Ba		0.39±0.03	0.11±0.02
$_{73}$Ta	Before [illegible] of iron shielding	0.26±0.04	0.13±0.02
	After [illegible] of iron shielding	0.27±0.02	0.12±0.01
$_{82}$Pb	target diameter [illegible] cm	0.39±0.03	0.15±0.02
	target diameter 1.5 cm	0.40±0.03	0.19±0.02
$_{83}$Bi		0.42±0.03	0.17±0.02

$a_0 + a_1 \cos\theta + a_2 \cos^2\theta$

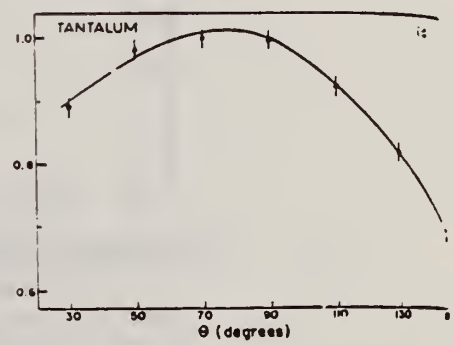

REF.

L. Green, D. J. Donahue
Phys. Rev. 135, B701-05 (1964)

ELEM. SYM.	A	Z
Ta	181	73

METHOD

Reactor; neutron capture gamma rays

REF. NO. 64 Gr 2 NVB

REACTION	RESULT	EXCITATION ENERGY	SOURCE TYPE	SOURCE RANGE	DETECTOR TYPE	DETECTOR RANGE	ANGLE
G,N	ABX	THR-11	D	THR-11	BF3-I		4PI

TABLE II. Summary of measured cross sections (millibarns).

Source	Energy[a] (MeV)	Targets Ta^{181}	Li^{7}	Li^{6}	C^{12}	B^{10}
Aluminum	7.72	4.1± 0.4	0.06 ±0.01	1.13±0.12	1.7 ±0.2	···
Copper	7.91	10.8±1.0	0.07 ±0.01	1.1 ±0.2	0.97±0.13	···
Chlorine	8.56	29 ± 6	0.17 ±0.12	···	···	···
Nickel	9.00	44 ± 6	0.16 ±0.06	1.6 ±0.3	0.6 ±0.1	0.11±0.01
Nitrogen	10.83	121 ±12	1.07 ±0.25	···	4 ±2	0.9 ±0.2
Chromium	9.72	84 ±25	0.55 ±0.25	···	···	0.23±0.05
Iron	7.64	9.0± 0.9	0.079±0.014	1.3 ±0.2	0.23±0.05	···
Iron	9.30	···	···	···	···	0.09±0.03
Lead	7.38	···	0.068±0.035	1.2 ±0.2	0.3 ±0.3	···
Sulphur	5.43	···	···	0.42±0.07		
Sodium	6.41	···	···	0.6 ±0.1		
Titanium	6.75	···	···	1.3 ±0.2	···	···
Titanium	6.61[b]	···	···	···	0.32±0.04	···
Manganese	7.16[c]	···	···	0.9 ±0.1	0.4 ±0.1	
Zinc	7.88	···	···	1.0 ±0.2	1.2 ±0.2	

[a] Energies taken from Refs. 4 and 5.
[b] Weighted average of 6.75-, 6.55-, and 6.41-MeV γ rays.
[c] Weighted average of 7.26-, 7.15-, and 7.05-MeV γ rays.

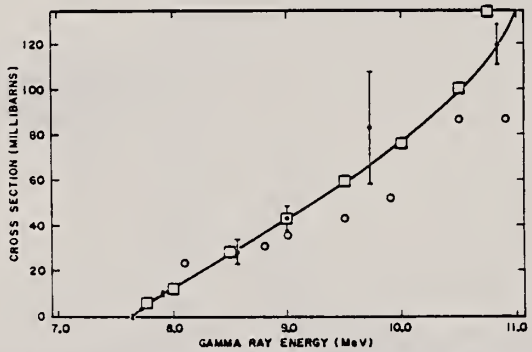

FIG. 2. Energy versus cross section, $Ta^{181}(\gamma,n)$. Boxes are data of Fuller and Weiss (Ref. 8), circles are data of Bramblett *et al.* (Ref. 1). The solid line is a smooth curve through the present cross-section measurements.

REF. M. Langevin, J. M. Loiseaux et J. M. Maison
Nucl. Phys. 54, 114-124 (1964)

ELEM. SYM.	A	Z
Ta	181	73

METHOD: Bremsstrahlung scattering [Page 1 of 2]

REF. NO.: 64 La 1 JOC

REACTION	RESULT	EXCITATION ENERGY	SOURCE		DETECTOR		ANGLE
			TYPE	RANGE	TYPE	RANGE	
G,G	ABX	10-25	C	32	NAI-D		DST

TABLEAU 1

Le paramètre $a(E)$ de la distribution angulaire

Noyau	11.5-14. MeV			14-17.5 MeV			17.5-20 MeV			20-30 MeV	
	Exp.	Ellipsoïdal	Triax.	Exp.	Ellips.	Triax.	Exp.	Ellips.	Triax.	Exp.	Ellips
							Contribution Quadrupolaire %				
Tb	$0.5^{+0.15}_{-0.1}$	0.41	0.39	$0.54^{+0.15}_{-0.1}$	0.70	0.50	25	0.97	0.85		1
Ho	$0.27^{+0.15}_{-0.1}$	0.44	0.407	$0.43^{+0.10}_{-0.05}$	0.71	0.53	25	0.95	0.9	0.4 ± 0.1	1
Er	$0.27^{+0.15}_{-0.1}$	0.44	0.407	$0.8^{+0.15}_{-0.1}$	0.71	0.53	25	0.95	0.9		1
Ta	$0.6^{+0.15}_{-0.1}$	0.58		$0.68^{+0.15}_{-0.1}$	0.81		20	0.96			
Au	a_{exp}(11-20 MeV) = 0.9									0.7 ± 0.1	1
	a_{th} (11-20 MeV) ≈ 1										

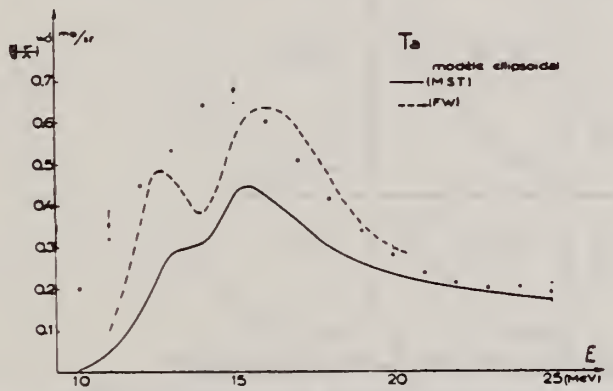

Fig. 4. Sections efficaces différentielles de diffusion obtenues pour le tantale. Les courbes tracées correspondent à l'application des relations de dispersion aux sections efficaces d'absorption obtenues par Fuller et Weiss [16]) (F.W.) et par Miller *et al.* [9]). (M.S.T.).

REF.

M. Langevin, J. M. Loiseaux et J. M. Maison
Nucl. Phys. 54, 114-124 (1964)

ELEM. SYM.	A	Z
Ta	181	73

METHOD

Bremsstrahlung scattering

REF. NO. 64 La 1 JOC

REACTION	RESULT	EXCITATION ENERGY	SOURCE		DETECTOR		ANGLE
			TYPE	RANGE	TYPE	RANGE	

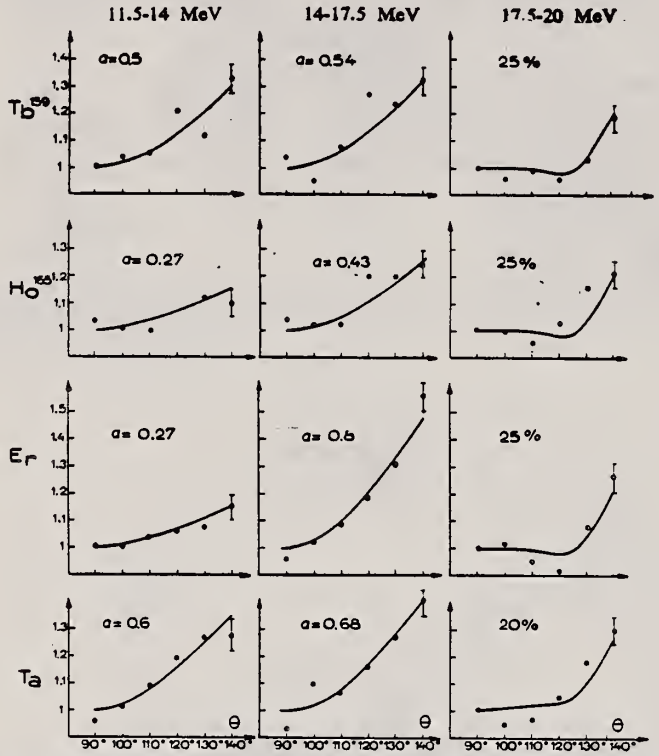

Fig. 8. Répartitions angulaires du rayonnement diffusé obtenues pour le terbium, l'holmium, l'erbium et le tantale dans les zones d'énergie 11.5-14 MeV, 14-17.5 MeV et 17.5-20 MeV.

REF. D. F. Herring, I. C. Nascimento, R. B. Walton, and R. E. Sund
Phys. Rev. 139, B562 (1965)

ELEM. SYM.	A	Z
Ta	181	73

METHOD

REF. NO. 65 He 1 EGF

REACTION	RESULT	EXCITATION ENERGY	SOURCE		DETECTOR		ANGLE
			TYPE	RANGE	TYPE	RANGE	
E,N	RLY	THR-32	D	14-32	ACT-I		4PI
E+,N	RLY	THR-32	D	14-32	ACT-I		4PI

Ratio of positron to electron induced activity determined.

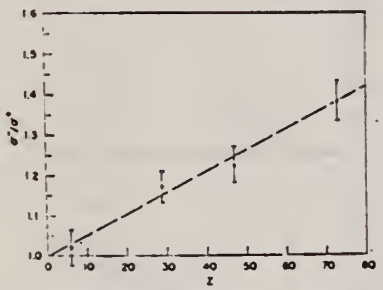

FIG. 4. The ratio σ^-/σ^+ as a function of atomic number at 27-MeV (total) bombarding energy. The straight line is for comparison purposes.

REF.

F. W. K. Firk
Proc. Gatlinburg Conference 352 (1966)

ELEM. SYM.	A	Z
Ta	181	73

METHOD

REF. NO. 66 Fi 2 hmg

REACTION	RESULT	EXCITATION ENERGY	SOURCE		DETECTOR		ANGLE
			TYPE	RANGE	TYPE	RANGE	
G,XN	SPC	THR-60	C	60	TOF-D	5-40	90

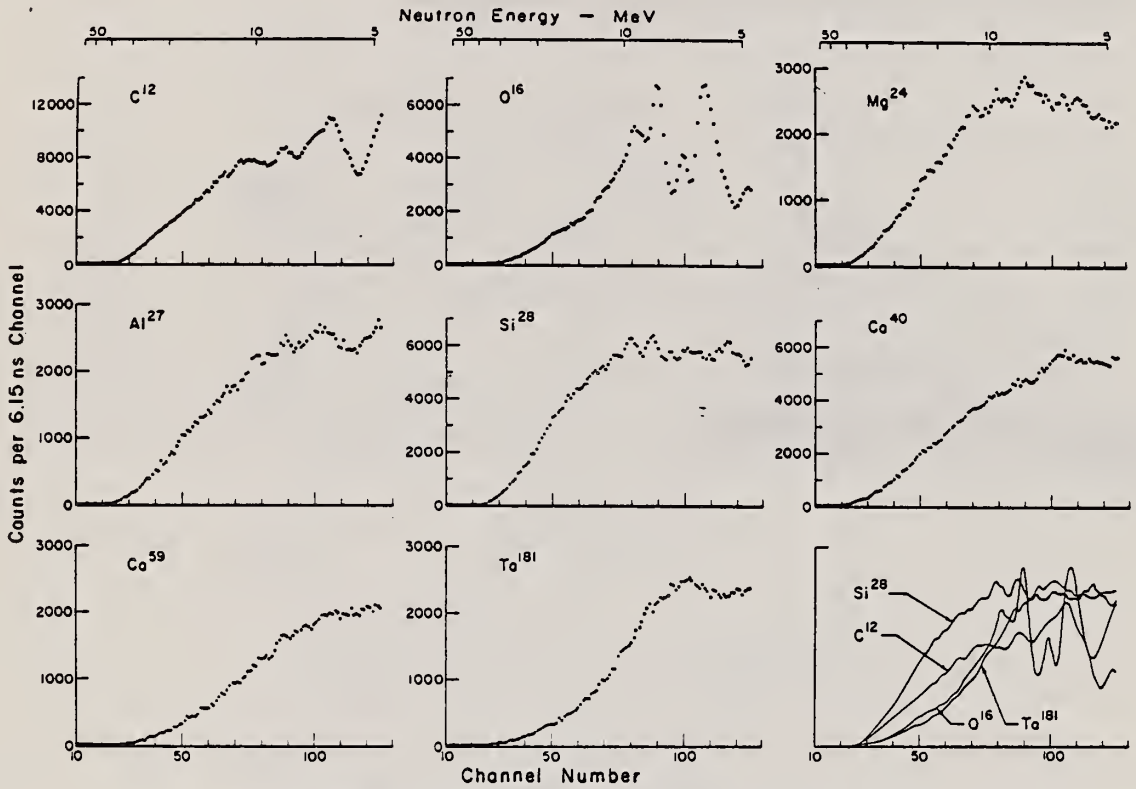

Fig. 1. Observed photoneutron time-of-flight spectra of C, O, Mg, Si, Ca, Co, V, and Ta.

REF.

G. P. Antropov, I. E. Mitrofanov, V. S. Russkikh
Izv. Akad. Nauk SSR Fiz. 31, 336 (1967)
Bull. Acad. Sci. USSR 31, 320 (1967)

ELEM. SYM.	A	Z
Ta	181	73

METHOD

REF. NO. 67 An 2 egf

REACTION	RESULT	EXCITATION ENERGY	SOURCE		DETECTOR		ANGLE
			TYPE	RANGE	TYPE	RANGE	
G,XN	ABX	THR-20	C	8-20	BF3-I		4PI

553

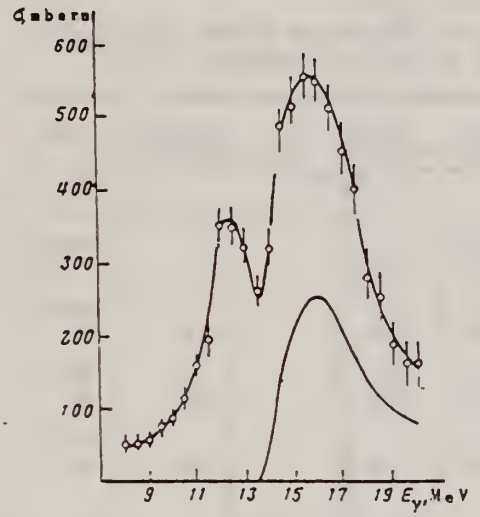

Fig.5

Fig.5. Experimentally determined cross section $\sigma_{(\gamma n)} + 2\sigma_{(\gamma, 2n)}$ for ^{181}Ta. The lower curve was calculated for $\sigma_{(\gamma, 2n)}$ with a = 18.1.

REF. H. M. Gerstenberg and E. G. Fuller
NBS Tech. Note 416, June 1967

ELEM. SYM.	A	Z
Ta	181	73

METHOD

REF. NO. 67 Ge 2 HMG

REACTION	RESULT	EXCITATION ENERGY	SOURCE		DETECTOR		ANGLE
			TYPE	RANGE	TYPE	RANGE	
G,N	ABY	THR-27	C	22,27	BF3-I		4PI

Table 7. Comparison of neutron yields. Yields are given in units of (neutron cm^2/MeV nucleus)$\times 10^{-28}$. The estimated uncertainties in Y and Y_c are of the order of 6% and 10%, respectively.

Element	E_o	$Y(E_o)$	Y_c UCRL	Y_c Saclay	Y_c Va.	Y_c NBS(Old)	Y_c/Y UCRL Exp	Y_c/Y Saclay Exp	Y_c/Y Va. Exp	Y_c/Y NBS(Old) Exp	Ref.
Pb	27	103	86				0.83				26,30
	22	111	92	116			0.83	1.05			
Au	27	89	97				1.09				24,30,
	22	92	98	88		115	1.07	0.96		1.25	38
Ta	27	81	82	77			1.01	0.95			27,30,
	22	85	79	80		113	0.93	0.94		1.33	38
Ho	27	67	75				1.12				27,31,
	22	69	77	82		103	1.12	1.19		1.49	39
Ag	27	36									
	22	34.8									
Cu	27	14.4	13.2				0.92				28,30
	22	12.6	11.5	12.4			0.91	0.98			
Co	27	12.7	12.1				0.95				29,34
	22	10.6	9.9		13.5		0.94		1.27		
Ca	27	1.69		1.13	1.01			0.67	0.60		32,35
P	27	2.35			1.76				0.75		36
Al	27	1.92	1.62		1.38		0.84		0.72		25,37
O^{16}	27	0.54	0.42	0.48	0.42		0.78	0.89			16,32, 37
C	27	0.50	0.35	0.33	0.46		0.70	0.66			25,32, 33

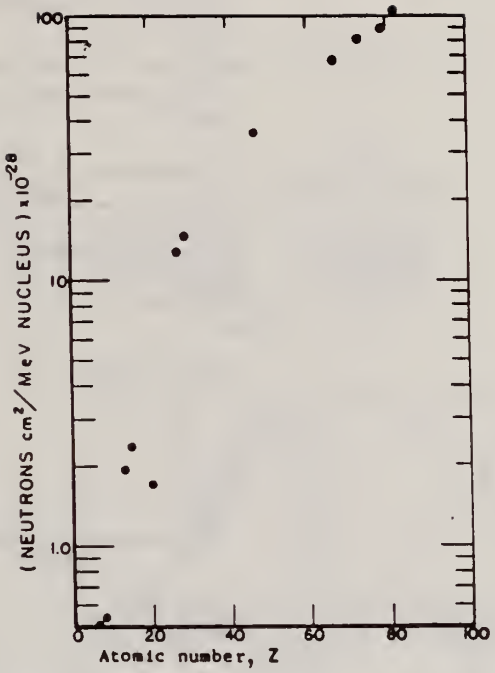

Fig. 31. Absolute neutron yield as a function of atomic number. The neutron yield from calcium (Z = 20) is particularly low in comparison with the other elements because its (γ,n) threshold is high compared to the mean energy of the giant resonance.

REF.

R. R. Hurst and D. J. Donahue
Nucl. Phys. A91, 365 (1967)

EL EM. SYM.	A	Z
Ta	181	73

METHOD

Neutron capture gamma rays

REF. NO.	
67 Hu 1	EGF

REACTION	RESULT	EXCITATION ENERGY	SOURCE		DETECTOR		ANGLE
			TYPE	RANGE	TYPE	RANGE	
G,N	ABX	8-11	D	8-11	BF3-I		4PI

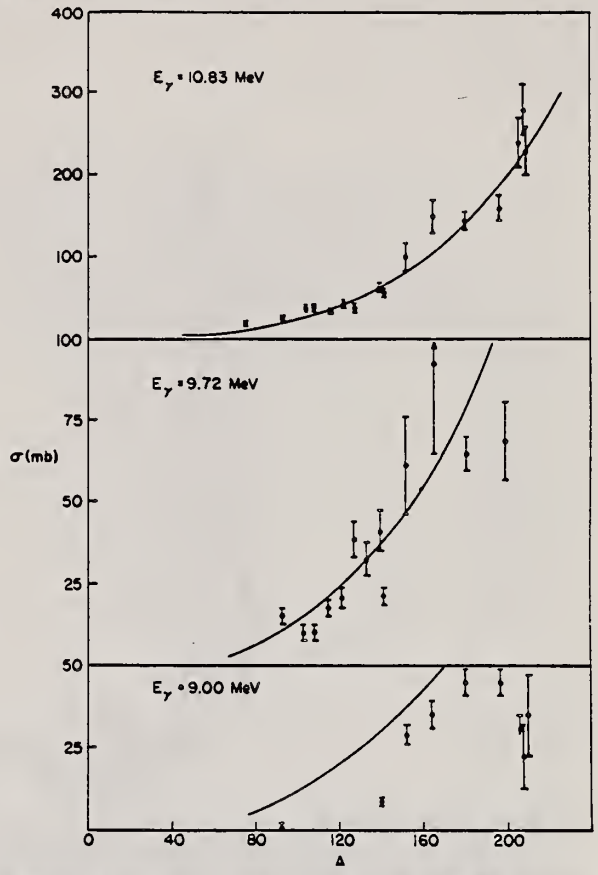

Fig. 1. Cross section (in mb) versus mass number of the target for gamma-ray energies of 9.00, 9.72 and 10.83 MeV. The solid lines are plots of eq. (1) in the text.

TABLE 1
Photoneutron cross sections (mb)

Target	7.72 MeV	9.00 MeV	9.72 MeV	10.83 MeV
^{59}Co				9.0± 0.8
^{75}As				20.4± 1.7
^{93}Nb		0.53± 0.10	14.6± 2.2	25.8± 2.1
^{103}Rh			10.6± 1.7	38.8± 3.1
^{107}Ag, ^{109}Ag			10.0± 1.5	37.6± 2.9
^{115}In			17.1± 2.6	33.3± 2.7
^{121}Sb, ^{123}Sb			20.7± 3.1	42.5± 3.6
^{127}I			38.7± 5.8	38.8± 3.1
^{133}Cs			31.7± 4.8	52.5± 3.8
^{139}La		8.61± 0.86	40.8± 6.5	63.0± 5.0
^{141}Pr			21.5± 3.2	58.3± 4.1
^{151}Eu, ^{153}Eu		28.9 ± 3.2	61.3±14.7	102 ±18
^{165}Ho		35.6 ± 4.3	92.2±27.6	150 ±20
^{181}Ta	4.14±0.36	45.4 ± 3.7	65.0± 5.5	146 ±12
^{197}Au		44.5 ± 3.6	68.4±13.5	160 ±15
^{206}Pb		<34.3		238 ±29
^{208}Pb		22.6 ±11.3		280 ±31
^{209}Bi		36.1 ±12.0		226 ±27

REF. A. V. Mitrofanova, Yu. N. Ranyuk, and P. V. Sorokin
J. Nucl. Phys. (USSR) 6, 703 (1967)
Sov. J. Nucl. Phys. 6, 512 (1968)

ELEM. SYM.	A	Z
Ta	181	73

METHOD

REF. NO.	
67 Mi 1	HMG

REACTION	RESULT	EXCITATION ENERGY	SOURCE		DETECTOR		ANGLE
			TYPE	RANGE	TYPE	RANGE	
G,F	ABX	300-999		300-999	TRK-I		

999 = 1600 MEV

Detector: Fission fragment tracks in glass.

Angular distribution measured for Pb was found isotropic; for other elements it was assumed isotropic.

Nucleus	Fissionability D	Cross section σ_A, $\mu\beta$	Nucleus	Fissionability D	Cross section σ_A, $\mu\beta$
Bi	0.11±0.01	7.8±0.6	Os	0.0058±0.0005	0,37±0.04
Pb	0.050±0.004	3.4±0.3	Re	0.0056±0.0006	0.35±0.04
Tl	0.031±0.003	2.1±0.2	Ta	0.0043±0.0005	0.27±0.03
Au	0.019±0.002	1.25±0.10	Hf	0.0042±0.0004	0.25±0.03
Pt	0.012±0.002	0.80±0.08			

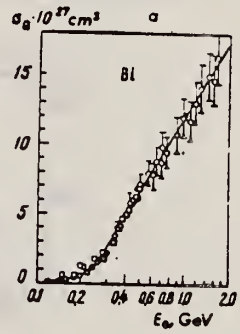

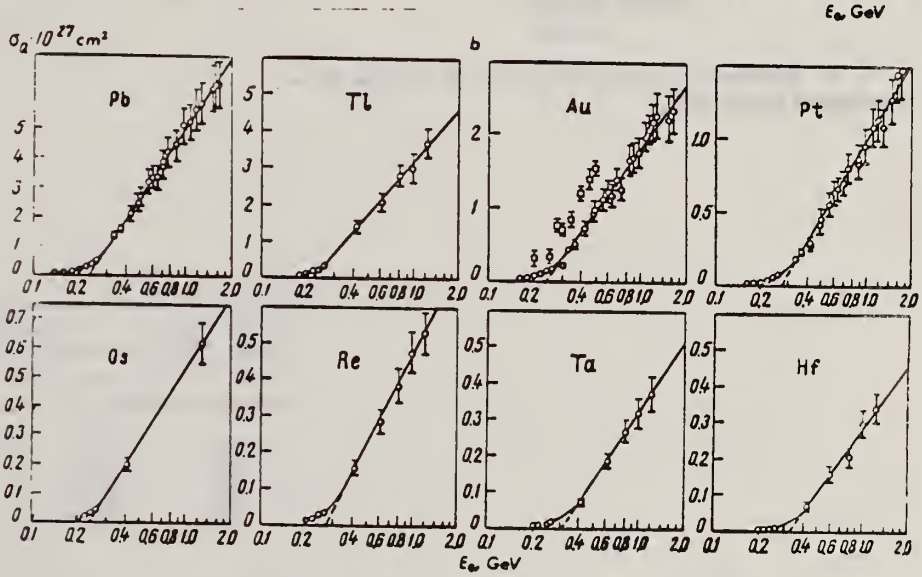

Fig. 1. Photofission fragment yields. ○-present work; □-Jungerman and Steiner.[1] The curves were plotted through the experimental points.

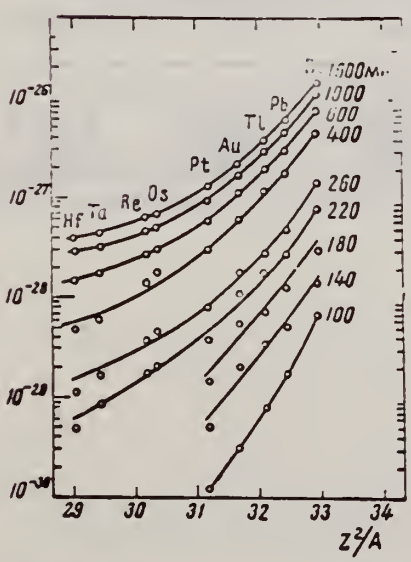

Fig. 2. Photofission fragment yields as a function of Z^2/A. The ordinates are values of σ_a in units of cm².

REF. Yu. N. Ranyuk and P. V. Sorokin
J. Nucl. Phys. (USSR) 5, 37 (1967)
Sov. J. Nucl. Phys. 5, 26 (1967)

ELEM. SYM.	A	Z
Ta	181	73

METHOD

REF. NO.	
67 Ra 2	HMG

REACTION	RESULT	EXCITATION ENERGY	SOURCE		DETECTOR		ANGLE
			TYPE	RANGE	TYPE	RANGE	
G,F	ABX	THR-260	C	200-260	EMU-I		4PI

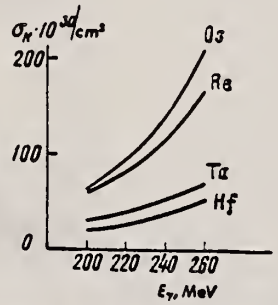

Fig. 4. Photofission cross sections of Os, Re, Ta, and Hf as functions of photon energy.

TABLE III

$E_{\gamma\ max}$, MeV	Cross section per equivalent γ quantum, 10^{-30} cm²			
	Os	Re	Ta	Hf
200	17±2	11.8±0.8	5.2±0.3	3.2±0.7
220	22±2	17±1	8.6±0.5	4.8±0.3
240	33±3	29±1	13.0±0.6	8.2±0.4
260	45±4	36±2	17.2±0.7	11.2±0.5

REF. S. Shimizu, Y. Isozumi and Y. Nakayama
Phys. Letters 25B, 124 (1967)

ELEM. SYM.	A	Z
Ta	181	73

METHOD

REF. NO. 67 Sh 3 EGF

REACTION	RESULT	EXCITATION ENERGY	SOURCE		DETECTOR		ANGLE
			TYPE	RANGE	TYPE	RANGE	
G,G/	ABX	18	D	18	NAI-D	0-18	90
		(17.6)		(17.6)			

Photon source: 1 MeV proton on Li metal

RAMAN SCATTERING

$\hat{\sigma}_{exp} = (9.6 \pm 3.9) \times 10^{-28} cm^2$

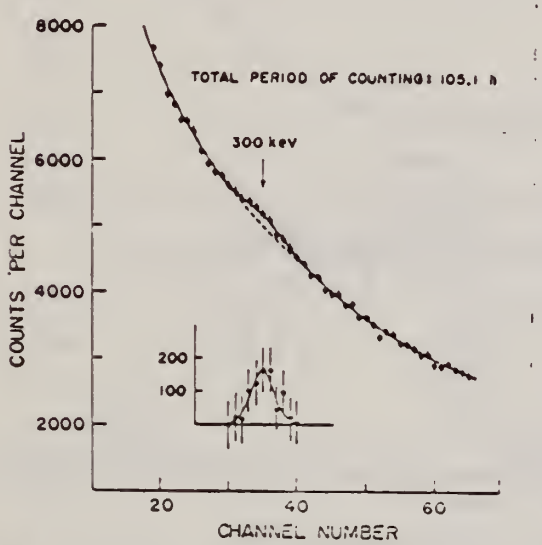

Fig. 1. The observed spectrum of photons from a transition of $\frac{11}{2}^+$ (303 keV) $\rightarrow$ $\frac{7}{2}^+$ (ground state) in coincidence with the nuclear Raman scattering of Li(p,γ) γ rays

REF. R. Bergère, H. Beil and A. Veyssière
Nucl. Phys. A121, 463 (1968)

ELEM. SYM.	A	Z
Ta	181	73

METHOD

REF. NO. 68 Be 5

egf

REACTION	RESULT	EXCITATION ENERGY	SOURCE		DETECTOR		ANGLE
			TYPE	RANGE	TYPE	RANGE	
G,N 85+	ABX	THR-30	D	7-30	MOD-I		4PI
G,2N 86	ABX	THR-30	D	7-30	MOD-I		4PI
G,3N 87	ABX	THR-30	D	7-30	MOD-I		4PI
G,4N 88	ABX	THR-36	D	7-36	MOD-I		4PI

85+

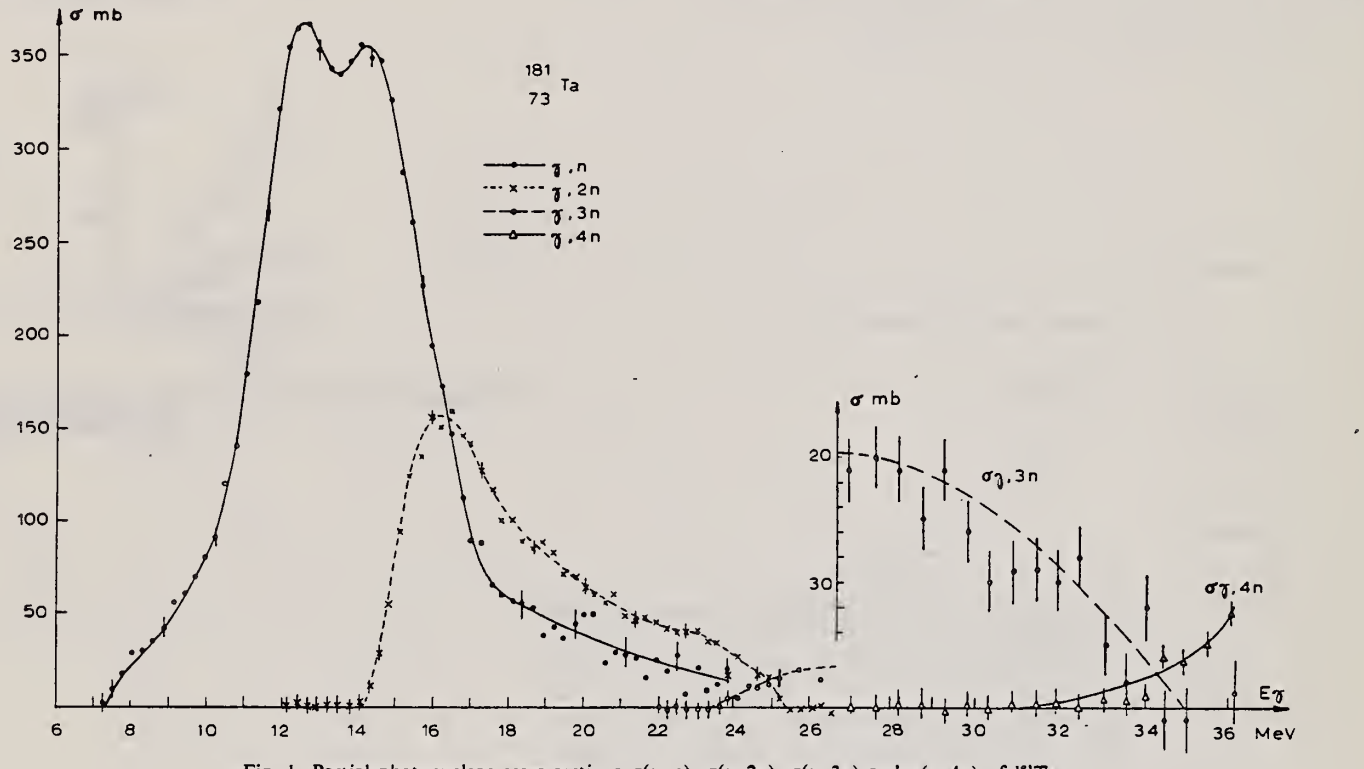

Fig. 1. Partial photonuclear cross sections $\sigma(\gamma, n)$, $\sigma(\gamma, 2n)$, $\sigma(\gamma, 3n)$ and $\sigma(\gamma, 4n)$ of $^{181}_{73}$Ta.

TABLE 2

Lorentz line paramcters for a two or three lines fit to the total cross section data of $^{181}_{73}$Ta

	E_1 (MeV)	σ_1 (mb)	Γ_1 (MeV)	$\sigma_1\Gamma_1$ (MeV·b)	E_2	σ_2	Γ_2	$\sigma_2\Gamma_2$	E_3	σ_3	Γ_3	$\sigma_3\Gamma_3$
2 Lorentz lines	12.35	270	2.57	0.693	15.30	330	4.47	1.47				
3 Lorentz lines	12.30	280	2.45	0.686	14.85	210	3.32	0.698	16.10	155	4.975	0.771

REF. R. Bergère, H. Beil and A. Veyssière
Nucl. Phys. A121, 463 (1968)

ELEM. SYM.	A	Z
Ta	181	73

METHOD

REF. NO. 68 Be 5

egf

REACTION	RESULT	EXCITATION ENERGY	SOURCE		DETECTOR		ANGLE
			TYPE	RANGE	TYPE	RANGE	

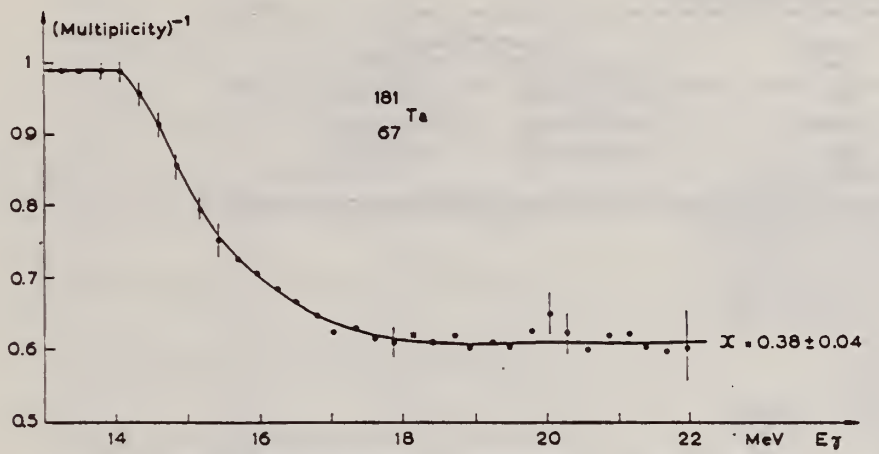

Fig. 2. Reciprocal neutron multiplicity as a function of γ energy for $^{181}_{73}$Ta.

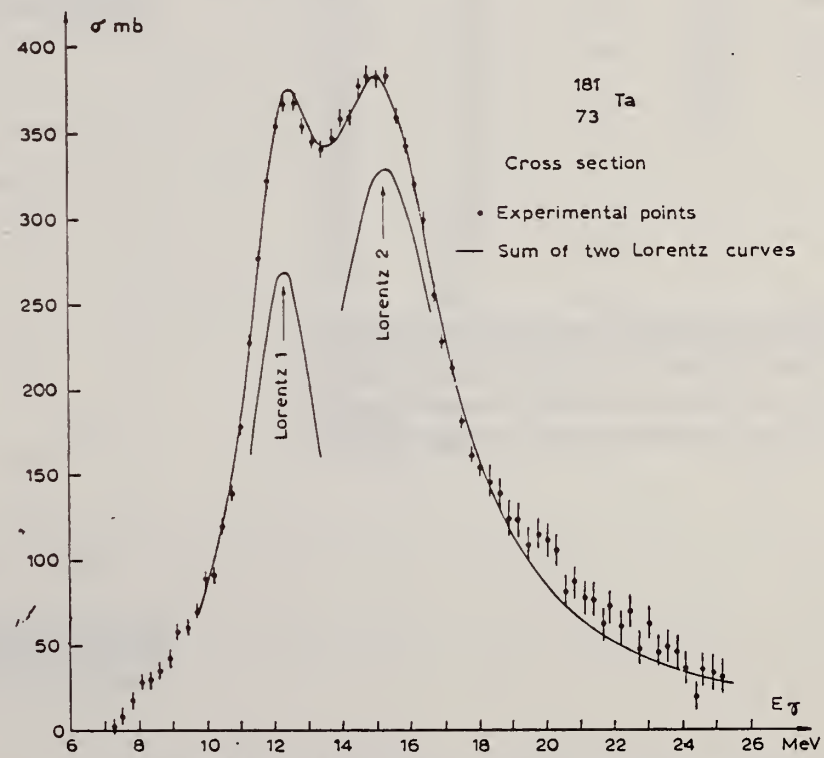

Fig. 3. Total cross section data showing a two Lorentz line fit for a $^{181}_{73}$Ta target.

REF. H. R. Bowman, R. C. Gatti, R. C. Jared, G. Kilian, L. G. Moretto, S. G. Thompson, M. R. Croissiaux, J. H. Heisenberg, R. Hofstadter, L. M. Middleman, and M. R. Yearian
Phys. Rev. 168, 1396 (1968)

ELEM. SYM.	A	Z
Ta	181	73

METHOD

REF. NO. 68 Bo 1 HMG

REACTION	RESULT	EXCITATION ENERGY	SOURCE		DETECTOR		ANGLE
			TYPE	RANGE	TYPE	RANGE	
E,F	ABI		D	250, 500	EMU-I		4PI
					(MICA)		

TABLE I. Experimental results.

Target	Thickness	Method used	Fission cross section 250 MeV e^- (cm²)	500 MeV e^- (cm²)
$_{92}U^{238}$ [a]	85 μg/cm²	Mica	$(6.0\pm1.2)\times10^{-27}$	$(9.4\pm1.9)\times10^{-27}$
$_{92}U^{238}$	162 μg/cm²	Counter	$(5.0\pm1.0)\times10^{-27}$	$(7.0\pm1.4)\times10^{-27}$
$_{83}Bi^{209}$	1 mg/cm²	Mica	$(2.3\pm0.5)\times10^{-30}$	$(1.4\pm0.3)\times10^{-29}$
$_{73}Ta^{181}$	4 mg/cm²	Mica		3.9×10^{-31} [b]

[a] U^{235}/U^{238} was 1.12×10^{-4} in target sample.
[b] Not corrected for photofission contribution [see (4) in text].

REF. N. N. Kaushal, E. J. Winhold, P. F. Yergin, H. A. Medicus and R. H. Augustson
Phys. Rev. 175, 1330 (1968)

ELEM. SYM.	A	Z
Ta	181	73

METHOD

REF. NO. 68 Ka 1 HMG

REACTION	RESULT	EXCITATION ENERGY	SOURCE		DETECTOR		ANGLE
			TYPE	RANGE	TYPE	RANGE	
G,N	ABX	50-85	C	55,85	TOF-D	10-35	90
							(67.5)

NEUT ENGY SPEC

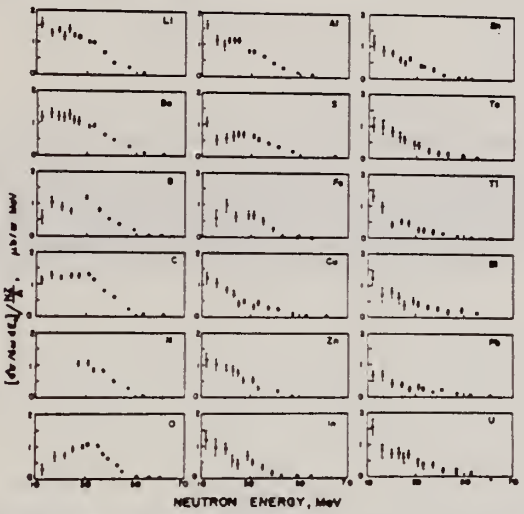

FIG. 6. Observed neutron spectra due to 55–85-MeV difference photon spectra. The effective cross sections have been divided by NZ/A.

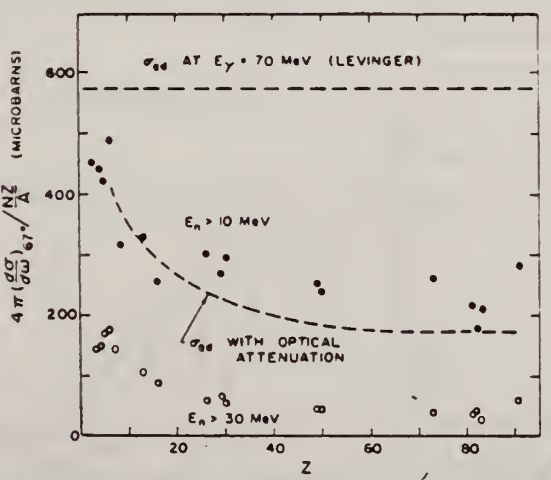

FIG. 7. Effective cross sections for production of fast neutrons with energies greater than 10 MeV (solid circles) and 30 MeV (open circles) by the 55–85-MeV photon difference spectrum. The dashed curves are modified quasideuteron model predictions as discussed in the text.

TABLE I. Comparison of present cross-section values in mb for production of high-energy photoneutrons by 55–85-MeV photons with measured cross sections $\sigma(\gamma,Tn)$, also in mb, for total photoneutron production. The present cross-section values are uncertain by 8 to 10% because of counting statistics and normalization errors; in addition all values depend on an absolute normalization in terms of the deuteron photodisintegration cross section, which is known to about 10% at these energies.

Target	$4\pi(d\sigma/d\omega)_{\sigma^0}$ ($E_n>10$ MeV) [Present experiment]	$\sigma(\gamma,Tn)$ Jones and Terwilliger[a]	$\sigma(\gamma,Tn)$ Costa *et al.*[b]	Other results
Li	0.75		1.0	
Be	1.0	2.7	2.3	2.3[c]
B	1.0		1.4	
C	1.5	1.3	1.4	2.4[d]
O	1.3		1.6	
Al	2.8	5.5	4.6	8[d]
S	2.1		4.4	6.5[d]
Fe	4.2	16	12	
Cu	4.3	20	19	
Zn	4.4		15	
In	7.4			
Sn	7.0			
Ta	10.7	95		
Tl	10.7			
Pb	8.3	100		
Bi	13			
U	16	65		

[a] Average cross sections between 55 and 85 MeV, as read from Figs. 4 and 5 of Ref. 4.
[b] $\int_0^{30}\sigma dE - \int_0^{30}\sigma dE/50$, as taken from Fig. 4 of Ref. 5 and Table I of Ref. 6.
[c] S. Costa, L. Pasqualini, G. Piragino, and L. Roasio, Nuovo Cimento 42, 306 (1966).
[d] G. Bishop, S. Costa, S. Ferroni, R. Malvano, and G. Ricco, Nuovo Cimento 42, 148 (1966).

REF. A. Veyssière, H. Beil and R. Bergère
C.R. Acad. Sc. Paris 267, 234(1968)

ELEM. SYM.	A	Z
Ta	181	73

METHOD

REF. NO.	
68 Ve 1	egf

REACTION	RESULT	EXCITATION ENERGY	SOURCE		DETECTOR		ANGLE
			TYPE	RANGE	TYPE	RANGE	
G,N	ABX	THR-36	D	7-36	MOD-I		4PI
G,2N	ABX	THR-36	D	7-36	MOD-I		4PI
G,3N	ABX	THR-36	D	7-36	MOD-I		4PI
G,4N	ABX	THR-36	D	7-36	MOD-I		4PI

$$\int_{\gamma}^{25} \frac{\sigma(\gamma,n)}{\sigma_T} dE = 72.5 \pm 3\% ,$$

$$\int_{\gamma}^{25} \frac{\sigma(\gamma,2n)}{\sigma_T} dE = 27 \pm 2\%.$$

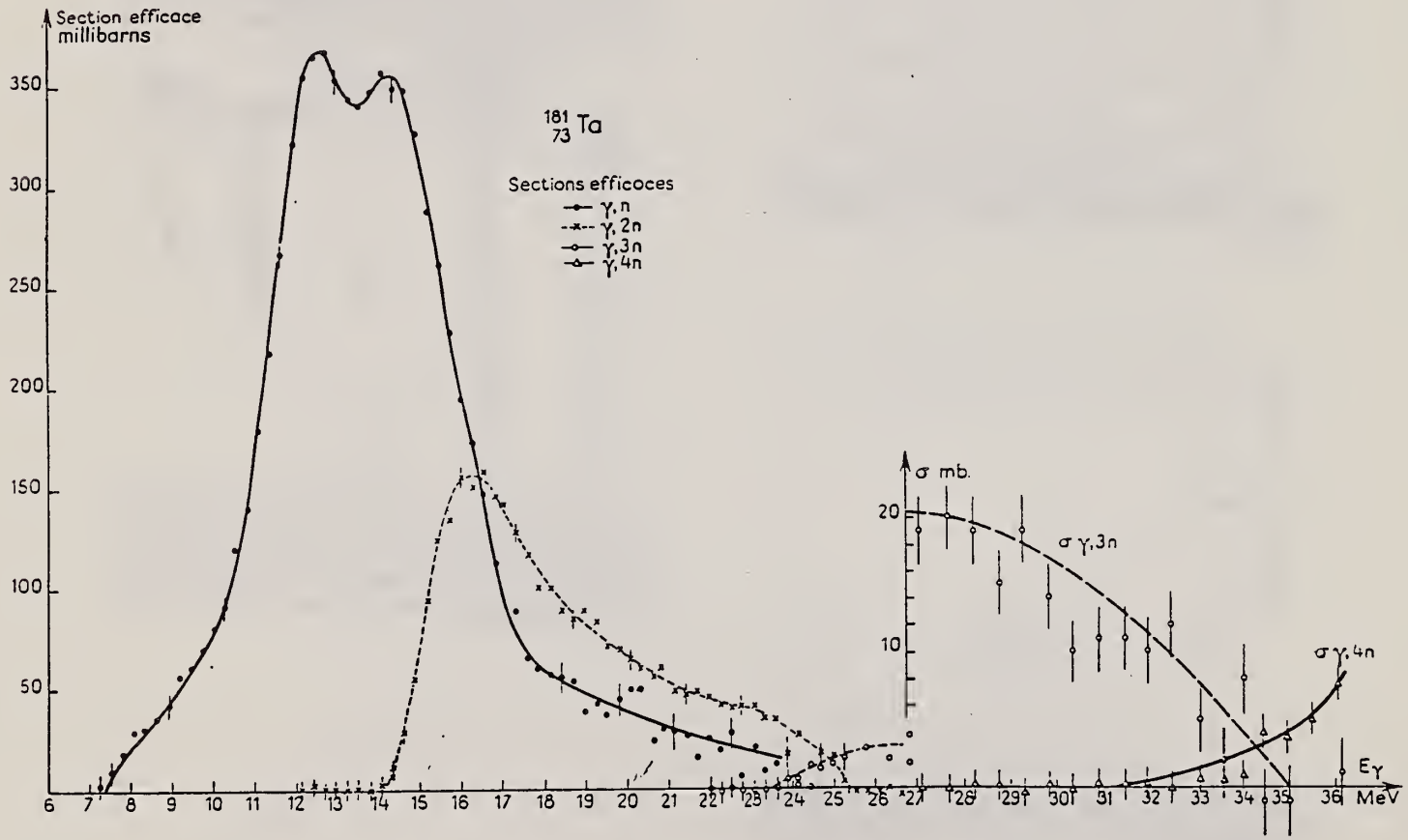

REF. Yu. P. Antuf'ev, V. L. Agranovich, V. B. Ganenko, V. S. Kuzmenko, I. I. Miroshnichenko, and P. V. Sorokin
Ukr. Fiz. Zh. 14, 248 (1969)

ELEM. SYM.	A	Z
Ta	181	73

METHOD

REF. NO. 69 An 6 egf

REACTION	RESULT	EXCITATION ENERGY	SOURCE		DETECTOR		ANGLE
			TYPE	RANGE	TYPE	RANGE	
G,P	ABY	103-999	C	700,999	TEL-D	97-230	DST
G,D	ABY	109-999	C	700,999	TEL-D	97-205	DST

999 = 1.2 GEV

Summary

The cross-sections of the (γ, p) (γ, d) reactions were investigated. Li^7, Be^9, C^{12}, Si^{28}, Cu^{63}, Mo^{96} and Ta^{181} targets were irradiated with the bremsstrahlung of 700 and 1200 MeV maximum energy from the Kharkov PhTI Ac. Sci. UkrSSR linear accelerator. The photoprotons and deuterons were detected by the scintillation telescope at 30°, 60°, and 120° with the beam. Possible mechanisms of the proton and deuteron photoproduction are discussed. The qualitative agreement of A dependence of the cross-sections is observed with a suggestion on the meson mechanism for these reactions.

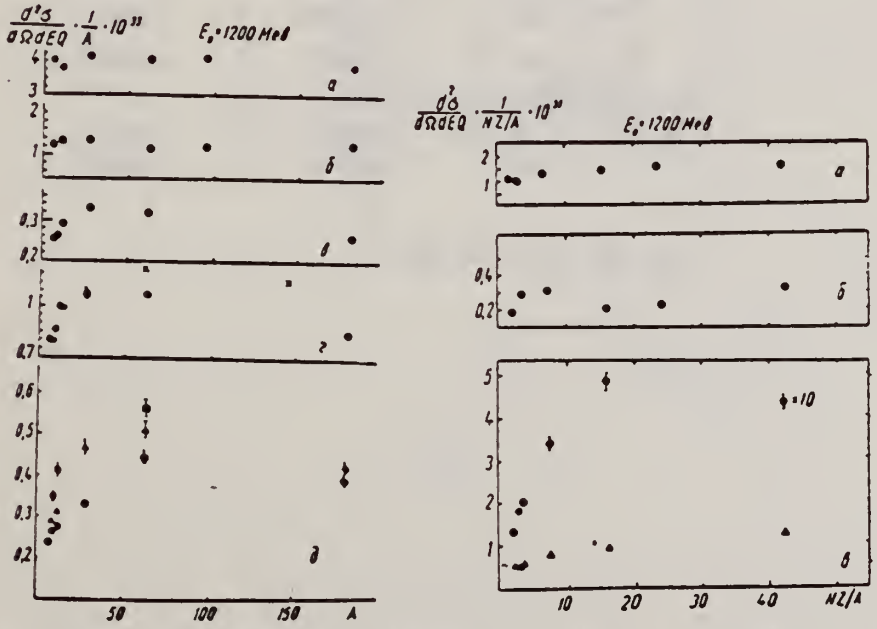

Рис. 1. Залежність перерізу (γ, p)-реакції від A: $а$ — ϑ=30°, E_p=97 *Мев*; $б$ — E_p=205 *Мев*; $в$ — ϑ=60°, E_p=230 *Мев*; $г$ — E_p=157 *Мев* (× — дані [3]); $д$ — ϑ=120°, ○ — E_p=120 *Мев*, △ — E_p=157 *Мев*, □ — E_p=230 *Мев*. Абсолютне значення перерізу наведено при енергії протонів E_p=120 *Мев*. Інші дані нормовані до перерізу для Li^7 при E_p=120 *Мев*.

Рис. 2. Залежність перерізу (γ, d)-реакції від NZ/A: $а$ — ϑ=30°, E_d=97 *Мев*; $б$ — ϑ=30°, E_d=205 *Мев*; $в$: △ — ϑ=60°, E_d=97 *Мев*, ○ — ϑ=120°, E_d=97 *Мев* (перерізи наведені в одиницях 10^{-32} *см²/стер · Мев · Q*).

REF. Yu. P. Antufyev, V. L. Agranovich, V. B. Ganenko, V. S. Kuzmenko, I.I. Miroshnichenko, P.V. Sorokin
Ukr. Fiz. 14, 496 (1969)

ELEM. SYM.	A	Z
Ta	181	73

METHOD

REF. NO. 69 An 8 hmg

	REACTION	RESULT	EXCITATION ENERGY	SOURCE		DETECTOR		ANGLE
				TYPE	RANGE	TYPE	RANGE	
1)	E,P	RLY	THR-999	C	999	MAG-D		DST
2)	E,D	RLY	THR-999	C	999	MAG-D		DST
3)	E,T	RLY	THR-999	C	999	MAG-D		DST

The differential cross-sections of (γ, p), (γ, d) and (γ, t) reactions on carbon for 700 and 1200 MeV maximum energies of photons and energy distributions of the secondary particles were measured at 30, 60 and 120° of particle emission angles. Excitation function for protons with the energy of 97 MeV is given for the maximum incident photon energy from 400 to 1300 MeV. Deuteron to proton and triton to deuteron yield ratios for various nuclei are also shown.

Experiment was carried out at the Kharkov linear accelerator. The particles were detected by scintillation counters after a magnetic spectrometer.

Possible mechanisms of the high energy photon-nuclei interactions are discussed. (6 Figs).

1) 999 = 1 GEV, REL P/D
2) 1.3 GEV, REL P/D, D/T
3) 999 = 1 GEV, REL D/T

Таблица 2

	θ°	$\left[\frac{d^2\sigma_d(2p)}{d\Omega dp}\Big/\frac{d^2\sigma_p(p)}{d\Omega dp}\right]\cdot 10^3$	$\left[\frac{d^2\sigma_t(3p)}{d\Omega dp}\Big/\frac{d^2\sigma_d(2p)}{d\Omega dp}\right]\cdot 10^3$
Li^7	60	1,94±0,19	2,1±0,3
	120	0,8±0,08	0,9±0,13
C^{12}	60	2,2±0,2	1,8±0,3
	120	—	—
Ta^{181}	60	3,1±0,3	2,8±0,4
	120	1,89±0,2	1,85±0,28

REF.

I.A. Grishaev, V.P. Efimov, V.I. Kasilov, V.I. Noga,
Yu.N. Ranyuk, P.V. Sorokin, A.N. Fisun
Ukr. Fiz. Zhur. 14, 1818 (1969)

ELEM. SYM.		
Ta	181	73

METHOD

REF. NO.	
69 Gr 2	egf

REACTION	RESULT	EXCITATION ENERGY	SOURCE		DETECTOR		ANGLE
			TYPE	RANGE	TYPE	RANGE	
E,N	RLY	THR-999	C	70-999	ACT-I		4PI

999= 1 GEV,RLY E-/E+

DISINTEGRATION OF HEAVY NUCLEI BY ELECTRONS AND POSITRONS

I. A. Grishaev, V. P. Efimov, V. I. Kasilov, V. I. Noga, Yu. N. Ranyuk, P. V. Sorokin, A. N. Fisun

Summary

Gross-section ratio for the uranium and tantalum disintegration by electrons and positrons is equal to unity within the experimental errors over the investigated energy range from 70 to 1000 MeV and is in agreement with Barber's measurements and Rodenberg's calculations.

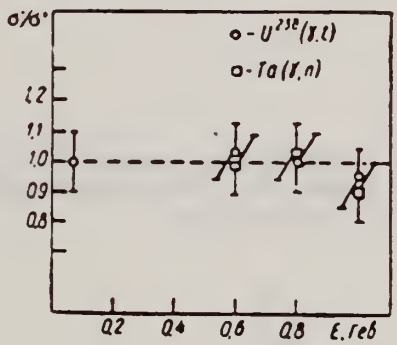

B. S. Ishkhanov, I. M. Kapitonov, E. V. Lazutin, I. M. Piskarev, and O. P. Shevchenko
ZhETP Pis. Red. 10, 80 (1969)
JETP Letters 10, 51 (1969)

ELEM. SYM.	MASS	Z
Ta	181	73

METHOD

REF. NO. 69 Is 1 hmg

REACTION	RESULT	EXCITATION ENERGY	SOURCE		DETECTOR		ANGLE
			TYPE	RANGE	TYPE	RANGE	
G,XN	ABX	7-30	C	7-30	MOD-I		4PI

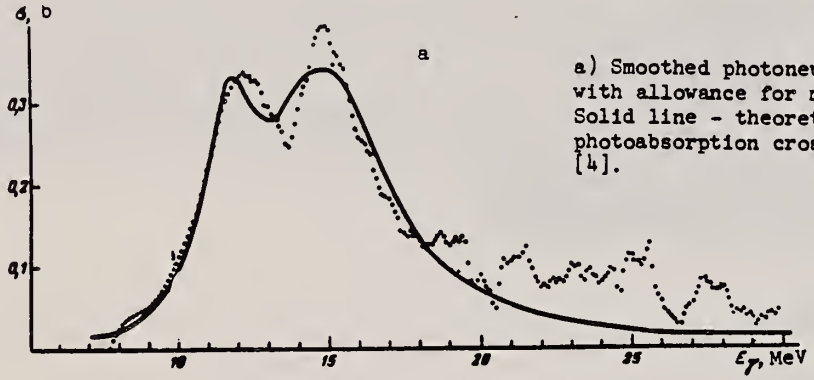

a) Smoothed photoneutron cross section w with allowance for multiplicity (points). Solid line - theoretically calculated photoabsorption cross section for ^{181}Ta [4].

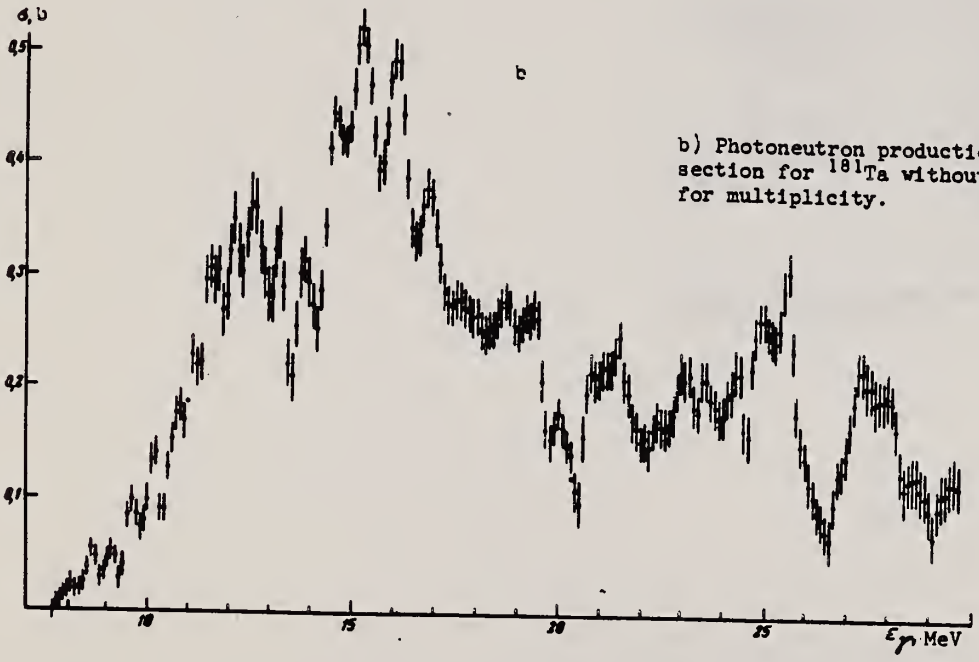

b) Photoneutron production cross section for ^{181}Ta without allowance for multiplicity.

REF. H. Tsubota, N. Fujiwara, H. Ishimaru, E. Tanaka, T. Aizawa, M. Kanazawa and N. Mutsuro
J. Phys. Soc. Japan 26, 1 (1969)

ELEM. SYM.	A	Z
Ta	181	73

METHOD

REF. NO.	
69 Ts 1	egf

REACTION	RESULT	EXCITATION ENERGY	SOURCE		DETECTOR		ANGLE
			TYPE	RANGE	TYPE	RANGE	
G,N	NOX	15-26	C	26	SCI-D	7-	DST
				(25.5)			

Paper gives summary of angular distribution measurements.

Table I. A summary of the results.
$W(\theta)=A+B\sin^2\theta+C\cos\theta$

Target	E_{max}(MeV)	A	B	C	B/A	C/A
Bi	7.4	0.65±0.02	0.35±0.11	0.16±0.05	0.55±0.20	0.24±0.10
	8.7	0.66±0.01	0.34±0.06	0.18±0.03	0.51±0.10	0.27±0.06
Pb	7.4	0.45±0.05	0.55±0.11	0.10±0.01	1.22±0.25	0.22±0.04
	8.7	0.75±0.03	0.26±0.03	0.17±0.03	0.22±0.03	0.22±0.03
Ta	7.4	0.69±0.02	0.32±0.03	0.03±0.01	0.46±0.05	0.05±0.02
	8.7	0.80±0.04	0.20±0.02	0.05±0.03	0.25±0.04	0.07±0.04

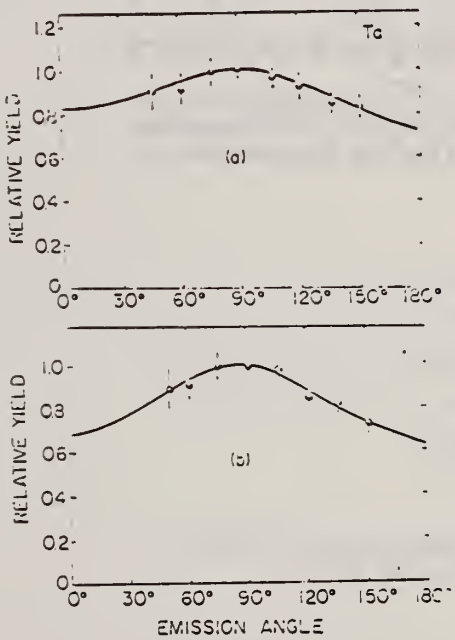

Fig. 7. The angular distributions of fast photoneutrons from Ta irradiated with 25.5 MeV bremsstrahlung.
(a) The neutron detecting bias energy is set at 8.7 MeV.
(b) The neutron detecting bias energy is set at 7.4 MeV.

REF.

Yu. P. Antuf'ev, V. L. Agranovich, V. G. Ganenko, V. S. Kuz'menko, I. I. Miroshnichenko, and P. V. Sorokin
Yad. Fiz. 12, 1143 (1970); Sov. J. Nucl. Phys. 12, 627 (1971)

ELEM. SYM.	A	Z
Ta	181	73

METHOD

REF. NO.	
70 An 5	hmg

REACTION	RESULT	EXCITATION ENERGY	SOURCE		DETECTOR		ANGLE
			TYPE	RANGE	TYPE	RANGE	
E,P	RLY	86-999	C	999	TEL-D	80-265	DST

999 = 1140 MEV

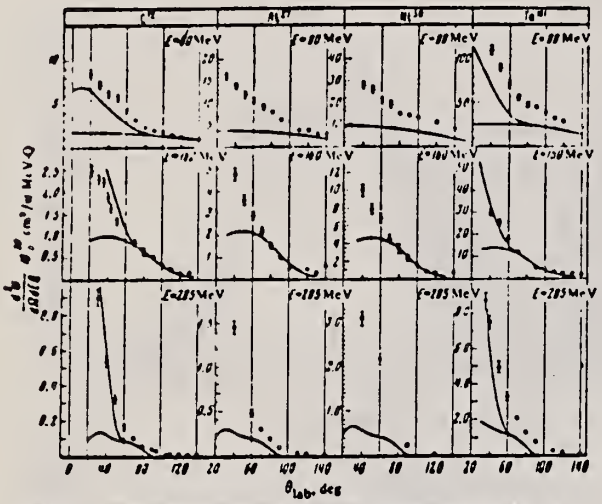

FIG. 1. Angular distributions of protons with energies of 80, 160, and 285 MeV produced from C^{12}, Al^{27}, Ni^{59}, and Ta^{181} nuclei by photons with maximum energy 1140 MeV. Only the statistical errors are shown.

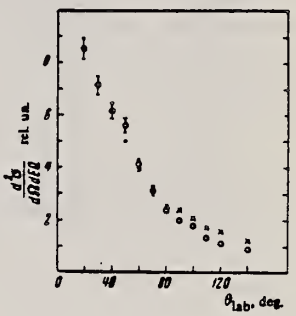

FIG. 2. Angular distributions of 80-MeV protons (normalized at θ = 40° (the solid circle) for C^{12} (O) and Ta^{181} (X), $E_{\gamma\,max}$ = 1140 MeV.

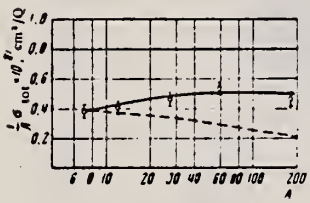

FIG. 3

FIG. 3. Total cross section for proton production per nucleon. $E_{\gamma\,max}$ = 1140 MeV. Dashed curve—theory from ref. 11.

11 K. S. Kölbig and B. Margolis, Nucl. Phys. B6, 85 (1968).

REF.

C. E. Burgart, E. A. Straker, T. A. Love, and R. M. Freestone, Jr.
Nucl. Sci. & Engr. 42, 421 (1970)

ELEM. SYM.	A	Z
Ta	181	73

METHOD

REF. NO.	
70 Bu 2	egf

REACTION	RESULT	EXCITATION ENERGY	SOURCE		DETECTOR		ANGLE
			TYPE	RANGE	TYPE	RANGE	
E,XN	SPC	7-140	C	140	TOF-D		165

THICK TARGET

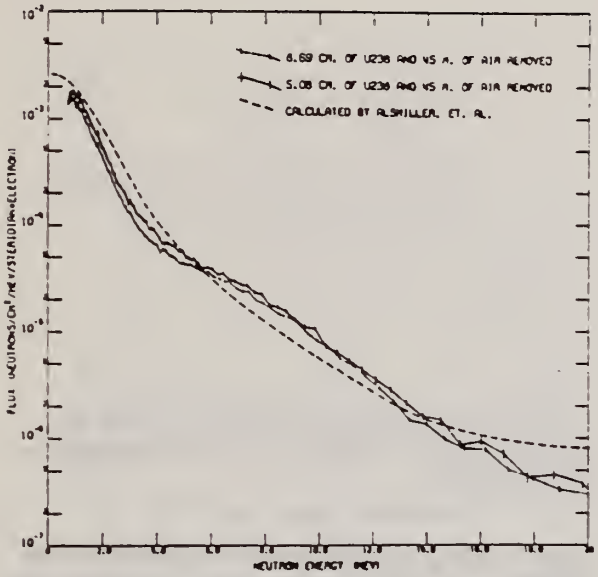

Fig. 2. Photoneutron energy spectrum produced by 140-MeV electrons incident on tantalum.

REF.

Yu. P. Antuf'ev, V. L. Agranovich, V. B. Ganenko, V. S. Kuz'menko
I. I. Miroshnichenko, and P. V. Sorokin
Yad. Fiz. 13, 473 (1971); Sov. J. Nucl. Phys. 13, 265 (1971)

ELEM. SYM.	A	Z
Ta	181	73

METHOD

REF. NO. 71 An 1 hmg

REACTION	RESULT	EXCITATION ENERGY	SOURCE		DETECTOR		ANGLE
			TYPE	RANGE	TYPE	RANGE	
G,P	SPC	36-999	C	700,999	TEL-D	25-400	DST
G,D	SPC	43-999	C	700,999	TEL-D	25-400	DST

Yield of protons 30-400 MeV, deuterons 30-200 MeV. 999=1.2 GEV,REL D/P

Table I. Values of the parameter τ, MeV

Target	E_0 = 700 MeV										E_0 = 1200 MeV					
	Protons					Deuterons					Protons			Deuterons		
	40°	60°	80°	100°	120°	40°	60°	80°	100°	120°	30°	60°	120°	30°	60°	120°
Li	46	42	34	30	27	28	24	22	21	20		45	28		27	24
Be	48	43	36	30	27	28	26	24	22	19		45	28		27	24
C	50	44	38	30	26	34	33	29	23	19	60	48	35	37	34	22
Si		43			28		27			22		46	35		28	25
Cu												45	29		27	24
Ta					28					21		45	34		27	24
Pb											51		29	36		22

The measured secondary-particle spectra for kinetic energies $T > 80$ MeV are well described by the expression

$$d^2\sigma / d\Omega dTQ = \text{const}\, T \exp(-T/\tau), \quad (1)$$

which is identical to the formula for the evaporation process.[4] In Table I we have given the values of the parameter τ for the nuclei studied, at various angles. The accuracy in determination of τ is about 10%.

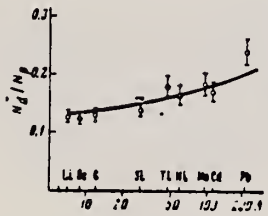

FIG. 4. The ratios N_d/N_p as a function of target-nucleus mass number A at an angle $\theta = 60°$ for E_0 = 1200 MeV. Solid curve - $A^{0.13}$.

REF.

Yu. P. Antuf ev, V.L. Agranovich, V.B. Ganenko, V.S. Kuz menko, I.I. Miroshnichenko, and P.V. Sorokin
Yad. Fiz. 14, 898 (1971)
Sov. J. Nucl. Phys. 14, 502 (1972)

ELEM. SYM.	A	Z
Ta	181	73

METHOD

REF. NO. 71 An 2 hmg

REACTION	RESULT	EXCITATION ENERGY	SOURCE		DETECTOR		ANGLE
			TYPE	RANGE	TYPE	RANGE	
G,XD	ABX	101-999	C	999	MAG-D		DST

999 = 1.14 GEV

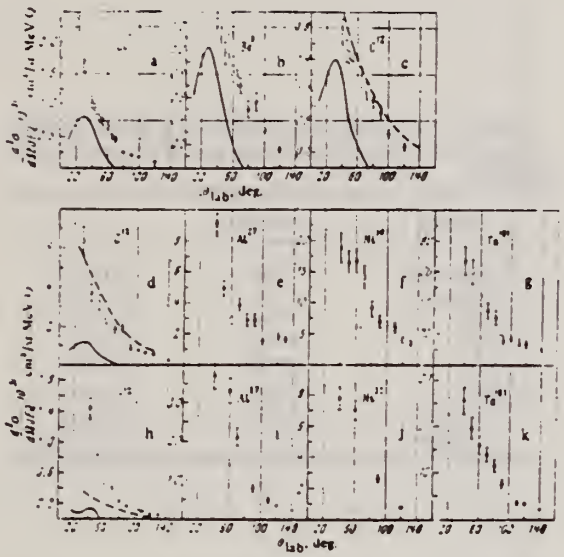

FIG. 1. Angular distributions of deuterons in (γ, d) reactions in nuclei for E_0 = 620 MeV (a–c) and E_0 = 1140 MeV (d–k). The statistical errors are shown. a–g–angular distributions of deuterons with energies of 90 MeV, h–k–with energy 160 MeV.

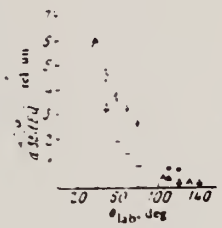

FIG. 2. Angular distributions of 160-MeV deuterons normalized at $\theta = 40°$ for C^{12} (Δ) and Ta^{181} (○) for E_0 = 1140 MeV.

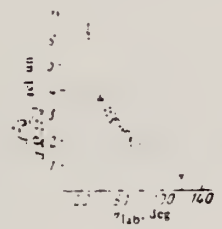

FIG. 3. Angular distributions of 90-MeV deuterons normalized at $\theta = 40°$ for E_0 = 1140 MeV (⊙) and E_0 = 620 MeV (Δ).

REF.

C. B. Fulmer, K. S. Toth, I. R. Williams, and G. F. Dell
Phys. Rev. C4, 2123 (1971)

ELEM. SYM.	A	Z
Ta	181	73

METHOD

REF. NO. 71 Fu 4 hmg

REACTION	RESULT	EXCITATION ENERGY	SOURCE		DETECTOR		ANGLE
			TYPE	RANGE	TYPE	RANGE	
G,SPL	RLX	THR-999	D	999	ACT-I		4PI
		(5 GEV)		(5 GEV)			

Measurement of F values (the ratio of photodisintegration to electrodisintegration cross sections).

999= 5 GEV

TABLE I. Experimentally measured *F* values for several nuclides produced in targets bombarded with 5-GeV electrons.

Target	Nuclide	*F*
Aluminum	^{24}Na	2.4 ± 0.4
Aluminum	^{7}Be	3.3 ± 0.5
Iron	^{52}Mn	2.0 ± 0.3
Iron	^{48}Cr	2.0 ± 0.2
Iron	^{46m}Sc	2.4 ± 0.4
Iron	^{24}Na	3.2 ± 0.4
Tantalum	^{175}Hf	2.0 ± 0.3
Tantalum	^{177}Lu	1.9 ± 0.4

REF. T. Methasiri and S. A. E. Johansson
Nucl. Phys. A167, 97 (1971)

ELEM. SYM.	A	Z
Ta	181	73

METHOD

REF. NO. 71 Me 1 egf

REACTION	RESULT	EXCITATION ENERGY	SOURCE		DETECTOR		ANGLE
			TYPE	RANGE	TYPE	RANGE	
G,F	ABY	THR-900	C	300-900	FRG-I		4PI

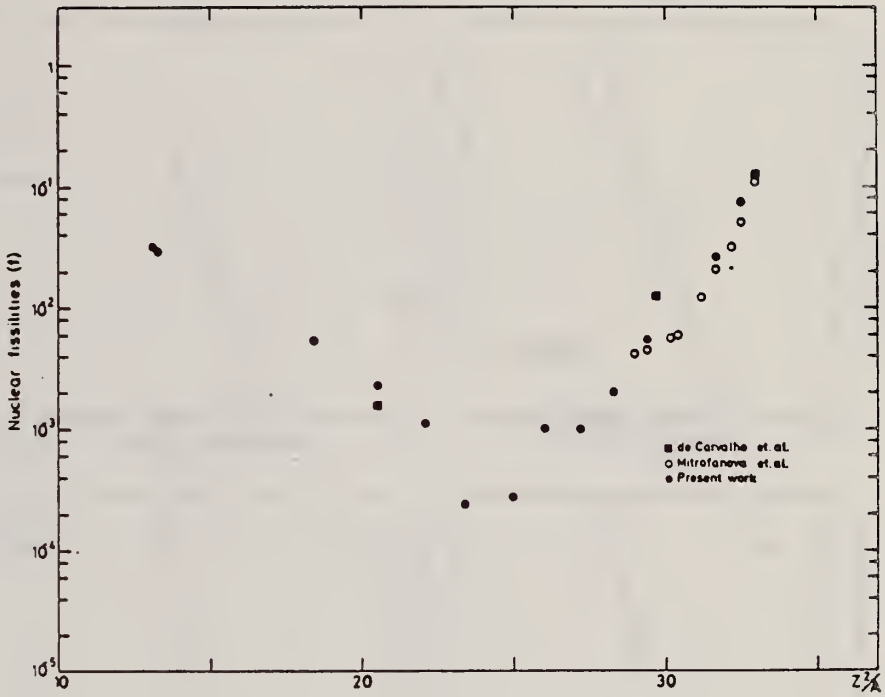

Fig. 2. Nuclear fissilities as a function of Z^2/A.

TABLE 1

The constant fission cross sections above the threshold

Element	σ_f (cm²)	Element	σ_f (cm²)
Pb	$(5.0\pm0.2)\times10^{-27}$	La	$(1.1\pm0.1)\times10^{-29}$
Au	$(1.7\pm0.1)\times10^{-27}$	Sn	$(4.3\pm1.1)\times10^{-29}$
Ta	$(3.3\pm0.2)\times10^{-28}$	Ag	$(8.4\pm2.0)\times10^{-29}$
Yb	$(1.2\pm0.2)\times10^{-28}$	Mo	$(1.7\pm0.4)\times10^{-28}$
Ho	$(5.5\pm0.3)\times10^{-29}$	Cu	$(6.6\pm1.2)\times10^{-28}$
Gd	$(5.3\pm0.8)\times10^{-29}$	Ni	$(5.8\pm0.1)\times10^{-28}$
Nd	$(1.3\pm0.2)\times10^{-29}$		

[over]

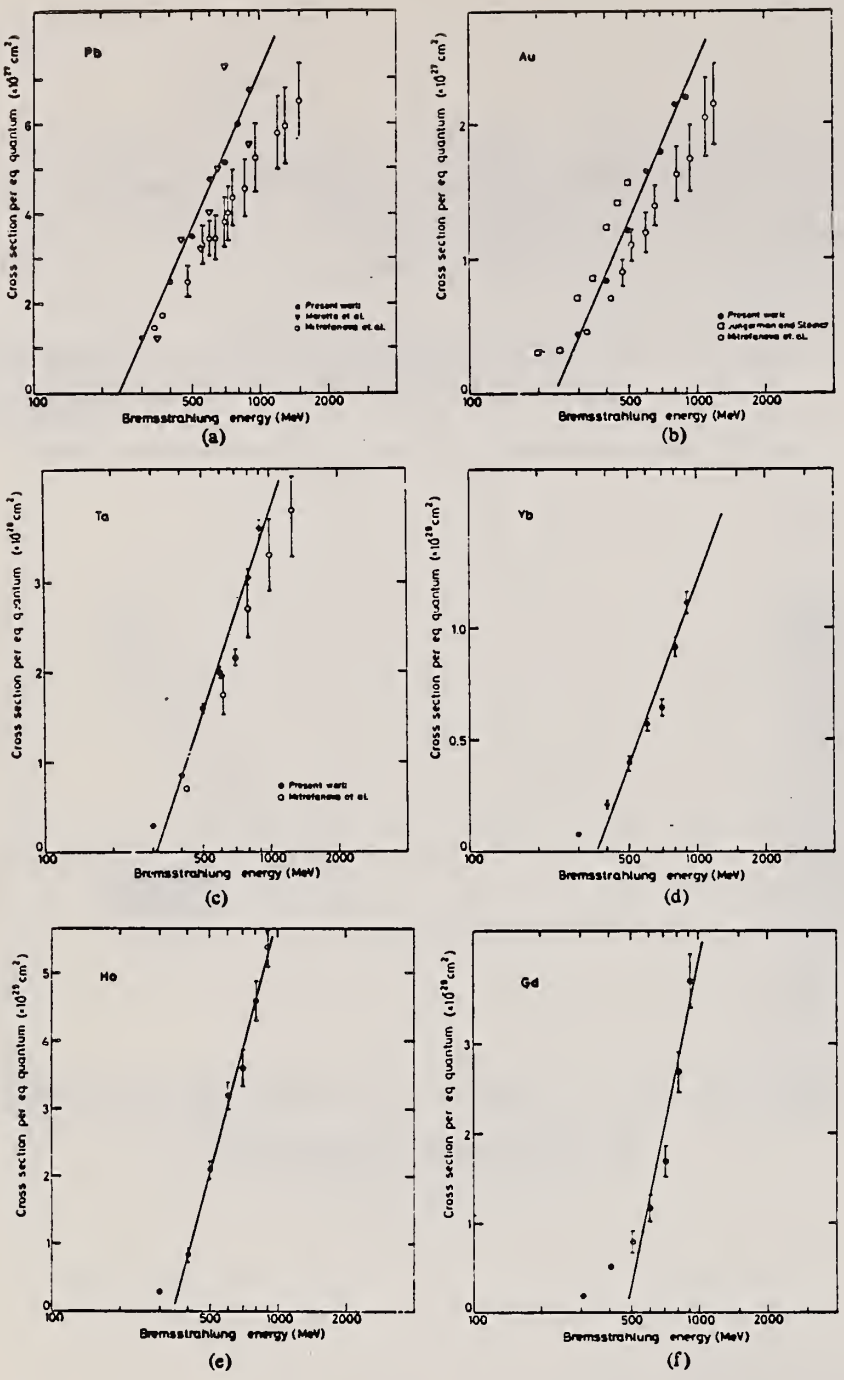

Fig. 1. Cross sections per equivalent quantum $\sigma_q(\bar{E})$ as a function of log $\bar{E}$.

REF.

E. J. Moniz, I. Sick, R. R. Whitney, J. R. Ficenec, R. G. Kephart and W. P. Trower
Phys. Rev. Letters 26, 445 (1971)

ELEM. SYM.	A	Z
Ta	181	73

METHOD

REF. NO.	
71 Mo 3	hmg

REACTION	RESULT	EXCITATION ENERGY	SOURCE		DETECTOR		ANGLE
			TYPE	RANGE	TYPE	RANGE	
E,E/	ABX	0-240	D	500	MAG-D		60

Table I. Nuclear Fermi momentum k_F and average nucleon interaction energy $\bar{\epsilon}$ determined by least-squares fit of theory to quasielastic peak.

Nucleus	k_F (MeV/c)[a]	$\bar{\epsilon}$ (MeV)[b]
$_3Li^6$	169	17
$_6C^{12}$	221	25
$_{12}Mg^{24}$	235	32
$_{20}Ca^{40}$	251	28
$_{28}Ni^{58.7}$	260	36
$_{39}Y^{89}$	254	39
$_{50}Sn^{118.7}$	260	42
$_{73}Ta^{181}$	265	42
$_{82}Pb^{208}$	265	44

[a]The fitting uncertainty in these numbers is approximately ±5 MeV/c.

[b]The fitting uncertainty in these numbers is approximately ±3 MeV. Simple estimates for $\bar{\epsilon}$ give numbers in reasonable agreement with those in the table

REF. G.A. Vartapetyan, N.A. Demekhina, V.I. Kasilov, Yu. N. Ranyuk, P.V. Sorokin and A.G. Khudaverdyan
Yad. Fiz. 14, 65 (1971)
Sov. J. Nucl. Phys. 14, 37 (1972)

ELEM. SYM.	A	Z
Ta	181	73

METHOD

REF. NO. 71 Va 4 egf

REACTION	RESULT	EXCITATION ENERGY	SOURCE		DETECTOR		ANGLE
			TYPE	RANGE	TYPE	RANGE	
G,F	ABX	100-999	C	100-999	TRK-I		4PI

999 = 5 GEV

$E_{\gamma max}$, MeV	Photofission yields per cm³ per equivalent photon					
	U^{238}	U^{235}	Th^{232}	Bi^{209}	Au^{197}	Ta^{181}
100	$(226\pm20)\cdot10^{-27}$	$(120\pm12)\cdot10^{-27}$	$(50\pm5)\cdot10^{-27}$	$(0.70\pm0.08)\cdot10^{-28}$	$(3.0\pm0.4)\cdot10^{-28}$	
120				$(1.5\pm0.2)\cdot10^{-28}$	$(1.8\pm0.2)\cdot10^{-28}$	
140				$(2.9\pm0.2)\cdot10^{-28}$	$(2.0\pm0.2)\cdot10^{-28}$	
150	$(240\pm20)\cdot10^{-27}$		$(63\pm7)\cdot10^{-27}$			
160				$(3.1\pm0.3)\cdot10^{-28}$	$(3.7\pm0.4)\cdot10^{-28}$	
180				$(4.6\pm0.5)\cdot10^{-28}$	$(5.5\pm0.6)\cdot10^{-28}$	
200	$(265\pm30)\cdot10^{-27}$	$(150\pm15)\cdot10^{-27}$	$(72\pm7)\cdot10^{-27}$	$(6.1\pm0.6)\cdot10^{-28}$	$(8.2\pm0.8)\cdot10^{-28}$	$(4.9\pm0.5)\cdot10^{-28}$
220				$(8.3\pm0.8)\cdot10^{-28}$	$(1.1\pm0.1)\cdot10^{-27}$	$(8.2\pm0.8)\cdot10^{-28}$
240				$(1.2\pm0.1)\cdot10^{-27}$	$(1.5\pm0.2)\cdot10^{-27}$	$(1.2\pm0.1)\cdot10^{-27}$
215		$(156\pm16)\cdot10^{-27}$				
260				$(1.5\pm0.2)\cdot10^{-27}$	$(1.8\pm0.2)\cdot10^{-27}$	$(1.6\pm0.2)\cdot10^{-27}$
280		$(160\pm16)\cdot10^{-27}$	$(85\pm9)\cdot10^{-27}$			
300				$(2.2\pm0.2)\cdot10^{-27}$	$(2.3\pm0.2)\cdot10^{-27}$	
340				$(3.5\pm0.4)\cdot10^{-27}$	$(4.4\pm0.4)\cdot10^{-27}$	
370				$(4.2\pm0.4)\cdot10^{-27}$	$(5.0\pm0.5)\cdot10^{-27}$	
400	$(318\pm30)\cdot10^{-27}$	$(175\pm20)\cdot10^{-27}$				
420			$(106\pm11)\cdot10^{-27}$			$(7.0\pm0.7)\cdot10^{-27}$
450				$(5.4\pm0.5)\cdot10^{-27}$	$(6.9\pm0.7)\cdot10^{-27}$	
480				$(6.7\pm0.7)\cdot10^{-27}$	$(9.1\pm0.9)\cdot10^{-27}$	
500		$(180\pm20)\cdot10^{-27}$	$(115\pm12)\cdot10^{-27}$	$(6.9\pm0.7)\cdot10^{-27}$	$(9.6\pm1)\cdot10^{-27}$	
520				$(7.9\pm0.8)\cdot10^{-27}$	$(1.1\pm0.1)\cdot10^{-26}$	
540	$(346\pm35)\cdot10^{-27}$					
570				$(8.7\pm0.8)\cdot10^{-27}$	$(1.2\pm0.1)\cdot10^{-26}$	$(1.1\pm0.2)\cdot10^{-27}$
645				$(8.5\pm0.9)\cdot10^{-27}$	$(1.1\pm0.1)\cdot10^{-26}$	
700		$(200\pm20)\cdot10^{-27}$	$(120\pm12)\cdot10^{-27}$	$(8.5\pm0.9)\cdot10^{-27}$	$(1.1\pm0.1)\cdot10^{-26}$	
750				$(9.2\pm0.9)\cdot10^{-27}$	$(1.2\pm0.1)\cdot10^{-26}$	
820						$(2.4\pm0.2)\cdot10^{-27}$
870				$(10.4\pm1)\cdot10^{-27}$	$(1.3\pm0.2)\cdot10^{-26}$	
900		$(220\pm22)\cdot10^{-27}$	$(135\pm14)\cdot10^{-27}$			
950	$(396\pm40)\cdot10^{-27}$					
1000		$(224\pm23)\cdot10^{-27}$	$(140\pm14)\cdot10^{-27}$			
1050						$(2.9\pm0.3)\cdot10^{-27}$
1100				$(11.3\pm1.1)\cdot10^{-27}$	$(1.9\pm0.2)\cdot10^{-26}$	
1150	$(480\pm40)\cdot10^{-27}$					
1200	$(490\pm40)\cdot10^{-27}$	$(217\pm23)\cdot10^{-27}$	$(136\pm14)\cdot10^{-27}$			
1250				$(12.5\pm1.3)\cdot10^{-27}$	$(1.7\pm0.2)\cdot10^{-26}$	
1300						$(3.3\pm0.3)\cdot10^{-27}$
1350				$(13.5\pm1.4)\cdot10^{-27}$	$2.\cdot10^{-26}$	
1400		$(193\pm20)\cdot10^{-27}$	$(132\pm13)\cdot10^{-27}$			
1450				$(14.3\pm1.4)\cdot10^{-27}$	$2.3\cdot10^{-26}$	
1500	$(445\pm45)\cdot10^{-27}$	$(228\pm24)\cdot10^{-27}$	$(155\pm15)\cdot10^{-27}$			
1550				$(14.9\pm1.4)\cdot10^{-27}$	$(2.1\pm0.2)\cdot10^{-26}$	
1600				$(15.5\pm1.6)\cdot10^{-27}$	$(2.2\pm0.2)\cdot10^{-26}$	
1650	$(510\pm45)\cdot10^{-27}$	$(207\pm21)\cdot10^{-27}$	$(139\pm14)\cdot10^{-27}$			
1700	$(535\pm45)\cdot10^{-27}$	$(242\pm24)\cdot10^{-27}$	$(155\pm16)\cdot10^{-27}$			
1750	$(580\pm50)\cdot10^{-27}$	$(215\pm22)\cdot10^{-27}$	$(152\pm15)\cdot10^{-27}$	$(18.1\pm1.8)\cdot10^{-27}$	$2.\cdot10^{-26}$	
1800	$(555\pm50)\cdot10^{-27}$	$(240\pm23)\cdot10^{-27}$	$(146\pm15)\cdot10^{-27}$			
1850	$(580\pm50)\cdot10^{-27}$	$(251\pm25)\cdot10^{-27}$	$(158\pm15)\cdot10^{-27}$		$(3.0\pm0.3)\cdot10^{-27}$	$(6.4\pm0.6)\cdot10^{-28}$
1900				$(15.6\pm1.6)\cdot10^{-27}$	$3.0\pm0.3)\cdot10^{-26}$	$(5.6\pm0.7)\cdot10^{-28}$
1950	$(476\pm50)\cdot10^{-27}$	$(264\pm27)\cdot10^{-27}$	$(182\pm18)\cdot10^{-27}$			
4000	$(477\pm50)\cdot10^{-27}$	$(280\pm28)\cdot10^{-27}$		$(20.2\pm2)\cdot10^{-27}$	$(2.8\pm0.3)\cdot10^{-26}$	$(6.8\pm0.7)\cdot10^{-28}$
5000	$(495\pm50)\cdot10^{-27}$	$(274\pm28)\cdot10^{-27}$	$(206\pm21)\cdot10^{-27}$	$(20.2\pm2)\cdot10^{-27}$	$(2.8\pm0.3)\cdot10^{-26}$	$(6.3\pm0.6)\cdot10^{-28}$

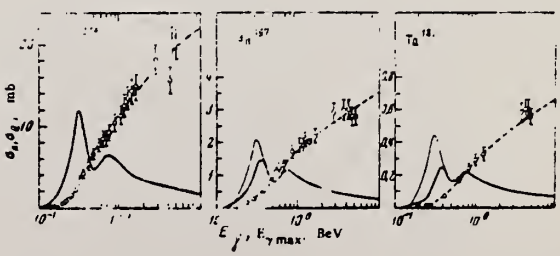

FIG. 3. Solid heavy curve – photofission cross section of Bi^{209}, Au^{197}, Ta^{181}. Dashed curve – the same cross section, integrated over the Schiff bremsstrahlung spectrum (yield per equivalent photon as a function of bremsstrahlung maximum energy). Thin line – cross section for γp interaction, multiplied by the number of nucleons in the nucleus and by the fissility.

(over)

REF. W. C. Barber, E. Hayward, J. Sazama
PICNS-72, p.313 Sendai

ELEM. SYM.	A	Z
Ta	181	73

METHOD

REF. NO. 72 Ba 16 hvm

REACTION	RESULT	EXCITATION ENERGY	SOURCE		DETECTOR		ANGLE
			TYPE	RANGE	TYPE	RANGE	
$ G,G	RLX	15.1	D	15.1	NAI-D		90

POL G; ALSO G/

$$\eta = \frac{(d\sigma/d\Omega)_{\parallel} \text{ to polarization vector}}{(d\sigma/d\Omega)_{\perp} \text{ to polarization vector}}$$

Table 1. Results and Comparison with Theory

Target	$d\sigma/d\Omega_{\perp}$ (Arbitrary Units)	η(exp)	η(DCM)	η(HD)
Cd	0.39±0.05	0.09±0.08	0.19	0
Sn	0.65±0.06	0.11±0.06	0.067	0
Ta	1.74±0.14	0.14±0.07	0.180	0.155
Au	2.08±0.15	0.17±0.06	0.067	0
Bi	2.65±0.26	0.02±0.06	0	0

REF.

N.A. Demekhina, V.I. Kasilov, A.V. Mitrofanova, Yu. N. Ranyuk, and P.V. Sorokin
Yad. Fiz. 16, 911 (1972)
Sov. J. Nucl. Phys. 16, 502 (1973)

EL.EM. SYM.	A	Z
Ta	181	73

METHOD

REF. NO.	
72 De 12	hmg

REACTION	RESULT	EXCITATION ENERGY	SOURCE		DETECTOR		ANGLE
			TYPE	RANGE	TYPE	RANGE	
G,F	NOX	THR* 6	C	1* 6	TRK-I		DST

$d\sigma/d\Omega \sim 1+2\ v/V \cos\theta - P \sin^2\theta$

*ENERGIES IN GEV

Table II

Element	$E_{\gamma max}$, MeV	χ^2	$w(\chi^2-\chi_q^2)$	$a = 2v/V$	$a = 2v/V$ [*]	v, (MeV/nucleon)$^{1/2}$	ε, MeV
U^{238}	3000	0.16	0.99	−0.031±0.025		0.042±0.005	0.160±0.020
	3800	0.55	0.85	0.013±0.017		0.018±0.002	0.045±0.005
	5100	0.59	0.85	0.040±0.017		0.054±0.006	0.096±0.031
Bi^{209}	700	0.93	0.45	0.155±0.017		0.091±0.009	0.251±0.052
	1000	1.14	0.3	−0.065±0.017		0.047±0.005	0.220±0.023
	1200	0.76	0.6	0.094±0.020		0.055±0.006	0.214±0.030
	1300	0.91	0.4	0.093±0.015		0.055±0.006	0.214±0.030
	1480	0.62	0.85	0.034±0.018		0.020±0.002	0.048±0.004
Au^{197}	350				0.097±0.010		
	450				0.102±0.010		
	600				0.090±0.010		
	645	0.87	0.55	0.084±0.018		0.044±0.004	0.187±0.018
	700				0.116±0.010		
	800	0.45	0.95	0.008±0.020		0.005±0.001	0.020±0.002
	850				0.121±0.010		
	900	4.50	0.001	0.124±0.018		0.064±0.005	0.400±0.040
	1000	0.95	0.4	0.101±0.017	0.090±0.010	0.052±0.005	0.262±0.025
	1360	0.87	0.4	0.094±0.017		0.049±0.005	0.234±0.024
	1400	0.90	0.5	0.075±0.018		0.039±0.004	0.147±0.015
	3000	1.34	0.15	0.122±0.017		0.065±0.006	0.410±0.040
	3800	0.7	0.65	0.093±0.17		0.048±0.005	0.223±0.022
Ta^{181}	600	0.8	0.5	0.087±0.018		0.044±0.004	0.176±0.018
	700				0.147±0.010		
	1145	5.2	0.001	0.144±0.018		0.072±0.007	0.468±0.047
	1480	1.25	0.15	0.127±0.018		0.064±0.006	0.370±0.037
	5100	2.02	0.001	0.200±0.020		0.100±0.010	0.940±0.090

Note. χ^2 is the value of χ^2 per degree of freedom, $w(\chi^2-\chi_q^2)$ is the probability of the value of χ^2, $a = 2v/V$ is the anisotropy coefficient, ε is the fissioning-nucleus kinetic energy, v is the fissioning-nucleus velocity.

Table III

$E_{\gamma max}$, MeV	χ^2	$w(\chi^2-\chi_q^2)$	$a = 2v/V$	v (MeV/nucleon)$^{1/2}$	ε, MeV	P
600	0.68	0.8	0.087±0.018	0.044±0.004	0.176±0.018	0.153±0.035
1145	4.23	0.001	0.136±0.017	0.068±0.007	0.416±0.042	0.170±0.030
1480	1.04	0.40	0.128±0.017	0.064±0.006	0.370±0.037	0.068±0.030
5100	1.83	0.015	0.195±0.015	0.098±0.009	0.805±0.080	−0.152±0.028

Note. χ^2 is the value of χ^2 per degree of freedom, $w(\chi^2-\chi_q^2)$ is the probability of the value of χ^2, $a = 2v/V$ is the anisotropy coefficient associated with transport velocity of the fissioning nucleus, v is the velocity of the fissioning nucleus, V is the kinetic energy of the fissioning nucleus, P is the anisotropy coefficient associated with angular momentum of the nucleus.

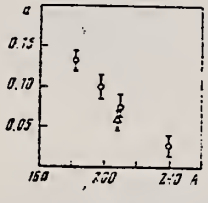

FIG. 3. Anisotropy coefficent as a function of target-nucleus atomic number. Points: O—results of the present work, Δ—results of Kroon and Forkman [16].

$$a = 2\frac{v}{V}$$

REF.		ELEM. SYM.	A	Z
	V.I. Kasilov, A.V. Mitrofanova, Yu. N. Ranyuk, P.V. Sorokin Yad. Fiz. 15, 406 (1972) Sov. J. Nucl. Phys. 15, 228 (1972)	Ta	181	73

METHOD	REF. NO.	
	72 Ka 5	hmg

REACTION	RESULT	EXCITATION ENERGY	SOURCE		DETECTOR		ANGLE
			TYPE	RANGE	TYPE	RANGE	
G,SPL	RLY	THR-999	C	600-999	TRK-I		DST
G,F	RLY	THR-999	C	600-999	TRK-I		DST

999 = 1.7 GEV

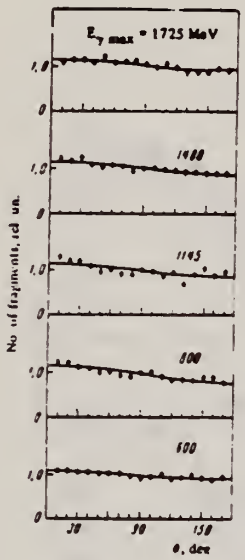

FIG. 4

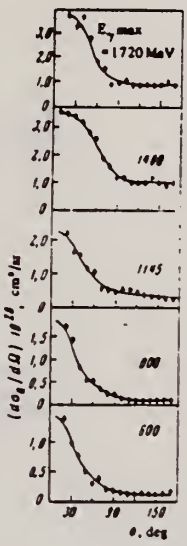

FIG. 5

FIG. 4. Angular distributions of fragments from photofission of tantalum.

FIG. 5. Angular distributions of fragmentation products.

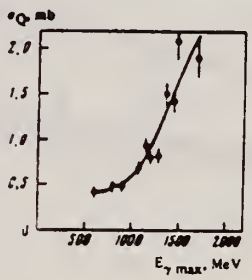

FIG. 6

FIG. 6. Yield of photofragmentation as a function of $E_{\gamma\,max}$.

REF.

I. Kroon and B. Forkman
Nucl. Phys. A179, 141 (1972)

ELEM. SYM.	A	Z
Ta	181	73

METHOD

REF. NO.: 72 Kr 3 | egf

REACTION	RESULT	EXCITATION ENERGY	SOURCE		DETECTOR		ANGLE
			TYPE	RANGE	TYPE	RANGE	
G,F	ABY	THR-999	C	350-999	TRK-I		DST

999= 1 GEV

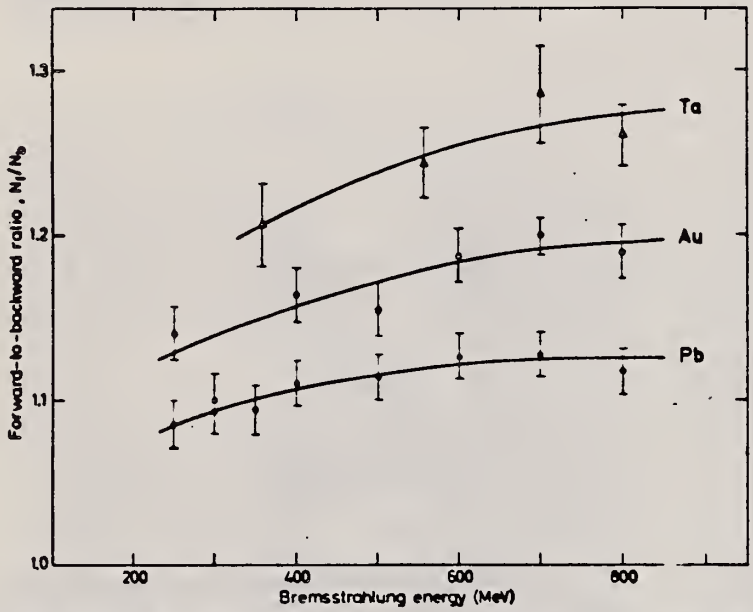

Fig. 4. The tantalum, gold and lead forward-to-backward ratios as a function of bremsstrahlung energy.

TABLE 1

Ratios between the number of fragments in the forward and backward directions recorded in glass detectors, N_f/N_b

Element	Present work		Proton sandwich experiment[c])
	from angular distribution[a])	sandwich experiment[b])	
Ta		1.29 ± 0.04	
Re			1.42 ± 0.08
Au	1.19 ± 0.02	1.20 ± 0.01	1.45 ± 0.07
Pb	1.11 ± 0.02	1.13 ± 0.01	1.61 ± 0.15
^{238}U			1.26 ± 0.05

[a]) Ratios calculated from the angular distributions at 700 MeV.
[b]) Ratios obtained with the sandwich technique, 700 MeV for Au and Pb, 800 MeV for Ta.
[c]) From ref. [9]). Proton induced fission at proton energy 660 MeV.

[9] V.A. Kon'shin, E.S. Matusevich, V.I. Regushevskii, Sov. J. Nucl. Phys. 2, 489 (1966).

REF.

N.A. Skakun and N.P. Dikii
Yad. Fiz. 15, 615 (1972)
Sov. J. Nucl. Phys. 15, 341 (1972)

ELEM. SYM.	A	Z
Ta	181	73

METHOD

REF. NO. 72 Sk 6 hmg

REACTION	RESULT	EXCITATION ENERGY	SOURCE		DETECTOR		ANGLE
			TYPE	RANGE	TYPE	RANGE	
G,F	LFT	THR-999	C	999	TRK-I		DST

Fission lifetime is 3.3×10^{-17} sec.

999 = 1.45 GEV

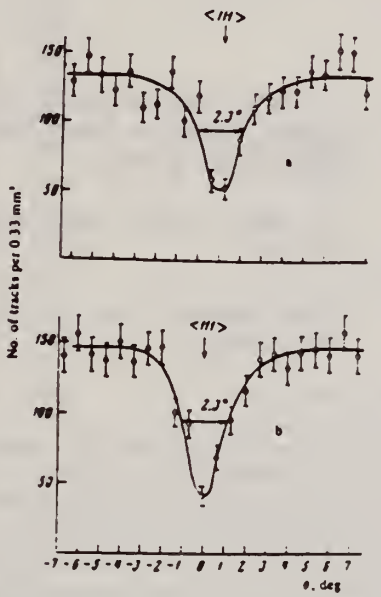

Angular distributions of fragments from photofission of tantalum: a—in the vicinity of the crystallographic (111) axis, directed at 90° to the beam; b—in the vicinity of the crystallographic (111) axis directed at 160° to the beam.

REF.

R.F. Barrett, J.R. Birkelund, B.J. Thomas, K.S. Lam, and H.H. Thies
Nucl. Phys. A210, 355 (1973)

ELEM. SYM.	A	Z
Ta	181	73

METHOD

REF. NO. 73 Ba 20 egf

REACTION	RESULT	EXCITATION ENERGY	SOURCE		DETECTOR		ANGLE
			TYPE	RANGE	TYPE	RANGE	
G,N	NOX	THR- 27	C	10- 27	BF3-I		4PI

MEAN NEUT ENERGY

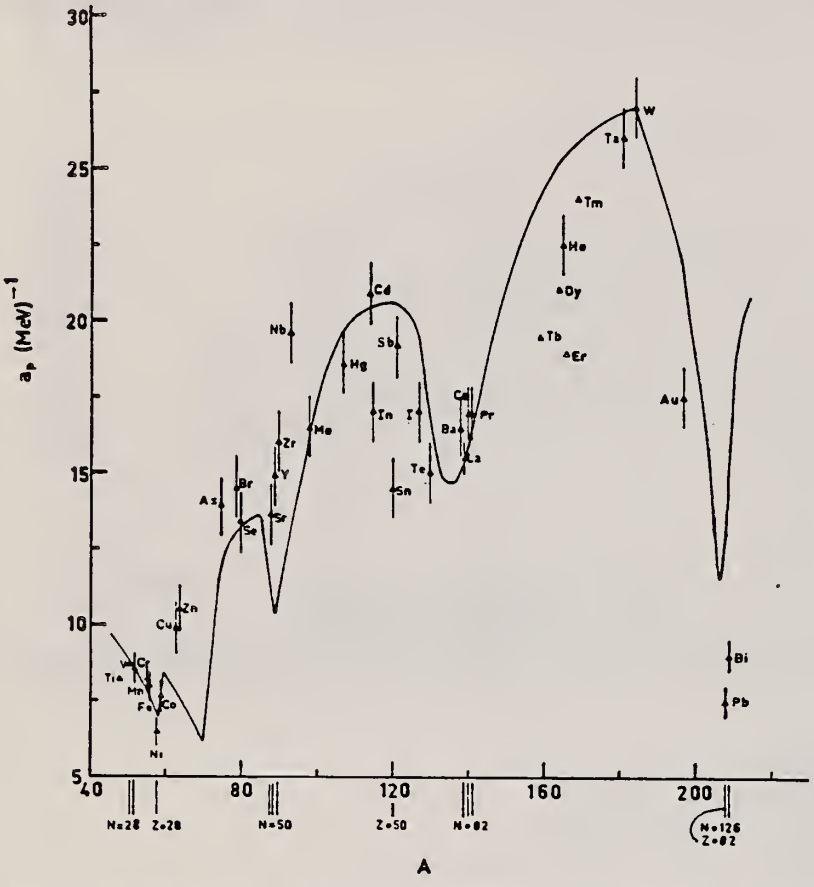

Fig. 12. Experimental values of the level density parameter a_p (Fermi gas formula plus pairing correction) versus atomic number A. The continuous curve is a least-squares fit to the data of a theoretical calculation from Newton [15]).

1
H. Baba and S. Baba, Japan Atomic Energy Research Institute report JAERI-1183 (1969).

2
H. Baba, Nucl. Phys. A159, 625 (1970).

15
T.D. Newton, Can. J. Phys. 34, 804 (1956).

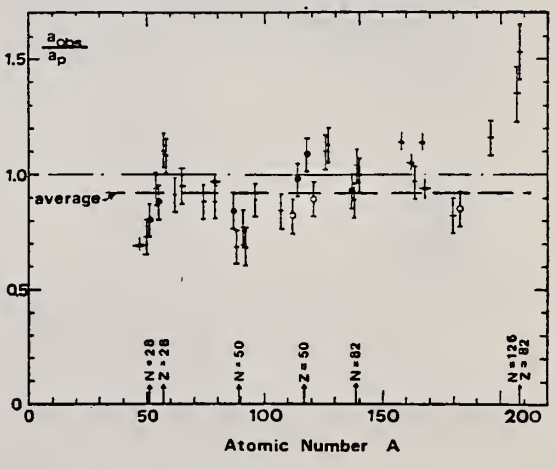

Fig. 15. Ratio a_{obs}/a_p versus atomic number A. Here a_{obs} is the level density parameter taken from the neutron resonance work of refs. [1,2]), and a_p is the level density parameter derived from the present (γ, n) work. Filled circles represent points where nuclei in the neutron resonance and in the (γ, n) experiment were the same. Open circles represent points where the respective nuclei were approximately matched. Triangles represent points which are based on measurement of neutron mean energies at two bremsstrahlung energies only.

(over)

TABLE 3 (continued)

Target	N (residual nucleus) [a]		Goodness of fit [b]		$\hat{E}_a(24)$ (MeV) [c]	T (MeV) [d]	a_p (MeV^{-1}) [e]	a_{obs} (MeV^{-1}) [f]	a_{obs}/a_p
			no p.c.	with p.c.					
Ba	75	1%		F	1.16		16.5–^{136}Ba	15.39–^{136}Ba	0.93
	77	2%							
	78	7%							
	79	8%							
	80	11%							
	81	71%							
La	80	100%	F	F	1.25	0.72	15.5–^{139}La	13.76–^{139}La	0.89
Ce	81	89%	F	G	1.24	0.70	17.0–^{139}Ce	17.8 –^{141}Ce	1.04
	83	11%							
Pr	81	100%	G	G	1.17	0.65	17.0–^{140}Pr	17.05–^{142}Pr	1.00
Tb [g]	93	100%			1.15		19.3–^{158}Tb	21.85–^{160}Tb	1.14
Dy [g]	93	2%			1.06		20.9–$^{161.5}$Dy	21.9 –^{162}Dy	1.05
	94	19%							
	95	25%							
	96	25%							
	97	28%							
Ho	97	100%	P	G	1.06	0.56	21.4–^{164}Ho	20.66–^{166}Ho	0.97
Er [g]	95	2%			1.11		19.2–^{166}Er	21.9 –^{166}Er	1.14
	97	33%							
	98	23%							
	99	27%							
	101	15%							
Tm [g]	99	100%			1.03		24.0–^{168}Tm	22.58–^{170}Tm	0.94
Ta	107	100%		G	1.00	0.49	26.0–^{180}Ta	21.2 –^{181}Ta	0.82
W	107	26%	G	F	0.98	0.50	27.0–^{183}W	23.0 –^{183}W	0.85
	108	14%							
	109	31%							
	111	28%							
Au	117	100%		G	1.19		17.5–^{196}Au	20.24–^{198}Au	1.16
Pb	123	24%		V.P.	1.87	1.20	7.5–^{206}Pb	10.1 –^{207}Pb	1.35
(Z = 82)	124	23%							
	125	52%							
Bi	125	100%		F	1.65	1.03	9.0–^{208}Bi	13.8 –^{210}Bi	1.53

[a]) Neutron numbers and abundances of respective residual nuclei in (γ, n) experiments.
[b]) These give an assessment of the goodness of fit of a calculated $\hat{E}_a$ versus E_0 curve to the observed data, using the Fermi gas level density formula both without and with pairing corrections.
[c]) Bremsstrahlung photoneutron mean energies $\hat{E}_a$ for peak bremsstrahlung energy E_0 = 24 MeV.
[d]) Nuclear temperature from fit with constant-temperature formula.
[e]) Level density parameter a_p derived from the present (γ, n) experiment, using a Fermi gas formula plus pairing correction, and corresponding residual nucleus (the atomic weight shown is the weighted average of atomic weights of the respective isotopes present).
[f]) As column 7, but using data on n-resonance absorption from refs. [1,2]).
[g]) Measurements of $\hat{E}_a(E_0)$ for these nuclei were made only for E_0 = 21, 23 and 24 MeV.

REF. N.V. Goncharov, A.I. Derebchinskii, O.G. Konovalov, S.G. Tonapetyan, and V.M. Khvorostyan
Yad. Fiz. 17, 242 (1973)
Sov. J. Nucl. Phys. 17, 124 (1973)

EL EM. SYM.	A	Z
Ta	181	73

METHOD

REF. NO. 73 Go 5 hmg

REACTION	RESULT	EXCITATION ENERGY	SOURCE		DETECTOR		ANGLE
			TYPE	RANGE	TYPE	RANGE	
G,PI+	ABY	170-400	C	400	BBL-D		90
G,PI-	ABY	170-400	C	400	BBL-D		90
G,P	ABY	76-400	C	400	BBL-D		90

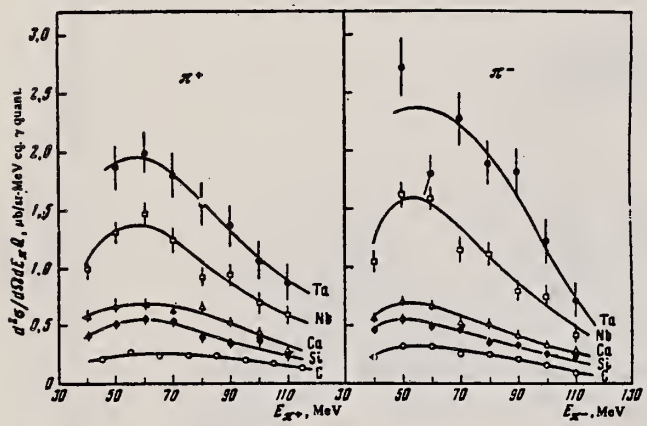

FIG. 2. Energy spectra of π^+ and π^- mesons, $E_\gamma^{max} = 400$ MeV, $\theta_{lab} = (90 \pm 7)°$.

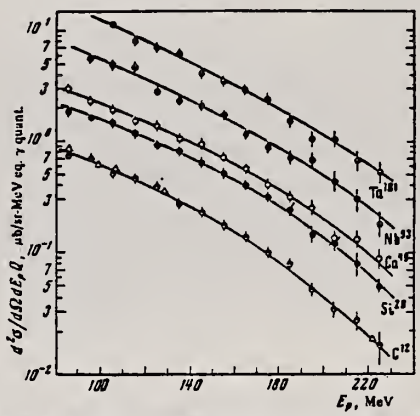

FIG. 3. Energy spectra of protons, $E_\gamma^{max} = 400$ MeV, $\theta_{lab} = (90 \pm 7)°$. Circles–present data, triangles–from [18].

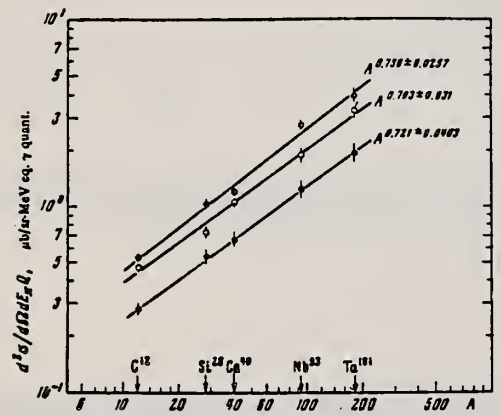

FIG. 4. Charged pion yield vs. the mass number of the nucleus: ●– $E_\pi = 105 \pm 10$ MeV, ○–$E_\pi = 85 \pm 10$ MeV, ◐–$E_\pi = 65 \pm 10$ MeV.

[18] P. Dougan, W. Stäefler, LUSY Preprint, 1001-1003. 1970.

(over)

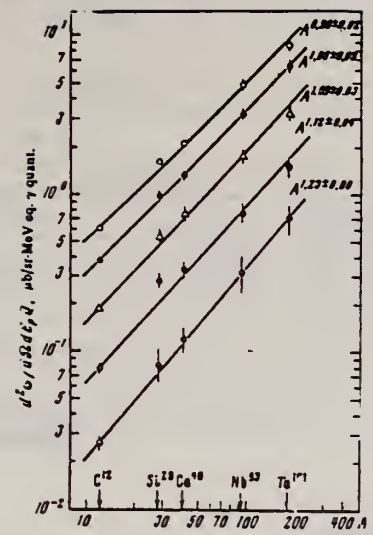

FIG. 5. Proton yields vs. mass number of the nucleus: O–E_p = 100 ± 10 MeV, ●–E_p = 125 ± 15 MeV, Δ–E_p = 155 ± 15 MeV, ◐–E_p = 185 ± 15 MeV, ◒–E_p = 215 ± 15 MeV.

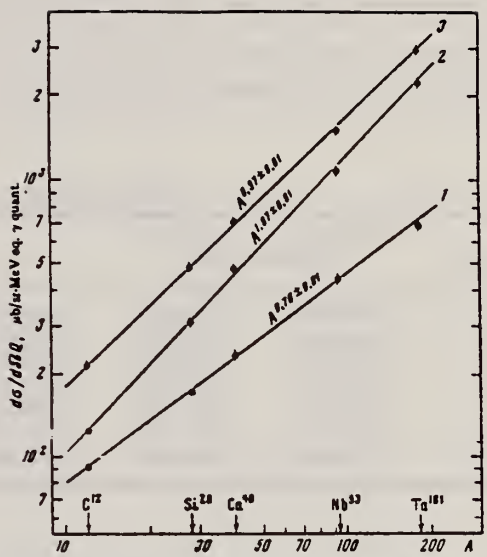

FIG. 6. Pion yield (1), proton yield (2), and summary pion and proton yield (3) vs. the mass number of the nucleus.

REF. E. Hayward, W. C. Barber, and Jed Sazama
Phys. Rev. C8, 1065 (1973)

ELEM. SYM.	A	Z
Ta	181	73

METHOD

REF. NO. 73 Ha 3 hmg

REACTION	RESULT	EXCITATION ENERGY	SOURCE		DETECTOR		ANGLE
			TYPE	RANGE	TYPE	RANGE	
$ G,G	RLY	15	D	15	NAI-D		90
		(15.1)		(15.1)			

POLARIZED PHOTONS

TABLE II. Results.

Target	$d\sigma^{\parallel}/d\Omega_F$ Arbitrary units	$d\sigma^{\perp}/d\Omega_F$	η_F	η	$\eta(DCM)$
Cd	0.042±0.028	0.39±0.05	0.11±0.07	0.09±0.07	0.19
Sn	0.084±0.036	0.65±0.06	0.13±0.06	0.11±0.06	0.07
Ta	0.24±0.10	1.47±0.14	0.16±0.07	0.14±0.07	0.20
W	0.52±0.10	1.66±0.12	0.31±0.07	0.29±0.07	0.20
Pt	0.23±0.08	1.94±0.13	0.12±0.04	0.10±0.04	0.08
Au	0.39±0.11	2.08±0.15	0.19±0.06	0.17±0.06	0.07
Bi	0.10±0.15	2.65±0.26	0.04±0.06	0.02±0.06	0

REF. R. S. Hicks and B. M. Spicer
Aust. J. Phys. 26, 585 (1973)

ELEM. SYM.	A	Z
Ta	181	73

METHOD

REF. NO. 73 Hi 6 egf

REACTION	RESULT	EXCITATION ENERGY	SOURCE		DETECTOR		ANGLE
			TYPE	RANGE	TYPE	RANGE	
G,XN	ABX	7- 29	C	7- 29	BF3-I		4PI

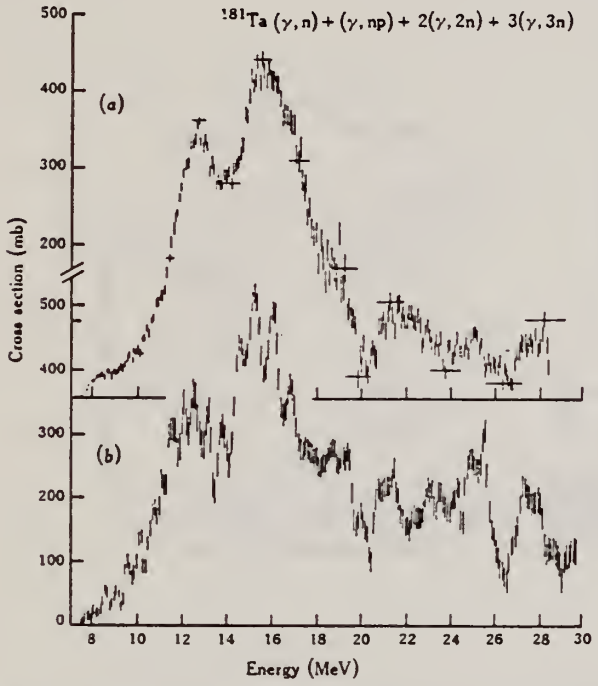

Fig. 1.—Comparison of (*a*) the present results with (*b*) those of Ishkhanov *et al.* (1969) for the cross section for photoneutron production in ^{181}Ta.

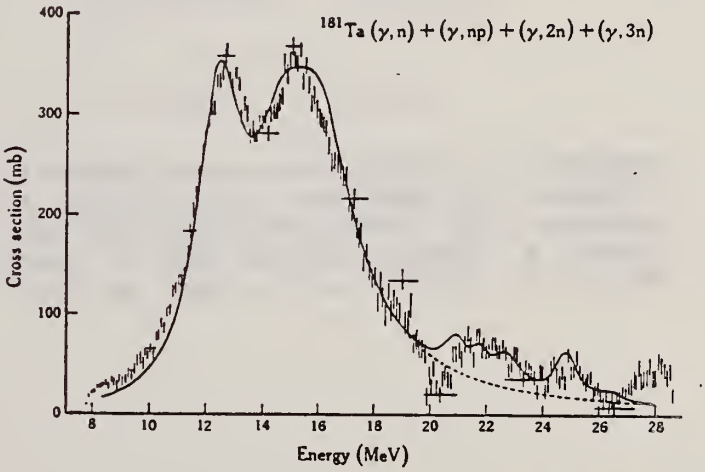

Fig. 3.—Multiplicity corrected ^{181}Ta photoneutron cross section as derived using the VBPL technique with analysis bin widths close to 1·5 times the Thies (1961) optimum value. The full curve represents the DCM predicted form, an incoherent sum of calculations by Arenhövel (1965) and Ligensa *et al.* (1966) for the E1 and E2 giant resonances respectively. The dashed curve is an extrapolation of the predicted dipole resonance.

(over)

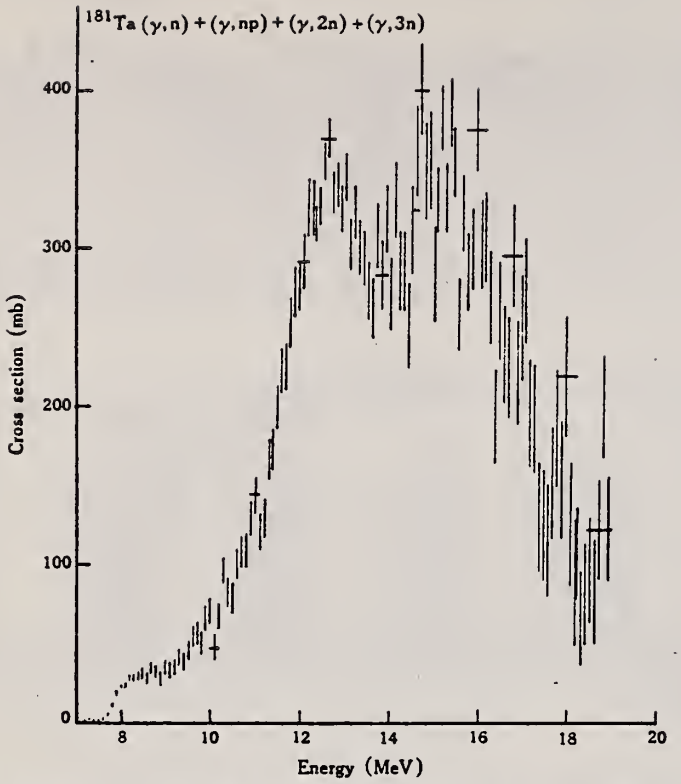

Fig. 4.—Multiplicity corrected ^{181}Ta photoneutron cross section obtained by a re-analysis of the data with bin widths close to the Thies (1961) optimum bin in order to examine the possibility of extensive fine structure within the dipole resonance.

Arenhövel, H. (1965).-Dissertation, University of Frankfurt am Main.
Ishkhanov, B.S., Kapitonov, I.M., Lazutin, E.V., Piskarev, I.M., and Shevchenko, O.P. (1969).-Sov. Phys. JETP Lett. 10, 51.
Ligensa, R., Greiner, W., and Danos, M. (1966).-Phys. Rev. Lett. 16, 363.
Thies, H.H. (1961).- Aust. J. Phys. 14, 174.

REF.	A. Suzuki, K. Shoda, M. Sugawara, T. Saito, H. Miyase, S. Oikawa, and J. Uegaki PICNS-73, Vol. I, p. 195 Asilomar	ELEM. SYM.	A	Z
		Ta	181	73

METHOD	REF. NO.	
	73 Su 10	hmg

REACTION	RESULT	EXCITATION ENERGY	SOURCE		DETECTOR		ANGLE
			TYPE	RANGE	TYPE	RANGE	
E,P	RLY	5- 20	D	15- 20	MAG-D		125

Fig 2

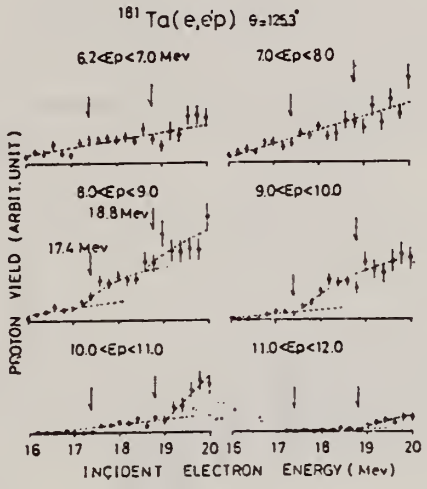

Fig 3

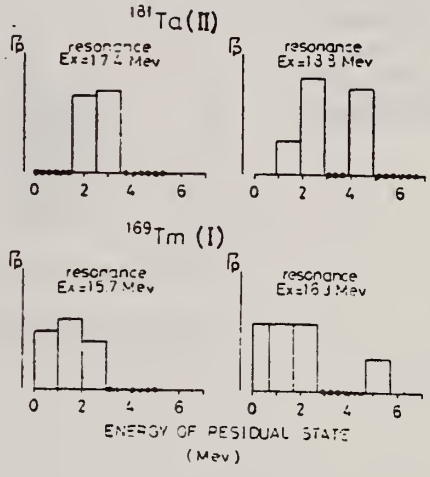

REF. A. Suzuki, K. Shoda, M. Sugawara, T. Saito, H. Miyase, S. Oikawa, J. Uegaki, M.N. Thompson, K.J.F. Allen, H.J. Askin, B.N. Sung PICNS-73, Vol.I, p.197 Asilomar

ELEM. SYM.	A	Z
Ta	181	73

METHOD

REF. NO. 73 Su 11 hmg

REACTION	RESULT	EXCITATION ENERGY	SOURCE		DETECTOR		ANGLE
			TYPE	RANGE	TYPE	RANGE	
E,P	RLY	5- 22	D	18- 22	MAG-D		90

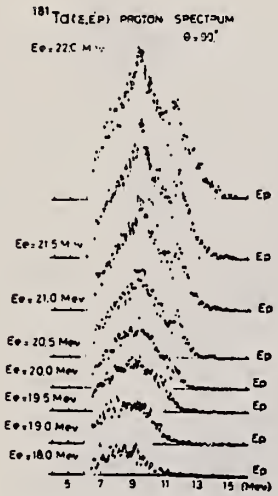

Fig.1

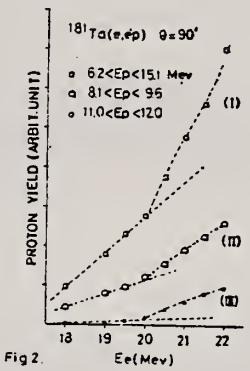

Fig 2.

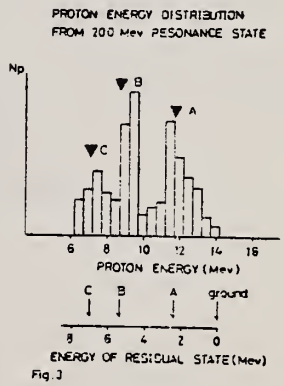

Fig.3

REF. P. David, J. Debrus, F. Lubke, H. Mommsen, R. Schoenmackers, and G. Stein
Nucl. Phys. A221, 145 (1974)

EL EM. SYM.	A	Z
Ta	181	73

METHOD

REF. NO. 74 Da 2 egf

REACTION	RESULT	EXCITATION ENERGY	SOURCE		DETECTOR		ANGLE
			TYPE	RANGE	TYPE	RANGE	
G,A	ABY	10-450	C	450	TEL-D		90

Data measured for p,t, and He3, but not given in paper.

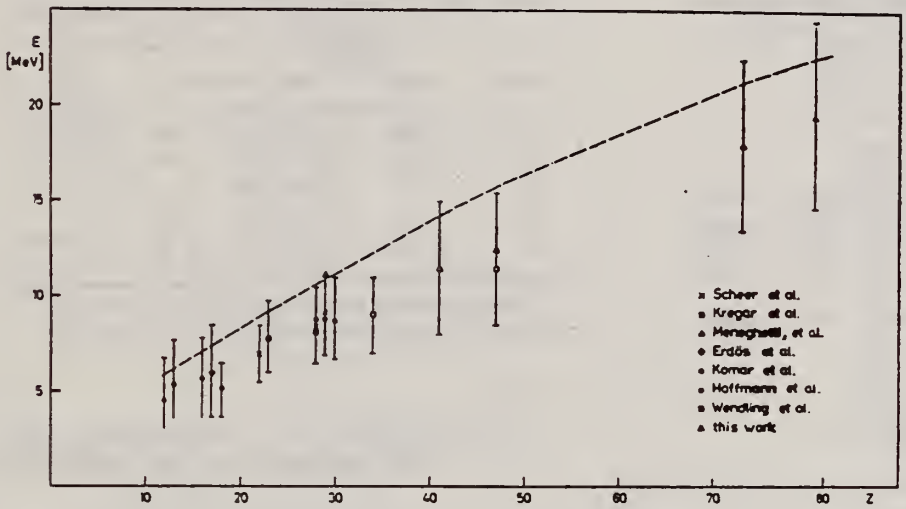

Fig. 8. The position of maxima of the (γ, α) spectra and the width of the spectra at half height. The broken line gives the height of the Coulomb barrier.

REF.

H.E. Jackson, G.E. Thomas, and K.J. Wetzel
Phys. Rev. C9, 1153 (1974)

ELEM. SYM.	A	Z
Ta	181	73

METHOD

REF. NO. 74 Ja 2 hmg

REACTION	RESULT	EXCITATION ENERGY	SOURCE TYPE	SOURCE RANGE	DETECTOR TYPE	DETECTOR RANGE	ANGLE
G,G	ABX	10	D	10	SCD-D		90
		(10.83)		(10.83)			

TABLE I. Differential cross sections measured for elastic and inelastic scattering of 10.83-MeV photons. State or states populated by inelastic scattering are indicated in parentheses below the target. The errors given result from the statistical error in the measurement of the cross section relative to the calibration value, the 90° uranium inelastic cross section.

Nucleus	θ (deg)	$d\sigma/d\omega$ (elastic) (mb/sr)	$d\sigma/d\omega$ (inelastic) (mb/sr)
^{238}U			
(2^+, 45 keV)	20	1.72 ± 0.17	
	30	0.97 ± 0.12	
	50	0.334 ± 0.039	
	60	0.23 ± 0.04	
	70	0.245 ± 0.024	0.136 ± 0.015
	90	0.182 ± 0.017	0.154 ± 0.012
	120	0.189 ± 0.017	0.160 ± 0.013
	150	0.303 ± 0.016	0.160 ± 0.015
^{232}Th			
(2^+, 45 keV)	90	0.129 ± 0.015	0.103 ± 0.007
Pb	20	1.28 ± 0.12	
	30	0.55 ± 0.07	
	50	0.289 ± 0.051	
	60	0.20 ± 0.04	
	70	0.087 ± 0.014	
	90	0.079 ± 0.005	
	120	0.060 ± 0.004	
	150	0.127 ± 0.008	
^{209}Bi			
($\frac{1}{2}^-$, 910 keV)	90	0.101 ± 0.0062	~0
^{181}Ta			
($\frac{9}{2}^+$, 136 keV)	90	0.0370 ± 0.003	0.006 56 ± 0.0015
^{159}Tb			
($\frac{5}{2}^+$, 58 keV)	90	0.0314 ± 0.003	0.0110 ± 0.0016
$\frac{7}{2}^+$, 138 keV)			0.005 11 ± 0.0011

TABLE III. Comparison of calculated and observed values of the 90° cross sections for elastic scattering and of the ratio at 90° of Raman to elastic scattering by various nuclei for 10.83-MeV photons. The parameters used in the calculations are given in Table II.

Target	$d\sigma_{elas}$ (90°)/$d\Omega$ (mb/sr) Calc	Exp	$d\sigma^{(90°)}_{Raman}/d\sigma^{(90°)}_{elas}$ Calc	Exp
Tb	0.036	0.031 ± 0.003	0.80	0.51 ± 0.06
Ta	0.055	0.037 ± 0.003	0.28	0.18 ± 0.04
Pb	0.076	0.079 ± 0.005	0	
Bi		0.101 ± 0.006	0	~0
Th	0.128	0.129 ± 0.015	0.91	0.80 ± 0.08
U	0.157 [a]	0.182 ± 0.017	1.03	0.85 ± 0.08

[a] If the Livermore parameters (Ref. 33) for ^{235}U are used then this calculated value would be 0.210 mb/sr.

33
C.D. Bowman, G.F. Auchampauch, and S.C. Fultz, Phys. Rev. 133, B676 (1964).

REF. S. Kahane and R. Moreh
Phys. Rev. C9, 2384 (1974)
(See also 73Mol3)

ELEM. SYM.	A	Z
Ta	181	73

METHOD

REF. NO. 74 Ka 9 egf

REACTION	RESULT	EXCITATION ENERGY	SOURCE TYPE	SOURCE RANGE	DETECTOR TYPE	DETECTOR RANGE	ANGLE
G,G	ABX	8	D	8	SCD-D		DST

Differential cross sections for elastic scattering of 7.9-MeV photons from ^{181}Ta have been measured at angles ranging from 25 to 140°. These results and previously measured differential cross sections from ^{238}U and ^{232}Th are compared with theoretical predictions taking into account Rayleigh scattering, nuclear Thomson scattering, nuclear resonance scattering, and Delbruck scattering. It is shown that at this energy the forward elastic scattering at angles ≤75° is due almost entirely to Delbruck scattering. The experimental results were found to deviate systematically from predicted values throughout most of the angular range. A striking agreement with theory was obtained only after excluding the contribution of the real part of the Delbruck scattering amplitude.

8=7.9 MEV

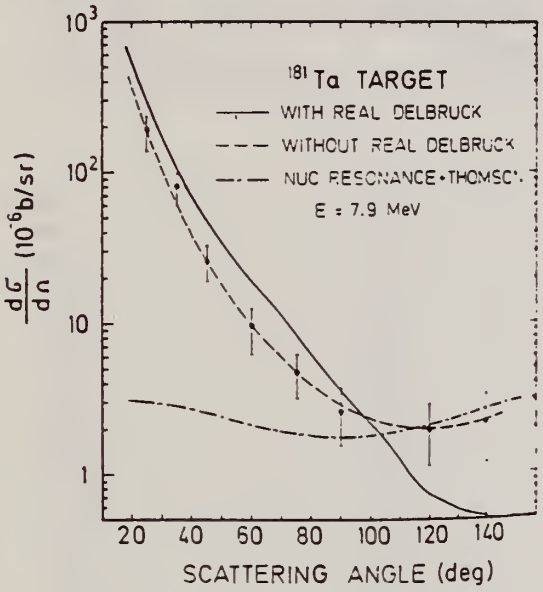

FIG. 4. Differential elastic scattering cross sections for 7.9-MeV photons from ^{181}Ta. The solid curve represents the calculated values obtained by including the amplitudes of Thomson, Rayleigh, nuclear resonance, and Delbruck scatterings. The dashed curve represents the result obtained after excluding the real Delbruck amplitudes while the dash-dot curve represents the result obtained by including nuclear resonance and Thomson scattering only. The incoherent contribution is included in all calculations.

TABLE I. Measured differential cross sections (μb/sr) for elastic scattering from a ^{181}Ta target at various angles. The calculated cross sections include the contributions of all scattering processes with and without the real part of the Delbruck scattering amplitude.

Angle (deg)	Experiment	Calculated Without real	Calculated With real
25	195 ±50	190	290
35	82 ±20	62	110
45	26 ± 7	25	48
60	9.7± 3.5	9.8	19
75	4.9± 1.5	4.8	8.5
90	2.6± 1.1	2.9	3.8
120	2.0± 0.9	2.1	0.76
140	2.2± 1.1	2.2	0.51

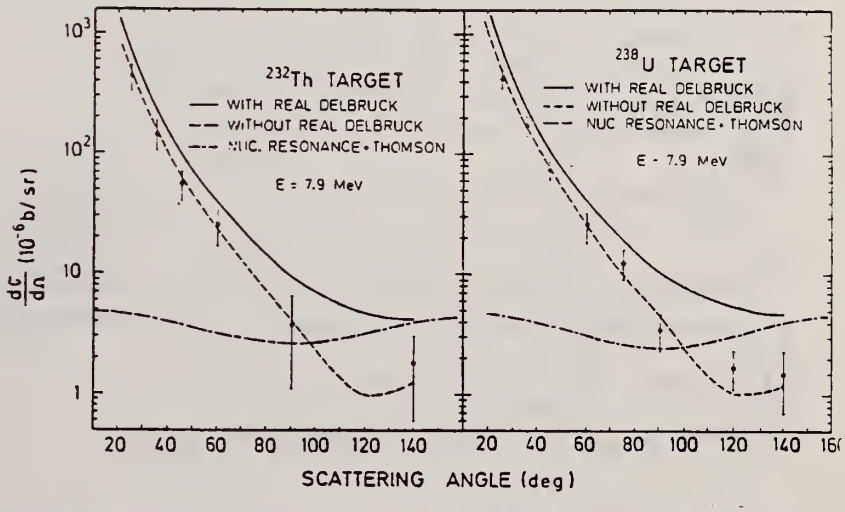

FIG. 5. Differential elastic scattering cross sections for 7.9-MeV photons from ^{232}Th and ^{238}U. The solid curve represents the calculated values obtained by including the amplitudes of Thomson, Rayleigh, nuclear resonance, and Delbruck scatterings. The dashed curve represents the result obtained after excluding the real Delbruck amplitudes while the dash-dot curve represents the result obtained by including nuclear resonance and Thomson scattering only.

REF.

L.E. Lazareva, A.I. Lepestkin, and V.I. Sidorov
Yad. Fiz. 20, 242 (1974)
Sov. J. Nucl. Phys. 20, 128 (1975)

ELEM. SYM.	A	Z
Ta	181	73

METHOD

REF. NO. 74 La 5 hmg

REACTION	RESULT	EXCITATION ENERGY	SOURCE		DETECTOR		ANGLE
			TYPE	RANGE	TYPE	RANGE	
G,XN	SPC	8- 29	C	29	EMU-D		DST
				(28.5)			

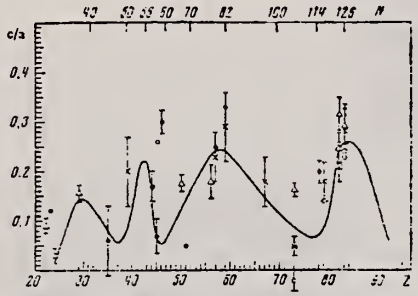

FIG. 2. Assymetry coefficients c/a obtained for nuclei with various Z in the following studies: ref. 10–$E_{\gamma\,max}$ = 25.5 MeV, $E_n > 7.4$ MeV (*); ref. 11–$E_{\gamma\,max}$ = 27–32 MeV, $E_n > \sim 5$ MeV (●); ref. 12–$E_{\gamma\,max}$ = 34 MeV, $E_n > \sim 8$ MeV (△); ref. 13–$E_{\gamma\,max}$ = 55 MeV, $E_n > \sim 5$ MeV (X); present work–$E_{\gamma\,max}$ = 28.5 MeV, $E_n > 5$ MeV (○). The smooth curve shows the coefficient b/a characterizing the photoneutron angular distribution anisotropy as a function of atomic number Z. (This has been converted from the curve given in ref. 11 and and is for the distribution $I(\vartheta) = a + b \sin^2\vartheta + c \cos\vartheta$, normalized at the points Z = 82–83.)

[11] J.W. Jury, J.S. Hewitt, K.G. McNeill, Can. J. Phys. 46, 1823 (1968).

[12] F.R. Allum, T.W. Quirk, B.M. Spicer, Nucl. Phys. 53, 545 (1964).

[13] G.C. Reinhardt and W.D. Whitehead, Nucl.Phys. 30, 201 (1962).

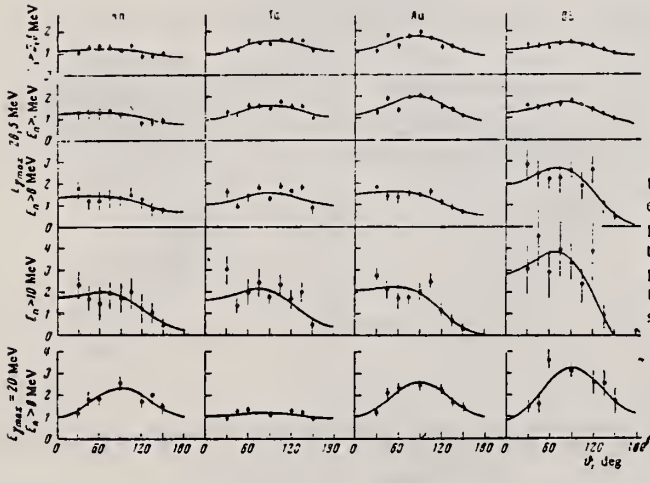

FIG. 1. Angular distributions of photoneutrons obtained in irradiation of Rh, Ta, Au, and Bi samples by bremsstrahlung with maximum energy $E_{\gamma\,max}$ = 28.5 MeV. The curves were calculated from the experimental points by the method of least squares for a distribution of the form $I(\vartheta) = a + b \sin^2\vartheta + c \cos\vartheta$ and normalized (a = 1). For comparison we have shown below the angular distributions of photoneutrons with energy $E_n > 8$ MeV obtained in irradiation of the same samples by bremsstrahlung with $E_{\gamma\,max}$ = 20 MeV.

(over)

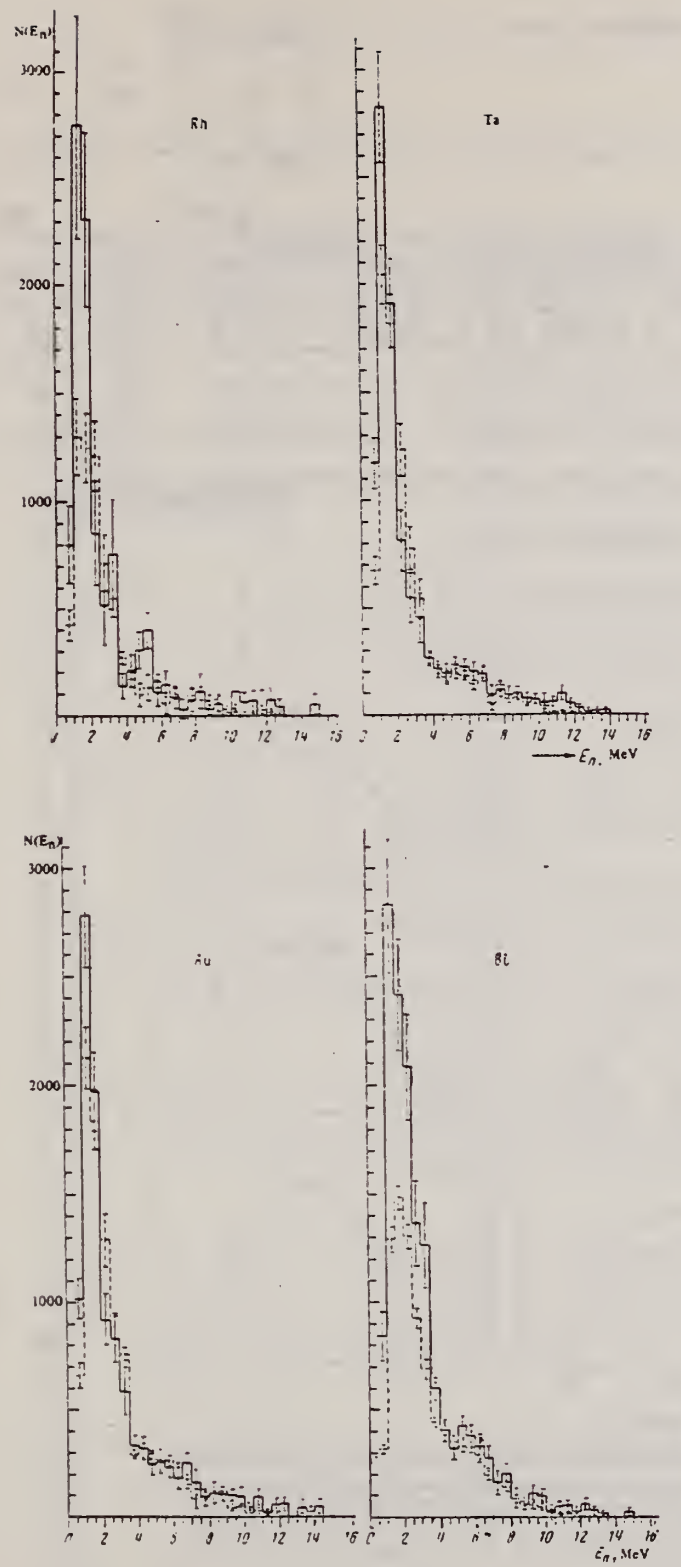

FIG. 3. Photoneutron energy spectra from Rh, Ta, Au, and Bi for irradiation of the samples by bremsstrahlung with maximum energy $E_{\gamma\,max}$ = 20 (dashed line) and 28.5 (solid line) MeV for angles ϑ with maximum neutron yield. For each nucleus the histograms given for $E_{\gamma\,max}$ = 20 and 28.5 MeV have been combined in the interval E_n = 4–4.5 MeV.

REF. R.R. Whitney, I. Sick, J.R. Ficenec, R.D. Kephart, and W.P. Trower
Phys. Rev. C9, 2230 (1974)

ELEM. SYM.	A	Z
Ta	181	73

METHOD

REF. NO. 74 Wh 3 hmg

REACTION	RESULT	EXCITATION ENERGY	SOURCE TYPE	SOURCE RANGE	DETECTOR TYPE	DETECTOR RANGE	ANGLE
E,E/	ABX	0-300	D	500	MAG-D		60

QUASIELASTIC SCAT

See further analysis of this data in reference 79Zil

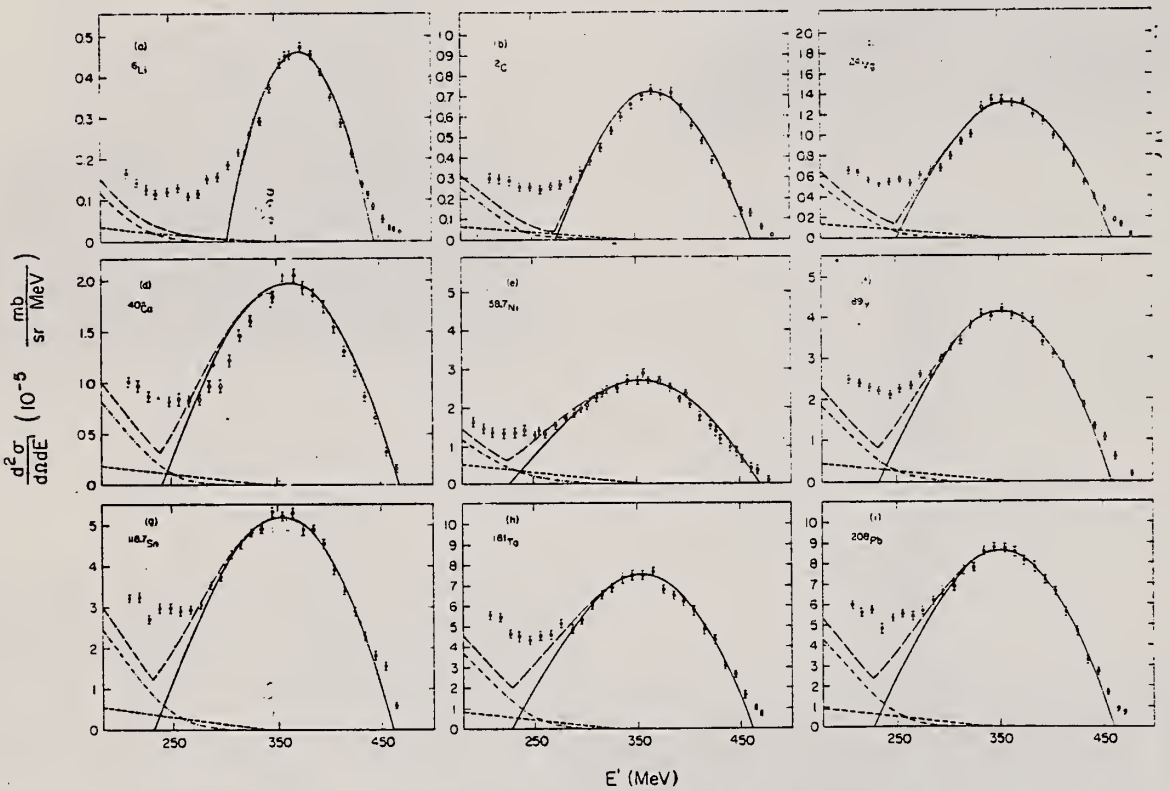

FIG. 1. The measured quasielastic peaks; the errors on the data points do not include an over-all 3% normalization uncertainty. The solid curve is a fit by the Fermi-gas model which yielded k_F (in MeV/c) and $\bar{\epsilon}$ (in MeV) as follows: (a) ^{6}Li (169, 17); (b) ^{12}C (221, 25); (c) ^{24}Mg (235, 32); (d) ^{40}Ca (249, 33); (e) $^{58.7}$Ni (260, 36); (f) ^{89}Y (254, 39); (g) $^{118.7}$Sm (260, 42); (h) ^{181}Ta (265, 42); (i) ^{208}Pb (265, 44). The fitting uncertainty in k_F is ±5 MeV/c and in $\bar{\epsilon}$ it is ±3 MeV. The small-amplitude dashed curve is the s-wave π-production contribution, the dot-dashed curve is the isobar excitation, and the large-amplitude dashed curve is the total result.

(over)

TABLE I. Proton-normalized and radiative-corrected cross sections $d^2\sigma/d\Omega dE' = (N \pm \Delta N) \times 10^{-n}$ in mb/sr MeV, for $E = 500$ MeV and $\theta = 60°$.

E'	^{6}Li			^{12}C			^{24}Mg			^{40}Ca			^{58,7}Ni			^{89}Y			^{118,7}Sn			^{180,95}Ta			^{208}Pb		
(MeV)	N	ΔN	n	N	ΔN	n	N	ΔN	n	N	ΔN	n	N	ΔN	n	N	ΔN	n	N	ΔN	n	N	ΔN	n	N	ΔN	n
480.0	···			1.79	0.19	7	3.83	0.42	7	···			1.22	0.17	6	1.71	0.19	6	···			···			···		
474.0	···			1.02	0.13	7	···			···			···			···			···			···			···		
470.0	1.72	0.18	7	5.75	0.52	7	1.55	0.15	6	···			3.90	0.29	6	5.85	0.41	6	···			7.09	0.67	6	7.00	0.68	6
464.0	2.49	0.29	7	1.38	0.11	6	1.91	0.17	6	2.72	0.15	6	4.48	0.33	6	5.68	0.37	6	8.32	0.71	6	1.16	0.08	5	9.82	0.79	6
460.0	2.96	0.30	7	1.20	0.09	6	2.58	0.19	6	···			···			···			···			1.54	0.10	5	1.81	0.10	5
454.1	5.02	0.17	7	9.21	0.71	7	2.96	0.20	6	4.20	0.17	6	7.00	0.41	6	1.07	0.05	5	1.85	0.09	5	1.70	0.11	5	2.31	0.11	5
450.0	···			···			···			···			8.92	0.47	6	1.03	0.05	5	1.83	0.09	5	···			···		
444.3	8.68	0.58	7	1.26	0.07	6	4.11	0.25	6	6.67	0.27	6	1.02	0.05	5	1.33	0.05	5	···			2.77	0.14	5	2.74	0.12	5
440.0	1.11	0.06	6	2.50	0.13	6	5.23	0.26	6	···			···			···			···			3.43	0.16	5	3.24	0.13	5
434.2	1.32	0.06	6	2.99	0.11	6	5.50	0.26	6	8.71	0.35	6	1.19	0.05	5	1.90	0.07	5	2.27	0.09	5	3.14	0.15	5	3.34	0.14	5
430.0	···			···			···			···			1.40	0.07	5	2.11	0.08	5	2.77	0.11	5	···			···		
424.3	2.12	0.08	6	3.75	0.15	6	7.31	0.29	6	1.12	0.04	5	1.54	0.08	5	2.31	0.09	5	2.88	0.12	5	4.43	0.18	5	4.74	0.19	5
414.4	2.88	0.12	6	4.75	0.19	6	8.78	0.35	6	1.32	0.05	5	1.78	0.10	5	2.88	0.11	5	3.40	0.14	5	4.98	0.20	5	5.64	0.23	5
404.5	3.51	0.11	6	5.46	0.22	6	1.02	0.04	5	1.56	0.06	5	2.09	0.08	5	3.09	0.12	5	3.90	0.16	5	5.89	0.24	5	6.57	0.26	5
400.0	···			6.25	0.25	6	1.09	0.01	5	···			2.35	0.09	5	3.34	0.13	5	4.29	0.17	5	6.56	0.27	5	7.00	0.28	5
394.7	4.16	0.17	6	6.32	0.26	6	1.15	0.05	5	1.75	0.07	5	2.22	0.09	5	3.41	0.14	5	4.56	0.18	5	6.29	0.25	5	7.25	0.29	5
385.7	4.55	0.18	6	7.09	0.28	6	1.21	0.05	5	1.86	0.07	5	2.51	0.10	5	3.91	0.16	5	4.88	0.19	5	6.36	0.26	5	7.88	0.32	5
374.9	4.76	0.19	6	6.97	0.28	6	1.33	0.05	5	1.91	0.08	5	2.72	0.11	5	4.02	0.16	5	4.88	0.19	5	6.87	0.28	5	8.19	0.33	5
365.0	4.56	0.18	6	7.28	0.29	6	1.32	0.05	5	2.08	0.08	5	2.69	0.10	5	4.04	0.16	5	5.34	0.21	5	7.77	0.31	5	8.61	0.34	5
360.0	4.50	0.18	6	6.61	0.28	6	1.32	0.05	5	···			2.88	0.11	5	4.11	0.16	5	5.69	0.23	5	7.92	0.33	5	8.42	0.34	5
355.2	4.35	0.17	6	6.97	0.28	6	1.36	0.05	5	2.08	0.08	5	2.69	0.11	5	4.23	0.17	5	5.22	0.21	5	7.51	0.30	5	···		
345.3	3.68	0.15	6	6.54	0.26	6	1.35	0.05	5	1.85	0.07	5	2.72	0.11	5	4.02	0.16	5	5.37	0.21	5	7.59	0.30	5	8.83	0.35	5
335.4	2.90	0.12	6	5.91	0.24	6	1.29	0.05	5	1.87	0.08	5	2.48	0.10	5	4.08	0.16	5	4.92	0.19	5	7.44	0.29	5	8.68	0.35	5
325.5	2.59	0.10	6	5.23	0.21	6	1.05	0.04	5	1.61	0.07	5	2.48	0.11	5	3.78	0.15	5	4.83	0.19	5	6.93	0.28	5	7.81	0.31	5
320.0	···			···			···			···			2.35	0.09	5	3.34	0.14	5	4.53	0.18	5	···			···		
315.7	2.16	0.10	6	4.43	0.18	6	9.41	0.38	6	1.47	0.06	5	2.26	0.09	5	3.43	0.14	5	4.34	0.17	5	6.61	0.26	5	7.76	0.31	5
305.8	1.84	0.09	6	3.79	0.15	6	8.61	0.32	6	1.23	0.05	5	2.03	0.08	5	3.27	0.13	5	4.32	0.17	5	6.11	0.24	5	6.92	0.28	5
300.0	···			···			···			···			1.97	0.08	5	3.11	0.12	5	4.03	0.16	5	···			···		
295.9	1.55	0.09	6	3.38	0.14	6	6.77	0.29	6	9.97	0.40	6	1.80	0.07	5	3.02	0.12	5	3.74	0.15	5	5.38	0.22	5	6.73	0.27	5
285.9	1.50	0.09	6	2.96	0.14	6	6.64	0.31	6	9.73	0.39	6	1.72	0.07	5	2.60	0.13	5	3.55	0.15	5	4.92	0.23	5	6.30	0.29	5
276.2	1.14	0.08	6	2.64	0.13	6	6.03	0.32	6	8.35	0.41	6	1.50	0.07	5	2.64	0.13	5	3.10	0.15	5	5.22	0.24	5	5.73	0.30	5
266.3	1.08	0.08	6	2.61	0.14	6	5.32	0.33	6	8.57	0.43	6	1.31	0.08	5	2.37	0.14	5	2.72	0.16	5	4.62	0.26	5	5.51	0.31	5
260.0	···			···			···			···			1.39	0.08	5	1.95	0.13	5	2.94	0.18	5	···			···		
256.4	1.28	0.09	6	2.43	0.15	6	5.71	0.35	6	8.33	0.45	6	1.27	0.08	5	2.27	0.14	5	2.87	0.18	5	4.57	0.28	5	5.63	0.33	5
246.6	1.20	0.09	6	2.55	0.16	6	5.47	0.36	6	8.55	0.48	6	1.39	0.09	5	2.14	0.14	5	2.95	0.19	5	4.33	0.28	5	5.40	0.35	5
236.7	1.15	0.10	6	2.54	0.16	6	5.18	0.38	6	8.71	0.51	6	1.34	0.09	5	2.24	0.15	5	3.02	0.20	5	4.35	0.30	5	4.90	0.34	5
226.8	1.27	0.11	6	2.88	0.19	6	5.62	0.42	6	8.72	0.51	6	1.29	0.10	5	2.29	0.16	5	2.73	0.20	5	4.57	0.30	5	5.88	0.37	5
216.9	1.43	0.14	6	2.91	0.21	6	6.35	0.49	6	9.81	0.56	6	1.34	0.10	5	2.38	0.17	5	3.26	0.22	5	5.42	0.36	5	5.76	0.38	5
207.0	1.66	0.16	6	2.91	0.21	6	6.59	0.52	6	1.02	0.06	5	1.43	0.11	5	2.51	0.18	5	3.24	0.22	5	5.58	0.37	5	6.11	0.40	5
197.2	1.78	0.17	6	3.42	0.24	6	7.01	0.59	6	···			1.59	0.12	5	2.77	0.20	5	3.43	0.24	5	5.67	0.38	5	5.99	0.41	5

REF.

V. S. Evseev, T. N. Mamedov, O. V. Selyugin
Yad. Fiz. 21, 245 (1975)
Sov. J. Nucl. Phys. 21, 129 (1975)

ELEM. SYM.	A	Z
Ta	181	73

METHOD

REF. NO.: 75 Ev 1 hmg

REACTION	RESULT	EXCITATION ENERGY	SOURCE		DETECTOR		ANGLE
			TYPE	RANGE	TYPE	RANGE	
G,N	SPC	7- 31	C	31	SCI-D		140

Neutron energy spectra have been measured in the energy range $2 \leq E_n \leq 5$ MeV for photoexcitation of the nuclei Ta, Pb, Bi, and Th by bremsstrahlung with maximum energy 31 MeV. From the neutron spectra we have determined values of the nuclear temperature T after emission of the first neutron: 1.01 ± 0.04, 1.12 ± 0.04, 1.11 ± 0.04, and 1.25 ± 0.05 MeV respectively for Ta, Pb, Bi, and Th. Comparison of the values obtained for the nuclear level-density parameter with the predictions of the statistical theory of nuclear reactions shows that this theory does not describe the decay of collective nuclear states of the giant dipole resonance type.

REF. H. E. Jackson, G. E. Thomas, K. J. Wetzel
Phys. Rev. C11, 1664 (1975)

ELEM. SYM.	A	Z
Ta	181	73

METHOD

REF. NO. 75 Ja 1 hmg

REACTION	RESULT	EXCITATION ENERGY	SOURCE		DETECTOR		ANGLE
			TYPE	RANGE	TYPE	RANGE	
G,G	ABX	11	D	11	SCD-D		DST
		(11.387)		(11.387)			

RATIO RAMAN/ELASTIC

TABLE I. Differential cross sections measured for elastic and inelastic scattering of 11.39-MeV photons. State or states populated by inelastic scattering are indicated in parentheses beside the target. The errors given result from the statistical error in the measurement of the cross section relative to the calibration value, the 90° uranium elastic cross section.

θ (deg)	$d\sigma/d\omega$ (elastic) (mb/sr)	$d\sigma/d\omega$ (inelastic) (mb/sr)
	^{238}U (2$^+$, 45 keV)	
90	0.169 ± 0.011	0.173 ± 0.016
150	0.355 ± 0.041	0.236 ± 0.24
	^{232}Th (2$^+$, 45 keV)	
150	0.331 ± 0.035	0.210 ± 0.022
	^{181}Ta ($\frac{9}{2}^+$, 136 keV) ($\frac{11}{2}^+$, 301 keV)	
90	0.073 ± 0.008	0.020 ± 0.004 0.009 ± 0.004
150	0.145 ± 0.015	0.017 ± 0.004 0.017 ± 0.004
	^{165}Ho ($\frac{9}{2}^+$, 95 keV) ($\frac{11}{2}^+$, 210 keV)	
150	0.141 ± 0.014	0.022 ± 0.004 0.013 ± 0.004
	^{159}Tb ($\frac{5}{2}^+$, 58 keV) ($\frac{7}{2}^+$, 138 keV)	
90	0.062 ± 0.006	0.024 ± 0.003 0.013 ± 0.003
150	0.134 ± 0.012	0.042 ± 0.004 0.019 ± 0.004
	^{141}Pr	
150	0.030 ± 0.008	...

TABLE II. Comparison of calculated and observed values of the cross sections for elastic scattering and of the ratio of Raman to elastic scattering by various nuclei for 11.387-MeV photons at 90 and 150°. The parameters used in the calculations for column 5 are given in Table II. Column 4 describes results obtained by perturbing those parameter to meet the constraint of Eq. (3) (see text).

Target	$d\sigma(\theta)d\Omega$ (mb/sr) Calc.	Exp.	$d\sigma_{Raman}(\theta)/d\sigma_{elastic}(\theta)$		
		$\theta = 150°$			
Pr	0.025	0.030 ± 0.008		0.0	0.0
Tb	0.094	0.134 ± 0.012	0.53	0.57	0.46 ± 0.04
Ho	0.170	0.141 ± 0.014	0.28	0.28	0.25 ± 0.04
Ta	0.160	0.145 ± 0.015	0.23	0.22	0.23 ± 0.04
Th	0.253	0.331 ± 0.035	0.59	0.63	0.64 ± 0.08
U	0.289	0.355 ± 0.041	0.78	0.73	0.67 ± 0.07
		$\theta = 90°$			
Tb	0.062	0.062 ± 0.006	0.76	0.82	0.60 ± 0.07
Ta	0.109	0.074 ± 0.008	0.32	0.30	0.38 ± 0.07
U	0.172	0.169 ± 0.008	1.29	1.15	1.03 ± 0.10

REF. S. G. Tonapetyan, N. V. Goncharov, and V. M. Khvorostyan
Yad. Fiz. 22, 440 (1975)
Sov. J. Nucl. Phys. 22, 226 (1976)

ELEM. SYM.	A	Z
Ta	181	73

METHOD

REF. NO. 75 To 4 hmg

REACTION	RESULT	EXCITATION ENERGY	SOURCE		DETECTOR		ANGLE
			TYPE	RANGE	TYPE	RANGE	
G,PI+	ABY	150-400	C	300,400	BBL-D		90
G,PI-	ABY	150-400	C	300,400	BBL-D		90
G,P	ABY	86-400	C	300,400	BBL-D		90

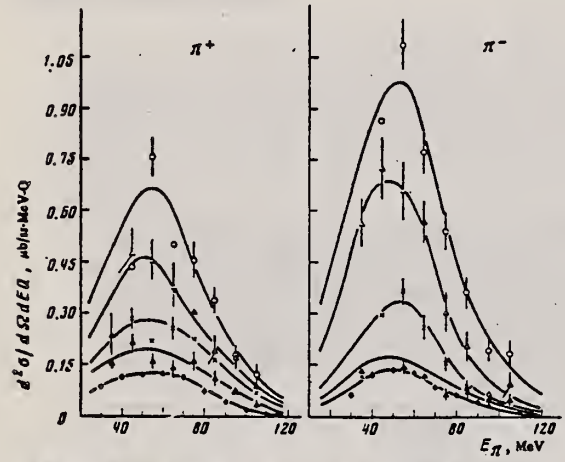

FIG. 1. Energy spectra of π^+ and π^- mesons. $E_\gamma^{max} = 300$ MeV, $\theta_{lab} = 90 \pm 7°$. Points: ●—^{12}C, ▲—^{28}Si, X—^{40}Ca, △—^{93}Nb, ○—^{181}Ta.

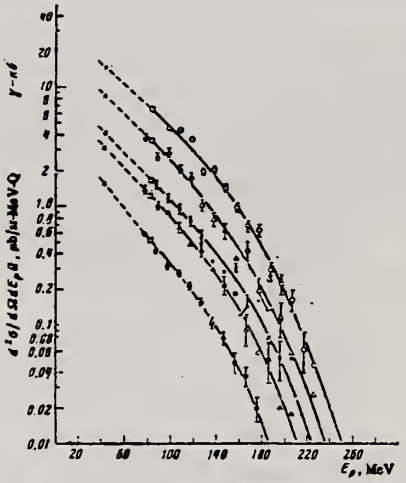

FIG. 3. Energy spectra of protons, $E_\gamma^{max} = 300$ MeV, $\theta_{lab} = 90 \pm 7°$. Points: ●—^{12}C, ▲—^{28}Si, X—^{40}Ca, △—^{93}Nb, ○—^{181}Ta, □—data from ref. 5, ³—data from ref. 5.

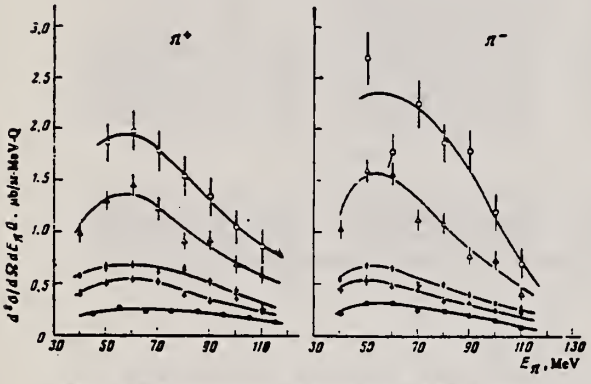

FIG. 2. Energy spectra of π^+ and π^- mesons. $E_\gamma^{max} = 400$ MeV, $\theta_{lab} = 90 \pm 7°$. The points are the same as in Fig. 1.

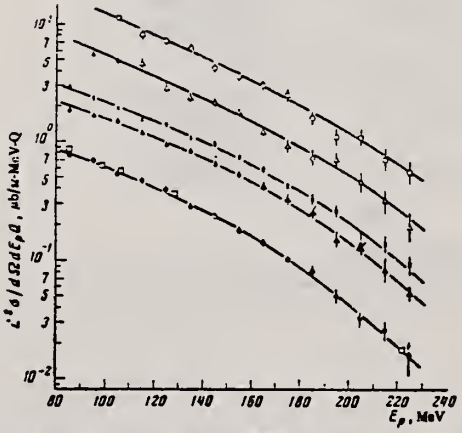

FIG. 4. Energy spectra of protons, $E_\gamma^{max} = 400$ MeV, $\theta_{lab} = 90 \pm 7°$. The points are the same as in Fig. 1; □—data from ref. 7.

FIG. 5. Dependence of yields of π mesons 1, protons 2, and the sum of π-meson and proton yields 4 as a function of mass number of the nucleus. The dashed line 3 is the theory. Points: □—experimental differential cross sections for pions of all signs, △—differential cross sections for protons emitted at the same angle $\theta_{lab} = 90°$, ○—combined values of these differential cross sections. The statistical errors are shown.

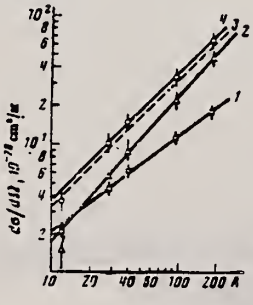

[5] P.C. Murray et al., Phys.Rev. 94, 764 (54).
[6] C.Levinthal et al., Phys.Rev.82, 822 (51)
[7] P.Dougan et al., LUSY Preprint 1002 (70).

REF. H. Bartsch, K. Huber, U. Kneissl, H. Krieger
Nucl. Phys. A256, 243 (1976)

ELEM. SYM.	A	Z
Ta	181	73

METHOD

REF. NO. 76 Ba 1 egf

REACTION	RESULT	EXCITATION ENERGY	SOURCE TYPE	SOURCE RANGE	DETECTOR TYPE	DETECTOR RANGE	ANGLE
G, 3N	RLY	THR-UKN	C	UKN	SCD-D		4PI

ISOMER RATIO

TABLE 1
Experimental and theoretical results

Process	Target-spin	E_γ (keV)	$T_{\frac{1}{2}}$	Spin high	Spin low	$R_{exp} = \frac{\sigma_{high}}{\sigma_{low}}$	SCOP ($\bar{h}$)
^{181}Ta(γ, 3n)	$\frac{7}{2}^+$	93	2.2 h 9.31 min 8.15 h	7^-	1^+	0.51 ±0.09	3.6 ±0.2
^{142}Nd(γ, n)	0^+	755 1100–1300, 145	63 s 2.5 h	$\frac{11}{2}^-$	$\frac{3}{2}^+$	0.055±0.006 0.19 ±0.01 [a])	2.20±0.06
^{92}Mo(γ, n)	0^+	652.9 1208, 1508, 1581, 1637	66 s 15.49 min	$\frac{3}{2}^+$	$\frac{1}{2}^-$	1.03 ±0.21 0.85 ±0.07 [b]) 1.92 ±0.15 [a])	5.03±0.75 4^{+6}_{-2}
^{100}Mo(γ, n)	0^+	97.3 140.5	16.8 μs 66.02 h	$\frac{1}{2}^+$	$\frac{1}{2}^+$	0.85 ±0.24	1.72±0.25
^{108}Pd(γ, n)	0^+	214.5 115	22 s 850 ns	$\frac{11}{2}^-$	$\frac{1}{2}^+$	0.5 ±0.2	3.4 ±0.5
^{110}Pd(γ, n)	0^+	188 113 87.7	4.7 min 390 ns 13.47 h	$\frac{11}{2}^-$ $\frac{11}{2}^-$ $\frac{3}{2}^+$	$\frac{3}{2}^+$ $\frac{1}{2}^+$ $\frac{1}{2}^+$	0.11 ±0.02 0.41 ±0.09 3.2 ±0.7	3.14±0.15 3.0 ±0.25 3.3 ±0.4
^{89}Y(γ, n)	$\frac{1}{2}^-$	231.7 442.3 392.5	14.2 ms 300 μs	8^+	1^+	0.056±0.008	

[a]) Ref. [14]). [b]) Ref. [15]).

14 P.E. Haustein et al., J. Inorg. Nucl. Chem. 33, 289 (1971)
15 J.H. Carver et al., Nucl. Phys. 37, 449 (1962)

REF.

V. Emma, S. Lo Nigro, C. Milone
Nucl. Phys. A257, 438 (1976)

ELEM. SYM.	A	Z
Ta	181	73

METHOD

REF. NO.: 76 Em 2 — egf

REACTION	RESULT	EXCITATION ENERGY	SOURCE TYPE	SOURCE RANGE	DETECTOR TYPE	DETECTOR RANGE	ANGLE
G,F	ABY	THR-999	C	999	TRK-I		4PI

999 = 1 GEV

TABLE 1
Measured values of σ_q at $E = 1000$ MeV and deduced values of σ_k assumed constant from E_0 to 1000 MeV

Element	Z^2/A	σ_q (mb)	E_0 (MeV)	σ_k (mb)
Bi	32.96	12.3 ± 0.6	200	7.6 ± 0.6
Pb	32.45	5.4 ± 0.4	220	3.6 ± 0.3
Tl	32.10	4.1 ± 0.3	230	2.8 ± 0.3
Au	31.68	2.0 ± 0.15	240	1.4 ± 0.2
Pt	31.18	1.1 ± 0.08	255	$(8 \pm 0.7) \times 10^{-1}$
Re	30.21	$(3.7 \pm 0.3) \times 10^{-1}$	280	$(2.9 \pm 0.3) \times 10^{-1}$
W	29.78	$(3.5 \pm 0.3) \times 10^{-1}$	290	$(2.8 \pm 0.3) \times 10^{-1}$
Ta	29.45	$(3.3 \pm 0.3) \times 10^{-1}$	300	$(2.7 \pm 0.3) \times 10^{-1}$
Hf	29.04	$(1.7 \pm 0.2) \times 10^{-1}$	310	$(1.4 \pm 0.2) \times 10^{-1}$
Yb	28.31	$(1.3 \pm 0.1) \times 10^{-1}$	330	$(1.2 \pm 0.1) \times 10^{-1}$
Tm	28.18	$(7.5 \pm 0.8) \times 10^{-2}$	335	$(6.8 \pm 0.8) \times 10^{-2}$
Ho	27.21	$(3.6 \pm 0.4) \times 10^{-2}$	355	$(3.5 \pm 0.4) \times 10^{-2}$
Dy	26.80	$(2.6 \pm 0.3) \times 10^{-2}$	360	$(2.5 \pm 0.3) \times 10^{-2}$
Tb	26.58	$(2.5 \pm 0.3) \times 10^{-2}$	370	$(2.5 \pm 0.3) \times 10^{-2}$
Gd	26.04	$(1.6 \pm 0.2) \times 10^{-2}$	380	$(1.7 \pm 0.2) \times 10^{-2}$
Sm	25.56	$(1.3 \pm 0.2) \times 10^{-2}$	390	$(1.4 \pm 0.2) \times 10^{-2}$
Nd	24.96	$(9.2 \pm 0.9) \times 10^{-3}$	405	$(1 \pm 0.1) \times 10^{-2}$
Ce	24.00	$(8 \pm 0.9) \times 10^{-3}$	420	$(9 \pm 1) \times 10^{-3}$
La	23.39	$(8.4 \pm 0.9) \times 10^{-3}$	430	$(1 \pm 0.1) \times 10^{-3}$
Sb	21.36	$(1.2 \pm 0.2) \times 10^{-2}$	460	$(1.5 \pm 0.3) \times 10^{-2}$
Te	21.19	$(8.8 \pm 1) \times 10^{-3}$	465	$(1.2 \pm 0.2) \times 10^{-2}$
Sn	21.06	$(1.3 \pm 0.2) \times 10^{-2}$	465	$(1.7 \pm 0.3) \times 10^{-2}$
Cd	20.49	$(1.7 \pm 0.3) \times 10^{-2}$	470	$(2.2 \pm 0.4) \times 10^{-2}$
Ag	20.47	$(2 \pm 0.3) \times 10^{-2}$	470	$(2.6 \pm 0.4) \times 10^{-2}$
Zn	13.76	$(2 \pm 0.4) \times 10^{-1}$	515	$(3 \pm 0.6) \times 10^{-1}$
Cu	13.44	$(2.4 \pm 0.5) \times 10^{-1}$	515	$(3.6 \pm 0.8) \times 10^{-1}$
Ni	13.35	$(2.4 \pm 0.5) \times 10^{-1}$	510	$(3.6 \pm 0.8) \times 10^{-1}$
Fe	12.10	$(3 \pm 0.6) \times 10^{-1}$	510	$(4.4 \pm 0.9) \times 10^{-1}$

[4] A.V. Mitrofanova et al. Sov. J. Nucl. Phys. 6, 512 (1968).

[7] T. Methasiri et al., Nucl. Phys. A167, 97 (1971).

[12] J.R. Nix et al., Nucl. Phys. 81, 61 (1966).

[20] N.A. Perifilov et al., JETP (Sov. Phys.) 14, 623 (1962); Proc. Symp. on the physics & chemistry of fission, Salzburg 1965, vol. 2 (IAEA) Vienna, 1965, p.283.

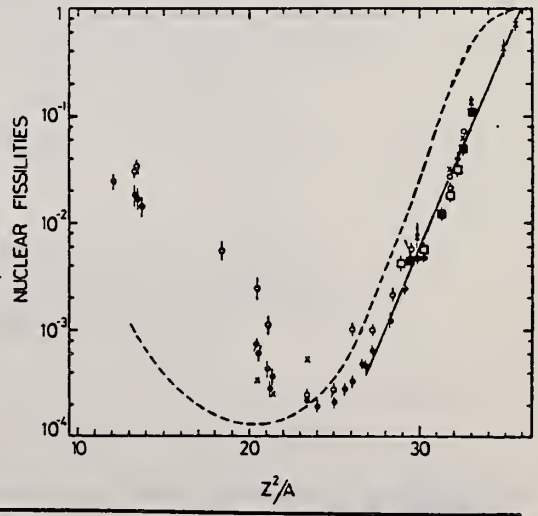

Fig. 2. Nuclear fissilities as a function of Z^2/A. Experimental points: solid circles represent our data: squares, the data from ref. [4]); open circles, the data from ref. [7]); and crosses, the data from (p,f) experiments[20]). The straight line is the best fit calculated from our data for $Z^2/A > 26$. The dashed curve is the curve VI calculated by Nix and Sassi[12]).

REF. G. M. Gurevich, L. E. Lazareva, V. M. Mazur and G. B. Solodukhov
JETP Lett. 23, 370 (1976)
Pis'ma Zh. Eksp. Teor. Fiz. 23, 411 (1976)

ELEM. SYM.	A	Z
Ta	181	73

METHOD

REF. NO. 76 Gu 5 hmg

REACTION	RESULT	EXCITATION ENERGY	SOURCE		DETECTOR		ANGLE
			TYPE	RANGE	TYPE	RANGE	
G,MU-T	ABX	8- 21	C	35	NAI-D		4PI

We measured the total cross section for the absorption of rays in the region of $E1$ resonance for the nuclei ^{165}Ho, ^{178}Hf, ^{180}Hf, ^{181}Ta, ^{182}W, ^{197}Au, and ^{209}Bi. The singularity in the behavior of the resonance widths, observed in the region $160 < A < 185$, is apparently due to the influence of the neutron subshell $N = 108$.

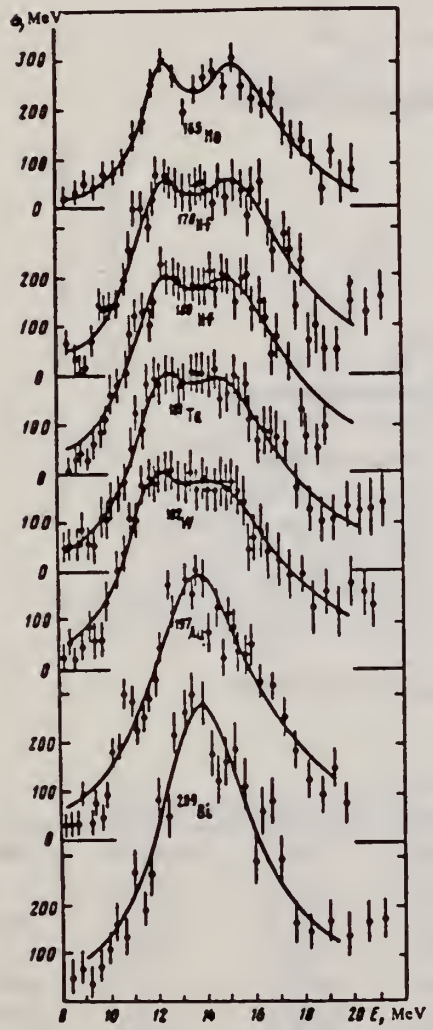

FIG. 1. Total photoabsorption cross sections for the nuclei ^{165}Ho, ^{178}Hf, ^{180}Hf, ^{181}Ta, ^{182}W, ^{197}Au, ^{209}Bi.

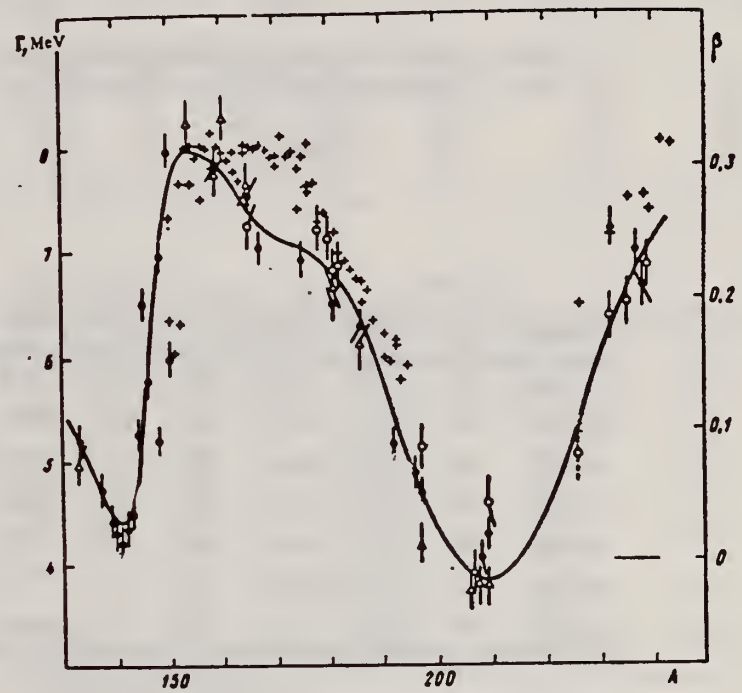

FIG. 2. Widths Γ of $E1$ giant resonance in the region of nuclei with $A > 150$ according to the data of Saclay (●), Livermore (Δ), and the Institute of Nuclear Research of the USSR Academy of Sciences (○). The crosses mark the deformation parameters β.

over

U.S. DEPARTMENT OF COMMERCE
NATIONAL BUREAU OF STANDARDS

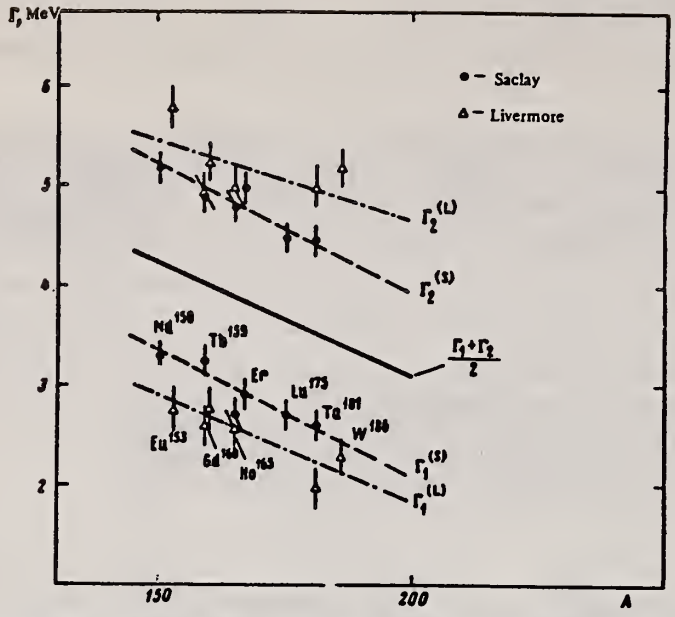

FIG. 3. Width of Lorentz lines approximating the photoabsorption cross sections, for deformed nuclei in the region $150 < A < 185$.

Nucleus	σ_1 mb	Γ_1 MeV	E_1 MeV	σ_2 mb	Γ_2 MeV	E_2 MeV	$\frac{\sigma_2\Gamma_2}{\sigma_1\Gamma_1}$	Q_0 b	β
Ho-165	235	2.0	12.2	272	4.0	15.5	2.3	6.8±0.8	0.29
Hf-178	291	3.1	12.2	334	4.9	15.5	1.8	7.5±0.8	0.28
Hf-180	286	3.2	12.2	324	5.1	15.3	1.8	7.2±0.8	0.27
Ta-181	272	3.0	12.1	316	5.1	15.0	2.0	6.8±0.8	0.26
W-182	267	3.2	11.9	303	5.6	14.8	2.0	7.2±0.8	0.26
Au-197	535	5.2	13.7	...	...	...	...	...	...
Bi-209	600	4.6	13.8	...	...	...	...	...	...

REF.		ELEM. SYM.	A	Z
	A. Suzuki and K. Shoda Nucl. Phys. A260, 172 (1976)	Ta	181	73

METHOD	REF. NO.	
	76 Su 2	egf

REACTION	RESULT	EXCITATION ENERGY	SOURCE		DETECTOR		ANGLE
			TYPE	RANGE	TYPE	RANGE	
E,P	ABX	12- 23	D	16- 23	MAG-D		125

Proton yields obtained by summing protons with energies above levels given in tables.

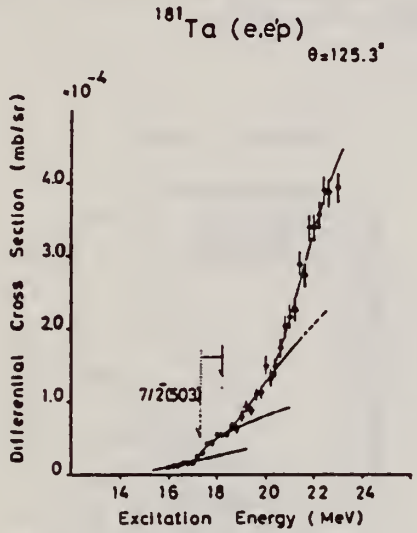

Fig. 6. Cross section of the ^{181}Ta(e, e'p) reaction. See also the caption to fig. 2.

TABLE 1

Parameters of the present experiment

Target	Atomic number	Purity (%)	Thickness (mg/cm²)	Lowest proton energy (MeV)	Bin size (keV)	Range of measurement (MeV)
^{159}Tb	65	99.9 (natural)	14.87	4.70	100	15.0 –17.5
^{165}Ho	67	99.9 (natural)	11.64	4.70	100	15.5 –17.5
^{169}Tm	69	99 (natural)	13.40	4.70	100	15.0 –18.0
^{175}Lu	71	99.87 (enriched)	5.24	5.34	150	15.05–20.0
^{181}Ta	73	99.9 (natural)	6.73	6.16	200	16.0 –23.0

TABLE 3

Displacement energies obtained from the present data and the estimates with eqs. (20) and (21)

Target	Resonance	E^* (MeV)	E_d (exp) (MeV)	E_d[a]) (MeV)	$E_d(\delta = 0.3)$[b]) (MeV)
^{159}Tb	1st	15.75±0.15	15.58	16.06	15.93
	2nd	16.50±0.15	15.46		
^{165}Ho	1st	16.15±0.14	15.64	16.38	16.25
^{169}Tm	1st	15.76±0.13	16.20	16.76	16.63
	2nd	16.34±0.14	16.22		
^{175}Lu	1st	16.44±0.13	16.75	17.07	16.93
	2nd	17.45±0.15	16.35		
^{181}Ta	1st	17.31±0.15	16.40	17.38	17.24

[a]) Estimated with eq. (20).
[b]) Estimated with eq. (21).

TABLE 4

Deformation parameters of IAS δ_{IAR} derived from the (e, e'p) result

Target	Resonance	IAS	Parent state	$\delta_{IAR}-\delta_p$[a])	δ_p (assumed)	δ_{IAR}[a])
^{159}Tb	1st	$\frac{3}{2}^-$[521]	ground	—0.008	0.31	0.30
	2nd	$\frac{1}{2}^-$[512]	875 keV	—0.016		0.29
^{165}Ho	1st	$\frac{7}{2}^+$[633]	ground	—0.023	0.30	0.28
^{169}Tm	1st	$\frac{1}{2}^-$[521]	ground	—0.018	0.29	0.27
	2nd	$\frac{1}{2}^-$[510]	565 keV	—0.019		0.27
^{175}Lu	1st	$\frac{7}{2}^-$[514]	ground	—0.010	0.28	0.27
	2nd	$\frac{7}{2}^-$[503]	1420 keV	—0.029		0.25
^{181}Ta	1st	$\frac{7}{2}^-$[503]	670 keV	—0.046	0.26	0.21

The assumed deformation parameters for the parent states δ_p are also shown.
[a]) The errors are about ±0.01.

REF. A. Suzuki, K. Shoda, M. Sugawara, T. Saito, H. Miyase, S. Oikawa, J. Uegaki, M.N. Thompson, K.J.F. Allen, H.J. Askin, and B.N. Sung
Nucl. Phys. A257, 477 (1976)

ELEM. SYM.	A	Z
Ta	181	73

METHOD

REF. NO. 76 Su 3 egf

REACTION	RESULT	EXCITATION ENERGY	SOURCE TYPE	SOURCE RANGE	DETECTOR TYPE	DETECTOR RANGE	ANGLE
E,P	ABX	16- 28	D	16- 28	MAG-D		90

G,P SIG DERIVED

TABLE 1

Parameters of the (γ, p) cross section of ^{181}Ta

	(γ, p)	(γ, n) ref. [11])	(γ, n) ref. [12])	Theory
$\int \frac{d\sigma}{d\Omega} dE$ (mb · MeV/sr)	0.75[a])			
$\int \sigma dE$ (mb · MeV)	9.36[b])	2983	2470 ± 350	
σ_{-1}[c]) (mb)	0.42	205	170	
E^R (MeV)	22.7[d])	12.30, 15.23	12.4, 15.1	
$\frac{\sigma_{-1}(T_>)}{\sigma_{-1}(T_<)}$		0.0020[e])	0.0025[e])	0.010[f])
ΔE (MeV)		8.4[g])	8.5[g])	6.1[h])

[a]) Integrated energy region is 16.5–28 MeV.
[b]) An isotropic angular distribution was assumed [2]).
[c]) $\sigma_{-1} = \int [\sigma/E] dE$.
[d]) Determined by $\int_{16.5}^{28} \sigma(\gamma, p) dE / \int_{16.5}^{28} [\sigma(\gamma, p)/E] dE$.
[e]) $\sigma_>$ and $\sigma_<$ were assumed equal to $\sigma(\gamma, p)$ and $\sigma(\gamma, n)$.
[f]) Ref. [15]).
[g]) $E_<$ was assumed as one-third of the lower E^R plus two-thirds of the upper E^R in $\sigma(\gamma, n)$ (see text).
[h]) Calculated with eq. (2).

[2] M.E. Toms et al., Phys. Rev. 98, 626 (1955).
[15] S. Fallieros et al., Nucl. Phys. A147, 593 (1970).

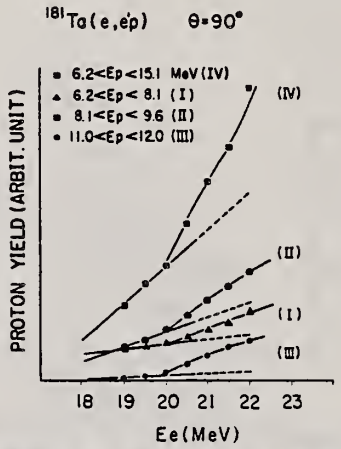

Fig. 5. The (e, e'p) cross sections for four energy regions at 90°. Statistical errors are included in each symbol.

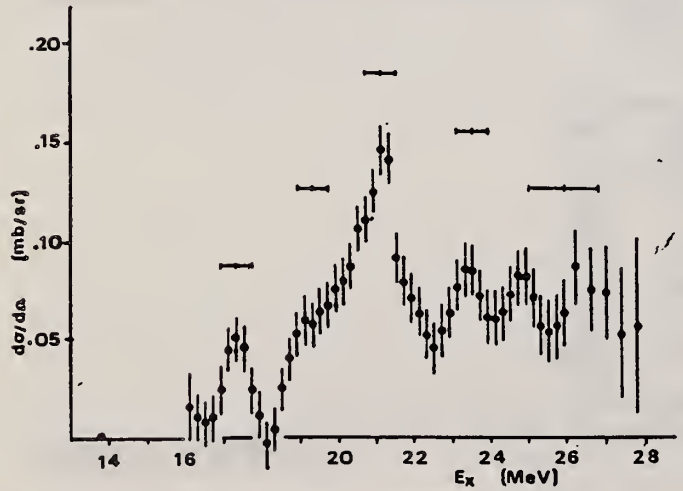

Fig. 3. The (γ, p) cross section of ^{181}Ta analysed by Cook's method from the (e, e'p) cross section shown in fig. 2.

REF. T. Bar-Noy and R. Moreh
Nucl. Phys. A288, 192 (1977)

ELEM. SYM.	A	Z
Ta	181	73

METHOD

REF. NO. 77 Ba 9 egf

REACTION	RESULT	EXCITATION ENERGY	SOURCE		DETECTOR		ANGLE
			TYPE	RANGE	TYPE	RANGE	
G,G	ABX	8- 12	D	8- 12	SCD-D		140

Abstract: Differential cross sections for elastic and inelastic Raman scattering from [illegible]Lu and [illegible]Ta were measured. Five photon energies between 8.5 and 11.4 MeV were used and were obtained from the (n,γ) reaction on Ni and Cr using thermal neutrons. The results are compared with calculations using a modified simple rotator model (SRM) of the giant dipole resonance (GDR) in which the effect of Delbrück scattering was incorporated. In general, fair agreement between theory and experiment is obtained. A new set of GDR parameters is extracted, based on photon scattering data and, as expected, yield better agreement between experimental and predicted cross sections.

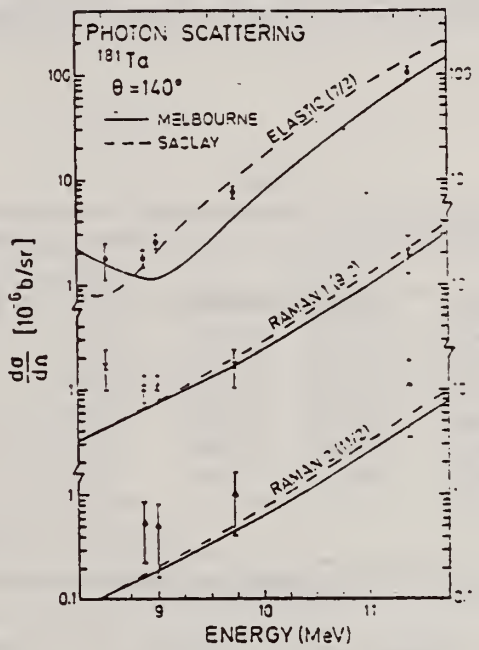

Fig. 3. Elastic and Raman inelastic differential cross sections for ^{181}Ta at 140°. The solid and dashed lines were calculated by using GDR parameters extracted from the photoneutron data of the Melbourne and Saclay groups (table 2). The elastic curves include contributions from Thomson, Delbrück and nuclear resonance scattering.

over

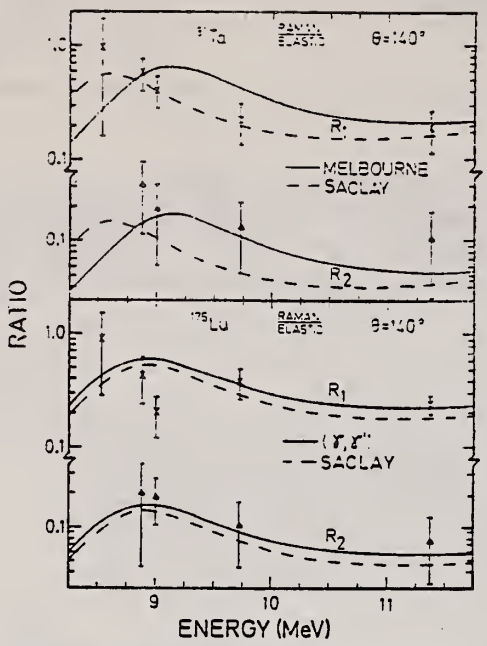

Fig. 5. Ratios of Raman/elastic scattering cross sections at 140° for ^{175}Lu and ^{181}Ta. R_1 and R_2 refer to the first and second Raman lines (fig. 1). The GDR parameters used in calculating the nuclear resonance amplitudes are explained in the captions to figs. 3 and 4.

TABLE 1

Differential cross sections (in μb/sr) of elastic and Raman inelastic scattering at $\theta = 140°$

E (MeV)	^{175}Lu elastic $I_0 = \frac{7}{2}^+$	^{175}Lu Raman 1 $\frac{5}{2}^+$, 114	^{175}Lu Raman 2 $\frac{11}{2}^+$, 251	^{181}Ta elastic $I_0 = \frac{7}{2}^+$	^{181}Ta Raman 1 $\frac{5}{2}^+$, 136	^{181}Ta Raman 2 $\frac{11}{2}^+$, 301
8.53	2.2±1.0	2.0±1.0	0.9±0.7	1.8±0.7	1.7±0.7	
8.88	2.3±0.6	1.0±0.5	0.5±0.3	1.8±0.4	1.0±0.3	0.5±0.3
9.00	3.5±1.0	0.7±0.2	0.7±0.2	2.5±0.3	1.0±0.3	0.5±0.3
9.72	6.2±1.1	2.4±0.7	0.7±0.4	7.6±1.0	1.7±0.7	1.0±0.6
11.39	120 ±20	31 ±7	10 ±5	107 ±15	21 ±8	11 ±8
11.39 [a])				131 ±14	17 ±4	17 ±4

[a]) Experimental results of ref. [3]) (calculated for 140° from measured values at 150°).

[3]H.E. Jackson, G.E. Thomas and K.J. Wetzel, Phys. Rev. C11, 1664 (1975)

R.S. Hicks, I.P. Auer, J.C. Bergstrom and H.S. Caplan
Nucl. Phys. A278, 261 (1977)

ELEM. SYM.	A	Z
Ta	181	73

METHOD

REF. NO.: 77 Hi 2 | egf

REACTION	RESULT	EXCITATION ENERGY	SOURCE TYPE	SOURCE RANGE	DETECTOR TYPE	DETECTOR RANGE	ANGLE
E,E/	LFT	3 - 30	D	79-118	MAG-D		DST

Abstract: The giant resonance region of ^{181}Ta has been investigated by means of inelastic electron scattering, with primary electron energies of 79.1 to 118.3 MeV. A peak-fitting procedure was employed to separate the measured spectrum into nine different resonance components. Multipolarity and strength assignments were deduced using DWBA analysis with the Goldhaber-Teller and Steinwedel-Jensen models. In addition to the well-known giant dipole structure, other resonances were identified at 23.2 ± 0.3 MeV (E2), 9.5 ± 0.2 and 11.5 ± 0.2 MeV (E2 or E0), 19.5 ± 0.8 MeV (E3), 3.70 ± 0.14 MeV (E3 or E4), and 5.40 ± 0.15 MeV (E4 or E5). The model dependence of the analysis is discussed.

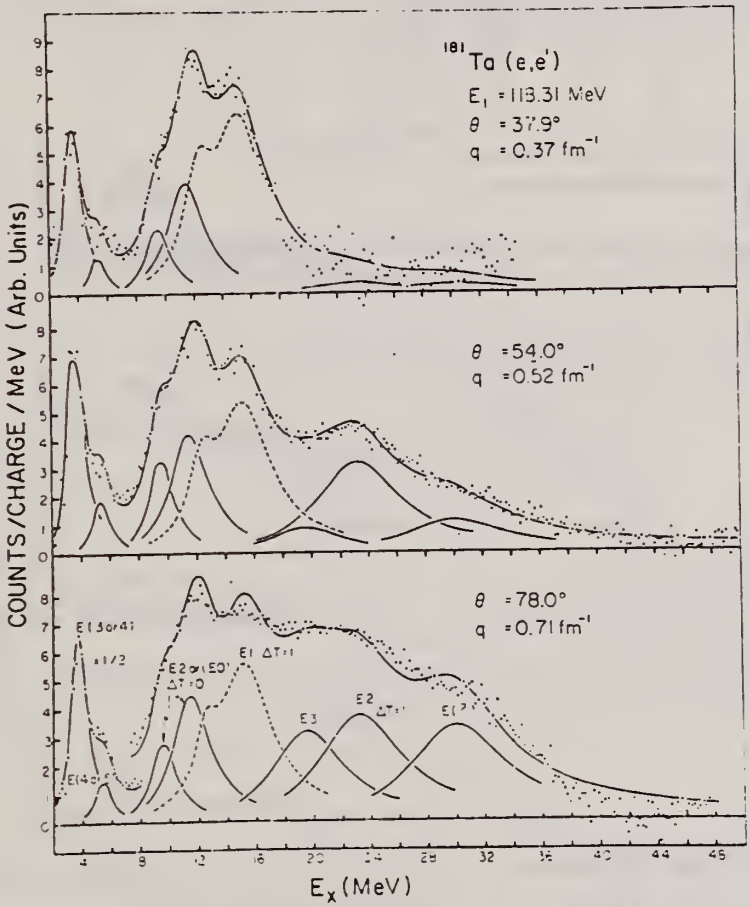

Fig. 5. Three spectra after subtraction of the mean fitted backgrounds. At low momentum transfer the dipole structure dominates the measured cross section, however, beginning with resonances centred at 9.5, 11.5 and 23.2 MeV, the importance of the other peaks grows with increasing q. In the determination of the errors in the peak parameters the uncertainty in the background was taken into account.

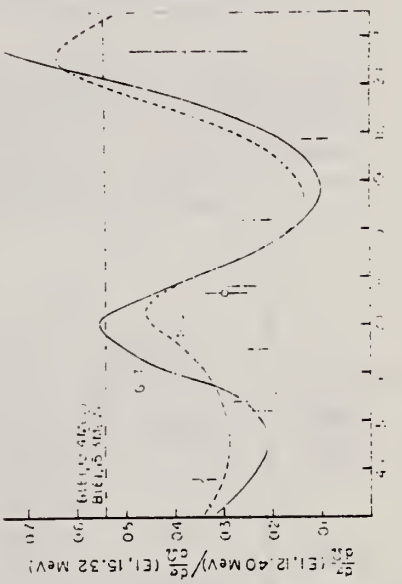

Fig. 7. Ratio of the electroexcitation cross sections for the 12.4 and 15.3 MeV dipole resonances of ^{181}Ta. The continuous (El. / ... 10) and dashed (Sl. / ... 115) curves were computed in DWBA, assuming pure proton charge exchange for the major and minor nuclear axes. The normalization of these curves is given by the ratio of the photonuclear transition probabilities (dot dash curve).

(over)

Results of DWBA analysis

E_x (MeV)	$E_x A^{1/3}$ (MeV)	Γ (MeV)	EL	ΔT	Analysis model [a]	f [b,c]	R_t [b] (fm)	$B(EL)$ ($e^2 \cdot fm^{2L}$) [c]	% EWSR	Weisskopf (s.p.u.)
3.70 ± 0.14	20.9	1.39 ± 0.23	(E3) [d]	0	GT	0.80	6.4	$(6.7 \pm 3.0) \times 10^4$	3.0 ± 1.5	3.8
			(E4) [d]	0	GT	0.94	8.0	$(2.6 \pm 1.4) \times 10^7$	11 ± 6	31.0
			(E2)	0	GT	0.85	6.4	$(9.2 \pm 3.4) \times 10^2$	5 ± 2	3.1
5.40 ± 0.15	30.5	1.38 ± 0.65	(E4) [d]	0	GT	0.90	6.8	$(1.40 \pm 0.25) \times 10^7$	0.8 ± 0.2	1.7
			(E5) [d]	0	GT	0.92	8.4	$(7.6 \pm 1.3) \times 10^8$	4 ± 1	19.0
			(E2)	0	GT	0.85	6.4	$(1.9 \pm 0.5) \times 10^2$	1.5 ± 0.4	0.5
9.54 ± 0.20	54.0	2.07 ± 0.35	E2	0	GT	0.80	6.0	$(5.8 \pm 3.2) \times 10^2$	8 ± 4	1.6
			(E0)	0	HBM	0.80	7.1	$(1.20 \pm 0.65) \times 10^3$	13 ± 7	
11.47 ± 0.22	64.9	3.13 ± 0.55	E2	0	GT	0.80	6.0	$(1.34 \pm 0.50) \times 10^3$	22 ± 8	3.7
			(E0)	0	HBM	0.80	7.1	$(3.0 \pm 1.0) \times 10^3$	40 ± 13	
(9.54, 11.47)	61.6		E2	0	GT	0.80	6.0	$(1.92 \pm 0.60) \times 10^3$	30 ± 9	5.3
			(E0)	0	HBM	0.80	7.1	$(4.2 \pm 1.2) \times 10^3$	53 ± 15	
12.40	70.1	2.33	E1	1	GT	1.00	8.1	26.0 ± 13.1	56 ± 22	4.2
					SJ	1.15	7.8	22.0 ± 13.2	47 ± 22	3.6
15.32	86.7	4.23	E1	1	GT	1.00	6.6	61.0 ± 18.7	119 ± 32	7.1
					SJ	1.15	6.3	54.0 ± 25.1	105 ± 43	6.3
(12.40, 15.32)	81.1		E1	1	GT	1.00		87.0 ± 22.8	175 ± 39	11.3
					SJ	1.15		76.0 ± 28.3	153 ± 58	9.9
19.5 ± 0.8	110.3	6.0 ± 1.5	E3	0	GT	0.80	6.4	$(5.2 \pm 3.3) \times 10^4$	12 ± 8	2.9
23.2 ± 0.3	131.2	7.0 ± 1.2	E2	1	GT	0.73	5.5	$(9.2 \pm 2.5) \times 10^2$	20 ± 5	2.5
					SJ	0.87	5.3	$(8.5 \pm 2.3) \times 10^2$	18 ± 5	2.3
30.0 ± 3.0	170	8^{+6}_{-4}	(E4) [d]	0	GT	0.80	6.8	$(4.7 \pm 2.2) \times 10^6$	15 ± 7	5.5
			(E2)	1	GT	0.73	5.5	$(1.1 \pm 0.6) \times 10^2$	3 ± 2	0.3

[a]) Indicated analysis models are Goldhaber-Teller, Steinwedel-Jensen, and hydrodynamic breathing mode.
[b]) Uncertainties in f and R_t are approximately 5 %.
[c]) Unit for the monopole matrix element, $|M_{if}|^2$, is $e^2 \cdot fm^4$.
[d]) For resonances containing possible E2 admixture, tabulated non-E2 strengths represent means of fits with and without quadrupole contributions.
[e]) For E1 transitions the ratio f is relative to ground-state semi-major or semi-minor radius; for all other transitions f refers to the averaged-over-orientation radius.

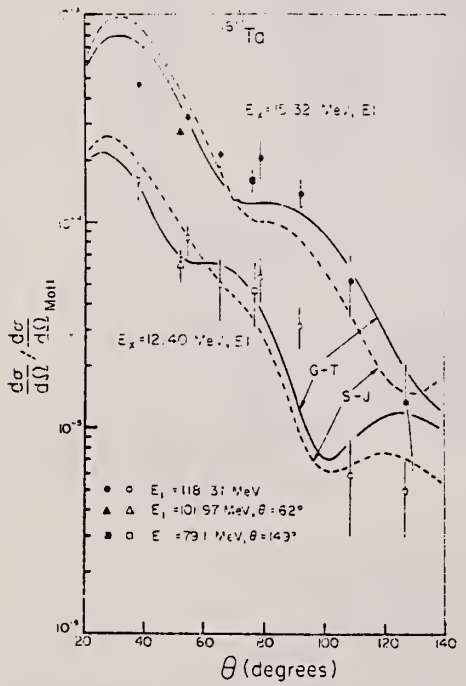

Fig. 6. Differential cross sections for 118.3 MeV electrons inelastically scattering from the 12.4 and 15.3 MeV components of the GDR of ^{181}Ta. The data points from measurements with 79.1 and 102.0 MeV electrons have been repositioned as described in the text. The continuous and dashed curves were computed in DWBA using the Goldhaber-Teller (f = 1.00) and Steinwedel-Jensen (f = 1.15) models.

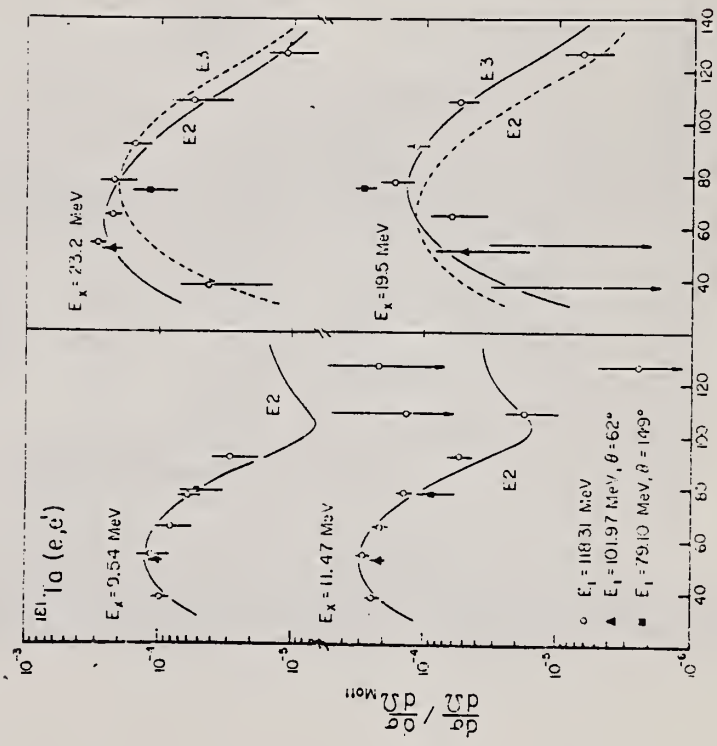

Fig. 8. Differential cross sections for 118.3 MeV electrons scattering from giant resonances of ^{181}Ta. Resonances fitted with E2 curves are equally well described by E0 calculations.

REF. H. Miura and Y. Torizuka
Phys. Rev. C 16, 1688 (1977)

ELEM. SYM.	A	Z
Ta	181	73

METHOD

REF. NO. 77 Mi 8 hmg

REACTION	RESULT	EXCITATION ENERGY	SOURCE		DETECTOR		ANGLE
			TYPE	RANGE	TYPE	RANGE	
E,E/	FMF	8- 30	D	150-250	MAG-D		DST

G-WIDTH,B(EL),J-PI

A new resonance peak has been found at 14.7 ± 0.2 MeV in spectra of inelastic electrons scattered from ^{181}Ta. The peak exhausts a significant part of the $E0$ sum rule and is characterized by a narrow width of about 2.1 MeV. The giant quadrupole resonances splits into two peaks at 9.5 ± 0.2 and 11.3 ± 0.2 MeV which deplete (29 ± 5)% and (63 ± 8)% of the isoscalar $E2$ energy-weighted sum rule, respectively.

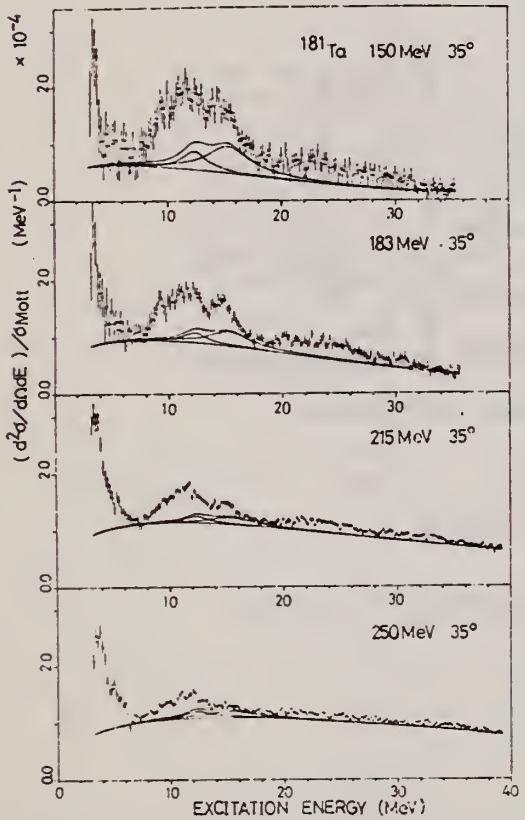

FIG. 1. Spectra of inelastic electrons scattered from ^{181}Ta. The radiation tail was subtracted by the calculation. Solid curves represent the giant dipole resonance and underlying background.

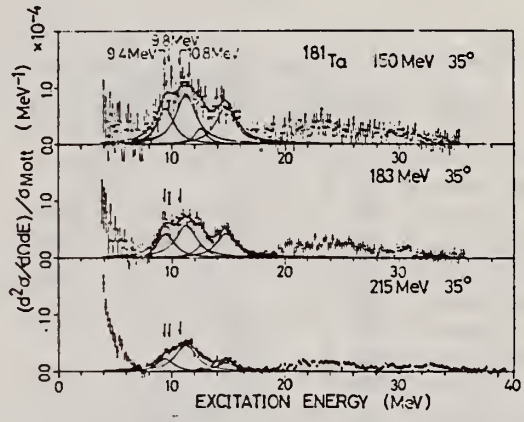

FIG. 2. After the subtraction of the GDR and underlying background the remaining cross section is displayed. The overlapping peaks were decomposed into 9.5-, 11.3-, and 12.6-MeV components and 14.7-MeV peak by a χ^2 fitting procedure. Arrows indicate the quadrupole $K=0$, 1, and 2 states at 9.4, 9.8, and 10.8 MeV, respectively, calculated from the dipole energies.

TABLE I. Line width Γ, $B(EL)$ values, and percentages of the EWSR in ^{181}Ta.

ω (MeV)	J^π	Mode	Γ (MeV)	$B(E2\uparrow)$ (e^2 fm^4)	$B(E0\uparrow)$ (fm^4)	EWSR (%)
9.5 ± 0.2	2^+	$T=0$	1.8 ± 0.6	2147 ± 334		29 ± 5
11.3 ± 0.2	2^+	$T=0$	2.2 ± 0.7	3975 ± 482		63 ± 8
12.6 ± 0.2	2^+	$T=0$	1.3 ± 0.8	634 ± 231		11 ± 5
14.7 ± 0.2	0^+	$T=0$	2.1 ± 0.3		4543 ± 371	94 ± 8
or	2^+	$T=0$		1971 ± 162		41 ± 4
18 ~ 30	2^+	$T=1$		3229 ± 194		74 ± 6

REF. A.V. Mitrofanova, V.I. Noga, A.I. Popov, Yu.N. Ranyuk and Yu.N. Telegin
Yad. Fiz. 25, 926 (1977)
Sov. J. Nucl. Phys. 25, 493 (1977)

ELEM. SYM.	A	Z
Ta	181	73

METHOD

REF. NO.	
77 Mi 11	hmg

REACTION	RESULT	EXCITATION ENERGY	SOURCE		DETECTOR		ANGLE
			TYPE	RANGE	TYPE	RANGE	
G,SPL	ABY	THR-999	C	600-999	ACT-I		4PI

The induced activity method has been used to measure the yields of 15 photonuclear reactions in tantalum and tungsten nuclei in the photon energy range 600–1300 MeV. The cross sections have been calculated in the approximation of a rectangular bremsstrahlung spectrum. Rudstam's semiempirical formula has been used to analyze the experimental data. For the reactions in tungsten the ratios of the yields produced by photons and electrons have been measured.

999=1.3 GEV

TABLE I.

№	Initial nucleus	Emitted nucleus	Residual nucleus	$\bar{\sigma}_k$ (600–1300 MeV), mb	$E_{\gamma\,max}$=1000 MeV: σ_Q, mb (exp)	σ_Q, mb (theory)	σ_Q, mb (Ref. 6)	$\frac{\sigma_Q}{\bar{\sigma}_k}$
1	$^{182-181,180}_{74}W$	4p, 9–13n	$^{169}_{70}Yb$	2.2	3.1±0.6	2.36	–	24.5±4.9
		3p, 10–15n	$^{169}_{71}Lu$					
2	$^{182-181,180}_{74}W$	2p, 5–9n	$^{173}_{72}Hf$	4.0	5.6±1.1	0.58	–	22±4
3	$^{182-184,186}_{74}W$	4p, 11–15n	$^{167}_{70}Yb$	2.0	1.9±0.4	1.58	–	27±5
4	$^{182-184,186}_{74}W$	3p, 8–12n	$^{171}_{71}Lu$	1.96*	2.2±0.4*	3.9	–	23±4
		2p, 9–13n	$^{171}_{72}Hf$					
5	$^{182-184,186}_{74}W$	3p, 6–10n	$^{173}_{71}Lu$	4.0	5.5±1.1	4.6	–	27±5
		2p, 7–11n	$^{173}_{72}Hf$					
6	$^{182-181,180}_{74}W$	10p, 26–30n	$^{146}_{61}Nd$	10.4	5.0±1.0	0.10	–	–
7	$^{183,182,180}_{74}W$	1p, 0–4n	$^{181}_{73}Ta$	1.63	2.3±0.5	–	–	26±5
8	$^{183,182,180}_{74}W$	2p, 0–3n	$^{181}_{72}Hf$	0.09	0.12±0.02	–	–	31±6
9	$^{181}_{73}Ta$	3p, 9n	$^{169}_{70}Yb$	2.3	3.6±0.7	3.2	7.07	–
		2p, 10n	$^{169}_{71}Lu$					
10	$^{181}_{73}Ta$	1p, 3n	$^{175}_{72}Hf$	3.3	5.8±1.1	0.7	8.9	–
11	$^{181}_{73}Ta$	2p, 6n	$^{173}_{71}Lu$	2.6	6.2±1.2	2.44	6.55	–
		1p, 7n	$^{173}_{72}Hf$					
12	$^{181}_{73}Ta$	3p, 11n	$^{167}_{70}Yb$	2.0	2.9±0.6	1.9	3.67	–
		4p, 10n	$^{167}_{69}Tm$					
13	$^{181}_{73}Ta$	2p, 8n	$^{171}_{71}Lu$	1.52*	2.4±0.5*	4.8	3.67	–
		1p, 9n	$^{171}_{72}Hf$					
14	$^{181}_{73}Ta$	9p, 26n	$^{146}_{64}Gd$	9.6	8.5±1.7	0.12	–	–

*In view of the absence of data on the absolute intensities of the γ lines in the spectrum of ^{171}Lu activity, in calculation of σ_Q the intensity of the peak E_γ = 739 keV was taken as 100%.

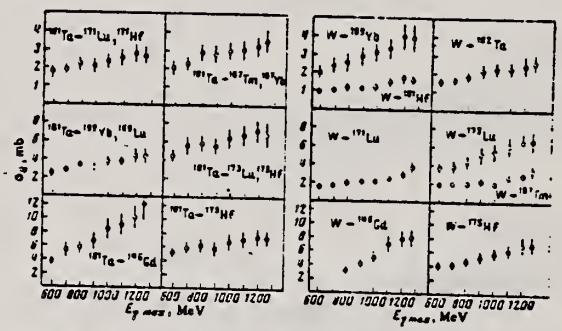

FIG. 2. Reaction yields: a) in ^{181}Ta, b) in W.

REF. J.J. Murphy II, H.J. Gehrhardt and D.M. Skopik
Nucl. Phys. A277, 69 (1977)

ELEM. SYM.	A	Z
Ta	181	73

METHOD

REF. NO. 77 Mu 3 egf

REACTION	RESULT	EXCITATION ENERGY	SOURCE		DETECTOR		ANGLE
			TYPE	RANGE	TYPE	RANGE	
E,A	ABX	14-100	D	100	MAG-D		50

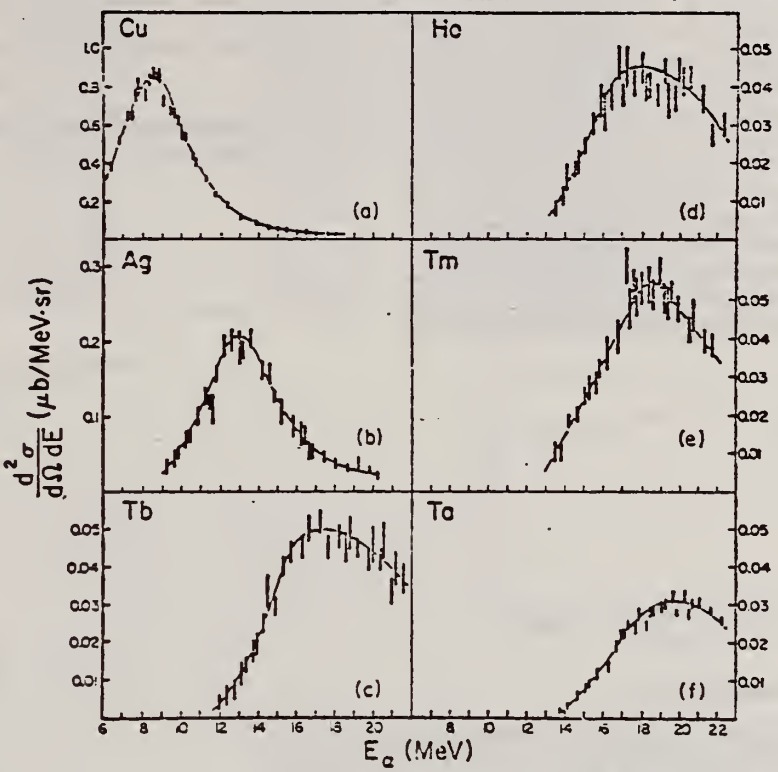

Fig. 1. The α-particle energy spectra at 50° in the lab for the six nuclei studied. Note that as Z increases, the cross section decreases and the energy of the peak increases. Errors are statistical. Curves are to guide the eye.

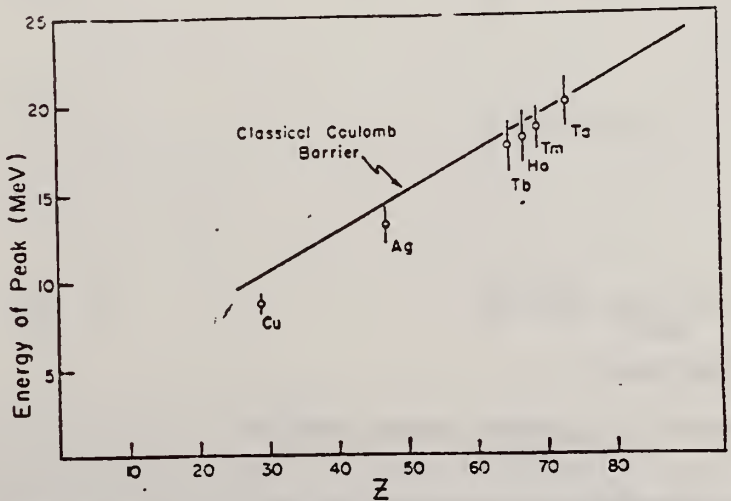

Fig. 2. Energy of the cross section peak as a function of Z. The solid line is the energy of the classical Coulomb barrier.

REF. V. Bellini, V. Emma, A.S. Figuera, S. Lo Nigro, C. Milone, G.S. Pappalardo, G. Bologna
Il Nuovo Cimento 47A, 529 (1978)

ELEM. SYM.	A	Z
Ta	181	73

METHOD

REF. NO. 78 Be 10 hg

REACTION	RESULT	EXCITATION ENERGY	SOURCE TYPE	SOURCE RANGE	DETECTOR TYPE	DETECTOR RANGE	ANGLE
G,F	RLX	180-999	C	220-999	TRK-D		4PI

Summary. — The photofission yields of Re, W and Ta induced by a coherent bremsstrahlung beam from 1000 MeV electrons striking a diamond single crystal have been measured. The experiment has been performed at eighteen different energies of the main peak of the photon spectrum, in the energy range between 220 MeV and 550 MeV, by detecting the fission fragments with glass sandwiches. The behaviour of the photofission cross-section has been deduced from the experimental yields by using an appropriate unfolding method. The obtained curves clearly show a first resonance centred at a photon energy $k \simeq 350$ MeV with a FWHM $\simeq 145$ MeV, while there is a hint of a second resonance at $k \simeq 750$ MeV. Information on the energy dependence of the nuclear fissility from 100 MeV to 1000 MeV has been deduced from the comparison of the estimated photofission cross-section with the total photon interaction cross-section. It has been found that the photomesonic model of the fission process permits to explain the energy dependence of our photofission cross-sections if a nuclear fissility increasing with photon energy is assumed.

COHERENT BREM.

Zero cross section assumed below 180 MeV.

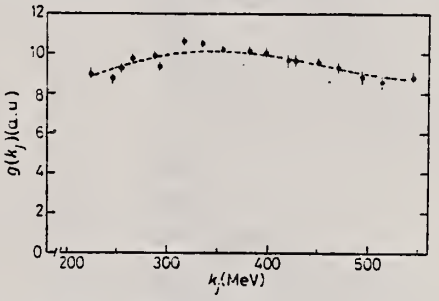

Fig. 5. – See caption to fig. 3. Results for Ta.

Fig. 3. – Photofission yields per equivalent quantum as a function of the first-peak energy k_f of photons. The dots are the experimental data; the dashed curve represents the yield function recalculated from the $f(k)$ data. Results for Re.

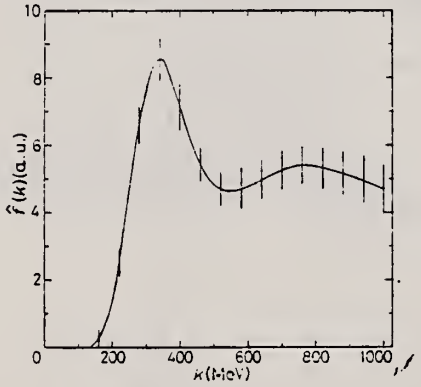

Fig. 8. – See caption to fig. 6. Result for Ta(γ, f).

Fig. 6. – Photofission cross-section estimated by our unfolding method. Results for Re (γ, f).

(over)

TABLE II. – *Estimated $\hat{f}_t$ values and corresponding errors.* All the data are given in arbitrary units.

k	$\hat{f}(k)$ (arbitrary units)		
(MeV)	Re	W	Ta
100	-0.31 ± 0.85	-0.14 ± 0.85	-0.49 ± 0.87
160	0.03 ± 0.31	0.24 ± 0.31	0.26 ± 0.33
220	1.95 ± 0.41	2.50 ± 0.41	2.51 ± 0.41
280	6.26 ± 0.53	6.51 ± 0.53	6.63 ± 0.55
340	8.90 ± 0.69	8.75 ± 0.69	8.56 ± 0.68
400	8.16 ± 0.72	8.38 ± 0.72	7.15 ± 0.70
460	6.10 ± 0.51	6.34 ± 0.51	5.43 ± 0.49
520	4.83 ± 0.47	5.04 ± 0.47	4.70 ± 0.48
580	4.70 ± 0.57	4.95 ± 0.57	4.72 ± 0.58
640	4.96 ± 0.59	5.20 ± 0.59	4.98 ± 0.60
700	5.41 ± 0.58	5.57 ± 0.58	5.29 ± 0.58
760	5.68 ± 0.57	5.78 ± 0.57	5.41 ± 0.57
820	5.65 ± 0.61	5.71 ± 0.61	5.32 ± 0.61
880	5.51 ± 0.67	5.53 ± 0.67	5.18 ± 0.67
940	5.38 ± 0.74	5.36 ± 0.74	4.98 ± 0.73
1000	5.23 ± 0.80	5.18 ± 0.80	4.70 ± 0.77

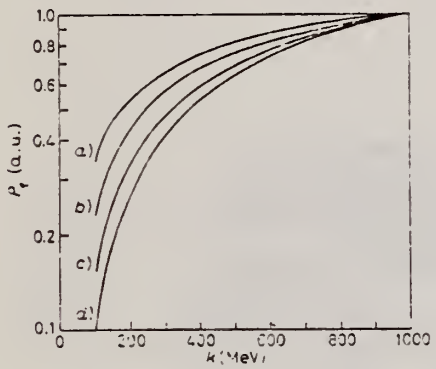

Fig. 11.

Fig. 11. – Nuclear fissility P_f as a function of the photon energy k. The curves are normalized at $k = 1000$ MeV. *a*) Bi, *b*) Pb, *c*) Au, *d*) Ta.

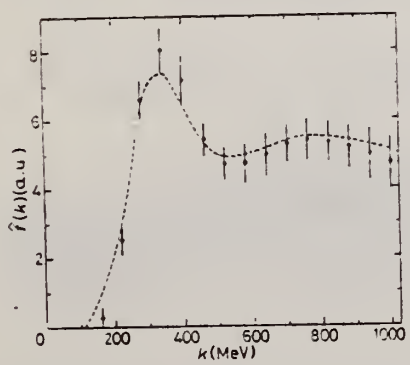

Fig. 12.

Fig. 12. – Photofission cross-section of Ta *vs.* the photon energy k. The dots are the $f(k)$ data of the present analysis; the dashed curve represents the cross-section calculated by using the P_f energy dependence of fig. 11.

REF. S. Kahane, R. Moreh, and O. Shahal
Phys. Rev. C 18, 1217 (1978)

ELEM. SYM.	A	Z
Ta	181	73

METHOD

REF. NO. 78 Ka 6 hg

REACTION	RESULT	EXCITATION ENERGY	SOURCE TYPE	SOURCE RANGE	DETECTOR TYPE	DETECTOR RANGE	ANGLE
G,G	ABX	6- 12	C	6- 12	SCD-D		DST
		(6.84-11.39)		(6.84-11.39)			

Monoenergetic photons at eight energies in the range 6.84–11.39 MeV were elastically scattered from targets of ^{181}Ta, Pb, and ^{238}U at $\theta = 1.21°$–$1.50°$. The differential scattering cross section at such angles was measured relative to the Compton cross section. The photon beam was obtained from the Ni(n,γ) reaction using thermal neutrons. Strong evidence for the contribution of both Rayleigh and the real Delbruck amplitudes and for their destructive interference was obtained.

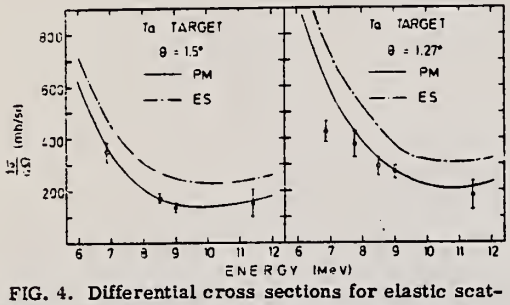

FIG. 4. Differential cross sections for elastic scattering of photons at $\theta = 1.27°$ and 1.50° from Ta. PM denotes theoretical values obtained using the Delbruck amplitudes based on Papatzacos and Mork (Refs. 3 and 4); ES denotes theoretical values obtained using the Delbruck amplitudes of Ehlotzky and Sheppey (Ref. 1).

TABLE II. Differential cross sections (mb/sr) of elastic photon scattering from Ta ($Z = 73$) at $\theta = 1.27° \pm 0.27°$ and $1.50 \pm 0.35°$. PM represent calculated values using the Delbruck amplitudes of Papatzacos and Mork; ES are those of Ehlotzky and Sheppey.

	$\theta = 1.27° \pm 0.27°$			$\theta = 1.50° \pm 0.35°$		
E (keV)	Exp.	PM	ES	Exp.	PM	ES
6 837	423 ± 40	658	773	349 ± 37	380	485
7 819	375 ± 51	415	560	...	...	...
8 533	291 ± 54	307	443	171 ± 17	168	273
8 999	270 ± 25	257	371	136 ± 15	148	243
11 388	179 ± 54	203	313	153 ± 54	162	248

[1] F. Ehlotzky and G.C. Sheppey, Nouvo Cimento 33, 1185 (1964).

[3] P. Papatzacos and K. Mork, Phys. Rev. D 12, 206 (1975); Phys. Rep. 21C, 81 (1975).

[4] T. Bar-Noy and S. Kahane, Nucl. Phys. A288, 132 (1977).

REF. J.J. Murphy, II, D.M. Skopik, J. Asai, and J. Uegaki
Phys. Rev. C 18, 736 (1978)

ELEM. SYM.	A	Z
Ta	181	73

METHOD

REF. NO. 78 Mu 9 hg

REACTION	RESULT	EXCITATION ENERGY	SOURCE		DETECTOR		ANGLE
			TYPE	RANGE	TYPE	RANGE	
E,A	ABX	5-100	D	100	MAG-D		DST

α particles from the electrodisintegration of seven nuclei with Z between 29 and 79 have been observed. Energy spectra at 50° in the laboratory for six nuclei and angular distributions for five nuclei are reported. The cross sections exhibit a broad peak whose magnitude decreases with increasing Z; the energy of the peak increases as Z increases. Angular distributions at the highest energies measured become increasingly forward peaked suggesting a direct-reaction process.

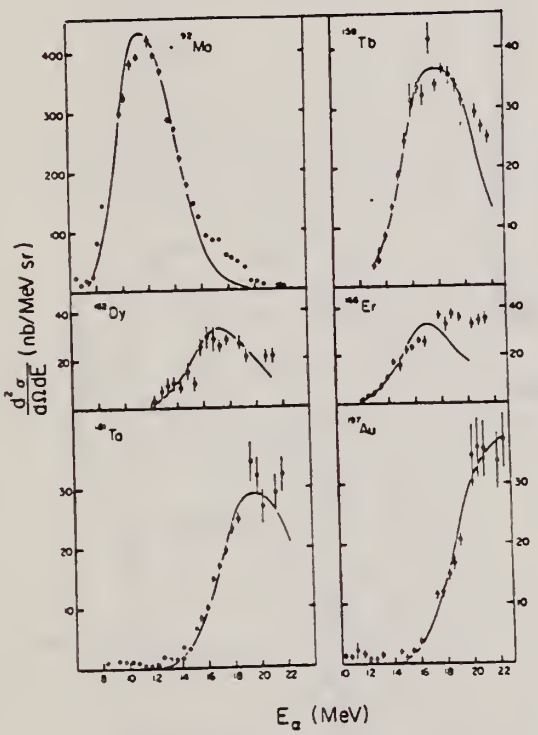

FIG. 2. The α-particle energy spectra at 50° in the laboratory for the four new nuclei studied as well as for two nuclei in which additional data have been obtained. The solid curves are the evaporation model fits described in text.

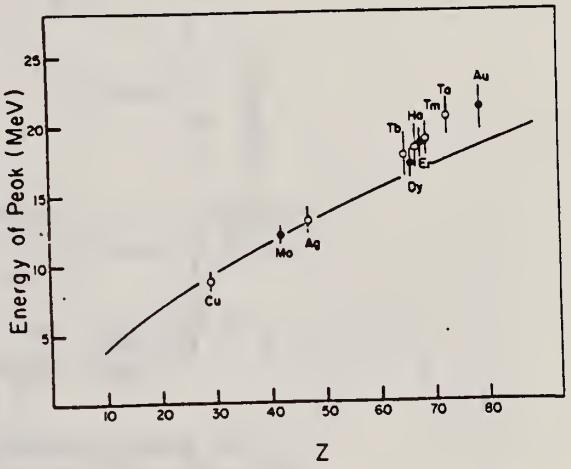

FIG. 3. Energy of the cross section peak as a function of Z. The solid line is the energy of the classical Coulomb barrier. The closed circles are the current work; the open circles are from Ref. 1.

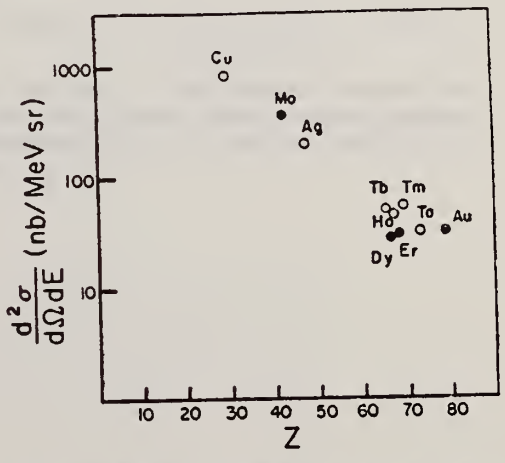

FIG. 4. Magnitude of cross section peak as a function of Z. The closed circles are the current work; the open circles are from Ref. 1.

[1] J.J. Murphy,II, H.J. Gehrhardt, and D.M. Skopik, Nucl. Phys. A277, 69 (1977)

over

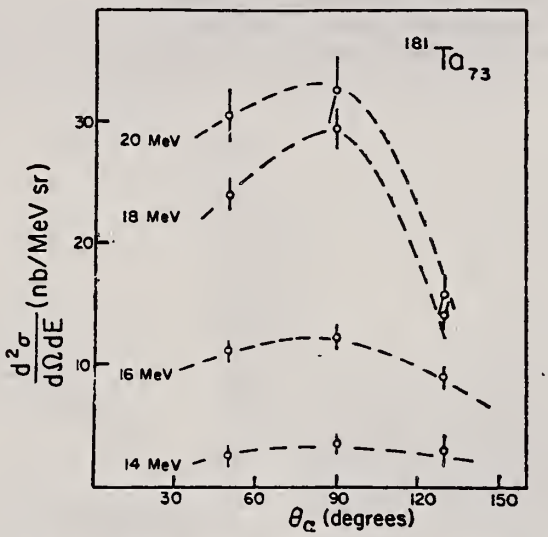

FIG. 8. Angular distributions for tantalum. The comments made for Fig. 5 apply here.

REF. F. N. Rad, T. Sasanuma, W. Bertozzi, J. Heisenberg, M. V. Hynes, S. Kowalski, H. Miska, B. Norum, C. P. Sargent, W. Turchinetz, and C. F. Williamson

Phys. Rev. Lett. 40, 368 (1978)

ELEM. SYM.	A	Z
Ta	181	73

METHOD

Remarks: *EFF. MOMENT. TRANS.

REF. NO. 78 Ra 1 hmg

REACTION	RESULT	EXCITATION ENERGY	SOURCE		DETECTOR		ANGLE
			TYPE	RANGE	TYPE	RANGE	
E,E/	FMF	0- 1	D	0*3	MAG-D	-	DST

* EFF. Q

Elastic and inelastic form factors for electron scattering from the ground-state rotational band of ^{181}Ta have been studied for momentum transfers 0.4 fm$^{-1} \leq q_{eff} \leq$ 2.7 fm^{-1} The data are shown to provide an independent check of the rotational assumption, thus adding confidence that the experimental form factors are characteristic of a stable intrinsic state associated with the rotational band. The data are also compared to a Hartree–Fock calculation using density-dependent interactions.

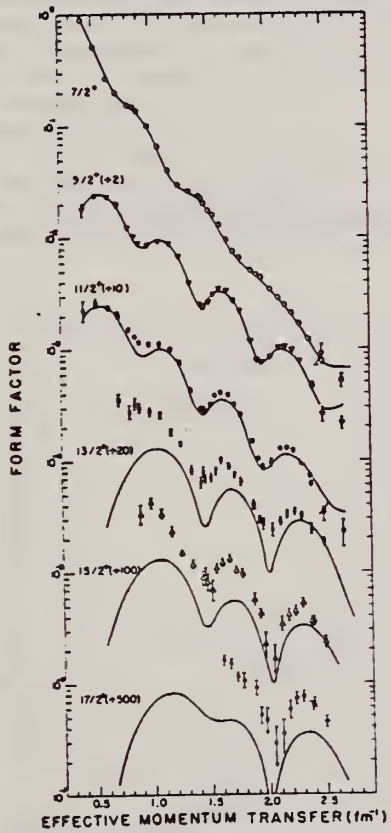

FIG. 1. Experimental "form factor" [$F = (\sigma/\sigma_{Mott})^{1/2}$] for the ground-state rotational band of ^{181}Ta as a function of effective momentum transfer. All data points were taken at 90° laboratory angle except those below $q_{eff} = 0.8$ fm^{-1} which were taken at 45°. The solid curves are the theoretical calculation based on the density-dependent interaction with filling approximation using the Hartree–Fock method.

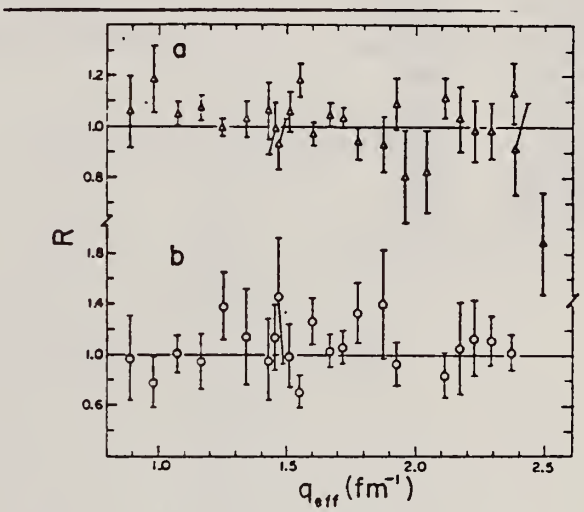

FIG. 2. The ratio (R) of the measured cross section (a) $\sigma_{11/2}$, and (b) $\sigma_{13/2}$ to that predicted by the rotational assumption from (a) $\sigma_{9/2}$, $\sigma_{13/2}$, and $\sigma_{15/2}$, and (b) $\sigma_{9/2}$, $\sigma_{11/2}$, and $\sigma_{15/2}$.

REF. P. Rulhusen, F. Smend and M. Schumacher
Z. Physik A288, 119 (1978)

ELEM. SYM.	A	Z
Ta	181	73

METHOD

REF. NO. 78 Ru 3 rs

REACTION	RESULT	EXCITATION ENERGY	SOURCE		DETECTOR		ANGLE
			TYPE	RANGE	TYPE	RANGE	
G,G	ABX	3	D	3	SCD-D		DST

Differential cross sections for the elastic scattering of 2.754 MeV photons by Ta have been measured for angles ranging from 30° to 150°. A comparison with lowest-order Delbrück theory reveals discrepancies of the same size as previously observed for Pb and Bi. Consideration is given to interference phenomena between Delbrück, Rayleigh and nuclear Thomson scattering.

3=2.754

Table 1. Differential cross sections for elastic scattering of 2.754 MeV photons by Ta ($Z=73$)

θ (deg)	$d\sigma/d\Omega_{exp}$ (μb/sr)	$d\sigma/d\Omega_{theor}$ (μb/sr)
30	76 ±30	77.6
45	43.7± 2.6	34.0
60	24.2± 1.3	18.8
75	20.4± 1.0	16.5
90	19.2± 0.6	17.9
120	25.0± 0.9	23.5
150	31.6± 2.0	29.7

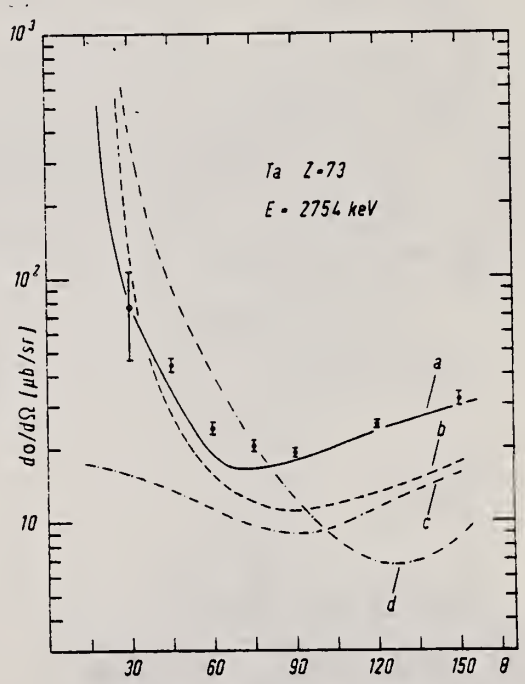

Fig. 3. Comparison of experimental differential cross sections with different predictions: (*a*): calculated from the N-, R-, T-, and D-amplitudes of Table 2. (*b*): calculated without including the real D-amplitudes. (*c*): calculated from the N- and T-amplitudes only. (*d*): calculated in the same way as (*a*) but with reversed signs of the real D-amplitudes

REF. S. A. Hayashi, S. Yamamoto, I. Kimura, K. Kobayashi, T. Mori, S. Kanazawa, H. Nishihara, S.A. Bokharee, R.W. Emmett, R.C. Block, M. Becker, D.R. Harris, B.K. Malaviya
Ann. Rpt. Res. Reac. Inst., Kyoto Univ. 13, 23 (1980)

ELEM. SYM.	A	Z
Ta	181	73

METHOD

REF. NO. 80 Ha 6 egf

REACTION	RESULT	EXCITATION ENERGY	SOURCE		DETECTOR		ANGLE
			TYPE	RANGE	TYPE	RANGE	
G,XN	SPC	7-60	C	30,60	TOF-D		DST

ANG DST WITH ACT DET

Three kinds of photoneutron targets, the cylindrical lead target, and the spherical and spheroidal tantalum targets were designed as pulsed-neutron sources with an electron linear accelerator for the fast neutron spectrum study in assemblies of reactor materials. Angular distributions of photoneutrons and X-rays from these targets bombarded by about 30- and 60-MeV electrons were obtained by the activation method and the results show fairly isotropic photoneutron distributions except to the forward and extraordinarily sharp forward peak of X-rays. Among these three targets the spheroidal tantalum target is seen to be superior to others from the viewpoints of the isotropy of photoneutrons and of a lower forward peak of X-rays even at the higher bombarding energy. However, for the lower electron energy, about 30 MeV, both the lead target and the spherical tantalum target can be usable for the above purpose, although the maximum beam power of the former is restricted to about 120 watts.

Neutron spectra from these targets were measured in the energy range from 20 keV to 10 MeV by the LINAC TOF method. It was found that neutron spectra from tantalum targets are apparently softer than that from the lead target.

With the above characteristics obtained experimentally, these targets will be used for the neutron spectra measurements in assemblies of reactor materials.

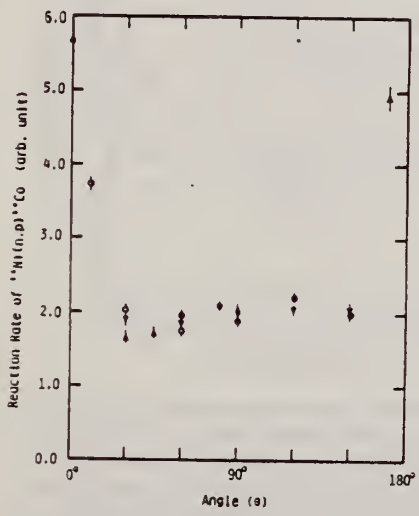

Fig. 7. Angular distribution of photoneutrons emanated from the spherical tantalum target bombarded by 36-MeV electrons. The ^{58}Co activities from Ni foils are shown. The symbols are the same as in Fig. 4.

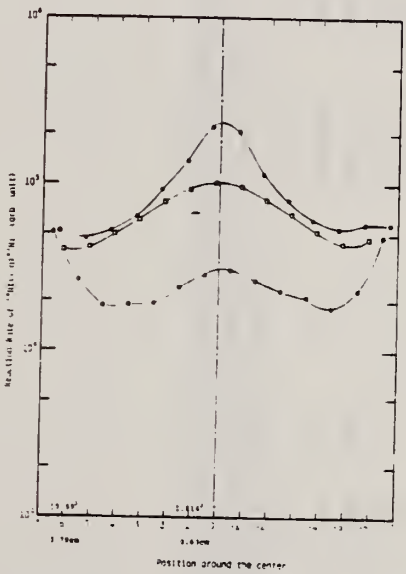

Fig. 12. Distributions of X-rays near the forward direction around the central axis of the electron beam from the spherical tantalum target bombarded by 36-MeV electrons and the spheroidal tantalum target by 64-MeV and 28-MeV electrons (*cf.* Fig. 1 (b)). The ^{57}Ni activities from Ni foils by 36-MeV, 64-MeV and 28-MeV electrons are shown as the symbols □, ● and ○, respectively.

(over)

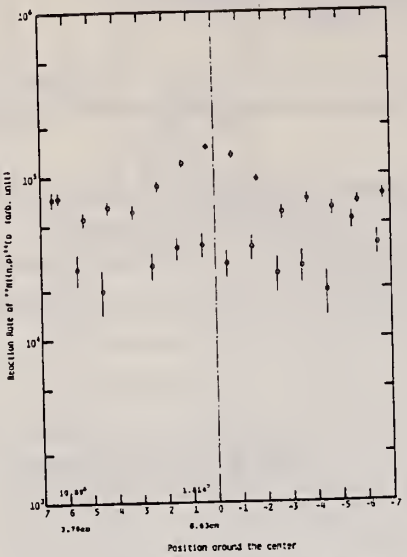

Fig. 13. Distributions of photoneutrons near the forward direction around the central axis of the electron beam from the spheroidal tantalum target bombarded by 64-MeV and 28-MeV electrons. The ^{58}Co activities from Ni foils by 64-MeV and 28-MeV electrons are shown as the symbols ● and ○, respectively.

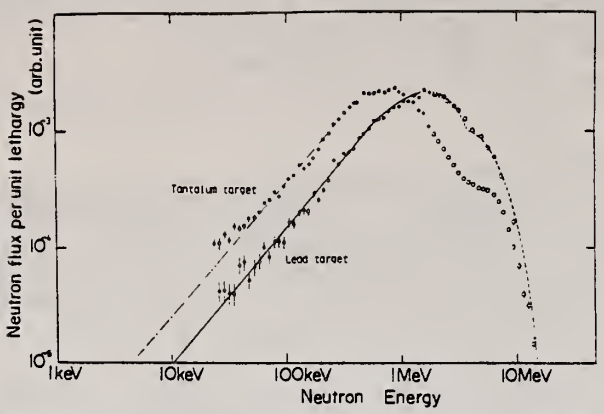

Fig. 14. Photoneutron spectra from the lead target and the spherical tantalum target bombarded hy approximately 30-MeV electrons.

—·— curve is obtained by eye guide fitting of the measured tantalum target data and —— curve is for the lead data. ---- curve is obtained by fitting the data of the lead target with nuclear temperatures of evaporation spectra, T_1=0.89 MeV ($\leqq$3.8 MeV neutrons) and T_2=1.70 MeV (>3.8 MeV neutrons). ●●●● shows data measured with the ^{6}Li glass scintillation or the ^{10}B-vaseline-plug NaI(Tl) detectors. ○○○○ shows data with the liquid scintillation detector.

REF. W. Muckenheim, P. Rullhusen, F. Smend, M. Schumacher
Phys. Lett. 92B, 71 (1980)

ELEM. SYM.	A	Z
Ta	181	73

METHOD

REF. NO. 80 Mu 4 hg

REACTION	RESULT	EXCITATION ENERGY	SOURCE		DETECTOR		ANGLE
			TYPE	RANGE	TYPE	RANGE	
G,G	ABX	3	D	2-4	UKN-D		DST
		(3.010)		(2.5-3.5)			

LFT, LEVEL AT 3.010

Elastic photon scattering investigated at energies of 2.5–3.5 MeV using radioactive sources has revealed a large probability for observing photoexcitation of nuclear levels. This finding removes inconsistencies in previously investigated properties of Delbrück scattering and provides a new access to nuclear resonance fluorescence.

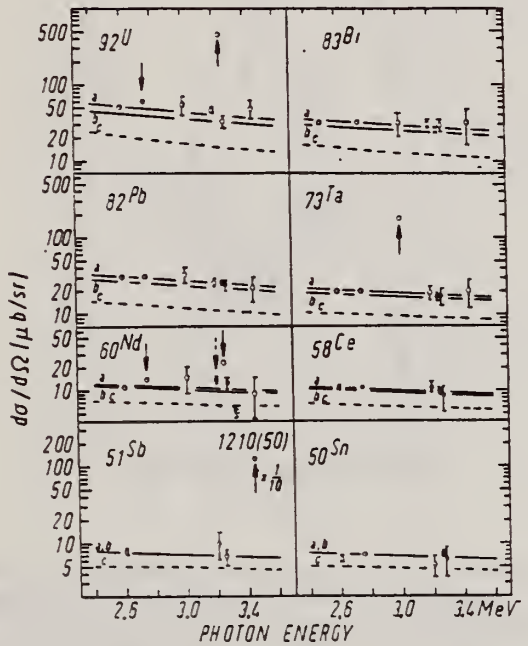

Fig. 1. Elastic differential cross sections versus photon energy. Unless error bars are given, the error intervals are at most equal to the diameter of the circles. Predicted differential cross sections: (a) including Coulomb corrections in addition to lowest-order D-, T-, R- and N-amplitudes, (b) including lowest-order D-, T-, R- and N-amplitudes, (c) including T-, R- and N-amplitudes.

Table 1
Levels observed via photoexcitation. ΔE: width of exciting photon line. D: predicted level spacing at 3 MeV. I^π: spin–parity. $(d\sigma/d\Omega)_{res}$: elastic differential cross section for resonance fluorescence by the identified isotope or element measured for $\theta = 90°$. Γ_0: partial width of the level for γ-transition to the ground state. Γ: total level width. $g = (2I_{ex}+1)/(2I_g+1)$. $W(\theta)$: angular correlation function.

Isotope	Level (MeV)	ΔE (eV)	D (eV)	I^π	$(d\sigma/d\Omega)_{res}$ (μb/sr)	$W(\theta)g\Gamma_0^2/\Gamma$ (meV)	Γ_0/Γ	Γ_0 (meV)
^{238}U	2.754	451	10^3	(1, 2)	13 ± 4	0.145	≲ 0.77	≳ 0.084 a)
	3.254	57		1^-	399 ± 5	0.79	0.24	1.5
^{181}Ta	3.010	81	5×10^2	–	165 ± 17	0.40	≲ 0.72	≳ 0.56 b)
nat Nd	2.754	451		–	2.6 ± 0.5	–	–	
	3.202	63	2×10^3	–	3.3 ± 1.5	–	–	
	3.254	57		–	12.8 ± 1.0	–	–	
^{121}Sb	3.452	35	10^3	$(3/2, 5/2)^+$	2100 ± 50	2.8	0.60	4.7 b)

a) $I = 1$ assumed. b) $gW(0) = 1$ assumed.

REF. F.N. Rad, W. Bertozzi, S. Kowalski, C.P. Sargent, C.F. Williamson, M.V. Hynes, B. Norum, B. Peterson, T. Sasanuma, W. Turchinetz
Phys. Rev. Lett. 45, 1758 (1980)

EL EM. SYM.	A	Z
Ta	181	73

METHOD

REF. NO.: 80 Ra 1 | hg

REACTION	RESULT	EXCITATION ENERGY	SOURCE		DETECTOR		ANGLE
			TYPE	RANGE	TYPE	RANGE	
E,E/	FMF	0-1	D	0*3	MAG-D		180
		(.136,.302)		(.7-2.5)			

Transverse electron scattering form factors from the ground-state rotational band of ^{181}Ta have been measured to study the single-particle contribution to the magnetization current density. The data are compared with a Hartree-Fock calculation by use of density matrix expansion with filling approximation.

TWO LEV .136, .302 MEV

PACS numbers: 25.30.Cg, 21.10.Ky, 27.70.+q

(OVER)

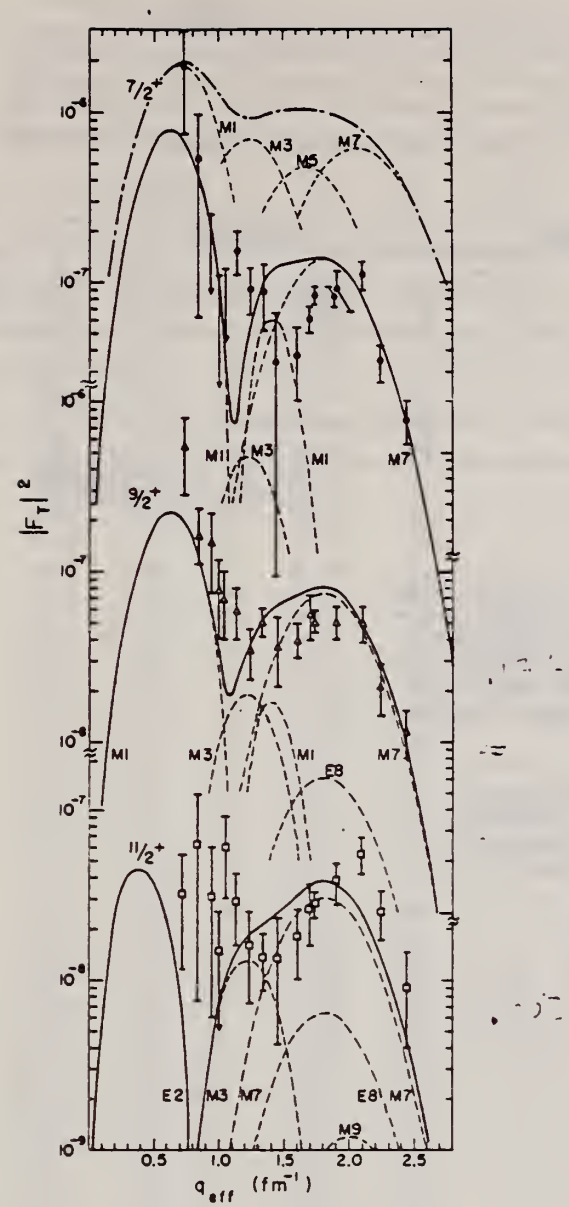

FIG. 1. Experimental results for $|F_T(q)|^2$ for electron scattering from the first three members of the ground-state rotational band of ^{181}Ta: circles, elastic; triangles, $\frac{7}{2}^+ \rightarrow \frac{3}{2}^+$; squares, $\frac{7}{2}^+ \rightarrow \frac{11}{2}^+$. The curves are the result of the H-F theory described in the text. The solid lines are the full results, and the dashed lines represent the contributions of the individual multipoles. The dash-dotted curve is the total elastic form factor of a $g_{7/2}$ proton in a spherical harmonic oscillator potential with oscillator parameter $b = 2$ fm. The individual multipoles, $M1$–$M7$, are shown as dashed curves.

REF. N.K. Sherman, C.K. Ross, K.H. Lokan
Phys. Rev. C21, 2328 (1980)

ELEM. SYM.	A	Z
Ta	181	73

METHOD

REF. NO. 80 Sh 10 egf

REACTION	RESULT	EXCITATION ENERGY	SOURCE		DETECTOR		ANGLE
			TYPE	RANGE	TYPE	RANGE	
G,MUT	ABX	3-30	C	42	TOF-D		4PI

D(G,N) SPECTROMETER

Photon absorption by Al, Ta, and Bi between 3 and 30 MeV was measured using as a photon spectrometer a photoneutron time-of-flight detector and a liquid deuterium target. The atomic cross sections of Ta and Bi at the lowest energies (and of Al at higher energies) agree with calculated values appearing in published tabulations but exceed them at 25 MeV by about 2% in Ta and 3% in Bi. Calculations by others using empirical Coulomb corrections and improved screening corrections to the cross section for pair production by the nucleus agree with experiment to within $(0.5 \pm 0.4)\%$. Best experimental values of the combined correction for Bi are given.

[NUCLEAR REACTIONS ^{27}Al, ^{181}Ta, ^{209}Bi; measured total photon absorption $\sigma_\gamma(E)$; observed GDR; deduced electron pair production $\sigma_K(E)$; $E = 3.0$ to 30.0 MeV; resolution 500 keV; deduced experimental values for Bi of the combined Coulomb and screening correction; ^{2}H(γ,n) LD_2/TOF spectrometer.]

(OVER)

TABLE III. Measured values σ_{exp}(Ta) of the absorption cross section of tantalum and their statistical errors ϵ_σ are listed against photon energy ω along with the atomic cross sections σ_Z(Ta) and nuclear pair cross sections σ_K(Ta) obtained from them. Values of σ_Z interpolated from measurements made at Mainz [a] are shown for comparison. The amounts $\delta\sigma_Z$ and $\delta\sigma_K$ by which σ_Z(Ta) and σ_K(Ta) exceed the calculated [b] values σ_Z(calc) and σ_K(calc) are also given.

ω (MeV)	σ_{exp}(Ta) (b)	ϵ_σ (mb)	σ_Z(Ta) [c] (b)	$\delta\sigma_Z$ (mb)	σ_Z(Mainz) (b)	σ_K(Ta) (b)	σ_K(calc) (b)	$\delta\sigma_K$ (b)
3.869	12.126	±56	12.123	−57		4.47	4.45	+0.02
4.327	12.128	30.5	12.124	−66		5.04	5.05	−0.01
4.830	12.258	23.5	12.252	+8		5.82	5.67	+0.15
5.333	12.394	21	12.386	−4		6.26	6.23	+0.03
5.837	12.561	20.5	12.551	0		6.80	6.75	+0.05
6.348	12.789	21.5	12.777	+60		7.35	7.27	+0.08
6.870	12.990	21.5	12.974	+70		7.84	7.77	+0.07
7.404	13.171	22.5	13.149	+40		8.26	8.24	+0.02
7.936	13.391	24.5	13.365	+40		8.69	8.66	+0.03
8.382	13.601	26.5	13.564	+11		9.11	9.07	+0.04
8.936	13.854	28.5	13.807	+70		9.55	9.46	+0.09
9.476	14.079	30	14.019	+70		9.92	9.84	+0.08
9.992	14.318	32	14.240	+70	14.19	10.30	10.22	+0.08
10.514	14.507	34	14.405	+30	14.40	10.61	10.56	+0.05
11.039	14.775	36.5	14.635	+60	14.58	10.98	10.90	+0.08
11.557	15.056	40	14.828	+40	14.79	11.30	11.23	+0.07
12.088	15.380	41.5	15.052	+60	14.98	11.63	11.58	+0.05
12.629	15.562	46	15.194	0	15.17	11.88	11.88	0.00
13.174	15.730	47.5	15.386	−20		12.18	12.18	0.00
13.715	15.947	54	15.605	−20		12.48	12.46	+0.02
14.253	16.124	56.5	15.764	−50	15.81	12.70	12.76	−0.06
14.780	16.303	63	15.921	−80	16.02	12.93	13.02	−0.09
15.293	16.522	64.5	16.137	−50	16.23	13.21	13.27	−0.06
15.840	16.683	67.5	16.333	−40	16.40	13.48	13.50	−0.02
16.422	16.841	68.5	16.541	−10	16.57	13.76	13.77	−0.01
16.977	16.924	78	16.684	−30		13.97	14.00	−0.03
17.500	17.093	82.5	16.895	+20		14.25	14.22	+0.03
18.078	17.188	84	17.026	−30		14.44	14.46	−0.02
18.665	17.324	86.5	17.188	−20	17.25	14.72 [d]	14.66	+0.06
19.286	17.412	±90	17.294	−100	17.45	14.96 [d]	14.90	+0.06
19.856	17.920	112	17.816	+260	17.62	15.17 [d]	15.11	+0.06
20.370	17.850	112	17.758	+70	17.75	15.35 [d]	15.28	+0.07
20.907	17.868	115	17.785	−50	17.88	15.53 [d]	15.47	+0.06
21.468	17.903	117.5	17.829	−140				
22.055	18.316	124	18.252	+130				
22.670	18.362	127.5	18.306	+50				
23.314	18.380	131	18.333	−90				
23.989	18.791	136.5	18.751	+170				
24.697	18.514	137.5	18.480	−250				
25.312	18.709	176	18.679	−190				
25.825	18.658	177.5	18.632	−360				
26.355	19.156	187.5	19.132	+30				
26.903	19.300	195.5	19.277	−50				
27.470	19.408	206.5	19.387	+30				

[a] J. Ahrens *et al.* (Ref. 3). Numerical values are given in Ref. 6.

[b] Calculated atomic cross section values σ_Z(calc) were obtained by interpolation of tables compiled by J. H. Hubbell, H. A. Gimm, and I. Øverbø (private communication).

[c] Obtained by subtracting the total photoneutron cross section measured (Ref. 17) by R. Bergere *et al.* from σ_{exp}(Ta). See also Ref. 16.

[d] Using the interpolated Mainz (Ref. 6) value.

REF. G.M. Gurevich, L.E. Lazareva, V.M. Mazur, S.Yu. Merkulov, G.V. Solodukhov, V.A. Tyutin
Nucl. Phys. A351, 257 (1981)

ELEM. SYM.	A	Z
Ta	181	73

METHOD

REF. NO. 81 Gu 2 hg

REACTION	RESULT	EXCITATION ENERGY	SOURCE		DETECTOR		ANGLE
			TYPE	RANGE	TYPE	RANGE	
G,MU-T	ABX	THR-20	C	27	NAI-D		4PI

Abstract: The curves of the total gamma-absorption cross sections (σ_{tot}) in the E1 giant resonance energy range for the nuclei ^{154}Sm, ^{156}Gd, ^{165}Ho, ^{168}Er, ^{174}Yb, ^{178}Hf, ^{180}Hf, ^{181}Ta, ^{182}W, ^{184}W, ^{186}W and ^{197}Au have been measured using the absorption method. Parameters of the Lorentz curves fitting the measured cross sections σ_{tot} are given. Quadrupole moments (Q_0) and nuclear deformation parameters (β) were obtained.

For deformed nuclei in the $\sim 155 < A < \sim 180$ region a violation of the correlation between giant resonance widths (Γ) and nuclear deformation parameters was found. Γ_1 and Γ_2, the widths of the resonances corresponding to vibrations of nucleons along and across the nuclear deformation axis, were observed to decrease with the increase of A which could be accounted for by the presence of an $N = 108$ subshell.

E NUCLEAR REACTIONS ^{154}Sm, ^{156}Gd, ^{165}Ho, ^{168}Er, ^{174}Yb, ^{178,180}Hf, ^{181}Ta, ^{182,184,186}W, ^{197}Au (γ, X). E = 7–20 MeV; measured total $\sigma(E)$; deduced integrated σ, Lorentz line parameters. ^{154}Sm, ^{156}Gd, ^{165}Ho, ^{168}Er, ^{174}Yb, ^{178,180}Hf, ^{181}Ta, ^{182,184,186}W, ^{197}Au deduced β, Q_0, Γ, giant resonance evolution. Enriched, natural targets.

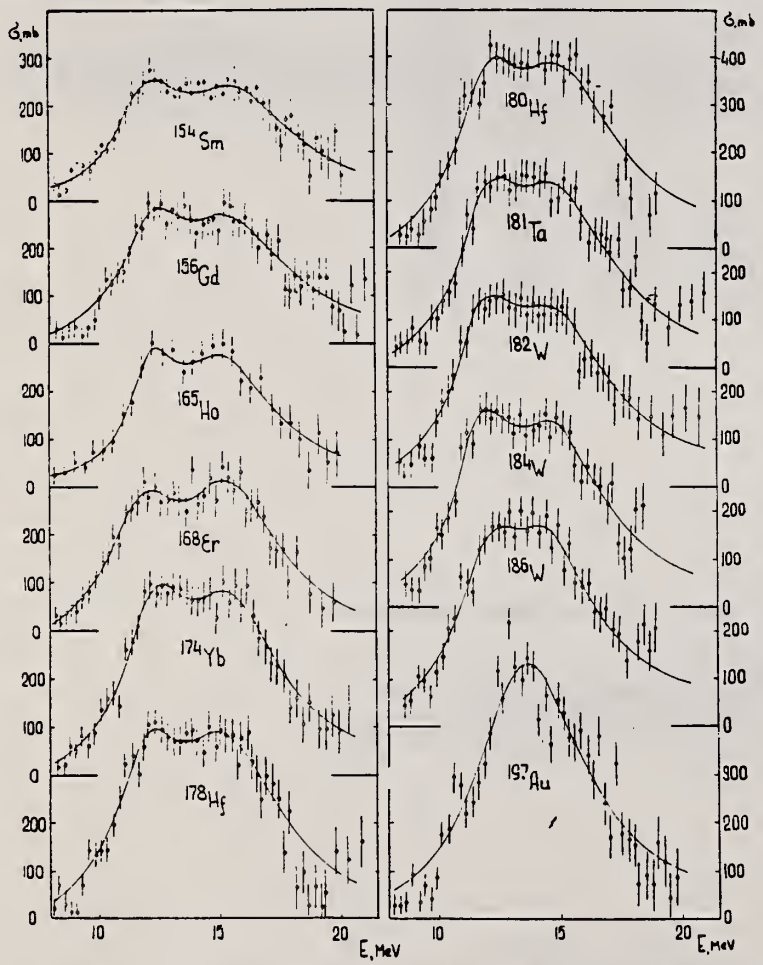

Fig. 2. Total nuclear γ-absorption cross sections (σ_{tot}) measured by the absorption method for ^{154}Sm, ^{156}Gd, ^{165}Ho, ^{168}Er, ^{174}Yb, ^{178}Hf, ^{180}Hf, ^{181}Ta, ^{182}W, ^{184}W, ^{186}W and ^{197}Au. Rms error bars are shown.

(OVER)

TABLE 2

Parameters of Lorentz curves fitting the experimental data on σ_{tot}

Nucleus	E_1 (MeV)	σ_1 (mb)	Γ_1 (MeV)	E_2 (MeV)	σ_2 (mb)	Γ_2 (MeV)	$\frac{\sigma_2\Gamma_2}{\sigma_1\Gamma_1}$	Γ (MeV)
^{154}Sm	12.2	188	3.4	15.7	207	5.7	1.85	8.1
^{156}Gd	12.3	206	3.2	15.7	220	5.5	1.81	7.7
^{165}Ho	12.3	202	2.3	15.2	239	4.8	2.47	7.0
^{168}Er	11.9	222	3.2	15.5	275	4.5	1.73	7.4
^{174}Yb	12.3	297	2.9	15.5	320	4.9	1.80	7.1
^{178}Hf	12.2	291	3.1	15.5	334	4.9	1.80	7.2
^{180}Hf	12.2	286	3.2	15.3	324	5.1	1.81	7.1
^{181}Ta	12.1	272	3.0	15.0	316	5.1	1.97	6.8
^{182}W	11.9	267	3.2	14.8	303	5.6	2.01	6.8
^{184}W	11.9	315	2.9	14.8	321	4.7	1.65	6.8
^{186}W	12.0	246	3.3	14.5	332	5.1	2.07	6.4
^{197}Au	13.7	535	5.2					
Average error	1.4 %	11.2 %	9.3 %	1.5 %	9.7 %	4.6 %	0.22	0.2 MeV

TABLE 3

Ratios of nuclear ellipsoid axes (λ), deformation parameters (β) and intrinsic quadrupole moments (Q_0), calculated from E_2/E_1

Nucleus	^{154}Sm	^{156}Gd	^{165}Ho	^{168}Er	^{174}Yb	^{178}Hf	^{180}Hf	^{181}Ta	^{182}W	^{184}W	^{186}W
λ	1.320	1.302	1.259	1.327	1.289	1.296	1.281	1.263	1.271	1.268	1.229
β	0.326 ±0.017	0.309 ±0.016	0.266 ±0.036	0.334 ±0.032	0.296 ±0.024	0.303 ±0.032	0.288 ±0.036	0.270 ±0.026	0.278 ±0.030	0.274 ±0.032	0.235 ±0.033
Q_0	6.3 ±0.3	6.2 ±0.3	5.8 ±0.8	7.5 ±0.7	7.0 ±0.6	7.5 ±0.8	7.2 ±0.9	6.9 ±0.7	7.2 ±0.8	7.1 ±0.8	6.2 ±0.9

TABLE 4

Integral characteristics of E1 giant resonance

Nucleus	$\sigma_{0,exp}$ (MeV·b)	$\sigma_{0,exp}$ / 0.06NZ/A	σ_{0t} (MeV·b)	σ_{0t} / 0.06NZ/A	σ_{-1} (mb)	σ_{-1L} (mb)	$\sigma_{-1L}A^{-1/3}$ (mb)	σ_{-2} (mb·MeV^{-1})	σ_{-2L} (mb·MeV^{-1})	$\sigma_{-2L}A^{-1/3}$ (μb·MeV^{-1})
^{154}Sm	1.94±0.06	0.87	2.86	1.29	117±3.5	156	0.189	9.1±0.3	14.3	3.23
^{156}Gd	2.07±0.07	0.91	2.95	1.30	143±4.6	163	0.194	10.5±0.4	14.9	3.30
^{165}Ho	1.86±0.06	0.78	2.53	1.06	155±4.4	160	0.177	10.1±0.3	12.6	2.54
^{168}Er	2.24±0.06	0.92	3.07	1.26	161±4.3	197	0.212	12.0±0.3	16.0	3.13
^{174}Yb	2.69±0.05	1.07	3.82	1.52	195±3.4	240	0.247	14.5±0.3	19.2	3.54
^{178}Hf	2.85±0.07	1.11	3.99	1.55	208±4.9	247	0.247	15.3±0.4	20.2	3.59
^{180}Hf	2.72±0.06	1.05	4.03	1.56	200±4.4	250	0.246	15.1±0.3	20.7	3.61
^{181}Ta	2.84±0.07	1.09	3.81	1.46	210±5.3	245	0.239	16.0±0.4	20.0	3.45
^{182}W	2.86±0.07	1.09	4.01	1.52	211±5.3	256	0.248	16.2±0.4	21.6	3.70
^{184}W	2.78±0.07	1.05	3.80	1.43	207±5.3	251	0.240	15.9±0.4	20.9	3.51
^{186}W	2.90±0.07	1.08	3.95	1.48	214±5.3	256	0.241	16.2±0.4	21.6	3.56
^{197}Au	3.12±0.06	1.10	4.37	1.54	229±4.2	276	0.241	18.6±0.4	23.3	3.49

REF. A. Leprêtre, H. Beil, R. Bergère, P. Carlos, J. Fagot, A. De Miniac, A. Veyssière
Nucl. Phys. A367, 237 (1981)

ELEM. SYM.	A	Z
Ta	181	73

METHOD

REF. NO. 81 Le 1 | egf

REACTION	RESULT	EXCITATION ENERGY	SOURCE		DETECTOR		ANGLE
			TYPE	RANGE	TYPE	RANGE	
G,SN	ABX	25-140	D	25-140	MOD-I		4PI
G,XN	ABX	25-140	D	25-140	MOD-I		4PI

(G,SN) NO G,1N IN G,SN

Abstract: The total photonuclear absorption cross section for Sn, Ce, Ta, Pb and U has been studied from 25 to 140 MeV using a continuously variable monochromatic photon beam obtained from the annihilation in flight of monoenergetic positrons. The basic experimental results are a set of data giving sums of inclusive multiple photoneutron production cross sections of the form $\sigma^{(i)}(E_\gamma) = \sum_{i=i}\sigma(\gamma, in: E_\gamma)$ for neutron multiplicities ranging from $i = 1$ to 12. From these data the total photonuclear absorption cross section $\sigma(\text{tot}: E_\gamma)$ has been deduced. It is concluded that Levinger's modified quasideuteron model describes the total cross sections reasonably well. When these data are combined with lower energy data and integrated to 140 MeV they indicate the need for an enhancement factor K for the Thomas-Reiche-Kuhn sum rule of 0.76 ± 0.10. No evidence was found that would indicate an A-dependence for the enhancement factor.

$$\sigma^{(i)}(E_\gamma) = \sum_{i=i}\sigma(\gamma, in: E_\gamma).$$

E PHOTONUCLEAR REACTIONS Sn, Ce, Ta, Pb, U(γ, xn), $E_\gamma = 25$–140↓ MeV· measured $a(E_\gamma)$ summed for $x = 1$–12; deduced $\sigma(E_\gamma$, total), integrated σ, interaction models. Monochromatic photons.

TABLE 3

Integrated cross sections

	Sn	Ce	Ta	Pb	U	U
$\sigma_0 = 0.06NZ/A$ (MeV · b)	1.74	2.04	2.61	2.97	3.40	3.40
$E_{\gamma 0}$(MeV)	29.7	25	25	25	18	18.30
$M = \int_{B_{1n}}^{E_{\gamma_0}} \sigma_{GDR}(E_\gamma)\,dE_\gamma$ (MeV · b)	2.0 ± 0.15 [a]	2.13 ± 0.15 [b]	2.90 ± 0.23 [b]	3.48 ± 0.23 [c]	2.98 ± 0.15 [d]	3.58 [e]
(σ_0 unit)	1.15 ± 0.09	1.04 ± 0.07	1.11 ± 0.09	1.17 ± 0.08	0.88 ± 0.05	1.05
$N = \int_{E_{\gamma 0}}^{140\,MeV} \sigma^{(2)}(E_\gamma)\,dE_\gamma$ (Mev · b)	0.96 ± 0.1	1.27 ± 0.1	1.73 ± 0.15	1.69 ± 0.15	2.59 ± 9.2	2.59 ± 0.2
(σ_0 unit)	0.55 ± 0.06	0.63 ± 0.05	0.66 ± 0.06	0.57 ± 0.05	0.76 ± 0.06	0.76 ± 0.06
$M+N$ (MeV · b)	2.96 ± 0.2	3.40 ± 0.2	4.63 ± 0.3	5.17 ± 0.3	5.57 ± 0.3	6.17 ± 0.3
(σ_0 unit)	1.70 ± 0.12	1.67 ± 0.10	1.77 ± 0.10	1.74 ± 0.10	1.64 ± 0.10	1.81 ± 0.10
$(M+N)$ + evaluation of the $\int_{E_{\gamma 0}}^{140\,MeV} \lvert\sigma^{(1)} - \sigma^{(2)}\rvert\,dE_\gamma$ contribution $= (1+K)$ (σ_0 unit)	1.74 ± 0.15	1.71 ± 0.15	1.81 ± 0.15	1.78 ± 0.15	1.68 ± 0.15	1.85 ± 0.15
$\int^{\infty} \sigma_L(E_\gamma)\,dE_\gamma$ (σ_0 unit)	1.28 [a]	1.24 [b]	1.30 [b]	1.35 [a]	1.18 [d]	1.43 [e]

[a]) Ref. [26]). [b]) Ref. [27]). [c]) Ref. [5]). [d]) Ref. [28]). [e]) Ref. [29]).

The symbols M and N are defined in the text. The last row gives the integrated cross sections for the Lorentz line fit, $\sigma_L(E_\gamma)$ to the GDR data, published in the above references.

(OVER)

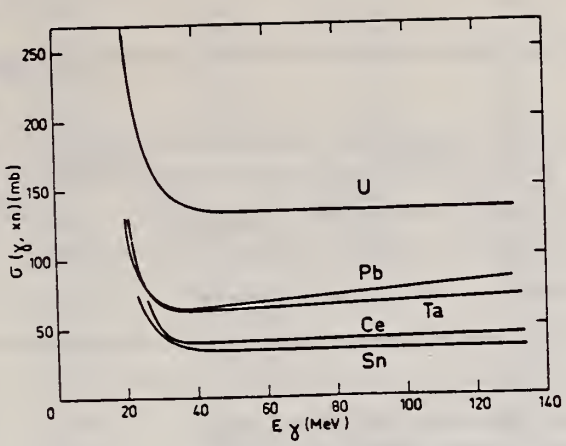

Fig. 11. The general behaviour of the "smoothed" average neutron yield cross sections $\sigma(\gamma, xn) = \sum_i i\sigma(\gamma, in: E_\gamma)$ for the Sn, Ce, Ta, Pb and U nuclei studied in the present paper (see text).

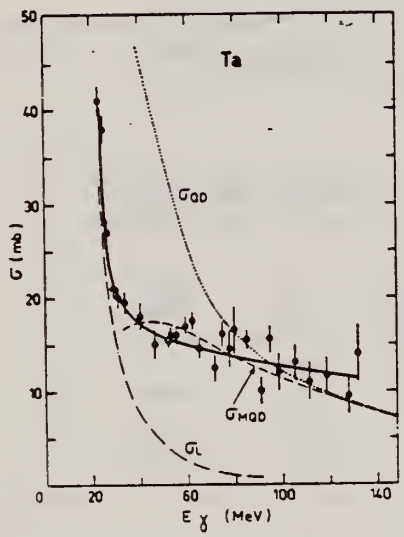

Fig. 15. Total photonuclear absorption cross sections $\sigma(\text{tot}: E_\gamma) \approx \sigma^{(2)}(E_\gamma)$ from the present paper, represented by the experimental points and the corresponding full lines, are shown for Pb, Sn, Ce, Ta and U. These experimental results for photon energies E_γ between 20 and 140 MeV are compared with: (a) Lorentz line fits to the GDR data of the appropriate nucleus represented by the dot-dash $\sigma_L(E_\gamma)$ plots. (b) Quasideuteron cross sections, $\sigma_{QD}(E_\gamma) = (4.6NZ/A)\sigma_D(E_\gamma)$ for the appropriate nuclei, represented by the dotted $\sigma_{QD}(E_\gamma)$ plots. Here $\sigma_D(E_\gamma)$ is the photodisintegration cross section of deuterium. (c) Modified quasideuteron cross sections, $\sigma_{QDM}(E_\gamma) = (8NZ/A)\sigma_D(E_\gamma) \exp(-D/E_\gamma)$ with $D = 60$ MeV, represented by the dashed $\sigma_{MQD}(E_\gamma)$ plots. Pertinent GDR data for Pb, Sn, Ce, Ta and U were taken from refs. [5,26–28]).

REF. M. Schumacher, F. Smend, W. Mückenheim, P. Rullhusen, H.G. Börner
Z. Phys. A300, 193 (1981)

ELEM. SYM.	A	Z
Ta	181	73

METHOD

REF. NO. 81 Sc 6 egf

REACTION	RESULT	EXCITATION ENERGY	SOURCE TYPE	SOURCE RANGE	DETECTOR TYPE	DETECTOR RANGE	ANGLE
G,G	ABX	2-7		2-7	SCD-D		90

2.60-6.76 MEV

Elastic scattering by nuclei in the range of mass numbers between 64 and 238 has been studied with monochromatic photons in the energy range between 2 and 8 MeV. These photons were provided either by a Ti(n,γ) source installed in the tangential through channel of the Grenoble high flux reactor, or by ^{24}Na and ^{56}Co sources produced by deuteron bombardment of Al or Fe at the Göttingen cyclotron. The photoexcitation of 23 nuclear levels has been observed and the decay properties and groundstate widths of the majority of these levels have been determined. For the lead scattering target the coherent elastic differential cross section has been studied in detail. There is evidence that below the photo-neutron threshold the elastic scattering via virtual photoexcitation of the nucleus can be approximated by extrapolating the real part of the Giant Dipole Resonance amplitude along a Lorentzian curve. Coulomb corrections to Delbrück scattering seem to play a small role at 6.5 MeV.

Table 4. Properties of levels observed by photoexcitation. $(d\sigma/d\Omega)^{NRF}$: experimental differential cross section per identified isotope or element for resonance scattering through $\Theta = 90°$. I^π: spin-parity of excited level; $W(\Theta)$: angular correlation function; $g = (2I_{ex}+1)/(2I_g+1)$; Γ_0: radiative groundstate transition width, Γ: total level width. Errors in the last digits are given in parentheses

Isotope	E_γ (MeV)	$(d\sigma/d\Omega)^{NRF}$ (μb/sr)	I^π	Γ_0/Γ [c]	$W(\Theta)g\Gamma_0^2/\Gamma$ (meV)	Γ_0 [f] (meV)	Γ_0 [g] (meV)
^{238}U	2.754	13 (4)	(1)	0.77	0.145	0.084	-
^{238}U	3.254	421 (5)	1^-	0.24	0.83	1.5	0.52(15)[d]
^{209}Bi	6.555	2.1 (4)·10^2	-	-	0.74	0.74[b]	-
^{209}Bi	7.168	1.7 (3)·10^5	$9/2^+$[a]	1.00	710	786	820 (40)[a]
^{203}Tl	6.418	8.75(30)·10^3	$1/2^+$[a]	0.28	30	102	82 (15)[a]
Tl	6.759	7 (3)	-	-	-	-	-
Hg	6.555	68 (17)	-	-	-	-	-
^{186}W	6.418	5.2 (3)·10^2	1^-[a]	0.32	1.75	2.4	-
^{184}W	6.555	9.8 (10)·10^2	(1)	0.52	3.44	2.9	-
^{184}W	6.759	46 (10)	(1)	0.58	0.17	0.13	-
^{181}Ta	3.010	174 (17)	-	0.72	0.42	0.59	-
^{181}Ta	6.418	62 (4)	-	0.73	0.2	0.27[c]	-
^{181}Ta	6.759	4.8 (12)	-	-	0.018	0.018[b]	-
^{165}Ho	6.418	10.3 (30)	-	-	0.035	0.035[b]	-
^{165}Ho	6.759	5.6 (14)	-	-	0.021	0.021[b]	-
Nd	2.754	2.6 (5)	-	-	-	-	-
Nd	3.254	14.0 (10)	-	-	-	-	-
Ce	6.759	13.4 (10)	-	-	-	-	-
^{121}Sb	3.452	2.20 (5)·10^3	-	0.60	2.9	4.9[b]	-
^{100}Mo	6.418	1.53 (4)·10^4	1^-[a]	0.88	52	26	25 (8)[a]
^{94}Mo	6.555	4.4 (4)·10^3	(1)	0.33	15	21	-
Mo	6.759	6.2 (15)	-	-	-	-	-
Mo	7.168	8.2 (26)·10^2	-	-	-	-	-

[a] [11] [b] $W(\Theta)g\Gamma_0/\Gamma = 1$ assumed [c] $W(\Theta)g = 1$ assumed
[d] [28] (a small correction has been applied to the data of [28])
[e] Upper limits in case not all the transitions to lower levels were observed
[f] Present work [g] Previous work

(OVER)

Table 1. Differential cross sections for elastic scattering $(d\sigma/d\Omega)^{exp}$ of photons from ^{56}Co and ^{24}Na sources by different scattering targets, in units of μb/sr. Errors in the last digits are given in parentheses.

Θ deg	Scattering targets	2.599[a] (MeV)	2.754[b] (MeV)	3.010[a] (MeV)	3.202[a] (MeV)	3.254[a] (MeV)	3.273[a] (MeV)	3.452[a] (MeV)
90	^{238}U	52.7(25)	57.5(25)[c]	56(16)	47(4)	456 (10)[c]	34(6)	49(14)
	^{209}Bi	33.1(30)	32 (2)	33(11)	32(4)	25.6(20)	29(6)	33(15)
	^{nat}Pb	31.5(23)	31.0(16)	35 (8)	27(3)	26.6(22)	25(4)	23 (8)
	^{nat}Tl	31.5(33)	-	27(12)	32(5)	24 (3)	22(7)	34(15)
	^{nat}Hg	30.0(27)	-	24(10)	28(5)	25.5(18)	26(8)	20 (8)
	^{nat}W	22.5(11)	-	17 (7)	19(3)	18.4(15)	18(5)	21 (6)
	^{181}Ta	20.0(15)	19.2 (6)	193(20)[c]	20(4)	17.3(21)	18(5)	21 (8)
	^{165}Ho	15.9(13)	-	17(10)	13(6)	15.6(20)	18(8)	-
	^{nat}Nd	11.4 (7)	14.2 (5)[d]	15 (7)	14(3)	24.2(12)[d]	13(3)	9 (6)
	^{nat}Ce	11.1 (9)	11.0 (5)	-	11(3)	9.5(13)	8(4)	-
	^{127}J	8.4(10)	8.6 (5)	-	9(2)	7 (1)	5(3)	-
	^{nat}Sb	8.0(11)	-	-	10(4)	6.8(19)	-	1,270(50)[c]
	^{nat}Sn	6.5 (7)	7.0 (5)	-	5(2)	7.6 (8)	6(3)	-
	^{nat}Cd	6.2 (5)	-	-	6(2)	6.6 (8)	7(3)	-
120	^{238}U	55.1(25)	64 (4)[c]	43(15)	55(5)	574 (10)[c]	48(5)	48(11)
	^{181}Ta	27.5(15)	25.0 (9)	227(20)[c]	22(5)	21 (2)	22(8)	-
	^{nat}Nd	17.9(30)	17.0 (9)[d]	-	-	29.8(47)[d]	-	-

[a] ^{56}Co source in Fe lattice [b] ^{24}Na source in Al lattice (part of data have been published elsewhere)
[c] Transitions to excited states observed in addition to the ground-state transition
[d] Photoexcitation of nuclear level identified from the size of the differential cross section

Table 2. Elastic differential cross sections $d\sigma/d\Omega(\Theta=90°)$ in μb/sr measured with the Ti(n,γ) source and compared with theoretical predictions. n: predicted number of levels in a $\Delta E=25$ eV interval at 6.5 MeV. Errors in the last digits are given in parentheses

Scattering target	6.418 MeV exp.	6.418 MeV th.	6.555 MeV exp.	6.555 MeV th.	6.759 MeV exp.	6.759 MeV th.	7.168 MeV exp.	7.168 MeV th.	n
^{238}U	23 (12)	10.3	-	-	-	-	-	-	45
^{209}Bi	-	-	219(39)[b,c]	8.0	12 (4)	7.4	1.5(3)·10^5[b,c]	5.7	0.1
^{nat}Pb	7.0(15)	8.6	-	-	6.5(11)	7.4	-	-	0.05
^{nat}Tl	2.586 (92)[a,c]	7.5	-	-	13 (3)[b]	6.0	-	-	0.4
^{nat}Hg	12 (3)	7.8	74(17)[b]	6.5	6.7(15)	6.4	-	-	3.4
^{nat}W	159 (10)[a,c]	6.6	306(33)[a,c]	6.3	20 (2)[a,c]	5.6	-	-	13
^{181}Ta	68 (4)[a,c]	6.3	-	-	10.1(12)[b,c]	5.3	-	-	28
^{165}Ho	15 (3)[b]	4.7	-	-	9.5(14)[b]	3.9	-	-	18
^{nat}Ce	4.1(21)	4.1	-	-	17 (1)[b,c]	3.6	-	-	0.04
^{nat}Sn	4.2(13)	3.0	-	-	2.5 (5)	2.7	-	-	1.9
^{nat}Mo	1.474 (44)[a,c]	2.5	407(39)[a,c]	2.5	8.5(15)[b,c]	2.3	817(258)[b,c]	2.0	0.5
^{nat}Zn	2.4 (8)	1.6	-	-	1.8 (5)	1.5	-	-	0.3

[a] Transitions to excited states observed [b] Photoexcitation identified from size of differential cross section
[c] Photoexcitation reported in [11]

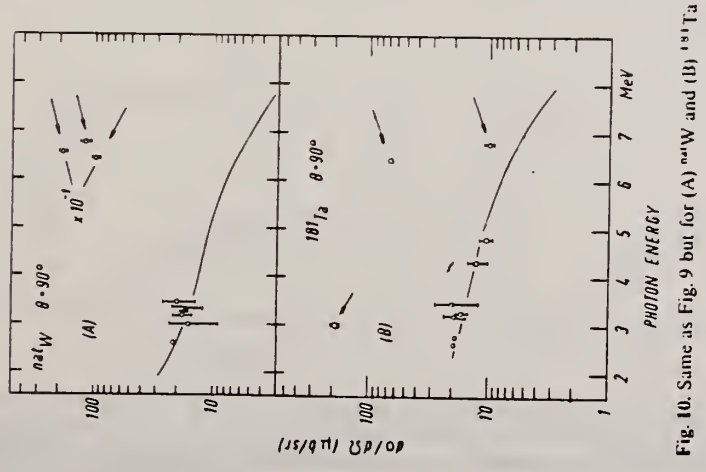

Fig. 10. Same as Fig. 9 but for (A) ^{nat}W and (B) ^{181}Ta

REF. A. Leprêtre, H. Beil, R. Bergère, P. Carlos, J. Fagot, A. Veyssière, I. Halpern
Nucl. Phys. A390, 221 (1982)

ELEM. SYM.	A	Z
Ta	181	73

METHOD

REF. NO.: 82 Le 3 | egf

REACTION	RESULT	EXCITATION ENERGY	SOURCE		DETECTOR		ANGLE
			TYPE	RANGE	TYPE	RANGE	
G,XN	NOX	30-140	D	30-140	MOD-I		4PI

See also A. Leprêtre et al. NP A390, 240 (1982) MULT ANAL 81LE1

Abstract: From event-by-event records of observed photoneutron multiplicities for photons from 30 to 140 MeV on several heavy targets (Sn, Ce, Ta and Pb), it was possible to determine the mean number of photoneutrons, $\bar{\nu}$, for each photon energy and the widths W of the multiplicity distributions. The mean neutron numbers increase smoothly from about three to six over the photon energy span for all four targets. The widths go from about one to two neutrons in the same interval. When these measurements are combined with other photonuclear information, it is possible to extract the average numbers of fast neutrons and fast protons and the average number of evaporation neutrons emitted per photoabsorption.

E PHOTONUCLEAR REACTIONS Sn, Ce, Ta, Pb(γ, xn), E = 25–140 MeV; measured photoneutron mean numbers, width distributions; deduced fast evaporation neutron, fast proton average numbers. Monochromatic photons.

TABLE 2

Photonucleon emission features for four targets at 70 MeV

	Sn	Ce	Ta	Pb
$\bar{\nu}$	4.3 ± 0.2	4 ± 0.2	4.5 ± 0.2	4.8 ± 0.2
$\overline{\nu_f}$	0.50 ± 0.11	0.59 ± 0.13	0.71 ± 0.16	0.66 ± 0.15
$\overline{\pi_f}$	0.24 ± 0.05	0.26 ± 0.05	0.27 ± 0.05	0.23 ± 0.04
$\overline{\nu_s}$	3.8 ± 0.3	3.4 ± 0.3	3.8 ± 0.3	4.1 ± 0.3
$\overline{E_f}$ (MeV)	23.4 ± 5	26.3 ± 6	28.7 ± 6	26.6 ± 6
$\overline{E^*}$ (MeV)	46.6 ± 6	43.7 ± 5	41.3 ± 5	43.4 ± 5

(See caption under table 1.)

Experimental data are taken from ref. [1]) and fig. 2 of this paper. ν stands for neutrons and π for protons; f stands for fast particles and s for evaporated particles. $\overline{E^*}$ is the residual excitation energy after all fast particles have escaped – carrying with them energy $\bar{E}_f$. The coefficients α and β have to do with the ratio of fast neutrons to fast protons that are emitted. They are explained in the text. The uncertainties in this table are statistical only.

(OVER)

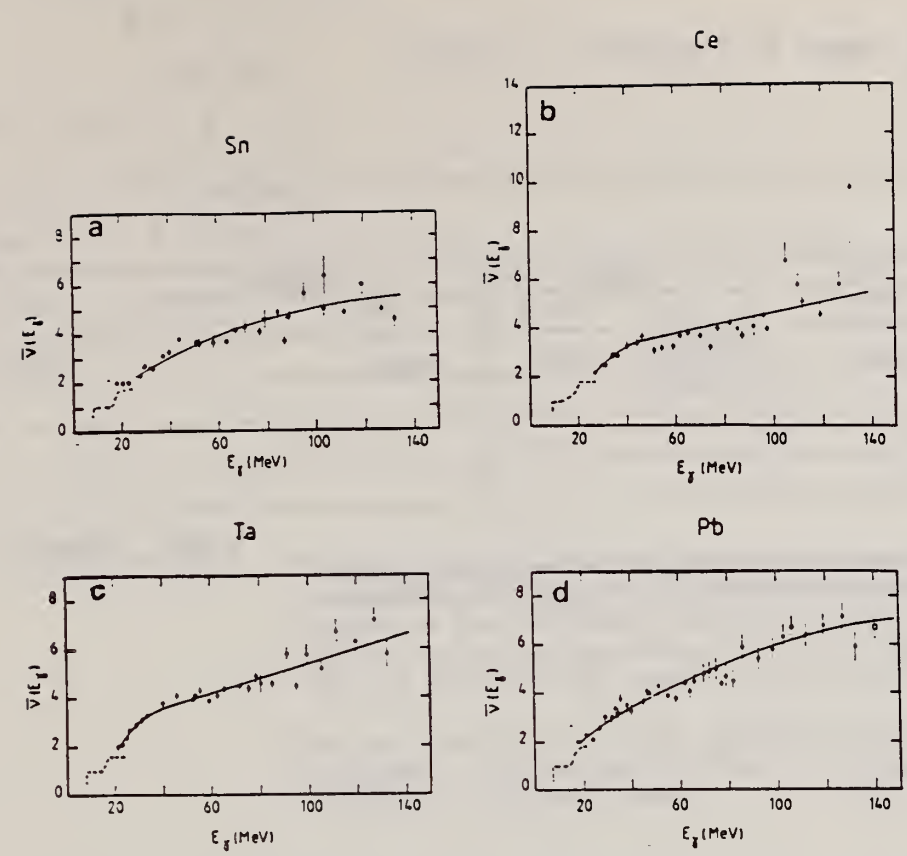

Fig. 2. Average experimental photoneutron multiplicities $\bar{\nu}(E_\gamma)$ plotted against photon energy E_γ, for 25 MeV $\leq E_\gamma \leq$ 140 MeV. Data points were evaluated using results from ref. [1]). The full line represents a smoothed average behaviour. The dashed line represents $\bar{\nu}(E_\gamma)$ values, measured in the giant dipole resonance (GDR) region, in previous Saclay experiments [7]). Fig. 2a: Sn; fig. 2b: Ce; fig. 2c: Ta; fig. 2d: Pb [where the $\square$ point refers to the SIN [19]) measurement with stopped π^-].

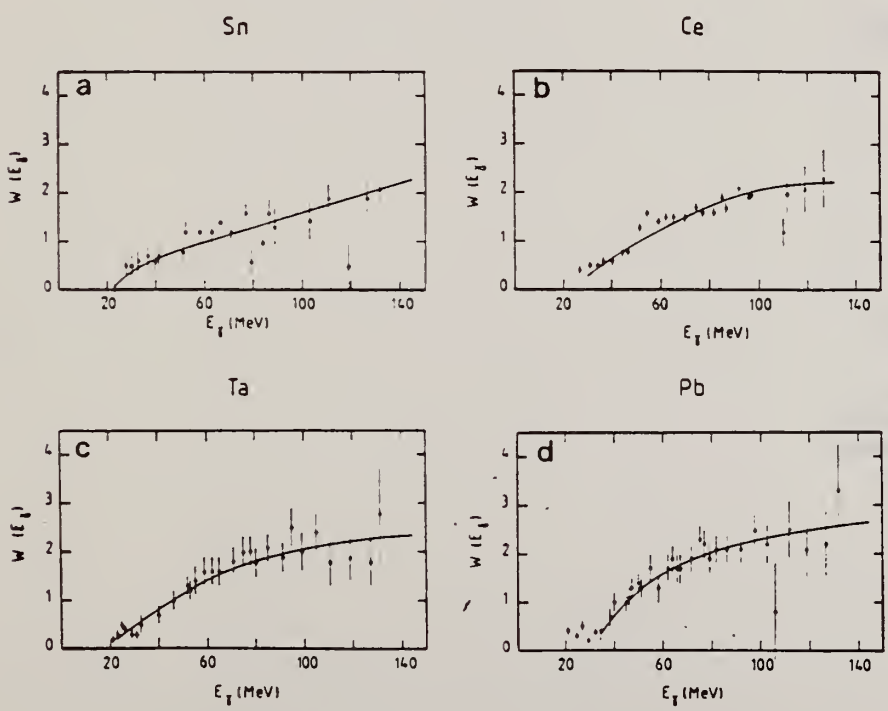

Fig. 3. Widths, $W(E_\gamma)$ of the experimental photoneutron multiplicity distributions as a function of the photon energy E_γ for 25 MeV $\leq E_\gamma \leq$ 140 MeV. Data points were evaluated using results from ref. [1]). The full line represents a smoothed average behaviour. Fig. 3a: Sn; fig. 3b: Ce; fig. 3c: Ta; fig. 3d: Pb.

REF. U. Zurmühl, P. Rullhusen, F. Smend, M. Schumacher, H.G. Börner
Phys. Lett. 114B, 99 (1982)

ELEM. SYM.	A	Z
Ta	181	73

METHOD

REF. NO.	
82 Zu 2	egf

REACTION	RESULT	EXCITATION ENERGY	SOURCE		DETECTOR		ANGLE
			TYPE	RANGE	TYPE	RANGE	
G,G	ABX	3-6	D	3-6	SCD-D		DST

SOURCE 141PR(N,G)

A procedure is presented to determine total photoabsorption cross sections σ_t by resonant scattering of γ-rays. It is shown that σ_t follows along the GDR lorentzian line down to 3.5 MeV. Indications for nonstatistical deviations from the lorentzian line are observed.

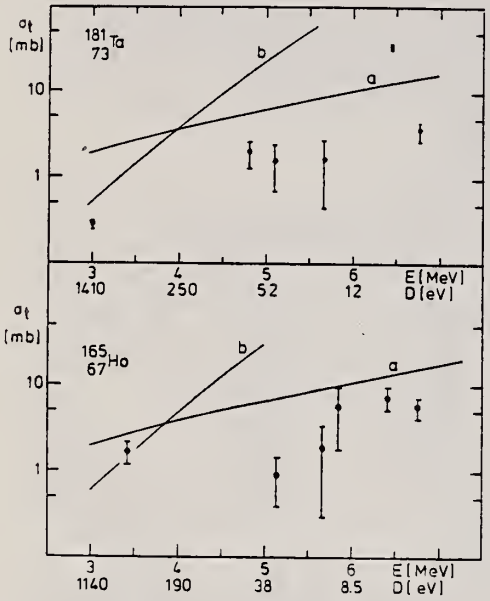

Fig. 2. Total photoabsorption cross section for ^{181}Ta and ^{165}Ho versus energy. Curve a: extrapolated lorentzian according to ref. [13]. Curve b: total photoabsorption cross section predicted by the Weisskopf model with hindrance factor 3×10^{-5}.

W

TUNGSTEN
Z=74

The word wolfram was first applied to the ore iron-manganese tungstate as described by Lazarus Ecker in 1574. The term refered to its "wolflike" nature in "devouring" tin and causing low recoverage rates in the tin smelting operation (the ore inhibits the reduction of tin oxides).

The word tungsten was first applied to the mineral calcium tungstate. The term was derived from the Swedish words tung(heavy) and sten(stone).

W

W

Ref. W.H. Hartley, W.E. Stephens, E.J. Winhold
Phys. Rev. 104, 178 (1956)

Elem. Sym.	A	Z
W		74

Method
Li (p,γ) source, 480 kev protons. BF_3 counters

Ref. No. 56 Ha 1 | EGF

Reaction	E or ΔE	E_o	Γ	$\int \sigma dE$	Jπ	Notes
(γ,xn)						Average Li cross section is 365 mb; cross section with detector response weighted for low energy neutrons, 355 mb. Assumed ratio 17.6/14.8 = 1.7. Calculated cross section at 14.8 and 17.6 MeV assuming cross section curves measured at Pennsylvania and Saskatchewan (refer Table I).

TABLE I. Cross sections for photoneutron emission induced by the lithium gamma rays. The results are compared with previous data

Element	Present cross-section data: Counter Group A	Present cross-section data: Counter Group B	Data of McDaniel et al.[a]	Betatron data: Pennsylvania $\sigma_{14.8}$	Pennsylvania $\sigma_{17.6}/\sigma_{14.8}$	Saskatchewan $\sigma_{14.8}$	Saskatchewan $\sigma_{17.6}/\sigma_{14.8}$		
$_{26}$Fe	38 mb	33 mb	37 mb			60[f] mb	0.5	23 mb	47 mb
$_{27}$Co	49	49	47	60[c] mb	0.5	95[f]	0.5	30	60
$_{28}$Ni	29	25	23			40[g]	0.7	22	32
$_{29}$Cu	64	61	55±12			95[f]	0.6	45	75
$_{30}$Zn	48	45	48			90[f]	0.7	38	54
$_{42}$Mo	175	170	135			240[f]	1.0	175	175
$_{50}$Sn	200	190	180						
$_{73}$Ta	355	360	260	350[d]	1.3	420[e]	2.3	420[h] 550[i]	320[h] 240[i]
$_{74}$W	365	355	325						
$_{79}$Au	330	295		315[c]	1.7	480[f]	1.9	460	255
$_{80}$Hg	365	340	290						
$_{82}$Pb	310	295	250	320[b]	1.6	440[f]	2.5	400[h] 500[i]	250[h] 290[i]
$_{83}$Bi	305	280	250	270[d]	2.6	550[f]	2.4	490	195

[a] See reference 3.
[b] Average of 14.8- and 17.6-Mev cross sections weighted with relative intensities of the lithium gamma-ray lines.
[c] See reference 24.
[d] R. Nathans, Ph.D. thesis, University of Pennsylvania, 1954 (unpublished).
[e] I. Halpern (private communication).
[f] See reference 23.
[g] See reference 32.
[h] Separate cross sections at 14.8 and 17.6 Mev as obtained from Group A data and 14.8/17.6 betatron cross-section ratios.
[i] Obtained using 14.8/17.6 cross-section ratio from Pennsylvania betatron data.
[j] Obtained using 14.8/17.6 cross-section ratio from Saskatchewan betatron data.

Ref. K. Reibel, A.K. Mann
Phys. Rev. 118, 701 (1960)

Elem. Sym.	A	Z
W		74

Method
γ's from $F^{19}(p,a\gamma)$ reaction; protons from Vande Graaff; NaI.

Ref. No. 60 Re 1 JHH

Reaction	E or ΔE	E_o	Γ	$\int \sigma dE$	Jπ	Notes
(γ,γ)	$\sim \bar{\Gamma}$					$\langle\bar{\sigma}\rangle$ (E_p = 2.05 MeV) = 1.8 ± 0.4 mb

REF.

R.G. Baker, K.G. McNeill
Can. J. Phys. 39, 1158 (1961)

ELEM. SYM.		
W		74

METHOD: Betatron; fast neutron yield, angular distribution; Si threshold detector; ion chamber

REF. NO.: 61 Ba 2 NVB

REACTION	RESULT	EXCITATION ENERGY	SOURCE		DETECTOR		ANGLE
			TYPE	RANGE	TYPE	RANGE	
G,XN	ABY	THR-22	C	22	THR-I	5-+	DST

In Table 4:

$\bar{\sigma}$ = average cross section of detector weighted with neutron spectrum

$\bar{q}$ = neutrons/100 roentgen/mole

$$W(\theta) = a_o \sum_{n=1}^{\infty} [1 + A_n P_n (\cos \theta)]$$

TABLE IV

I Element	II a_0	III a_1	IV a_2	V $(\bar{\sigma}\Phi)\times 10^{26}$	VI Φ_{total} (22 Mev) $\times 10^{2}$	VII Φ_{fast}/Φ_{total}
[illegible]	245 (1±0.06)	0.01±0.08	−0.00±0.10	6.05	0.21	0.12
[illegible]	164 (1±0.03)	0.04±0.04	−0.05±0.05	4.05	0.17	0.10
Manganese	308 (1±0.02)	0.07±0.03	−0.09±0.04	7.61	0.25	0.12
Iron	200 (1±0.03)	0.05±0.04	−0.17±0.05	4.94	0.18	0.11
Cobalt	390 (1±0.02)	0.08±0.03	−0.22±0.04	9.63	0.26	0.15
Nickel	145 (1±0.05)	0.07±0.07	−0.23±0.09	3.58	0.12	0.12
Copper	347 (1±0.02)	0.05±0.03	−0.29±0.04	8.57	0.30	0.12
Arsenic	482 (1±0.03)	0.11±0.04	−0.24±0.05	11.91	0.33	0.15
Rubidium	638 (1±0.05)	0.13±0.06	−0.14±0.08	15.76		
Strontium	409 (1±0.05)	0.10±0.06	−0.17±0.08	10.10		
Yttrium	290 (1±0.10)	0.08±0.12	−0.12±0.15	7.16		
Silver	590 (1±0.04)	0.10±0.06	−0.22±0.08	14.57	0.87	0.07
Cadmium	905 (1±0.02)	0.02±0.02	−0.26±0.03	22.35		
Iodine	1133 (1±0.03)	0.04±0.04	−0.29±0.05	27.99	1.42	0.08
Barium	1048 (1±0.04)	0.10±0.06	−0.38±0.08	25.89		
Lanthanum	1595 (1±0.02)	0.02±0.03	−0.42±0.04	39.40	1.04	0.15
Cerium	1316 (1±0.05)	0.05±0.06	−0.39±0.08	32.50		
Dysprosium	1652 (1±0.08)	0.04±0.10	−0.34±0.13	40.80		
Tantalum	1558 (1±0.02)	0.04±0.03	−0.22±0.04	38.48	2.50	0.06
Tungsten	1365 (1±0.02)	−0.07±0.03	−0.24±0.04	33.71		
Mercury	1345 (1±0.02)	0.04±0.03	−0.31±0.04	33.22		
Lead	2274 (1±0.01)	0.02±0.02	−0.42±0.03	56.17	2.72	0.08
Bismuth	2162 (1±0.02)	0.05±0.03	−0.45±0.04	53.40	3.36	0.06
Thorium	3031 (1±0.04)	0.06±0.05	−0.32±0.07	74.87		
Uranium	4630 (1±0.02)	0.05±0.03	−0.17±0.04	114.36		

*$(\bar{\sigma}\Phi) = 2.47\times 10^{2}$ ev millibarn-neutron. Errors are standard errors due to counting statistics only.

Ref. V.G. Shevchenko, B.A. Yurev
Nuclear Phys. 37, 495 (1962)

Elem. Sym.	A	Z
W		74

Method
35 MeV betatron; emulsions

Ref. No.
62 Sh 4
JHH

Reaction	E or ΔE	E_o	Γ	$\int \sigma dE$	Jπ	Notes
W (γ,p)	Bremss. 22.5 33.5					Parameters a, b and p for $\omega(\theta_p) = a + b \sin^2\theta (1 + p \cos\theta)^2$ in Table I.

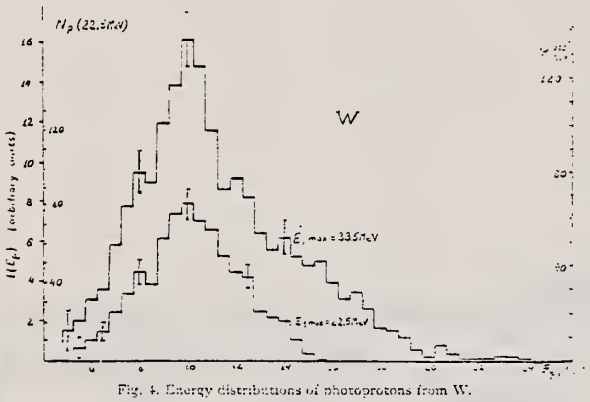

Fig. 4. Energy distributions of photoprotons from W.

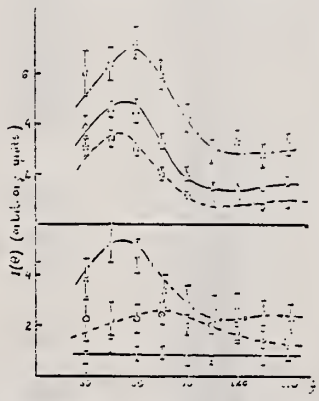

Fig. 9. Angular distributions of photoprotons from W. The experimental points for $E_{\gamma max}$ = 22.5 MeV are denoted by solid dots for E_p = 0.25-8.75 MeV, by solid squares for E_p = 8.75-12.75 MeV and by crosses for E_p > 12.75 MeV. For the case of $E_{\gamma max}$ = 33.5 MeV circled circles denote E_p = 0.25-8.75 MeV, open triangles E_p = 8.75-12.75 MeV and open squares denote E_p > 12.75 MeV.

Coefficients of expressions of type (1 [illegible]) and estimates of the contribution from the [illegible]

Element	Z	$E_{\gamma max}$ (MeV)	E_p (MeV)	a	b	p	$\sigma_{E1}/(\sigma_{E1}-\sigma_{E2})$ (...)
Rh	45	22.5	3.25-9.25	1.9	0	0	0
			> 9.25	2.8	1.0	0.2	1
		33.5	3.25- 9.25	12.2	0	0	0
			> 9.25	4.5	3.7	1.2	≈20
Pr	59	22.5	4.5-7.25	1.4	0.7	0.42	0
			7.25-11.25	2.0	4.4	0.82	2
			> 11.25	1.5	3.4	0.44	1
		33.5	4.5-7.25	3.3	1.2	1.0	≈15
			7.25-11.25	4.2	1.55	2.2	≈50
			> 11.25	0.8	1.2	1.8	≈50
W	74	22.5	6.25-8.75	0.8	0	0	0
			8.75-12.75	2.8	1.6	1.6	≈55
			> 12.75	2.2	0.5	2.0	≈55
		33.5	6.25-8.75	1.2	0.95	0.44	0
			8.75-12.75	1.5	0.85	2.0	≈55
			> 12.75	0.55	0.5	3.4	≈70
Pt	78	22.5	6.25-8.75	0.6	1.0	0.4	0
			8.75-11.75	2.5	1.0	1.2	≈20
			> 11.75	1.4	0.56	2.0	≈55
		33.5	7.25-11.25	2.1	1.1	2.0	≈55
			> 14.25	0.5	0.8	3.0	≈70
Pb	82	22.5	5.25-10.25	1.05	0.75	0.8	≈10
			> 10.25	0.75	0.75	2.2	≈50
		33.5	5.25-10.25	1.9	1.2	1.2	≈20
			10.25-14.25	1.15	0.65	2.0	≈65
			> 14.25	1.3	1.3	3.3	≈70

Table 2

Measured photoproton yields and comparison with estimates by the models of evaporation and [illegible]

Element	$E_{\gamma max}$ (MeV)	Y_{exp} *	[illegible]	[illegible]
Rh[illegible]	22.5	[illegible]	≤ 3	≤ 0
	33.5	[illegible]	≤ 0	≤ 4.5
Pr[illegible]	22.5	[illegible]	≤ 10	≤ 1.5
	33.5	[illegible]	≤ 45	≤ 0
W	22.5	[illegible]	[illegible]	≤ 0
	33.5	[illegible]	[illegible]	≤ 45
Pt	22.5	[illegible]	[illegible]	≤ 0
	33.5	[illegible]	[illegible]	≤ 20
Pb	22.5	[illegible]	≤ 1.5 [illegible]	≤ 11
	33.5	[illegible]	≤ 4 [illegible]	≤ 25

*. The yield Y_{exp} is expressed in protons per mol per [illegible].

References

1) M. E. Toms and W. E. Stephens, Phys. Rev. 98 (1955) 626
2) M. M. Hoffman and A. G. W. Cameron, Phys. Rev. 92 (1953) 1184
3) W. C. Barber and V. J. Vanhuyse, Nuclear Physics 16 (1960) 381
4) M. E. Toms and W. E. Stephens, Phys. Rev. 92 (1953) 362
5) E. D. Makhnovskiy, JETP 33 (1960) 95
6) R. B. Taylor, Nuclear Physics 19 (1960) 453
7) A. G. W. Cameron, W. Harms and L. Katz, Phys. Rev. 83 (1951) 1264
8) V. G. Neudachin, V. G. Shevchenko and N. P. Yudin, Report at the Second All-Union Conf. for Nuclear Reactions at Low and Medium Energies, Moscow, 1960
9) E. D. Courant, Phys. Rev. 82 (1951) 703
10) V. V. Balashov, V. G. Shevchenko and N. P. Yudin, JETP 41 (1961) 1929

Ref. V.G. Shevchenko, B.A. Yur'ev
Vesta. Mosk. Univ., Ser. III, No. 3, 90 (1962)

Elem. Sym.	A	Z
W		74

Method
35-MeV betatron

Ref. No.
62 Sh 6

JHH

Reaction	E or ΔE	E_0	Γ	$\int \sigma dE$	Jπ	Notes
W(γ,p)	Bremss.:					Angular distribution fitted to $a + b \sin^2\theta (1+p\cos\theta)^2$.
	22.5	10.0				
	33.5	10.0				

На рис. 2 представлены полученные угловые распределения фотопротонов различных энергий. На обоих рисунках приведены только статистические ошибки измерений. Через экспериментальные точки на рис. 2 проведены аппроксимирующие кривые типа $a - b\sin^2\theta(1 - p\cos\theta)^2$, параметры которых приведены в таблице. Приведенное выражение приближенно описывает угловые распределения при условии интерференции $E1$ и $E2$ поглощения, причем $p = \sigma_{E_1}/\sigma_{E_2}$. Исходя из этого были сделаны оценки вклада $E2$ поглощения, приведенные в таблице. Из рис. 2 видно, что линии наиболее низкой группы протонов (6,25—8,75 *Мэв*) имеет симметричное относительно 90° угловое распределение как при облучении с $E_{\gamma max} = 22.5$ *Мэв* так и в случае $E_{\gamma max} = 33.5$ *Мэв*. Это указывает на дипольный характер поглощения γ-квантов при образовании малоэнергичных протонов. Однако группы более энергичных протонов имеют угловые распределения с максимумами, вытянутыми вперед, причем сильнее вытянут как с увеличением энергии протонов, так и с увеличением $E_{\gamma max}$. Это связано, как видно из таблицы, с ростом вклада квадрупольного поглощения, который достигает ~ 70% в случаях наиболее энергичных протонов при облучении с $E_{\gamma max} = 33.5$ *Мэв*.

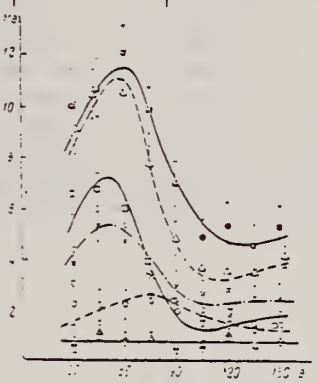

Рис. 2. Угловые распределения фотопротонов с $E_{\gamma max} = 22.5$ *Мэв*: ○ — $E_{прот} = 6.25 - 8.75$ *Мэв*; □ — $E_{прот} = 8.75 - 12.75$ *Мэв*; △ — $E_{прот} > 12.75$ *Мэв*; и с $E_{\gamma max} = 33.5$ *Мэв*: ● — $E_{прот} = 6.25 - 8.75$ *Мэв*; ■ — $E_{прот} = 8.75 - 12.75$ *Мэв*; ▲ — $E_{прот} > 12.75$ *Мэв*

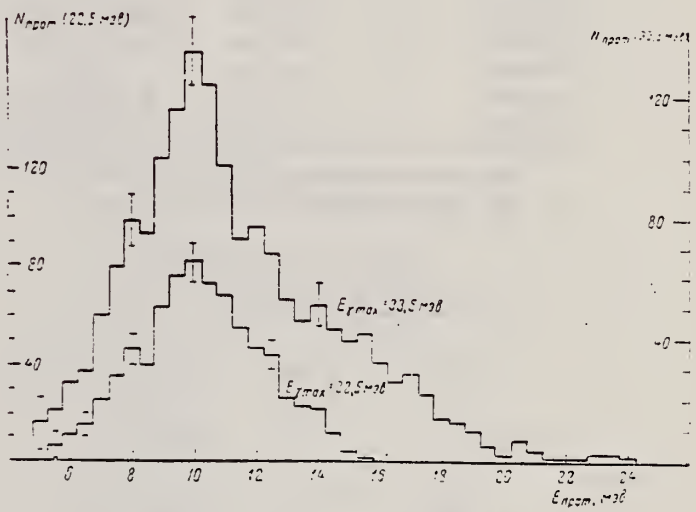

Рис. 1. Энергетические распределения фотопротонов из W

$E_{\gamma max}$, *Мэв*	$E_{прот}$, *Мэв*	a	b	p	$\sigma_{E1} : \sigma_{E2}$, %
22,5	6,25—8,75	0,8	0	0	0
	8,75—12,75	1,7	2,7	1,6	~35
	12,75	2,2	0,5	2,6	~20
33,5	6,75—8,75	1,2	0,05	0,44	1
	8,75—12,75	3,1	2,0	2,6	~35
	12,75	1,1	1,0	3,4	~70

Сечения выхода фотопротонов из W для энергий $2.6 \cdot 10^4$ и $6.5 \cdot 10^4$ протон/молль — рентген при $E_{\gamma max} = 22.5$ и 33.5 *Мэв* соответственно. Такой значительный рост выхода указывает на существенное увеличение сечения при $E_\gamma > 22.5$ *Мэв*, т. е. позволяет сделать вывод о том, что максимум сечения образования фотопротонов из W находится выше 22,5 *Мэв*. Это находится в согласии с результатами, полученными для Pb[206] [2], и с данными о сечениях (γ, n)-реакции на тяжелых ядрах [3—5]. Таким образом, полученные результаты указывают, что сечение реакции (γ, p) на W имеет максимум при $E_\gamma > 22.5$ *Мэв* и что поглощение γ-квантов в этой области имеет в основном квадрупольный характер.

ЛИТЕРАТУРА

T. Kaminishi, C. Kojima
Jap. J. Appl. Phys. 2, 399 (1963)

ELEM. SYM.	A	
W		74

METHOD: Linac; isomer yield; activity

REF. NO.: 63 Ka 2 · NVB

REACTION	RESULT	EXCITATION ENERGY	SOURCE TYPE	SOURCE RANGE	DETECTOR TYPE	DETECTOR RANGE	ANGLE
G,G/	RLY	1	C 5		ACT-I		4PI
		(0.20, 0.17,					
		0.12)					

Table II. The isomers observed

Isomer	Observed value		Referenced value[1)13)]	
	Half-life	Energy (MeV)	Half-life	Energy (MeV)
Se-77m	17.5 sec	0.160	17.5 sec	0.161
Br-79m	4.80 sec	0.209	4.8 sec	0.208
Sr-87m	2.3 hr	0.390	2.8 hr	0.388
Y-89m	15.0 sec	0.920	14 sec	0.915
Rh-103m	58 min	*	57 min	0.040
Ag-107m	} 42 sec	} 0.95	44 sec	0.094
Ag-109m			40 sec	0.088
Cd-111m	47 min	0.150,0.255	49 min	0.150,0.247
In-115m	4.5 hr	0.335	4.5 hr	0.335
Sn-117m	17 day	0.160	14 day	0.159,0.161
Ba-137m	2.6 min	0.660	2.6 min	0.662
Er-167m	2.10 sec	0.209	2.5 sec	0.208
Hf-179m	18.5 sec	0.157,0.215	19 sec	0.161,0.217
W-183m	5.4 sec	0.200,0.170,0.115	5.5 sec	0.1025,0.2915 others
Ir-191m	4.90 sac	0.129, <0.07	4.9 sec	0.042-0.129
Pt-195m	4.5 day	0.065**	4.1 day	0.031-0.130
Au-197m	7.0 sec	0.10,0.27,0.40	7.2 sec	0.130,0.270,0.407
Hg-199m	43 min	0.160,0.370	42 min	0.158,0.368

* This isomer was measured with a G-M flow counter.
** This value corresponds to Pt-K X-ray energy.

Table III. Induced activation rate

Element	Beam energy (MeV)	Counting rate (×10000 cpm)	Sample form
Se	5	1300	metallic [illegible]
Br	4	1600	NaBr grain
Sr	6	0.3	$SrCO_3$ powder
Y	5	90	metallic grain
Rh	5	0.2*	$RhCl_3$ grain
Ag	5	180	metallic plate
Cd	6	0.5	$CdCl_2$ grain
In	6	8	metallic plate
Sn	6	0.0005	metallic plate
Ba	5	0.6	BaS powder
Er	4	4900	Er_2O_3 powder
Hf	5	1600	metallic plate
W	5	120	metallic powder
Ir	5	2100	metallic powder
Pt	5	0.3	metallic plate
Au	4	4300	metallic plate
Hg	6	0.09	metallic liquid

* The value measured with a G-M flow counter.

Ref. V.G. Shevchenko, B.A. Yur'ev, B.P. Levkin
Zhur. Eksp. i Teoret. Fiz. 44, 808 (1963)
Soviet Phys. JETP 17, 547 (1963)

Elem. Sym.	A	Z
W		74

Method
35 MeV betatron; thin CsI(Tl) proton counters.

Ref. No. 63 Sh 1 | JHH

Reaction	E or ΔE	E_o	Γ	$\int \sigma dE$	Jπ	Notes
(γ,p)	15.5-33.5	E_γ = ~20.5 = ~ 28		~ 50±10MevMb $\Big|_{24}^{33}$ ~ 30MeV-mb $\Big|_{24}^{33}$ $^{15.5}$		E = 7MeV. σ_{max} = ~ 2.2mb; E1 + E2 σ_{max} = ~ 4.3 mb; mainly E2 Yields measured at 120° and 150°; background subtracted; corrected assuming (γ,p) angular distribution from Shevchenko and Yur'ev, JETP 16, 609 (1963). (See 62 Sh 3)

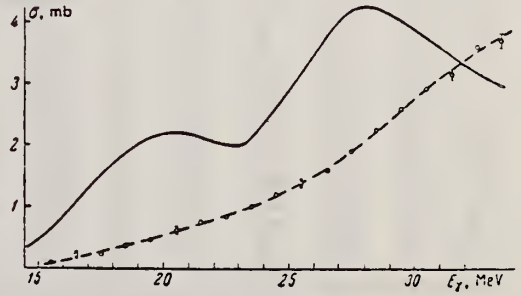

Measured reaction yields (in relative units). A smoothed yield curve is drawn through the experimental point (dashed). The excitation function $\sigma(E_\gamma)$ is represented by the continuous curve.

REF. H. G. De Carvalho, G. Cortini, E. Del Giudice, G. Potenza, R. Rinzivillo, and G. Ghigo
Nuovo Cimento 32, 293 (1964)

EL EM. SYM.	A	Z
W		74

METHOD

REF. NO. 64 De 4 HMG

REACTION	RESULT	EXCITATION ENERGY	SOURCE		DETECTOR		ANGLE
			TYPE	RANGE	TYPE	RANGE	
G,F	ABX	300-999	C	300-999	EMU-D	300-999	4PI

TABLE I.

Nuclide	Bi 209	W 184	Ag
Number of runs	3	2	1
Number of atoms cm^{-3}	$\sim 2 \cdot 10^{20}$	$\sim 5 \cdot 10^{19}$	10^{22}
Total number of tracks	~ 6000	~ 500	~ 100
Cross-sections per equivalent quantum, σ_Q, at 1000 MeV (millibarns)	12.2 ± 0.7	1 ± 0.1	0.1
Cross-sections per photon, σ_k, between 300 and 1000 MeV (millibarns)	7.8 ± 0.8	0.65 ± 0.11	~ 0.05
Fissility	0.12	0.012	< 0.0015

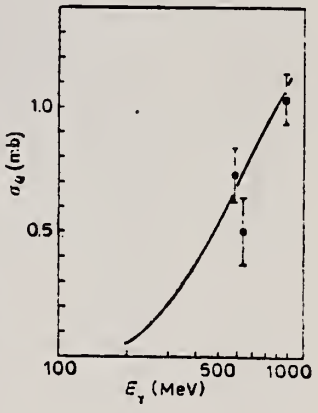

Fig. 4. – The W photofission cross-sections per quantum equivalent at 600, 650 and 1000 MeV are given by the full squares. The data can be fitted roughly with a curve corresponding to a constant value of the fissility.

REF. G. Ben-David, B. Arad, J. Balderman, and Y. Schlesinger
Phys. Rev. 146, B852 (1966)

ELEM. SYM.	A	Z
W		74

METHOD

Nuclear Resonance Scattering using N,G reactions.

REF. NO. 66 Be 3 JDM

REACTION	RESULT	EXCITATION ENERGY	SOURCE TYPE	SOURCE RANGE	DETECTOR TYPE	DETECTOR RANGE	ANGLE
G,G	RLX	5 - 10	D	5 - 10	NAI-D	5 - 10	135

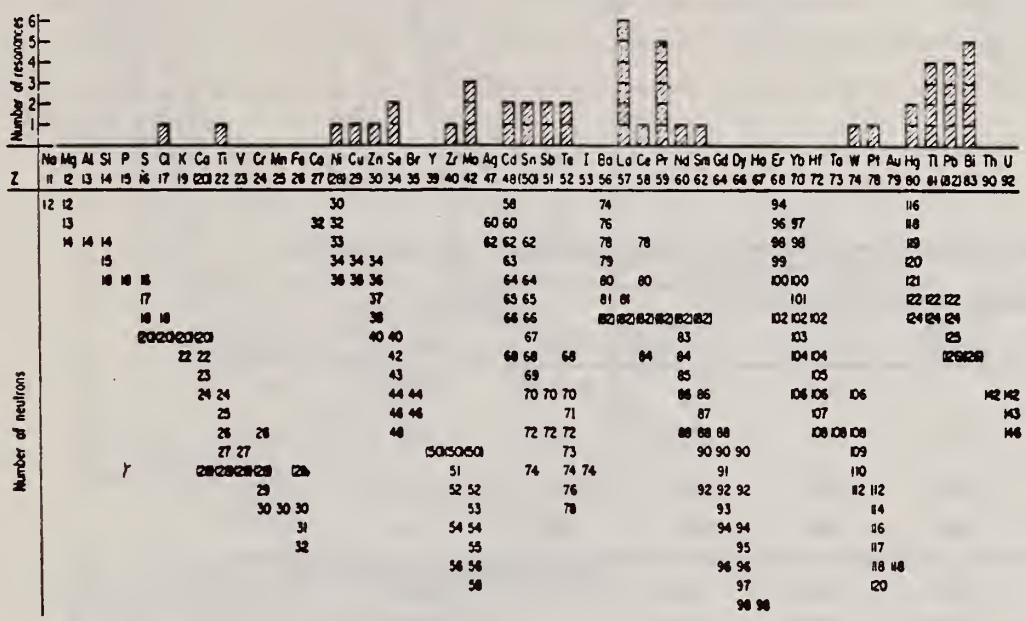

FIG. 3. Histogram of distribution of observed resonances among the different targets. The atomic number is given directly beneath the chemical symbol followed by the neutron numbers of the naturally occurring isotopes. Magic numbers are shown in brackets.

TABLE III. List of effective cross sections.

Scatterer	Energy (MeV)	Gamma source	δ (mb)	Scatterer	Energy (MeV)	Gamma source	δ (mb)
Sm^{144}	8.997	Ni	100	Sn	7.01	Cu	110
Pr^{141}	8.881	Cr	9	Nd	6.867	Co	30
La	8.532	Ni	6	Pr^{141}	6.867	Co	3
Te	8.532	Ni	3[a]	Te	6.7	Ni	...
Cu	8.499	Cr	24	La	6.54	Ag	12
Zr	8.496	Se	3050	Cd	6.474	Co	110
Zn	8.119	Ni	13	Mo	6.44	Hg	25[g]
Se	7.817	Ni	50	La	6.413	Ti	72
Se	7.76	K	90	Mo	6.413	Ti	10
Sb	7.67	V	...[b]	Tl	6.413	Ti	25
Cd	7.64	Fe	40[c]	W	~6.3	Ti	...[b]
Ni	7.64	Fe	7[c]	Sb	6.31	Hg	6[c]
Pr^{141}	7.64	Fe	12[c]	Ti	6.31	Hg	2[c]
Tl	7.64	Fe	370[c]	Sn	6.27	Ag	75
La	7.634	Cu	7	Pb^{206}	6.15	Gd	...[e]
Mo	7.634	Cu	11	Te	5.8	Ni	...[f]
Bi^{209}	7.634	Cu	4	La	6.12	Cl	35
Te	7.528	Ni	66[d]	Pr^{141}	6.12	Cl	110
Bi^{209}	7.416	Se	100	Pt	5.99	Hg	40[a,g]
Bi^{209}	7.300	As	80[c]	Tl	5.99	Hg	5[g]
Pb^{206}	7.285	Fe	4100	Pb^{206}	5.9	Sr	...[b]
Cl	7.285	Fe	34	Ce	5.646	Co	17
Pr^{141}	7.185	Se	80	Bi^{209}	5.646	Co	55
Tl	7.16	Cu	120	Pb^{206}	5.53	Ag	70
La	7.15	Mn	50	Hg	5.44	Hg	75[g]
Bi^{209}	7.149	Tl	2000	Hg	4.903	Co	385

[a] High-energy component of a complex spectrum.
[b] A broad scattered spectrum with no observable peak structure.
[c] There are actually two lines of energies 7.647 and 7.633 MeV having equal intensities in the iron capture gamma spectrum. The cross section has therefore been corrected, although there is no possibility at present of deciding which line is responsible for each resonance.
[d] Is probably an independent level in the complex spectrum of Ni γ rays on Te.
[e] Rough estimate.
[f] May be inelastic component from 7.528 level in Te.
[g] The relative line intensities in this case are due to Grosbev and co-workers.
[h] No line is known for the source at this energy.
[i] Difficult to resolve among the many source lines present at this energy.

REF. J. Maly
Phys. Letters 35B, 148 (1971)

EL EM. SYM.	A	Z
W		74

METHOD

REF. NO.	
71 Ma 2	egf

REACTION	RESULT	EXCITATION ENERGY	SOURCE		DETECTOR		ANGLE
			TYPE	RANGE	TYPE	RANGE	
E,F	SPC	THR-999	D	500,999	FRG-I		4PI

999 = 1.3 GEV

Table 1
Estimated energies and cross-sections of fission fragment formations produced by 1300 MeV electrons (detected on (D) foils)

Range in mylar (μm) (passing foil No.)	Estimated energy of fragment in MeV				Cross section in μb		
	$A = 25$ $Z = 10$	$A = 50$ $Z = 20$	$A = 75$ $Z = 30$	$A = 100$ $Z = 40$	U	Pb	W
(0.foil)					3×10^6	6×10^3	400
53 μm (4. foil)	79	185	294	391	1.7	2.2	4.1
67 μm (5. foil)	89	222	362	484	1.8	1.0	1.2
79 μm (6. foil)	105	260	422	576	3.6	1.2	1.8
E_{kin} from Q values (MeV)					Kinetic energy from fission of:		
	23.6	60.1	60.0	49.8	^{186}W		
	22.4	61.6	80.0	66.9	^{208}Pb		
	49.2	92.0	111.0	111.3	^{238}U		
B_{lab} (MeV)					B_{lab} for fusion with:		
	92.6	192	302	433	^{186}W		
	99.7	203.5	315	442	^{208}Pb		
	107	209	334	462	^{238}U		

[over]

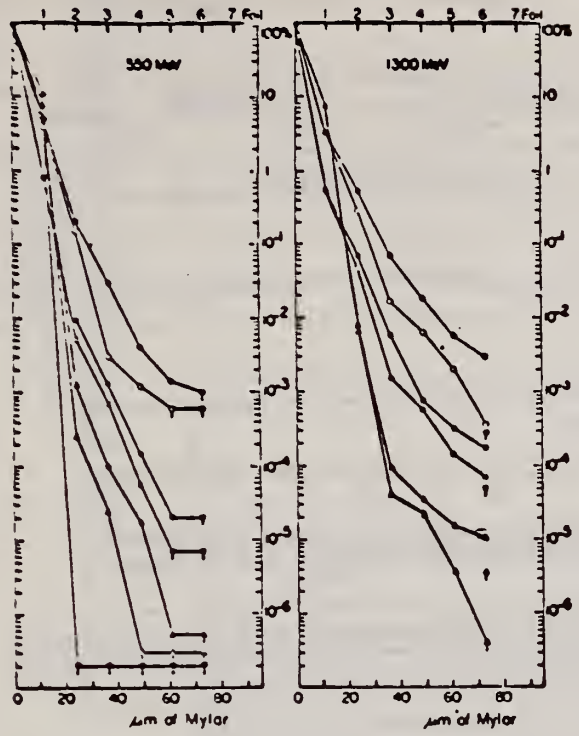

Fig. 1. Penetration of fission fragments through mylar foils from fission induced in U, Pb and W by electrons and bremsstrahlung. Explanation of symbols:
Cf spontaneous fission ○; U fission front foils △ and back foils ▲; Pb fission front foils □ and back foils ■; W fission front foils ○ and back foils ○ .
Symbols with arrows (e.g. ♀) denote background level.

REF. V.P. Kovalev, V.P. Kharits, V.V. Gordeev, V.I. Isaev (USSR)
Atomnaya Energiya 32, 496 (1972)

ELEM. SYM.	A	Z
W		74

METHOD

REF. NO. 72 Ko 8 hmg

REACTION	RESULT	EXCITATION ENERGY	SOURCE		DETECTOR		ANGLE
			TYPE	RANGE	TYPE	RANGE	
G,N	NOX	6- 22	C	22	THR-I		DST

Мишень	Энергия электронов, Мэв	Детектор	Угол, град							B/A
			30	50	70	90	110	130	150	
Al	22,5	$P^{31}(n,p)$	1,05±0,08	1,03±0,08	0,97±0,08	1,0±0,08	0,98±0,08	1,02±0,08	1,04±0,08	Изотропно
	22,5	$Al^{27}(n,p)$	0,90±0,15	0,95±0,15	1,02±0,15	1,00±0,14	0,96±0,13	1,07±0,13	1,01±0,13	»
Ti	22,5	$P^{31}(n,p)$	1,04±0,07	0,96±0,07	1,03±0,07	1,00±0,07	0,98±0,07	1,05±0,07	1,03±0,07	»
	22,5	$Al^{27}(n,p)$	1,06±0,13	0,94±0,13	1,04±0,12	1,00±0,12	0,95±0,11	0,98±0,11	1,02±0,10	»
Cu	12,8	$P^{31}(n,p)$	0,97±0,10	1,04±0,10	1,02±0,10	1,00±0,10	1,01±0,10	0,99±0,10	0,96±0,10	»
	17,0	$P^{31}(n,p)$	1,03±0,07	0,97±0,07	1,00±0,07	1,00±0,07	1,06±0,07	0,95±0,07	0,88±0,07	»
	22,5	$P^{31}(n,p)$	0,87±0,05	0,94±0,05	0,97±0,05	1,00±0,05	0,99±0,05	0,93±0,05	0,91±0,05	0,18±0,04
	22,5	$Al^{27}(n,p)$	0,75±0,09	0,86±0,07	0,93±0,06	1,00±0,05	1,02±0,05	0,94±0,04	0,90±0,04	0,28±0,06
Mo	22,5	$P^{31}(n,p)$	0,90±0,05	0,93±0,05	0,98±0,05	1,00±0,05	0,99±0,05	0,92±0,05	0,84±0,05	0,21±0,04
	22,5	$Al^{27}(n,p)$	0,80±0,08	0,95±0,08	0,95±0,07	1,00±0,06	0,94±0,05	0,83±0,04	0,72±0,04	0,44±0,08
	22,5	$Al^{27}(n,\alpha)$	0,72±0,08	0,84±0,08	0,89±0,08	1,00±0,08	0,95±0,08	0,87±0,08	0,63±0,08	0,78±0,18
W	22,5	$P^{31}(n,p)$	0,85±0,04	0,90±0,04	0,98±0,04	1,00±0,04	0,98±0,04	0,92±0,04	0,087±0,04	0,25±0,04
	22,5	$Al^{27}(n,p)$	0,78±0,06	0,84±0,06	0,89±0,05	1,00±0,05	0,97±0,04	0,86±0,04	0,75±0,04	0,54±0,06
Pb	22,5	$P^{31}(n,p)$	0,79±0,04	0,85±0,04	0,96±0,04	1,00±0,04	0,98±0,04	0,88±0,04	0,84±0,04	0,36±0,05
	22,5	$Al^{27}(n,p)$	0,70±0,09	0,81±0,08	0,94±0,07	1,00±0,06	0,94±0,06	0,80±0,05	0,69±0,05	0,69±0,12

(Over)

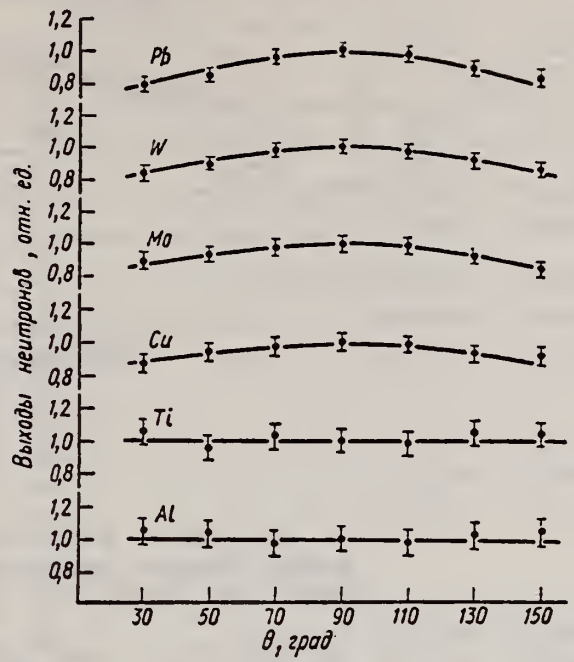

Угловые распределения быстрых фотонейтронов из Al, Ti, Cu, Mg, W, Pb, облучаемых электронами с энергией 22,5 *Мэв*. Детектор I^{131} (γ, p) Si^{31}.

REF.

R.F. Barrett, J.R. Birkelund, B.J. Thomas, K.S. Lam, and H.H. Thies
Nucl. Phys. A210, 355 (1973)

ELEM. SYM.	A	Z
W		74

METHOD

REF. NO.	
73 Ba 20	egf

REACTION	RESULT	EXCITATION ENERGY	SOURCE		DETECTOR		ANGLE
			TYPE	RANGE	TYPE	RANGE	
G,N	NOX	THR- 27	C	10- 27	BF3-I		4PI

MEAN NEUT ENERGY

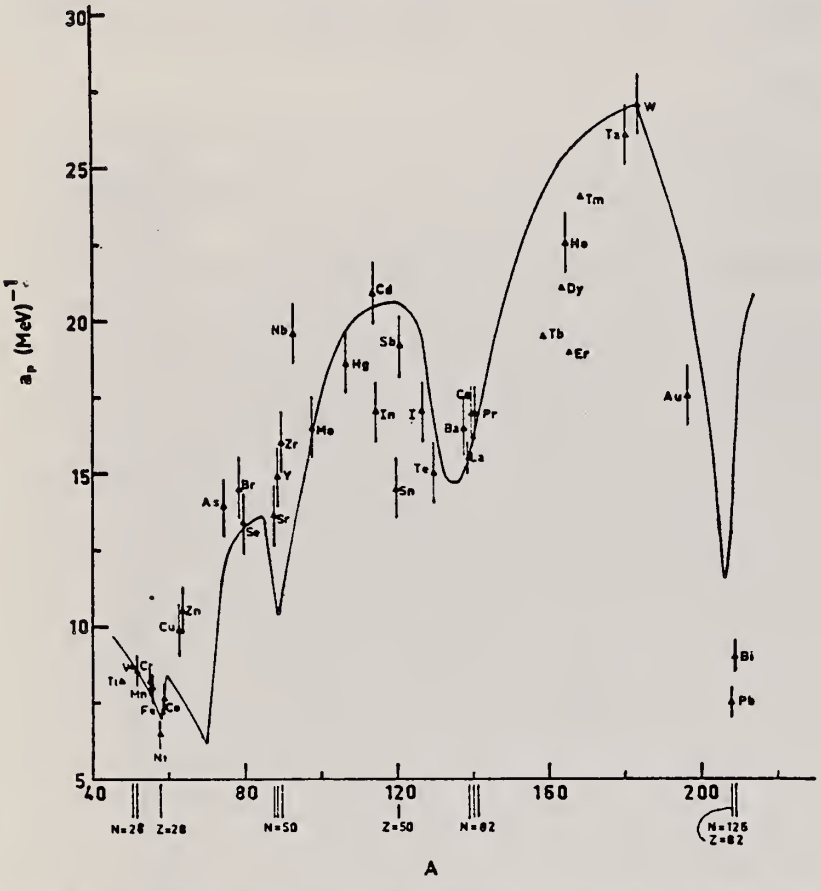

Fig. 12. Experimental values of the level density parameter a_p (Fermi gas formula plus pairing correction) versus atomic number A. The continuous curve is a least-squares fit to the data of a theoretical calculation from Newton [15].

1
H. Baba and S. Baba, Japan Atomic Energy Research Institute report JAERI-1183 (1969).
2
H. Baba, Nucl. Phys. A159, 625 (1970).
15
T.D. Newton, Can. J. Phys. 34, 804 (1956).

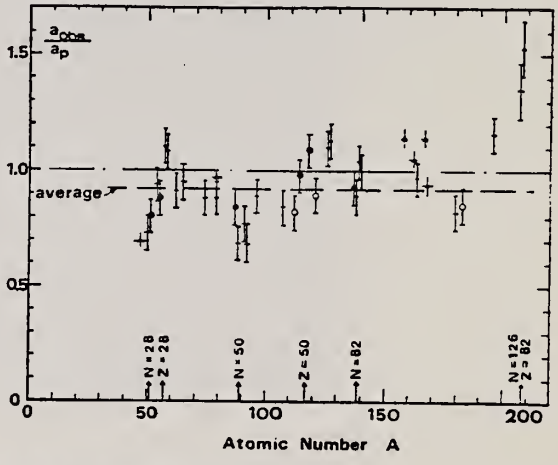

Fig. 15. Ratio a_{obs}/a_p versus atomic number A. Here a_{obs} is the level density parameter taken from the neutron resonance work of refs. [1,2]), and a_p is the level density parameter derived from the present (γ, n) work. Filled circles represent points where nuclei in the neutron resonance and in the (γ, n) experiment were the same. Open circles represent points where the respective nuclei were approximately matched. Triangles represent points which are based on measurement of neutron mean energies at two bremsstrahlung energies only.

(over)

TABLE 3 (continued)

Target	N (residual nucleus) [a]		Goodness of fit [b]		$\hat{E}_0(24)$ (MeV) [c]	T (MeV) [d]	a_p (MeV^{-1}) [e]	a_{obs} (MeV^{-1}) [f]	a_{obs}/a_p
			no p.c.	with p.c.					
Ba	75	1%		F	1.16		16.5–^{136}Ba	15.39–^{136}Ba	0.93
	77	2%							
	78	7%							
	79	8%							
	80	11%							
	81	71%							
La	80	100%	F	F	1.25	0.72	15.5–^{138}La	13.76–^{139}La	0.89
Ce	81	89%	F	G	1.24	0.70	17.0–^{139}Ce	17.8 –^{141}Ce	1.04
	83	11%							
Pr	81	100%	G	G	1.17	0.65	17.0–^{140}Pr	17.05–^{142}Pr	1.00
Tb [g]	93	100%			1.15		19.3–^{158}Tb	21.85–^{160}Tb	1.14
Dy [g]	93	2%			1.06		20.9–$^{161.5}$Dy	21.9 –^{162}Dy	1.05
	94	19%							
	95	25%							
	96	25%							
	97	28%							
Ho	97	100%	P	G	1.06	0.56	21.4–^{164}Ho	20.66–^{166}Ho	0.97
Er [g]	95	2%			1.11		19.2–^{166}Er	21.9 –^{166}Er	1.14
	97	33%							
	98	23%							
	99	27%							
	101	15%							
Tm [g]	99	100%			1.03		24.0–^{168}Tm	22.58–^{170}Tm	0.94
Ta	107	100%		G	1.00	0.49	26.0–^{180}Ta	21.2 –^{181}Ta	0.82
W	107	26%	G	F	0.98	0.50	27.0–^{183}W	23.0 –^{183}W	0.85
	108	14%							
	109	31%							
	111	28%							
Au	117	100%		G	1.19		17.5–^{196}Au	20.24–^{198}Au	1.16
Pb	123	24%		V.P.	1.87	1.20	7.5–^{206}Pb	10.1 –^{207}Pb	1.35
(Z = 82)	124	23%							
	125	52%							
Bi	125	100%		F	1.65	1.03	9.0–^{208}Bi	13.8 –^{210}Bi	1.53

[a] Neutron numbers and abundances of respective residual nuclei in (γ, n) experiments.

[b] These give an assessment of the goodness of fit of a calculated $\hat{E}_0$ versus E_0 curve to the observed data, using the Fermi gas level density formula both without and with pairing corrections.

[c] Bremsstrahlung photoneutron mean energies $\hat{E}_0$ for peak bremsstrahlung energy E_0 = 24 MeV.

[d] Nuclear temperature from fit with constant-temperature formula.

[e] Level density parameter a_p derived from the present (γ, n) experiment, using a Fermi gas formula plus pairing correction, and corresponding residual nucleus (the atomic weight shown is the weighted average of atomic weights of the respective isotopes present).

[f] As column 7, but using data on n-resonance absorption from refs. [1, 2]).

[g] Measurements of $\hat{E}_0(E_0)$ for these nuclei were made only for E_0 = 21, 23 and 24 MeV.

REF. E. Hayward, W. C. Barber, and Jed Sazama
Phys. Rev. C8, 1065 (1973)

ELEM. SYM.	A	Z
W		74

METHOD

REF. NO. 73 Ha 3 hmg

REACTION	RESULT	EXCITATION ENERGY	SOURCE		DETECTOR		ANGLE
			TYPE	RANGE	TYPE	RANGE	
$ G,G	RLY	15	D	15	NAI-D		90
		(15.1)		(15.1)			

POLARIZED PHOTONS

TABLE II. Results.

Target	$d\sigma^{\parallel}/d\Omega_F$ Arbitrary units	$d\sigma^{\perp}/d\Omega_F$ Arbitrary units	η_F	η	$\eta(DCM)$
Cd	0.042 ± 0.028	0.39 ± 0.05	0.11 ± 0.07	0.09 ± 0.07	0.19
Sn	0.084 ± 0.036	0.65 ± 0.06	0.13 ± 0.06	0.11 ± 0.06	0.07
Ta	0.24 ± 0.10	1.47 ± 0.14	0.16 ± 0.07	0.14 ± 0.07	0.20
W	0.52 ± 0.10	1.66 ± 0.12	0.31 ± 0.07	0.29 ± 0.07	0.20
Pt	0.23 ± 0.08	1.94 ± 0.13	0.12 ± 0.04	0.10 ± 0.04	0.08
Au	0.39 ± 0.11	2.08 ± 0.15	0.19 ± 0.06	0.17 ± 0.06	0.07
Bi	0.10 ± 0.15	2.65 ± 0.26	0.04 ± 0.06	0.02 ± 0.06	0

REF. A. Veyssiere, H. Beil, R. Bergere, P. Carlos, A. Lepretre, A. De Miniac
J. Phys. Lett. 36, L267 (1975)

ELEM. SYM.	A	Z
W		74

METHOD

REF. NO. 75 Ve 5 egf

REACTION	RESULT	EXCITATION ENERGY	SOURCE		DETECTOR		ANGLE
			TYPE	RANGE	TYPE	RANGE	
G,N *	ABX	8- 22	D	8- 22	MOD-I		4PI
G,2N **	ABX	13- 22	D	8- 22	MOD-I		4PI

Abstract. — Partial photoneutron cross-sections [$\sigma(\gamma, n) + \sigma(\gamma, pn)$], and $\sigma(\gamma, 2n)$ of W, Re, Ir, Pt and Hg were measured by means of monochromatic photons of 8 MeV $\leq E \leq$ 22 MeV so as to study the giant resonance. The experimentally observed evolution of the shape of the GDR, as one proceeds from permanently deformed prolate nuclei (W and Re) towards oblate or even triaxial gamma unstable nuclei (Pt), corresponds to the theoretical predictions of the dynamic collective model.

* 1020+
** 1021

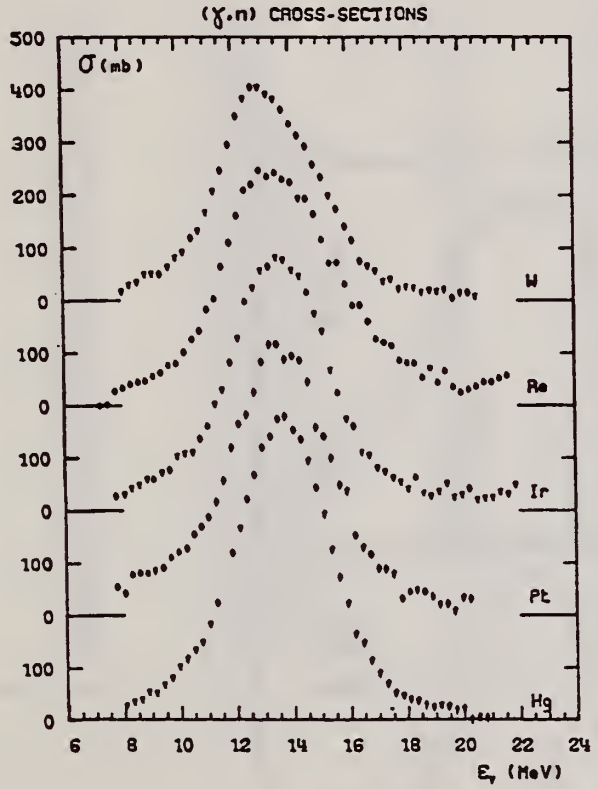

FIG. 1. — Sections efficaces partielles $\sigma(\gamma, n) + \sigma(\gamma, pn)$ des noyaux W, Re, Ir, Pt, Hg.

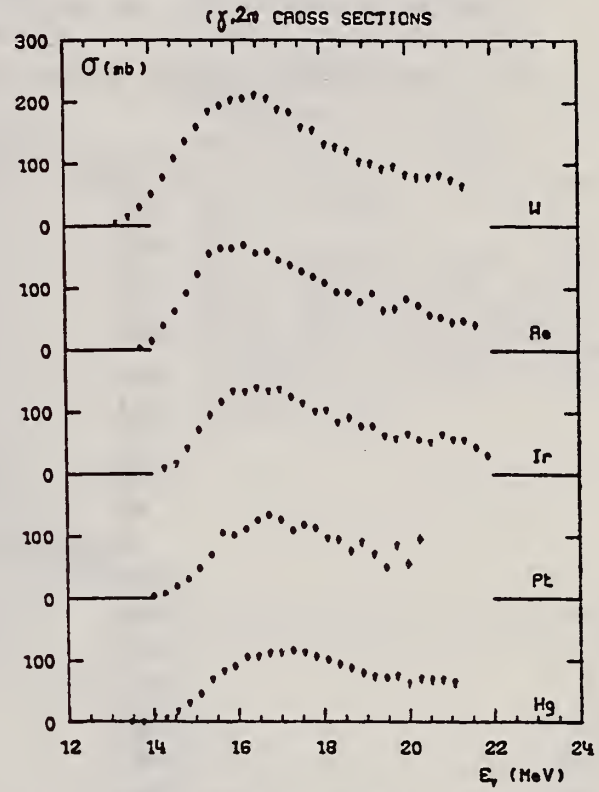

FIG. 2. — Sections efficaces partielles $\sigma(\gamma, 2n)$ des noyaux W, Re, Ir, Pt, Hg.

(over)

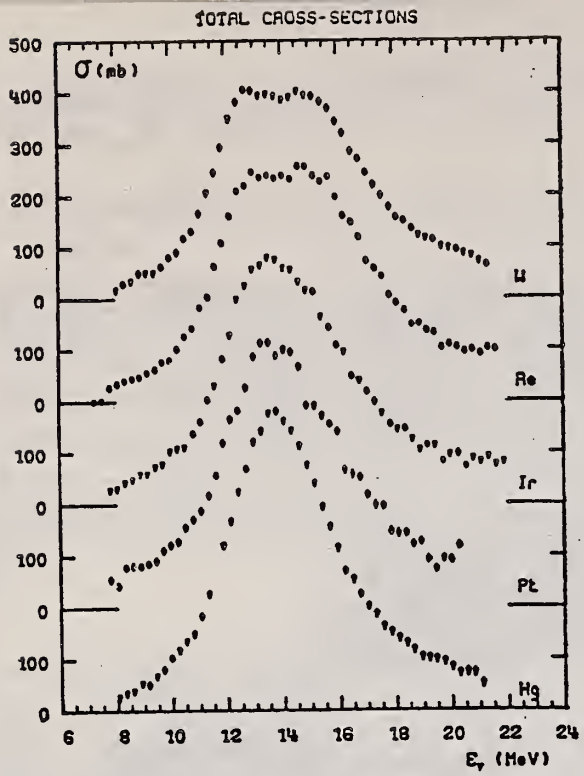

FIG. 3. — Sections efficaces totales $\sigma_T(E)$ des noyaux W, Re, Ir, Pt, Hg.

TABLEAU I

	σ_1 mb	Γ_1 MeV	E_1 MeV	σ_2 mb	Γ_2 MeV	E_2 MeV
W	300	3,2	12,7	290	4,3	15,4
Re	310	3,3	12,8	330	4,45	15,4

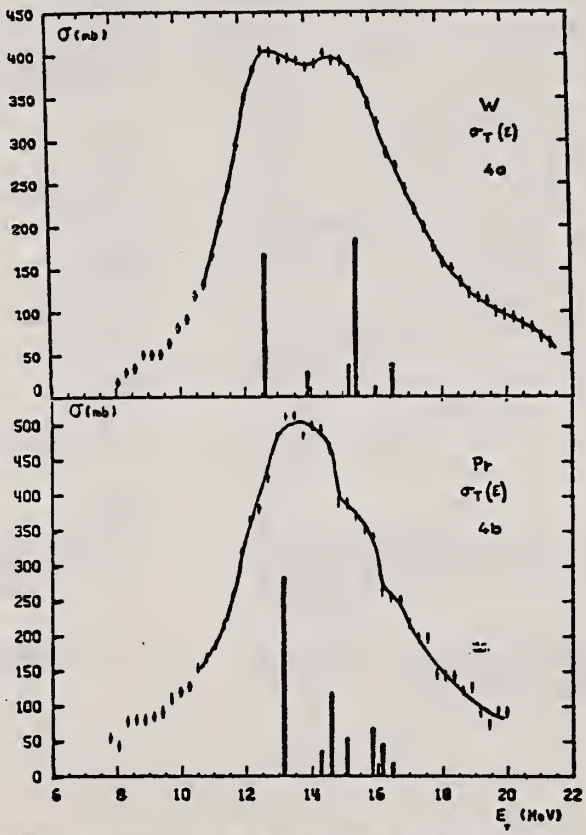

FIG. 4. — Comparaison des sections efficaces totales expérimentales $\sigma_T(E)$ des noyaux W et Pt avec les prédictions du modèle collectif dynamique [12] positionnées de façon à faire coïncider les énergies moyennes observées et calculées de la RGD.

REF.

V. Emma, S. Lo Nigro, C. Milone
Nucl. Phys. A257, 438 (1976)

ELEM. SYM.	A	Z
W		74

METHOD

REF. NO. 76 Em 2 egf

REACTION	RESULT	EXCITATION ENERGY	SOURCE TYPE	SOURCE RANGE	DETECTOR TYPE	DETECTOR RANGE	ANGLE
G,F	ABY	THR-999	C	999	TRK-I		4PI

TABLE I

Measured values of σ_q at $E = 1000$ MeV and deduced values of σ_k assumed constant from E_0 to 1000 MeV

Element	Z^2/A	σ_q (mb)	E_0 (MeV)	σ_k (mb)
Bi	32.96	12.3 ± 0.6	200	7.6 ± 0.6
Pb	32.45	5.4 ± 0.4	220	3.6 ± 0.3
Tl	32.10	4.1 ± 0.3	230	2.8 ± 0.3
Au	31.68	2.0 ± 0.15	240	1.4 ± 0.2
Pt	31.18	1.1 ± 0.08	255	$(8 \pm 0.7) \times 10^{-1}$
Re	30.21	$(3.7 \pm 0.3) \times 10^{-1}$	280	$(2.9 \pm 0.3) \times 10^{-1}$
W	29.78	$(3.5 \pm 0.3) \times 10^{-1}$	290	$(2.8 \pm 0.3) \times 10^{-1}$
Ta	29.45	$(3.3 \pm 0.3) \times 10^{-1}$	300	$(2.7 \pm 0.3) \times 10^{-1}$
Hf	29.04	$(1.7 \pm 0.2) \times 10^{-1}$	310	$(1.4 \pm 0.2) \times 10^{-1}$
Yb	28.31	$(1.3 \pm 0.1) \times 10^{-1}$	330	$(1.2 \pm 0.1) \times 10^{-1}$
Tm	28.18	$(7.5 \pm 0.8) \times 10^{-2}$	335	$(6.8 \pm 0.8) \times 10^{-2}$
Ho	27.21	$(3.6 \pm 0.4) \times 10^{-2}$	355	$(3.5 \pm 0.4) \times 10^{-2}$
Dy	26.80	$(2.6 \pm 0.3) \times 10^{-2}$	360	$(2.5 \pm 0.3) \times 10^{-2}$
Tb	26.58	$(2.5 \pm 0.3) \times 10^{-2}$	370	$(2.5 \pm 0.3) \times 10^{-2}$
Gd	26.04	$(1.6 \pm 0.2) \times 10^{-2}$	380	$(1.7 \pm 0.2) \times 10^{-2}$
Sm	25.56	$(1.3 \pm 0.2) \times 10^{-2}$	390	$(1.4 \pm 0.2) \times 10^{-2}$
Nd	24.96	$(9.2 \pm 0.9) \times 10^{-3}$	405	$(1 \pm 0.1) \times 10^{-2}$
Ce	24.00	$(8 \pm 0.9) \times 10^{-3}$	420	$(9 \pm 1) \times 10^{-3}$
La	23.39	$(8.4 \pm 0.9) \times 10^{-3}$	430	$(1 \pm 0.1) \times 10^{-3}$
Sb	21.36	$(1.2 \pm 0.2) \times 10^{-2}$	460	$(1.5 \pm 0.3) \times 10^{-2}$
Te	21.19	$(8.8 \pm 1) \times 10^{-3}$	465	$(1.2 \pm 0.2) \times 10^{-2}$
Sn	21.06	$(1.3 \pm 0.2) \times 10^{-2}$	465	$(1.7 \pm 0.3) \times 10^{-2}$
Cd	20.49	$(1.7 \pm 0.3) \times 10^{-2}$	470	$(2.2 \pm 0.4) \times 10^{-2}$
Ag	20.47	$(2 \pm 0.3) \times 10^{-2}$	470	$(2.6 \pm 0.4) \times 10^{-2}$
Zn	13.76	$(2 \pm 0.4) \times 10^{-1}$	515	$(3 \pm 0.6) \times 10^{-1}$
Cu	13.44	$(2.4 \pm 0.5) \times 10^{-1}$	515	$(3.6 \pm 0.8) \times 10^{-1}$
Ni	13.35	$(2.4 \pm 0.5) \times 10^{-1}$	510	$(3.6 \pm 0.8) \times 10^{-1}$
Fe	12.10	$(3 \pm 0.6) \times 10^{-1}$	510	$(4.4 \pm 0.9) \times 10^{-1}$

999 = 1 GEV

[4] A.V. Mitrofanova et al. Sov. J. Nucl. Phys. 6, 512 (1968).

[7] T. Methasiri et al., Nucl. Phys. A167, 97 (1971).

[12] J.R. Nix et al., Nucl. Phys. 81, 61 (1966).

[20] N.A. Perifilov et al., JETP (Sov. Phys.) 14, 623 (1962); Proc. Symp. on the physics & chemistry of fission, Salzburg 1965, vol. 2 (IAEA) Vienna, 1965, p.283.

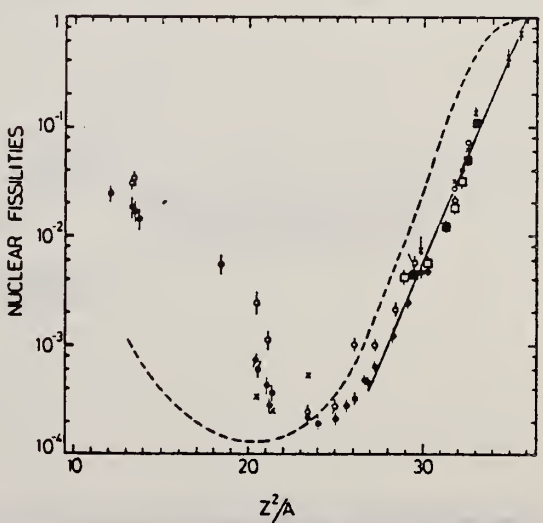

Fig. 2. Nuclear fissilities as a function of Z^2/A. Experimental points: solid circles represent our data; squares, the data from ref. [4]); open circles, the data from ref. [7]); and crosses, the data from (p,f) experiments[20]). The straight line is the best fit calculated from our data for $Z^2/A > 26$. The dashed curve is the curve VI calculated by Nix and Sassi[12]).

REF.		ELEM. SYM.	A	Z
	V.G. Vlasenko, V.A. Gol'dshtein, A.V. Mitrofanova, V.I. Noga, Yu.N. Ranuuk, V.I. Startsev, P.V. Sorokin, Yu.N. Telegin Yad. Fiz. 23, 504 (1976) Sov. J. Nucl. Phys. 23, 265 (1976)	W		74
METHOD		REF. NO.		
		76 V1 1		hmg

REACTION	RESULT	EXCITATION ENERGY	SOURCE		DETECTOR		ANGLE
			TYPE	RANGE	TYPE	RANGE	
E,E/	ABX	100-500	D	1* 2	MAG-D		DST

Inelastic electron scattering has been used to measure the total hadronic cross sections for absorption of photons with energy 150–500 MeV by nuclei of C, Al, Ni, Mo, and W. The results obtained are compared with calculations carried out in the impulse approximation.

*E IN GEV,1.2,1.36

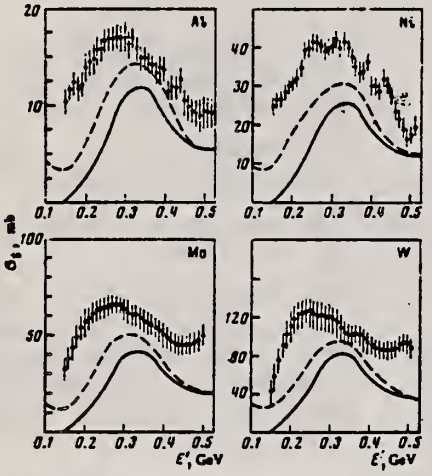

FIG. 5. Total hadronic cross sections for absorption of photons by nuclei.

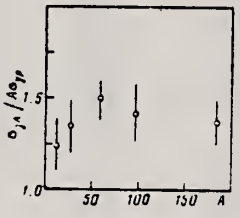

FIG. 6. The ratio $\sigma_{\gamma A}/A\sigma_{\gamma p}$ as a function of A for $k=0.32$ GeV.

REF. A.V. Mitrofanova, V.I. Noga, A.I. Popov, Yu.N. Ranyuk and Yu.N. Telegin
Yad. Fiz. 25, 926 (1977)
Sov. J. Nucl. Phys. 25, 493 (1977)

ELEM. SYM.	A	Z
W		74

METHOD

REF. NO.	
77 Mi 11	hmg

REACTION	RESULT	EXCITATION ENERGY	SOURCE TYPE	SOURCE RANGE	DETECTOR TYPE	DETECTOR RANGE	ANGLE
1. G,SPL	ABY	THR-999	C	600-999	ACT-I		4PI
2. E,SPL	ABY	THR-999	D	999	ACT-I		4PI

The induced activity method has been used to measure the yields of 15 photonuclear reactions in tantalum and tungsten nuclei in the photon energy range 600–1300 MeV. The cross sections have been calculated in the approximation of a rectangular bremsstrahlung spectrum. Rudstam's semiempirical formula has been used to analyze the experimental data. For the reactions in tungsten the ratios of the yields produced by photons and electrons have been measured.

1. 999=1.3 GEV DST NA24
2. 999=1.27 GEV

TABLE I.

№	Initial nucleus	Emitted nucleus	Residual nucleus	$\bar{\sigma}_k$ (600–1300 MeV), mb	$E_{\gamma max}$=1000 MeV: σ_Q, mb (exp)	σ_Q, mb (theory)	σ_Q, mb (Ref. 6)	$\frac{\sigma_Q}{\bar{\sigma}_k}$
1	$^{180-181,186}_{74}W$	4p, 9–13n	$^{169}_{70}Yb$	2.2	3.1±0.6	2.36	–	24.5±4.9
		3p, 10–15n	$^{169}_{71}Lu$					
2	$^{182-181,186}_{74}W$	2p, 5–9n	$^{173}_{72}Hf$	4.0	3.6±1.1	0.58	–	22±4
3	$^{182-184,186}_{74}W$	4p, 11–15n	$^{167}_{70}Yb$	2.0	1.9±0.4	1.58	–	27±5
4	$^{182-184,186}_{74}W$	3p, 8–12n	$^{171}_{71}Lu$	1.96 *	2.2±0.4 *	3.9	–	23±4
		2p, 9–13n	$^{171}_{72}Hf$					
5	$^{182-184,186}_{74}W$	3p, 6–10n	$^{173}_{71}Lu$	4.0	5.5±1.1	4.6	–	27±5
		2p, 7–11n	$^{173}_{72}Hf$					
6	$^{182-184,186}_{74}W$	10p, 26–30n	$^{146}_{64}Gd$	10.4	5.0±1.0	0.10	–	–
7	$^{182, 183, 184, 186}_{74}W$	1p, 0–4n	$^{182}_{73}Ta$	1.63	2.3±0.5	–	–	28±5
8	$^{182, 183, 184, 186}_{74}W$	2p, 0–3n	$^{181}_{72}Hf$	0.09	0.12±0.02	–	–	31±6
9	$^{181}_{73}Ta$	3p, 9n	$^{169}_{70}Yb$	2.3	3.8±0.7	3.2	7.07	–
		2p, 10n	$^{169}_{71}Lu$					
10	$^{181}_{73}Ta$	1p, 5n	$^{175}_{72}Hf$	3.3	5.8±1.1	0.7	8.9	–
11	$^{181}_{73}Ta$	2p, 6n	$^{173}_{71}Lu$	2.6	6.2±1.2	2.44	6.55	–
		1p, 7n	$^{173}_{72}Hf$					
12	$^{181}_{73}Ta$	3p, 11n	$^{167}_{70}Yb$	2.0	2.9±0.6	1.9	3.67	–
		4p, 10n	$^{167}_{69}Tm$					
13	$^{181}_{73}Ta$	2p, 8n	$^{171}_{71}Lu$	1.52 *	2.4±0.5 *	4.8	3.67	–
		1p, 9n	$^{171}_{72}Hf$					
14	$^{181}_{73}Ta$	9p, 25n	$^{146}_{64}Gd$	9.6	8.5±1.7	0.12	–	–

*In view of the absence of data on the absolute intensities of the γ lines in the spectrum of ^{171}Lu activity, in calculation of σ_Q the intensity of the peak E_γ = 739 keV was taken as 100%.

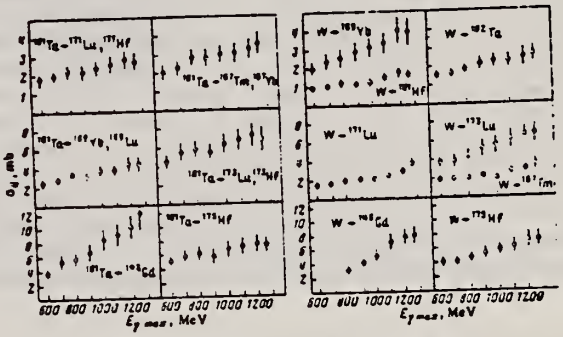

FIG. 2. Reaction yields: a) in ^{181}Ta, b) in W.

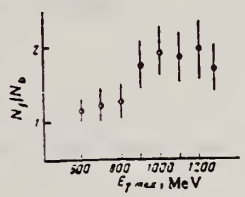

FIG. 3. Anisotropy of the yield of the fragment ^{24}Na from W.

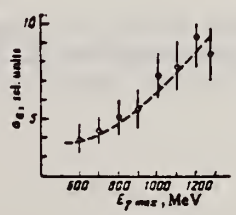

FIG. 4. Yield of the reaction W $\rightarrow$ ^{24}Na as a function of bremsstrahlung maximum energy.

REF. V. Bellini, V. Emma, A.S. Figuera, S. Lo Nigro, C. Milone, G.S. Pappalardo, G. Bologna
Il Nuovo Cimento 47A, 529 (1978)

ELEM. SYM.	A	Z
W		74

METHOD

REF. NO. 78 Be 10 hg

REACTION	RESULT	EXCITATION ENERGY	SOURCE		DETECTOR		ANGLE
			TYPE	RANGE	TYPE	RANGE	
G,F	RLX	180-999	C	220-999	TRK-D		4PI

Zero cross section assumed below 180 MeV.

COHERENT BREM.

Summary. — The photofission yields of Re, W and Ta induced by a coherent bremsstrahlung beam from 1000 MeV electrons striking a diamond single crystal have been measured. The experiment has been performed at eighteen different energies of the main peak of the photon spectrum, in the energy range between 220 MeV and 550 MeV, by detecting the fission fragments with glass sandwiches. The behaviour of the photofission cross-section has been deduced from the experimental yields by using an appropriate unfolding method. The obtained curves clearly show a first resonance centred at a photon energy $k \simeq 350$ MeV with a FWHM $\simeq 145$ MeV, while there is a hint of a second resonance at $k \simeq 750$ MeV. Information on the energy dependence of the nuclear fissility from 100 MeV to 1000 MeV has been deduced from the comparison of the estimated photofission cross-section with the total photon interaction cross-section. It has been found that the photomesonic model of the fission process permits to explain the energy dependence of our photofission cross-sections if a nuclear fissility increasing with photon energy is assumed.

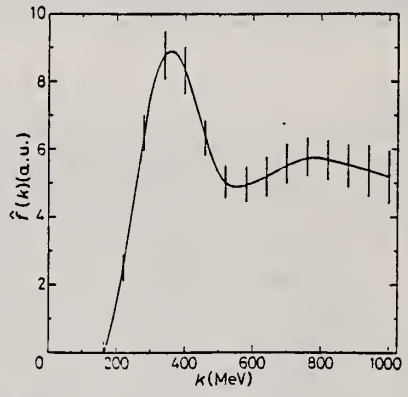

Fig. 7.

Fig. 7. – See caption to fig. 6. Result for W(γ, f).

Fig. 6. – Photofission cross-section estimated by our unfolding method. Results for Re (γ, f).

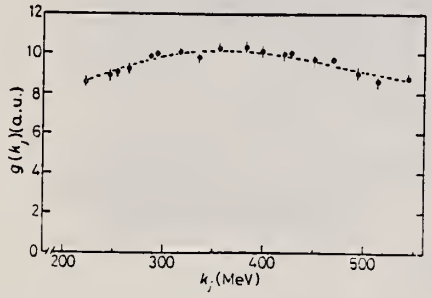

Fig. 4.

Fig. 4. – See caption to fig. 3. Results for W.

Fig. 3. – Photofission yields per equivalent quantum as a function of the first-peak energy k_i of photons. The dots are the experimental data; the dashed curve represents the yield function recalculated from the $f(k)$ data. Results for Re.

(over)

TABLE II. – *Estimated $\hat{f}_i$ values and corresponding errors.* All the data are given in arbitrary units.

k	$\hat{f}(k)$ (arbitrary units)		
(MeV)	Re	W	Ta
100	-0.31 ± 0.85	-0.14 ± 0.85	-0.49 ± 0.87
160	0.03 ± 0.31	0.24 ± 0.31	0.26 ± 0.33
220	1.95 ± 0.41	2.50 ± 0.41	2.51 ± 0.41
280	6.26 ± 0.53	6.51 ± 0.53	6.63 ± 0.55
340	8.90 ± 0.69	8.75 ± 0.69	8.56 ± 0.68
400	8.16 ± 0.72	8.38 ± 0.72	7.15 ± 0.70
460	6.10 ± 0.51	6.34 ± 0.51	5.43 ± 0.49
520	4.83 ± 0.47	5.04 ± 0.47	4.70 ± 0.48
580	4.70 ± 0.57	4.95 ± 0.57	4.72 ± 0.58
640	4.96 ± 0.59	5.20 ± 0.59	4.98 ± 0.60
700	5.41 ± 0.58	5.57 ± 0.58	5.29 ± 0.58
760	5.68 ± 0.57	5.78 ± 0.57	5.41 ± 0.57
820	5.65 ± 0.61	5.71 ± 0.61	5.32 ± 0.61
880	5.51 ± 0.67	5.53 ± 0.67	5.18 ± 0.67
940	5.38 ± 0.74	5.36 ± 0.74	4.98 ± 0.73
1000	5.23 ± 0.80	5.18 ± 0.80	4.70 ± 0.77

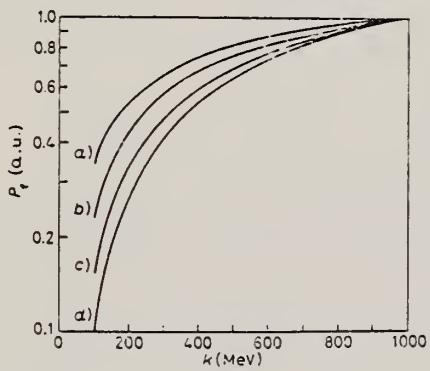

Fig. 11.

Fig. 11. – Nuclear fissility P_f as a function of the photon energy k. The curves are normalized at $k = 1000$ MeV. *a*) Bi, *b*) Pb, *c*) Au, *d*) Ta.

W
A=182

W
A=182

W
A=182

REF.

Yu. I. Sorokin, V.A. Khrushchev, and B.A. Yur'ev
Yad. Fiz. 17, 3 (1973)
Sov. J. Nucl. Phys. 17, 1 (1973)

ELEM. SYM.	A	Z
W	182	74

METHOD

REF. NO.: 73 So 16 hmg

REACTION	RESULT	EXCITATION ENERGY	SOURCE		DETECTOR		ANGLE
			TYPE	RANGE	TYPE	RANGE	
G,XN	ABX	8- 28	C	0- 28	BF3-I		4PI

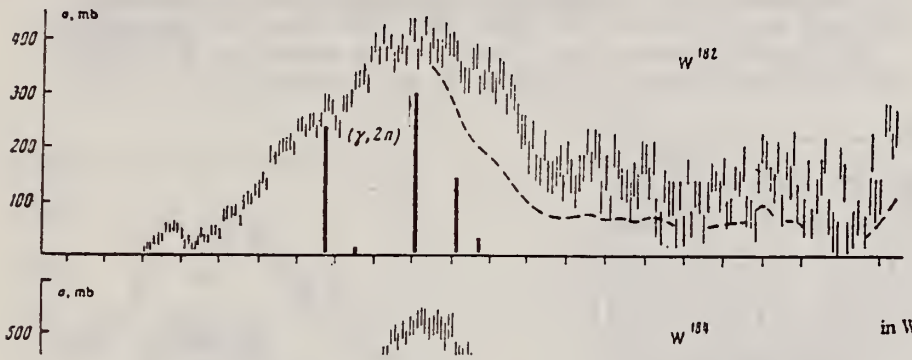

Cross sections for photoneutron reactions in W^{182} and W^{184}.

Figure gives σ(sn) obtained by correcting σ(xn) for neutron multiplicity. Berman's statistical factors for W-186 used.

TABLE 1. Giant-resonance characteristics of W^{182} and W^{184}

	W^{182}	W^{184}		W^{182}	W^{184}
E_1, MeV	12,1±0.1	12.2±0.1	$R_A = \sigma_1\Gamma_1 / \sigma_2\Gamma_2$	0.28±0.03	0.17±0.02
σ_1, mb	145±7	145±7	e	0.473±0.07	0.45±0.07
Γ_1, MeV	2,7±0,1	2±0.1	$Q_2 = 0{,}4ZR^2e$, b	7.2±0.9	6.8±0.9
E_2, MeV	14,8±0.1	14.7±0.1	Q_3 [9], b	6.57	6.21
σ_2, mb	337±8	428±9			
Γ_2, MeV	3.5±0.1	4.0±0.1			

TABLE 2. Integrated cross sections of W^{182} and W^{184}

		W^{182}	W^{184}
$\sigma(\gamma, Tn)$	From threshold to 27.4 MeV	3.68	4.88
	From threshold to 20 MeV	2.75	3.46
σ_γ	From threshold to 20 MeV	2.32	2.33
	From 20 to 27.4 MeV	0.46	0.72
	From threshold to 27.4 MeV	2.78	2.95
$0{,}06\,NZ/A$		2.63	2.65
$\sigma(E2)$		0.45	0.48

REF.

Yu. I. Sorokin and B. A. Yur'ev
Izv. Akad. Nauk SSSR. Ser. Fiz. 39, 114 (1975)
Bull. Acad. Sci. (USSR) Phys. Ser. 39, 98 (1975)

ELEM. SYM.	A	Z
W	182	74

METHOD

REF. NO.: 75 So 12 | hmg

REACTION	RESULT	EXCITATION ENERGY	SOURCE		DETECTOR		ANGLE
			TYPE	RANGE	TYPE	RANGE	
G,XN	ABI	8- 27	C	8- 27	BF3-I		4PI

SEE 73SO16

Table 1

Element	A	σ_0, (γ, Tn) MeV · b	$\sigma_{\sigma\gamma}$ MeV · b		σ_{-1}, mb	σ_{-2}, mb × MeV^{-1}	E_m, MeV	K, MeV	$\alpha(A-1)$ MeV^{-1}	Threshold (γ,2n), MeV	σ_0 (E1), MeV × b
		to 27 MeV	to 20 MeV	20–27 MeV							
Sn	112	2,23	1,80	1,49	0,41	112	6,7	15,8	20,1	10,2	19,2	1,66
	114	2,26	1,86	1,55	0,47	108	6,5	15,7	21,5	10,2	18,1	1,68
	116	2,40	1,85	1,40	0,45	110	6,6	15,6	21,7	8,1	17,1	1,71
	117	2,52	1,86	1,39	0,47	110	6,7	15,4	21,6	7,3	16,5	1,72
	118	2,46	1,92	1,53	0,39	115	7,1	15,5	20,7	5,6	16,3	1,71
	119	2,64	1,86	1,42	0,44	111	6,8	15,4	22,0	13,2	15,8	1,74
	120	2,69	2,07	1,69	0,38	127	7,9	15,3	19,1	3,6	15,6	1,75
	122	2,94	2,01	1,51	0,52	119	7,1	15,6	21,8	4,5	15,0	1,77
	124	2,90	1,93	1,44	0,49	114	6,9	15,5	23,2	5,4	14,4	1,79
W	182	3,68	2,78	2,32	0,46	184	12,5	-	24,2	5,2	14,9	2,63
	184	4,88	2,95	2,34	0,72	196	13,0	--	23,7	5,2	13,6	2,65
Au	197	4,06	3,15	2,81	0,34	226	15,5	13,3	20,9	17,1	14,8	2,84
Pb	206	3,93	3,21	2,80	0,41	225	16,1	13,5	23,1	6,5	14,8	2,96
	208	4,32	3,28	2,81	0,47	231	16,7	13,3	22,6	9,6	14,1	2,98
Bi	209	4,59	3,47	2,96	0,51	246	17,9	13,2	21,3	10,2	14,3	3,00

REF. G. M. Gurevich, L. E. Lazareva, V. M. Mazur, and G. B. Solodukhov
JETP Lett. 23, 370 (1976)
Pis'ma Zh. Eksp. Teor. Fiz. 23, 411 (1976)

ELEM. SYM.	A	Z
W	182	74

METHOD

REF. NO. 76 Gu 5 hmg

REACTION	RESULT	EXCITATION ENERGY	SOURCE		DETECTOR		ANGLE
			TYPE	RANGE	TYPE	RANGE	
G,MU-T	ABX	8- 21	C	35	NAI-D		4PI

We measured the total cross section for the absorption of rays in the region of $E1$ resonance for the nuclei ^{165}Ho, ^{178}Hf, ^{180}Hf, ^{181}Ta, ^{182}W, ^{197}Au, and ^{209}Bi. The singularity in the behavior of the resonance widths, observed in the region $160 < A < 185$, is apparently due to the influence of the neutron subshell $N = 108$.

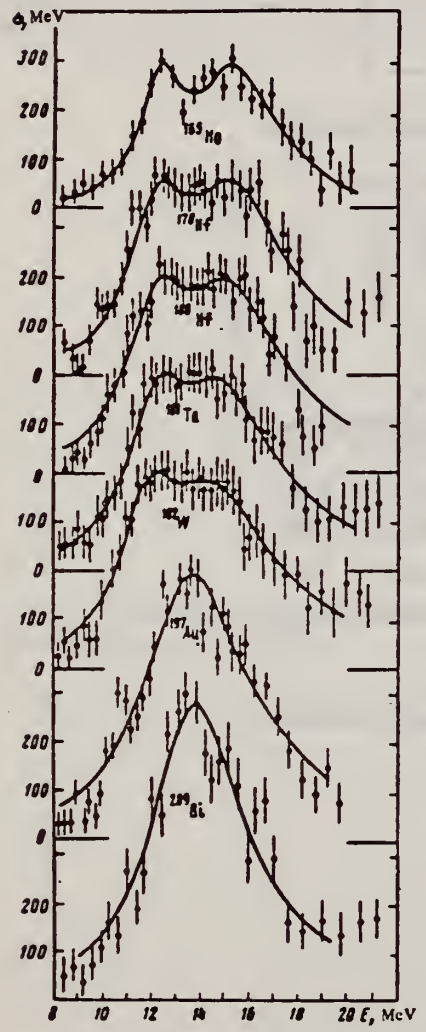

FIG. 1. Total photoabsorption cross sections for the nuclei ^{165}Ho, ^{178}Hf, ^{180}Hf, ^{181}Ta, ^{182}W, ^{197}Au, ^{209}Bi.

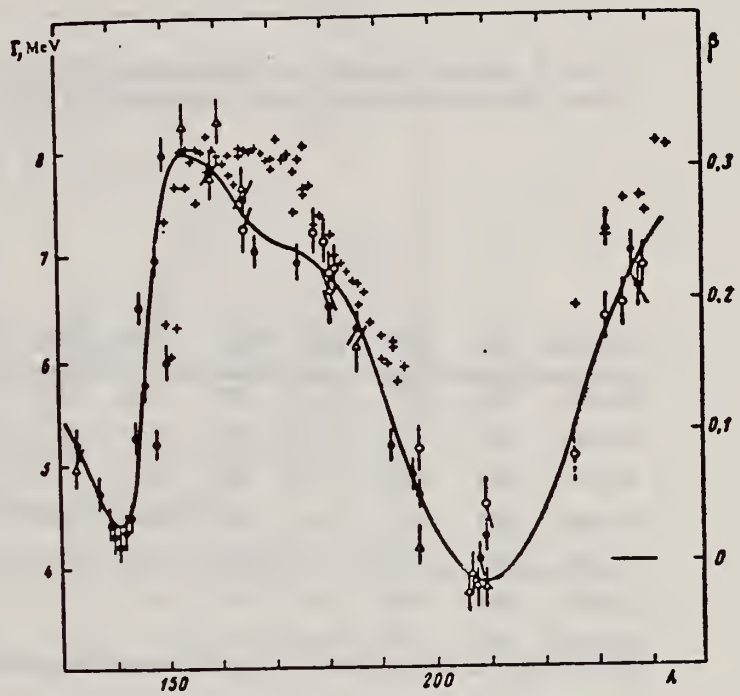

FIG. 2. Widths Γ of $E1$ giant resonance in the region of nuclei with $A > 150$ according to the data of Saclay (●), Livermore (Δ), and the Institute of Nuclear Research of the USSR Academy of Sciences (○). The crosses mark the deformation parameters β.

Over

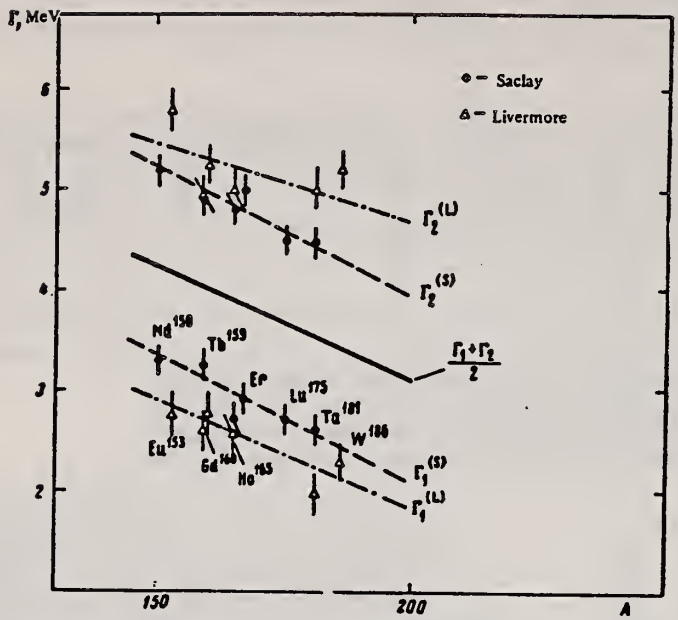

FIG. 3. Width of Lorentz lines approximating the photoabsorption cross sections, for deformed nuclei in the region $150 < A < 185$.

Nucleus	σ_1 mb	Γ_1 MeV	E_1 MeV	σ_2 mb	Γ_2 MeV	E_2 MeV	$\frac{\sigma_2\Gamma_2}{\sigma_1\Gamma_1}$	Q_0 b	β
Ho-165	235	2.0	12.2	272	4.0	15.5	2.3	6.8±0.8	0.29
Hf-178	291	3.1	12.2	334	4.9	15.5	1.8	7.5±0.8	0.28
Hf-180	286	3.2	12.2	324	5.1	15.3	1.8	7.2±0.8	0.27
Ta-181	272	3.0	12.1	316	5.1	15.0	2.0	6.8±0.8	0.26
W-182	267	3.2	11.9	303	5.6	14.8	2.0	7.2±0.8	0.26
Au-197	535	5.2	13.7	...	...	...	...	...	...
Bi-209	600	4.6	13.8	...	...	...	...	...	...

REF. W. Günther, R. Haag, K. Huber, U. Kneissl, H. Krieger, H.J. Maier, H. Ströher
Phys. Rev. Lett. 44, 716 (1980)

ELEM. SYM.	A	Z
W	182	74

METHOD

REF. NO.	
80 Gu 1	hg

REACTION	RESULT	EXCITATION ENERGY	SOURCE		DETECTOR		ANGLE
			TYPE	RANGE	TYPE	RANGE	
E,F	NOX	THR-55	D	35-55	TRK-D		4PI

Low end of experimental arrows in Fig. 1 indicated lower limit for fission barriers established by this experiment.

The electroinduced fission of ^{182,184,186}W has been investigated in the energy range from 35 to 55 MeV. The fission barriers, estimated by a statistical-model analysis of the measured cross sections, are compared with theoretical predictions and are only consistent with the assumption of a constant pairing strength.

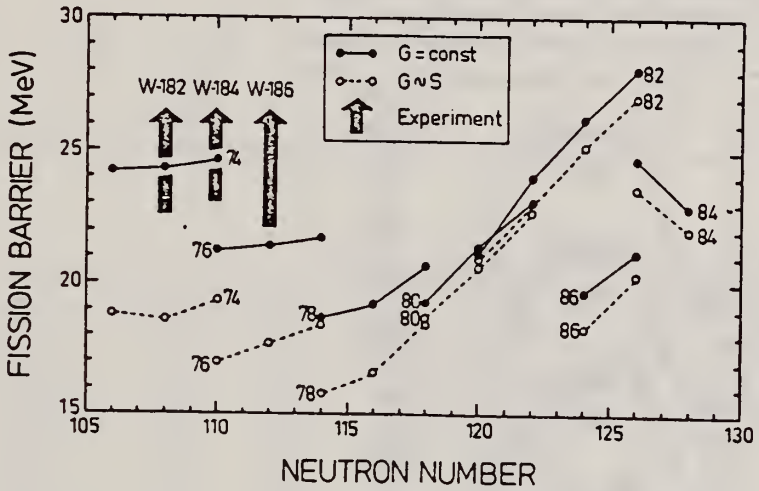

FIG. 1. Calculated fission barriers (Ref. 3) (full lines, G = const; dashed lines, $G \sim S$) and limits deduced from our experiments on ^{182,184,186}W.

REF. G.M. Gurevich, L.E. Lazareva, V.M. Mazur, S.Yu. Merkulov, G.V. Solodukhov, V.A. Tyutin
Nucl. Phys. A351, 257 (1981)

ELEM. SYM	A	Z
W	182	74

METHOD

REF. NO.	
81 Gu 2	hg

REACTION	RESULT	EXCITATION ENERGY	SOURCE		DETECTOR		ANGLE
			TYPE	RANGE	TYPE	RANGE	
G,MU-T	ABX	THR-20	C	27	NAI-D		4PI

Abstract: The curves of the total gamma-absorption cross sections (σ_{tot}) in the E1 giant resonance energy range for the nuclei ^{154}Sm, ^{156}Gd, ^{165}Ho, ^{168}Er, ^{174}Yb, ^{178}Hf, ^{180}Hf, ^{181}Ta, ^{182}W, ^{184}W, ^{186}W and ^{197}Au have been measured using the absorption method. Parameters of the Lorentz curves fitting the measured cross sections σ_{tot} are given. Quadrupole moments (Q_0) and nuclear deformation parameters (β) were obtained.

For deformed nuclei in the $\sim 155 < A < \sim 180$ region a violation of the correlation between giant resonance widths (Γ) and nuclear deformation parameters was found. Γ_1 and Γ_2, the widths of the resonances corresponding to vibrations of nucleons along and across the nuclear deformation axis, were observed to decrease with the increase of A which could be accounted for by the presence of an $N = 108$ subshell.

E NUCLEAR REACTIONS ^{154}Sm, ^{156}Gd, ^{165}Ho, ^{168}Er, ^{174}Yb, ^{178,180}Hf, ^{181}Ta, ^{182,184,186}W, ^{197}Au (γ, X), E = 7–20 MeV; measured total $\sigma(E)$; deduced integrated σ. Lorentz line parameters. ^{154}Sm, ^{156}Gd, ^{165}Ho, ^{168}Er, ^{174}Yb, ^{178,180}Hf, ^{181}Ta, ^{182,184,186}W, ^{197}Au deduced β, Q_0, Γ, giant resonance evolution. Enriched, natural targets.

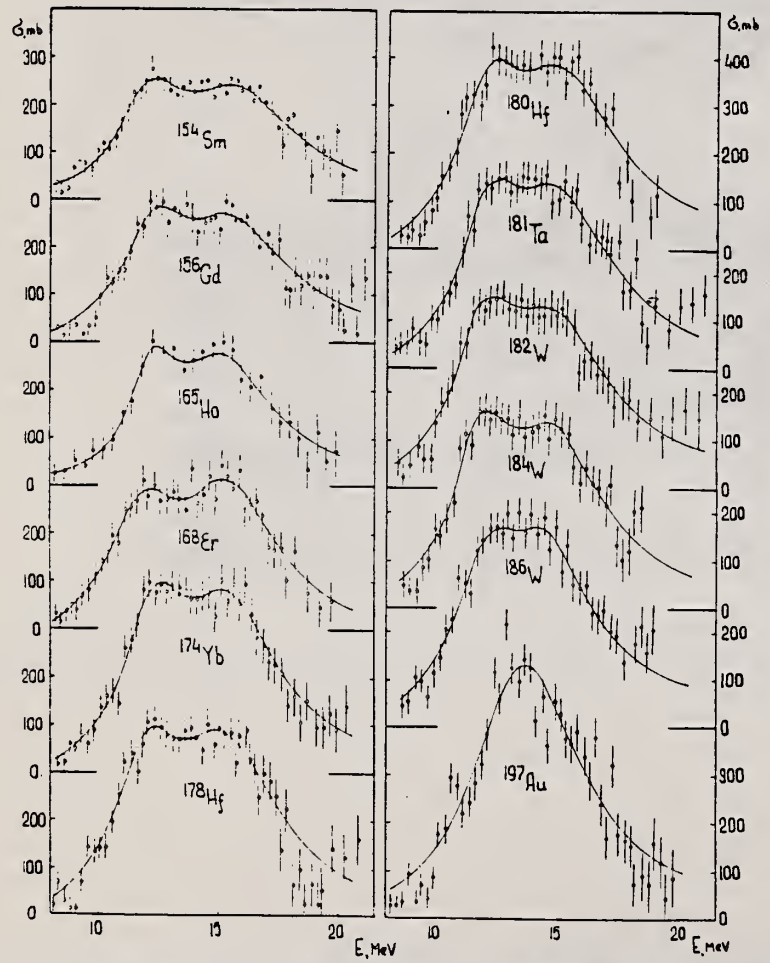

Fig. 2. Total nuclear γ-absorption cross sections (σ_{tot}) measured by the absorption method for ^{154}Sm, ^{156}Gd, ^{165}Ho, ^{168}Er, ^{174}Yb, ^{178}Hf, ^{180}Hf, ^{181}Ta, ^{182}W, ^{184}W, ^{186}W and ^{197}Au. Rms error bars are shown.

(OVER)

TABLE 2

Parameters of Lorentz curves fitting the experimental data on σ_{tot}

Nucleus	E_1 (MeV)	σ_1 (mb)	Γ_1 (MeV)	E_2 (MeV)	σ_2 (mb)	Γ_2 (MeV)	$\frac{\sigma_2\Gamma_2}{\sigma_1\Gamma_1}$	Γ (MeV)
^{154}Sm	12.2	188	3.4	15.7	207	5.7	1.85	8.1
^{156}Gd	12.3	206	3.2	15.7	220	5.5	1.81	7.7
^{165}Ho	12.3	202	2.3	15.2	239	4.8	2.47	7.0
^{168}Er	11.9	222	3.2	15.5	275	4.5	1.73	7.4
^{174}Yb	12.3	297	2.9	15.5	320	4.9	1.80	7.1
^{178}Hf	12.2	291	3.1	15.5	334	4.9	1.80	7.2
^{180}Hf	12.2	286	3.2	15.3	324	5.1	1.81	7.1
^{181}Ta	12.1	272	3.0	15.0	316	5.1	1.97	6.8
^{182}W	11.9	267	3.2	14.8	303	5.6	2.01	6.8
^{184}W	11.9	315	2.9	14.8	321	4.7	1.65	6.8
^{186}W	12.0	246	3.3	14.5	332	5.1	2.07	6.4
^{197}Au	13.7	535	5.2					
Average error	1.4 %	11.2 %	9.3 %	1.5 %	9.7 %	4.6 %	0.22	0.2 MeV

TABLE 3

Ratios of nuclear ellipsoid axes (k), deformation parameters (β) and intrinsic quadrupole moments (Q_0), calculated from E_2, E_1

Nucleus	^{154}Sm	^{156}Gd	^{165}Ho	^{168}Er	^{174}Yb	^{178}Hf	^{180}Hf	^{181}Ta	^{182}W	^{184}W	^{186}W
k	1.320	1.302	1.259	1.327	1.289	1.296	1.281	1.263	1.271	1.268	1.229
β	0.326 ±0.017	0.309 ±0.016	0.266 ±0.036	0.334 ±0.032	0.296 ±0.024	0.303 ±0.032	0.288 ±0.036	0.270 ±0.026	0.278 ±0.030	0.274 ±0.032	0.235 ±0.033
Q_0	6.3 ±0.3	6.2 ±0.3	5.8 ±0.8	7.5 ±0.7	7.0 ±0.6	7.5 ±0.8	7.2 ±0.9	6.9 ±0.7	7.2 ±0.8	7.1 ±0.8	6.2 ±0.9

TABLE 4

Integral characteristics of E1 giant resonance

Nucleus	$\sigma_{0\,exp}$ (MeV · b)	$\sigma_{0\,exp}$ $0.06NZ/A$	σ_{01} (MeV · b)	σ_{01} $0.06NZ/A$	σ_{-1} (mb)	σ_{-1L} (mb)	$\sigma_{-1L}A^{-4/3}$ (mb)	σ_{-2} (mb · MeV^{-1})	σ_{-2L} (mb · MeV^{-1})	$\sigma_{-2L}A^{-5/3}$ (μb · MeV^{-1})
^{154}Sm	1.94 ± 0.06	0.87	2.86	1.29	117 ± 3.5	156	0.189	9.1 ± 0.3	14.3	3.23
^{156}Gd	2.07 ± 0.07	0.91	2.95	1.30	143 ± 4.6	163	0.194	10.5 ± 0.4	14.9	3.30
^{165}Ho	1.86 ± 0.06	0.78	2.53	1.06	155 ± 4.4	160	0.177	10.1 ± 0.3	12.6	2.54
^{168}Er	2.24 ± 0.06	0.92	3.07	1.26	161 ± 4.3	197	0.212	12.0 ± 0.3	16.0	3.13
^{174}Yb	2.69 ± 0.05	1.07	3.82	1.52	195 ± 3.4	240	0.247	14.5 ± 0.3	19.2	3.54
^{178}Hf	2.85 ± 0.07	1.11	3.99	1.55	208 ± 4.9	247	0.247	15.3 ± 0.4	20.2	3.59
^{180}Hf	2.72 ± 0.06	1.05	4.03	1.56	200 ± 4.4	250	0.246	15.1 ± 0.3	20.7	3.61
^{181}Ta	2.84 ± 0.07	1.09	3.81	1.46	210 ± 5.3	245	0.239	16.0 ± 0.4	20.0	3.45
^{182}W	2.86 ± 0.07	1.09	4.01	1.52	211 ± 5.3	256	0.248	16.2 ± 0.4	21.6	3.70
^{184}W	2.78 ± 0.07	1.05	3.80	1.43	207 ± 5.3	251	0.240	15.9 ± 0.4	20.9	3.51
^{186}W	2.90 ± 0.07	1.08	3.95	1.48	214 ± 5.3	256	0.241	16.2 ± 0.4	21.6	3.56
^{197}Au	3.12 ± 0.06	1.10	4.37	1.54	229 ± 4.2	276	0.241	18.6 ± 0.4	23.3	3.49

W
A=183

W
A=183

W
A=183

A. H. Geller, J. Halpern, and E. G. Muirhead
Phys. Rev. 118, 1302-12 (1960)

ELEM.	M.	A
W	183	74

METHOD

Betatron; neutron threshold; ion chamber

REF. NO. 60 Ge 3 NVB

REACTION	RESULT	EXCITATION ENERGY	SOURCE		DETECTOR		ANGLE
			TYPE	RANGE	TYPE	RANGE	
G,N	NØX	THR	C THR		BF3-I		4 PI

THRESHØLD

TABLE I. Summary and comparison of neutron separation energies inferred from present threshold measurements with values predicted from mass data and reaction energies. All energies are expressed in the center-of-mass system in Mev.

Reaction	No. runs	Present results	Other results	Method	Reference
$W^{183}(\gamma,n)W^{182}$	1	6.29 ±0.05	6.29 ±0.06	mass data	q

q W. H. Johnson, Jr., and V. B. Bhanot, Phys. Rev. 107, 6 (1957).

FORM NBS-418
U.S. DEPARTMENT OF COMMERCE
NATIONAL BUREAU OF STANDARDS

REF.

N. Shikazono, H. Takekoshi and T. Shoji
J. Phys. Soc. Japan 21, 829 (1966)

ELEM. SYM.	A	Z
W	183	74

METHOD

Mössbauer Effect

REF. NO.

66 Sh 2 JDM

REACTION	RESULT	EXCITATION ENERGY	SOURCE		DETECTOR		ANGLE
			TYPE	RANGE	TYPE	RANGE	
G,G	LFT	1	D	1	NAI-D	1	4PI

Γ_γ(46.48 keV) = (2.4 ± .1) x 10^{-7} eV

E2/M1 = 0.5%

W
A=184

W
A=184

W
A=184

Ref. J.H. Carver, D.C. Peaslee, R.B. Taylor
Phys. Rev. 127, 2198 (1962)

Elem. Sym.	A	Z
W	184	74

Method: 33 MeV electron synchrotron; activation; Be - window NaI

Ref. No.: 62 Ca 2 JHH

Reaction	E or ΔE	E_o	Γ	$\int \sigma dE$	Jπ	Notes
(γ,p)	Bremss. 32	22.5		$65 \int_0^{32}$ MeV-mb		Absolute yields by comparison with $Ta^{181}(\gamma,n)$, $Cu^{63}(\gamma,n)Cu^{62}$ and results of Berman and Brown [Phys. Rev. 96, 83 (1954)].

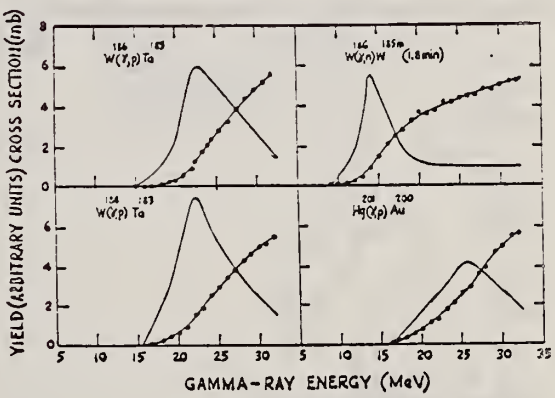

FIG. 7. Excitation functions and derived cross sections for the photodisintegration of tungsten and mercury.

REF. A.M. Goryachev, G.N. Zalesnyi, S.F. Semenko, and B.A. Tulupov
Yad. Fiz. 17, 463 (1973)
Sov. J. Nucl. Phys. 17, 236 (1973)

ELEM. SYM.	A	Z
W	184	74

METHOD

REF. NO. 73 Go 6 hmg

REACTION	RESULT	EXCITATION ENERGY	SOURCE TYPE	SOURCE RANGE	DETECTOR TYPE	DETECTOR RANGE	ANGLE
G,XN	ABX	8- 20	C	8- 20	BF3-I		4PI

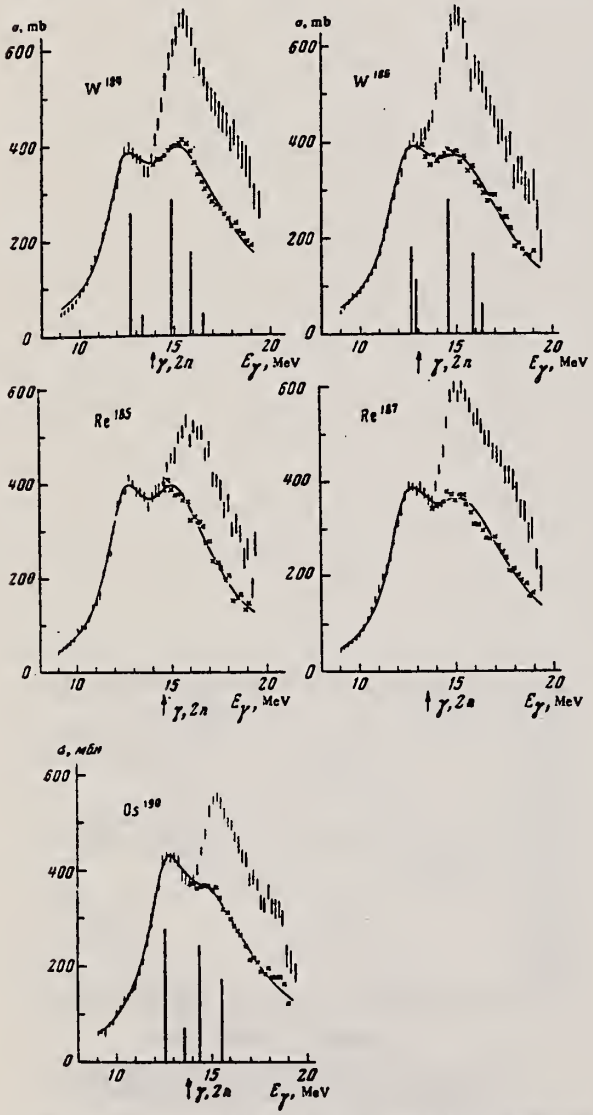

FIG. 2. Cross sections for $W^{184,186}$, Os^{190}, and $Re^{185,187}$. The cross section $\sigma_{\gamma,n} + 2\sigma_{\gamma,2n}$ is denoted by vertical lines whose lengths are twice the rms errors. The crosses represent the cross sections, corrected for multiplicity, above the threshold of the (γ, 2n) reaction. The solid curves are Lorentz curve approximations. For $W^{184,186}$ and Os^{190} the calculated dipole transition strengths are shown.

TABLE III

	W^{184}	W^{186}	Os^{190}	Re^{185}	Re^{187}	W^{184} [?]
Γ_1, MeV	2.33	2.55	2,13	2.51	2.83	2.29
E_1, MeV	12.5	12.5	12.6	12.7	12.6	12.50
σ_1, mb	241	225	223	262	250	211
Γ_2, MeV	5.1	5.4	5.7	5.2	5.3	5.18
E_2, MeV	15.6	15.2	14.8	15.4	15.6	14.88
σ_2, mb	338	317	318	315	296	334
0.06 NZ/A, MeV-mb	2.65	2.67	2.74	2.68	2.69	2.67
$S_1 + S_2$, MeV − mb	4.0	3.9	3.9	3.6	3.8	3.47
S_2 / S_1	2,8	3.0	3.8	2.5	2.2	3,6

Note. $S_i = (\pi/2)\sigma_i\Gamma_i$ is the Lorentz area.

REF.

Yu. I. Sorokin, V.A. Khrushchev, and B.A. Yur'ev
Yad. Fiz. 17, 3 (1973)
Sov. J. Nucl. Phys. 17, 1 (1973)

ELEM. SYM.	A	Z
W	184	74

METHOD

REF. NO.: 73 So 16 hmg

REACTION	RESULT	EXCITATION ENERGY	SOURCE		DETECTOR		ANGLE
			TYPE	RANGE	TYPE	RANGE	
G,XN	ABX	8- 28	C	0- 28	BF3-I		4PI

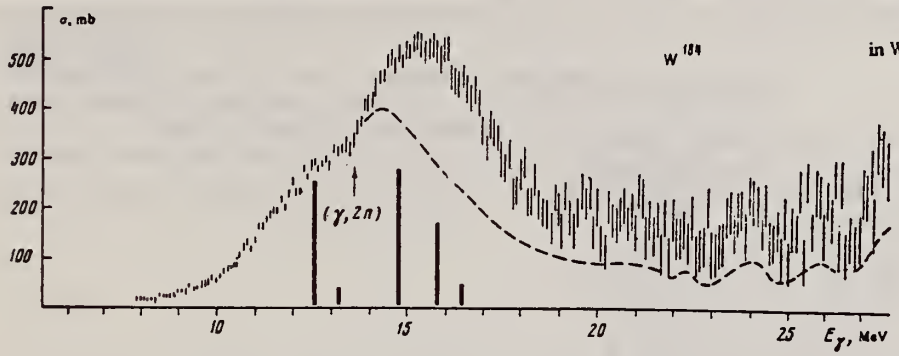

Cross sections for photoneutron reactions in W^{182} and W^{184}.

TABLE 1. Giant-resonance characteristics of W^{182} and W^{184}

	W^{182}	W^{184}		W^{182}	W^{184}
E_1, MeV	12,1±0.1	12.2±0.1	$R_A = \sigma_1\Gamma_1 / \sigma_2\Gamma_2$	0.238±0.03	0.17±0.02
σ_1, mb	145±7	145±7	e	0,478±0.07	0.45±0.07
Γ_1, MeV	2,7±0,1	2±0.1	$Q_0 = 0{,}4ZR^2\alpha$, b	7.2±0.9	6.8±0.9
E_2, MeV	14,8±0,1	14.7±0.1	Q_0 [7], b	6.57	6.21
σ_2, mb	387±8	428±9			
Γ_2, MeV	3.5±0.1	4.0±0.1			

Figure gives σ(sn) obtained by correcting σ(xn) for neutron multiplicity. Berman's statistical factors for W-186 used.

TABLE 2. Integrated cross sections of W^{182} and W^{184}

		W^{182}	W^{184}
$\sigma(\gamma, T\pi)$	From threshold to 27.4 MeV	3.68	4.88
	From threshold to 20 MeV	2.75	3.16
σ_T	From threshold to 20 MeV	2.32	2.33
	From 20 to 27.4 MeV	0.46	0.72
	From threshold to 27.4 MeV	2.73	2.95
$0{,}06\,NZ/A$		2.63	2.65
$\sigma(E2)$		0.45	0.43

REF.

Yu. I. Sorokin and B. A. Yur'ev
Izv. Akad. Nauk SSSR. Ser. Fiz. 39, 114 (1975)
Bull. Acad. Sci. (USSR) Phys. Ser. 39, 98 (1975)

ELEM. SYM.	A	Z
W	184	74

METHOD

REF. NO. 75 So 12 hmg

REACTION	RESULT	EXCITATION ENERGY	SOURCE		DETECTOR		ANGLE
			TYPE	RANGE	TYPE	RANGE	
G,XN	ABI	7- 27	C	7- 27	BF3-I		4PI

SEE 73SO16

Table 1

Element	A	σ_0, (γ, Tn) MeV · b: to 27 MeV	$\sigma_{0\gamma}$, MeV · b: to 20 MeV	$\sigma_{0\gamma}$, MeV · b: 20–27 MeV	σ_{-1}, mb	σ_{-2}, mb × MeV^{-1}	E_m, MeV	K, MeV	σ_{0A-1}, MeV^{-1}	Threshold (γ,2n), MeV	σ_0 (E1), MeV × b
Sn	112	2,23	1,80	1,49	0,41	112	6,7	15,8	20,1	10,2	19,2	1,66
	114	2,26	1,86	1,39	0,47	108	6,5	15,7	21,5	10,2	18,1	1,68
	116	2,40	1,85	1,40	0,45	110	6,6	15,6	21,7	8,1	17,1	1,71
	117	2,52	1,86	1,39	0,47	110	6,7	15,4	21,6	7,3	16,5	1,72
	118	2,46	1,92	1,53	0,39	115	7,1	15,5	20,7	7,6	16,3	1,71
	119	2,63	1,86	1,42	0,44	111	6,8	15,4	22,0	13,2	15,8	1,74
	120	2,69	2,07	1,69	0,38	127	7,9	15,3	19,1	4,6	15,6	1,75
	122	2,94	2,01	1,51	0,52	119	7,1	15,6	21,8	4,5	15,0	1,77
	124	2,90	1,93	1,44	0,49	114	6,9	15,5	23,2	5,4	14,4	1,79
W	182	3,68	2,78	2,32	0,46	184	12,5	-	24,2	5,2	14,9	2,63
	184	4,88	2,95	2,33	0,72	196	13,0	--	23,7	5,2	13,6	2,65
Au	197	4,06	3,15	2,81	0,34	226	15,5	13,3	20,9	17,1	11,8	2,84
Pb	206	3,93	3,21	2,80	0,41	225	16,1	13,5	23,1	6,5	14,8	2,96
	208	4,32	3,28	2,81	0,47	231	16,7	13,3	22,6	9,6	14,1	2,98
Bi	209	4,59	3,47	2,96	0,51	216	17,9	13,2	21,3	10,2	14,3	3,09

REF. G.M. Gurevich, L.E. Lazareva, V.M. Mazur, S.Yu. Merkulov, G.V. Solodukhov, V.A. Tyutin
JETP Lett. 28, 168 (1978)
Pis'ma Zh. Eksp. Teor. Fiz. 28, 168 (1978)

ELEM. SYM.	A	Z
W	184	74

METHOD

REF. NO.	
78 Gu 7	hg

REACTION	RESULT	EXCITATION ENERGY	SOURCE		DETECTOR		ANGLE
			TYPE	RANGE	TYPE	RANGE	
G,MU-T	ABX	THR-37	C	UKN	NAI-D		4PI

The absorption method is used to measure the total photoabsorption cross section curves for deformed ^{154}Sm, ^{156}Gd, ^{168}Er, ^{174}Yb, ^{184}W, and ^{186}W nuclei in the region of the $E1$ giant resonance. The behavior of the resonance widths for nuclei in the interval $A = 153$ to 186 is discussed.

PACS numbers: 24.30.Cz, 25.20.+y, 27.70.+q

TABLE I.

Nucleus	E_1 MeV	σ_1 mb	Γ_1 MeV	E_2 MeV	σ_2 mb	Γ_2 MeV	Γ MeV	Q_o b	β	$\sigma_{oL}/0.06\frac{ZN}{A}$
^{154}Sm	12.2	188	3.4	15.7	207	5.7	8.1 ± 0.2	6.3 ± 0.3	0.32 ± 0.02	1.28
^{156}Gd	12.3	206	3.2	15.7	229	5.5	7.7 ± 0.2	6.2 ± 0.3	0.31 ± 0.02	1.30
^{168}Er	11.9	222	3.2	15.5	275	4.5	7.4 ± 0.2	7.5 ± 0.7	0.32 ± 0.03	1.26
^{174}Yb	12.3	297	2.9	15.5	320	4.9	7.1 ± 0.2	7.0 ± 0.6	0.30 ± 0.02	1.52
^{184}W	11.9	315	2.9	14.8	321	4.7	6.8 ± 0.2	7.2 ± 0.8	0.27 ± 0.03	1.50
^{186}W	12.0	246	3.3	14.5	332	5.1	6.4 ± 0.2	6.2 ± 0.8	0.23 ± 0.03	1.48
Average error	±1.3%	±10.5%	±7.5%	±1.3%	±9.4%	±3.8%	—	—	—	—

(over)

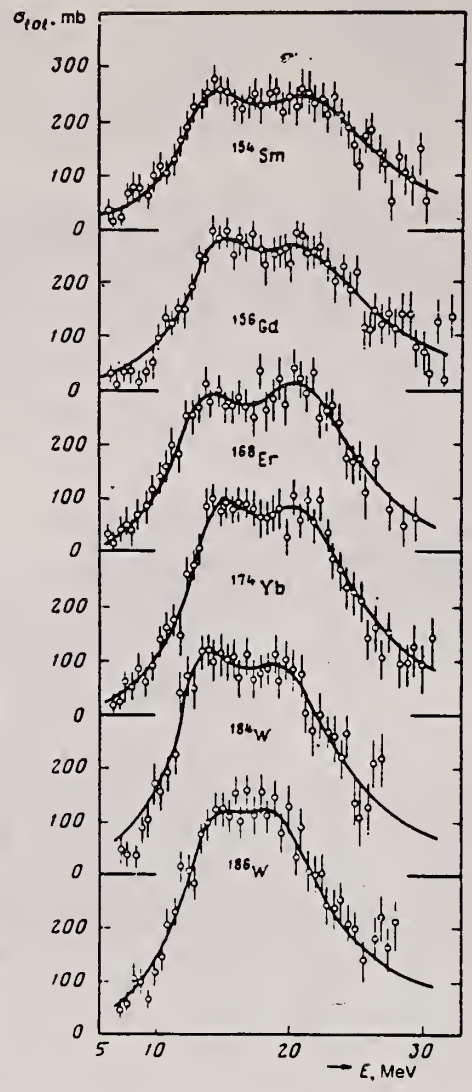

FIG. 2. Total cross sections of the photoabsorption of the nuclei ^{154}Sm, ^{156}Gd, ^{168}Er, ^{174}Yb, ^{184}W, and ^{186}W. The mean squared errors are shown.

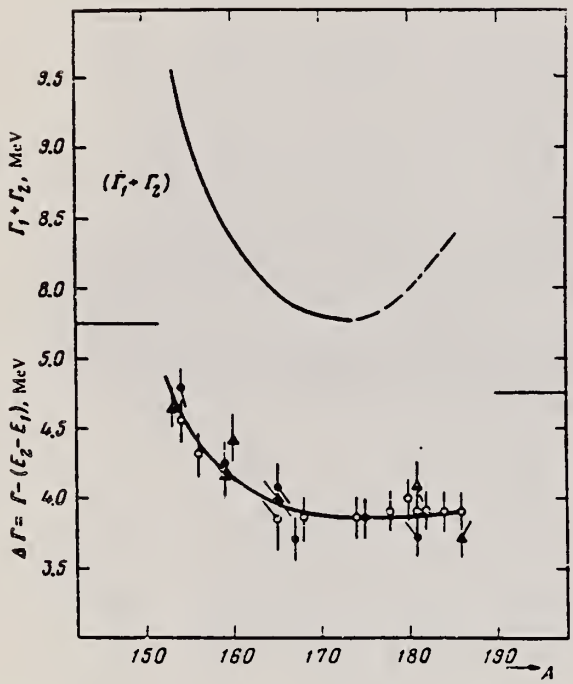

FIG. 3. Experimental values of $\Delta\Gamma = \Gamma - (E_2 - E_1)$ in the region of deformed nuclei with $A = 153$–186: ○—present work and[11]; ●—Saclay group; ▲—Livermore group. Owing to a small systematic deviations of the absolute values, the ordinate scales for the Saclay and Livermore data are shifted 0.15 MeV upward and downward, respectively. The $(\Gamma_1 + \Gamma_2)$ curve was obtained from the $\Delta\Gamma$ curve after introduction of corrections in the interval $A = 175$–186.

REF. W. Günther, R. Haag, K. Huber, U. Kneissl, H. Krieger, H.J. Maier, H. Ströher
Phys. Rev. Lett. 44, 716 (1980)

ELEM. SYM.	A	Z
W	184	74

METHOD

REF. NO. 80 Gu 1 hg

REACTION	RESULT	EXCITATION ENERGY	SOURCE		DETECTOR		ANGLE
			TYPE	RANGE	TYPE	RANGE	
E,F	ABX	THR-55	D	35-55	TRK-D		4PI

Low end of experimental arrows in Fig. 1 indicated lower limit for fission barriers established by this experiment.

The electroinduced fission of $^{182,184,186}W$ has been investigated in the energy range from 35 to 55 MeV. The fission barriers, estimated by a statistical-model analysis of the measured cross sections, are compared with theoretical predictions and are only consistent with the assumption of a constant pairing strength.

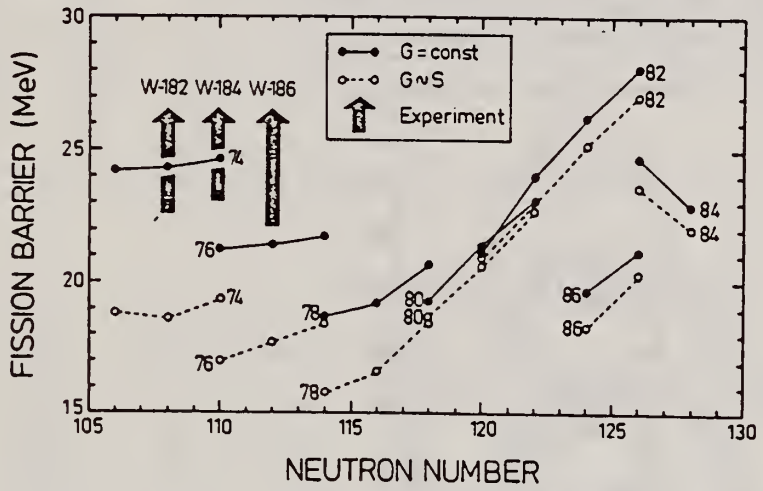

FIG. 1. Calculated fission barriers (Ref. 3) (full lines, G=const; dashed lines, $G \sim S$) and limits deduced from our experiments on $^{182,184,186}W$.

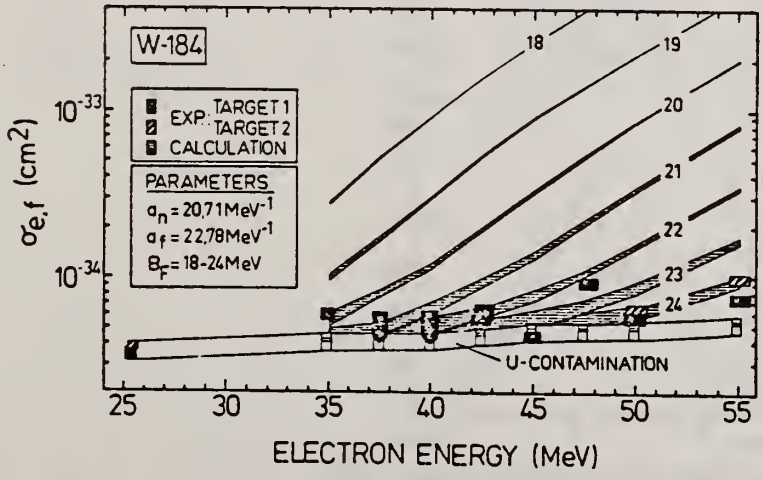

FIG. 2. Measured cross sections for ^{184}W and statistical-model calculations for different barrier heights (B_f = 18–24 MeV); full and hatched rectangles, experimental points for different targets; open rectangles, cross section for U normalized to the 25-MeV point.

REF. G.M. Gurevich, L.E. Lazareva, V.M. Mazur, S.Yu. Merkulov, G.V. Solodukhov, V.A. Tyutin
Nucl. Phys. A351, 257 (1981)

ELEM. SYM.	A	Z
W	184	74

METHOD

REF. NO. 81 Gu 2 hg

REACTION	RESULT	EXCITATION ENERGY	SOURCE		DETECTOR		ANGLE
			TYPE	RANGE	TYPE	RANGE	
G,MU-T	ABX	THR-20	C	27	NAI-D		4PI

Abstract: The curves of the total gamma-absorption cross sections (σ_{tot}) in the E1 giant resonance energy range for the nuclei ^{154}Sm, ^{156}Gd, ^{165}Ho, ^{168}Er, ^{174}Yb, ^{178}Hf, ^{180}Hf, ^{181}Ta, ^{182}W, ^{184}W, ^{186}W and ^{197}Au have been measured using the absorption method. Parameters of the Lorentz curves fitting the measured cross sections σ_{tot} are given. Quadrupole moments (Q_0) and nuclear deformation parameters (β) were obtained.

For deformed nuclei in the $\sim 155 < A < \sim 180$ region a violation of the correlation between giant resonance widths (Γ) and nuclear deformation parameters was found. Γ_1 and Γ_2, the widths of the resonances corresponding to vibrations of nucleons along and across the nuclear deformation axis, were observed to decrease with the increase of A which could be accounted for by the presence of an $N = 108$ subshell.

E NUCLEAR REACTIONS ^{154}Sm, ^{156}Gd, ^{165}Ho, ^{168}Er, ^{174}Yb, ^{178,180}Hf, ^{181}Ta, ^{182,184,186}W, ^{197}Au (γ, X), E = 7–20 MeV; measured total $\sigma(E)$; deduced integrated σ, Lorentz line parameters. ^{154}Sm, ^{156}Gd, ^{165}Ho, ^{168}Er, ^{174}Yb, ^{178,180}Hf, ^{181}Ta, ^{182,184,186}W, ^{197}Au deduced β, Q_0, Γ, giant resonance evolution. Enriched, natural targets.

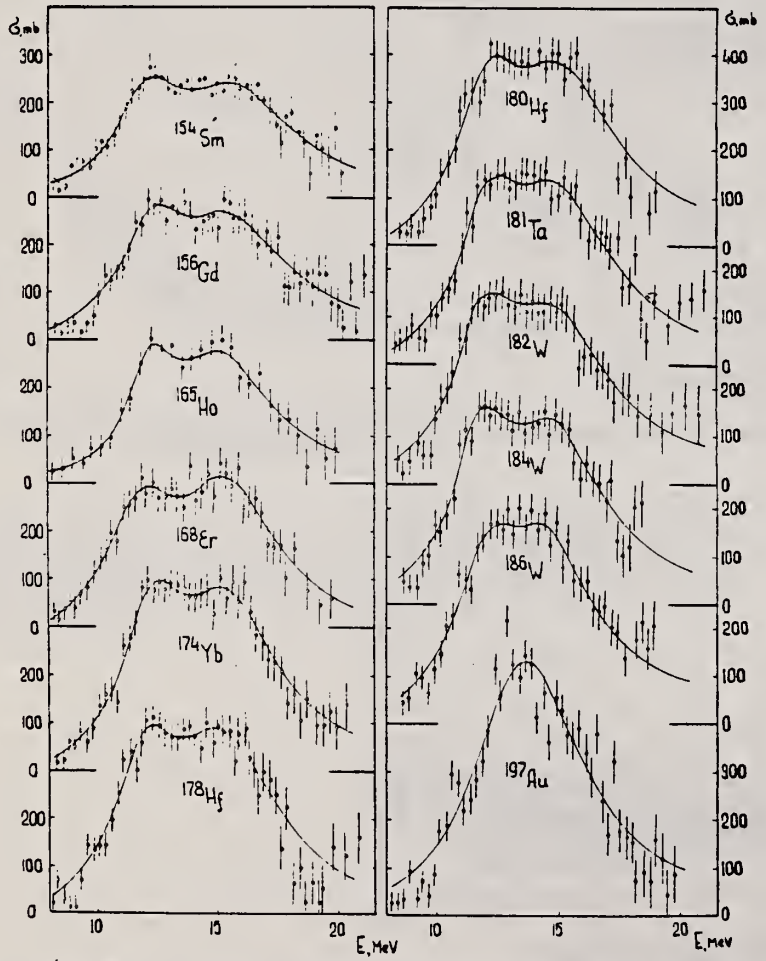

Fig. 2. Total nuclear γ-absorption cross sections (σ_{tot}) measured by the absorption method for ^{154}Sm, ^{156}Gd, ^{165}Ho, ^{168}Er, ^{174}Yb, ^{178}Hf, ^{180}Hf, ^{181}Ta, ^{182}W, ^{184}W, ^{186}W and ^{197}Au. Rms error bars are shown.

(OVER)

TABLE 2

Parameters of Lorentz curves fitting the experimental data on σ_{tot}

Nucleus	E_1 (MeV)	σ_1 (mb)	Γ_1 (MeV)	E_2 (MeV)	σ_2 (mb)	Γ_2 (MeV)	$\frac{\sigma_2\Gamma_2}{\sigma_1\Gamma_1}$	Γ (MeV)
^{154}Sm	12.2	188	3.4	15.7	207	5.7	1.85	8.1
^{156}Gd	12.3	206	3.2	15.7	220	5.5	1.81	7.7
^{165}Ho	12.3	202	2.3	15.2	239	4.8	2.47	7.0
^{168}Er	11.9	222	3.2	15.5	275	4.5	1.73	7.4
^{174}Yb	12.3	297	2.9	15.5	320	4.9	1.80	7.1
^{178}Hf	12.2	291	3.1	15.5	334	4.9	1.80	7.2
^{180}Hf	12.2	286	3.2	15.3	324	5.1	1.81	7.1
^{181}Ta	12.1	272	3.0	15.0	316	5.1	1.97	6.8
^{182}W	11.9	267	3.2	14.8	303	5.6	2.01	6.8
^{184}W	11.9	315	2.9	14.8	321	4.7	1.65	6.8
^{186}W	12.0	246	3.3	14.5	332	5.1	2.07	6.4
^{197}Au	13.7	535	5.2					
Average error	1.4 %	11.2 %	9.3 %	1.5 %	9.7 %	4.6 %	0.22	0.2 MeV

TABLE 3

Ratios of nuclear ellipsoid axes (k), deformation parameters (β) and intrinsic quadrupole moments (Q_0), calculated from E_2, E_1

Nucleus	^{154}Sm	^{156}Gd	^{165}Ho	^{168}Er	^{174}Yb	^{178}Hf	^{180}Hf	^{181}Ta	^{182}W	^{184}W	^{186}W
k	1.320	1.302	1.259	1.327	1.289	1.296	1.281	1.263	1.271	1.268	1.229
β	0.326 ±0.017	0.309 ±0.016	0.266 ±0.036	0.334 ±0.032	0.296 ±0.024	0.303 ±0.032	0.288 ±0.036	0.270 ±0.026	0.278 ±0.030	0.274 ±0.032	0.235 ±0.033
Q_0	6.3 ±0.3	6.2 ±0.3	5.8 ±0.8	7.5 ±0.7	7.0 ±0.6	7.5 ±0.8	7.2 ±0.9	6.9 ±0.7	7.2 ±0.8	7.1 ±0.8	6.2 ±0.9

TABLE 4

Integral characteristics of E1 giant resonance

Nucleus	$\sigma_{0\,exp}$ (MeV · b)	$\sigma_{0\,exp}$ $0.06NZ/A$	σ_{0L} (MeV · b)	σ_{01} $0.06NZ/A$	σ_{-1} (mb)	σ_{-1L} (mb)	$\sigma_{-1L}A^{-1/3}$ (mb)	σ_{-2} (mb · MeV^{-1})	σ_{-2L} (mb · MeV^{-1})	$\sigma_{-2L}A^{-1/3}$ (μb · MeV^{-1})
^{154}Sm	1.94 ± 0.06	0.87	2.86	1.29	117 ± 3.5	156	0.189	9.1 ± 0.3	14.3	3.23
^{156}Gd	2.07 ± 0.07	0.91	2.95	1.30	143 ± 4.6	163	0.194	10.5 ± 0.4	14.9	3.30
^{165}Ho	1.86 ± 0.06	0.78	2.53	1.06	155 ± 4.4	160	0.177	10.1 ± 0.3	12.6	2.54
^{168}Er	2.24 ± 0.06	0.92	3.07	1.26	161 ± 4.3	197	0.212	12.0 ± 0.3	16.0	3.13
^{174}Yb	2.69 ± 0.05	1.07	3.82	1.52	195 ± 3.4	240	0.247	14.5 ± 0.3	19.2	3.54
^{178}Hf	2.85 ± 0.07	1.11	3.99	1.55	208 ± 4.9	247	0.247	15.3 ± 0.4	20.2	3.59
^{180}Hf	2.72 ± 0.06	1.05	4.03	1.56	200 ± 4.4	250	0.246	15.1 ± 0.3	20.7	3.61
^{181}Ta	2.84 ± 0.07	1.09	3.81	1.46	210 ± 5.3	245	0.239	16.0 ± 0.4	20.0	3.45
^{182}W	2.86 ± 0.07	1.09	4.01	1.52	211 ± 5.3	256	0.248	16.2 ± 0.4	21.6	3.70
^{184}W	2.78 ± 0.07	1.05	3.80	1.43	207 ± 5.3	251	0.240	15.9 ± 0.4	20.9	3.51
^{186}W	2.90 ± 0.07	1.08	3.95	1.48	214 ± 5.3	256	0.241	16.2 ± 0.4	21.6	3.56
^{197}Au	3.12 ± 0.06	1.10	4.37	1.54	229 ± 4.2	276	0.241	18.6 ± 0.4	23.3	3.49

REF. M. Schumacher, F. Smend, W. Mückenheim, P. Rullhusen, H.G. Börner
A. Phys. A300, 193 (1981)

ELEM. SYM.	A	Z
W	184	74

METHOD

REF. NO. 81 Sc 6 egf

REACTION	RESULT	EXCITATION ENERGY	SOURCE		DETECTOR		ANGLE
			TYPE	RANGE	TYPE	RANGE	
G,G	ABX	2-7		2-7	SCD-D		90

2.60-6.76 MEV

Elastic scattering by nuclei in the range of mass numbers between 64 and 238 has been studied with monochromatic photons in the energy range between 2 and 8 MeV. These photons were provided either by a Ti(n,γ) source installed in the tangential through channel of the Grenoble high flux reactor, or by ^{24}Na and ^{56}Co sources produced by deuteron bombardment of Al or Fe at the Göttingen cyclotron. The photoexcitation of 23 nuclear levels has been observed and the decay properties and groundstate widths of the majority of these levels have been determined. For the lead scattering target the coherent elastic differential cross section has been studied in detail. There is evidence that below the photo-neutron threshold the elastic scattering via virtual photoexcitation of the nucleus can be approximated by extrapolating the real part of the Giant Dipole Resonance amplitude along a Lorentzian curve. Coulomb corrections to Delbrück scattering seem to play a small role at 6.5 MeV.

Table 4. Properties of levels observed by photoexcitation. $(d\sigma/d\Omega)^{NRF}$: experimental differential cross section per identified isotope or element for resonance scattering through $\Theta = 90°$. I^π: spin-parity of excited level; $W(\Theta)$: angular correlation function: $g = (2I_{ex}+1)/(2I_g+1)$; Γ_0: radiative groundstate transition width, Γ: total level width. Errors in the last digits are given in parentheses

Isotope	E_γ (MeV)	$(d\sigma/d\Omega)^{NRF}$ (μb/sr)	I^π	Γ_0/Γ [c]	$W(\Theta)g\Gamma_0^2/\Gamma$ (meV)	Γ_0 [f] (meV)	Γ_0 [g] (meV)
^{238}U	2.754	13 (4)	(1)	0.77	0.145	0.084	-
^{238}U	3.254	421 (5)	1^-	0.24	0.83	1.5	0.52(15)[d]
^{209}Bi	6.555	2.1 (4)·10^2	-	-	0.74	0.74[b]	-
^{209}Bi	7.168	1.7 (3)·10^5	$9/2^-$[a]	1.00	710	786	820 (40)[a]
^{203}Tl	6.418	8.75(30)·10^3	$1/2^+$[a]	0.28	30	102	82 (15)[a]
Tl	6.759	7 (3)	-	-	-	-	-
Hg	6.555	68 (17)	-	-	-	-	-
^{186}W	6.418	5.2 (3)·10^2	1^-[a]	0.32	1.75	2.4	-
^{184}W	6.555	9.8 (10)·10^2	(1)	0.52	3.44	2.9	-
^{184}W	6.759	46 (10)	(1)	0.58	0.17	0.13	-
^{181}Ta	3.010	174 (17)	-	0.72	0.42	0.59	-
^{181}Ta	6.418	62 (4)	-	0.73	0.2	0.27[c]	-
^{181}Ta	6.759	4.8 (12)	-	-	0.018	0.018[b]	-
^{165}Ho	6.418	10.3 (30)	-	-	0.035	0.035[b]	-
^{165}Ho	6.759	5.6 (14)	-	-	0.021	0.021[b]	-
Nd	2.754	2.6 (5)	-	-	-	-	-
Nd	3.254	14.0 (10)	-	-	-	-	-
Ce	6.759	13.4 (10)	-	-	-	-	-
^{121}Sb	3.452	2.20 (5)·10^3	-	0.60	2.9	4.9[b]	-
^{100}Mo	6.418	1.53 (4)·10^4	1^-[a]	0.88	52	26	25 (8)[a]
^{94}Mo	6.555	4.4 (4)·10^3	(1)	0.33	15	21	-
Mo	6.759	6.2 (15)	-	-	-	-	-
Mo	7.168	8.2 (26)·10^2	-	-	-	-	-

[a] [11] [b] $W(\Theta)g\Gamma_0/\Gamma = 1$ assumed [c] $W(\Theta)g = 1$ assumed
[d] [28] (a small correction has been applied to the data of [28])
[e] Upper limits in case not all the transitions to lower levels were observed
[f] Present work [g] Previous work

(OVER)

Table 1. Differential cross sections for elastic scattering $(d\sigma/d\Omega)^{exp}$ of photons from ^{56}Co and ^{24}Na sources by different scattering targets, in units of μb/sr. Errors in the last digits are given in parentheses.

Θ deg	Scattering targets	2.599[a] (MeV)	2.754[b] (MeV)	3.010[a] (MeV)	3.202[a] (MeV)	3.254[a] (MeV)	3.273[a] (MeV)	3.452[a] (MeV)
90	^{238}U	52.7(25)	57.5(25)[c]	56(16)	47(4)	456 (10)[c]	34(6)	49(14)
	^{209}Bi	33.1(30)	32 (2)	33(11)	32(4)	25.6(20)	29(6)	33(15)
	^{nat}Pb	31.5(23)	31.0(16)	35 (8)	27(3)	26.6(22)	25(4)	23 (8)
	^{nat}Tl	31.5(33)	-	27(12)	32(5)	24 (3)	22(7)	34(15)
	^{nat}Hg	30.0(27)	-	24(10)	28(5)	25.5(18)	26(8)	20 (8)
	^{nat}W	22.5(11)	-	17 (7)	19(3)	18.4(15)	18(5)	21 (6)
	^{181}Ta	20.0(15)	19.2 (6)	193(20)[c]	20(4)	17.3(21)	18(5)	21 (8)
	^{165}Ho	15.9(13)	-	17(10)	13(6)	15.6(20)	18(8)	-
	^{nat}Nd	11.4 (7)	14.2 (5)[d]	15 (7)	14(3)	24.2(12)[d]	13(3)	9 (6)
	^{nat}Ce	11.1 (9)	11.0 (5)	-	11(3)	9.5(13)	8(4)	-
	^{127}J	8.4(10)	8.6 (5)	-	9(2)	7 (1)	5(3)	-
	^{nat}Sb	8.0(11)	-	-	10(4)	6.8(19)	-	1,270(50)[c]
	^{nat}Sn	6.5 (7)	7.0 (5)	-	5(2)	7.6 (8)	6(3)	-
	^{nat}Cd	6.2 (5)	-	-	6(2)	6.6 (8)	7(3)	-
120	^{238}U	55.1(25)	64 (4)[c]	43(15)	55(5)	574 (10)[c]	48(5)	48(11)
	^{181}Ta	27.5(15)	25.0 (9)	227(20)[c]	22(5)	21 (2)	22(8)	-
	^{nat}Nd	17.9(30)	17.0 (9)[d]	-	-	29.8(47)[d]	-	-

[a] ^{56}Co source in Fe lattice [b] ^{24}Na source in Al lattice (part of data have been published elsewhere)
[c] Transitions to excited states observed in addition to the ground-state transition
[d] Photoexcitation of nuclear level identified from the size of the differential cross section

Table 2. Elastic differential cross sections $d\sigma/d\Omega(\Theta=90°)$ in μb/sr measured with the Ti(n,γ) source and compared with theoretical predictions. n: predicted number of levels in a $\Delta E=25$ eV interval at 6.5 MeV. Errors in the last digits are given in parentheses

Scattering target	6.418 MeV		6.555 MeV		6.759 MeV		7.168 MeV		n
	exp.	th.	exp.	th.	exp.	th.	exp.	th.	
^{238}U	23 (12)	10.3	-	-	-	-	-	-	45
^{209}Bi	-	-	219(39)[b,c]	8.0	12 (4)	7.4	1.5(3)·10^5[b,c]	5.7	0.1
^{nat}Pb	7.0(15)	8.6	-	-	6.5(11)	7.4	-	-	0.05
^{nat}Tl	2,586 (92)[a,c]	7.5	-	-	13 (3)[b]	6.0	-	-	0.4
^{nat}Hg	12 (3)	7.8	74(17)[b]	6.5	6.7(15)	6.4	-	-	3.4
^{nat}W	159 (10)[a,c]	6.6	306(33)[a,c]	6.3	20 (2)[a,c]	5.6	-	-	13
^{181}Ta	68 (4)[a,c]	6.3	-	-	10.1(12)[b,c]	5.3	-	-	28
^{165}Ho	15 (3)[b]	4.7	-	-	9.5(14)[b]	3.9	-	-	18
^{nat}Ce	4.1(21)	4.1	-	-	17 (1)[b,c]	3.6	-	-	0.04
^{nat}Sn	4.2(13)	3.0	-	-	2.5 (5)	2.7	-	-	1.9
^{nat}Mo	1,474 (44)[a,c]	2.5	407(39)[a,c]	2.5	8.5(15)[b,c]	2.3	817(258)[b,c]	2.0	0.5
^{nat}Zn	2.4 (8)	1.6	-	-	1.8 (5)	1.5	-	-	0.3

[a] Transitions to excited states observed [b] Photoexcitation identified from size of differential cross section
[c] Photoexcitation reported in [11]

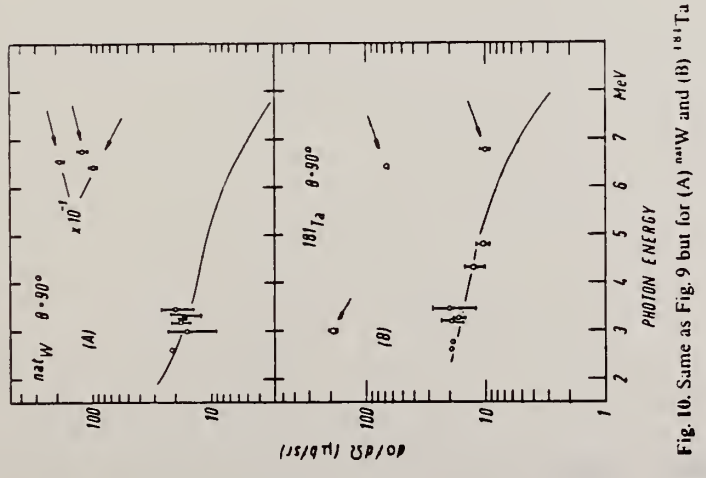

Fig. 10. Same as Fig. 9 but for (A) ^{nat}W and (B) ^{181}Ta

W
A=186

W
A=186

W
A=186

.. .. Geller, J. Halpern, and E. G. Muirhead
Phys. Rev. 118, 1302-12 (1960)

ELEM. SYM.	A	Z
W	186	74

METHOD

Betatron; neutron threshold; ion chamber

REF. NO. 60 Ge 3 NVB

REACTION	RESULT	EXCITATION ENERGY	SOURCE		DETECTOR		ANGLE
			TYPE	RANGE	TYPE	RANGE	
G,N	NØX	THR	C THR		BF3-I		4 PI

THRESHØLD

TABLE I. Summary and comparison of neutron separation energies inferred from present threshold measurements with values predicted from mass data and reaction energies. All energies are expressed in the center-of-mass system in Mev.

Reaction	No. runs	Present results	Other results	Method	Reference
$W^{186}(\gamma,n)W^{185}$	1	7.28 ±0.06			

Ref. J.H. Carver, D.C. Peaslee, R.B. Taylor
Phys. Rev. 127, 2198 (1962)

Elem. Sym.	A	Z
W	186	74

Method 33 MeV electron synchrotron; activation; Be-windown NaI

Ref. No. 62 Ca 2 JHH

Reaction	E or ΔE	E_o	Γ	$\int \sigma dE$	Jπ	Notes
$(\gamma,p)Ta^{185}$	Bremss. 32	22.5		$55\int_0^{32}$ MeV-mb		Absolute yields by comparison with $Ta^{181}(\gamma,n)$, $Cu^{63}(\gamma,n)Cu^{62}$ and results of Berman and Brown [Phys. Rev. 96, 83 (1954)].
$(\gamma,n)W^{185}$ [74 day]		14		$3500\int_0^{32}$ MeV-mb		
$(\gamma,n)W^{185}$ [1.8 min]		14		$40\int_0^{32}$ MeV-mb		

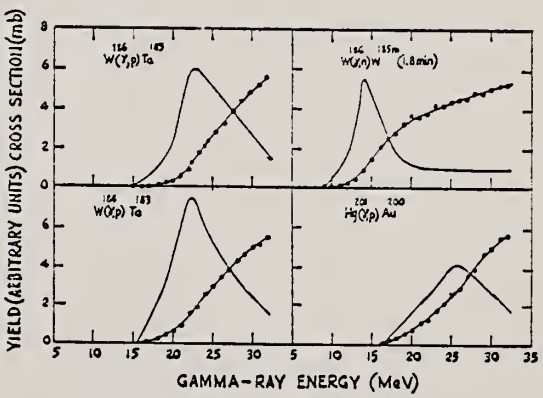

FIG. 7. Excitation functions and derived cross sections for the photodisintegration of tungsten and mercury.

REF.

B. L. Berman, M. A. Kelly, R. L. Bramblett, J. T. Caldwell, H. S. Davis, and S. C. Fultz
Phys. Rev. 185, 1576 (1969)

ELEM. SYM.	A	Z
W	186	74

METHOD

REF. NO. 69 Be 8 hmg

REACTION	RESULT	EXCITATION ENERGY	SOURCE TYPE	SOURCE RANGE	DETECTOR TYPE	DETECTOR RANGE	ANGLE
G,N* 167+	ABX	8-29	D	8-29	BF3-I		4PI
G,2N** 168	ABX	8-29	D	8-29	BF3-I		4PI
G,3N 169	ABX	8-29	D	8-29	BF3-I		4PI

* INCLUDES NP
** INCLUDES 2NP
166+

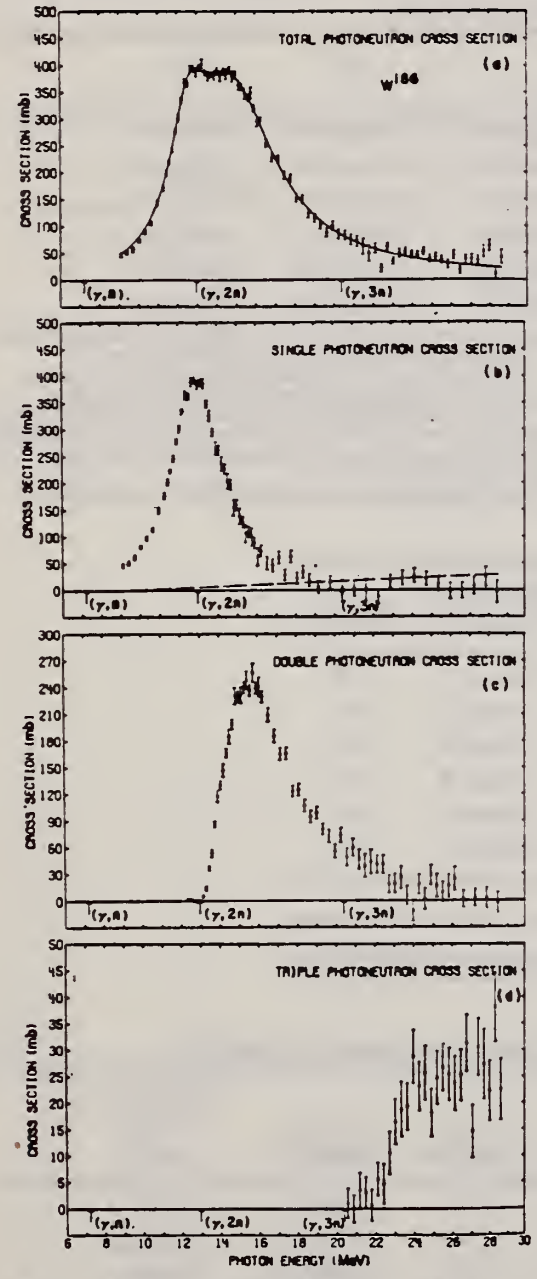

FIG. 8. Photoneutron cross sections for W^{186}: (a) $\sigma[(\gamma,n)+(\gamma,pn)+(\gamma,2n)+(\gamma,p2n)+(\gamma,3n)]$, (b) $\sigma[(\gamma,n)+(\gamma,pn)]$, (c) $\sigma[(\gamma,2n)+(\gamma,p2n)]$, (d) $\sigma(\gamma,3n)$.

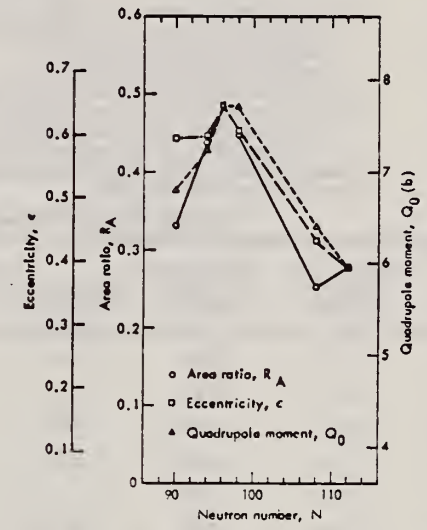

FIG. 9. The area ratio R_A, nuclear eccentricity ϵ, and intrinsic quadrupole moment Q_0 plotted versus neutron number N. The data were scaled between the value for Gd^{160} and that for W^{186}. The absolute scale for Q_0 is based on a mean radius parameter $R_0 = 1.26$ F. The lines merely connect the three sets of data points. The experimental uncertainties have been omitted for clarity but are given in Tables VII and VIII; their average values are 0.065 (17%) for R_A, 0.010 (1.9%) for ϵ, and 0.26b (3.7%) for Q_0.

[over]

TABLE V. Parameters of Lorentz-curve fits to the giant resonance.

Nucleus	$E_m(1)$ (MeV)	$\sigma_m(1)$ [a] (mb)	$\Gamma(1)$ (MeV)	$E_m(2)$ (MeV)	$\sigma_m(2)$ [a] (mb)	$\Gamma(2)$ (MeV)
Eu^{153}	12.33±0.06	155±9	2.75±0.26	15.79±0.10	222±6	5.83±0.30
Tb^{159} [b]	12.22±0.04	181±6	2.64±0.16	15.67±0.06	220±4	4.97±0.19
Gd^{160}	12.23±0.06	215±9	2.77±0.25	15.96±0.09	233±6	5.28±0.30
Ho^{165}	12.28±0.02	214±5	2.57±0.11	15.78±0.04	246±3	5.00±0.17
Ta^{181} [c]	12.59±0.03	171±8	1.94±0.12	15.13±0.12	265±6	4.98±0.23
W^{186}	12.59±0.03	211±14	2.29±0.14	14.88±0.08	334±8	5.18±0.14

[a] The uncertainties for σ_m given here are relative. The absolute uncertainty is 7% (10% for Tb^{159} and Ta^{181}).
[b] The data of Ref. 10 were reanalysed to obtain the values given in this and subsequent tables (see text).
[c] The data of Ref. 11 were reanalysed to obtain the values given in this and subsequent tables (see text).

[10] R.L. Bramblett, J. T. Caldwell, R. R. Harvey, S.C. Fultz, Phys.Rev.133, B869 (1964).
[11] R.L. Bramblett, J.T. Caldwell, G.F. Auchampaugh, S.C. Fultz, Phys.Rev.129, 2723 (1963)

TABLE VIII. Nuclear radius parameters.

Nucleus	Q_0 [a] (b)	Refs.	ϵ [b]	R_0 [c] (F)	Q_0 [d] (b)
Eu^{153}	6.99±0.08	e, f	0.595±0.015	1.276±0.018	6.80±0.28
Tb^{159}	7.41±0.11	e	0.598±0.009	1.274±0.013	7.23±0.26
Gd^{160}	7.55±0.17	g	0.645±0.014	1.245±0.020	7.71±0.30
Ho^{165}	7.56±0.11	e	0.604±0.006	1.246±0.011	7.71±0.26
Ta^{181}	6.89±0.21	h, i	0.433±0.010	1.306±0.025	6.43±0.26
W^{186}	5.96±0.05	g, j, k	0.390±0.006	1.259±0.011	5.96±0.21

[a] Values taken from or computed from the references listed in column 3.
[b] Values from present data (Table VII).
[c] Computed from Eq. (2) in the text.
[d] The "best" values for Q_0 deduced from the present data, computed from Eq. (2) in the text, taking R_0 to be 1.26±0.02 F.
[e] M. C. Oleson and B. Elbek, Nucl. Phys. 15, 134 (1960).
[f] R. A. Carrigan, Jr., P. D. Gupta, R. B. Sutton, M. N. Suzuki, A. C. Thompson, R. E. Coté, W. V. Prestwich, A. K. Gaigalas, and S. Raboy, Phys. Rev. Letters 20, 874 (1968).
[g] P. H. Stelson and L. Grodzins, Nucl. Data A1, 21 (1965).
[h] F. K. McGowan and P. H. Stelson, Phys. Rev. 109, 901 (1958).
[i] E. M. Bernstein and R. Graetzer, Phys. Rev. 119, 1321 (1960).
[j] R. C. Barrett, S. Bernow, S. Devons, I. Duerdoth, D. Hitlin, J. W. Kast, W. Y. Lee, E. R. Macagno, J. Rainwater, and C. S. Wu, Columbia University Pegram Nuclear Physics Lab. Report No. NYO-72-191, 1968, p. 74 (unpublished).
[k] R. G. Stokstad and B. Persson, Phys. Rev. 170, 1072 (1968).

TABLE IX. Integrated cross sections.

Nucleus	$E_{\gamma\,max}$ (MeV)	$\sigma_{int}[(\gamma,n)+(\gamma,pn)]$ [a] (MeV-b)	$\sigma_{int}[(\gamma,2n)+(\gamma,p2n)]$ [a] (MeV-b)	$\sigma_{int}(\gamma,3n)$ [a] (MeV-b)	$\frac{\sigma_{int}[(\gamma,2n)+(\gamma,p2n)]}{\sigma_{int}(\gamma,\text{total})}$ [b]	$\frac{1}{2}\pi[\sigma_m(1)\Gamma(1)+\sigma_m(2)\Gamma(2)]$ [a] (MeV-b)	$0.06\,NZ/A$ (MeV-b)
Eu^{153}	28.9	1.57	0.67	0.04	0.29±0.04	2.70±0.19	2.22
Tb^{159}	28.0	1.41	0.89	d	0.39±0.08	2.47±0.12	2.31
Gd^{160}	29.5	1.45	1.00	0.08	0.39±0.05	2.87±0.20	2.30
Ho^{165}	28.9	1.73	0.74	0.04	0.29±0.04	2.80±0.09	2.39
Ta^{181}	24.6	1.31	0.88 [e]	f	0.40 [e]±0.08	2.59±0.15	2.61
W^{186}	28.6	1.66	1.19	0.15	0.40±0.05	3.47±0.17	2.67

[a] All measured integrated cross-section values are given for an energy region from threshold to $E_{\gamma\,max}$.
[b] The word "total" in this table refers to the total photoneutron cross section, $\sigma[(\gamma,n)+(\gamma,pn)+(\gamma,2n)+(\gamma,p2n)+(\gamma,3n)]$.
[c] The uncertainties listed here are relative; to get the absolute uncertainty, a systematic uncertainty of 7% (10% for Tb^{159} and Ta^{181}) must be folded into the values for σ_m.
[d] Not measured in Ref. 10; $\sigma_{int}[(\gamma,2n)+(\gamma,p2n)]$ contains $\frac{1}{2}\sigma_{int}(\gamma,3n)$.
[e] Because $E_{\gamma\,max}$ is so low, these values cannot be compared to the rest.
[f] Not measured in Ref. 11; the $(\gamma,3n)$ cross section below 24.6 is MeV probably negligible.

TABLE X. Integrated moments[a] of the measured photoneutron cross section and sum rules.

Nucleus	σ_{-1} (mb)	$\sigma_{-1}A^{-1/3}$ (mb)	σ_{-2} (mb-MeV^{-1})	$\frac{\sigma_{-2}}{0.00225\,A^{5/3}}$	$\frac{\sigma_{-2}K}{0.05175\,A^{5/3}}$	$\frac{0.05175\,A^{5/3}}{\sigma_{-2}}$ (MeV)
Eu^{153}	148	0.181	10.18	1.03	1.16±0.11	22.2±1.6
Tb^{159}	151	0.175	10.49	1.00	1.14±0.13	23.0±2.3
Gd^{160}	169	0.195	12.09	1.14	1.35±0.13	20.2±1.4
Ho^{165}	166	0.183	11.56	1.04	1.23±0.10	22.2±1.6
Ta^{181} [b]	(149)	(0.145)	(10.66)	(0.82)	(0.97±0.13)	(28.1±2.8)
W^{186}	203	0.191	14.51	1.06	1.26±0.11	21.6±1.5

[a] $\sigma_{-1}=\int_{E_{thr}}^{E_{\gamma\,max}}\sigma E^{-1}\,dE$ and $\sigma_{-2}=\int_{E_{thr}}^{E_{\gamma\,max}}\sigma E^{-2}\,dE$, where σ is the total photoneutron cross section.
[b] Because $E_{\gamma\,max}$ is so low, the values for Ta^{181} cannot be compared to the rest.

REF.	ELEM. SYM.	A	Z
R. Moreh, A. Nof, O. Shahal and A. Wolf Phys. Letters 36B, 71 (1971)	W	186	74
METHOD	REF. NO.		
	71 Mo 2		egf

REACTION	RESULT	EXCITATION ENERGY	SOURCE		DETECTOR		ANGLE
			TYPE	RANGE	TYPE	RANGE	
G,G/	LFT	6	D	6,8	SCD-D		DST

6.418 MEV

Table 1
Summary of the experimental and theoretical decay properties of the resonance levels excited by nuclear photo-excitation.

Scatterer	Transition $1^- \rightarrow 2^+$ (keV)	A $(1^- \rightarrow 2^+)$	Γ_γ (meV)	Γ(M2) (μeV)	Γ(M2) (W.u.)	δ^2(M2/E1) ($\times 10^3$)	δ^2(M2/E1) Weisskopf estimate ($\times 10^6$)
^{74}Ge	6018 → 2200	0.14 ± 0.04	120 ± 15	190	0.89	17^{+23}_{-12}	3.2
^{100}Mo	6418 → 1064	0.20 ± 0.08	50 ± 45	110	0.079	46^{+53}_{-33}	6.3
^{112}Cd	7632 → 617	0.09 ± 0.02	86 ± 15	36	0.006	$3.6^{+4.5}_{-2.7}$	10.8
^{186}W	6418 → 122	-0.011 ± 0.014	46 ± 35	110	0.023	$9.0^{+5.4}_{-4.1}$	8.7

A.M. Goryachev, G.N. Zalesnyi, S.F. Semenko, and B.A. Tulupov

REF. Yad. Fiz. 17, 463 (1973)
Sov. J. Nucl. Phys. 17, 236 (1973)

ELEM. SYM.	A	Z
W	186	74

METHOD

REF. NO. 73 Go 6 hmg

REACTION	RESULT	EXCITATION ENERGY	SOURCE		DETECTOR		ANGLE
			TYPE	RANGE	TYPE	RANGE	
G,XN	ABX	8- 20	C	8- 20	BF3-I		4PI

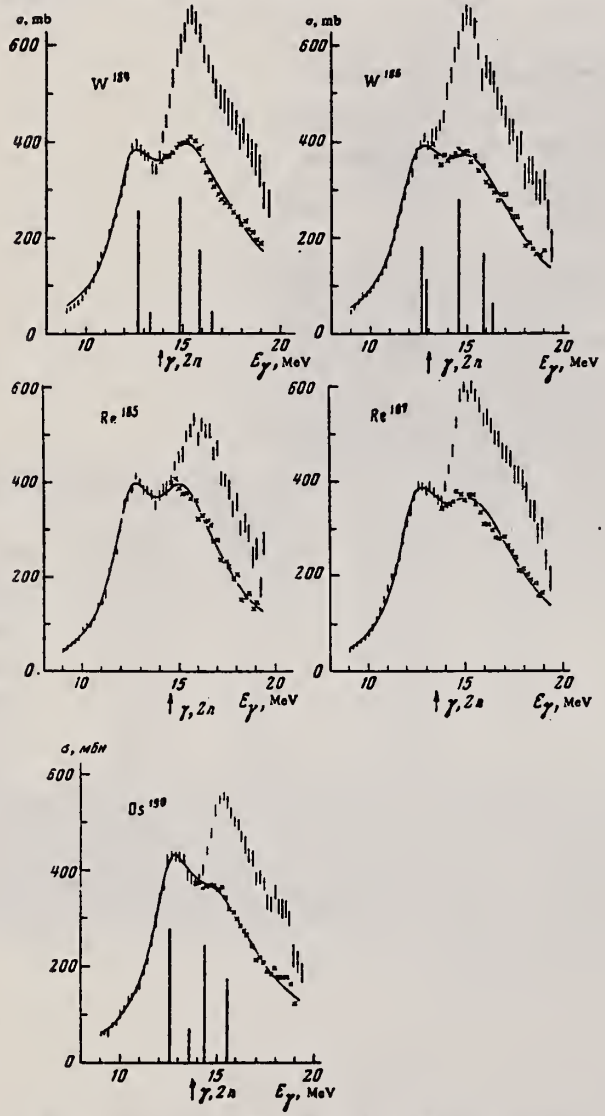

FIG. 2. Cross sections for $W^{184,186}$, Os^{190}, and $Re^{185,187}$. The cross section $\sigma_{\gamma,n} + 2\sigma_{\gamma,2n}$ is denoted by vertical lines whose lengths are twice the rms errors. The crosses represent the cross sections, corrected for multiplicity, above the threshold of the (γ, 2n) reaction. The solid curves are Lorentz curve approximations. For $W^{184,186}$ and Os^{190} the calculated dipole transition strengths are shown.

TABLE III

	W^{184}	W^{186}	Os^{190}	Re^{185}	Re^{187}	W^{186} [7]
Γ_1, MeV	2.33	2.55	2.13	2.51	2.83	2.20
E_1, MeV	12.5	12.5	12.6	12.7	12.6	12.59
σ_1, mb	241	225	223	262	250	211
Γ_2, MeV	5.1	5.4	5.7	5.2	5.3	5.18
E_2, MeV	15.6	15.2	14.8	15.4	15.6	14.88
σ_2, mb	338	317	318	315	296	334
0.06 NZ/A, MeV·mb	2.65	2.67	2.74	2.68	2.69	2.67
$S_1 + S_2$, MeV − mb	4.0	3.9	3.9	3.6	3.8	3.47
S_2 / S_1	2.8	3.0	3.8	2.5	2.2	3.6

Note. $S_i = (\pi/2)\sigma_i\Gamma_i$ is the Lorentz area.

REF.

A. Wolf, R. Moreh, and O. Shahal
Nucl. Phys. A227, 373 (1974)

ELEM. SYM.	A	Z
W	186	74

METHOD

REF. NO. 74 Wo 2 egf

REACTION	RESULT	EXCITATION ENERGY	SOURCE TYPE	SOURCE RANGE	DETECTOR TYPE	DETECTOR RANGE	ANGLE
$ G,G	LFT	6- 8	D	6- 8	SCD-D		DST

δ = Doppler width

6.418

TABLE 4

Upper limit of Γ_0/Γ, the temperature variation ratio R_T, and the self-absorption ratio R

Scatterer (γ-source)	E_0 (MeV)	Γ_0/Γ (±15%)	R_T [a]	R(%) [b]
^{65}Cu(Ti)	6.556	0.80	0.94 ±0.02	1.1±0.5
^{69}Ga(Cu)	7.306	0.52	1.035±0.004	3.5±0.5
^{100}Mo(Cu)	7.637	0.28	1.043±0.007	0.8±0.3
^{100}Mo(Ti)	6.418	0.85	1.032±0.003	0.6±0.3
^{113}Sn(Cu)	6.988	0.84	1.020±0.009	5.7±0.2
^{126}Te(Cu)	7.915	0.4 ±0.1	0.95 ±0.05	6 ±5
^{130}Te(Cu)	7.637	0.45±0.10	0.84 ±0.05	0.9±1.5
^{139}La(Cu)	7.637	0.55	0.95 ±0.01	2.2±0.3
^{139}La(Ti)	6.418	0.78	0.968±0.008	6.4±0.8
^{141}Pr(Cu)	7.915	0.25	1.02 ±0.01	0.9±0.9
^{141}Pr(Cu)	7.252	0.51	1.005±0.003	5.9±0.4
^{144}Nd(Cu)	7.915	0.27	0.89 ±0.05	< 0.5
^{186}W(Ti)	6.418	0.31	1.030±0.004	< 0.5
^{203}Tl(Ti)	6.418	0.28	1.03 ±0.01	1.6±0.3
^{205}Tl(Cu)	7.252	0.58	1.02 ±0.01	1.6±0.7
^{209}Bi(Cu)	7.637	1.00	1.00 ±0.02	2 ±1
^{209}Bi(Ti)	7.168	1.00	0.971±0.005	28.0±0.6

[a]) The values of R_T are given for 10 g/cm² thick scatterers placed at an angle of 60° and a detector angle of 135°.

[b]) The values of R are given for the same scatterer-detector geometry as that of R_T and a 20 g/cm² thick absorber.

TABLE 7

Summary of Γ, Γ_0 and δ of resonance levels measured in the present work and in earlier works [8, 16, 17]

Isotope	Energy (MeV)	Γ (meV)	Γ_0 (meV)	δ (eV)	Ground state transition
^{65}Cu	6.556	70^{+60}_{-20}	28^{+15}_{-5}	11.2 ±0.8	
^{69}Ga [a])	7.306	105±40	48± 7	6.2 ±0.5	E1
^{100}Mo [c])	7.637	140±40	40± 5	4.5 ±0.5	E1
^{100}Mo [c])	6.418	50±35	25± 8	4.25±0.25	E1
^{118}Sn	6.988	152± 5	128± 3	5.5 ±0.5	E1
^{126}Te	7.915	12± 6	5± 2	11 ±2	M1
^{130}Te	7.637	60±30	30±10	15 ±2	E1
^{139}La [b])	7.637	170±40	47± 6	10.5 ±0.5	E1
^{139}La [b])	6.418	85^{+13}_{-7}	67± 8	9.5 ±0.5	E1
^{141}Pr [b])	7.915	7± 3	2± 1	6.6 ±1.0	M1
^{141}Pr [b])	7.252	290±30	110±10	6.4 ±0.5	E1
^{144}Nd [b])	7.915	30±10	8± 3	14.0 ±0.5	M1
^{186}W	6.418	46±35	6± 3	1 ±1	E1
^{203}Tl [b])	6.418	350±60	82±15	0.5 ±0.5	
^{205}Tl [b])	7.252	50±30	25± 6	5.2 ±1.5	M1
^{209}Bi	7.637	> 500	> 30		
^{209}Bi [b])	7.168	820±40	820±40	5.8 ±0.8	E1

[a]) Ref. [16]). [b]) Ref. [8]). [c]) Ref. [17]).

(over)

TABLE 6

Values of A_2, $N_{\parallel}/N_{\perp}$, spins, and mixing amplitudes x

Scatterer (γ-source)	E_0 (MeV)	A_2	$N_{\parallel}/N_{\perp}$	J_0^{π}	J^{π}	J_f^{π}	x
^{65}Cu(Ti)	6.556	0		$\frac{3}{2}^-$	$\frac{1}{2}$	$\frac{3}{2}^-$	0
^{69}Ga(Cu)	7.306	0.14 ±0.01	1.046±0.022	$\frac{3}{2}^-$	$\frac{3}{2}^+$	$\frac{1}{2}^-$	0
^{100}Mo(Cu)	7.637	0.49 ±0.05	1.17 ±0.05	0^+	1^-	0^+	0
^{100}Mo(Cu)	7.102 [a])	0.013±0.016		0^+	1^-	2^-	−0.06±0.02 [b])
^{100}Mo(Ti)	6.418	0.52 ±0.02	1.15 ±0.03	0^+	1^-	0^+	0
^{100}Mo(Ti)	5.355 [a])	0.19 ±0.08		0^+	1^-	2^+	0.21±0.12 [b])
^{118}Sn(Cu)	6.988	0.48 ±0.02	1.12 ±0.05	0^+	1^-	0^+	0
^{126}Te(Cu)	7.915	0.46 ±0.11	0.86 ±0.10	0^+	1^+	0^+	0
^{130}Te(Cu)	7.637	0.48 ±0.04	1.12 ±0.04	0^+	1^-	0^+	0
^{139}La(Cu)	7.637	0.16 ±0.02	1.024±0.015	$\frac{7}{2}^+$	$\frac{5}{2}^-$	$\frac{7}{2}^+$	0
^{139}La(Ti)	6.418	0.093±0.004	1.018±0.006	$\frac{7}{2}^+$	$\frac{5}{2}^-$	$\frac{7}{2}^+$	0
^{141}Pr(Cu)	7.915	0.41 ±0.06	0.94 ±0.03	$\frac{5}{2}^+$	$\frac{5}{2}^+$	$\frac{5}{2}^+$	$0.2^{+0.3}_{-0.3}$
^{141}Pr(Cu)	7.252	0.23 ±0.06	1.03 ±0.02	$\frac{5}{2}^+$	$\frac{3}{2}^-$	$\frac{5}{2}^+$	0
^{144}Nd(Cu)	7.915	0.50 ±0.03	0.92 ±0.09	0^+	1^+	0^+	0
^{186}W(Ti)	6.418	0.49 ±0.05	1.15 ±0.06	0^+	1^-	0^+	0
^{186}W(Ti)	6.296 [a])	−0.011±0.014		0^+	1^-	2^+	−0.10±0.0[illegible] [c])
^{203}Tl(Ti)	6.418	0	1.01 ±0.01	$\frac{1}{2}^+$	$\frac{1}{2}$	$\frac{1}{2}^-$	0
^{205}Tl(Cu)	7.252	0.71 ±0.08	0.90 ±0.02	$\frac{1}{2}^+$	$\frac{3}{2}^+$	$\frac{1}{2}^+$	−0.25±0.0[illegible]
^{205}Tl(Cu)	7.047 [a])	−0.69 ±0.03		$\frac{1}{2}^+$	$\frac{3}{2}^+$	$\frac{3}{2}^+$	0.33±0.04
^{209}Bi(Cu)	7.637	0.24 ±0.04		$\frac{9}{2}^-$	$(\frac{7}{2})$	$\frac{9}{2}^-$	
^{209}Bi(Ti)	7.168	0.20 ±0.02	1.040±0.015	$\frac{9}{2}^-$	$\frac{7}{2}^+$	$\frac{9}{2}^-$	

Errors refer to one standard deviation.
[a]) Inelastic transitions.
[b]) Ref. [17]).
[c]) Ref. [15]).

1) R. Moreh et al., Phys. Rev. C2 (1970) 1144
8) A. Wolf, et al., Phys. Rev. C6 (1972) 2276
15) R. Moreh et al., Phys. Lett. 36B (1971) 71
16) R. Moreh et al., Phys. Rev. C7 (1973) 1385
17) R. Moreh et al., Nucl. Phys. A217 (1973) 477
29) R. Moreh et al., Phys. Rev. C4 (1971) 2265
30) R. Moreh et al., Phys. Rev. 178 (1969) 1961

TABLE 8

Values of Γ_0, D, k_{E1} and k_{M1}

E1 transitions					M1 transitions				
scatterer (γ-source)	$E_0 \rightarrow E_f$ (MeV)	Γ_0 (meV)	D (eV)	k_{E1} (10^{-9} MeV^{-3})	scatterer (γ-source)	$E_0 \rightarrow E_f$ (MeV)	Γ_0 (meV)	D (eV)	k_{M1} (10^{-9} MeV^{-3})
^{62}Ni(Fe) [a])	7.646		12300		^{126}Te(Cu)	7.915		260	
	→ 1.172	24		0.5		→ 0.666	2.3		[illegible]
^{69}Ga(Cu)	7.306		660			→ 1.421	1.7		[illegible]
	→ 0.572	3.2		1.0	^{141}Pr(Cu)	7.915		90	
	→ 0.872	2.7		0.9		→ 1.298	1.3		[illegible]
^{100}Mo(Cu)	7.637		670			→ 1.437	0.8		[illegible]
	→ 0.535	40		7.7		→ 1.580	1.4		[illegible]
	→ 1.063	5.7		1.4		→ 1.655	1.0		[illegible]
	→ 1.461	1.4		0.4	^{141}Pr(Fe) [c])	7.632		170	
^{112}Cd(Fe) [b])	7.632		350			→ 0.145	5.6		[illegible]
	→ 0.617	11		4		→ 1.130	6.4		[illegible]
	→ 1.223	7.3		3.4		→ 1.293	0.4		[illegible]
	→ 1.429	2		1		→ 1.437	5.6		[illegible]
	→ 1.468	1.7		0.9		→ 1.451	6.8		[illegible]
^{130}Te(Cu)	7.637		360			→ 1.582	1.1		[illegible]
	→ 0.837	16		5.5	^{144}Nd(Cu)	7.915		380	
	→ 1.589	18		8.8		→ 0.697	13		[illegible]
^{139}La(Cu)	7.637		190			→ 1.041	2.7		[illegible]
	→ 1.384	3		2.5		→ 1.564	6.2		[illegible]
	→ 1.538	3		2.7	^{205}Tl(Cu)	7.252		1200	
^{141}Pr(Cu)	7.252		220			→ 0.205	4		[illegible]
	→ 0.146	82		38					
	→ 1.120	8.6		6.5					
^{186}W(Cu)	6.418		110						
	→ 0.122	12		14					

The values of D refer to an excitation energy E_0.
[a]) Ref. [1]). [b]) Ref. [29]). [c]) Ref. [30]).

REF. G.M. Gurevich, L.E. Lazareva, V.M. Mazur, S.Yu. Merkulov, G.V. Solodukhov, V.A. Tyutin
JETP Lett. 28, 157 (1978)
Pis'ma Zh. Eksp. Teor. Fiz. 28, 168 (1978)

ELEM. SYM.	A	Z
W	186	74

METHOD

REF. NO. 78 Gu 7 hg

REACTION	RESULT	EXCITATION ENERGY	SOURCE		DETECTOR		ANGLE
			TYPE	RANGE	TYPE	RANGE	
G,MU-T	ABX	THR-28	C	UKN	NAI-D		4PI

The absorption method is used to measure the total photoabsorption cross section curves for deformed ^{154}Sm, ^{156}Gd, ^{168}Er, ^{174}Yb, ^{184}W, and ^{186}W nuclei in the region of the $E1$ giant resonance. The behavior of the resonance widths for nuclei in the interval $A = 153$ to 186 is discussed.

PACS numbers: 24.30.Cz, 25.20.+y, 27.70.+q

TABLE I.

Nucleus	E_1 MeV	σ_1 mb	Γ_1 MeV	E_2 MeV	σ_2 mb	Γ_2 MeV	Γ MeV	Q_o b	β	$\sigma_{o\,L}/0.06\frac{ZN}{A}$
^{154}Sm	12.2	188	3.4	15.7	207	5.7	8.1 ± 0.2	6.3 ± 0.3	0.32 ± 0.02	1.28
^{156}Gd	12.3	206	3.2	15.7	220	5.5	7.7 ± 0.2	6.2 ± 0.3	0.31 ± 0.02	1.30
^{168}Er	11.9	222	3.2	15.5	275	4.5	7.4 ± 0.2	7.5 ± 0.7	0.32 ± 0.03	1.26
^{174}Yb	12.3	297	2.9	15.5	320	4.9	7.1 ± 0.2	7.0 ± 0.6	0.30 ± 0.02	1.52
^{184}W	11.9	315	2.9	14.8	321	4.7	6.8 ± 0.2	7.2 ± 0.8	0.27 ± 0.03	1.50
^{186}W	12.0	246	3.3	14.5	332	5.1	6.4 ± 0.2	6.2 ± 0.8	0.23 ± 0.03	1.48
Average error	±1.3%	±10.5%	±7.5%	±1.3%	±9.4%	±3.8%	—	—	—	—

(over)

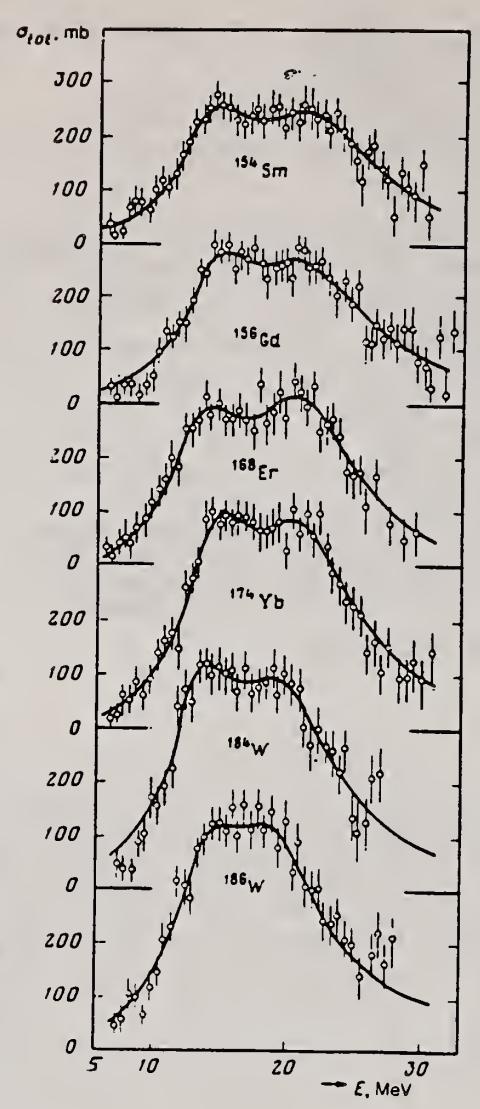

FIG. 2. Total cross sections of the photoabsorption of the nuclei ^{154}Sm, ^{156}Gd, ^{168}Er, ^{174}Yb, ^{184}W, and ^{186}W. The mean squared errors are shown.

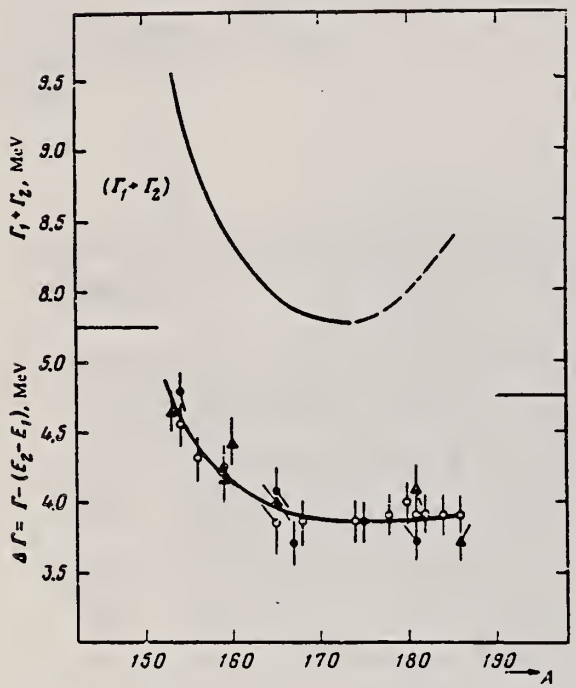

FIG. 3. Experimental values of $\Delta\Gamma = \Gamma - (E_2 - E_1)$ in the region of deformed nuclei with $A = 153$–186: ○—present work and[11]; ●—Saclay group; ▲—Livermore group. Owing to a small systematic deviations of the absolute values, the ordinate scales for the Saclay and Livermore data are shifted 0.15 MeV upward and downward, respectively. The $(\Gamma_1 + \Gamma_2)$ curve was obtained from the $\Delta\Gamma$ curve after introduction of corrections in the interval $A = 175$–186.

REF.	ELEM. SYM.	A	Z
W. Günther, R. Haag, K. Huber, U. Kneissl, H. Krieger, H.J. Maier, H. Ströher Phys. Rev. Lett. 44, 716 (1980)	W	186	74

METHOD	REF. NO.
	80 Gu 1 hg

REACTION	RESULT	EXCITATION ENERGY	SOURCE		DETECTOR		ANGLE
			TYPE	RANGE	TYPE	RANGE	
E,F	NOX	THR-55	D	35-55	TRK-D		4PI

Low end of experimental arrows in Fig. 1 indicated lower limit for fission barriers established by this experiment.

The electroinduced fission of ^{182,184,186}W has been investigated in the energy range from 35 to 55 MeV. The fission barriers, estimated by a statistical-model analysis of the measured cross sections, are compared with theoretical predictions and are only consistent with the assumption of a constant pairing strength.

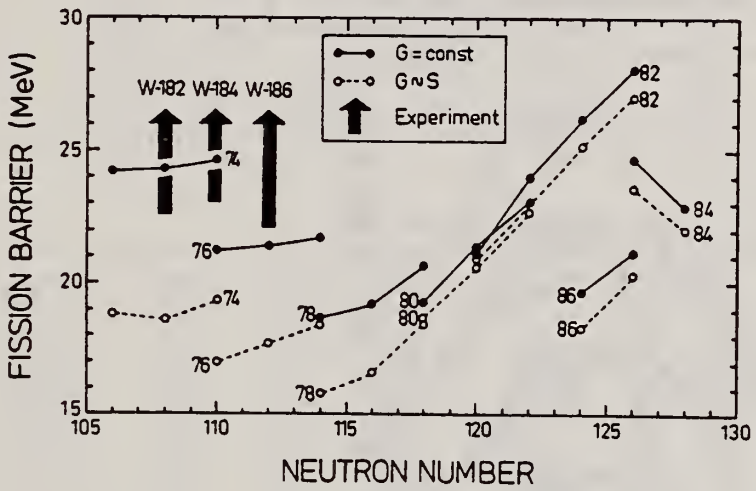

FIG. 1. Calculated fission barriers (Ref. 3) (full lines, G = const; dashed lines, $G \sim S$) and limits deduced from our experiments on ^{182,184,186}W.

REF. G.M. Gurevich, L.E. Lazareva, V.M. Mazur, S.Yu. Merkulov, G.V. Solodukhov, V.A. Tyutin
Nucl. Phys. A351, 257 (1981)

ELEM. SYM.	A	Z
W	186	74

METHOD

REF. NO. 81 Gu 2 hg

REACTION	RESULT	EXCITATION ENERGY	SOURCE TYPE	SOURCE RANGE	DETECTOR TYPE	DETECTOR RANGE	ANGLE
G,MU-T	ABX	THR-20	C	27	NAI-D		4PI

Abstract: The curves of the total gamma-absorption cross sections (σ_{tot}) in the E1 giant resonance energy range for the nuclei ^{154}Sm, ^{156}Gd, ^{165}Ho, ^{168}Er, ^{174}Yb, ^{178}Hf, ^{180}Hf, ^{181}Ta, ^{182}W, ^{184}W, ^{186}W and ^{197}Au have been measured using the absorption method. Parameters of the Lorentz curves fitting the measured cross sections σ_{tot} are given. Quadrupole moments (Q_0) and nuclear deformation parameters (β) were obtained.

For deformed nuclei in the $\sim 155 < A < \sim 180$ region a violation of the correlation between giant resonance widths (Γ) and nuclear deformation parameters was found. Γ_1 and Γ_2, the widths of the resonances corresponding to vibrations of nucleons along and across the nuclear deformation axis, were observed to decrease with the increase of A which could be accounted for by the presence of an $N = 108$ subshell.

E NUCLEAR REACTIONS ^{154}Sm, ^{156}Gd, ^{165}Ho, ^{168}Er, ^{174}Yb, ^{178,180}Hf, ^{181}Ta, ^{182,184,186}W, ^{197}Au (γ, X), E = 7–20 MeV; measured total $\sigma(E)$; deduced integrated σ, Lorentz line parameters. ^{154}Sm, ^{156}Gd, ^{165}Ho, ^{168}Er, ^{174}Yb, ^{178,180}Hf, ^{181}Ta, ^{182,184,186}W, ^{197}Au deduced β, Q_0, Γ, giant resonance evolution. Enriched, natural targets.

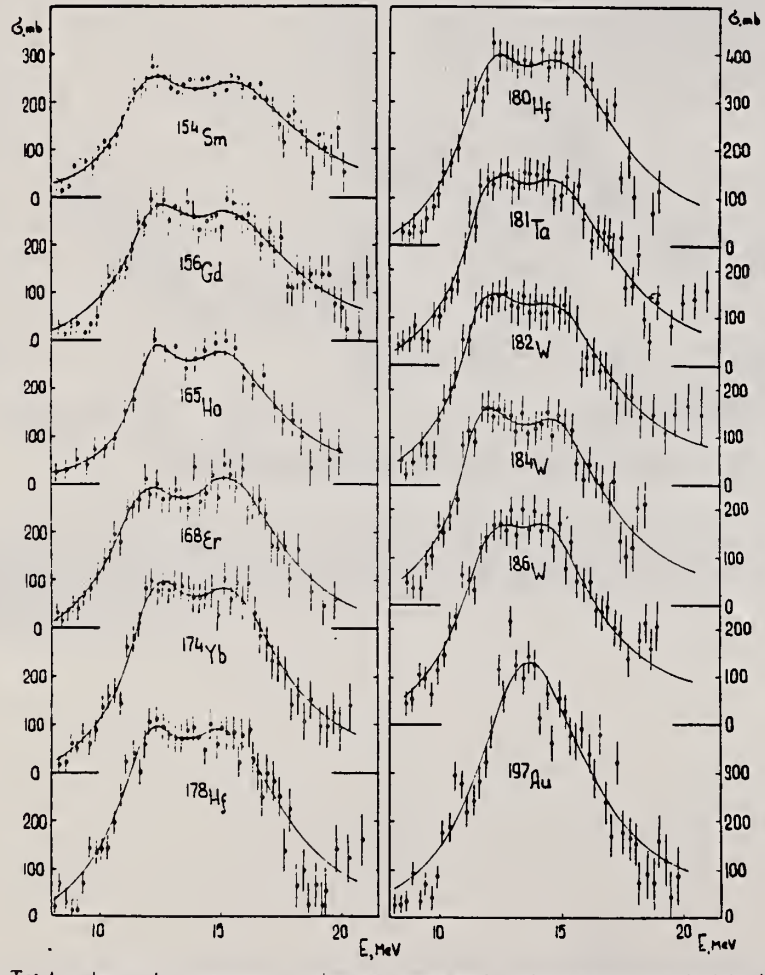

Fig. 2. Total nuclear γ-absorption cross sections (σ_{tot}) measured by the absorption method for ^{154}Sm, ^{156}Gd, ^{165}Ho, ^{168}Er, ^{174}Yb, ^{178}Hf, ^{180}Hf, ^{181}Ta, ^{182}W, ^{184}W, ^{186}W and ^{197}Au. Rms error bars are shown.

(OVER)

TABLE 2

Parameters of Lorentz curves fitting the experimental data on $\sigma_{(\gamma,n)}$

Nucleus	E_1 (MeV)	σ_1 (mb)	Γ_1 (MeV)	E_2 (MeV)	σ_2 (mb)	Γ_2 (MeV)	$\frac{\sigma_2\Gamma_2}{\sigma_1\Gamma_1}$	Γ (MeV)
^{154}Sm	12.2	188	3.4	15.7	207	5.7	1.85	8.1
^{156}Gd	12.3	206	3.2	15.7	220	5.5	1.81	7.7
^{165}Ho	12.3	202	2.3	15.2	239	4.8	2.47	7.0
^{168}Er	11.9	222	3.2	15.5	275	4.5	1.73	7.4
^{174}Yb	12.3	297	2.9	15.5	320	4.9	1.80	7.1,
^{178}Hf	12.2	291	3.1	15.5	334	4.9	1.80	7.2
^{180}Hf	12.2	286	3.2	15.3	324	5.1	1.81	7.1
^{181}Ta	12.1	272	3.0	15.0	316	5.1	1.97	6.8
^{182}W	11.9	267	3.2	14.8	303	5.6	2.01	6.8
^{184}W	11.9	315	2.9	14.8	321	4.7	1.65	6.8
^{186}W	12.0	246	3.3	14.5	332	5.1	2.07	6.4
^{197}Au	13.7	535	5.2					
Average error	1.4 %	11.2 %	9.3 %	1.5 %	9.7 %	4.6 %	0.22	0.2 MeV

TABLE 3

Ratios of nuclear ellipsoid axes (k), deformation parameters (β) and intrinsic quadrupole moments (Q_0), calculated from E_2/E_1

Nucleus	^{154}Sm	^{156}Gd	^{165}Ho	^{168}Er	^{174}Yb	^{178}Hf	^{180}Hf	^{181}Ta	^{182}W	^{184}W	^{186}W
k	1.320	1.302	1.259	1.327	1.289	1.296	1.281	1.263	1.271	1.268	1.229
β	0.326 ±0.017	0.309 ±0.016	0.266 ±0.036	0.334 ±0.032	0.296 ±0.024	0.303 ±0.032	0.288 ±0.036	0.270 ±0.026	0.278 ±0.030	0.274 ±0.032	0.235 ±0.033
Q_0	6.3 ±0.3	6.2 ±0.3	5.8 ±0.8	7.5 ±0.7	7.0 ±0.6	7.5 ±0.8	7.2 ±0.9	6.9 ±0.7	7.2 ±0.8	7.1 ±0.8	6.2 ±0.9

TABLE 4

Integral characteristics of E1 giant resonance

Nucleus	$\sigma_{0\,exp}$ (MeV · b)	$\sigma_{0\,exp}$ $0.06NZ/A$	σ_{0L} (MeV · b)	σ_{01} $0.06NZ/A$	σ_{-1} (mb)	σ_{-1L} (mb)	$\sigma_{-1L}A^{-4/3}$ (mb)	σ_{-2} (mb · MeV^{-1})	σ_{-2L} (mb · MeV^{-1})	$\sigma_{-2L}A^{5/3}$ (μb · MeV^{-1})
^{154}Sm	1.94 ± 0.06	0.87	2.86	1.29	117 ± 3.5	156	0.189	9.1 ± 0.3	14.3	3.23
^{156}Gd	2.07 ± 0.07	0.91	2.95	1.30	143 ± 4.6	163	0.194	10.5 ± 0.4	14.9	3.30
^{165}Ho	1.86 ± 0.06	0.78	2.53	1.06	155 ± 4.4	160	0.177	10.1 ± 0.3	12.6	2.54
^{168}Er	2.24 ± 0.06	0.92	3.07	1.26	161 ± 4.3	197	0.212	12.0 ± 0.3	16.0	3.13
^{174}Yb	2.69 ± 0.05	1.07	3.82	1.52	195 ± 3.4	240	0.247	14.5 ± 0.3	19.2	3.54
^{178}Hf	2.85 ± 0.07	1.11	3.99	1.55	208 ± 4.9	247	0.247	15.3 ± 0.4	20.2	3.59
^{180}Hf	2.72 ± 0.06	1.05	4.03	1.56	200 ± 4.4	250	0.246	15.1 ± 0.3	20.7	3.61
^{181}Ta	2.84 ± 0.07	1.09	3.81	1.46	210 ± 5.3	245	0.239	16.0 ± 0.4	20.0	3.45
^{182}W	2.86 ± 0.07	1.09	4.01	1.52	211 ± 5.3	256	0.248	16.2 ± 0.4	21.6	3.70
^{184}W	2.78 ± 0.07	1.05	3.80	1.43	207 ± 5.3	251	0.240	15.9 ± 0.4	20.9	3.51
^{186}W	2.90 ± 0.07	1.08	3.95	1.48	214 ± 5.3	256	0.241	16.2 ± 0.4	21.6	3.56
^{197}Au	3.12 ± 0.06	1.10	4.37	1.54	229 ± 4.2	276	0.241	18.6 ± 0.4	23.3	3.49

RHENIUM
Z=75

Credit for the discovery of rhenium goes to the German chemists Walter Noddack, Ida Tacke —— later Ida Noddack, and Otto Berg. Their discovery, based on the x-ray examinations of columbite and various platinum ores, was not accidental but the result of a three year search begun by studying the relative frequencies of known elements in the earth's crust. Noddack, Tacke, and Berg found that elements of odd atomic number are less common than those of even number. Using this information combined with the known frequency of occurance of platinum ores and of columbite, they obtained an approximate idea of the extent of the extraction process. In May of 1925, they accomplished a 100,000-fold concentration of element 75 and established the existence of the new element. They named it rhenium —— derived from the Latin word *Rhenus* for the German Rhine river.

Re

Re

REF. A. V. Mitrofanova, Yu. N. Ranyuk, and P. V. Sorokin
J. Nucl. Phys. (USSR) 6, 703 (1967)
Sov. J. Nucl. Phys. 6, 512 (1968)

ELEM. SYM.	A	Z
Re		75

METHOD

REF. NO.	
67 Mi 1	HMG

REACTION	RESULT	EXCITATION ENERGY	SOURCE		DETECTOR		ANGLE
			TYPE	RANGE	TYPE	RANGE	
G,F	ABX	300-999		300-999	TRK-I		

Detector: Fission fragment tracks in glass.

999 = 1600 MEV

Angular distribution measured for Pb was found isotropic; for other elements it was assumed isotropic.

Nucleus	Fissionability D	Cross section σ_A, $\mu\beta$	Nucleus	Fissionability D	Cross section σ_K, $\mu\beta$
Bi	0.11±0.01	7.8±0.6	Os	0.0058±0.0005	0.37±0.04
Pb	0.050±0.004	3.4±0.3	Re	0.0056±0.0006	0.35±0.04
Tl	0.031±0.003	2.1±0.2	Ta	0.0045±0.0005	0.27±0.03
Au	0.019±0.002	1.25±0.10	Hf	0.0042±0.0004	0.25±0.03
Pt	0.012±0.002	0.80±0.08			

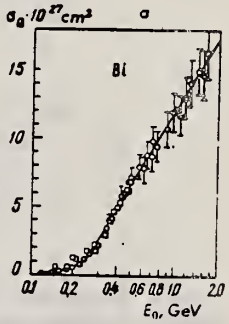

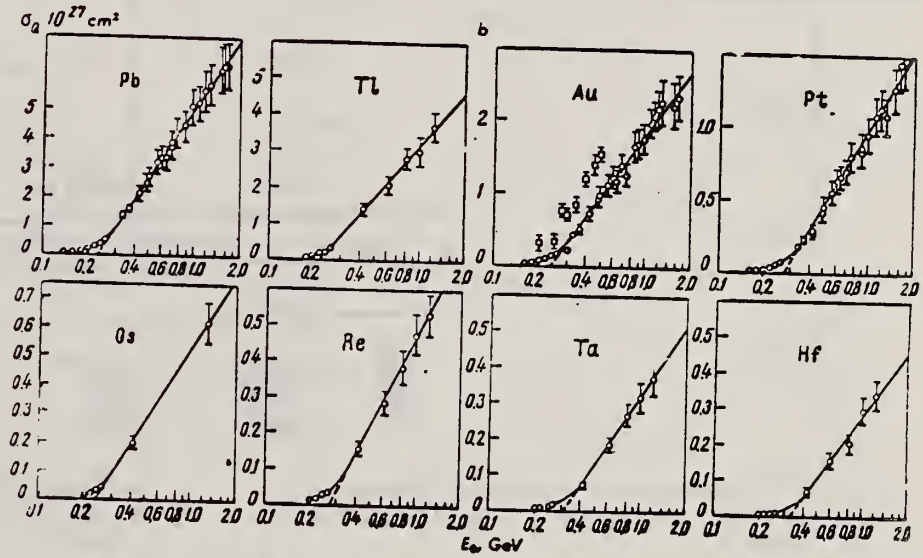

Fig. 1. Photofission fragment yields. ○-present work; □-Jungerman and Steiner.[1] The curves were plotted through the experimental points.

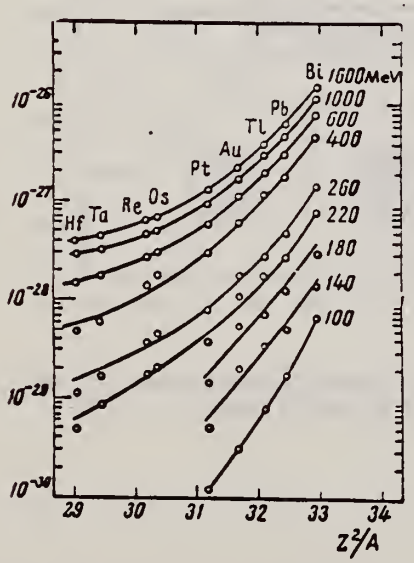

Fig. 2. Photofission fragment yields as a function of Z^2/A. The ordinates are values of σ_γ in units of cm².

REF. Yu. N. Ranyuk and P. V. Sorokin
J. Nucl. Phys. (USSR) 5, 37 (1967)
Sov. J. Nucl. Phys. 5, 26 (1967)

ELEM. SYM.	A	Z
Re		75

METHOD

REF. NO.	
67 Ra 2	HMG

REACTION	RESULT	EXCITATION ENERGY	SOURCE		DETECTOR		ANGLE
			TYPE	RANGE	TYPE	RANGE	
G, F	ABX	THR-260	C	200-260	EMU-I		4PI

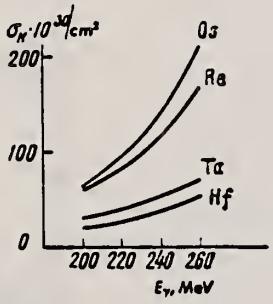

Fig. 4. Photofission cross sections of Os, Re, Ta, and Hf as functions of photon energy.

TABLE III

$E_{\gamma\ max}$, MeV	Cross section per equivalent γ quantum, 10^{-30} cm²			
	Os	Re	Ta	Hf
200	17±2	11.8±0.8	5.2±0.3	3.2±0.7
220	22±2	17±1	8.6±0.5	4.8±0.3
240	33±3	29±1	13.0±0.6	8.2±0.4
260	45±4	36±2	17.2±0.7	11.2±0.5

REF. A. Veyssiere, H. Beil, R. Bergere, P. Carlos, A. Lepretre, A. De Miniac
J. Phys. Lett. 36, L267 (1975)

ELEM. SYM.	A	Z
Re		75

METHOD

REF. NO. 75 Ve 5 egf

REACTION	RESULT	EXCITATION ENERGY	SOURCE		DETECTOR		ANGLE
			TYPE	RANGE	TYPE	RANGE	
G,N*	ABX	8- 22	D	8- 22	MOD-I		4PI
G,2N**	ABX	13- 22	D	8- 22	MOD-I		4PI

Abstract. — Partial photoneutron cross-sections $[\sigma(\gamma, n) + \sigma(\gamma, pn)]$, and $\sigma(\gamma, 2n)$ of W, Re, Ir, Pt and Hg were measured by means of monochromatic photons of 8 MeV $\leqslant E \leqslant$ 22 MeV so as to study the giant resonance. The experimentally observed evolution of the shape of the GDR, as one proceeds from permanently deformed prolate nuclei (W and Re) towards oblate or even triaxial gamma unstable nuclei (Pt), corresponds to the theoretical predictions of the dynamic collective model.

*1023+
**1024

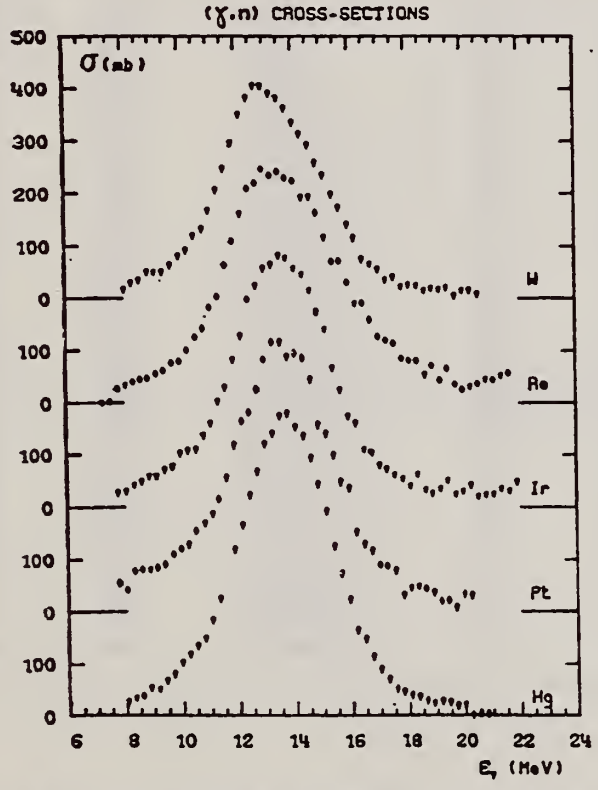

FIG. 1. — Sections efficaces partielles $\sigma(\gamma, n) + \sigma(\gamma, pn)$ des noyaux W, Re, Ir, Pt, Hg.

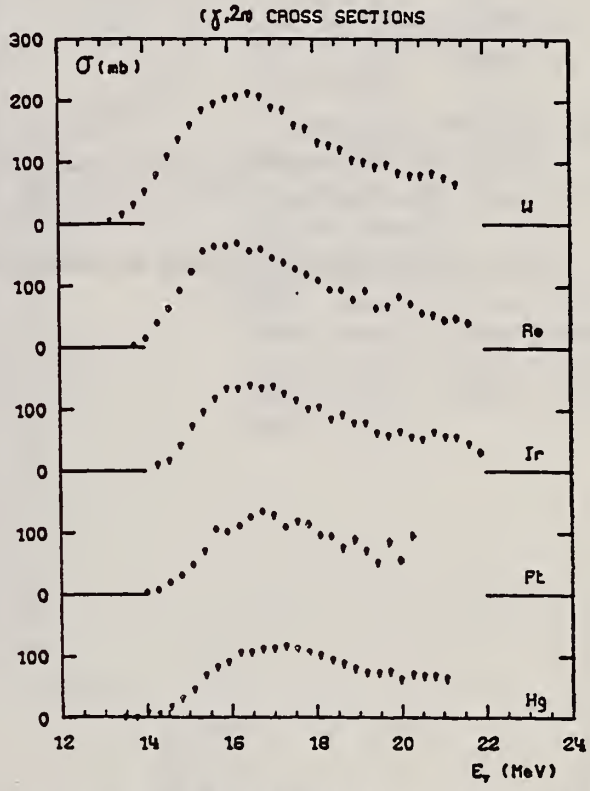

FIG. 2. — Sections efficaces partielles $\sigma(\gamma, 2n)$ des noyaux W, Re, Ir, Pt, Hg.

(over)

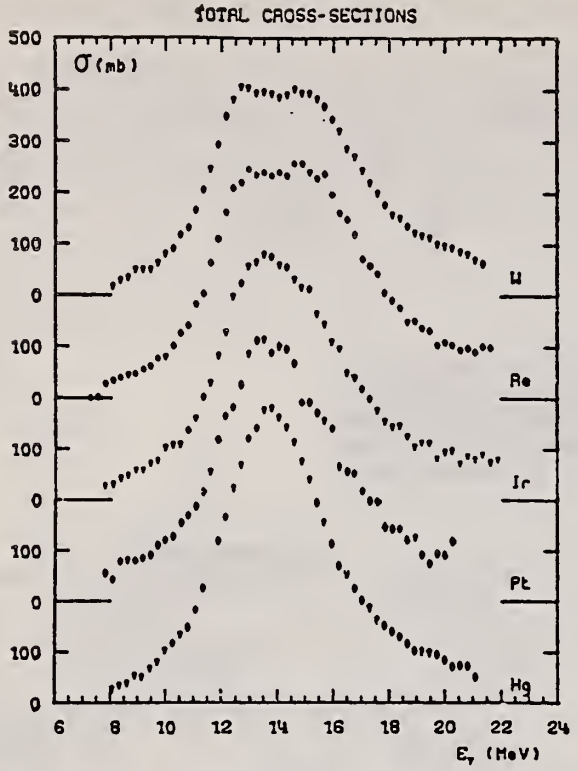

FIG. 3. — Sections efficaces totales $\sigma_T(E)$ des noyaux W, Re, Ir, Pt, Hg.

TABLEAU I

	σ_1 mb	Γ_1 MeV	E_1 MeV	σ_2 mb	Γ_2 MeV	E_2 MeV
W	300	3,2	12,7	290	4,3	15,4
Re	310	3,3	12,8	330	4,45	15,4

REF.

V. Emma, S. Lo Nigro, C. Milone
Nucl. Phys. A257, 438 (1976)

ELEM. SYM.	A	Z
Re		75

METHOD

REF. NO.: 76 Em 2 | egf

REACTION	RESULT	EXCITATION ENERGY	SOURCE		DETECTOR		ANGLE
			TYPE	RANGE	TYPE	RANGE	
G,F	ABY	THR-999	C	999	TRK-I		4PI

999 = 1 GEV

TABLE I

Measured values of σ_q at $E = 1000$ MeV and deduced values of σ_k assumed constant from E_0 to 1000 MeV

Element	Z^2/A	σ_q (mb)	E_0 (MeV)	σ_k (mb)
Bi	32.96	12.3±0.6	200	7.6±0.6
Pb	32.45	5.4±0.4	220	3.6±0.3
Tl	32.10	4.1±0.3	230	2.8±0.3
Au	31.68	2.0±0.15	240	1.4±0.2
Pt	31.18	1.1±0.08	255	(8 ±0.7)×10^{-1}
Re	30.21	(3.7±0.3)×10^{-1}	280	(2.9±0.3)×10^{-1}
W	29.78	(3.5±0.3)×10^{-1}	290	(2.8±0.3)×10^{-1}
Ta	29.45	(3.3±0.3)×10^{-1}	300	(2.7±0.3)×10^{-1}
Hf	29.04	(1.7±0.2)×10^{-1}	310	(1.4±0.2)×10^{-1}
Yb	28.31	(1.3±0.1)×10^{-1}	330	(1.2±0.1)×10^{-1}
Tm	28.18	(7.5±0.8)×10^{-2}	335	(6.8±0.8)×10^{-2}
Ho	27.21	(3.6±0.4)×10^{-2}	355	(3.5±0.4)×10^{-2}
Dy	26.80	(2.6±0.3)×10^{-2}	360	(2.5±0.3)×10^{-2}
Tb	26.58	(2.5±0.3)×10^{-2}	370	(2.5±0.3)×10^{-2}
Gd	26.04	(1.6±0.2)×10^{-2}	380	(1.7±0.2)×10^{-2}
Sm	25.56	(1.3±0.2)×10^{-2}	390	(1.4±0.2)×10^{-2}
Nd	24.96	(9.2±0.9)×10^{-3}	405	(1 ±0.1)×10^{-2}
Ce	24.00	(8 ±0.9)×10^{-3}	420	(9 ±1)×10^{-3}
La	23.39	(8.4±0.9)×10^{-3}	430	(1 ±0.1)×10^{-3}
Sb	21.36	(1.2±0.2)×10^{-2}	460	(1.5±0.3)×10^{-2}
Te	21.19	(8.8±1)×10^{-3}	465	(1.2±0.2)×10^{-2}
Sn	21.06	(1.3±0.2)×10^{-2}	465	(1.7±0.3)×10^{-2}
Cd	20.49	(1.7±0.3)×10^{-2}	470	(2.2±0.4)×10^{-2}
Ag	20.47	(2 ±0.3)×10^{-2}	470	(2.6±0.4)×10^{-2}
Zn	13.76	(2 ±0.4)×10^{-1}	515	(3 ±0.6)×10^{-1}
Cu	13.44	(2.4±0.5)×10^{-1}	515	(3.6±0.8)×10^{-1}
Ni	13.35	(2.4±0.5)×10^{-1}	510	(3.6±0.8)×10^{-1}
Fe	12.10	(3 ±0.6)×10^{-1}	510	(4.4±0.9)×10^{-1}

4 A.V. Mitrofanova et al. Sov. J. Nucl. Phys. 6, 512 (1968).

7 T. Methasiri et al., Nucl. Phys. A167, 97 (1971).

12 J.R. Nix et al., Nucl. Phys. 81, 61 (1966).

20 N.A. Perifilov et al., JETP (Sov. Phys.) 14, 623 (1962); Proc. Symp. on the physics & chemistry of fission, Salzburg 1965, vol. 2 (IAEA) Vienna, 1965, p.283.

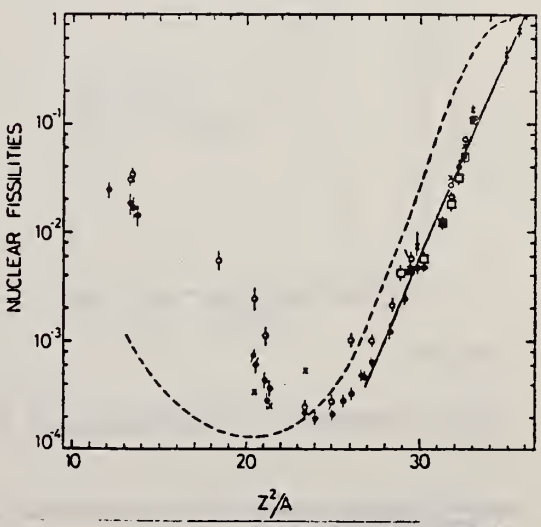

Fig. 2. Nuclear fissilities as a function of Z^2/A. Experimental points: solid circles represent our data; squares, the data from ref. [4]; open circles, the data from ref. [7]; and crosses, the data from (p,f) experiments[20]. The straight line is the best fit calculated from our data for $Z^2/A > 26$. The dashed curve is the curve VI calculated by Nix and Sassi[12].

REF. V. Bellini, V. Emma, A.S. Figuera, S. Lo Nigro, C. Milone, G.S. Pappalardo, G. Bologna
Il Nuovo Cimento 47A, 529 (1978)

ELEM. SYM.	A	Z
Re		75

METHOD

REF. NO. 78 Be 10

REACTION	RESULT	EXCITATION ENERGY	SOURCE		DETECTOR		ANGLE
			TYPE	RANGE	TYPE	RANGE	
G,F	RLX	180-999	C	220-999	IRK-D		4PI

Zero cross section assumed below 180 MeV.

COHERENT BREM.

Summary. — The photofission yields of Re, W and Ta induced by a coherent bremsstrahlung beam from 1000 MeV electrons striking a diamond single crystal have been measured. The experiment has been performed at eighteen different energies of the main peak of the photon spectrum, in the energy range between 220 MeV and 550 MeV, by detecting the fission fragments with glass sandwiches. The behaviour of the photofission cross-section has been deduced from the experimental yields by using an appropriate unfolding method. The obtained curves clearly show a first resonance centred at a photon energy $k \simeq 350$ MeV with a FWHM $\simeq 145$ MeV, while there is a hint of a second resonance at $k \simeq 750$ MeV. Information on the energy dependence of the nuclear fissility from 100 MeV to 1000 MeV has been deduced from the comparison of the estimated photofission cross-section with the total photon interaction cross-section. It has been found that the photomesonic model of the fission process permits to explain the energy dependence of our photofission cross-sections if a nuclear fissility increasing with photon energy is assumed.

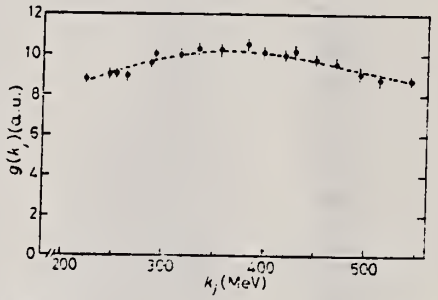

Fig. 3.

Fig. 3. – Photofission yields per equivalent quantum as a function of the first-peak energy k_i of photons. The dots are the experimental data; the dashed curve represents the yield function recalculated from the $f(k)$ data. Results for Re.

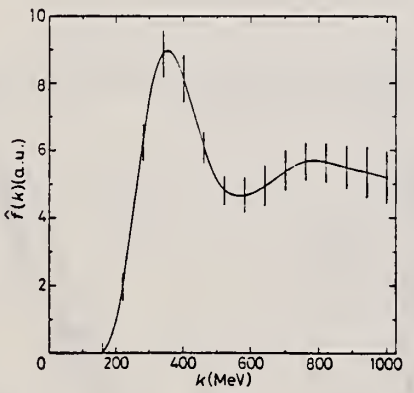

Fig. 6.

Fig. 6. – Photofission cross-section estimated by our unfolding method. Results for Re (γ, f).

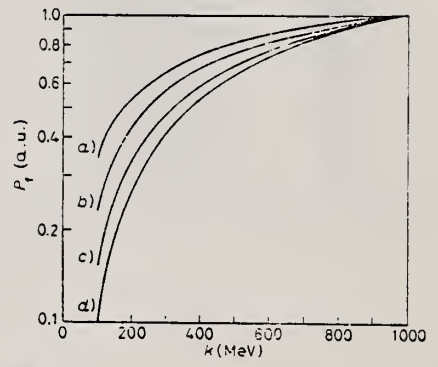

Fig. 11.

Fig. 11. – Nuclear fissility P_f as a function of the photon energy k. The curves are normalized at $k = 1000$ MeV. *a*) Bi, *b*) Pb, *c*) Au, *d*) Ta.

(over)

TABLE II. – *Estimated $\hat{f}_i$ values and corresponding errors.* All the data are given in arbitrary units.

k	$\hat{f}(k)$ (arbitrary units)		
(MeV)	Re	W	Ta
100	-0.31 ± 0.85	-0.14 ± 0.85	-0.49 ± 0.87
160	0.03 ± 0.31	0.24 ± 0.31	0.26 ± 0.33
220	1.95 ± 0.41	2.50 ± 0.41	2.51 ± 0.41
280	6.26 ± 0.53	6.51 ± 0.53	6.63 ± 0.55
340	8.90 ± 0.69	8.75 ± 0.69	8.56 ± 0.68
400	8.16 ± 0.72	8.38 ± 0.72	7.15 ± 0.70
460	6.10 ± 0.51	6.34 ± 0.51	5.43 ± 0.49
520	4.83 ± 0.47	5.04 ± 0.47	4.70 ± 0.48
580	4.70 ± 0.57	4.95 ± 0.57	4.72 ± 0.58
640	4.96 ± 0.59	5.20 ± 0.59	4.98 ± 0.60
700	5.41 ± 0.58	5.57 ± 0.58	5.29 ± 0.58
760	5.68 ± 0.57	5.78 ± 0.57	5.41 ± 0.57
820	5.65 ± 0.61	5.71 ± 0.61	5.32 ± 0.61
880	5.51 ± 0.67	5.53 ± 0.67	5.18 ± 0.67
940	5.38 ± 0.74	5.36 ± 0.74	4.98 ± 0.73
1000	5.23 ± 0.80	5.18 ± 0.80	4.70 ± 0.77

RE
A=185

RE
A=185

RE
A=185

REF.
F. R. Metzger
Phys. Rev. 157, 1060 (1967)

ELEM. SYM.	A	Z
Re	185	75

METHOD

REF. NO. 67 Me 1 HMG

REACTION	RESULT	EXCITATION ENERGY	SOURCE		DETECTOR		ANGLE
			TYPE	RANGE	TYPE	RANGE	
G,G	LFT	0-1	D	0-1	SCD-D	0-1	DST

J-PI

TABLE II. Summary of the results of the resonance-scattering experiments. The factor g in columns 2 and 4 is the ratio of the statistical weights of the excited state and the ground state, i.e., $g=(2I_{ex}+1)/(2I_{gs}+1)$. For the 646- and 874-keV transitions, the internal conversion is responsible for the small difference between Γ_0 and Γ.

Level energy (keV)	$g\Gamma_0^2/\Gamma$ (10^{-6} eV)	Γ_0/Γ	$g\Gamma_0$ (10^{-6} eV)
646	2.37±0.15	0.99	2.39±0.15
718	4.8 ±1.0	0.70[a]	6.9 ±1.4
874	27 ±3	0.99	27.3 ±3

[a] The 72-keV transition from the 718-keV level was assumed to account for 0.4% of the Os^{188} disintegrations (Ref. 1).

[1] M. W. Johns, S. V. Nablo, and W. J. King, Can. J. Phys. 35, 1159 (1957).

TABLE III. Transition probabilities for the γ transitions in Re^{188} studied in this paper and listed in column 1. The spin assignments and branching ratios used to arrive at these transition probabilities are listed in columns 2 and 3. The information available on the reduced $E2$ transition probabilities is listed in the last column.

Transition energy (keV)	Spins $I_i \rightarrow I_f$	Γ_i/Γ_0	Transition probability (sec^{-1})	$B(E2)$ (10^{-50} e^2 cm^4)
592	$\frac{4}{3}$-$\frac{7}{3}$	0.32	5.0 ×10^{10}	5.6±1.3
646	$\frac{1}{3}$-$\frac{4}{3}$	1	10.9 ×10^{10}	7.9±0.6
718	$\frac{3}{3}$-$\frac{6}{3}$	1	15.6 ×10^{10}	≤6.6±2.3
749	$\frac{4}{3}$-$\frac{7}{3}$	<0.002	<0.13×10^{10}	<0.02
874	$\frac{3}{3}$-$\frac{6}{3}$	1	62.3 ×10^{10}	<1.0[a]

[a] According to Ref. 4.

[4] K. Maack Bisgård (private communication).

A.M. Goryachev, G.N. Zalesnyi, S.F. Semenko, and B.A. Tulupov

REF. Yad. Fiz. 17, 463 (1973)
Sov. J. Nucl. Phys. 17, 236 (1973)

ELEM. SYM.	A	Z
Re	185	75

METHOD

REF. NO.	
73 Go 6	hmg

REACTION	RESULT	EXCITATION ENERGY	SOURCE		DETECTOR		ANGLE
			TYPE	RANGE	TYPE	RANGE	
G,XN	ABX	8- 20	C	8- 20	BF3-I		4PI

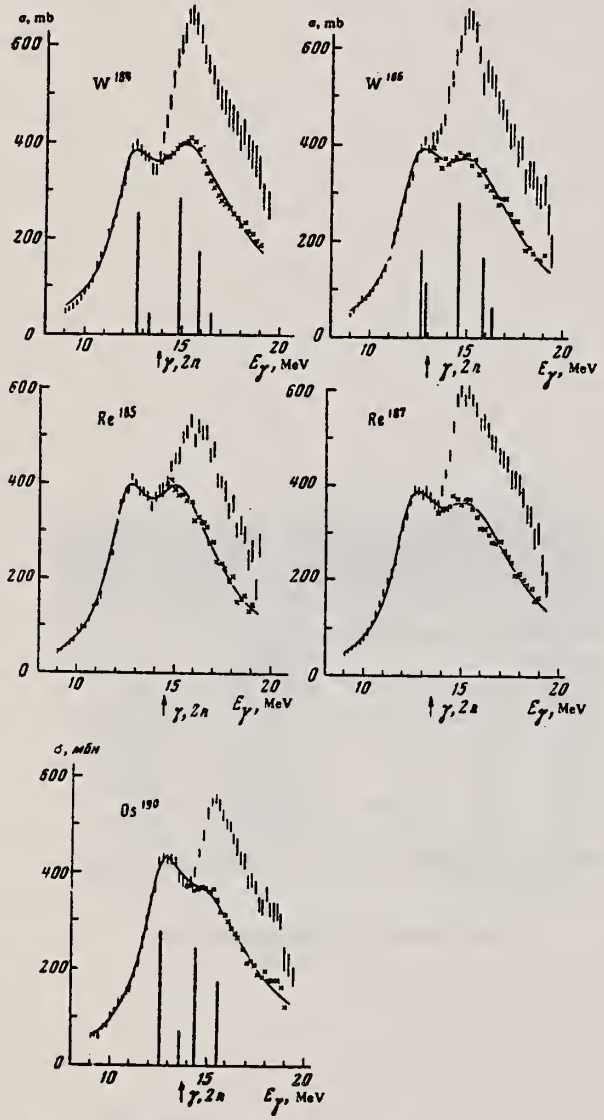

FIG. 2. Cross sections for $W^{184,186}$, Os^{190}, and $Re^{185,187}$. The cross section $\sigma_{\gamma,n} + 2\sigma_{\gamma,2n}$ is denoted by vertical lines whose lengths are twice the rms errors. The crosses represent the cross sections, corrected for multiplicity, above the threshold of the $(\gamma, 2n)$ reaction. The solid curves are Lorentz curve approximations. For $W^{184,186}$ and Os^{190} the calculated dipole transition strengths are shown.

TABLE III

	W^{184}	W^{186}	Os^{190}	Re^{185}	Re^{187}	W^{184} [7]
Γ_1, MeV	2.33	2.55	2.13	2.51	2.83	2.20
E_1, MeV	12.5	12.5	12.6	12.7	12.6	12.59
σ_1, mb	241	225	223	262	250	211
Γ_2, MeV	5.1	5.4	5.7	6.2	5.3	5.18
E_2, MeV	15.6	15.2	14.8	15.4	15.6	14.88
σ_2, mb	338	317	318	315	296	334
0.06 NZ/A, MeV·mb	2.65	2.67	2.74	2.68	2.69	2.67
$S_1 + S_2$, MeV − mb	4.0	3.9	3.9	3.6	3.8	3.47
S_2 / S_1	2.8	3.0	3.8	2.5	2.2	3.6

Note. $S_i = (\pi/2)\sigma_i\Gamma_i$ is the Lorentz area.

RE
A=187

RE
A=187

RE
A=187

K. N. Geller, J. Halpern, and E. G. Muirhead
Phys. Rev. 118, 1302-12 (1960)

ELEM. SYM.	A	Z
Re	187	75

METHOD

Betatron; neutron threshold; ion chamber

REF. NO.

60 Ge 3 NVB

REACTION	RESULT	EXCITATION ENERGY	SOURCE		DETECTOR		ANGLE
			TYPE	RANGE	TYPE	RANGE	
G,N	NØX	THR	C THR		BF3-I		4 PI

THRESHØLD

TABLE I. Summary and comparison of neutron separation energies inferred from present threshold measurements with values predicted from mass data and reaction energies. All energies are expressed in the center-of-mass system in Mev.

Reaction	No. runs	Present results	Other results	Method	Reference
$Re^{187}(\gamma,n)Re^{186}$	1	7.18 ±0.08			

REF.

H. Langhoff
Phys. Rev. 135, B1-8 (1964)

ELEM. SYM.	A	Z
Re	187	75

METHOD

Radioactive source: $W^{187} \rightarrow Re^{187*} + e'$; centrifuge technique

REF. NO.: 64 La 3 | NVB

REACTION	RESULT	EXCITATION ENERGY	SOURCE TYPE	SOURCE RANGE	DETECTOR TYPE	DETECTOR RANGE	ANGLE
G,G	LFT	0-1	D	0-1	NAI-D		DST

MIXING AMPLITUDES

TABLE I. Summary of the experimental results. From the results of the resonance fluorescence experiments listed in columns 2 and 3, the data in columns 6 and 8 have been calculated using spins, multipole orders, and branching ratios given by Gallagher *et al.* (Ref. 4) and reproduced in columns 4, 5, and 7.

E_γ (keV)	Angular distribution $A2$	$g_2\Gamma_0^2/g_1\Gamma$ (eV)	Assumed spins	Multipole order	Mixing amplitude δ	Γ_0/Γ	τ_{level} (sec)
864.5	...	$<1.3\times10^{-4}$	$\frac{5}{2}^+,\frac{3}{2}^+ \rightarrow \frac{5}{2}^+$	$M1$		0.54	$>1.0\times10^{-12}$
773	$+(0.03\pm0.05)$	$(1.75\pm0.22)\times10^{-3}$	$\frac{3}{2}^+ \rightarrow \frac{5}{2}^+$	$>85\%\ M1$, $<15\%\ E2$	$-0.40<\delta<0.15$	1	$(2.5\pm0.3)\times10^{-13}$
686.1	$+(0.21\pm0.10)$	$(1.82\pm0.16)\times10^{-5}$	$\frac{5}{2}^- \rightarrow \frac{5}{2}^+$	$E1$	$-0.10<\delta<0.15$	0.49	$(8.5\pm0.7)\times10^{-13}$
551.7	<0	...	$\frac{5}{2}^- \rightarrow \frac{3}{2}^+$	$E1$, $<1\%\ M2$			
479.4	$-(0.10\pm0.24)$	...	$\frac{5}{2}^- \rightarrow \frac{9}{2}^-$	$E2$			
625.3	$-(0.17\pm0.25)$	$(2.5\pm0.3)\times10^{-5}$	$\frac{5}{2}^+ \rightarrow \frac{5}{2}^+$	$E2$		0.82	
618.2	$-(0.17\pm0.25)$	$(2.5\pm0.3)\times10^{-5}$	$\frac{3}{2}^+ \rightarrow \frac{5}{2}^+$	$>85\%\ M1$	$-0.40<\delta<0.15$	0.96	$(1.6\pm0.2)\times10^{-11}$
511.3	...	$<4\times10^{-5}$	$\frac{3}{2}^+ \rightarrow \frac{5}{2}^+$	$>99\%\ E2$		1	$>6\times10^{-12}$

TABLE II. Summary of the known transition probabilities in Re^{187}. The experimental results T_{exp} are compared with theoretical predictions: $T_{Weisskopf}$ calculated with the Weisskopf formula omitting spin factors and $T_{Nilsson}$ calculated using Nilsson wave functions.

E_γ (keV)	Assumed Spins	Assumed Multipole order	T_{exp} (sec^{-1}) This experiment	T_{exp} (sec^{-1}) Others	$\frac{T_{exp}}{T_{Weisskopf}}$	Nilsson Model Assumed states	Nilsson Model $T_{Nilsson}$	Nilsson Model $\frac{T_{exp}}{T_{Nilsson}}$
134.3	$\frac{7}{2}^+ \rightarrow \frac{5}{2}^+$	$M1$	...	2.4×10^{10}[a]	1/2	31 rot → 31	2.8×10^{10}	1
		$E2$	...	7.1×10^{8}[a]	200	31 rot → 31	7.0×10^{8}	1
206.3	$\frac{9}{2}^- \rightarrow \frac{5}{2}^+$	$M2$	...	6.0×10^{3}[b]	1/88	32 → 31	1.2×10^{4}	1/2
72.0	$\frac{9}{2}^- \rightarrow \frac{7}{2}^+$	$E1$	...	6.1×10^{5}[b]	$1/2\times10^{-6}$	K forbidden	0	f
618.2	$\frac{3}{2}^+ \rightarrow \frac{5}{2}^-$	$M1$	5.9×10^{10}		1/80	K forbidden	0	f
106.6	$\frac{3}{2}^+ \rightarrow \frac{5}{2}^+$	$M1+(E2)$	3.9×10^{8}		1/70	43 → γ vibr.	0	f
625.3	$\frac{1}{2}^+ \rightarrow \frac{5}{2}^+$	$E2$	...		...	43 → 31	4.3×10^{7}	...
113.7	$\frac{7}{2}^+ \rightarrow \frac{9}{2}^-$	$M1+(E2)$	...		...	43 → γ vibr.	0	...
773	$\frac{1}{2}^+ \rightarrow \frac{5}{2}^+$	$M1$	4.0×10^{12}		1/2	42 → 31	2.0×10^{13}	1/5
		$E2$	$<8\times10^{11}$			42 → 31	5.2×10^{7}	...
864.5	$\frac{3}{2}^+ \rightarrow \frac{5}{2}^+$	$M1+(E2)$	$<5.5\times10^{11}$		<1/23	33 → 31	8.1×10^{12}	<1/15
	$\frac{5}{2}^+ \rightarrow \frac{5}{2}^+$	$M1+(E2)$	$<2.5\times10^{11}$[c]		<1/50	27 → 31	1.4×10^{12}	<1/5
246.3	$\frac{3}{2}^+ \rightarrow \frac{3}{2}^+$	$M1+(E2)$	$<1.9\times10^{11}$			33 → 43 rot	2.0×10^{11}	...
239.3	$\frac{3}{2}^+ \rightarrow \frac{3}{2}^+$	$M1+(E2)$	$<1.2\times10^{11}$			33 → 43	2.2×10^{11}	...
880	→ $\frac{5}{2}^+$	$E2$		3×10^{11}[d]		...	...	...
686.1	$\frac{5}{2}^- \rightarrow \frac{5}{2}^+$	$E1$	5.7×10^{10}[e]		$1/2\times10^{-4}$	36 → 31	1.8×10^{10}	(3)
551.7	$\frac{5}{2}^- \rightarrow \frac{3}{2}^+$	$E1$	1.0×10^{10}[e]		$1/6\times10^{-4}$	36 → 31 rot	3.6×10^{9}	(3)
479.4	$\frac{5}{2}^- \rightarrow \frac{9}{2}^-$	$E2$	4.9×10^{10}[e]		24	...	...	...
511.3	$\frac{1}{2}^+ \rightarrow \frac{5}{2}^+$	$E2$		5.1×10^{10}	18	...	...	...

[a] Refs. 10, 13, and 17.
[b] Refs. 14 and 15.
[c] Computed with branching ratios of Ref. 6.
[d] Calculated from the result given in Ref. 11, assuming $g_1\Gamma_0/g_2\Gamma = 1$.
[e] The result of Vartapetyan is about 1/30 of this value (see discussion).
[f] Comparison with column 6 shows that the experimental transition probabilities are small.

REF.

Yu. K. Shubnyĭ, D. K. Kaipov, and R.B. Begzhanov
J. Exptl. Theoret. Phys. (USSR) 47, 16 (1964)
Soviet Phys. JETP 20, 11 (1965)

ELEM. SYM.	A	Z
Re	187	75

METHOD

Resonance scattering; high temperature source

REF. NO.	
64 Sh 5	JOC

REACTION	RESULT	EXCITATION ENERGY	SOURCE		DETECTOR		ANGLE
			TYPE	RANGE	TYPE	RANGE	
G,G	LFT	1	D	1	NAI-D		122

$\tau_\gamma(E1) = (4.1 \pm 2.0) \times 10^{-10}$ sec for .686 MeV level.

REF. H. Langhoff
Phys. Rev. 159, 1033 (1967)

ELEM. SYM.	A	Z
Re	187	75

METHOD

REF. NO. 67 La 2 HMG

REACTION	RESULT	EXCITATION ENERGY	SOURCE		DETECTOR		ANGLE
			TYPE	RANGE	TYPE	RANGE	
G,G	LFT	0 - 1	D	0 - 1	SCD-D		

TABLE I. Results of the resonance-fluorescence experiment. The results of the present experiment, $(g_2\Gamma_0\Gamma_i/g_1\Gamma)_{Ge}$, are compared with the results of the previous study $(g_2\Gamma_0\Gamma_i/g_1\Gamma)_{NaI}$. Using spins and branching ratios, Γ_i/Γ, from Ref. 2, the mean lifetimes τ_{level}, in column 7 have been obtained.

E_{level} (keV)	E_γ (keV)	$(g_2\Gamma_0\Gamma_i/g_1\Gamma)_{Ge}$ (10^{-3} eV)	$(g_2\Gamma_0\Gamma_i/g_1\Gamma)_{NaI}$ (10^{-3} eV)	Assumed spins	Γ_i/Γ	τ_{level} (psec)
512	512	0.9 ± 0.3	<4	$\frac{1}{2}^+ \rightarrow \frac{1}{2}^+$	0.98	23 ±8
589	589	<8	···	$\frac{3}{2}^+ \rightarrow \frac{1}{2}^+$	0.99	>5
618	618	2.5 ± 0.2	2.5 ± 0.3	$\frac{3}{2}^+ \rightarrow \frac{1}{2}^+$	0.95	15.7 ±1.3
625	625	<1	···	$\frac{1}{2}^+ \rightarrow \frac{1}{2}^+$	~0.76	>12
686	686	1.84± 0.10	1.82± 0.16	$\frac{5}{2}^- \rightarrow \frac{1}{2}^+$	0.49	8.6 ±0.5
	552	0.35± 0.05	···	$\rightarrow \frac{7}{2}^+$	0.10	9.2 ±1.3
	480	1.52± 0.20	···	$\rightarrow \frac{3}{2}^-$	0.40	8.5 ±1.1
773	773	170 ±12	175 ±22.	$\frac{3}{2}^+ \rightarrow \frac{1}{2}^+$	0.99	0.25±0.02
865	865	6 ±2	<13	$\frac{3}{2}^+ \rightarrow \frac{1}{2}^+$	0.61	2.7 ±0.9
880	880	24 ±8	···	$\frac{5}{2}^+ \rightarrow \frac{1}{2}^+$	0.40	0.44±0.13

REF. A.M. Goryachev, G.N. Zalesnyi, S.F. Semenko, and B.A. Tulupov
Yad. Fiz. 17, 463 (1973)
Sov. J. Nucl. Phys. 17, 236 (1973)

ELEM. SYM.	A	Z
Re	187	75

METHOD

REF. NO. 73 Go 6 hmg

REACTION	RESULT	EXCITATION ENERGY	SOURCE TYPE	SOURCE RANGE	DETECTOR TYPE	DETECTOR RANGE	ANGLE
G,XN	ABX	8- 20	C	8- 20	BF3-I		4PI

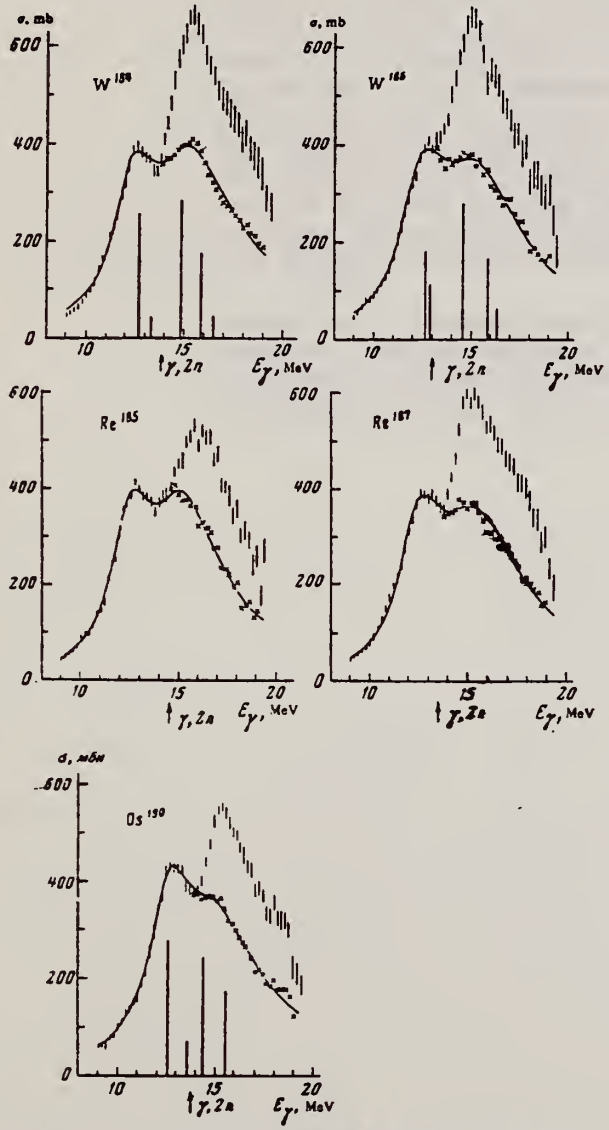

FIG. 2. Cross sections for $W^{184,186}$, Os^{190}, and $Re^{185,187}$. The cross section $\sigma_{\gamma,n} + 2\sigma_{\gamma,2n}$ is denoted by vertical lines whose lengths are twice the rms errors. The crosses represent the cross sections, corrected for multiplicity, above the threshold of the (γ, 2n) reaction. The solid curves are Lorentz curve approximations. For $W^{184,186}$ and Os^{190} the calculated dipole transition strengths are shown.

TABLE III

	W^{184}	W^{186}	Os^{190}	Re^{185}	Re^{187}	W^{nat} [7]
Γ_1, MeV	2.33	2.55	2.13	2.51	2.83	2.29
E_1, MeV	12.5	12.5	12.6	12.7	12.6	12.59
σ_1, mb	241	225	223	262	250	211
Γ_2, MeV	5.1	5.4	5.7	5.2	5.3	5.18
E_2, MeV	15.6	15.2	14.8	15.4	15.6	14.88
σ_2, mb	338	317	318	315	296	334
0.06 NZ/A, MeV-mb	2.65	2.67	2.74	2.68	2.69	2.67
$S_1 + S_2$, MeV − mb	4.0	3.9	3.9	3.6	3.8	3.47
S_2 / S_1	2.8	3.0	3.8	2.5	2.2	3.6

Note. $S_i = (\pi/2)\sigma_i\Gamma_i$ is the Lorentz area.

OSMIUM
Z=76

Osmium is noted for its great density, considerable hardness (it will scratch glass), high melting point, and low ductility. It was the first commercially successful metal to be used in an incandescent electric bulb. The alloys of osmium are used as bearings in fine instruments as well as for fountain pens because of the alloy's resistance to wear and corrosion. It is used as a catalyst and the metal, when used in a finely divided form, will cause the union of hydrogen and oxygen to become explosive at temperatures as low as 40 or 50 degrees Celsius.

Osmium was discovered and first described by the English amateur scientist Smithson Tennant. He noted the oxide possessed a pungent and peculiar smell and thus called the new element osmium, from the Greek *osmé*, a smell.

Os

Os

REF. A. V. Mitrofanova, Yu. N. Ranyuk, and P. V. Sorokin
J. Nucl. Phys. (USSR) 6, 703 (1967)
Sov. J. Nucl. Phys. 6, 512 (1968)

ELEM. SYM.	A	Z
Os		76

METHOD

REF. NO.	
67 Mi 1	HMG

REACTION	RESULT	EXCITATION ENERGY	SOURCE		DETECTOR		ANGLE
			TYPE	RANGE	TYPE	RANGE	
G,F	ABX	300-999		300-999	TRK-I		

Detector: Fission fragment tracks in glass.

999 = 1600 MEV

Angular distribution measured for Pb was found isotropic; for other elements it was assumed isotropic.

Nucleus	Fissionability D	Cross section σ_K, $\mu\beta$	Nucleus	Fissionability D	Cross section σ_K, $\mu\beta$
Bi	0.11±0.01	7.8±0.6	Os	0.0058±0.0005	0.37±0.04
Pb	0.050±0.004	3.4±0.3	Re	0.0056±0.0006	0.35±0.04
Tl	0.031±0.003	2.1±0.2	Ta	0.0045±0.0005	0.27±0.03
Au	0.019±0.002	1.25±0.10	Hf	0.0042±0.0004	0.25±0.03
Pt	0.012±0.002	0.80±0.08			

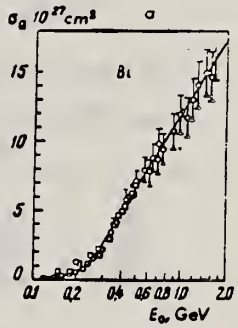

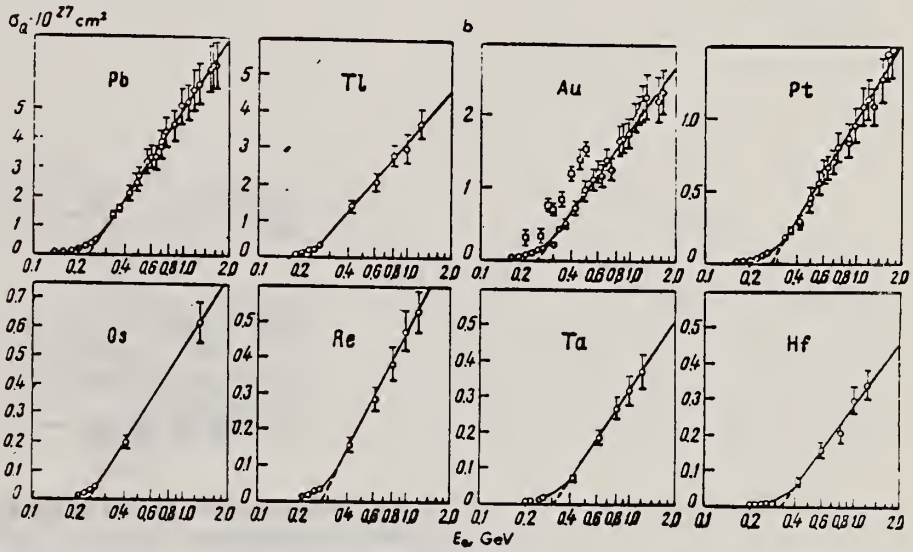

Fig. 1. Photofission fragment yields. ○-present work; □-Jungerman and Steiner.[11] The curves were plotted through the experimental points.

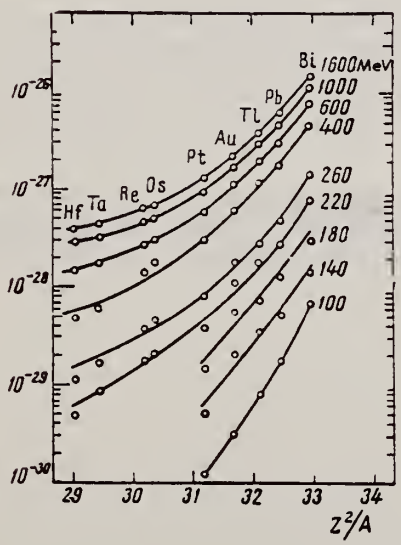

Fig. 2. Photofission fragment yields as a function of Z^2/A. The ordinates are values of σ_a in units of cm².

REF. Yu. N. Ranyuk and P. V. Sorokin
J. Nucl. Phys. (USSR) 5, 37 (1967)
Sov. J. Nucl. Phys. 5, 26 (1967)

ELEM. SYM.	A	Z
Os		76

METHOD

REF. NO. 67 Ra 2 HMG

REACTION	RESULT	EXCITATION ENERGY	SOURCE		DETECTOR		ANGLE
			TYPE	RANGE	TYPE	RANGE	
G,F	ABX	THR-260	C	200-260	EMU-I		4PI

TABLE III

$E_{\gamma\ max}$, MeV	Cross section per equivalent γ quantum, 10^{-30} cm²			
	Os	Re	Ta	Hf
200	17±2	11.8±0.8	5.2±0.3	3.2±0.7
220	22±2	17±1	8.6±0.5	4.8±0.3
240	33±3	29±1	13.0±0.6	8.2±0.4
260	45±4	36±2	17.2±0.7	11.2±0.5

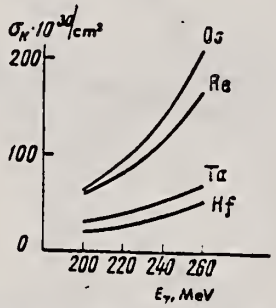

Fig. 4. Photofission cross sections of Os, Re, Ta, and Hf as functions of photon energy.

REF. Su Su, R.H. Sambell, E.G. Muirhead, B.M. Spicer
Aust. J. Phys. 30, 677 (1977)

ELEM. SYM.	A	Z
Os		76

METHOD

REF. NO.	
77 Su 10	hg

REACTION	RESULT	EXCITATION ENERGY	SOURCE		DETECTOR		ANGLE
			TYPE	RANGE	TYPE	RANGE	
G, SN	ABX	6-27	C	7-27	BF3-I		4PI

The absolute (γ,xn) cross section of natural osmium is extracted from bremsstrahlung yield curves measured from the lowest (γ,n) threshold of osmium isotopes up to 28 MeV in energy steps of 0·2 MeV. The VBPL method of Brannanis *et al.* (1972) has been used to unfold the cross section from bremsstrahlung yield data. The results do not show evidence of significant amounts of splitting of the giant dipole resonance, as might be expected from the theoretical predictions of Sedlmayr *et al.* (1974), but at the same time are not inconsistent with their general features.

STAT MODEL XN TO SN

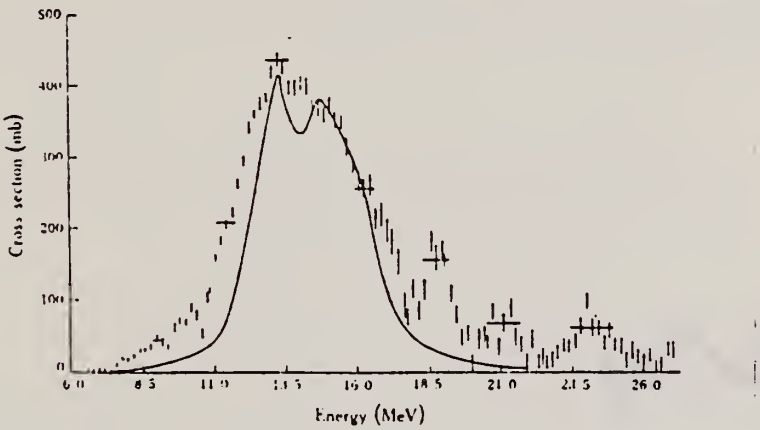

Fig. 1. Comparison of the absolute (γ,xn) cross section of natural osmium from the present measurements with the curve resulting from the theoretical predictions of Sedlmayr *et al.* (1974), after suitable weighting for isotopic abundances. The vertical bars representing the experimental results are each equal in length to two standard deviations obtained from the statistical errors on the yield points; the occasional horizontal bars give the energy resolution of neighbouring cross section points emerging from the VBPL analysis.

Correction for the neutron multiplicity effect was made using the usual statistical model approach. Cross section shown is probably the (γ,sn).

REF. Su Su, R.H. Sambell, E.G. Muirhead, B.M. Spicer
Aust. J. Phys. 30, 677 (1977)

ELEM. SYM.	A	Z
Os		76

METHOD

REF. NO. 77 Su 10 hg

REACTION	RESULT	EXCITATION ENERGY	SOURCE		DETECTOR		ANGLE
			TYPE	RANGE	TYPE	RANGE	
G,XN	ABX	6-27	C	6-28	BF3-I		4PI

The absolute (γ,xn) cross section of natural osmium is extracted from bremsstrahlung yield curves measured from the lowest (γ,n) threshold of osmium isotopes up to 28 MeV in energy steps of 0·2 MeV. The VBPL method of Bramanis *et al.* (1972) has been used to unfold the cross section from bremsstrahlung yield data. The results do not show evidence of significant amounts of splitting of the giant dipole resonance, as might be expected from the theoretical predictions of Sedlmayr *et al.* (1974), but at the same time are not inconsistent with their general features.

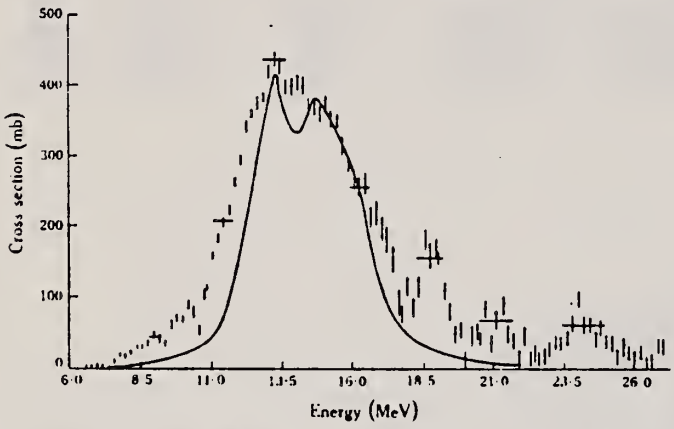

Fig. 1. Comparison of the absolute (γ,xn) cross section of natural osmium from the present measurements with the curve resulting from the theoretical predictions of Sedlmayr *et al.* (1974), after suitable weighting for isotopic abundances. The vertical bars representing the experimental results are each equal in length to two standard deviations obtained from the statistical errors on the yield points; the occasional horizontal bars give the energy resolution of neighbouring cross section points emerging from the VBPL analysis.

Correction for the neutron multiplicity effect was made using the usual statistical model approach. Cross section shown is probably the (γ,sn).

Os
A=186

Os
A=186

Os
A=186

REF. B.L. Berman, D.D. Faul, R.A. Alvarez, P. Meyer, D.L. Olson
Phys. Rev. C19, 1205 (1979)

ELEM. SYM.	A	Z
Os	186	76

METHOD

REF. NO. 79 Be 4 hg

REACTION	RESULT	EXCITATION ENERGY	SOURCE		DETECTOR		ANGLE
			TYPE	RANGE	TYPE	RANGE	
G,1N	ABX	11-20	D	11-20	BF3-I		4PI
G,2N	ABX	14-20	D	14-20	BF3-I		4PI

Photoneutron cross sections, including $\sigma[(\gamma,n) + (\gamma,pn)]$, $\sigma[(\gamma,2n) + (\gamma,p2n)]$, and $\sigma(\gamma,3n)$, were measured for ^{188}Os, ^{189}Os, ^{190}Os, and ^{192}Os from 7 to 30 MeV and for ^{186}Os from 11 to 20 MeV, with a photon energy resolution of about 300 keV. The source of radiation was the monoenergetic photon beam obtained from the annihilation in flight of fast positrons. The partial photoneutron cross sections were determined by neutron multiplicity counting, and the average neutron energies for each multiplicity were determined simultaneously with the cross-section data by the ring-ratio technique. Nuclear information extracted from the data includes parameters of the giant dipole and giant quadrupole resonances, integrated cross sections and their moments, nuclear symmetry energies, and nuclear deformation parameters and intrinsic quadrupole moments. No fewer than eight kinds of evidence point to a sudden change of behavior between ^{189}Os and ^{190}Os, which could be interpreted as a phase transition from a statically deformed prolate nucleus to a γ-unstable one, in general (but not detailed) agreement with the prediction of a dynamic-collective-model calculation.

[NUCLEAR REACTIONS ^{186,188,189,190,192}Os$(\gamma,n,2n,3n)$, E_γ=7–30 MeV; measured 4π neutron yield, multiplicities, average energies for monenergetic photons; $\sigma(E_\gamma,1n)$, $\sigma(E_\gamma,2n)$, $\sigma(E_\gamma,3n)$, GDR parameters, nuclear shape parameters, integrated cross sections and moments, GQR parameters, nuclear phase transition.]

TABLE IV. Parameters for classical theories (given in MeV).

Nucleus	E_m [a]	α [b]	β [c]	K [d]
^{186}Os	14.21 ± 0.06	81.1 ± 0.3	34.0 ± 0.1	28.9 ± 0.9
^{188}Os	14.19 ± 0.05	81.3 ± 0.3	34.0 ± 0.1	27.8 ± 0.5
^{189}Os	14.01 ± 0.04	80.4 ± 0.2	33.6 ± 0.1	27.3 ± 0.4
^{190}Os	13.83 ± 0.06	79.5 ± 0.3	33.1 ± 0.1	26.6 ± 0.7
^{192}Os	13.79 ± 0.04	79.6 ± 0.2	33.1 ± 0.1	26.8 ± 0.7

[a] Mean energy of the giant resonance, defined as $E_m = [E_m(1) + 2E_m(2)]/3$, except for ^{186}Os, for which $E_m = [E_m(1) + E_m(2)]/2$.
[b] Hydrodynamic parameter, defined by $E_m = \alpha A^{-1/3}$.
[c] Collective parameter, defined by $E_m = \beta A^{-1/6}$.
[d] Nuclear symmetry energy, computed from Eq. (2).

TABLE V. Nuclear shape parameters.

Nucleus	R_A [a]	η [b]	ϵ	β_2 [d]	Q_0 [e] (b)
^{186}Os	0.95 ± 0.27	1.188 ± 0.016	0.366 ± 0.031	0.194 ± 0.016	5.76 ± 0.49
^{188}Os	0.44 ± 0.08	1.177 ± 0.011	0.346 ± 0.021	0.183 ± 0.011	5.49 ± 0.33
^{189}Os	0.51 ± 0.07	1.173 ± 0.008	0.338 ± 0.015	0.179 ± 0.008	5.38 ± 0.24
^{190}Os	0.32 ± 0.10	1.149 ± 0.015	0.312 ± 0.029	0.155 ± 0.015	4.65 ± 0.46
^{192}Os	0.30 ± 0.11	1.145 ± 0.016	0.283 ± 0.031	0.150 ± 0.016	4.55 ± 0.50

[a] Area ratio, defined as $\sigma_m(1)\Gamma(1)/\sigma_m(2)\Gamma(2)$.
[b] Deformation parameter, computed from $E_m(2)/E_m(1) = 0.911\eta - 0.089$.
[c] Nuclear eccentricity, computed from $\epsilon = (\eta^2 - 1)^{1/2}/\eta$.
[d] Deformation parameter, defined as $\frac{2}{3}(\pi/5)^{1/2}\beta$.
[e] Intrinsic quadrupole moment, computed from Eq. [illegible], with R_0 taken to be 1.26 fm.

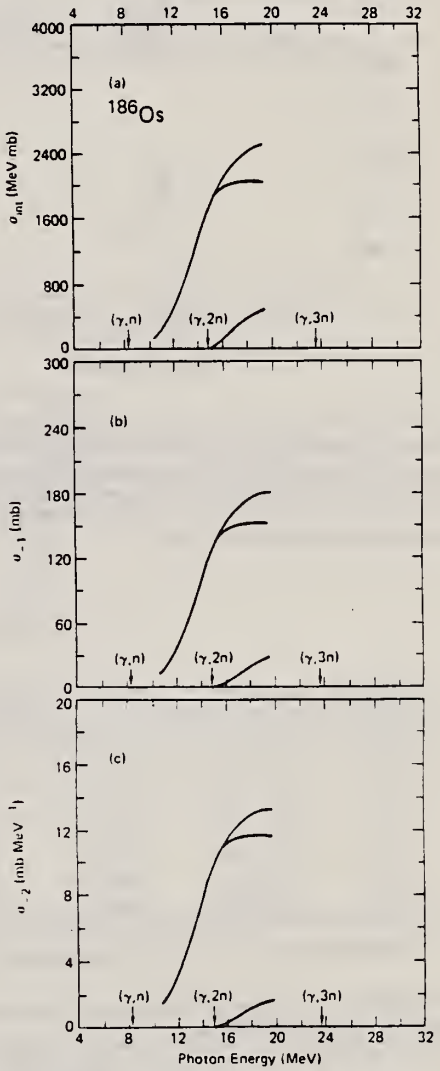

FIG. 8. Running sums of integrated photoneutron cross sections and their moments for ^{186}Os: (a) $\sigma_{int} = \int \sigma d E_\gamma$ for $\sigma(\gamma,n_1)$ (top), $\sigma(\gamma,1n)$ (middle), and $\sigma(\gamma,2n)$ (bottom); (b) $\sigma_{-1} = \int \sigma E_\gamma^{-1} dE_\gamma$; (c) $\sigma_{-2} = \int \sigma E_\gamma^{-2} dE_\gamma$.

(over)

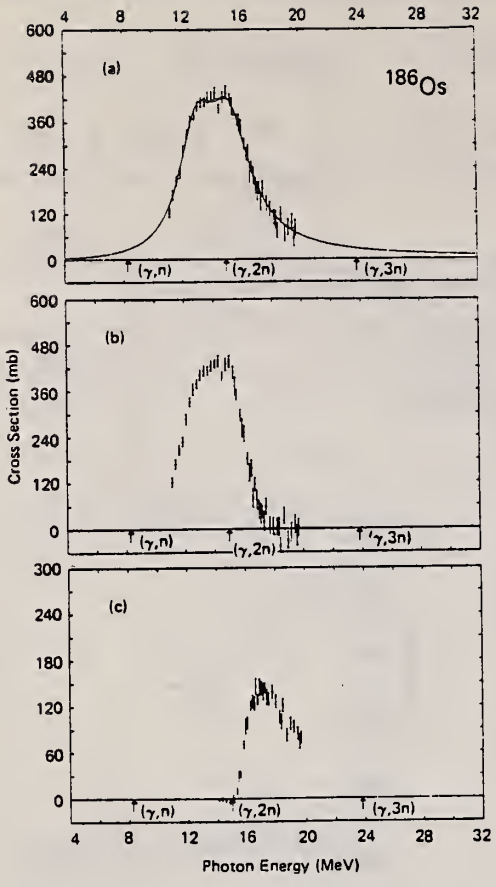

FIG. 2. Photoneutron cross sections for ^{186}Os: (a) total photoneutron cross section $\sigma(\gamma,n_t)=\sigma[(\gamma,1n)+(\gamma,2n)]$, together with a two-component Lorentz-curve fit to the data (solid line); (b) single-photoneutron cross section $\sigma(\gamma,1n)=\sigma[(\gamma,n)+(\gamma,pn)]$; (c) double-photoneutron cross section $\sigma(\gamma,2n)$.

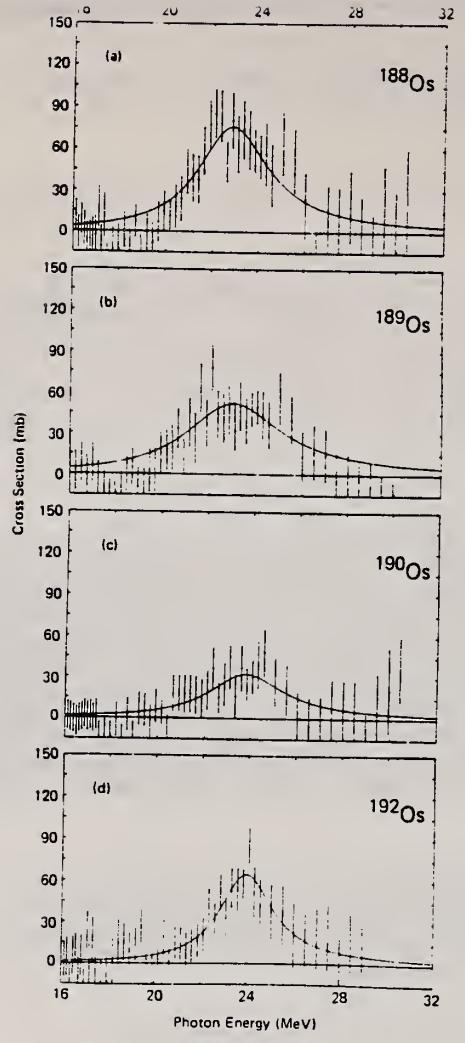

FIG. 14. Cross-section differences above the GDR; the two-component Lorentz-curve fits to $\sigma(\gamma,n_t)$ shown in part (a) of Figs. 3–6 were subtracted from the data points to give these differences, which were in turn fitted with the single-component Lorentz curves shown here as solid lines: (a) for ^{188}Os; (b) for ^{189}Os; (c) for ^{190}Os; (d) for ^{192}Os.

TABLE VI. Values for $B(E2,0^+\rightarrow 2^+)$ (in units of b^2).

Nucleus	Present experiment [a]	μ-mesic x rays [b]	Coulomb excitation [c]	Theory [d]	Theory [e]
^{186}Os	3.30 ± 0.56	3.15 ± 0.03	3.08 ± 0.21	2.96	3.05
^{188}Os	3.00 ± 0.36	2.84 ± 0.03	2.75 ± 0.12	2.72	2.75
^{190}Os	2.15 ± 0.43	2.48 ± 0.02	2.40 ± 0.11	2.59	2.54
^{192}Os	2.06 ± 0.46	2.10 ± 0.02	2.02 ± 0.09	2.56	2.34

[a] Computed from Eq. (9), using the values for Φ_0 from Table V.
[b] From Ref. 26.
[c] Weighted average from Refs. 27 and 28.
[d] From Ref. 5.
[e] From Ref. 6.

TABLE III. Parameters of Lorentz-curve fits to the giant dipole resonance. Lorentz parameters defined by Eq. (1); the fitting interval for all cases is 10.8 to 18.8 MeV.

Nucleus	$E_m(1)$ (MeV)	$\sigma_m(1)$ [a] (mb)	$\Gamma(1)$ (MeV)	$E_m(2)$ (MeV)	$\sigma_m(2)$ [a] (mb)	$\Gamma(2)$ (MeV)	χ^2
^{186}Os	13.03 ± 0.09	308 ± 21	3.13 ± 0.24	15.26 ± 0.09	302 ± 23	3.38 ± 0.21	0.88
^{188}Os	12.81 ± 0.05	260 ± 15	2.76 ± 0.13	14.88 ± 0.07	390 ± 14	4.19 ± 0.13	0.96
^{189}Os	12.68 ± 0.04	268 ± 14	2.71 ± 0.10	14.68 ± 0.05	395 ± 11	3.62 ± 0.10	0.75
^{190}Os	12.68 ± 0.07	206 ± 29	2.60 ± 0.21	14.40 ± 0.09	401 ± 24	4.16 ± 0.11	1.19
^{192}Os	12.68 ± 0.06	206 ± 34	2.49 ± 0.23	14.35 ± 0.12	389 ± 26	4.41 ± 0.13	0.95

[a] Uncertainties for σ_m given here are relative. The absolute uncertainties are 7% (10% for ^{186}Os).

TABLE IX. Integrated cross sections, $\sigma_{\rm int}(\gamma,x)=\int\sigma(\gamma,x)dE_\gamma$, integrated from threshold to $E_{\gamma\max}$. Uncertainties are discussed in Sec. II of the text.

Nucleus	$E_{\gamma\max}$ (MeV)	$\sigma_{\rm int}(\gamma,1n)$ (MeV b)	$\sigma_{\rm int}(\gamma,2n)$ (MeV b)	$\sigma_{\rm int}(\gamma,3n)$ (MeV b)	$\frac{\sigma_{\rm int}(\gamma,2n)}{\sigma_{\rm int}(\gamma,n_t)}$	$\frac{\sigma_{\rm int}(\gamma,n_t)}{0.06NZ/A}$	$\frac{\frac{1}{2}\pi[\sigma_m(1)\Gamma(1)+\sigma_m(2)\Gamma(2)]}{0.06NZ/A}$ [a]
^{186}Os	19.67 [b]	2.04	0.46	···	0.19	0.93 ± 0.09	1.15 ± 0.12
^{188}Os	30.42	2.62	0.88	0.12	0.24	1.33 ± 0.09	1.36 ± 0.08
^{189}Os	29.92	2.13	1.00	0.21	0.30	1.23 ± 0.09	1.24 ± 0.06
^{190}Os	30.42	2.01	1.08	0.14	0.33	1.18 ± 0.08	1.27 ± 0.10
^{192}Os	29.92	1.92	1.20	0.19	0.36	1.20 ± 0.08	1.27 ± 0.11

[a] Uncertainties listed here are relative; to obtain the absolute uncertainty a systematic uncertainty of 7% (10% for ^{186}Os) must be folded into the values for σ_m.
[b] Care must be used comparing values for ^{186}Os with the rest because $E_{\gamma\max}$ is so much different.

ELEM. SYM.	A	Z
Os	186	76

METHOD

REF. NO. 79 Be 4 hg

REACTION	RESULT	EXCITATION ENERGY	SOURCE		DETECTOR		ANGLE
			TYPE	RANGE	TYPE	RANGE	
G,1N	ABX	11-20	D	11-20	BF3-I		4PI
G,2N	ABX	14-20	D	14-20	BF3-I		4PI

TABLE X. Integrated cross-section moments, $\sigma_{-1} = \int \sigma(\gamma, n_t) E_\gamma^{-1} dE_\gamma$ and $\sigma_{-2} = \int \sigma(\gamma, n_t) E_\gamma^{-2} dE_\gamma$, integrated from threshold to $E_{\gamma max}$.

Nucleus	σ_{-1} (mb)	$\sigma_{-1}A^{-4/3}$ (mb)	σ_{-2} (mb MeV^{-1})	$\frac{\sigma_{-2}}{0.00225A^{5/3}}$	$\frac{\sigma_{-2}K}{0.05175A^{5/3}}$	$\frac{0.05175A^{5/3}}{\sigma_{-2}}$ (MeV)
^{186}Os[a]	179	0.168	13.2	0.97	1.22	23.8 ± 2.4
^{188}Os	239	0.222	16.7	1.20	1.45	19.1 ± 1.3
^{189}Os	228	0.210	16.7	1.19	1.41	19.3 ± 1.4
^{190}Os	220	0.202	15.8	1.12	1.30	20.6 ± 1.4
^{192}Os	224	0.203	16.0	1.12	1.31	20.6 ± 1.4

[a] Care must be used in comparing values for ^{186}Os with the rest because $E_{\gamma max}$ is so much different.

TABLE XII. Characteristics of the giant quadrupole resonance. The fitting interval used for the Lorentz-curve fits is 20–28 MeV.

Nucleus	E_q (MeV)	σ_q [a] (MeV)	Γ_q (MeV)	$E_q A^{1/3}$ (MeV)	$(1.60E_m)$ [b] (MeV)	$\frac{1}{2}\pi\sigma_q\Gamma_q$ (MeV mb)	(S_q/S_d) [c]	σ_{-2}(expt) [d] (mb MeV^{-1})	σ_{-2}(thy) [e] (mb MeV^{-1})
^{188}Os	22.8 ± 0.2	76 ± 6	3.8 ± 0.6	131	22.7	453 ± 107	0.12	0.87	0.49
^{189}Os	23.0 ± 0.3	51 ± 5	5.0 ± 1.0	132	22.4	407 ± 121	0.12	0.77	0.45
^{190}Os	23.8 ± 0 3	32 ± 4	4.0 ± 0.9	137	22.1	202 ± 71	0.06	0.36	0.47
^{192}Os	23.9 ± 0.1	65 ± 4	2.8 ± 0.4	138	22.1	288 ± 59	0.08	0.50	0.47

[a] Relative uncertainties.
[b] Theoretical prediction of Ref. 42 (see text). E_m is the GDR energy from Table IV.
[c] S_q is the quadrupole strength defined as $\frac{1}{2}\pi\sigma_q\Gamma_q$; S_d is the dipole strength defined as $\frac{1}{2}\pi[\sigma_m(1)\Gamma(1) + \sigma_m(2)\Gamma(2)]$.
[d] Computed as S_q/E_q^2.
[e] Computed from Eq. (12).

Os
A=188

Os
A=188

Os
A=188

REF. B.L. Berman, D.D. Faul, R.A. Alvarez, P. Meyer, D.L. Olson
Phys. Rev. C19, 1205 (1979)

ELEM. SYM.	A	Z
Os	188	76

METHOD

REF. NO.	
79 Be 4	hg

REACTION	RESULT	EXCITATION ENERGY	SOURCE		DETECTOR		ANGLE
			TYPE	RANGE	TYPE	RANGE	
G,1N	ABX	8-30	D	8-30	BF3-I		4PI
G,2N	ABX	14-30	D	14-30	BF3-I		4PI
G,3N	ABX	21-30	D	21-30	BF3-I		4PI

Photoneutron cross sections, including $\sigma[(\gamma,n) + (\gamma,pn)]$, $\sigma[(\gamma,2n) + (\gamma,p2n)]$, and $\sigma(\gamma,3n)$, were measured for ^{188}Os, ^{189}Os, ^{190}Os, and ^{192}Os from 7 to 30 MeV and for ^{186}Os from 11 to 20 MeV, with a photon energy resolution of about 300 keV. The source of radiation was the monoenergetic photon beam obtained from the annihilation in flight of fast positrons. The partial photoneutron cross sections were determined by neutron multiplicity counting, and the average neutron energies for each multiplicity were determined simultaneously with the cross-section data by the ring-ratio technique. Nuclear information extracted from the data includes parameters of the giant dipole and giant quadrupole resonances, integrated cross sections and their moments, nuclear symmetry energies, and nuclear deformation parameters and intrinsic quadrupole moments. No fewer than eight kinds of evidence point to a sudden change of behavior between ^{189}Os and ^{190}Os, which could be interpreted as a phase transition from a statically deformed prolate nucleus to a γ-unstable one, in general (but not detailed) agreement with the prediction of a dynamic-collective-model calculation.

[NUCLEAR REACTIONS ^{186,188,189,190,192}Os$(\gamma,n,2n,3n)$, E_γ=7–30 MeV; measured 4π neutron yield, multiplicities, average energies for monenergetic photons; $\sigma(E_\gamma,1n)$, $\sigma(E_\gamma,2n)$, $\sigma(E_\gamma,3n)$, GDR parameters, nuclear shape parameters, integrated cross sections and moments, GQR parameters, nuclear phase transition.]

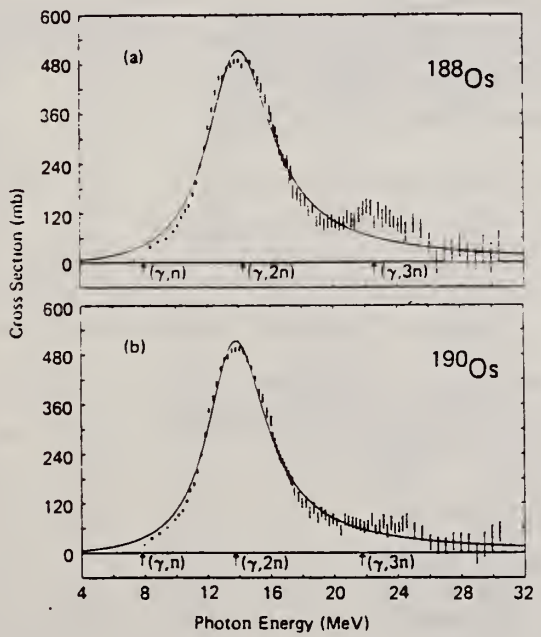

FIG. 7. Total photoneutron cross sections, together with single-component Lorentz-curve fits to the data: (a) for ^{188}Os; (b) for ^{190}Os.

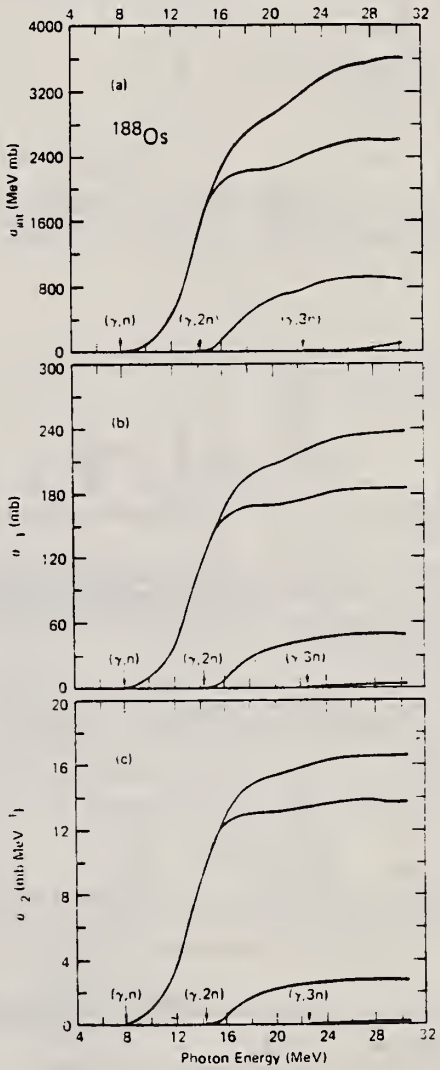

FIG. 9. Running sums of integrated cross sections for ^{188}Os: (a) σ_{int} for $\sigma(\gamma,n_t)$ (top), $\sigma(\gamma,1n)$ (next to top), $\sigma(\gamma,2n)$ (next to bottom), and $\sigma(\gamma,3n)$ (bottom); (b) σ_{-1}; (c) σ_{-2}.

(over)

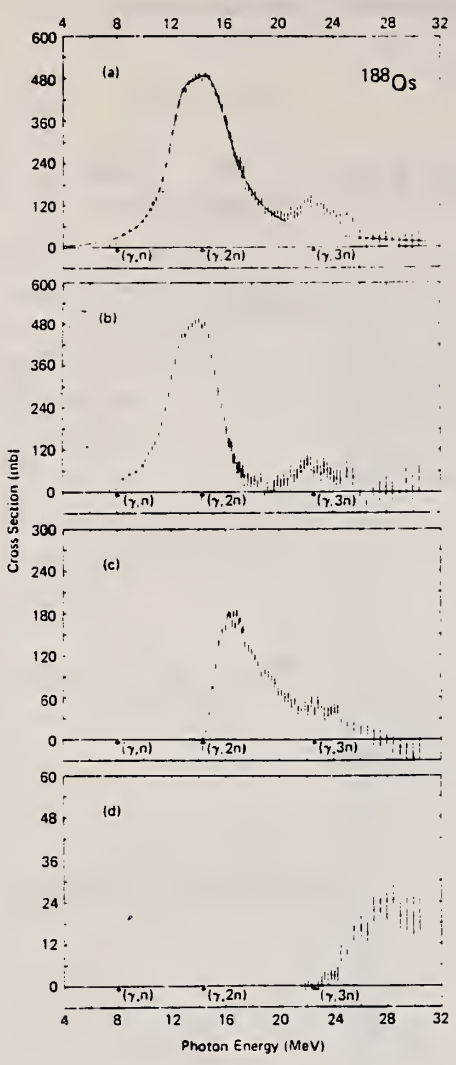

FIG. 3. Photoneutron cross sections for ^{188}Os: (a) $\sigma(\gamma,n_t)$, with a two-component Lorentz-curve fit; (b) $\sigma(\gamma,1n)$; (c) $\sigma(\gamma,2n)$; (d) triple-photoneutron cross section $\sigma(\gamma,3n)$.

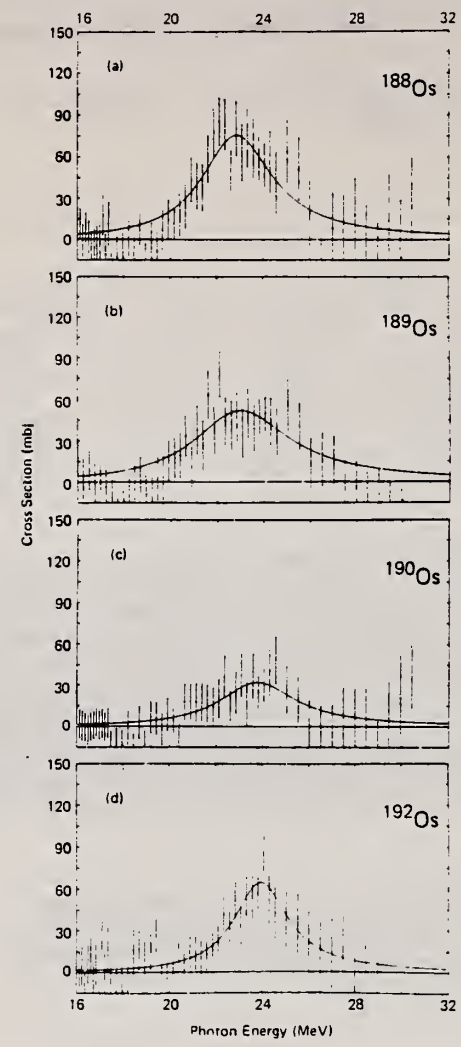

FIG. 14. Cross-section differences above the GDR; the two-component Lorentz-curve fits to $\sigma(\gamma,n_t)$ shown in part (a) of Figs. 3–6 were subtracted from the data points to give these differences, which were in turn fitted with the single-component Lorentz curves shown here as solid lines: (a) for ^{188}Os; (b) for ^{189}Os; (c) for ^{190}Os; (d) for ^{192}Os.

TABLE VI. Values for $B(E2, 0^+ \rightarrow 2^+)$ (in units of b^2).

Nucleus	Present experiment [a]	μ-mesic x rays [b]	Coulomb excitation [c]	Theory [d]	Theory [e]
^{188}Os	3.30 ± 0.56	3.15 ± 0.03	3.08 ± 0.21	2.96	3.05
^{189}Os	3.00 ± 0.36	2.84 ± 0.03	2.75 ± 0.12	2.72	2.75
^{190}Os	2.15 ± 0.43	2.48 ± 0.02	2.40 ± 0.11	2.59	2.54
^{192}Os	2.06 ± 0.46	2.10 ± 0.02	2.02 ± 0.09	2.56	2.34

[a] Computed from Eq. (5), using the values for Q_0 from Table V.
[b] From Ref. 26.
[c] Weighted average from Refs. 27 and 28.
[d] From Ref. 5.
[e] From Ref. 6.

TABLE III. Parameters of Lorentz-curve fits to the giant dipole resonance. Lorentz parameters defined by Eq. (1); the fitting interval for all cases is 10.8 to 18.8 MeV.

Nucleus	$E_m(1)$ (MeV)	$\sigma_m(1)$ [a] (mb)	$\Gamma(1)$ (MeV)	$E_m(2)$ (MeV)	$\sigma_m(2)$ [a] (mb)	$\Gamma(2)$ (MeV)	χ^2
^{186}Os	13.03 ± 0.09	308 ± 21	3.13 ± 0.24	15.26 ± 0.09	302 ± 23	3.38 ± 0.21	0.88
^{188}Os	12.81 ± 0.05	260 ± 18	2.76 ± 0.13	14.88 ± 0.07	390 ± 14	4.19 ± 0.13	0.96
^{189}Os	12.68 ± 0.04	268 ± 14	2.71 ± 0.10	14.68 ± 0.05	395 ± 11	3.62 ± 0.10	0.75
^{190}Os	12.68 ± 0.07	206 ± 29	2.60 ± 0.21	14.40 ± 0.09	401 ± 24	4.16 ± 0.11	1.19
^{192}Os	12.68 ± 0.06	206 ± 34	2.49 ± 0.23	14.35 ± 0.12	389 ± 26	4.41 ± 0.13	0.95

[a] Uncertainties for σ_m given here are relative. The absolute uncertainties are 7.7 (10.7)% for ^{186}Os).

TABLE V. Nuclear shape parameters.

Nucleus	R_A [a]	η [b]	ϵ [c]	β_2 [d]	Q_0 [e] (b)
^{186}Os	0.95 ± 0.27	1.188 ± 0.016	0.366 ± 0.031	0.194 ± 0.016	5.76 ± 0.49
^{188}Os	0.44 ± 0.08	1.177 ± 0.011	0.346 ± 0.021	0.183 ± 0.011	5.49 ± 0.33
^{189}Os	0.51 ± 0.07	1.173 ± 0.008	0.338 ± 0.015	0.179 ± 0.008	5.38 ± 0.24
^{190}Os	0.32 ± 0.10	1.149 ± 0.015	0.292 ± 0.029	0.155 ± 0.015	4.65 ± 0.46
^{192}Os	0.30 ± 0.11	1.145 ± 0.016	0.283 ± 0.031	0.150 ± 0.016	4.55 ± 0.50

[a] Area ratio, defined as $\sigma_m(1)\Gamma(1)/\sigma_m(2)\Gamma(2)$.
[b] Deformation parameter, computed from $E_m(2)/E_m(1) = 0.911\eta - 0.089$.
[c] Nuclear eccentricity, computed from $\epsilon = (\eta^2 - 1)\eta^{-2/3}$.
[d] Deformation parameter, defined as $\frac{2}{3}(\pi/5)^{1/2}\epsilon$.
[e] Intrinsic quadrupole moment, computed from Eq. (8), with R_0 taken to be 1.26 fm.

ELEM. SYM.	A	Z
Os	188	76

METHOD

REF. NO. 79 Be 4 hg

REACTION	RESULT	EXCITATION ENERGY	SOURCE		DETECTOR		ANGLE
			TYPE	RANGE	TYPE	RANGE	
G,1N	ABX	8-30	D	8-30	BF3-I		4PI
G,2N	ABX	14-30	D	14-30	BF3-I		4PI
G,3N	ABX	21-30	D	21-30	BF3-I		4PI

TABLE IV. Parameters for classical theories (given in MeV).

Nucleus	E_m [a]	α [b]	β [c]	K [d]
^{186}Os	14.21 ± 0.06	81.1 ± 0.3	34.0 ± 0.1	28.9 ± 0.9
^{188}Os	14.19 ± 0.05	81.3 ± 0.3	34.0 ± 0.1	27.8 ± 0.5
^{189}Os	14.01 ± 0.04	80.4 ± 0.2	33.6 ± 0.1	27.3 ± 0.4
^{190}Os	13.83 ± 0.06	79.5 ± 0.3	33.1 ± 0.1	26.6 ± 0.7
^{192}Os	13.79 ± 0.04	79.6 ± 0.2	33.1 ± 0.1	26.8 ± 0.7

[a] Mean energy of the giant resonance, defined as $E_m = [E_m(1) - 2E_m(2)]/3$, except for ^{186}Os, for which $E_m = [E_m(1) + E_m(2)]/2$.
[b] Hydrodynamic parameter, defined by $E_m = \alpha A^{-1/3}$.
[c] Collective parameter, defined by $E_m = \beta A^{-1/6}$.
[d] Nuclear symmetry energy, computed from Eq. (2).

TABLE IX. Integrated cross sections, $\sigma_{int}(\gamma,x) = \int \sigma(\gamma,x)dE_\gamma$, integrated from threshold to $E_{\gamma max}$. Uncertainties are discussed in Sec. II of the text.

Nucleus	$E_{\gamma max}$ (MeV)	$\sigma_{int}(\gamma,1n)$ (MeV b)	$\sigma_{int}(\gamma,2n)$ (MeV b)	$\sigma_{int}(\gamma,3n)$ (MeV b)	$\frac{\sigma_{int}(\gamma,2n)}{\sigma_{int}(\gamma,n_t)}$	$\frac{\sigma_{int}(\gamma,n_t)}{0.06NZ/A}$	$\frac{\frac{1}{2}\pi[\sigma_m(1)\Gamma(1) - \sigma_m(2)\Gamma(2)]}{0.06NZ/A}$ [a]
^{186}Os	19.67 [b]	2.04	0.46	···	0.19	0.93 ± 0.09	1.15 ± 0.12
^{188}Os	30.42	2.62	0.88	0.12	0.24	1.33 ± 0.09	1.36 ± 0.08
^{189}Os	29.92	2.13	1.00	0.21	0.30	1.23 ± 0.09	1.24 ± 0.06
^{190}Os	30.42	2.01	1.08	0.14	0.33	1.18 ± 0.08	1.27 ± 0.10
^{192}Os	29.92	1.92	1.20	0.19	0.36	1.20 ± 0.08	1.27 ± 0.11

[a] Uncertainties listed here are relative; to obtain the absolute uncertainty a systematic uncertainty of 7% (10% for ^{186}Os) must be folded into the values for σ_m.
[b] Care must be used comparing values for ^{186}Os with the rest because $E_{\gamma max}$ is so much different.

TABLE X. Integrated cross-section moments, $\sigma_{-1} = \int \sigma(\gamma,n_t)E_\gamma^{-1}dE_\gamma$ and $\sigma_{-2} = \int \sigma(\gamma,n_t)E_\gamma^{-2}dE_\gamma$, integrated from threshold to $E_{\gamma max}$.

Nucleus	σ_{-1} (mb)	$\sigma_{-1}A^{-4/3}$ (mb)	σ_{-2} (mb MeV^{-1})	$\frac{\sigma_{-2}}{0.00225A^{5/3}}$	$\frac{\sigma_{-2}}{\sigma_{-2K}}$	$\frac{\sigma_{-2}}{0.05175A^{5/3}}$	$\frac{0.05175A^{5/3}}{\sigma_{-2}}$ (MeV)
^{186}Os [a]	179	0.168	13.2	0.97	1.22		23.8 ± 2.4
^{188}Os	239	0.222	16.7	1.20	1.45		19.1 ± 1.3
^{189}Os	223	0.210	16.7	1.19	1.41		19.3 ± 1.4
^{190}Os	220	0.202	15.8	1.12	1.30		20.6 ± 1.4
^{192}Os	224	0.203	16.0	1.12	1.31		20.6 ± 1.4

[a] Care must be used in comparing values for ^{186}Os with the rest because $E_{\gamma max}$ is so much different.

TABLE XII. Characteristics of the giant quadrupole resonance. The fitting interval used for the Lorentz-curve fits is 20–28 MeV.

Nucleus	E_q (MeV)	σ_q [a] (MeV)	Γ_q (MeV)	$E_q A^{1/3}$ (MeV)	$(1.60E_m)$ [b] (MeV)	$\frac{1}{2}\pi\sigma_q\Gamma_q$ (MeV mb)	(S_q/S_d) [c]	σ_{-2}(expt) [d] (mb MeV^{-1})	σ_{-2}(thy) [e] (mb MeV^{-1})
^{188}Os	22.8 ± 0.2	76 ± 6	3.8 ± 0.6	131	22.7	453 ± 107	0.12	0.87	0.49
^{189}Os	23.0 ± 0.3	51 ± 5	5.0 ± 1.0	132	22.4	407 ± 121	0.12	0.77	0.45
^{190}Os	23.8 ± 0.3	32 ± 4	4.0 ± 0.9	137	22.1	202 ± 71	0.06	0.36	0.47
^{192}Os	23.9 ± 0.1	65 ± 4	2.8 ± 0.4	138	22.1	288 ± 59	0.08	0.50	0.47

[a] Relative uncertainties.
[b] Theoretical prediction of Ref. 42 (see text). E_m is the GDR energy from Table IV.
[c] S_q is the quadrupole strength defined as $\frac{1}{2}\pi\sigma_q\Gamma_q$; S_d is the dipole strength defined as $\frac{1}{2}\pi[\sigma_m(1)\Gamma(1) + \sigma_m(2)\Gamma(2)]$.
[d] Computed as S_q/E_q^2.
[e] Computed from Eq. (12).

Os
A=189

Os
A=189

REF. B.L. Berman, D.D. Faul, R.A. Alvarez, P. Meyer, D.L. Olson
Phys. Rev. C19, 1205 (1979)

ELEM. SYM.	A	Z
Os	189	76

METHOD

REF. NO. 79 Be 4 hg

REACTION	RESULT	EXCITATION ENERGY	SOURCE		DETECTOR		ANGLE
			TYPE	RANGE	TYPE	RANGE	
G,1N	ABX	6-30	D	6-30	BF3-I		4PI
G,2N	ABX	14-30	D	14-30	BF3-I		4PI
G,3N	ABX	19-30	D	19-30	BF3-I		4PI

Photoneutron cross sections, including $\sigma[(\gamma,n) + (\gamma,pn)]$, $\sigma[(\gamma,2n) + (\gamma,p2n)]$, and $\sigma(\gamma,3n)$, were measured for ^{188}Os, ^{189}Os, ^{190}Os, and ^{192}Os from 7 to 30 MeV and for ^{186}Os from 11 to 20 MeV, with a photon energy resolution of about 300 keV. The source of radiation was the monoenergetic photon beam obtained from the annihilation in flight of fast positrons. The partial photoneutron cross sections were determined by neutron multiplicity counting, and the average neutron energies for each multiplicity were determined simultaneously with the cross-section data by the ring-ratio technique. Nuclear information extracted from the data includes parameters of the giant dipole and giant quadrupole resonances, integrated cross sections and their moments, nuclear symmetry energies, and nuclear deformation parameters and intrinsic quadrupole moments. No fewer than eight kinds of evidence point to a sudden change of behavior between ^{189}Os and ^{190}Os, which could be interpreted as a phase transition from a statically deformed prolate nucleus to a γ-unstable one, in general (but not detailed) agreement with the prediction of a dynamic-collective-model calculation.

[NUCLEAR REACTIONS ^{186,188,189,190,192}Os$(\gamma,n,2n,3n)$, E_γ=7–30 MeV; measured 4π neutron yield, multiplicities, average energies for monenergetic photons; $\sigma(E_\gamma,1n)$, $\sigma(E_\gamma,2n)$, $\sigma(E_\gamma,3n)$, GDR parameters, nuclear shape parameters, integrated cross sections and moments, GQR parameters, nuclear phase transition.]

TABLE IV. Parameters for classical theories (given in MeV).

Nucleus	E_m [a]	α [b]	β [c]	K [d]
^{186}Os	14.21 ± 0.06	81.1 ± 0.3	34.0 ± 0.1	28.9 ± 0.9
^{188}Os	14.19 ± 0.05	81.3 ± 0.3	34.0 ± 0.1	27.3 ± 0.5
^{189}Os	14.01 ± 0.04	80.4 ± 0.2	33.6 ± 0.1	27.3 ± 0.4
^{190}Os	13.83 ± 0.06	79.5 ± 0.3	33.1 ± 0.1	26.6 ± 0.7
^{192}Os	13.79 ± 0.04	79.6 ± 0.2	33.1 ± 0.1	26.8 ± 0.7

[a] Mean energy of the giant resonance, defined as $E_m = [E_m(1) + 2E_m(2)]/3$, except for ^{186}Os, for which $E_m = [E_m(1) + E_m(2)]/2$.
[b] Hydrodynamic parameter, defined by $E_m = \alpha A^{-1/3}$.
[c] Collective parameter, defined by $E_m = \beta A^{-1/6}$.
[d] Nuclear symmetry energy, computed from Eq. (2).

TABLE V. Nuclear shape parameters.

Nucleus	R_A [a]	η [b]	ϵ [c]	β_2 [d]	Q_0 [e] (b)
^{186}Os	0.95 ± 0.27	1.188 ± 0.016	0.366 ± 0.031	0.194 ± 0.016	5.76 ± 0.49
^{188}Os	0.44 ± 0.08	1.177 ± 0.011	0.346 ± 0.021	0.183 ± 0.011	5.49 ± 0.33
^{189}Os	0.51 ± 0.07	1.173 ± 0.008	0.338 ± 0.015	0.179 ± 0.008	5.38 ± 0.24
^{190}Os	0.32 ± 0.10	1.149 ± 0.015	0.292 ± 0.029	0.155 ± 0.015	4.65 ± 0.46
^{192}Os	0.30 ± 0.11	1.145 ± 0.016	0.283 ± 0.031	0.150 ± 0.016	4.55 ± 0.50

[a] Area ratio, defined as $\sigma_m(1)\Gamma(1)/\sigma_m(2)\Gamma(2)$.
[b] Deformation parameter, computed from $E_m(2)/E_m(1) = 0.911\eta - 0.089$.
[c] Nuclear eccentricity, computed from $\epsilon = (\eta^2 - 1)\eta^{-2/3}$.
[d] Deformation parameter, defined as $\frac{2}{3}(\pi/5)^{1/2}\epsilon$.
[e] Intrinsic quadrupole moment, computed from Eq. (8), with R_0 taken to be 1.26 fm.

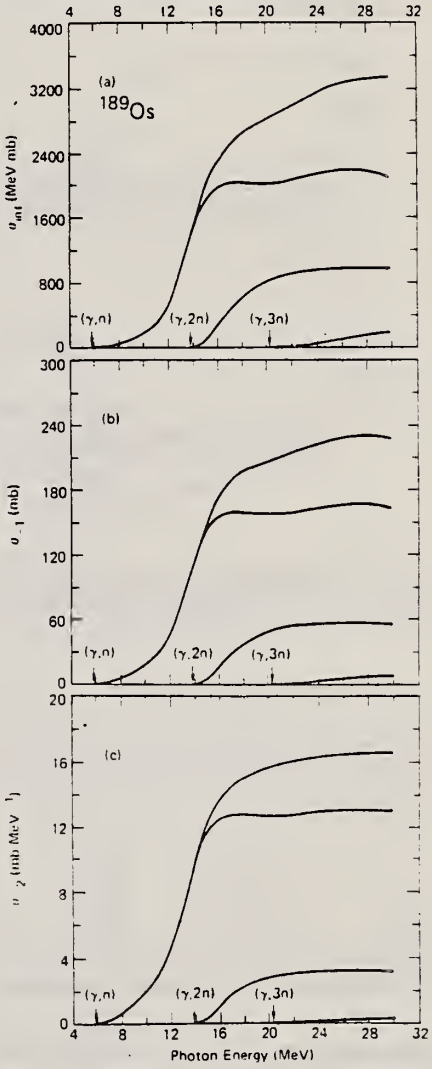

FIG. 10. Running sums of integrated cross sections for ^{189}Os: (a) σ_{int}; (b) σ_{-1}; (c) σ_{-2}.

(over)

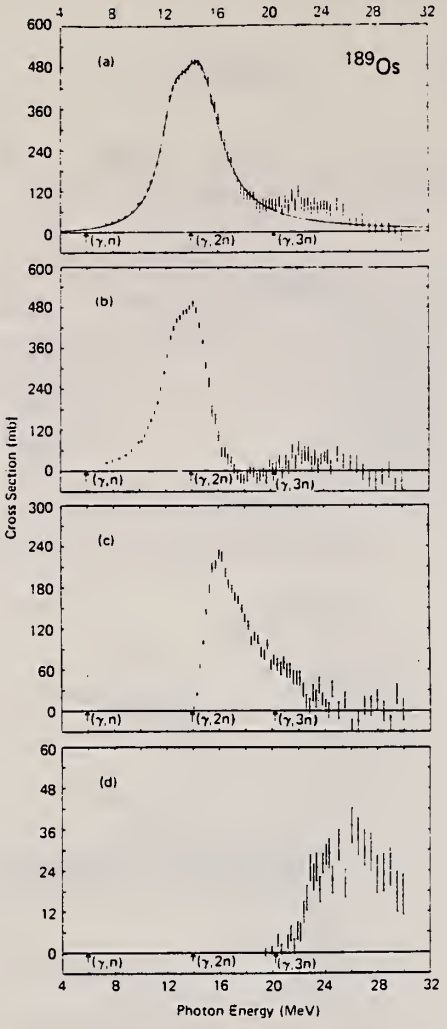

FIG. 4. Photoneutron cross sections for ^{189}Os: (a) $\sigma(\gamma,n_t)$, with a two-component Lorentz-curve fit; (b) $\sigma(\gamma,1n)$; (c) $\sigma(\gamma,2n)$; (d) $\sigma(\gamma,3n)$.

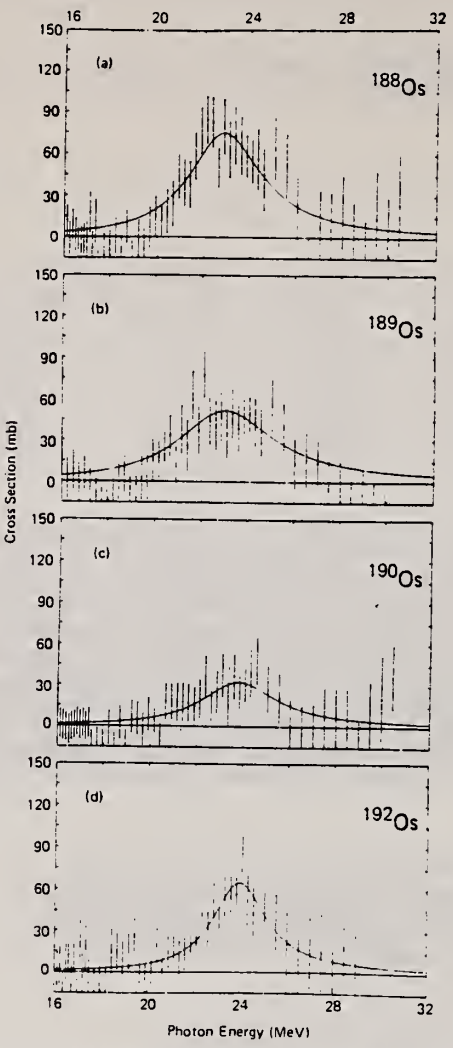

FIG. 14. Cross-section differences above the GDR; the two-component Lorentz-curve fits to $\sigma(\gamma,n_t)$ shown in part (a) of Figs. 3–6 were subtracted from the data points to give these differences, which were in turn fitted with the single-component Lorentz curves shown here as solid lines: (a) for ^{188}Os; (b) for ^{189}Os; (c) for ^{190}Os; (d) for ^{192}Os.

TABLE IX. Integrated cross sections, $\sigma_m(\gamma,x)\equiv\int\sigma(\gamma,x)dE_\gamma$, integrated from threshold to $E_{\gamma\,max}$. Uncertainties are discussed in Sec. II of the text.

Nucleus	$E_{\gamma\,max}$ (MeV)	$\sigma_m(\gamma,1n)$ (MeV b)	$\sigma_m(\gamma,2n)$ (MeV b)	$\sigma_m(\gamma,3n)$ (MeV b)	$\frac{\sigma_m(\gamma,2n)}{\sigma_m(\gamma,n_t)}$	$\frac{\sigma_m(\gamma,nt)}{0.06NZ/A}$	$\frac{\frac{1}{2}\pi[\sigma_m(1)\Gamma(1)+\sigma_m(2)\Gamma(2)]^a}{0.06NZ/A}$
^{186}Os	19.67[b]	2.04	0.46	...	0.19	0.93 ± 0.09	1.15 ± 0.12
^{188}Os	30.42	2.62	0.88	0.12	0.24	1.33 ± 0.09	1.36 ± 0.08
^{189}Os	29.92	2.13	1.00	0.21	0.30	1.23 ± 0.09	1.24 ± 0.06
^{190}Os	30.42	2.01	1.08	0.14	0.33	1.18 ± 0.08	1.27 ± 0.10
^{192}Os	29.92	1.92	1.20	0.19	0.36	1.20 ± 0.08	1.27 ± 0.11

[a] Uncertainties listed here are relative; to obtain the absolute uncertainty a systematic uncertainty of 7% (10% for ^{186}Os) must be folded into the values for σ_m.
[b] Care must be used comparing values for ^{186}Os with the rest because $E_{\gamma\,max}$ is so much different.

TABLE III. Parameters of Lorentz-curve fits to the giant dipole resonance. Lorentz parameters defined by Eq. 1; the fitting interval for all cases is 10.8 to 18.8 MeV.

Nucleus	$E_m(1)$ (MeV)	$\sigma_m(1)$[a] (mb)	$\Gamma(1)$ (MeV)	$E_m(2)$ (MeV)	$\sigma_m(2)$[a] (mb)	$\Gamma(2)$ (MeV)	χ^2
^{186}Os	13.03 ± 0.09	308 ± 21	3.13 ± 0.24	15.26 ± 0.09	302 ± 23	3.38 ± 0.21	0.88
^{188}Os	12.81 ± 0.05	260 ± 18	2.76 ± 0.13	14.88 ± 0.07	390 ± 14	4.19 ± 0.13	0.96
^{189}Os	12.68 ± 0.04	268 ± 14	2.71 ± 0.10	14.68 ± 0.05	395 ± 11	3.62 ± 0.10	0.75
^{190}Os	12.68 ± 0.07	206 ± 29	2.60 ± 0.21	14.40 ± 0.09	401 ± 24	4.16 ± 0.11	1.19
^{192}Os	12.68 ± 0.06	206 ± 34	2.49 ± 0.23	14.35 ± 0.12	389 ± 26	4.41 ± 0.13	0.95

[a] Uncertainties for σ_m given here are relative. The absolute uncertainties are 7% (10% for ^{186}Os).

TABLE VI. Values for $B(E2,0^+\rightarrow 2^+)$ (in units of b^2).

Nucleus	Present experiment[a]	μ-mesic x rays[b]	Coulomb excitation[c]	Theory[d]	Theory[e]
^{186}Os	3.30 ± 0.56	3.15 ± 0.03	3.08 ± 0.21	2.96	3.05
^{188}Os	3.00 ± 0.36	2.84 ± 0.03	2.75 ± 0.12	2.72	2.75
^{190}Os	2.15 ± 0.43	2.48 ± 0.02	2.40 ± 0.11	2.59	2.54
^{192}Os	2.06 ± 0.46	2.10 ± 0.02	2.02 ± 0.09	2.56	2.34

[a] Computed from Eq. (9), using the values for Ψ_0 from Table V.
[b] From Ref. 26.
[c] Weighted average from Refs. 27 and 28.
[d] From Ref. 5.
[e] From Ref. 6.

ELEM. SYM.	A	Z
Os	189	76

METHOD

REF. NO. 79 Be 4 hg

REACTION	RESULT	EXCITATION ENERGY	SOURCE		DETECTOR		ANGLE
			TYPE	RANGE	TYPE	RANGE	
G,1N	ABX	6-30	D	6-30	BF3-I		4PI
G,2N	ABX	14-30	D	14-30	BF3-I		4PI
G,3N	ABX	19-30	D	19-30	BF3-I		4PI

TABLE X. Integrated cross-section moments, $\sigma_{-1} = \int \sigma(\gamma, n_t) E_\gamma^{-1} dE_\gamma$ and $\sigma_{-2} = \int \sigma(\gamma, n_t) E_\gamma^{-2} dE_\gamma$, integrated from threshold to $E_{\gamma max}$.

Nucleus	σ_{-1} (mb)	$\sigma_{-1}A^{-4/3}$ (mb)	σ_{-2} (mb MeV^{-1})	$\frac{\sigma_{-2}}{0.00225A^{5/3}}$	$\frac{\sigma_{-2}K}{0.05175A^{5/3}}$	$\frac{0.05175A^{5/3}}{\sigma_{-2}}$ (MeV)
^{186}Os[a]	179	0.168	13.2	0.97	1.22	23.8 ± 2.4
^{188}Os	239	0.222	16.7	1.20	1.45	19.1 ± 1.3
^{189}Os	228	0.210	16.7	1.19	1.41	19.3 ± 1.4
^{190}Os	220	0.202	15.8	1.12	1.30	20.6 ± 1.4
^{192}Os	224	0.203	16.0	1.12	1.31	20.6 ± 1.4

[a] Care must be used in comparing values for ^{186}Os with the rest because $E_{\gamma max}$ is so much different.

TABLE XII. Characteristics of the giant quadrupole resonance. The fitting interval used for the Lorentz-curve fits is 20–28 MeV.

Nucleus	E_q (MeV)	σ_q [a] (MeV)	Γ_q (MeV)	$E_q A^{1/3}$ (MeV)	$(1.60E_m)$ [b] (MeV)	$\frac{1}{2}\pi\sigma_q\Gamma_q$ (MeV mb)	(S_q/S_d) [c]	σ_{-2}(expt) [d] (mb MeV^{-1})	σ_{-2}(thy) [e] (mb MeV^{-1})
^{188}Os	22.8 ± 0.2	76 ± 6	3.8 ± 0.6	131	22.7	453 ± 107	0.12	0.87	0.49
^{189}Os	23.0 ± 0.3	51 ± 5	5.0 ± 1.0	132	22.4	407 ± 121	0.12	0.77	0.45
^{190}Os	23.8 ± 0.3	32 ± 4	4.0 ± 0.9	137	22.1	202 ± 71	0.06	0.36	0.47
^{192}Os	23.9 ± 0.1	65 ± 4	2.8 ± 0.4	138	22.1	288 ± 59	0.08	0.50	0.47

[a] Relative uncertainties.
[b] Theoretical prediction of Ref. 42 (see text). E_m is the GDR energy from Table IV.
[c] S_q is the quadrupole strength defined as $\frac{1}{2}\pi\sigma_q\Gamma_q$; S_d is the dipole strength defined as $\frac{1}{2}\pi[\sigma_m(1)\Gamma(1) + \sigma_m(2)\Gamma(2)]$.
[d] Computed as S_q/E_q^2.
[e] Computed from Eq. (12).

Os
A=190

Os
A=190

Os
A=190

A.M. Goryachev, G.N. Zalesnyi, S.F. Semenko, and B.A. Tulupov

REF. Yad. Fiz. 17, 463 (1973)
Sov. J. Nucl. Phys. 17, 236 (1973)

ELEM. SYM.	A	Z
Os	190	76

METHOD

REF. NO.	
73 Go 6	hmg

REACTION	RESULT	EXCITATION ENERGY	SOURCE		DETECTOR		ANGLE
			TYPE	RANGE	TYPE	RANGE	
G,XN	ABX	8- 20	C	8- 20	BF3-I		4PI

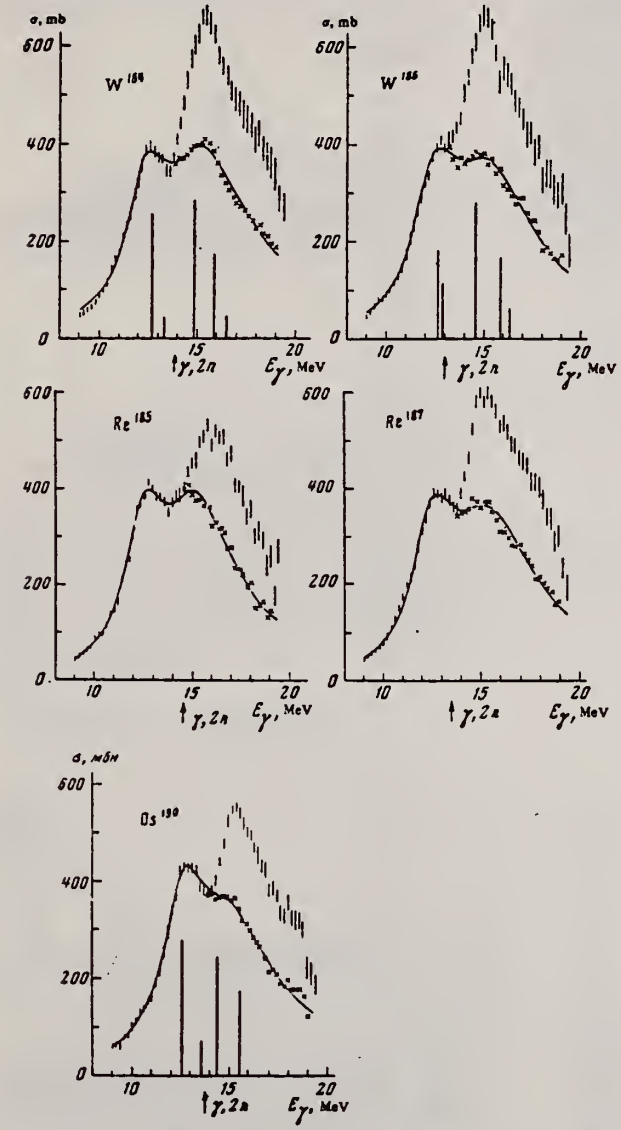

FIG. 2. Cross sections for $W^{184,186}$, Os^{190}, and $Re^{185,187}$. The cross section $\sigma_{\gamma,n} + 2\sigma_{\gamma,2n}$ is denoted by vertical lines whose lengths are twice the rms errors. The crosses represent the cross sections, corrected for multiplicity, above the threshold of the (γ, 2n) reaction. The solid curves are Lorentz curve approximations. For $W^{184,186}$ and Os^{190} the calculated dipole transition strengths are shown.

TABLE III

	W^{184}	W^{186}	Os^{190}	Re^{185}	Re^{187}	W^{184} [7]
Γ_1, MeV	2.33	2.55	2.13	2.51	2.83	2.29
E_{1}, MeV	12.5	12.5	12.6	12.7	12.6	12.50
σ_1, mb	241	225	223	262	250	211
Γ_2, MeV	5.1	5.4	5.7	5.2	5.3	5.18
E_2, MeV	15.6	15.2	14.8	15.4	15.6	14.88
σ_2, mb	338	317	318	315	296	334
0.06 NZ/A, MeV-mb	2.65	2.67	2.74	2.68	2.69	2.67
$S_1 + S_2$, MeV − mb	4.0	3.9	3.9	3.6	3.8	3.47
S_2 / S_1	2.8	3.0	3.8	2.5	2.2	3.6

Note. $S_i = (\pi/2)\sigma_i\Gamma_i$ is the Lorentz area.

REF. B.L. Berman, D.D. Faul, R.A. Alvarez, P. Meyer, D.L. Olson
Phys. Rev. C19, 1205 (1979)

ELEM. SYM.	A	Z
Os	190	76

METHOD

REF. NO. 79 Be 4 hg

REACTION	RESULT	EXCITATION ENERGY	SOURCE		DETECTOR		ANGLE
			TYPE	RANGE	TYPE	RANGE	
G,1N	ABX	8-30	D	8-30	BF3-I		4PI
G,2N	ABX	14-30	D	14-30	BF3-I		4PI
G,3N	ABX	20-30	D	20-30	BF3-I		4PI

Photoneutron cross sections, including $\sigma[(\gamma,n) + (\gamma,pn)]$, $\sigma[(\gamma,2n) + (\gamma,p2n)]$, and $\sigma(\gamma,3n)$, were measured for ^{188}Os, ^{189}Os, ^{190}Os, and ^{192}Os from 7 to 30 MeV and for ^{186}Os from 11 to 20 MeV, with a photon energy resolution of about 300 keV. The source of radiation was the monoenergetic photon beam obtained from the annihilation in flight of fast positrons. The partial photoneutron cross sections were determined by neutron multiplicity counting, and the average neutron energies for each multiplicity were determined simultaneously with the cross-section data by the ring-ratio technique. Nuclear information extracted from the data includes parameters of the giant dipole and giant quadrupole resonances, integrated cross sections and their moments, nuclear symmetry energies, and nuclear deformation parameters and intrinsic quadrupole moments. No fewer than eight kinds of evidence point to a sudden change of behavior between ^{189}Os and ^{190}Os, which could be interpreted as a phase transition from a statically deformed prolate nucleus to a γ-unstable one, in general (but not detailed) agreement with the prediction of a dynamic-collective-model calculation.

[NUCLEAR REACTIONS ^{186,188,189,190,192}Os$(\gamma,n,2n,3n)$, E_γ=7–30 MeV; measured 4π neutron yield, multiplicities, average energies for monenergetic photons; $\sigma(E_\gamma,1n)$, $\sigma(E_\gamma,2n)$, $\sigma(E_\gamma,3n)$, GDR parameters, nuclear shape parameters, integrated cross sections and moments, GQR parameters, nuclear phase transition.]

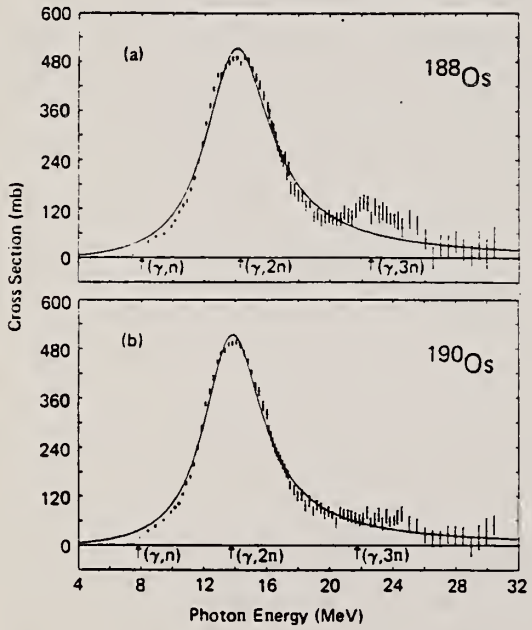

FIG. 7. Total photoneutron cross sections, together with single-component Lorentz-curve fits to the data: (a) for ^{188}Os; (b) for ^{190}Os.

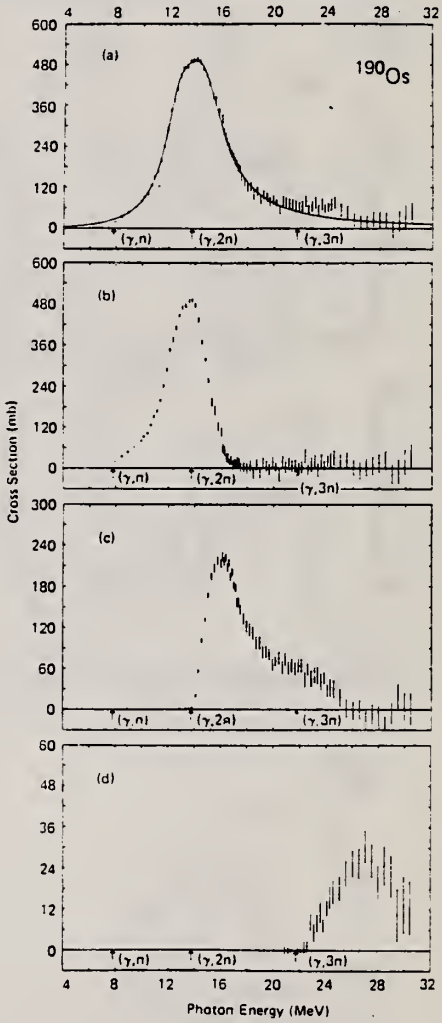

FIG. 5. Photoneutron cross sections for ^{190}Os: (a) $\sigma(\gamma,n_t)$, with a two-component Lorentz-curve fit; (b) $\sigma(\gamma,1n)$; (c) $\sigma(\gamma,2n)$; (d) $\sigma(\gamma,3n)$.

(over)

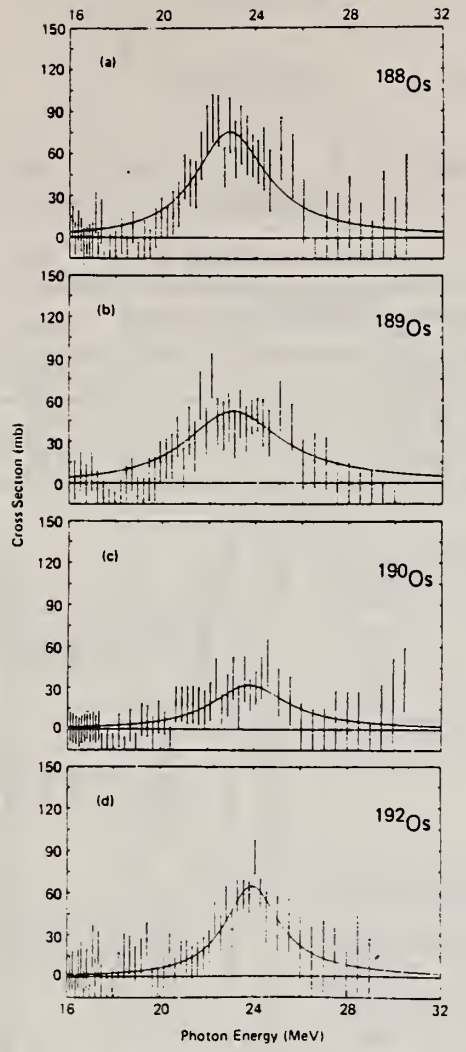

FIG. 14. Cross-section differences above the GDR; the two-component Lorentz-curve fits to $\sigma(\gamma, n_1)$ shown in part (a) of Figs. 3–6 were subtracted from the data points to give these differences, which were in turn fitted with the single-component Lorentz curves shown here as solid lines: (a) for ^{188}Os; (b) for ^{189}Os; (c) for ^{190}Os; (d) for ^{192}Os.

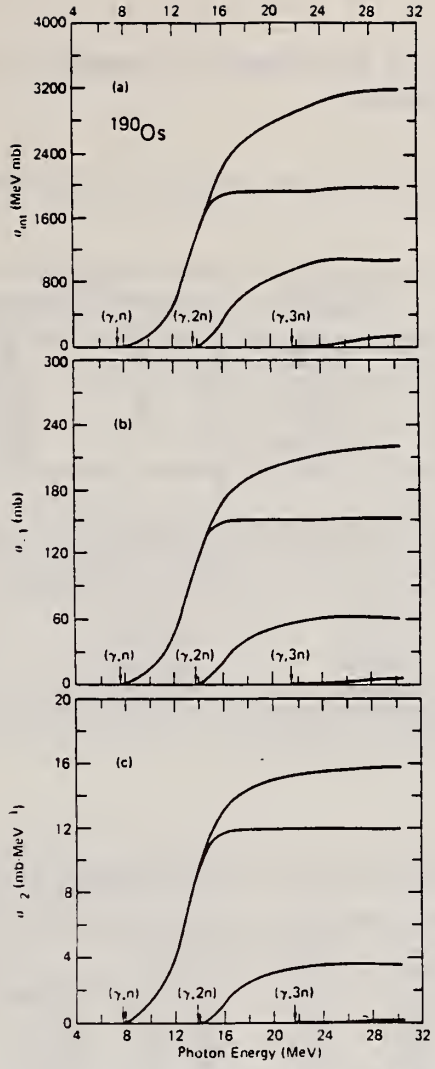

FIG. 11. Running sums of integrated cross sections for ^{190}Os: (a) $\sigma_{\rm int}$; (b) σ_{-1}; (c) σ_{-2}.

TABLE III. Parameters of Lorentz-curve fits to the giant dipole resonance. Lorentz parameters defined by Eq. (1); the fitting interval for all cases is 10.8 to 18.8 MeV.

Nucleus	$E_m(1)$ (MeV)	$\sigma_m(1)\Gamma(1)$ (mb)	$\Gamma(1)$ (MeV)	$E_m(2)$ (MeV)	$\sigma_m(2)\Gamma(2)$ (mb)	$\Gamma(2)$ (MeV)	χ^2
^{186}Os	13.03 ± 0.09	308 ± 21	3.13 ± 0.24	15.26 ± 0.09	302 ± 23	3.35 ± 0.21	0.88
^{188}Os	12.81 ± 0.05	260 ± 18	2.76 ± 0.13	14.88 ± 0.07	350 ± 11	4.19 ± 0.13	0.96
^{189}Os	12.68 ± 0.04	268 ± 14	2.71 ± 0.10	14.68 ± 0.05	395 ± 11	3.62 ± 0.10	0.75
^{190}Os	12.68 ± 0.07	206 ± 29	2.60 ± 0.21	14.40 ± 0.09	401 ± 24	4.16 ± 0.11	1.19
^{192}Os	12.68 ± 0.06	206 ± 34	2.49 ± 0.23	14.35 ± 0.12	389 ± 26	4.41 ± 0.13	0.95

[a] Uncertainties for σ_m given here are relative. The absolute uncertainties are 7% (10% for ^{186}Os).

TABLE IV. Parameters for classical theories (given in MeV).

Nucleus	E_m [a]	α [b]	β [c]	K [d]
^{186}Os	14.21 ± 0.06	81.1 ± 0.3	34.0 ± 0.1	28.9 ± 0.9
^{188}Os	14.19 ± 0.05	81.3 ± 0.3	34.0 ± 0.1	27.8 ± 0.5
^{189}Os	14.01 ± 0.04	80.4 ± 0.2	33.6 ± 0.1	27.3 ± 0.4
^{190}Os	13.83 ± 0.06	79.5 ± 0.3	33.1 ± 0.1	26.6 ± 0.7
^{192}Os	13.79 ± 0.04	79.6 ± 0.2	33.1 ± 0.1	26.8 ± 0.7

[a] Mean energy of the giant resonance, defined as $E_m = [E_m(1) + 2E_m(2)]/3$, except for ^{186}Os, for which $E_m = [E_m(1) + E_m(2)]/2$.
[b] Hydrodynamic parameter, defined by $E_m = \alpha A^{-1/3}$.
[c] Collective parameter, defined by $E_m = \beta A^{-1/6}$.
[d] Nuclear symmetry energy, computed from Eq. (2).

TABLE V. Nuclear shape parameters.

Nucleus	R_A [a]	η [b]	ϵ [c]	β_2 [d]	Q_0 [e] (b)
^{186}Os	0.95 ± 0.27	1.188 ± 0.016	0.366 ± 0.031	0.194 ± 0.016	5.76 ± 0.49
^{188}Os	0.44 ± 0.08	1.177 ± 0.011	0.346 ± 0.021	0.183 ± 0.011	5.49 ± 0.33
^{189}Os	0.51 ± 0.07	1.173 ± 0.008	0.338 ± 0.015	0.179 ± 0.008	5.38 ± 0.24
^{190}Os	0.32 ± 0.10	1.149 ± 0.015	0.292 ± 0.029	0.155 ± 0.015	4.65 ± 0.46
^{192}Os	0.30 ± 0.11	1.145 ± 0.016	0.283 ± 0.031	0.150 ± 0.016	4.55 ± 0.50

[a] Area ratio, defined as $\sigma_m(1)\Gamma(1)/\sigma_m(2)\Gamma(2)$.
[b] Deformation parameter, computed from $E_m(2)/E_m(1) = 0.911\eta - 0.089$.
[c] Nuclear eccentricity, computed from $\epsilon = (\eta^2 - 1)\eta^{-2/3}$.
[d] Deformation parameter, defined as $\frac{3}{5}(\pi/5)^{1/2}\epsilon$.
[e] Intrinsic quadrupole moment, computed from Eq. (8), with R_0 taken to be 1.26 fm.

ELEM. SYM.	A	Z
Os	190	76

METHOD

REF. NO. 79 Be 4 hg

REACTION	RESULT	EXCITATION ENERGY	SOURCE		DETECTOR		ANGLE
			TYPE	RANGE	TYPE	RANGE	
G, 1N	ABX	8-30	D	8-30	BF3-I		4PI
G,2N	ABX	14-30	D	14-30	BF3-I		4PI
G,3N	ABX	20-30	D	20-30	BF3-I		4PI

TABLE VI. Values for $B(E2, 0^+ \rightarrow 2^+)$ (in units of b^2).

Nucleus	Present experiment [a]	μ-mesic x rays [b]	Coulomb excitation [c]	Theory [d]	Theory [e]
^{186}Os	3.30 ± 0.56	3.15 ± 0.03	3.08 ± 0.21	2.96	3.05
^{188}Os	3.00 ± 0.36	2.84 ± 0.03	2.75 ± 0.12	2.72	2.75
^{190}Os	2.15 ± 0.43	2.48 ± 0.02	2.40 ± 0.11	2.59	2.54
^{192}Os	2.06 ± 0.46	2.10 ± 0.02	2.02 ± 0.09	2.56	2.34

[a] Computed from Eq. (9), using the values for Q_0 from Table V.
[b] From Ref. 26.
[c] Weighted average from Refs. 27 and 28.
[d] From Ref. 5.
[e] From Ref. 6.

TABLE XII. Characteristics of the giant quadrupole resonance. The fitting interval used for the Lorentz-curve fits is 20–28 MeV.

Nucleus	E_q (MeV)	σ_q [a] (MeV)	Γ_q (MeV)	$E_q A^{1/3}$ (MeV)	$(1.60E_m)$ [b] (MeV)	$\frac{1}{2}\pi\sigma_q\Gamma_q$ (MeV mb)	(S_q/S_d) [c]	σ_{-2}(expt) [d] (mb MeV^{-1})	σ_{-2}(thy) [e] (mb MeV^{-1})
^{188}Os	22.8 ± 0.2	76 ± 6	3.8 ± 0.6	131	22.7	453 ± 107	0.12	0.87	0.49
^{189}Os	23.0 ± 0.3	51 ± 5	5.0 ± 1.0	132	22.4	407 ± 121	0.12	0.77	0.45
^{190}Os	23.8 ± 0.3	32 ± 4	4.0 ± 0.9	137	22.1	202 ± 71	0.06	0.36	0.47
^{192}Os	23.9 ± 0.1	65 ± 4	2.8 ± 0.4	138	22.1	288 ± 59	0.08	0.50	0.47

[a] Relative uncertainties.
[b] Theoretical prediction of Ref. 42 (see text). E_m is the GDR energy from Table IV.
[c] S_q is the quadrupole strength defined as $\frac{1}{2}\pi\sigma_q\Gamma_q$; S_d is the dipole strength defined as $\frac{1}{2}\pi[\sigma_m(1)\Gamma(1) - \sigma_m(2)\Gamma(2)]$.
[d] Computed as S_q/E_q^2.
[e] Computed from Eq. (12).

TABLE X. Integrated cross-section moments, $\sigma_{-1} = \int\sigma(\gamma,n_t)E_\gamma^{-1}dE_\gamma$ and $\sigma_{-2} = \int\sigma(\gamma,n_t)E_\gamma^{-2}dE_\gamma$, integrated from threshold to $E_{\gamma\max}$.

Nucleus	σ_{-1} (mb)	$\sigma_{-1}A^{-4/3}$ (mb)	σ_{-2} (mb MeV^{-1})	$\frac{\sigma_{-2}}{0.00225A^{5/3}}$	$\frac{\sigma_{-2K}}{0.05175A^{5/3}}$	$\frac{\sigma_{-2}}{0.05175A^{5/3}}$ σ_{-2} (MeV)
^{186}Os [a]	179	0.168	13.2	0.97	1.22	23.8 ± 2.4
^{188}Os	239	0.222	16.7	1.20	1.45	19.1 ± 1.3
^{189}Os	228	0.210	16.7	1.19	1.41	19.3 ± 1.4
^{190}Os	220	0.202	15.8	1.12	1.30	20.6 ± 1.4
^{192}Os	224	0.203	16.0	1.12	1.31	20.6 ± 1.4

[a] Care must be used in comparing values for ^{186}Os with the rest because $E_{\gamma\max}$ is so much different.

TABLE IX. Integrated cross sections, $\sigma_{\rm int}(\gamma,x) = \int\sigma(\gamma,x)dE_\gamma$, integrated from threshold to $E_{\gamma\max}$. Uncertainties are discussed in Sec. II of the text.

Nucleus	$E_{\gamma\max}$ (MeV)	$\sigma_{\rm int}(\gamma,1n)$ (MeV b)	$\sigma_{\rm int}(\gamma,2n)$ (MeV b)	$\sigma_{\rm int}(\gamma,3n)$ (MeV b)	$\frac{\sigma_{\rm int}(\gamma,2n)}{\sigma_{\rm int}(\gamma,n_t)}$	$\frac{\sigma_{\rm int}(\gamma,n_t)}{0.06NZ/A}$	$\frac{\frac{1}{2}\pi[\sigma_m(1)\Gamma(1)+\sigma_m(2)\Gamma(2)]}{0.06NZ/A}$ [a]
^{186}Os	19.67 [b]	2.04	0.46	···	0.19	0.93 ± 0.09	1.15 ± 0.12
^{188}Os	30.42	2.62	0.88	0.12	0.24	1.33 ± 0.09	1.36 ± 0.08
^{189}Os	29.92	2.13	1.00	0.21	0.30	1.23 ± 0.09	1.24 ± 0.06
^{190}Os	30.42	2.01	1.08	0.14	0.33	1.18 ± 0.08	1.27 ± 0.10
^{192}Os	29.92	1.92	1.20	0.19	0.36	1.20 ± 0.08	1.27 ± 0.11

[a] Uncertainties listed here are relative; to obtain the absolute uncertainty a systematic uncertainty of 7% (10% for ^{186}Os) must be folded into the values for σ_m.
[b] Care must be used comparing values for ^{186}Os with the rest because $E_{\gamma\max}$ is so much different.

Os
A=192

Os
A=192

Os
A=192

REF. B.L. Berman, D.D. Faul, R.A. Alvarez, P. Meyer, D.L. Olson
Phys. Rev. C19, 1205 (1979)

ELEM. SYM.	A	Z
Os	192	76

METHOD

REF. NO.	
79 Be 4	hg

REACTION	RESULT	EXCITATION ENERGY	SOURCE		DETECTOR		ANGLE
			TYPE	RANGE	TYPE	RANGE	
G, 1N	ABX	7-30	D	7-30	BF3-I		4PI
G, 2N	ABX	13-30	D	13-30	BF3-I		4PI
G, 3N	ABX	20-30	D	20-30	BF3-I		4PI

Photoneutron cross sections, including $\sigma[(\gamma,n) + (\gamma,pn)]$, $\sigma[(\gamma,2n) + (\gamma,p2n)]$, and $\sigma(\gamma,3n)$, were measured for ^{188}Os, ^{189}Os, ^{190}Os, and ^{192}Os from 7 to 30 MeV and for ^{186}Os from 11 to 20 MeV, with a photon energy resolution of about 300 keV. The source of radiation was the monoenergetic photon beam obtained from the annihilation in flight of fast positrons. The partial photoneutron cross sections were determined by neutron multiplicity counting, and the average neutron energies for each multiplicity were determined simultaneously with the cross-section data by the ring-ratio technique. Nuclear information extracted from the data includes parameters of the giant dipole and giant quadrupole resonances, integrated cross sections and their moments, nuclear symmetry energies, and nuclear deformation parameters and intrinsic quadrupole moments. No fewer than eight kinds of evidence point to a sudden change of behavior between ^{189}Os and ^{190}Os, which could be interpreted as a phase transition from a statically deformed prolate nucleus to a γ-unstable one, in general (but not detailed) agreement with the prediction of a dynamic-collective-model calculation.

[NUCLEAR REACTIONS ^{186,188,189,190,192}Os$(\gamma,n,2n,3n)$, E_γ=7–30 MeV; measured 4π neutron yield, multiplicities, average energies for monenergetic photons; $\sigma(E_\gamma,1n)$, $\sigma(E_\gamma,2n)$, $\sigma(E_\gamma,3n)$, GDR parameters, nuclear shape parameters, integrated cross sections and moments, GQR parameters, nuclear phase transition.]

TABLE IV. Parameters for classical theories (given in MeV).

Nucleus	E_m [a]	α [b]	β [c]	K [d]
^{186}Os	14.21 ± 0.06	81.1 ± 0.3	34.0 ± 0.1	28.9 ± 0.9
^{188}Os	14.19 ± 0.05	81.3 ± 0.3	34.0 ± 0.1	27.8 ± 0.5
^{189}Os	14.01 ± 0.04	80.4 ± 0.2	33.6 ± 0.1	27.3 ± 0.4
^{190}Os	13.83 ± 0.06	79.3 ± 0.3	33.1 ± 0.1	26.6 ± 0.7
^{192}Os	13.79 ± 0.04	79.6 ± 0.2	33.1 ± 0.1	26.3 ± 0.7

[a] Mean energy of the giant resonance, defined as $E_m = [E_m(1) + 2E_m(2)]/3$, except for ^{186}Os, for which $E_m = [E_m(1) + E_m(2)]/2$.
[b] Hydrodynamic parameter, defined by $E_m = \alpha A^{-1/3}$.
[c] Collective parameter, defined by $E_m = \beta A^{-1/6}$.
[d] Nuclear symmetry energy, computed from Eq. (2).

TABLE V. Nuclear shape parameters.

Nucleus	R_A [a]	η [b]	ϵ [c]	β_2 [d]	Q_0 [e] (b)
^{186}Os	0.95 ± 0.27	1.188 ± 0.016	0.366 ± 0.031	0.194 ± 0.016	5.76 ± 0.49
^{188}Os	0.44 ± 0.08	1.177 ± 0.011	0.346 ± 0.021	0.183 ± 0.011	5.49 ± 0.33
^{189}Os	0.51 ± 0.07	1.173 ± 0.008	0.338 ± 0.015	0.179 ± 0.008	5.38 ± 0.24
^{190}Os	0.32 ± 0.10	1.149 ± 0.015	0.292 ± 0.029	0.155 ± 0.015	4.65 ± 0.46
^{192}Os	0.30 ± 0.11	1.145 ± 0.016	0.283 ± 0.031	0.150 ± 0.016	4.55 ± 0.50

[a] Area ratio, defined as $\sigma_m(1)\Gamma(1)/\sigma_m(2)\Gamma(2)$.
[b] Deformation parameter, computed from $E_m(2)/E_m(1) = 0.911\eta - 0.089$.
[c] Nuclear eccentricity, computed from $\epsilon = (\eta^2 - 1)\eta^{-2/3}$.
[d] Deformation parameter, defined as $\frac{2}{3}(\pi/5)^{1/2}\epsilon$.
[e] Intrinsic quadrupole moment, computed from Eq. (8), with R_0 taken to be 1.26 fm.

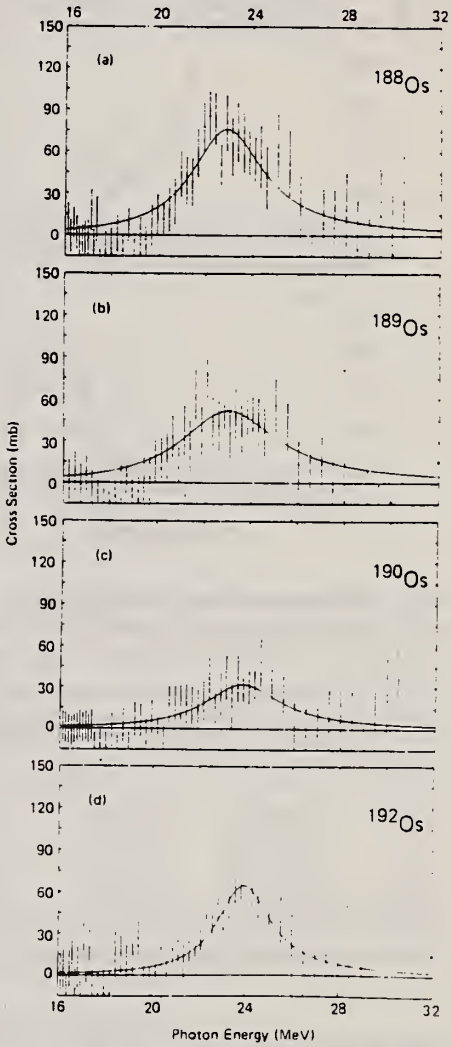

FIG. 14. Cross-section differences above the GDR; the two-component Lorentz-curve fits to $\sigma(\gamma,n_1)$ shown in part (a) of Figs. 3–6 were subtracted from the data points to give these differences, which were in turn fitted with the single-component Lorentz curves shown here as solid lines: (a) for ^{188}Os; (b) for ^{189}Os; (c) for ^{190}Os; (d) for ^{192}Os.

(over)

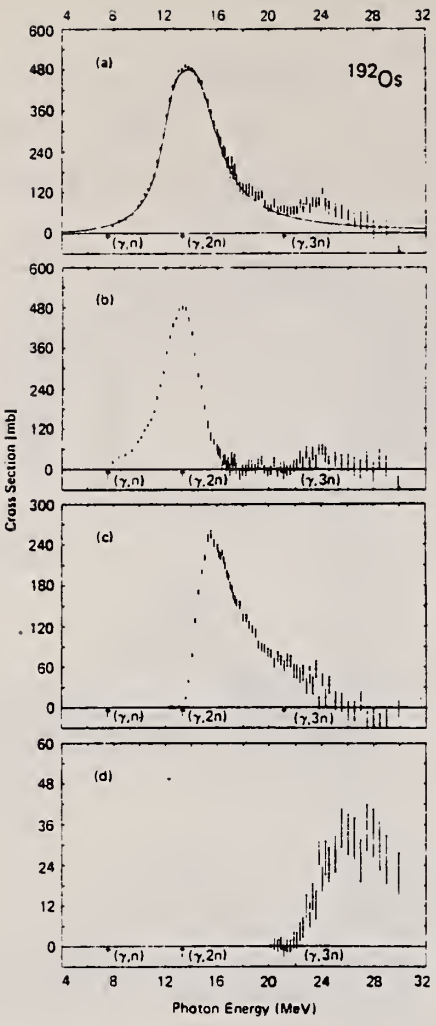

FIG. 6. Photoneutron cross sections for ^{192}Os: (a) $\sigma(\gamma,n_t)$, with a two-component Lorentz-curve fit; (b) $\sigma(\gamma,1n)$; (c) $\sigma(\gamma,2n)$; (d) $\sigma(\gamma,3n)$.

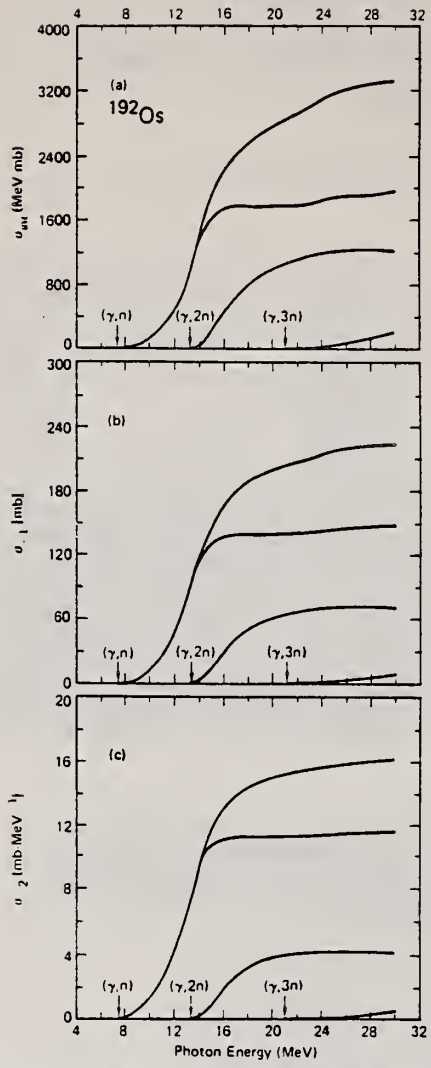

FIG. 12. Running sums of integrated cross sections for ^{192}Os: (a) σ_{int}; (b) σ_{-1}; (c) σ_{-2}.

TABLE IX. Integrated cross sections, $\sigma_{int}(\gamma,x)=\int\sigma(\gamma,x)dE_\gamma$, integrated from threshold to $E_{\gamma max}$. Uncertainties are discussed in Sec. II of the text.

Nucleus	$E_{\gamma max}$ (MeV)	$\sigma_{int}(\gamma,1n)$ (MeVb)	$\sigma_{int}(\gamma,2n)$ (MeVb)	$\sigma_{int}(\gamma,3n)$ (MeVb)	$\frac{\sigma_{int}(\gamma,2n)}{\sigma_{int}(\gamma,n_t)}$	$\frac{\sigma_{int}(\gamma,n_t)}{0.06NZ/A}$	$\frac{\frac{1}{2}\pi[\sigma_m(1)\Gamma(1)+\sigma_m(2)\Gamma(2)]}{0.06NZ/A}$
^{192}Os	19.67[b]	2.04	0.46	...	0.19	0.93 ± 0.09	1.15 ± 0.12
^{188}Os	30.42	2.62	0.88	0.12	0.24	1.33 ± 0.09	1.36 ± 0.08
^{190}Os	29.92	2.13	1.00	0.21	0.30	1.23 ± 0.09	1.24 ± 0.06
^{190}Os	30.42	2.01	1.08	0.14	0.33	1.18 ± 0.08	1.27 ± 0.10
^{192}Os	29.92	1.92	1.20	0.19	0.36	1.20 ± 0.08	1.27 ± 0.11

[a] Uncertainties listed here are relative; to obtain the absolute uncertainty a systematic uncertainty of 7% (10% for ^{186}Os) must be folded into the values for σ_m.
[b] Care must be used comparing values for ^{186}Os with the rest because $E_{\gamma max}$ is so much different.

TABLE III. Parameters of Lorentz-curve fits to the giant dipole resonance. Lorentz parameters defined by Eq. (1); the fitting interval for all cases is 10.8 to 18.8 MeV.

Nucleus	$E_m(1)$ (MeV)	$\sigma_m(1)$[a] (mb)	$\Gamma(1)$ (MeV)	$E_m(2)$ (MeV)	$\sigma_m(2)$[a] (mb)	$\Gamma(2)$ (MeV)	χ^2
^{186}Os	13.03 ± 0.09	308 ± 21	3.13 ± 0.24	15.26 ± 0.09	302 ± 23	3.38 ± 0.21	0.88
^{188}Os	12.81 ± 0.05	260 ± 18	2.76 ± 0.13	14.88 ± 0.07	390 ± 14	4.19 ± 0.13	0.96
^{190}Os	12.68 ± 0.04	268 ± 14	2.71 ± 0.10	14.68 ± 0.05	395 ± 11	3.62 ± 0.10	0.75
^{190}Os	12.68 ± 0.07	206 ± 29	2.60 ± 0.21	14.40 ± 0.09	401 ± 24	4.16 ± 0.11	1.10
^{192}Os	12.68 ± 0.06	206 ± 34	2.49 ± 0.23	14.35 ± 0.12	389 ± 26	4.41 ± 0.13	0.95

[a] Uncertainties for σ_m given here are relative. The absolute uncertainties are 7.7 (10.5 for ^{186}Os).

TABLE VI. Values for $B(E2,0^+\rightarrow 2^+)$ (in units of b^2).

Nucleus	Present experiment[a]	μ-mesic x rays[b]	Coulomb excitation[c]	Theory[d]	Theory[e]
^{186}Os	3.30 ± 0.56	3.15 ± 0.03	3.08 ± 0.21	2.96	3.05
^{188}Os	3.00 ± 0.36	2.84 ± 0.03	2.75 ± 0.12	2.72	2.75
^{190}Os	2.15 ± 0.43	2.48 ± 0.02	2.40 ± 0.11	2.59	2.54
^{192}Os	2.06 ± 0.46	2.10 ± 0.02	2.02 ± 0.09	2.56	2.34

[a] Computed from Eq. (9), using the values for Q_0 from Table V.
[b] From Ref. 26.
[c] Weighted average from Refs. 27 and 28.
[d] From Ref. 5.
[e] From Ref. 6.

REF. B.L. Berman, D.D. Faul, R.A. Alvarez, P. Meyer, D.L. Olson
Phys. Rev. C19, 1205 (1979)

ELEM. SYM.	A	Z
Os	192	76

METHOD

REF. NO.	
79 Be 4	hg

REACTION	RESULT	EXCITATION ENERGY	SOURCE		DETECTOR		ANGLE
			TYPE	RANGE	TYPE	RANGE	
G,1N	ABX	7-30	D	7-30	BF3-I		4PI
G,2N	ABX	13-30	D	13-30	BF3-I		4PI
G,3N	ABX	20-30	D	20-30	BF3-I		4PI

TABLE X. Integrated cross-section moments. $\sigma_{-1} = \int \sigma(\gamma, n_t) E_\gamma^{-1} dE_\gamma$ and $\sigma_{-2} = \int \sigma(\gamma, n_t) E_\gamma^{-2} dE_\gamma$, integrated from threshold to $E_{\gamma max}$.

Nucleus	σ_{-1} (mb)	$\sigma_{-1}A^{-4/3}$ (mb)	σ_{-2} (mb MeV^{-1})	$\frac{\sigma_{-2}}{0.00225A^{5/3}}$	$\frac{\tau_{-2}K}{0.05175A^{5/3}}$	$\frac{0.05175A^{5/3}}{\sigma_{-2}}$ (MeV)
^{186}Os[a]	179	0.168	13.2	0.97	1.22	23.8 ± 2.4
^{188}Os	239	0.222	16.7	1.20	1.45	19.1 ± 1.3
^{189}Os	228	0.210	16.7	1.19	1.41	19.3 ± 1.4
^{190}Os	220	0.202	15.8	1.12	1.30	20.6 ± 1.4
^{192}Os	224	0.203	16.0	1.12	1.31	20.6 ± 1.4

[a] Care must be used in comparing values for ^{186}Os with the rest because $E_{\gamma max}$ is so much different.

TABLE XII. Characteristics of the giant quadrupole resonance. The fitting interval used for the Lorentz-curve fits is 20–28 MeV.

Nucleus	E_q (MeV)	σ_q [a] (MeV)	Γ_q (MeV)	$E_q A^{1/3}$ (MeV)	$(1.60E_m)$ [b] (MeV)	$\frac{1}{2}\pi\sigma_q\Gamma_q$ (MeV mb)	(S_q/S_d) [c]	σ_{-2}(expt) [d] (mb MeV^{-1})	σ_{-2}(thy) [e] (mb MeV^{-1})
^{188}Os	22.8 ± 0.2	76 ± 6	3.8 ± 0.6	131	22.7	453 ± 107	0.12	0.87	0.49
^{189}Os	23.0 ± 0.3	51 ± 5	5.0 ± 1.0	132	22.4	407 ± 121	0.12	0.77	0.45
^{190}Os	23.8 ± 0.3	32 ± 4	4.0 ± 0.9	137	22.1	202 ± 71	0.06	0.36	0.47
^{192}Os	23.9 ± 0.1	65 ± 4	2.8 ± 0.4	138	22.1	288 ± 59	0.08	0.50	0.47

[a] Relative uncertainties.
[b] Theoretical prediction of Ref. 42 (see text). E_m is the GDR energy from Table IV.
[c] S_q is the quadrupole strength defined as $\frac{1}{2}\pi\sigma_q\Gamma_q$; S_d is the dipole strength defined as $\frac{1}{2}\pi[\sigma_m(1)\Gamma(1) + \sigma_m(2)\Gamma(2)]$.
[d] Computed as S_q/E_q^2.
[e] Computed from Eq. (12).

IRIDIUM
Z=77

Iridium is a precious heavy white metal with a density only exceeded by osmium. The metal is insoluble in acids and is not even attacked by aqua regia. The metal has no important applications because of difficulties in preparation and fabrication. The elements prinicipal use is in the preparation of platinum alloys.

Smithson Tennant, a British scientist, discovered the element by studying the small black residue —— for a time thought to be graphite —— which resulted from dissolving native platinum in aqua regia. Tennant named the material iridium because of the range of colors associated with its compounds.

T. Kaminishi, C. Kojima
Jap. J. Appl. Phys. 2, 399 (1963)

Ir		77

METHOD: Linac; isomer yield; activity

REF. NO.: 63 Ka 2 | NVB

REACTION	RESULT	EXCITATION ENERGY	SOURCE TYPE	SOURCE RANGE	DETECTOR TYPE	DETECTOR RANGE	ANGLE
G,G/	RLY	1	C 5		ACT-I		4PI
		(0.129, < 0.07)					

Table II. The isomers observed

Isomer	Observed value		Referenced value[11)13)]	
	Half-life	Energy (MeV)	Half-life	Energy (MeV)
Se-77m	17.5 sec	0.160	17.5 sec	0.161
Br-79m	4.80 sec	0.209	4.8 sec	0.208
Sr-87m	2.3 hr	0.390	2.8 hr	0.388
Y-89m	15.0 sec	0.920	14 sec	0.915
Rh-103m	58 min	*	57 min	0.040
Ag-107m	42 sec	0.95	44 sec	0.094
Ag-109m			40 sec	0.088
Cd-111m	47 min	0.150,0.255	49 min	0.150,0.247
In-115m	4.5 hr	0.335	4.5 hr	0.335
Sn-117m	17 day	0.160	14 day	0.159,0.161
Ba-137m	2.6 min	0.660	2.6 min	0.662
Er-167m	2.10 sec	0.209	2.5 sec	0.208
Hf-179m	18.5 sec	0.157,0.215	19 sec	0.161,0.217
W-183m	5.4 sec	0.200,0.170,0.115	5.5 sec	0.1025,0.2915 others
Ir-191m	4.90 sac	0.129, <0.07	4.9 sec	0.042-0.129
Pt-195m	4.5 day	0.065**	4.1 day	0.031-0.130
Au-197m	7.0 sec	0.10,0.27,0.40	7.2 sec	0.130,0.270,0.407
Hg-199m	43 min	0.160,0.370	42 min	0.158,0.368

* This isomer was measured with a G-M flow counter.
** This value corresponds to Pt-K X-ray energy.

Table III. Induced activation rate

Element	Beam energy (MeV)	Counting rate (×10000 cpm)	Sample form
Se	5	1300	metallic pellet
Br	4	1600	NaBr grain
Sr	6	0.3	$SrCO_3$ powder
Y	5	90	metallic grain
Rh	5	0.2 *	$RhCl_3$ grain
Ag	5	180	metallic plate
Cd	6	0.5	$CdCl_2$ grain
In	6	8	metallic plate
Sn	6	0.0005	metallic plate
Ba	5	0.6	BaS powder
Er	4	4900	Er_2O_3 powder
Hf	5	1600	metallic plate
W	5	120	metallic powder
Ir	5	2100	metallic powder
Pt	5	0.3	metallic plate
Au	4	4300	metallic plate
Hg	6	0.09	metallic liquid

* The value measured with a G-M flow counter.

REF.

A. Veres
Acta Phys. Acad. Sci. Hung. 16, 261-73 (1963)

ELEM. SYM.	A	Z
Ir		77

METHOD

Radioactive source

REF. NO. 63 Ve 2 NVB

REACTION	RESULT	EXCITATION ENERGY	SOURCE TYPE	SOURCE RANGE	DETECTOR TYPE	DETECTOR RANGE	ANGLE
G,G/	ABX	0-1	D	0-1	NAI-D		

ISØMERS

Таблица II

Измеренные значения после облучения, сравниваемые с другими литературными данными

Элемент	Активность облучения после первого измерения (имп/мин.)	Активн. экстрп. в конце облуч. (имп/мин.)	Лутературные данные $T_{1/2}$	Лутературные данные E (кэв)	Данные измерений $T_{1/2}$	Данные измерений E (кэв)	σ_m (10^{-28} см^2)	$\Gamma_{\gamma m}$ (10^{-4} эв)
Se-77m	3842±96	5400	17,5 сек.	160	18,1±1 сек.	160±10	9,5	1,75
Sr-87m	191±5	200	2,8 ч.	390	2,9±0,1 ч.	365±25	0,85	0,2
У-89m	96±20	170	16 сек.	910	16,7±5 сек.		0,08	0,02
Rh-103m	28±5	31	57 мин.	40	58±2 мин.	20,5±0,5	0,08	0,01
Ag-107m	220±14	250	44 сек.	93	43,8±0,6 сек	91±10	0,8	0,2
Ag-109m			39 сек.	88				
Hf-179m	80±18	155	19 сек.	160; 215	19±2 сек.		1	0,2
Ir-191m	90±20	250	4,9 сек.	42; 130	5±2 сек.		5,6	1
Pt-195m	90±9	100	3,5 д.	31; 100; 130;	3,5±0,2 д.	32±3 67,5±5 96±5 130±10	0,2	0,04
Au-197m	240±16	520	7,2 сек.	130; 277; 407	7,2±1 сек.	68:130: 280±20 390±20	0,07	0,01
Hg-199m	9,6±3,2		42 мин.	160; 370			0,005	0,001

Acta Phys. Hung. Tom. XVI. Fasc. 3.

REF. A. Veyssiere, H. Beil, R. Bergere, P. Carlos, A. Lepretre, A. De Miniac
J. Phys. Lett. 36, L267 (1975)

ELEM. SYM.	A	Z
Ir		77

METHOD

REF. NO. 75 Ve 5 egf

REACTION	RESULT	EXCITATION ENERGY	SOURCE		DETECTOR		ANGLE
			TYPE	RANGE	TYPE	RANGE	
G,N*	ABX	8- 22	D	8- 22	MOD-I		4PI
G,2N**	ABX	13- 22	D	8- 22	MOD-I		4PI

*1026+
**1027

Abstract. — Partial photoneutron cross-sections [$\sigma(\gamma, n) + \sigma(\gamma, pn)$], and $\sigma(\gamma, 2n)$ of W, Re, Ir, Pt and Hg were measured by means of monochromatic photons of 8 MeV $\leqslant E \leqslant$ 22 MeV so as to study the giant resonance. The experimentally observed evolution of the shape of the GDR, as one proceeds from permanently deformed prolate nuclei (W and Re) towards oblate or even triaxial gamma unstable nuclei (Pt), corresponds to the theoretical predictions of the dynamic collective model.

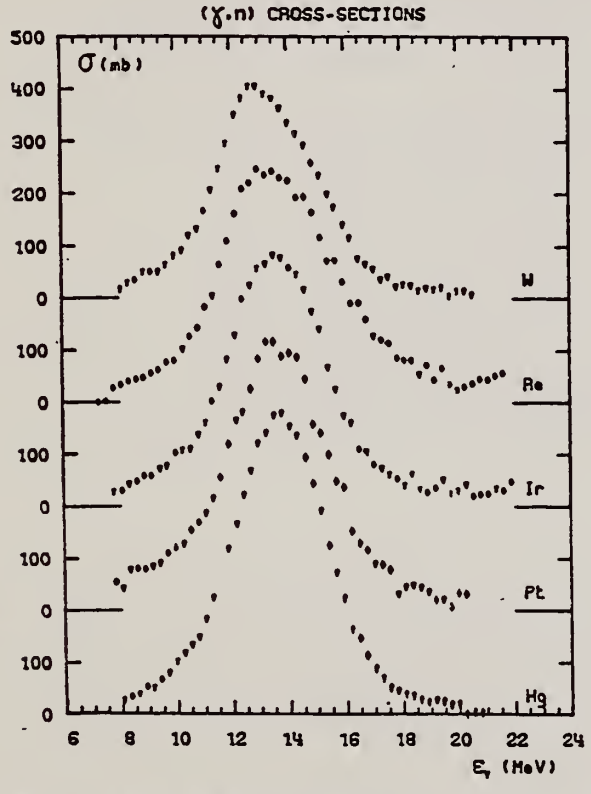

FIG. 1. — Sections efficaces partielles $\sigma(\gamma, n) + \sigma(\gamma, pn)$ des noyaux W, Re, Ir, Pt, Hg.

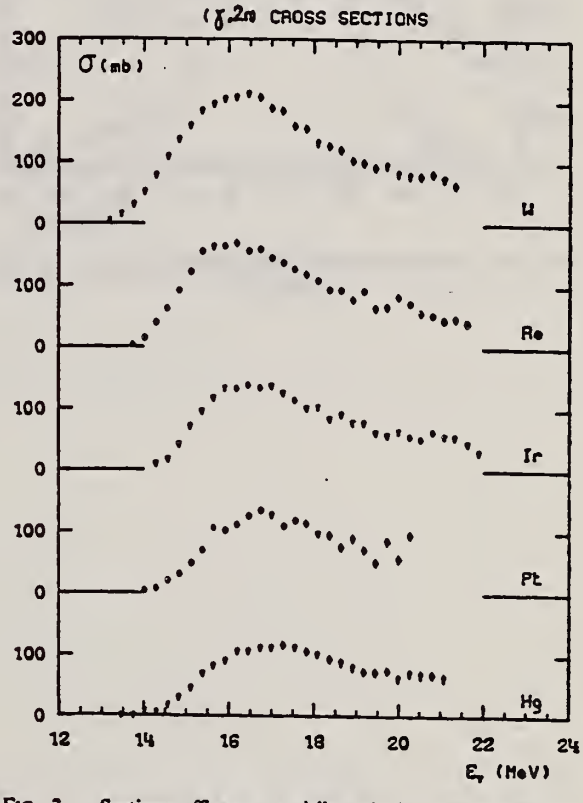

FIG. 2. — Sections efficaces partielles $\sigma(\gamma, 2n)$ des noyaux W, Re, Ir, Pt, Hg.

(over)

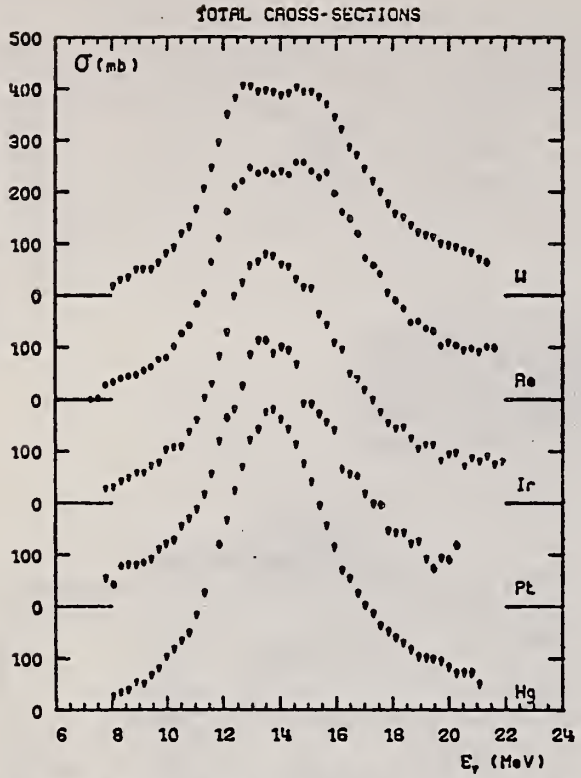

FIG. 3. — Sections efficaces totales $\sigma_T(E)$ des noyaux W, Re, Ir, Pt, Hg.

IR
A=191

IR
A=191

REF.
H. Langhoff
Phys. Rev. 136, B1590-93 (1964)

ELEM. SYM.	A	Z
Ir	191	77

METHOD
Radioactive source; centrifuge compensation

REF. NO. 64 La 4 NVB

REACTION	RESULT	EXCITATION ENERGY	SOURCE TYPE	SOURCE RANGE	DETECTOR TYPE	DETECTOR RANGE	ANGLE
G,G	LFT	0-1	D	0-1	NAI-D		125

539 keV level $\tau = (1.1^{+0.7}_{-0.3}) \times 10^{-11}$ sec.

(590 ± 15) keV level $5 \times 10^{-13} < \tau < 1.5 \times 10^{-11}$ sec.

TABLE I. $M1$ transition probabilities in Ir^{191}. The experimental information about the $M1$ transition probabilities T_{exp} (column 5) is obtained from the resonance fluorescence investigation and from lifetime measurements of the 129.5- and the 82.5-keV level. The assumed branching ratios $\Gamma_{\gamma M1}/\Gamma$ ($\Gamma_{\gamma M1}$ partial width for the $M1$ transitions, Γ total width) and spins are listed in columns 3 and 4. The results are compared with the transition probabilities expected from the Weisskopf formula and from the Nilsson model, T_{Wk} and $T_{Nilsson}$.

E_{level} (keV)	E_γ (keV)	$\Gamma_{\gamma M1}/\Gamma$	Assumed spins	T_{exp} 10^9 sec^{-1}	T_{Wk}/T_{exp}	Assignment	$T_{Nilsson}$ 10^9 sec^{-1}	$T_{Nilsson}/T_{exp}$
625	625	0.43	$\frac{5}{2} \rightarrow \frac{3}{2}$	<40	>110	(411)↑ − (402)↓	445	>11
	495	0.16	$\frac{5}{2} \rightarrow \frac{5}{2}$	<13	>180	− (402)↓	215	>16
	85	0.038	$\frac{5}{2} \rightarrow \frac{7}{2}$	< 3	> 4	− (411)↑	4.4	> 1.5
590	590					(402)↑ − (402)↓	5700	
539	539	0.35	$\frac{3}{2} \rightarrow \frac{3}{2}$	33	91	(411)↑ − (402)↓	640	19
	410	0.25	$\frac{3}{2} \rightarrow \frac{5}{2}$	23	57	− (402)↓	190	8
	457	0.09	$\frac{3}{2} \rightarrow \frac{1}{2}$	8.4	218	− (400)↑	40	5
	360	0.20	$\frac{3}{2} \rightarrow \frac{7}{2}$	19	47	− (400)↑	16	1
	188	0.012	$\frac{3}{2} \rightarrow \frac{9}{2}$	1.1	115	− (400)↑	0.6	0.5
129.5	129.5	0.23	$\frac{3}{2} \rightarrow \frac{3}{2}$	1.6[a]	26	(402)↓ − (402)↓	2.3	1
82.5	82.5	0.056	$\frac{1}{2} \rightarrow \frac{3}{2}$	0.010[b]	1000	(400)↓ − (402)↓	0.019	2

[a] Reference 13.
[b] Reference 14.

REF.

M. Schumacher, H. Langhoff
Phys. Rev. 162, 1153 (1967)

ELEM. SYM.	A	Z
Ir	191	77

METHOD

REF. NO.: 67 Sc 1 | egf

REACTION	RESULT	EXCITATION ENERGY	SOURCE		DETECTOR		ANGLE
			TYPE	RANGE	TYPE	RANGE	
G,G	LFT	0-1	D	0-1	SCD-D	0-1	125

539, 588 KEV

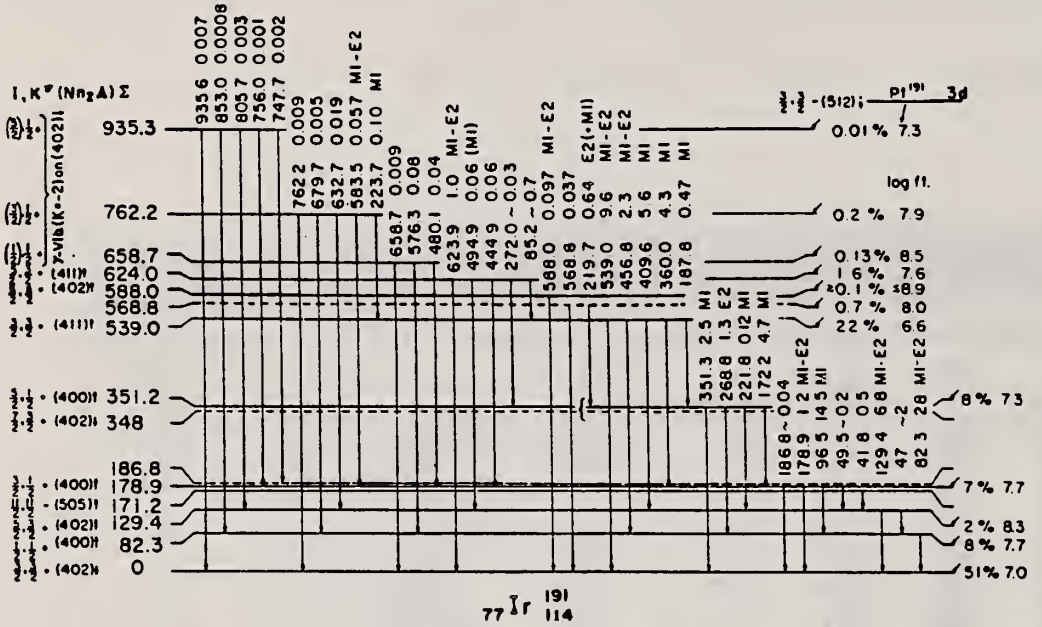

FIG. 5. Level scheme of Ir^{191} based on the presently available information, including the results of this investigation. The numbers associated with the transitions are the energies (keV) and the (γ+ce) intensities per 100 Pt^{191} decays. The quantum numbers assigned in terms of the Nilsson model are given on the left side. The transitions at 41.8, 47, 49.5, 85.2, 186.8, and 272.0 keV are taken from previous investigations (Refs. 2–4). Levels for which the existing evidence is weak are indicated by dashed lines. A detailed discussion is given in the text.

TABLE I. Results of the resonance-fluorescence experiment. g_1 and g_2 are the statistical weights of the ground state and excited state, respectively. Γ_0 represents the level width for the γ transition to the ground state and Γ the total level width. τ_{level} is the mean lifetime of the level. $(g_2\Gamma_0^2/g_1\Gamma)_{539\ keV}$ and $(g_2\Gamma_0^2/g_1\Gamma)_{588\ keV}$ are the weighted averages of the results of the present and the previous measurements.[a] Γ_0/Γ is calculated from the γ intensities given in Table II and from the conversion electron intensities given by Harmatz *et al.*[b]

E_γ(keV)	$g_2\Gamma_0^2/g_1\Gamma$(eV)	Γ_0/Γ	$I_i \rightarrow I_f$	τ_{level}(sec)
539	$(7.84\pm0.54)\times10^{-9}$	0.41 ± 0.02	$3/2 \rightarrow 3/2$	$(1.44\pm0.11)\times10^{-11}$
588	$(3.74\pm0.42)\times10^{-4}$	>0.5	$(5/2) \rightarrow 3/2$	$(1.76\pm0.20)(g_2/g_1)(\Gamma_0/\Gamma)^2\times10^{-11}$
624	$<1.5\times10^{-9}$	0.60	$5/2 \rightarrow 3/2$	$>2.4\times10^{-11}$
659	$<1.9\times10^{-8}$	7.0×10^{-2}		$>1.7g_2/g_1\times10^{-10}$

[a] Reference 1.
[b] Reference 2.

[1] H. Langhoff, Phys. Rev. 136, B1590 (1964).
[2] B. Harmatz, T. H. Handley, and J. W. Mihelich, Phys. Rev. 128, 1186 (1962).

REF. A. V. Davydov, G. R. Kartashov and Yu. V. Khrudev
Yad. Fiz. 7, 735 (1968)
Sov. J. Nucl. Phys. 7, 447 (1968)

ELEM. SYM.	A	Z
Ir	191	77

METHOD

REF. NO. 68 Da 1 hmg

REACTION	RESULT	EXCITATION ENERGY	SOURCE TYPE	SOURCE RANGE	DETECTOR TYPE	DETECTOR RANGE	ANGLE
$G,G	NOX	1	D	1	NAI-D		DST
		(129 keV)		(129 keV)			

Magnetic moment measured to be 3.00±0.58 nm MAG MOM

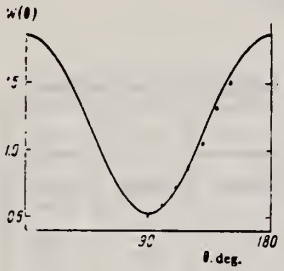

FIG. 3. Angular distribution of 129-keV γ quanta resonantly scattered by Ir^{191}. The experimental points are plotted for angles $\theta = \theta_0$ (see Fig. 2). The solid curves is the result of the reduction of the experimental data in accordance with formula (4).

REF. A.M. Goryachev and G.N. Zalesnyi
Yad. Fiz. 27, 1479 (June 1978)
Sov. J. Nucl. Phys. 27, 779 (June 1978)

ELEM. SYM.	A	Z
Ir	191	77

METHOD

REF. NO. 78 Go 3

hmg 11/17/80

REACTION	RESULT	EXCITATION ENERGY	SOURCE		DETECTOR		ANGLE
			TYPE	RANGE	TYPE	RANGE	
G,XN	ABX	8(8.1)-21	C	8-21	BF3-I	---	4PI

Photoneutron yield curves have been measured for the isotopes ^{191,193}Ir and ^{194,195,196,198}Pt in the bremsstrahlung beam of a betatron in the energy range 8–21 MeV with a 0.2-MeV step. For the isotopes ^{194,196,198}Pt we have also measured the photoneutron multiplicity curves. The measurements were made on-line with a computer. The cross sections were calculated from the yield curves by the Penfold-Leiss method with a 1.0-MeV step. The multiplicty curves were used to separate the contributions of (γ,n) and $(\gamma,2n)$ reactions. On the basis of the photoabsorption cross sections we have calculated the integrated cross sections, deformation parameters, and average energies. The existence of oblate deformation in these nuclei is not confirmed by the analysis of the measured cross sections.

n multiplicity measurement

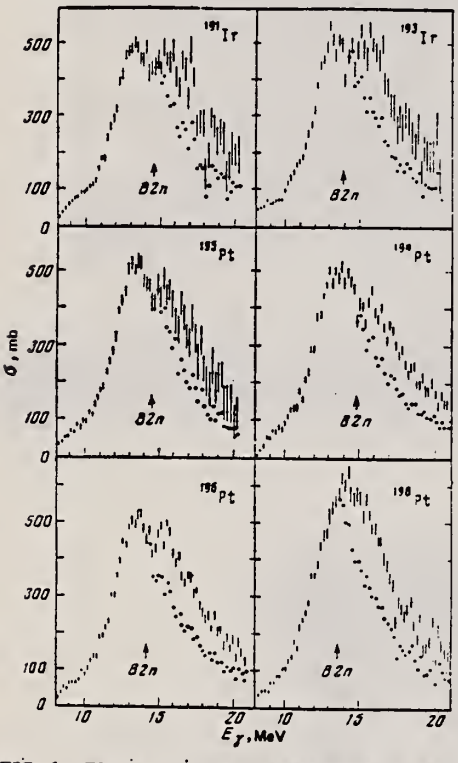

FIG. 1. Photoabsorption cross sections for the isotopes ^{191,193}Ir and ^{194,195,196,198}Pt. The vertical lines, whose length is equal to two standard deviations, show the experimental cross section. Above the $(\gamma,2n)$ threshold the photoabsorption cross section is designated by circles.

TABLE III. Integrated cross sections.

	^{191}Ir	^{193}Ir	^{194}Pt	^{195}Pt	^{196}Pt	^{198}Pt
σ_{int}, MeV·mb	2757±23	2835±30	2861±27	2797±25	2944±21	2813±32
$\sigma_{int}(\gamma, 2n)$, MeV·mb	–	–	626±9	–	744±9	1023±14
$\sigma_{int}L$, MeV·mb*	– 3741	– 3899	0.22 3759	– 3786	0.25 3884	0.36 3841
$\sigma_{int}L/60\,NZ/A$	1.38	1.40	1.34	1.34	1.38	1.35
σ_{-1}, mb	199±2.5	205±2	210±2	204±3	213±2.5	236±2
$\sigma_{-1}\cdot A^{-1/3}$	0.181	0.184	0.187	0.180	0.187	0.204
σ_{-2}, MeV^{-1}·mb	14.85±0.15	15.33±0.13	15.35±0.14	15.39±0.12	15.96±0.11	15.43±0.18
$\sigma_{-2}\cdot A^{-1/3}$	0.00234	0.00238	0.00236	0.00235	0.00241	0.00229

*Calculated in the case of validity of hypothesis 2) on the basis of the formula $\sigma_{int}\ L = (\pi/2)(\sigma_1\Gamma_1 + \sigma_2\Gamma_2)$.

σ_{int} corrected for neutron multiplicity

TABLE IV. Parameters of Lorentz curves.

Nucleus	E_1, MeV	Γ_1, MeV	σ_1, mb	E_2, MeV	Γ_2, MeV	σ_2, mb	$\sigma_1\Gamma_1/\sigma_2\Gamma_2$
^{191}Ir	12.85±0.04	2.70±0.07	294±8	14.82±0.09	5.30±0.21	299±10	0.5
^{193}Ir	13.01±0.04	2.61±0.06	317±10	14.77±0.09	6.44±0.31	257±12	0.5
^{194}Pt	12.98±0.04	2.59±0.07	308±10	14.54±0.10	5.33±0.22	299±11	0.5
^{195}Pt	12.99±0.05	2.70±0.07	296±10	14.59±0.11	5.46±0.27	293±15	0.5
^{196}Pt	13.07±0.05	2.72±0.08	303±11	14.40±0.12	5.97±0.29	276±13	0.5
^{198}Pt	13.06±0.05	2.87±0.09	284±12	14.34±0.14	6.27±0.34	260±16	0.5
^{198}Pt	13.58±0.02	4.45±0.06	514±6	–	–	–	–

TABLE V. Average energies.

Nucleus	E_M, MeV*	$E_M A^{1/3}$	$E_M A^{1/3}$	Nucleus	E_M, MeV*	$E_M A^{1/3}$	$E_M A^{1/3}$
^{191}Ir	14.16	81.6	34.0	^{195}Pt	14.06	81.5	33.9
^{193}Ir	14.18	82.0	34.1	^{196}Pt	13.96	81.1	33.6
^{194}Pt	14.01	81.1	33.7	^{198}Pt	13.91	81.1	33.6

*Calculated in the case of validity of hypothesis 2) according to the formula $E_M = (1/3)E_1 + (2/3)E_2$.

IR
A=193

IR
A=193

REF.

K. N. Geller, J. Halpern, and E. G. Muirhead
Phys. Rev. 118, 1302-12 (1960)

ELEM. SYM.	A	Z
Ir	193	77

METHOD

Betatron; neutron threshold; ion chamber

REF. NO.	
60 Ge 3	NVB

REACTION	RESULT	EXCITATION ENERGY	SOURCE		DETECTOR		ANGLE
			TYPE	RANGE	TYPE	RANGE	
G,N	NØX	THR	C THR		BF3-I		4 PI

THRESHØLD

TABLE I. Summary and comparison of neutron separation energies inferred from present threshold measurements with values predicted from mass data and reaction energies. All energies are expressed in the center-of-mass system in Mev.

Reaction	No. runs	Present results	Other results	Method	Reference
$Ir^{193}(\gamma,n)Ir^{192}$	1	7.79 ±0.05			

REF. F. R. Metzger
Phys. Rev. 161, 1249 (1967)
[See F. R. Metzger
Phys. Rev. C2, 2024 (1970)]

ELEM. SYM.	A	Z
Ir	193	77

METHOD

REF. NO. 67 Me 2 HMG

REACTION	RESULT	EXCITATION ENERGY	SOURCE		DETECTOR		ANGLE
			TYPE	RANGE	TYPE	RANGE	
G,G	LFT	0-1	D	0-1	SCD-D	0-1	105

TABLE II. Radiative widths of the Ir^{193} levels studied in this paper. The value of the partial radiative width for the transition listed in column 2 is given in column 6. The spin value assumed for the resonantly excited level is given in column 3, the ground-state branching ratio in column 4. The relative γ intensity used for the calculation of the radiative width is listed in column 5. For comparison purposes, columns 7 and 8 provide the single-particle estimates[a] for the $M1$ and $E2$ widths.

Level (keV)	E_γ (keV)	Spin	Γ_0/Γ	γ intensity in Os^{193} decay	Radiative width (10^{-6} eV)	$\Gamma(M1)_{sp}$ (10^{-6} eV)	$\Gamma(E2)_{sp}$ (10^{-6} eV)
559	559	$(\frac{9}{2})$	0.73	13	27±6	320	0.3
	486			<1.2	<10	210	0.14
	420			5.1[b]	10±2	140	0.07
557	557	$(\frac{7}{2})$	0.73	38	<12	320	0.3
	484			4.6[b]	<1.5	210	0.14
	418			<1.3	<0.4	140	0.07
460	460	$\frac{5}{2}$	0.48	100	1.6±0.3	180	0.11

[a] J. M. Blatt and V. F. Weisskopf, *Theoretical Nuclear Physics* (John Wiley & Sons, Inc., New York, 1952), Chap. 12.
[b] This intensity was calculated under the assumption that the corresponding transition from the other member of the 557–559 keV doublet is absent.

REF. F. R. Metzger
Phys. Rev. C2, 2024 (1970)

ELEM. SYM.	A	Z
Ir	193	77

METHOD

REF. NO. 70 Me 6 hmg

REACTION	RESULT	EXCITATION ENERGY	SOURCE		DETECTOR		ANGLE
			TYPE	RANGE	TYPE	RANGE	
G,G	LFT	0-1	D	0-1	SCD-D	0-1	105

SEE 67ME2

TABLE I. Mean lives of Ir^{193} levels. The values listed in columns 5–7 were determined using the delayed-coincidence technique. Multiplication by $(\Gamma_0/\Gamma)^2_{new}/(\Gamma_0/\Gamma)^2_{old}$ will adjust the lifetimes listed in column 4 to new values for the branching ratios.

Level energy (keV)	Spin	Γ_0/Γ	Res. scatt.	Mean lives in psec Avida *et al.* (Ref. 1)	Lindskog *et al.* (Ref. 2)	Välivaara *et al.* (Ref. 3)
460	$\frac{3}{2}$	0.43±0.02	16±3	27±7	20±13	22±8
557	$\frac{1}{2}$	0.54±0.04	<6		≤67	49±12
559	$\frac{5}{2}$	0.70±0.04	1.65±0.24	≤300	≤280	≤110

REF. A.M. Goryachev and G.N. Zalesnyi
Yad. Fiz. 27, 1479 (June 1978)
Sov. J. Nucl. Phys. 27, 779 (June 1978)

ELEM. SYM.	A	Z
193	Ir	77

METHOD

REF. NO. 78 Go 3

hmg 11/17/80

REACTION	RESULT	EXCITATION ENERGY	SOURCE		DETECTOR		ANGLE
			TYPE	RANGE	TYPE	RANGE	
G,XN	ABX	7(7.8)-21	C	8-21	BF3-I	---	4PI

Photoneutron yield curves have been measured for the isotopes ^{191,193}Ir and ^{194,195,196,198}Pt in the bremsstrahlung beam of a betatron in the energy range 8–21 MeV with a 0.2-MeV step. For the isotopes ^{194,196,198}Pt we have also measured the photoneutron multiplicity curves. The measurements were made on-line with a computer. The cross sections were calculated from the yield curves by the Penfold-Leiss method with a 1.0-MeV step. The multiplicty curves were used to separate the contributions of (γ,n) and $(\gamma,2n)$ reactions. On the basis of the photoabsorption cross sections we have calculated the integrated cross sections, deformation parameters, and average energies. The existence of oblate deformation in these nuclei is not confirmed by the analysis of the measured cross sections.

n multiplicity measurement

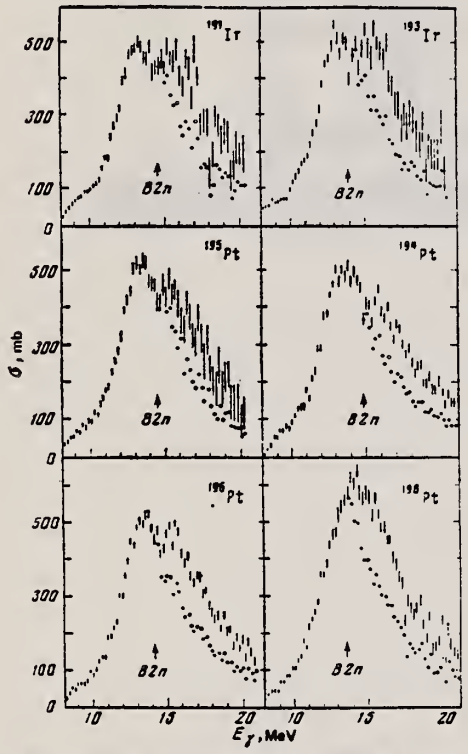

FIG. 1. Photoabsorption cross sections for the isotopes ^{191,193}Ir and ^{194,195,196,198}Pt. The vertical lines, whose length is equal to two standard deviations, show the experimental cross section. Above the $(\gamma,2n)$ threshold the photoabsorption cross section is designated by circles.

TABLE III. Integrated cross sections.

	^{191}Ir	^{193}Ir	^{194}Pt	^{195}Pt	^{196}Pt	^{198}Pt
σ_{int}, MeV·mb	2757±23	2835±30	2861±27	2797±25	2944±21	2813±32
$\sigma_{int}(\gamma,2n)$, MeV·mb	–	–	628±9	–	744±9	1023±14
	–	–	0.22	–	0.25	0.36
$\sigma_{int}L$, MeV·mb*	3741	3899	3759	3768	3884	3841
$\sigma_{int}L/60\,NZ/A$	1.36	1.40	1.34	1.34	1.38	1.35
σ_{-1}, mb	199±2.5	206±2	210±2	204±3	213±2.5	236±2
$\sigma_{-1}\cdot A^{-1/3}$	0.181	0.184	0.187	0.180	0.187	0.204
σ_{-2}, MeV^{-1}·mb	14.85±0.15	15.33±0.13	15.35±0.14	15.39±0.12	15.96±0.11	15.43±0.18
$\sigma_{-2}\cdot A^{-1/3}$	0.00234	0.00238	0.00236	0.00235	0.00241	0.00229

*Calculated in the case of validity of hypothesis 2) on the basis of the formula $\sigma_{int}\ L=(\pi/2)(\sigma_1\Gamma_1+\sigma_2\Gamma_2)$.

σ_{int} is corrected for neutron multiplicity

TABLE IV. Parameters of Lorentz curves.

Nucleus	E_1, MeV	Γ_1, MeV	σ_1, mb	E_2, MeV	Γ_2, MeV	σ_2, mb	$\sigma_1\Gamma_1/\sigma_2\Gamma_2$
^{191}Ir	12.85±0.04	2.70±0.07	294±8	14.82±0.09	5.30±0.21	299±10	0.5
^{193}Ir	13.01±0.04	2.61±0.06	317±10	14.77±0.09	6.44±0.31	257±12	0.5
^{194}Pt	12.96±0.04	2.59±0.07	308±10	14.54±0.10	5.33±0.22	299±11	0.5
^{195}Pt	12.99±0.05	2.70±0.07	296±10	14.59±0.11	5.46±0.27	293±15	0.5
^{196}Pt	13.07±0.05	2.72±0.08	303±11	14.40±0.12	5.97±0.29	276±13	0.5
^{198}Pt	13.06±0.05	2.87±0.09	284±12	14.34±0.14	6.27±0.34	260±16	0.5
^{198}Pt	13.58±0.02	4.45±0.08	514±6	–	–	–	–

TABLE V. Average energies.

Nucleus	E_M, MeV*	$E_M A^{1/3}$	$E_M A^{1/3}$	Nucleus	E_M, MeV*	$E_M A^{1/3}$	$E_M A^{1/3}$
^{191}Ir	14.16	81.6	34.0	^{194}Pt	14.08	81.5	33.9
^{193}Ir	14.18	82.0	34.1	^{195}Pt	13.96	81.1	33.6
^{194}Pt	14.01	81.1	33.7	^{196}Pt	13.91	81.1	33.6

*Calculated in the case of validity of hypothesis 2) according to the formula $E_M=(1/3)E_1+(2/3)E_2$.

PLATINUM
Z=78

Platinum is a silvery white, soft, ductile, metal valued as a powerful catalyst with a high resistance to chemical corrosion. The first known reference to the material was by Julius Caesar Scaliger (1557) who wrote about a substance found in the mines of Central America "which it has not hitherto been possible to melt by fire or by any of the Spanish arts". In the 18th Century there were references to *platina* —— an unwanted adjunct of gold in the mines of Columbia. The name *platina* is thought to have been a derogatory diminutive of plata, silver.

William Brownrigg, an English physician, did the first recorded experiments on platinum; the results were reported to the Royal Society in 1750. This publication stimulated other European scientists to study the new metal.

Pt

Pt

Ref. V.G. Shevchenko, B.A. Tur'ev

Zhur. Eksptl. i Teoret. Fiz. 42, 707 (1962)
Soviet Phys. JETP 15, 492 (1962)

Elem. Sym.	A	Z
Pt		78

Method: 35 MeV Betatron

Ref. No.: 62Sh2 — BG

Reaction	E or ΔE	E_o	Γ	$\int \sigma dE$	Jπ	Notes
(γ,p)	$E_{\gamma max}$= 22.5 33.5					Angular distribution of photoproton fitted to $a \pm b\sin^2\theta(1 + p\cos\theta)^2$ where a,b and p are given in the article. Quadrupole absorption is estimated to be about 60-70%.

Table II. Measured yields Y of photoprotons from Rh, Pt, and Pb, and estimates based on the evaporation model and on the direct photoeffect

Element	Rh		Pt	Pb
$E_{\gamma max}$, MeV	22.5	33.5	33.5	22.5
Y_{exp}, protons/mole-roentgen	$1.3 \cdot 10^3$	$2.8 \cdot 10^3$	$9.6 \cdot 10^4$	$2.9 \cdot 10^4$
Y_{exp}/Y_{evap}	~3	~6	~2000	~1500
Y_{exp}/Y_{direct}	~3	~4.5	~20	~11

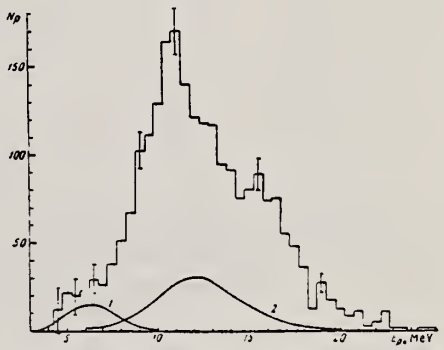

FIG. 3. Energy distribution of 2364 photoprotons from Pt for $E_{\gamma max}$ = 33.5 MeV. Same notation as in Figs. 1 and 2. The scale of curve 1 has been enlarged 50 times.

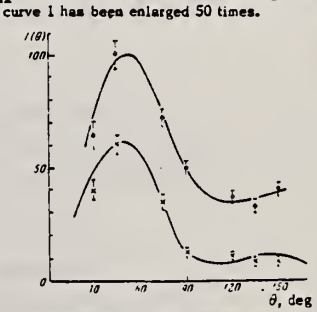

FIG. 7. Angular distributions of photoprotons from Pt for $E_{\gamma max}$ = 33.5 MeV. ●–E_p = 7.25–14.25 MeV; ×–E_p > 14.25 MeV.

Ref. V.G. Shevchenko, B.A. Yurev Nuclear Phys. 37, 495 (1962)	Elem. Sym. Pt	A	Z 78
Method: 35 MeV betatron; emulsions	Ref. No. 62 Sh 4		JHH

Reaction	E or ΔE	E_o	Γ	$\int \sigma dE$	Jπ	Notes
Pt (γ,p)	Bremss. 22.5 33.5					Parameters a, b and p for $\omega(\theta_p) = a + b \sin^2\theta\,(1 + p \cos\theta)^2$ in Table I.

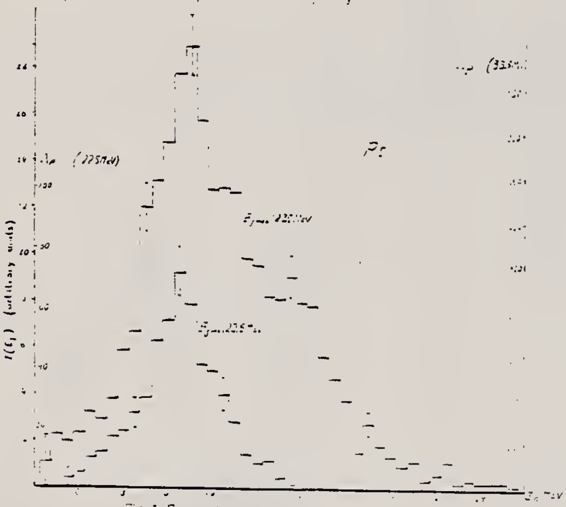

Fig. 5. Energy distribution [illegible]

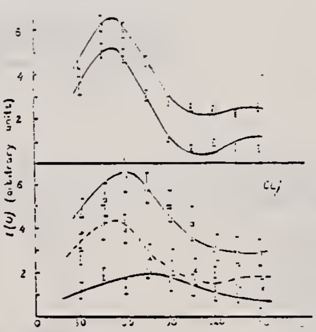

Fig. 10. Angular distributions of photoprotons [illegible]
a) The experimental points for $E_{\gamma max}$ = 22.5 MeV are [illegible] MeV, by solid squares for E_p = 8.75-11.75 MeV [illegible]
b) For the case of $E_{\gamma max}$ = 33.5 MeV crosses [illegible] 14.25 MeV

Coefficients of expressions of type [illegible] and estimates of the [illegible]

Element	Z	$E_{\gamma max}$ (MeV)	E_p (MeV)	a	b	p	[illegible]
Rh	45	22.5	3.25-9.25	1.9	0	0	0
			> 9.25	2.5	1.9	0.2	1
		33.5	3.25-9.25	12.2	0	0	[illegible]
			> 9.25	4.5	5.7	1.2	≈ 20
Pr	59	22.5	[illegible]-7.25	[illegible]	[illegible]	[illegible]	[illegible]
			7.25-11.25	2.9	[illegible]	0.32	[illegible]
			> 11.25	1.5	[illegible]	[illegible]	[illegible]
		33.5	4.5-7.25	[illegible]	[illegible]	[illegible]	≈ 15
			7.25-11.25	[illegible]	[illegible]	2.2	≈ 50
			> 11.25	[illegible]	[illegible]	1.5	≈ 40
W	74	22.5	6.25-8.75	3.5	[illegible]	0	[illegible]
			8.75-12.75	2.8	[illegible]	[illegible]	≈ 65
			> 12.75	2.2	[illegible]	[illegible]	≈ 75
		33.5	6.25-8.75	1.2	[illegible]	[illegible]	[illegible]
			8.75-12.75	1.8	[illegible]	2.0	≈ 55
			> 12.75	[illegible]	0.5	4.4	≈ 70
Pt	78	22.5	6.25-8.75	[illegible]	[illegible]	0.4	3
			8.75-11.75	2.5	[illegible]	1.2	≈ 20
			> 11.75	[illegible]	[illegible]	[illegible]	≈ 55
		33.5	7.25-11.25	[illegible]	[illegible]	[illegible]	≈ 55
			> 14.25	[illegible]	[illegible]	[illegible]	≈ 70
Pb	82	22.5	[illegible]	[illegible]	[illegible]	[illegible]	[illegible]
			[illegible]	[illegible]	[illegible]	[illegible]	≈ [illegible]
		33.5	[illegible]	[illegible]	[illegible]	[illegible]	[illegible]
			[illegible]	[illegible]	[illegible]	[illegible]	[illegible]
			[illegible]	[illegible]	[illegible]	[illegible]	[illegible]

Measured photoproton [illegible]

[illegible]	[illegible]	[illegible]	[illegible]	[illegible]

a) The yield Y_{exp} is expressed in protons per Mev per [illegible]

References

1) M. E. Toms and W. E. Stephens, Phys. Rev. 95 (1955) 926
2) M. M. Hoffman and A. G. W. Cameron, Phys. Rev. 92 (1953) 1184
3) W. C. Barber and V. I. [illegible], Nuclear Physics 16 [illegible] 651
4) M. E. Toms and W. E. Stephens, Phys. Rev. 92 (1953) 362
5) E. D. [illegible], JETP 33 [illegible]
6) R. B. Taylor, Nuclear Physics 19 [illegible] 478
7) A. G. W. Cameron, W. Harms and L. Katz, Phys. Rev. 83 (1951) [illegible]
8) V. G. [illegible], V. G. Shevchenko and N. P. Yudin, [illegible] at the Second All-Union Conf. for Nuclear Reactions at Low and Medium Energies, [illegible]
9) E. D. Courant, Phys. Rev. 82 (1951) 703
10) V. V. Balashov, V. G. Shevchenko and N. P. Yudin, JETP 41 (1961) [illegible]

Ref. V.G. Shevchenko, B.A. Yurev
Zhur. Eksp. i Teoret. Fiz. 42, 707 (1962);
Soviet Phys. JETP 15, 492 (1962)

Elem. Sym.	A	Z
Pt		78

Meth.
35 MeV betatron; emulsions

Ref. No.
62 Sh 7
JHH

Reaction	E or ΔE	E_0	Γ	$\int \sigma dE$	Jπ	Notes
Pt(γ,p)	Bremss. 33.5					

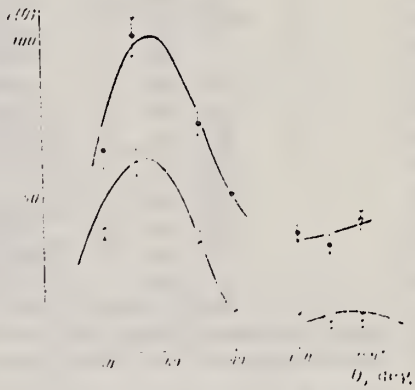

... Angular distributions of photoprotons from Pt for ... E_p 7.25–14.25 MeV; ×–E_p = 14.25 MeV.

Table I. Parameters of curves of $a + b\sin^2\vartheta(1 - p\cos\vartheta)^2$ and estimated contributions of E2 transitions

Element	Z	A	$E_{\gamma max}$, MeV	E_p, MeV	a	b	p	E2, %
[illegible]								

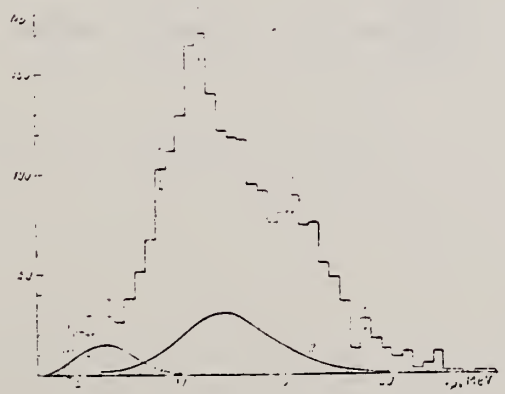

FIG. 3. Energy distribution of 2364 photoprotons from Pt for $E_{\gamma max}$ 33.5 MeV. Same notation as in Figs. 1 and 2. The scale of curve 1 has been enlarged 50 times.

Table II. Measured yields Y of photoprotons from Rh, Pt, and Pb, and estimates based on the evaporation model and on the direct photoeffect

Element	Rh	Pt	Pb
$E_{\gamma max}$, MeV	33.5	33.5	33.5
Y_{exp}, protons/mole-roentgen	[illegible]	[illegible]	[illegible]
Y_{exp}/Y_{evap}	~1	~6	~[illegible]
Y_{exp}/Y_{direct}	~1	~1.5	~20

T. Kamiishi, C. Kojima
Jap. J. Appl. Phys. 2, 399 (1963)

Pt		78

METHOD: Linac; isomer yield; activity

REF. NO.: 63 Ka 2 | NVB

REACTION	RESULT	EXCITATION ENERGY	SOURCE TYPE	SOURCE RANGE	DETECTOR TYPE	DETECTOR RANGE	ANGLE
G,G/	RLY	1	C 5		ACT-I		4PI
		(0.065)					

Table II. The isomers observed

Isomer	Observed value		Referenced value[11)13)]	
	Half-life	Energy (MeV)	Half-life	Energy (MeV)
Se-77m	17.5 sec	0.160	17.5 sec	0.161
Br-79m	4.80 sec	0.209	4.8 sec	0.208
Sr-87m	2.3 hr	0.390	2.8 hr	0.388
Y-89m	15.0 sec	0.920	14 sec	0.915
Rh-103m	58 min	*	57 min	0.040
Ag-107m	42 sec	0.95	44 sec	0.094
Ag-109m			40 sec	0.088
Cd-111m	47 min	0.150,0.255	49 min	0.150,0.247
In-115m	4.5 hr	0.335	4.5 hr	0.335
Sn-117m	17 day	0.160	14 day	0.159,0.161
Ba-137m	2.6 min	0.660	2.6 min	0.662
Er-167m	2.10 sec	0.209	2.5 sec	0.208
Hf-179m	18.5 sec	0.157,0.215	19 sec	0.161,0.217
W-183m	5.4 sec	0.200,0.170,0.115	5.5 sec	0.1025,0.2915 others
Ir-191m	4.90 sac	0.129, <0.07	4.9 sec	0.042-0.129
Pt-195m	4.5 day	0.065**	4.1 day	0.031-0.130
Au-197m	7.0 sec	0.10,0.27,0.40	7.2 sec	0.130,0.270,0.407
Hg-199m	43 min	0.160,0.370	42 min	0.158,0.368

* This isomer was measured with a G-M flow counter.
** This value corresponds to Pt-K X-ray energy.

Table III. Induced activation rate

Element	Beam energy (MeV)	Counting rate (×10000 cpm)	Sample form
Se	5	1300	metallic pellet
Br	4	1600	NaBr grain
Sr	6	0.3	$SrCO_3$ powder
Y	5	90	metallic grain
Rh	5	(0.2)*	$RhCl_3$ grain
Ag	5	180	metallic plate
Cd	6	0.5	$CdCl_2$ grain
In	6	8	metallic plate
Sn	6	0.0005	metallic plate
Ba	5	0.6	BaS powder
Er	4	4900	Er_2O_3 powder
Hf	5	1600	metallic plate
W	5	120	metallic powder
Ir	5	2100	metallic powder
Pt	5	0.3	metallic plate
Au	4	4300	metallic plate
Hg	6	0.09	metallic liquid

* The value measured with a G-M flow counter.

REF.

A. Veres
Acta Phys. Acad. Sci. Hung. 16, 261-73 (1963)

ELEM. SYM.	A	Z
Pt		78

METHOD

Radioactive source

REF. NO. 63 Ve 2 NVB

REACTION	RESULT	EXCITATION ENERGY	SOURCE		DETECTOR		ANGLE
			TYPE	RANGE	TYPE	RANGE	
G,G/	ABX	0-1	D	0-1	NAI-D		

ISØMERS

Таблица II

Измеренные значения после облучения, сравниваемые с другими литературными данными

Элемент	Активность облучения после первого измерения (имп/мин.)	Активн. экстрп. в конце облуч. (имп/мин.)	Литературные данные		Данные измерений		σ_m (10^{-28} см^2)	Γ_{ym} (10^{-3} эв)
			$T_{1/2}$	E (кэв)	$T_{1/2}$	E (кэв)		
Se-77m	3842±96	5400	17,5 сек.	160	18,1±1 сек.	160±10	9,5	1,75
Sr-87m	191±5	200	2,8 ч.	390	2,9±0,1 ч.	365±25	0,85	0,2
Y-89m	96±20	170	16 сек.	910	16,7±5 сек.		0,08	0,02
Rh-103m	28±5	31	57 мин.	40	58±2 мин.	20,5±0,5	0,08	0,01
Ag-107m	220±14	250	44 сек.	93	43,8±0,6 сек	91±10	0,8	0,2
Ag-109m			39 сек.	88				
Hf-179m	80±18	155	19 сек.	160; 215	19±2 сек.		1	0,2
Ir-191m	90±20	250	4,9 сек.	42; 130	5±2 сек.		5,6	1
Pt-195m	90±9	100	3,5 д.	31; 100; 130;	3,5±0,2 д.	32±3 67,5±5 96±5 130±10	0,2	0,04
Au-197m	240±16	520	7,2 сек.	130; 277; 407	7,2±1 сек.	68:130: 280±20 390±20	0,07	0,01
Hg-199m	9,6±3,2	-	42 мин.	160; 370			0,005	0,001

REF.

Yu.Ya. Glazunov, M.V. Savin, I.N. Safina, E.F. Fomushkin, Yu.A. Khokhlov
Zhur. Eksp. i Teoret. Fiz. 46, 1906-08 (1964)
Soviet Phys. JETP 19, 1284 (1964)

ELEM. SYM.	A	Z
Pt		78

METHOD

Linac

REF. NO.	
64 G1 1	NVB

REACTION	RESULT	EXCITATION ENERGY	SOURCE		DETECTOR		ANGLE
			TYPE	RANGE	TYPE	RANGE	
G,N	SPC	16	D	16	TØF-D	0-5	90

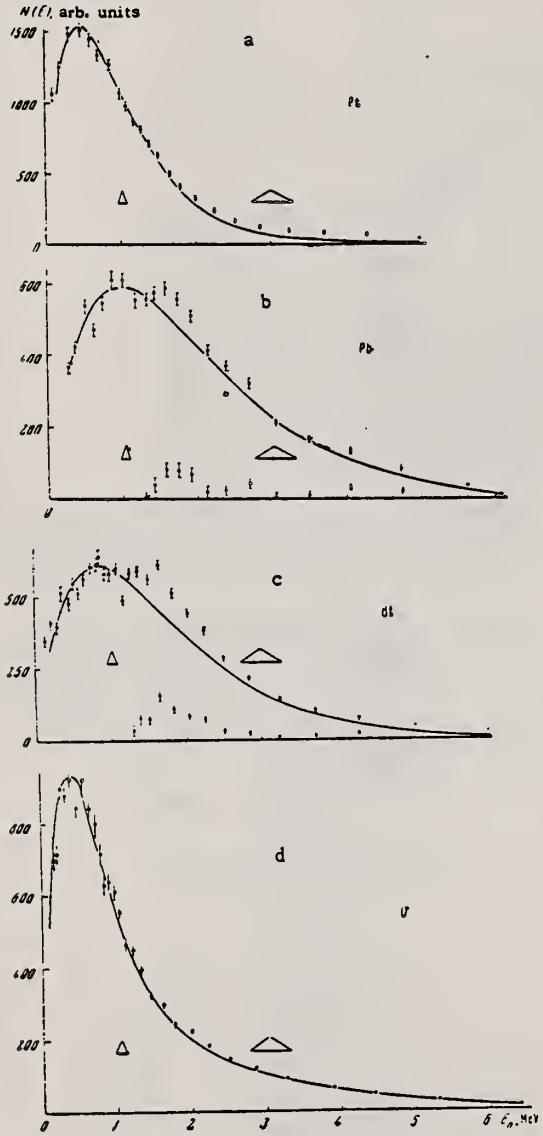

Photoneutron energy distributions.

shown in the figure. The solid curves a, b, and c are the evaporation spectra

$$N(E) \sim \frac{E}{T} \exp\left(-\frac{E}{T}\right)$$

with the temperature T = 0.48 ± 0.03 MeV for platinum, 0.84 ± 0.04 MeV for Bi, and 0.98 ± 0.04 MeV for lead.

The solid curve d is the sum of the evaporation spectrum and the fission spectrum of uranium:

$$N(E) = \alpha \frac{E}{T} \exp\left(-\frac{E}{T}\right) + (1-\alpha) \exp\left(-\frac{E}{T}\right) \times \frac{1}{\sqrt{\pi \omega T_f}} \exp\left(-\frac{E}{T_f}\right) \sinh \frac{\sqrt{\omega E}}{T_f}$$

with the parameters: T = 0.33 ± 0.03 MeV, T_f = 1.05 ± 0.04 MeV, ω = 0.5 MeV, α = 0.49 ± 0.01.

REF. G. Ben-David, B. Arad, J. Balderman, and Y. Schlesinger
Phys. Rev. 146, B852 (1966)

ELEM. SYM.	A	Z
Pt		78

METHOD

Nuclear Resonance Scattering using N,G reactions.

REF. NO. 66 Be 3 JDM

REACTION	RESULT	EXCITATION ENERGY	SOURCE TYPE	SOURCE RANGE	DETECTOR TYPE	DETECTOR RANGE	ANGLE
G,G	RLX	5 - 10	D	5 - 10	NAI-D	5 - 10	135

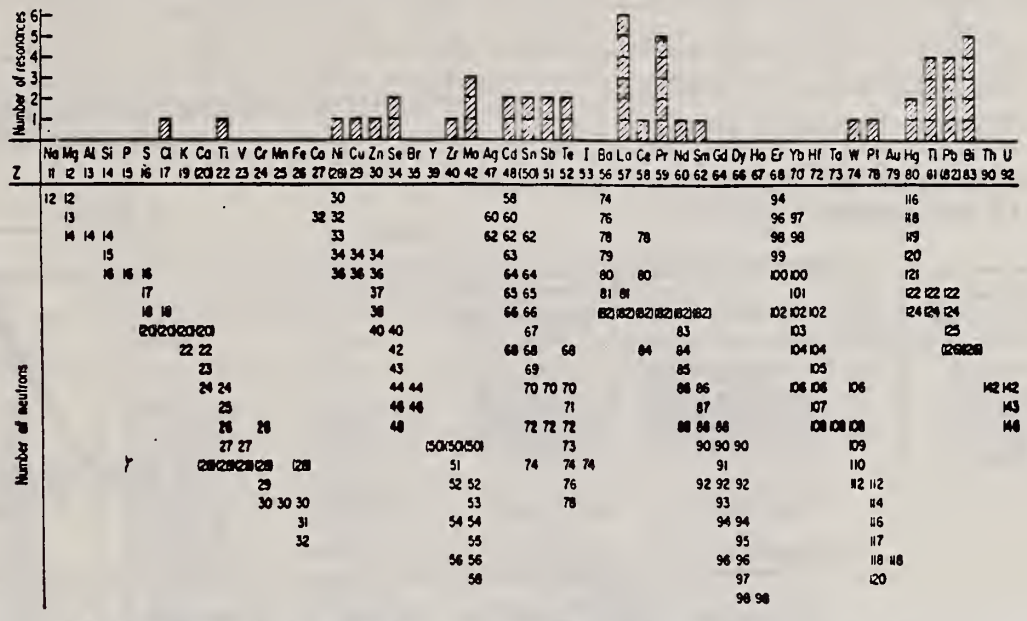

FIG. 3. Histogram of distribution of observed resonances among the different targets. The atomic number is given directly beneath the chemical symbol followed by the neutron numbers of the naturally occurring isotopes. Magic numbers are shown in brackets.

TABLE III. List of effective cross sections.

Scatterer	Energy (MeV)	Gamma source	δ (mb)	Scatterer	Energy (MeV)	Gamma source	δ (mb)
Sm^{144}	8.997	Ni	100	Sn	7.01	Cu	110
Pr^{141}	8.881	Cr	9	Nd	6.867	Co	30
La	8.532	Ni	6	Pr^{141}	6.867	Co	3
Te	8.532	Ni	3[a]	Te	6.7	Ni	...
Cu	8.499	Cr	24	La	6.54	Ag	12
Zr	8.496	Se	3050	Cd	6.474	Co	110
Zn	8.119	Ni	13	Mo	6.44	Hg	25[g]
Se	7.817	Ni	50	La	6.413	Ti	72
Se	7.76	K	90	Mo	6.413	Ti	10
Sb	7.67	V	...[b]	Tl	6.413	Ti	25
Cd	7.64	Fe	40[a]	W	~6.3	Ti	...[b]
Ni	7.64	Fe	7[a]	Sb	6.31	Hg	6[a]
Pr^{141}	7.64	Fe	12[a]	Ti	6.31	Hg	2[a]
Tl	7.64	Fe	370[a]	Sn	6.27	Ag	75
La	7.634	Cu	7	Pb^{206}	6.15	Gd	...[e]
Mo	7.634	Cu	11	Te	5.8	Ni	...[f]
Bi^{209}	7.634	Cu	4	La	6.12	Cl	35
Te	7.528	Ni	66[d]	Pr^{141}	6.12	Cl	110
Bi^{209}	7.416	Se	100	Pt	5.99	Hg	40[a,c]
Bi^{209}	7.300	As	80[a]	Tl	5.99	Hg	5[g]
Pb^{206}	7.285	Fe	4100	Pb^{206}	5.9	Sr	...[b]
Cl	7.285	Fe	34	Ce	5.646	Co	17
Pr^{141}	7.185	Se	80	Bi^{209}	5.646	Co	55
Tl	7.16	Cu	120	Pb^{206}	5.53	Ag	70
La	7.15	Mn	50	Hg	5.44	Hg	75[g]
Bi^{209}	7.149	Ti	2000	Hg	4.903	Co	385

[a] High-energy component of a complex spectrum.
[b] A broad scattered spectrum with no observable peak structure.
[c] There are actually two lines of energies 7.647 and 7.633 MeV having equal intensities in the iron capture gamma spectrum. The cross section has therefore been corrected, although there is no possibility at present of deciding which line is responsible for each resonance.
[d] Is probably an independent level in the complex spectrum of Ni γ rays on Te.
[e] Rough estimate.
[f] May be inelastic component from 7.528 level in Te.
[g] The relative line intensities in this case are due to Groshev and co-workers.
[h] No line is known for the source at this energy.
[i] Difficult to resolve among the many source lines present at this energy.

REF. A. V. Mitrofanova, Yu. N. Ranyuk, and P. V. Sorokin
J. Nucl. Phys. (USSR) 6, 703 (1967)
Sov. J. Nucl. Phys. 6, 512 (1968)

ELEM. SYM.	A	Z
Pt		78

METHOD

REF. NO.	
67 Mi 1	HMG

REACTION	RESULT	EXCITATION ENERGY	SOURCE		DETECTOR		ANGLE
			TYPE	RANGE	TYPE	RANGE	
G,F	ABX	300-999		300-999	TRK-I		

Detector: Fission fragment tracks in glass.

999 = 1600 MEV

Angular distribution measured for Pb was found isotropic; for other elements it was assumed isotropic.

Nucleus	Fissionability D	Cross section σ_K, $\mu\beta$	Nucleus	Fissionability D	Cross section σ_K, $\mu\beta$
Bi	0.11±0.01	7.8±0.6	Os	0.0058±0.0005	0.37±0.04
Pb	0.050±0.004	3.4±0.3	Re	0.0056±0.0006	0.35±0.04
Tl	0.031±0.003	2.1±0.2	Ta	0.0045±0.0005	0.27±0.03
Au	0.019±0.002	1.25±0.10	Hf	0.0042±0.0004	0.25±0.03
Pt	0.012±0.002	0.80±0.08			

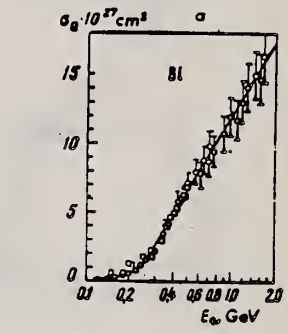

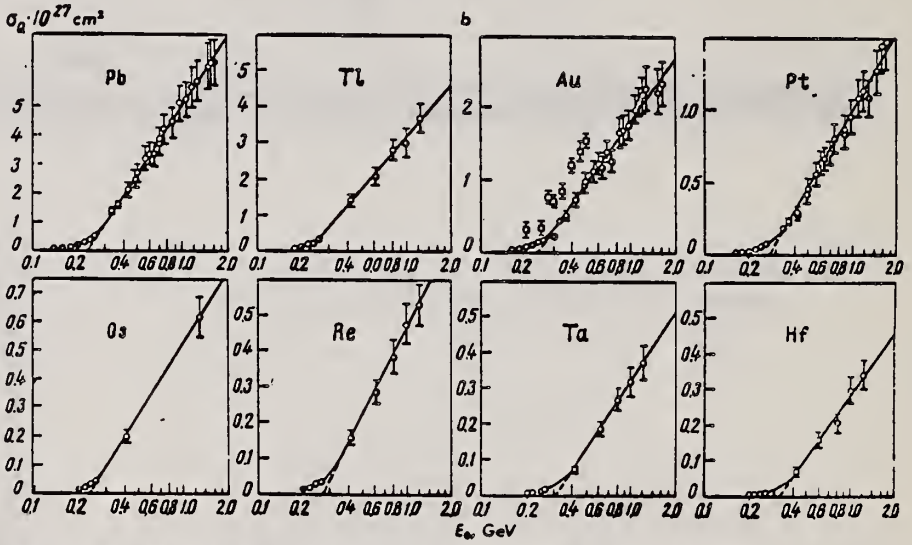

Fig. 1. Photofission fragment yields. ○-present work; □-Jungerman and Steiner.[1] The curves were plotted through the experimental points.

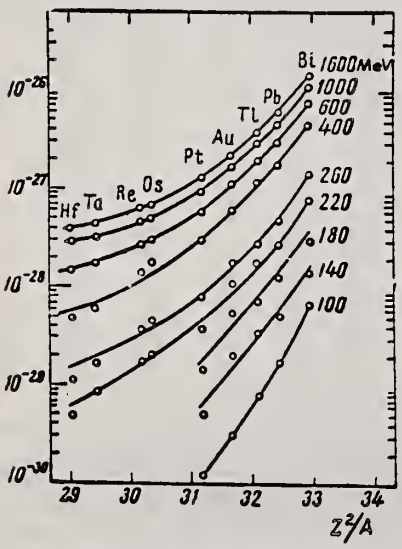

Fig. 2. Photofission fragment yields as a function of Z^2/A. The ordinates are values of σ_0 in units of cm².

REF. Yu. N. Ranyuk and P. V. Sorokin
J. Nucl. Phys. (USSR) 5, 37 (1967)
Sov. J. Nucl. Phys. 5, 26 (1967)

ELEM. SYM.	A	Z
Pt		78

METHOD

REF. NO. 67 Ra 2 HMG

REACTION	RESULT	EXCITATION ENERGY	SOURCE		DETECTOR		ANGLE
			TYPE	RANGE	TYPE	RANGE	
G,F	ABX	THR-260	C	100-260	EMU-I		DST

Angular distribution isotropic to 5%.

Table II

$E_{\gamma\,max}$, MeV	Cross section per equivalent γ quantum, 10^{-27} cm²			
	Bi	Pb	Au	Pt
100	0.07±0.005	0.017±0.002	0.003±0.0005	0.0012±0.0002
120	0.15±0.01	0.032±0.003	0.014±0.001	0.0035±0.0003
140	0.20±0.01	0.054±0.004	0.020±0.001	0.0053±0.0006
150 *	0.61±0.12	—	—	—
160	0.31±0.01	0.096±0.005	0.037±0.001	0.012±0.0005
180	0.46±0.02	0.13±0.01	0.055±0.001	0.015±0.001
180 *	0.68±0.09	—	—	—
200	0.62±0.02	0.20±0.01	0.082±0.002	0.031±0.001
200 *	1.3 ±0.24	—	0.31±0.09	—
200 **	0.7	—	—	—
220	0.83±0.03	0.28±0.01	0.108±0.003	0.039±0.001
240	1.22±0.03	0.36±0.01	0.146±0.003	0.063±0.001
240 **	1.5	—	—	—
250 *	1.78±0.22	—	0.33 ±0.07	—
260	1.50±0.04	0.50±0.02	0.180±0.004	0.085±0.002

* From [3].
** From [1].

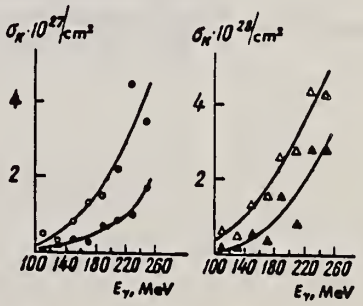

Fig. 3. Photofission cross sections. ○ – Bi, ● – Pb, △ – Au, ▲ – Pt. The curves were calculated from smoothed yield curves.

REF. J. W. Jury, J. S. Hewitt, and K. G. McNeill
Can. J. Phys. 46, 1823 (1968)

ELEM. SYM.	A	Z
Pt		78

METHOD

REF. NO. 68 Ju 1 EGF

REACTION	RESULT	EXCITATION ENERGY	SOURCE		DETECTOR		ANGLE
			TYPE	RANGE	TYPE	RANGE	
G,N	NOX	THR-27	C	27	THR	5-	DST

$$W(\theta) = a_0 + a_1 P_1 + a_2 P_2$$

TABLE I

Target element	Z	Energy	a_0*	a_1/a_0	a_2/a_0
Vanadium	23	32	640 ± 50	0.11 ± 0.10	−0.09 ± 0.11
Chromium	24	22	365 ± 39	0.02 ± 0.08	0.00 ± 0.10
Manganese	25	22	450 ± 33	0.07 ± 0.05	−0.11 ± 0.06
Bromine	35	27	874 ± 54	0.05 ± 0.06	−0.15 ± 0.08
Molybdenum	42	22	610 ± 60	0.09 ± 0.05	−0.35 ± 0.06
Ruthenium	44	27	1100 ± 25	0.12 ± 0.02	−0.29 ± 0.03
Rhodium	45	27	1270 ± 47	0.06 ± 0.03	−0.14 ± 0.03
Palladium	46	27	1350 ± 29	0.26 ± 0.02	−0.12 ± 0.02
Antimony	51	27	2140 ± 62	0.04 ± 0.08	−0.25 ± 0.11
Lanthanum	57	27	1940 ± 70	0.12 ± 0.10	−0.52 ± 0.14
Praseodymium	59	30	1800 ± 58	0.20 ± 0.08	−0.40 ± 0.09
Platinum	78	27	2600 ± 52	0.17 ± 0.02	−0.15 ± 0.03
Lead	82	22	2274 ± 59	0.08 ± 0.08	−0.46 ± 0.09

*The yield per mole per 100 r was normalized to a yield of 2274 for the lead sample at the same energy.

REF.

Yu. N. Ranyuk, V.M. Sanin, P.V. Sorokin
Ukr. Fiz. Zhur. 14, 408 (1969)

ELEM. SYM.	A	Z
Pt		78

METHOD

REF. NO.	
69 Ra 4	egf

REACTION	RESULT	EXCITATION ENERGY	SOURCE		DETECTOR		ANGLE
			TYPE	RANGE	TYPE	RANGE	
G,F	ABX	35-140	C	40-140	TRK-I		4PI

Yields of nuclear fission reaction for Bi, Au and Pt by bremsstrahlung were measured by means of solid state track detectors in the energy range from 40 to 140 MeV. The fission threshold for these nuclei is higher than the giant resonance energy which allowed total photofission cross-sections to be calculated by the yield curves.

A rapid increase of the cross-sections with the photon energy testifies to the preference of the statistical model within which the fission thresholds of target nuclei were calculated.

The results of the present experiment may be used to obtain information on the photon interaction mechanism in the energy region between the giant resonance and the threshold of meson production where this problem is still obscure.

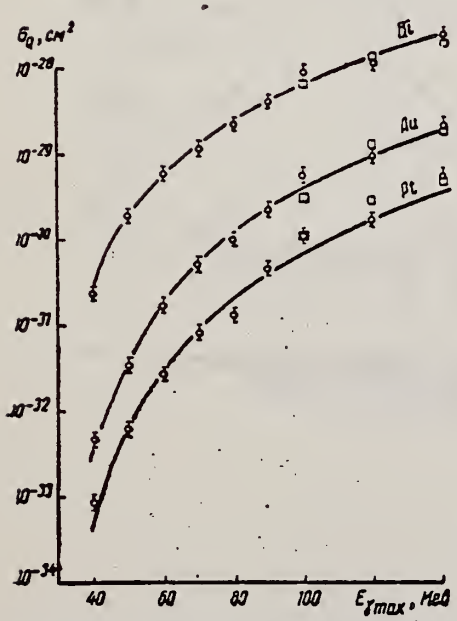

Рис. 2. Виходи уламків поділу: ○ — дані даної роботи, □ — дані роботи [3]. Суцільні криві одержані підгонкою за формулою (4).

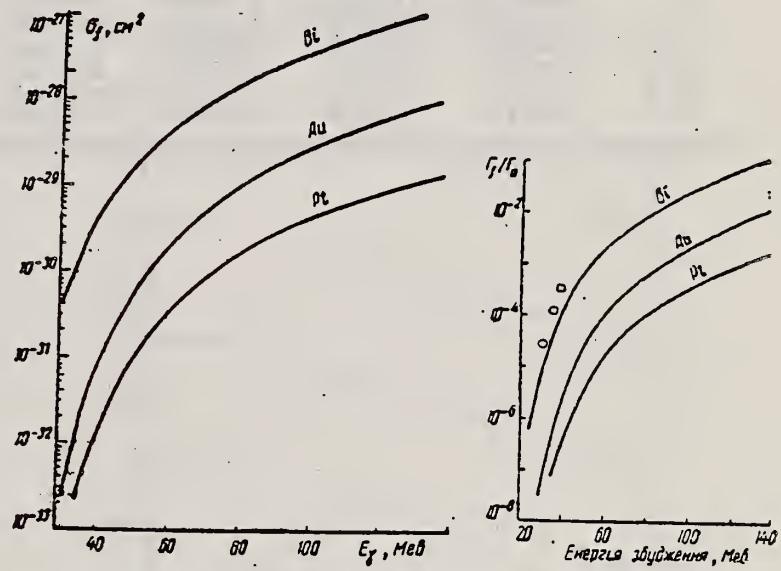

Рис. 3. Перерізи фотоподілу, розраховані на один реальний γ-квант підгонкою за формулою (4).

Рис. 4. Відношення ділильної і нейтронної ширин: □ — дані роботи [5] для суміші ізотопів Bi^{207} і Bi^{209}.

REF. E. Hayward, W. C. Barber, and Jed Sazama
Phys. Rev. C8, 1065 (1973)

ELEM. SYM.	A	Z
Pt		78

METHOD

REF. NO. 73 Ha 3 hmg

REACTION	RESULT	EXCITATION ENERGY	SOURCE		DETECTOR		ANGLE
			TYPE	RANGE	TYPE	RANGE	
$ G,G	RLY	15	D	15	NAI-D		90
		(15.1)		(15.1)			

POLARIZED PHOTONS

TABLE II. Results.

Target	$d\sigma^{\parallel}/d\Omega_F$ Arbitrary units	$d\sigma^{\perp}/d\Omega_F$ Arbitrary units	η_F	η	η(DCM)
Cd	0.042 ± 0.028	0.39 ± 0.05	0.11 ± 0.07	0.09 ± 0.07	0.19
Sn	0.084 ± 0.036	0.65 ± 0.06	0.13 ± 0.06	0.11 ± 0.06	0.07
Ta	0.24 ± 0.10	1.47 ± 0.14	0.16 ± 0.07	0.14 ± 0.07	0.20
W	0.52 ± 0.10	1.66 ± 0.12	0.31 ± 0.07	0.29 ± 0.07	0.20
Pt	0.23 ± 0.08	1.94 ± 0.13	0.12 ± 0.04	0.10 ± 0.04	0.08
Au	0.39 ± 0.11	2.08 ± 0.15	0.19 ± 0.06	0.17 ± 0.06	0.07
Bi	0.10 ± 0.15	2.65 ± 0.26	0.04 ± 0.06	0.02 ± 0.06	0

REF. A. Veyssiere, H. Beil, R. Bergere, P. Carlos, A. Lepretre, A. De Miniac
J. Phys. Lett. 36, L267 (1975)

ELEM. SYM.	A	Z
Pt		78

METHOD

REF. NO. 75 Ve 5 egf

REACTION	RESULT	EXCITATION ENERGY	SOURCE TYPE	SOURCE RANGE	DETECTOR TYPE	DETECTOR RANGE	ANGLE
G,N*	ABX	8- 22	D	8- 22	MOD-I		4PI
G,2N**	ABX	13- 21	D	8- 22	MOD-I		4PI

Abstract. — Partial photoneutron cross-sections [$\sigma(\gamma, n) + \sigma(\gamma, pn)$], and $\sigma(\gamma, 2n)$ of W, Re, Ir, Pt and Hg were measured by means of monochromatic photons of 8 MeV $\leq E \leq$ 22 MeV so as to study the giant resonance. The experimentally observed evolution of the shape of the GDR, as one proceeds from permanently deformed prolate nuclei (W and Re) towards oblate or even triaxial gamma unstable nuclei (Pt), corresponds to the theoretical predictions of the dynamic collective model.

*1029+
**1030

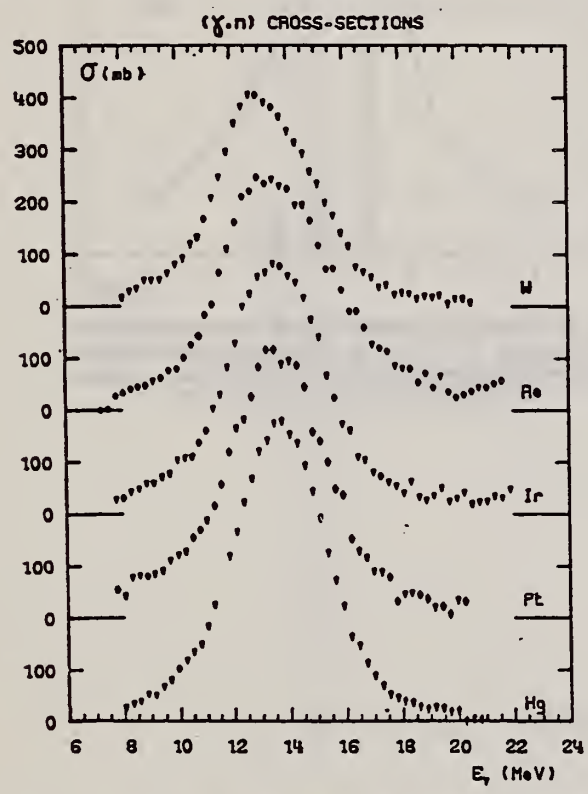

FIG. 1. — Sections efficaces partielles $\sigma(\gamma, n) + \sigma(\gamma, pn)$ des noyaux W, Re, Ir, Pt, Hg.

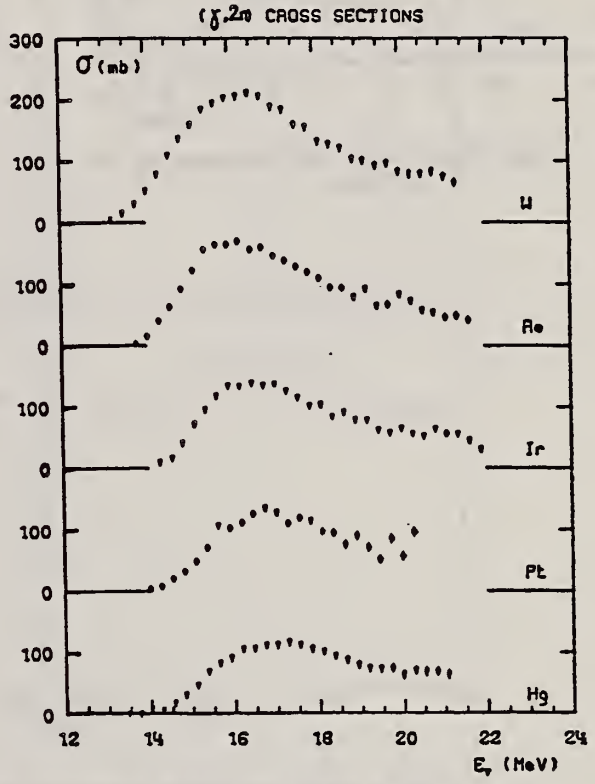

FIG. 2. — Sections efficaces partielles $\sigma(\gamma, 2n)$ des noyaux W, Re, Ir, Pt, Hg.

(over)

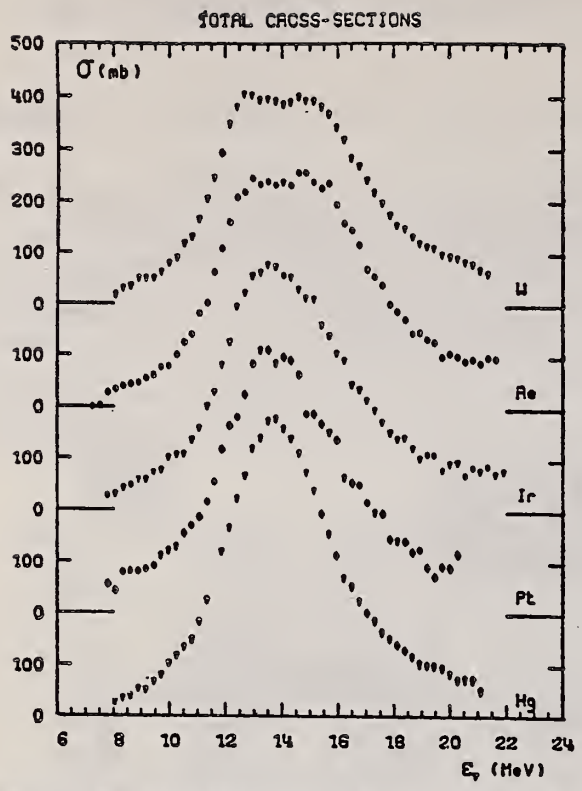

FIG. 3. — Sections efficaces totales $\sigma_T(E)$ des noyaux W, Re, Ir, Pt, Hg.

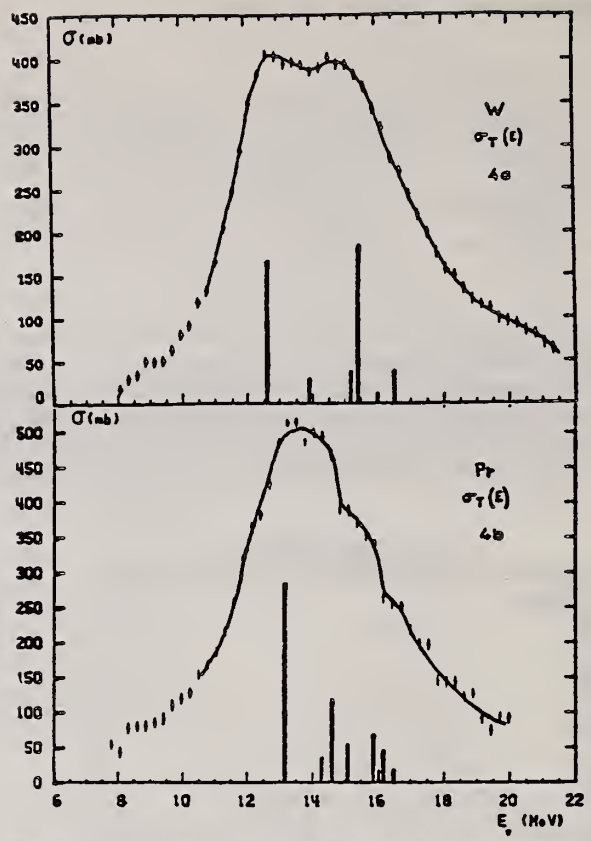

FIG. 4. — Comparaison des sections efficaces totales expérimentales $\sigma_T(E)$ des noyaux W et Pt avec les prédictions du modèle collectif dynamique [12] positionnées de façon à faire coïncider les énergies moyennes observées et calculées de la RGD.

REF. G. Bologna, V. Bellini, V. Emma, A.S. Figuera, S. Lo Nigro, C. Milone and G.S. Pappalardo
Il Nuovo Cimento 35A, 91 (1976)

ELEM. SYM.	A	Z
Pt		78

METHOD

REF. NO. 76 Bo 15 egf

REACTION	RESULT	EXCITATION ENERGY	SOURCE TYPE	SOURCE RANGE	DETECTOR TYPE	DETECTOR RANGE	ANGLE
G,F	RLX	220-500	D	220-500	TRK-I		4PI

COHERENT BREMS

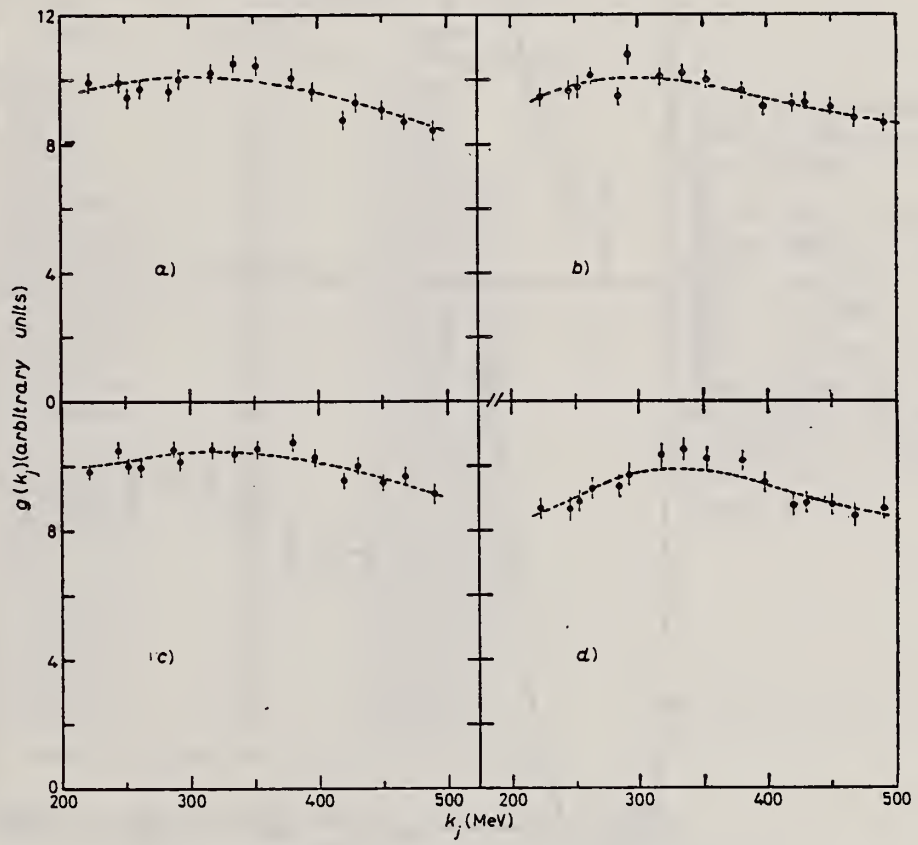

Fig. 6. – Photofission yields per equivalent quantum of Bi, Pb, Au and Pt as a function of the first peak energy k_j of photons. The dots are the experimental data; the dashed curves represent the yield functions estimated as described in sect. 5. *a*) Bi (γ, f), *b*) Pb (γ, f), *c*) Au (γ, f), *d*) Pt (γ, f).

over

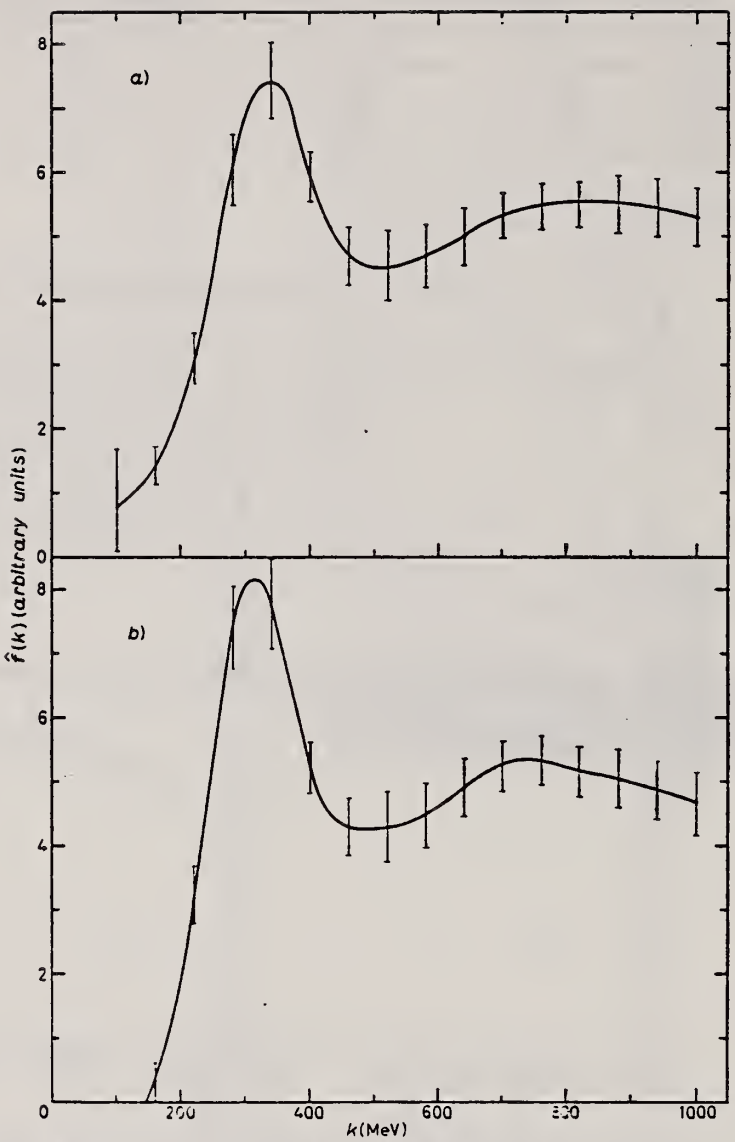

Fig. 8. – See caption to fig. 7. *a*) Au (γ, f), *b*) Pt (γ, f).

REF.	ELEM. SYM.	A	Z
V. Emma, S. Lo Nigro, C. Milone Nucl. Phys. A257, 438 (1976)	Pt		78

METHOD	REF. NO.	
	76 Em 2	egf

REACTION	RESULT	EXCITATION ENERGY	SOURCE		DETECTOR		ANGLE
			TYPE	RANGE	TYPE	RANGE	
G,F	ABY	THR-999	C	999	TRK-I		4PI

999 = 1 GEV

TABLE 1

Measured values of σ_q at $E = 1000$ MeV and deduced values of σ_k assumed constant from E_0 to 1000 MeV

Element	Z^2/A	σ_q (mb)	E_0 (MeV)	σ_k (mb)
Bi	32.96	12.3 ± 0.6	200	7.6 ± 0.6
Pb	32.45	5.4 ± 0.4	220	3.6 ± 0.3
Tl	32.10	4.1 ± 0.3	230	2.8 ± 0.3
Au	31.68	2.0 ± 0.15	240	1.4 ± 0.2
Pt	31.18	1.1 ± 0.08	255	$(8 \pm 0.7) \times 10^{-1}$
Re	30.21	$(3.7 \pm 0.3) \times 10^{-1}$	280	$(2.9 \pm 0.3) \times 10^{-1}$
W	29.78	$(3.5 \pm 0.3) \times 10^{-1}$	290	$(2.8 \pm 0.3) \times 10^{-1}$
Ta	29.45	$(3.3 \pm 0.3) \times 10^{-1}$	300	$(2.7 \pm 0.3) \times 10^{-1}$
Hf	29.04	$(1.7 \pm 0.2) \times 10^{-1}$	310	$(1.4 \pm 0.2) \times 10^{-1}$
Yb	28.31	$(1.3 \pm 0.1) \times 10^{-1}$	330	$(1.2 \pm 0.1) \times 10^{-1}$
Tm	28.18	$(7.5 \pm 0.8) \times 10^{-2}$	335	$(6.8 \pm 0.8) \times 10^{-2}$
Ho	27.21	$(3.6 \pm 0.4) \times 10^{-2}$	355	$(3.5 \pm 0.4) \times 10^{-2}$
Dy	26.80	$(2.6 \pm 0.3) \times 10^{-2}$	360	$(2.5 \pm 0.3) \times 10^{-2}$
Tb	26.58	$(2.5 \pm 0.3) \times 10^{-2}$	370	$(2.5 \pm 0.3) \times 10^{-2}$
Gd	26.04	$(1.6 \pm 0.2) \times 10^{-2}$	380	$(1.7 \pm 0.2) \times 10^{-2}$
Sm	25.56	$(1.3 \pm 0.2) \times 10^{-2}$	390	$(1.4 \pm 0.2) \times 10^{-2}$
Nd	24.96	$(9.2 \pm 0.9) \times 10^{-3}$	405	$(1 \pm 0.1) \times 10^{-2}$
Ce	24.00	$(8 \pm 0.9) \times 10^{-3}$	420	$(9 \pm 1) \times 10^{-3}$
La	23.39	$(8.4 \pm 0.9) \times 10^{-3}$	430	$(1 \pm 0.1) \times 10^{-3}$
Sb	21.36	$(1.2 \pm 0.2) \times 10^{-2}$	460	$(1.5 \pm 0.3) \times 10^{-2}$
Te	21.19	$(8.8 \pm 1) \times 10^{-3}$	465	$(1.2 \pm 0.2) \times 10^{-2}$
Sn	21.06	$(1.3 \pm 0.2) \times 10^{-2}$	465	$(1.7 \pm 0.3) \times 10^{-2}$
Cd	20.49	$(1.7 \pm 0.3) \times 10^{-2}$	470	$(2.2 \pm 0.4) \times 10^{-2}$
Ag	20.47	$(2 \pm 0.3) \times 10^{-2}$	470	$(2.6 \pm 0.4) \times 10^{-2}$
Zn	13.76	$(2 \pm 0.4) \times 10^{-1}$	515	$(3 \pm 0.6) \times 10^{-1}$
Cu	13.44	$(2.4 \pm 0.5) \times 10^{-1}$	515	$(3.6 \pm 0.8) \times 10^{-1}$
Ni	13.35	$(2.4 \pm 0.5) \times 10^{-1}$	510	$(3.6 \pm 0.8) \times 10^{-1}$
Fe	12.10	$(3 \pm 0.6) \times 10^{-1}$	510	$(4.4 \pm 0.9) \times 10^{-1}$

[4] A.V. Mitrofanova et al. Sov. J. Nucl. Phys. 6, 512 (1968).

[7] T. Methasiri et al., Nucl. Phys. A167, 97 (1971).

[12] J.R. Nix et al., Nucl. Phys. 81, 61 (1966).

[20] N.A. Perifilov et al., JETP (Sov. Phys.) 14, 623 (1962); Proc. Symp. on the physics & chemistry of fission, Salzburg 1965, vol. 2 (IAEA) Vienna, 1965, p.283.

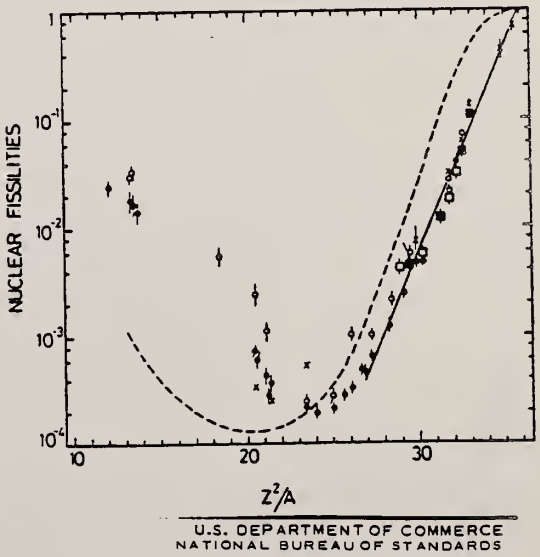

Fig. 2. Nuclear fissilities as a function of Z^2/A. Experimental points: solid circles represent our data; squares, the data from ref. [4]); open circles, the data from ref. [7]), and crosses, the data from (p,f) experiments[20]). The straight line is the best fit calculated from our data for $Z^2/A > 26$. The dashed curve is the curve VI calculated by Nix and Sassi[12]).

Pt
A=194

Pt
A=194

REF.

Yu. K. Shubnyi and Yu. A. Lysikov
Izv. Akad. Nauk SSSR Ser. Fiz. 36, 2531 (1972)
Bull. Acad. Sci. USSR Phys. Ser. 36, 2199 (1972)

ELEM. SYM.	A	Z
Pt	194	78

METHOD

REF. NO.: 72 Sh 13 hmg

REACTION	RESULT	EXCITATION ENERGY	SOURCE		DETECTOR		ANGLE
			TYPE	RANGE	TYPE	RANGE	
G,G	ABX	99*328	D	99*328	SCD-D		UKN

*ENERGY IN KEV

328 keV $\sigma = (3.5 \pm .5) \cdot 10^{-26} cm^2 \cdot sr^{-1}$
98.7 keV $\sigma = (1.8 \pm .3) \cdot 10^{-26} cm^2 \cdot sr^{-1}$

328 keV $\Gamma_{0\gamma} = (5.1 \pm .7) \cdot 10^{-11}$ sec

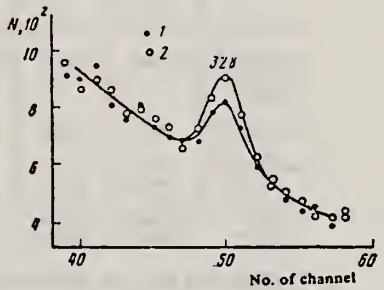

^{194}Pt

Fig. 1. Spectrum of the scattered radiation of ^{194}Ir for a source temperature of 1200° C. 1) Scattering by Ta; 2) scattering by Pt.

REF. A.M. Goryachev and G.N. Zalesnyi
Yad. Fiz. 27, 1479 (June 1978)
Sov. J. Nucl. Phys. 27, 779 (June 1978)

ELEM. SYM.	A	Z
Pt	194	78

METHOD

REF. NO. 78 Go 3

hmg 11/17/80

REACTION	RESULT	EXCITATION ENERGY	SOURCE		DETECTOR		ANGLE
			TYPE	RANGE	TYPE	RANGE	
G,XN	ABX	8(8.4)-21	C	8-21	BF3-I	---	4PI

Photoneutron yield curves have been measured for the isotopes ^{191,193}Ir and ^{190,195,196,198}Pt in the bremsstrahlung beam of a betatron in the energy range 8–21 MeV with a 0.2-MeV step. For the isotopes ^{194,196,198}Pt we have also measured the photoneutron multiplicity curves. The measurements were made on-line with a computer. The cross sections were calculated from the yield curves by the Penfold-Leiss method with a 1.0-MeV step. The multiplicity curves were used to separate the contributions of (γ,n) and $(\gamma,2n)$ reactions. On the basis of the photoabsorption cross sections we have calculated the integrated cross sections, deformation parameters, and average energies. The existence of oblate deformation in these nuclei is not confirmed by the analysis of the measured cross sections.

n multiplicity measurement

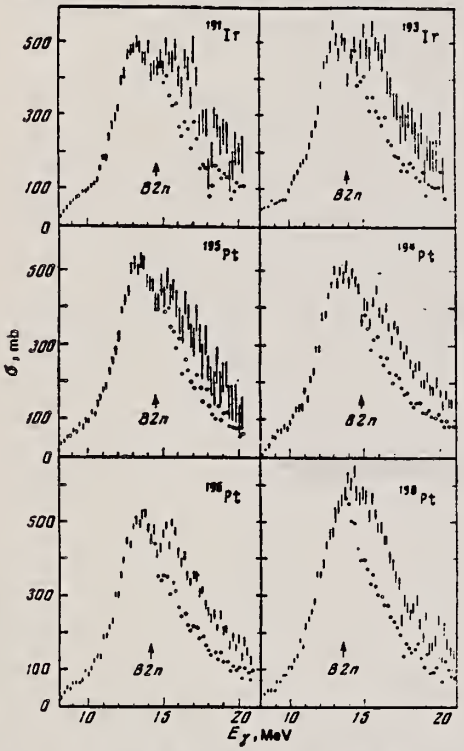

FIG. 1. Photoabsorption cross sections for the isotopes ^{191,193}Ir and ^{194,195,196,198}Pt. The vertical lines, whose length is equal to two standard deviations, show the experimental cross section. Above the $(\gamma,2n)$ threshold the photoabsorption cross section is designated by circles.

TABLE II. Parameters of photoneutron multiplicity curves.

Nucleus	σ, MeV^{-1}	W	χ^2/f	ϵ, MeV^{-1}	W	χ^2/f
^{194}Pt	6.3±0.7	0	1.07	21.16*	0.37±0.03	1.13
^{196}Pt	7.9±0.5	0	0.98	21.19*	0.29±0.02	1.04
^{198}Pt	8.2±0.6	0	1.15	20.2*	0.28±0.03	1.21

Note. Here f is the number of degrees of freedom; the asterisks denote level-density parameter values taken from Ref. 16.

TABLE III. Integrated cross sections.

	^{191}Ir	^{193}Ir	^{194}Pt	^{195}Pt	^{196}Pt	^{198}Pt
σ_{int}, MeV-mb	2757±23	2835±30	2861±27	2797±25	2944±21	2813±32
$\sigma_{int}(\gamma,2n)$, MeV-mb	–	–	626±9	–	744±9	1023±14
$\sigma_{int}L$, MeV-mb*	3741	3899	0.22 3759	– 3768	0.25 3884	0.36 3841
$\sigma_{int}L/60\,NZ/A$	1.36	1.40	1.34	1.34	1.38	1.35
σ_{-1}, mb	199±2.5	205±2	210±2	204±3	213±2.5	236±2
$\sigma_{-1}\cdot A^{-1/3}$	0.181	0.184	0.187	0.180	0.187	0.204
σ_{-2}, MeV^{-1}·mb	14.85±0.15	15.33±0.13	15.35±0.14	15.39±0.12	15.96±0.11	15.43±0.18
$\sigma_{-2}\cdot A^{-1/3}$	0.00234	0.00238	0.00236	0.00235	0.00241	0.00229

*Calculated in the case of validity of hypothesis 2) on the basis of the formula $\sigma_{int}\ L=(\pi/2)(\sigma_1\Gamma_1+\sigma_2\Gamma_2)$.

σ_{int} corrected for neutron multiplicity

TABLE IV. Parameters of Lorentz curves.

Nucleus	E_1, MeV	Γ_1, MeV	σ_1, mb	E_2, MeV	Γ_2, MeV	σ_2, mb	$\sigma_1\Gamma_1/\sigma_2\Gamma_2$
^{191}Ir	12.85±0.04	2.70±0.07	294±8	14.82±0.09	5.30±0.21	299±10	0.5
^{193}Ir	13.01±0.04	2.61±0.06	317±10	14.77±0.09	6.44±0.31	257±12	0.5
^{194}Pt	12.96±0.04	2.59±0.07	308±10	14.54±0.10	5.33±0.22	299±11	0.5
^{195}Pt	12.99±0.05	2.70±0.07	296±10	14.59±0.11	5.46±0.27	293±15	0.5
^{196}Pt	13.07±0.05	2.72±0.08	303±11	14.40±0.12	5.97±0.29	276±13	0.5
^{198}Pt	13.06±0.05	2.87±0.09	284±12	14.34±0.14	6.27±0.34	260±16	0.5
^{198}Pt	13.58±0.02	4.45±0.06	514±6	–	–	–	–

TABLE V. Average energies.

Nucleus	E_M, MeV*	$E_M A^{1/3}$	$E_M A^{1/3}$	Nucleus	E_M, MeV*	$E_M A^{1/3}$	$E_M A^{1/3}$
^{191}Ir	14.16	81.6	34.0	^{196}Pt	14.06	81.5	33.9
^{193}Ir	14.18	82.0	34.1	^{198}Pt	13.96	81.1	33.6
^{198}Pt	14.01	81.1	33.7	^{198}Pt	13.91	81.1	33.6

*Calculated in the case of validity of hypothesis 2) according to the formula $E_M=(1/3)E_1+(2/3)E_2$.

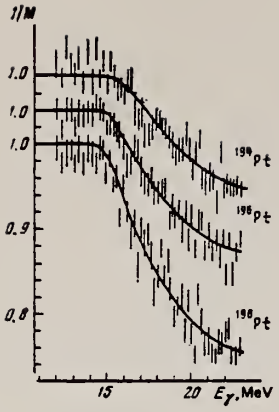

FIG. 2. Multiplicity of photoneutrons for the isotopes ^{194,196,198}Pt. The length of the vertical lines is equal to two standard deviations. The curves are a fit with the parameters given in Table II.

Pt
A=195

Pt
A=195

REF.

K. N. Geller, J. Halpern, and E. G. Muirhead
Phys. Rev. 118, 1302-12 (1960)

ELEM. SYM.	A	Z
Pt	195	78

METHOD

Betatron; neutron threshold; ion chamber

REF. NO. 60 Ge 3 NVB

REACTION	RESULT	EXCITATION ENERGY	SOURCE		DETECTOR		ANGLE
			TYPE	RANGE	TYPE	RANGE	
G,N	NØX	THR	C THR		BF3-I		4 PI

THRESHØLD

TABLE I. Summary and comparison of neutron separation energies inferred from present threshold measurements with values predicted from mass data and reaction energies. All energies are expressed in the center-of-mass system in Mev.

Reaction	No. runs	Present results	Other results	Method	Reference
$Pt^{196}(\gamma,n)Pt^{194}$	2	6.205±0.044	6.09 ±0.06	mass data	q
			6.07 ±0.04	$Pt^{194}(n,\gamma)Pt^{195}$	e

[q] W. H. Johnson, Jr., and V. B. Bhanot, Phys. Rev. 107, 6 (1957).

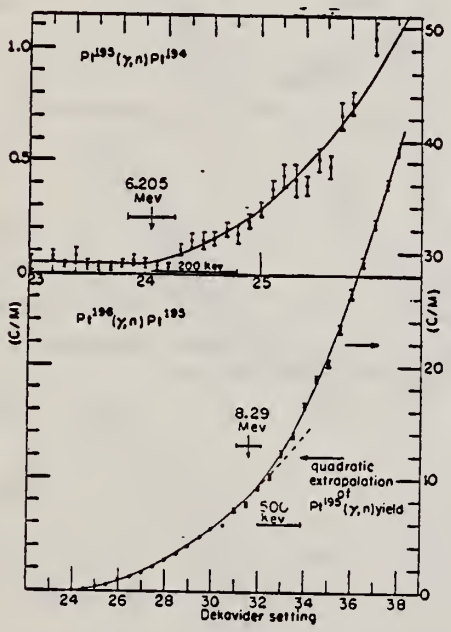

FIG. 9. Neutron yield data for platinum from 5.94 Mev to 9.96 Mev.

REF.

Yu. K. Shubnyi and Yu. A. Lysikov
Izv. Akad. Nauk SSSR Ser. Fiz. 36, 2531 (1972)
Bull. Acad. Sci. USSR Phys. Ser. 36, 2199 (1972)

ELEM. SYM.	A	Z
Pt	195	78

METHOD

REF. NO. 72 Sh 13 hmg

REACTION	RESULT	EXCITATION ENERGY	SOURCE		DETECTOR		ANGLE
			TYPE	RANGE	TYPE	RANGE	
G,G	ABX	99*328	D	99*328	SCD-D		UKN

*ENERGY IN KEV

98.7 keV $\Gamma_{0\gamma} = (1.2 \pm .2) \cdot 10^{-9}$ sec

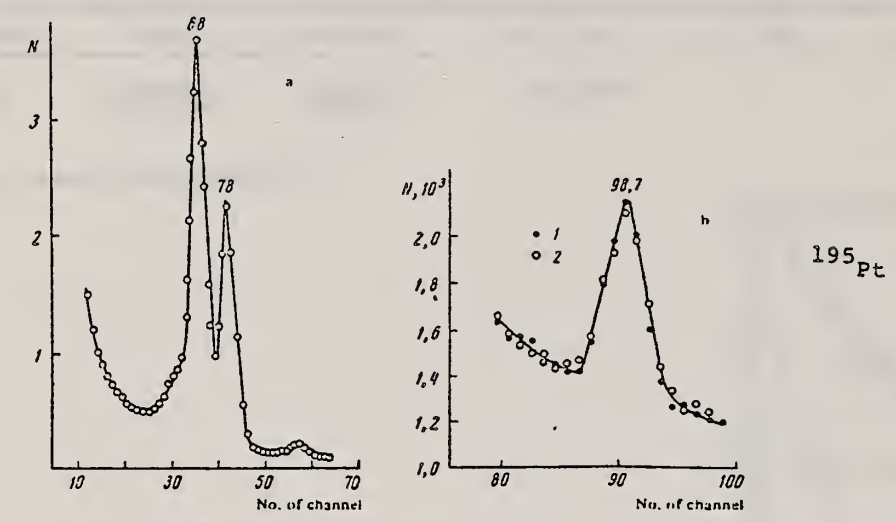

Fig. 2. Spectrum of scattered γ-radiation of ^{195}Au: a) 40-110 keV; b) scattering of 98.7 keV γ-quanta (1) scattering by Pt; 2) scattering by Ta).

REF. A.M. Goryachev and G.N. Zalesnyi
Yad. Fiz. 27, 1479 (June 1978)
Sov. J. Nucl. Phys. 27, 779 (June 1978)

ELEM. SYM.	A	Z
Pt	195	78

METHOD

REF. NO. 78 Go 3

hmg 11/17/80

REACTION	RESULT	EXCITATION ENERGY	SOURCE		DETECTOR		ANGLE
			TYPE	RANGE	TYPE	RANGE	
G,XN	ABX	6(6.1)-21	C	8-21	BF3-I	---	4PI

Photoneutron yield curves have been measured for the isotopes ^{191,193}Ir and ^{194,195,196,198}Pt in the bremsstrahlung beam of a betatron in the energy range 8–21 MeV with a 0.2-MeV step. For the isotopes ^{194,196,198}Pt we have also measured the photoneutron multiplicity curves. The measurements were made on-line with a computer. The cross sections were calculated from the yield curves by the Penfold-Leiss method with a 1.0-MeV step. The multiplicty curves were used to separate the contributions of (γ,n) and $(\gamma,2n)$ reactions. On the basis of the photoabsorption cross sections we have calculated the integrated cross sections, deformation parameters, and average energies. The existence of oblate deformation in these nuclei is not confirmed by the analysis of the measured cross sections.

n multiplicity measurement

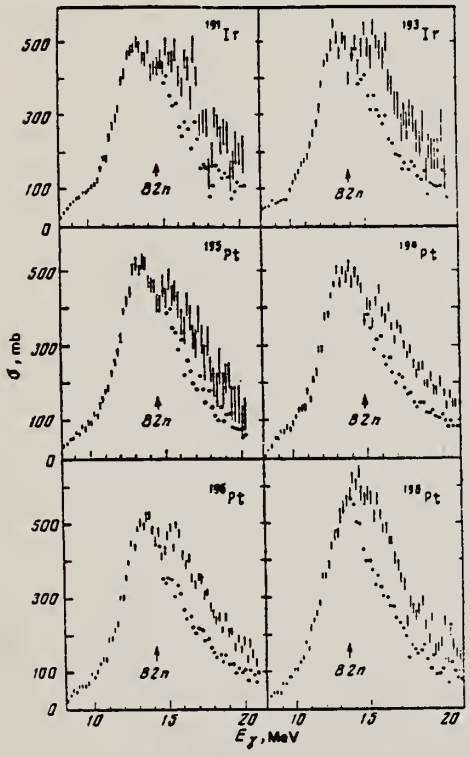

FIG. 1. Photoabsorption cross sections for the isotopes ^{191,193}Ir and ^{194,195,196,198}Pt. The vertical lines, whose length is equal to two standard deviations, show the experimental cross section. Above the $(\gamma,2n)$ threshold the photoabsorption cross section is designated by circles.

TABLE II. Parameters of photoneutron multiplicity curves.

Nucleus	ϵ, MeV^{-1}	w	χ^2/f	ϵ, MeV^{-1}	w	χ^2/f
^{194}Pt	8.3±0.7	0	1.07	21.16 *	0.37±0.03	1.13
^{196}Pt	7.9±0.5	0	0.98	21.19 *	0.29±0.02	1.04
^{198}Pt	8.2±0.6	0	1.15	20.2 *	0.28±0.03	1.21

Note. Here f is the number of degrees of freedom; the asterisks denote level-density parameter values taken from Ref. 16.

TABLE III. Integrated cross sections.

	^{191}Ir	^{193}Ir	^{194}Pt	^{196}Pt	^{198}Pt	^{198}Pt
σ_{int}, MeV-mb	2757±23	2835±30	2861±27	2797±25	2944±21	2813±32
$\sigma_{int}(\gamma,2n)$, MeV-mb	–	–	826±9	–	744±9	1023±14
	–	–	0.22	–	0.25	0.36
$\sigma_{int}L$, MeV-mb*	3741	3899	3759	3766	3884	3841
$\sigma_{int}L/60\,NZ/A$	1.36	1.40	1.34	1.34	1.38	1.35
σ_{-1}, mb	199±2.5	205±2	210±2	204±3	213±2.5	236±2
$\sigma_{-1}\cdot A^{-1/3}$	0.181	0.184	0.187	0.180	0.187	0.204
σ_{-2}, MeV^{-1}· mb	14.85±0.15	15.33±0.13	15.35±0.14	15.30±0.12	15.96±0.11	15.43±0.18
$\sigma_{-2}\cdot A^{-1/3}$	0.00234	0.00238	0.00236	0.00235	0.00241	0.00229

*Calculated in the case of validity of hypothesis 2) on the basis of the formula $\sigma_{int}\,L=(\pi/2)(\sigma_1\Gamma_1+\sigma_2\Gamma_2)$.

σ_{int} corrected for neutron multiplicity

TABLE IV. Parameters of Lorentz curves.

Nucleus	E_1, MeV	Γ_1, MeV	σ_1, mb	E_2, MeV	Γ_2, MeV	σ_2, mb	$\sigma_1\Gamma_1/\sigma_2\Gamma_2$
^{191}Ir	12.85±0.04	2.70±0.07	294±8	14.82±0.09	5.30±0.21	299±10	0.5
^{193}Ir	13.01±0.04	2.61±0.06	317±10	14.77±0.09	6.44±0.31	257±12	0.5
^{194}Pt	12.96±0.04	2.59±0.07	308±10	14.54±0.10	5.33±0.22	299±11	0.5
^{196}Pt	12.99±0.05	2.70±0.07	296±10	14.59±0.11	5.46±0.27	293±15	0.5
^{198}Pt	13.07±0.05	2.72±0.08	303±11	14.40±0.12	5.97±0.29	276±13	0.5
^{198}Pt	13.06±0.05	2.87±0.09	284±12	14.34±0.14	6.27±0.34	260±16	0.5
^{198}Pt	13.58±0.02	4.45±0.06	514±6	–	–	–	–

TABLE V. Average energies.

Nucleus	E_M, MeV*	$E_M A^{1/3}$	$E_M A^{1/3}$	Nucleus	E_M, MeV*	$E_M A^{1/3}$	$E_M A^{1/3}$
^{191}Ir	14.16	81.8	34.0	^{194}Pt	14.06	81.5	33.9
^{193}Ir	14.18	82.0	34.1	^{196}Pt	13.96	81.1	33.6
^{194}Pt	14.01	81.1	33.7	^{198}Pt	13.91	81.1	33.6

*Calculated in the case of validity of hypothesis 2) according to the formula $E_M=(1/3)E_1+(2/3)E_2$.

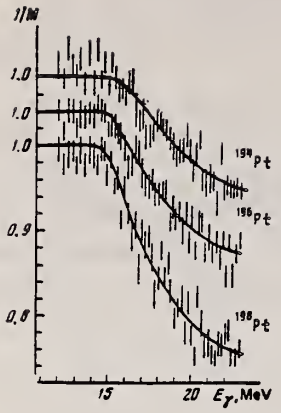

FIG. 2. Multiplicity of photoneutrons for the isotopes ^{194,196,198}Pt. The length of the vertical lines is equal to two standard deviations. The curves are a fit with the parameters given in Table II.

Pt
A=196

Pt
A=196

A. M. Gellier, J. Halpern, and E. G. Muirhead
Phys. Rev. 118, 1302-12 (1960)

ELEM. SYM.	A	Z
Pt	196	78

METHOD

Betatron; neutron threshold; ion chamber

REF. NO. 60 Ge 3 NVB

REACTION	RESULT	EXCITATION ENERGY	SOURCE		DETECTOR		ANGLE
			TYPE	RANGE	TYPE	RANGE	
G,N	NØX	THR	C THR		BF3-I		4 PI

THRESHØLD

TABLE I. Summary and comparison of neutron separation energies inferred from present threshold measurements with values predicted from mass data and reaction energies. All energies are expressed in the center-of-mass system in Mev.

Reaction	No. runs	Present results	Other results	Method	Reference
$Pt^{196}(\gamma,n)Pt^{195}$	2	8.29 ±0.14	7.91 ±0.06	mass data	q
			7.920±0.012	$Pt^{198}(n,\gamma)Pt^{196}$	e

q W. H. Johnson, Jr., and V. B. Bhanot, Phys. Rev. 107, 6 (1957).

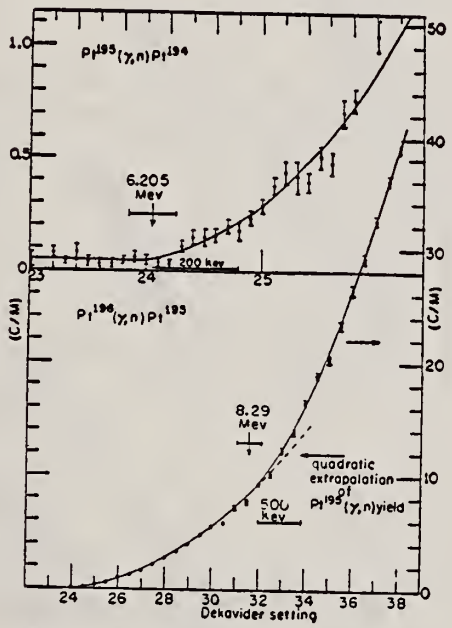

FIG. 9. Neutron yield data for platinum from 5.94 Mev to 9.96 Mev.

Ref. R. E. Chrien, H. H. Bolotin, H. Palevsky

Phys. Rev. 127, 1680 (1962)

Elem. Sym.	A	Z
Pt	196	78

Method
Reactor, fast chopper (Chalk River) - 6 NaI

Ref. No.
62Ch1

BG

Reaction	E or ΔE	E_o	Γ	∫σdE	Jπ	Notes
		E_n = (eV)				
(n,γ)		11.9				0^+ ground state
		19				Relative transition probabilities
		68				are given.
		113				
		121				
		(140)				
		(152)				
		189				
		223				
		277				

TABLE I. Pt^{196} transition probabilities.

Level (eV)	7.92-MeV transition	7.6-MeV transition	7.26-MeV transition	Sum
11.9	2.84 ±0.12	0.43 ±0.27	<0.24	3.33 ±0.21
19	0.57 ±0.12	0.28 ±0.18	0.62 ±0.18	1.69 ±0.16
68	1.83 ±0.14	2.14 ±0.22	0.26 ±0.22	4.59 ±0.19
113	0.62 ±0.10	0.85 ±0.17	0.62 ±0.18	2.39 ±0.15
121	1.48 ±0.14	0.30 ±0.22	0.18 ±0.18	2.05 ±0.18
140	0.28 ±0.09	0.09 ±0.14	2.85 ±0.21	4.08 ±0.15
152	0.29 ±0.12	0.28 ±0.22	0.53 ±0.27	1.29 ±0.20
189	1.02 ±0.16	0.43 ±0.27	0.98 ±0.27	2.78 ±0.23
223	1.39 ±0.32	3.65 ±0.66	1.75 ±0.71	7.79 ±0.57
252	0.04 ±0.12	0.18 ±0.16	0.56 ±0.19	0.97 ±0.15
277	1.60 ±0.29	0.22 ±0.57	0.22 ±0.41	2.13 ±0.44
296	0.03 ±0.08	1.87 ±0.19	0.11 ±0.21	2.29 ±0.16
Mean	1.000±0.048	0.893±0.091	0.723±0.088	2.948±0.077

FIG. 5. The decay scheme for Pt^{196}.

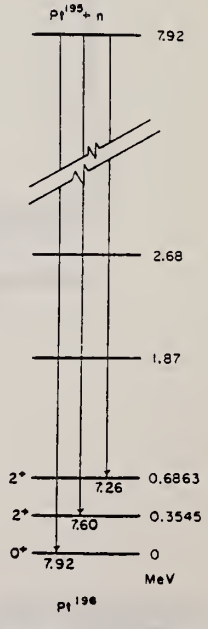

FORM NBS-418
(8-1-63)
USCOMM-DC 18556-P63

U.S. DEPARTMENT OF COMMERCE
NATIONAL BUREAU OF STANDARDS

REF. A.M. Goryachev and G.N. Zalesnyi
Yad. Fiz 27, 1479 (June 1978)
Sov. J. Nucl. Phys. 27, 779 (June 1978)

ELEM. SYM.	A	Z
Pt	196	78

METHOD

REF. NO. 78 Go 3

hmg 11/17/80

REACTION	RESULT	EXCITATION ENERGY	SOURCE		DETECTOR		ANGLE
			TYPE	RANGE	TYPE	RANGE	
G,XN	ABX	7(7.9)-21	C	8-21	BF3-I	---	4PI

Photoneutron yield curves have been measured for the isotopes ^{191,193}Ir and ^{194,195,196,198}Pt in the bremsstrahlung beam of a betatron in the energy range 8–21 MeV with a 0.2-MeV step. For the isotopes ^{194,196,198}Pt we have also measured the photoneutron multiplicity curves. The measurements were made on-line with a computer. The cross sections were calculated from the yield curves by the Penfold-Leiss method with a 1.0-MeV step. The multiplicty curves were used to separate the contributions of (γ,n) and $(\gamma,2n)$ reactions. On the basis of the photoabsorption cross sections we have calculated the integrated cross sections, deformation parameters, and average energies. The existence of oblate deformation in these nuclei is not confirmed by the analysis of the measured cross sections.

n multiplicity measurement

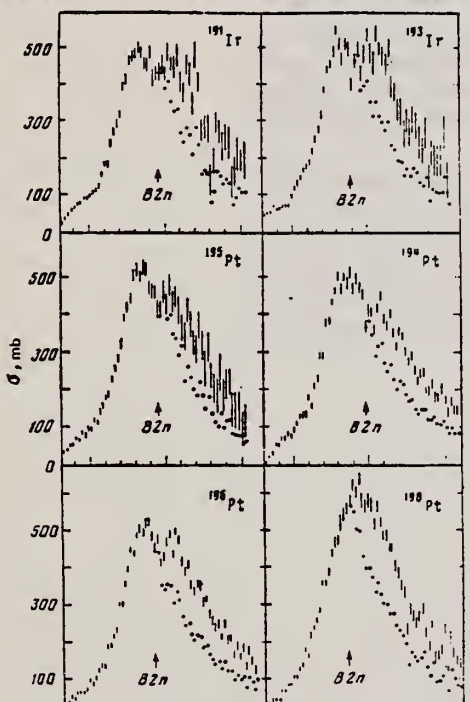

FIG. 1. Photoabsorption cross sections for the isotopes ^{191,193}Ir and ^{194,195,196,198}Pt. The vertical lines, whose length is equal to two standard deviations, show the experimental cross section. Above the $(\gamma,2n)$ threshold the photoabsorption cross section is designated by circles.

TABLE II. Parameters of photoneutron multiplicity curves.

Nucleus	a, MeV^{-1}	w	χ^2/f	a, MeV^{-1}	w	χ^2/f
^{196}Pt	6.3±0.7	0	1.07	21.16*	0.37±0.03	1.13
^{196}Pt	7.9±0.5	0	0.98	21.19*	0.29±0.02	1.04
^{196}Pt	8.2±0.6	0	1.15	20.2*	0.28±0.03	1.21

Note. Here f is the number of degrees of freedom; the asterisks denote level-density parameter values taken from Ref. 16.

TABLE III. Integrated cross sections.

	^{191}Ir	^{193}Ir	^{194}Pt	^{195}Pt	^{196}Pt	^{198}Pt
σ_{int}, MeV-mb	2757±23	2835±30	2861±27	2797±25	2944±21	2813±32
$\sigma_{int}(\gamma,2n)$, MeV-mb	–	–	626±9	–	744±9	1023±14
$\sigma_{int}L$, MeV-mb*	– 3741	– 3899	0.22 3759	– 3766	0.25 3884	0.36 3841
$\sigma_{int}L/60\,NZ/A$	1.36	1.40	1.34	1.34	1.38	1.35
σ_{-1}, mb	199±2.5	205±2	210±2	204±3	213±2.5	236±2
$\sigma_{-1}\cdot A^{-1/3}$	0.181	0.184	0.187	0.180	0.187	0.204
σ_{-2}, MeV^{-1} · mb	14.85±0.15	15.33±0.13	15.35±0.14	15.39±0.12	15.96±0.11	15.43±0.18
$\sigma_{-2}\cdot A^{-1/3}$	0.00234	0.00238	0.00236	0.00235	0.00241	0.00229

*Calculated in the case of validity of hypothesis 2) on the basis of the formula $\sigma_{int}\ L=(\pi/2)(\sigma_1\Gamma_1+\sigma_2\Gamma_2)$.

σ_{int} corrected for neutron multiplicity

TABLE IV. Parameters of Lorentz curves.

Nucleus	E_1, MeV	Γ_1, MeV	σ_1, mb	E_2, MeV	Γ_2, MeV	σ_2, mb	$\sigma_1\Gamma_1/\sigma_2\Gamma_2$
^{191}Ir	12.85±0.04	2.70±0.07	294±8	14.82±0.09	5.30±0.21	299±10	0.5
^{193}Ir	13.01±0.04	2.61±0.06	317±10	14.77±0.09	6.44±0.31	257±12	0.5
^{194}Pt	12.96±0.04	2.59±0.07	308±10	14.54±0.10	5.33±0.22	299±11	0.5
^{195}Pt	12.99±0.05	2.70±0.07	296±10	14.59±0.11	5.46±0.27	293±15	0.5
^{196}Pt	13.07±0.05	2.72±0.08	303±11	14.40±0.12	5.97±0.29	276±13	0.5
^{198}Pt	13.06±0.05	2.87±0.09	284±12	14.34±0.14	6.27±0.34	260±16	0.5
^{198}Pt	13.58±0.02	4.45±0.06	514±6	–	–	–	–

TABLE V. Average energies.

Nucleus	E_M, MeV*	$E_M A^{1/3}$	$E_M A^{1/3}$	Nucleus	E_M, MeV*	$E_M A^{1/3}$	$E_M A^{1/3}$
^{191}Ir	14.16	81.6	34.0	^{196}Pt	14.06	81.5	33.9
^{193}Ir	14.18	82.0	34.1	^{196}Pt	13.96	81.1	33.6
^{194}Pt	14.01	81.1	33.7	^{198}Pt	13.91	81.1	33.6

*Calculated in the case of validity of hypothesis 2) according to the formula $E_M=(1/3)E_1+(2/3)E_2$.

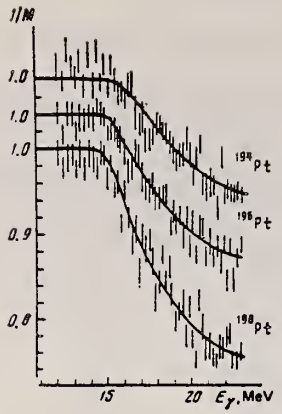

FIG. 2. Multiplicity of photoneutrons for the isotopes ^{194,196,198}Pt. The length of the vertical lines is equal to two standard deviations. The curves are a fit with the parameters given in Table II.

# GOLD
Z=79

The symbol Au for gold comes from the Latin *aurum* and is probably the first metal discovered by man. The goldsmith's art dates from at least 4000 B. C. in Mesopotamia and it then spread throughout the acient civilizations near the eastern Mediterranean and Egypt. It occurred in the Asian civilizations as well as in the cultures of Peru and Mexico. In the later years of history, alchemy, or the search for the Philosopher's Stone which would convert base metals to gold, contributed much to our early understanding of chemistry, medicine, and metallurgy.

Au
A=197

Estimates have been made to show that the greatest part of all the gold won from the earth in the last 10,000 years could still be accounted for in private and government vaults and in the wide private distribution of jewelery and artifacts throughout the world. No other possession is so zealously and effectively guarded.

Au
A=197

Ref. W.K. Dawson
Can. J. Phys. 34, 1480 (1956)

Elem. Sym.	A	Z
Au	197	79

Method Synchrotron; proton yield, spectrum; angular distribution; nuclear emulsion; ion chamber.

Ref. No. 56 Da 2 C S | NVB

Reaction	E or ΔE	E_o	Γ	$\int \sigma dE$	Jπ	Notes
$Au^{197}(\gamma, xp)$	70					Yield = 6.8×10^4 protons (up to 17 MeV)/r-mole ±30% for 70 MeV bremss.

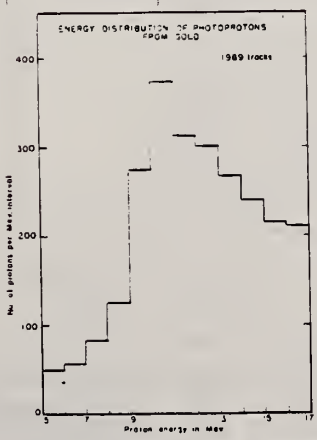

FIG. 5. The energy distribution of photoprotons from gold shown here cannot be explained on the basis of the theories outlined in the text.

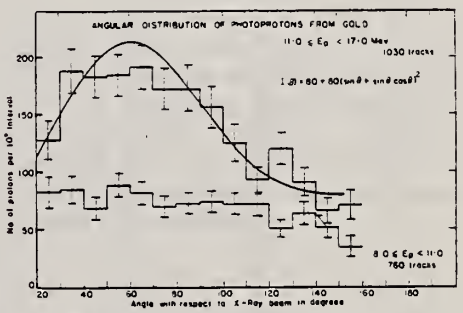

FIG. 9. The angular distributions of photoprotons of various energies from gold. Standard deviations are shown. The smooth curve for the higher energy group ($11.0 \leq E_\gamma < 17.0$ Mev) was calculated from equation (6).

Ref. E.G. Fuller, E. Hayward
Phys. Rev. 101, 692 (1956)

Elem. Sym.	A	Z
Au	197	79

Method
Betatron; photon scattering; NaI spectrometer

Ref. No. 56 Fu 1 NVB

Reaction	E or ΔE	E_o	Γ	$\int \sigma dE$	Jπ	Notes
$Au^{197}(\gamma,\gamma)$	Bremss. 4-40					Detector at 120°. Cross sections given here are 13% too high due to erroneous cosβ factor in denominator of Eq. 5. [See footnote 8 in Phys. Rev. 106, 993 (1957)].

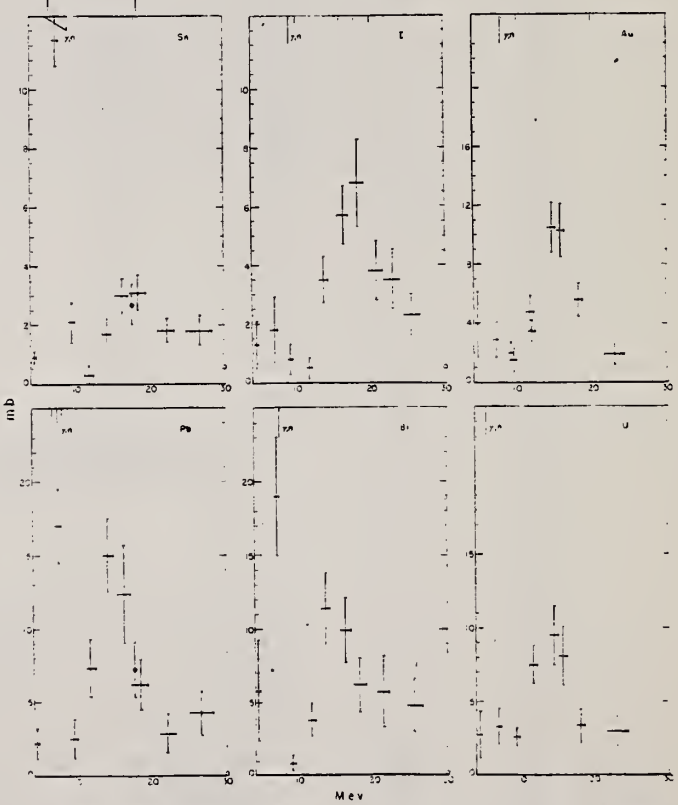

FIG. 6. The elastic scattering cross sections for Sn, I, Au, Pb, Bi, and U. The points at 17.6 Mev are those of Stearns.[4]

[4] E. R. Gaerttner and G. L. Yeater, Phys. Rev. 76, 363 (1949).
[5] Dressel, Goldhaber, and Hanson, Phys. Rev. 77, 754 (1950).
[6] M. B. Stearns, Phys. Rev. 87, 706 (1952).

Ref. B.I. Ga[illegible]lov, L.E. Lazareva
Zhur. Eksp. i Teoret. Fiz. 30, 855 (1956);
Soviet Phys. JETP 3, 871 (1957)

Elem. Sym.	A	Z
Au	197	79

Method γ-Bremsstrahlung; synchrotron; BF_3 counter

Ref. No. 56 Ga 1 EGF

Reaction	E or ΔE	E_0	Γ	$\int \sigma dE$	Jπ	Notes
$Au^{197}(\gamma, xn)$	~ 7.5-27	14.2	6.0	4.37 MeV-b		(567) 567
$Au^{197}(\mu_t)$	~ 7.5-27	14.2	4.7	3.49 MeV-b		

TABLE I. Fundamental characteristics of photoneutron cross sections.

Element	$E_{\sigma_n \max}$ in mev	$\sigma_n \max$ in barns	Half width in mev	$\int_{E_n}^{E_0} \sigma_n(E)\,dE$ in mev-barns	$\int_{E_n}^{E_0} \sigma_n(E)\,dE / \sigma_n \max$
Copper	17.2	0.126	4.3	0.93	7.4
Zinc	16.3	0.082	6.3	0.66	8.1
Cadmium	16.0	0.270	8.4	2.28	8.4
Iodine	15.5	0.288	6.0	2.35	8.2
Tantalum	14.5	0.452	6.8	3.87	8.6
Gold	14.2	0.571	6.0	4.37	7.6
Thallium	14.6	0.655	5.4	4.99	7.6
Bismuth	13.9	0.537	5.9	3.96	7.4
Thorium	14.5	0.796	5.6	6.33	8.0
Uranium	14.9	1.18	6.8	12.5	10.6

TABLE II. Threshold of photoneutron reactions (mev).

Element	(γ, n)	$(\gamma, 2n)$	$(\gamma, 3n)$	$(\gamma, 4n)$
Cadmium	8.7	14.6	23.0	>30
Iodine	9.4	16.2	26.0	32.9
Tantalum	7.6	13.9	21.6	28.2
Gold	8.1	14.9	23.9	>30
Thallium	7.5	14.0	22	28.8
Bismuth	7.4	14.2	22.5	29.6

TABLE III. Characteristics of the cross section of absorption of γ-quanta by nuclei.

Element	E_{res} in mev	$\sigma_\gamma(E=E_{res})$ in barns	Half width in mev	$\int_{E_n}^{E_0} \sigma_\gamma dE$ in mev-barns	$\int_{E_n}^{E_0} \sigma_\gamma dE / 0.05 \times E_n \times (ZN/A)$	$\int_{E_n}^{E_0} \sigma_\gamma(E)\,dE$	$\int_{E_n}^{E_0} \sigma_\gamma(E^*)\,dE$	$r_0 \times 10^3$ in cm
Cadmium	15.6	0.263	5.1	1.76	1.06	0,111	0.00745	1,26
Iodine	15.5	0,288	4.9	1.86	1,00	0,117	0,00768	1,16
Tantalum	13.9	0.448	4.5	2.74	1,05	0,190	0,0139	1,15
Gold	14.2	0.571	5.1	3.49	1.23	0.244	0,0182	1,23
Thallium	14.0	0,648	4.6	3.77	1,28	0.266	0,0200	1.25
Bismuth	13.8	0,537	4.8	3.12	1,04	0.230	0,0178	1.16

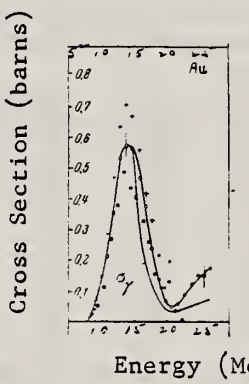

Figure 2: Photoneutron cross section σ_n, computed from the yield curves by the "photon difference method." "+" -- cross sections obtained in Ref 8 [Montalbetti, Katz and Goldemberg, Phys. Rev. 91, 659 (1959)]; "●" -- cross sections obtained in Ref. 9 [Nathans and Halpern Phys. Rev. 93, 437 (1954)]. Curve is presented for the cross section of γ-quanta, computed from the statistical theory of nuclei.

B.G. Chidley, L. Katz, S. Kowalski
Can. J. Phys. 36, 407 (1958)

ELEM. SYM.	A	Z
Au	197	79

Betatron

REF. NO. 58 Ch 2 NVB

REACTION	RESULT	EXCITATION ENERGY	SOURCE		DETECTOR		ANGLE
			TYPE	RANGE	TYPE	RANGE	
G,N	RLY	THR	C	THR	BF3-I		4PI

See 58 Ka 1 for cross sections

THRESHOLD

TABLE I

MEASURED PHOTONEUTRON THRESHOLDS

Reaction	Measured Q value, Mev.	Other Q values, Mev.	Method	Reference
$Au^{197}(\gamma, n)Au^{196}$	7.96±0.07			
		8.00 ±0.15	Threshold	Hanson *et al.* (1949)
		8.1 ± 0.1	Threshold	Parsons and Collie (1950)
		7.90 ±0.20	Threshold	Sher *et al.* (1951)
		7.78 ±0.40	Mass data	Hay (1955)

R. Fuller, B. Petree, M.S. Weiss
Phys. Rev. 112, 554 (1958)

ELEM. SYM.	A	Z
Au	197	79

Betatron; ion chamber

REF. NO. 58 Fu 1 NVB

REACTION	RESULT	EXCITATION ENERGY	SOURCE		DETECTOR		ANGLE
			TYPE	RANGE	TYPE	RANGE	
G,XN	ABY	7-40	C	7-40	BF3-I		4PI

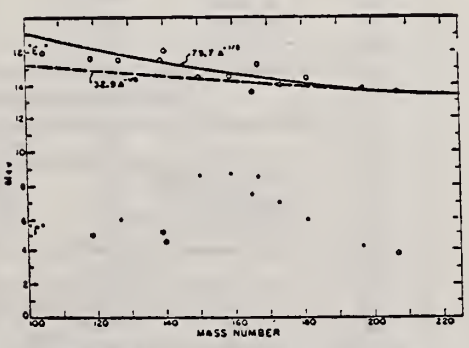

FIG. 6. Mean energy and width of giant resonances. "E_0" and "Γ" are the mean energy for photon absorption and the full width at half maximum of the giant resonance obtained from dashed histograms as in Fig. 5. No attempt was made to fit data with resonance curves to obtain these parameters.

TABLE I. Target properties and results.

Element	Form used	Weight grams	$\sigma^0(\gamma,n)$[a] barns	$\frac{S\sigma dE^b}{NZ/A}$ Mev-b	"Γ"[a] Mev
Sn	Sn	4.81	0.30	0.064	5.0
I	I	8.55	0.36	0.085	6.0
La	La	10.43	0.34	0.063	5.2
Ce	Ce	4.99	0.45	0.080	4.5
Sm	Sm_2O_2	2.90	0.26	0.073	8.6
Tb	Tb_4O_7	3.04	0.39	0.087	8.7
Ho	Ho_2O_3	1.87	0.41	0.079	7.5
Er	Er_2O_3	5.41	0.50	0.100	8.5
Yb	Yb_2O_3	5.37	0.50	0.090	7.0
Ta	Ta	8.41	0.49	0.077	6.0
Au	Au	3.16	0.68	0.085	4.2
Pb	Pb	8.05	0.75	0.081	3.8

[a] $\sigma^0(\gamma,n)$ is the maximum value and "Γ" the full width at $\sigma^0(\gamma,n)/2$ of the neutron production cross section corrected for multiple neutron emission. Data were not fitted with resonance lines to determine these values.
[b] Integrated neutron production cross sections corrected for multiple neutrons above $(\gamma,2n)$ threshold.

TABLE II. Energies of resonances in deformed nuclei.[a]

Nucleus	E_m Mev	Q_0 barns	Method	E_a Mev	E_b Mev	$E_{1/2}^-$ Mev	$E_{1/2}^+$ Mev
$_{65}Tb^{159}$	14.7	6.9[b]	CE	11.9	16.2	10.8	19.5
$_{67}Ho^{165}$	14.5	7.8[b]	CE	11.5	16.0	11.0	18.5
$_{68}Er^{167}$	14.5	21[b]	SC	8.5	17.5	11.5	20.0
$_{68}Er^{166}$	14.5	7.8[b]	CE	11.6	15.9	11.5	20.0
$_{73}Ta^{181}$	14.1	12.6[c]	SC	10.5	15.9	11.3	17.3
$_{73}Ta^{181}$	14.1	6.8[b]	CE	11.9	15.2	11.3	17.3
$_{79}Au^{197}$	13.6	3.75[c]	SC	12.5	14.1	11.8	16.2

[a] CE—Coulomb excitation; SC—spectroscopic; $E_{1/2}^-$, $E_{1/2}^+$—energies at which giant resonance drops to half its maximum value.
[b] Adler, Bohr, Huus, Mottelson, and Winther, Revs. Modern Phys. 28, 432 (1956).
[c] M. L. Pool and D. N. Kundu, *Chart of Atomic Nuclei* (Longs College Book Company, Columbus, 1955).

REF.

E.G. Fuller, M.S. Weiss
Phys. Rev. 112, 560 (1958)

ELEM. SYM.	A	Z
Au	197	79

METHOD

Betatron; ion chamber

REF. NO. 58 Fu 2 NVB

REACTION	RESULT	EXCITATION ENERGY	SOURCE TYPE	SOURCE RANGE	DETECTOR TYPE	DETECTOR RANGE	ANGLE
G,XN	ABX	8-23	C	THR-25	BF3-I		4PI

CF DANØS THEØRY 583

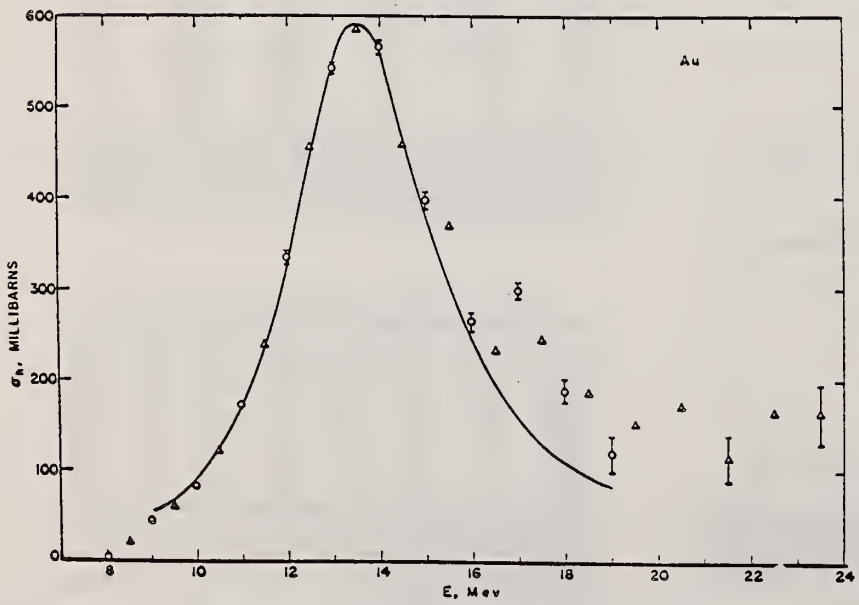

FIG. 7. Neutron cross section for gold. See Fig. 5 for description.

TABLE I. Resonance parameters.

	Tb^{159}	Ta^{181}	Au^{197}
B_{2n} (Mev)	15.2	14.0	14.2
E_a (Mev)	12.5	12.45	13.15
σ_a^0 (Mb)	258	308	255
Γ_a (Mev)	2.4	2.3	2.9
E_b (Mev)	16.3	15.45	13.90
σ_b^0 (Mb)	310	348	365
Γ_b (Mev)	4.0	4.4	4.0

TABLE II. Integral cross sections.

	Tb^{159}	Ta^{181}	Au^{197}
$A\int_0^{24}\sigma_a dE/0.06NZ$	1.27	1.30	1.29
$\int\sigma_b dE/\int\sigma_a dE$	2.00	2.16	1.97
$A\int_0^{\infty}(\sigma_a+\sigma_b)dE/0.06NZ$	1.27	1.35	1.22

TABLE III. Intrinsic quadrupole moments, in barns.

	Tb^{159}	Ta^{181}	Au^{197}
E_b/E_a	1.30±0.05	1.25±0.01	1.06±0.03
$Q_0(R_0=1.09\times10^{-13}$ cm)	5.6 ±0.6	5.7 ±0.3	1.6 ±0.6
Q_0 (Coulomb excitation)	6.9[a]	6.8[a]	2.6[b]

[a] Adler, Bohr, Huus, Mottelson, and Winter, Revs. Modern Phys. 28, 432 (1956).
[b] P. H. Stelson and F. K. McGowan, Phys. Rev. 99, 112 (1955).

L. Katz, G.B. Chidley
Nuclear Reactions at Low and Medium Energies (Academy of Science, USSR: 1958) 371

ELEM. SYM.	MASS	ATOMIC NO.
Au	197	79

METHOD: Betatron; neutron cross section; BF_3 counters; ion chamber monitor

REF. NO.: 58 Ka 1 | NVB

REACTION	RESULT	EXCITATION ENERGY	SOURCE		DETECTOR		ANGLE
			TYPE	RANGE	TYPE	RANGE	
G,XN	ABX	8-22	C	8-22	BF3-I		4PI

Таблица 2

Пороги испускания фотонейтронов

Изотоп	B_n, *Мэв*	B_{2n}, *Мэв*	Изотоп	B_n, *Мэв*	B_{2n}, *Мэв*
V^{51}	11,16	20,5	La^{139}	8,81	16,1
Mn^{55}	10,14	19,2	Pr^{141}	9,46	17,6
Co^{59}	10,44	18,6	Tb^{159}	8,16	14,8
As^{75}	10,24	18,1	Ho^{165}	8,10	14,6
Y^{89}	11,82	20,7	Tm^{169}	8,00	14,7
Nb^{93}	8,86	17,1	Lu^{175}	7,77	14,2
Rh^{103}	9,46	16,8	Ta^{181}	7,66	13,8
J^{127}	9,14	16,2	Au^{197}	7,96	13,3
Cs^{133}	9,11	16,5	Bi^{209}	7,43	14,5

THRESHOLDS

не приведены, поскольку они превышают 22 *Мэв* во всех случаях, кроме золота, для которого E_{2n}=21 *Мэв*. Свойства сечений $\sigma_C(\gamma)$ сведены в табл. 3.

Таблица 1

Изотоп	$E_{макс}$, *Мэв*	$\sigma_n(E_\gamma)$, барн	Γ, *Мэв*	Γ^{22}, *Мэв·барн*	$Y(22)$, 10^6 нейтрон/100 р·моль
V^{51}	18,4	0,062	5,2	0,33	1,62
Mn^{55}	20,2	0,060	7,0	0,39	2,01
Co^{59}	18,3	0,068	6,3	0,44	2,30
As^{75}	16,4	0,090	9,5	0,74	4,25
Y^{89}	17,1	0,172	5,2	0,93	5,33
Nb^{93}	18,0	0,156	7,5	1,17	6,80
Rh^{103}	17,5	0,160	9,4	1,40	8,28
J^{127}	15,2	0,273	6,8	1,76	11,9
Cs^{133}	16,5	0,238	7,7	1,59	10,7
La^{139}	15,5	0,325	3,8	1,55	11,2
Pr^{141}	15,0	0,320	4,9	1,93	13,1
Tb^{159}	15,6	0,274	9,8	2,49	18,1
Ho^{165}	13,5	0,305	8,9	2,52	18,7
Tm^{169}	16,4	0,250	8,4	1,91	14,9
Lu^{175}	16,0	0,225	8,4	1,90	23,0
Ta^{181}	14,5	0,380	8,5	3,15	22,0
Au^{197}	13,8	0,475	4,7	3,04	22,6
Bi^{209}	13,2	0,455	5,9	2,89	23,2

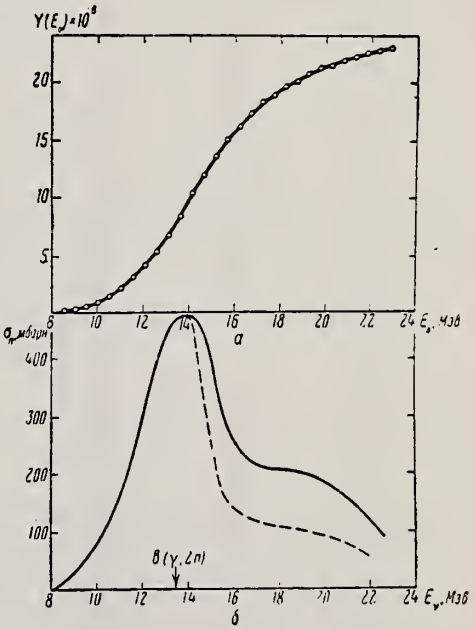

Рис. 16.

а — Выход фотонейтронов для Au; *б* — $\sigma_n(E_\gamma)$ и $\sigma_C(\gamma)$ для Au

Ref. W.H. Hartley, W.E. Stephens, E.J. Winholc
Phys. Rev. 104, 17[illegible] (1956)

Elem. Sym.	A	Z
Au	197	79

Method
Li (p,γ) source, 480 kev protons. BF_3 counters

Ref. No.
56 Ha 1

EGF

Reaction	E or ΔE	E_o	Γ	$\int \sigma dE$	Jπ	Notes
(γ,xn)						Average Li cross section is 330 mb; cross section with detector response weighted for low energy neutrons, 295 mb. Assumed ratio 17.6/14.8 = 1.7. Calculated cross section at 14.8 and 17.6 MeV assuming cross section curves measured at Pennsylvania and Saskatchewan (refer Table I).

TABLE I. Cross sections for photoneutron emission induced by the lithium gamma rays. The results are compared with previous data

Element	Present cross-section data		Data of McDaniel et al.[a]	Betatron data					
				Pennsylvania		Saskatchewan			
	Counter Group A	Counter Group B		$\sigma_{14.8}$	$\frac{\sigma_{14.8}}{\sigma_{17.6}}$	$\sigma_{14.8}$	$\frac{\sigma_{14.8}}{\sigma_{17.6}}$	$\sigma_{14.8}$	$\sigma_{17.6}$
$_{26}$Fe	38 mb	33 mb	37 mb			60[f] mb	0.5	23 mb	47 mb
$_{27}$Co	49	49	47	60[e] mb	0.5	95[f]	0.5	30	60
$_{28}$Ni	28	25	23			40[e]	0.7	22	32
$_{29}$Cu	64	61	55±12			95[f]	0.6	43	75
$_{30}$Zn	48	45	48			90[f]	0.7	38	54
$_{47}$Ag	175	170	135			240[f]	1.0	175	175
$_{50}$Sn	200	190	180						
$_{73}$Ta	355	360	260	350[d]	1.3	420[g]	2.3	420[i]	320[i]
$_{74}$W	365	355	325					550[i]	240[i]
$_{79}$Au	330	295		315[c]	1.7	480[f]	1.9	460	255
$_{80}$Hg	365	340	290						
$_{82}$Pb	310	295	250	320[e]	1.6	440[f]	2.5	400[i]	250[i]
$_{83}$Bi	305	280	250	270[d]	2.6	550[f]	2.4	550[i]	200[i]
								490	195

[a] See reference 3.
[b] Average of 14.8- and 17.6-Mev cross sections weighted with relative intensities of the lithium gamma-ray lines.
[c] See reference 24.
[d] K. Nathans, Ph.D. thesis, University of Pennsylvania, 1954 (unpublished).
[e] I. Halpern (private communication).
[f] See reference 25.
[g] See reference 32.
[h] Separate cross sections at 14.8 and 17.6 Mev as obtained from Group A data and 14.8/17.6 betatron cross-section ratios.
[i] Obtained using 14.8/17.6 cross-section ratio from Pennsylvania betatron data.
[j] Obtained using 14.8/17.6 cross-section ratio from Saskatchewan betatron data.

Ref. F. Ferrero, L. Gonella, R. Malvano, C. Tribuno, A.O. Hanson
Nuovo Cimento 5, 242 (1957)

Elem. Sym.	A	Z
Au	197	79

Method: 31 MeV betatron; neutron yield, angular distribution; threshold detector, $Si^{28}(n,p)Al^{27}$ reaction.

Ref. No.: 57 Fe 1 EGF

Reaction	E or ΔE	E_o	Γ	$\int \sigma dE$	Jπ	Notes
Au(γ,n!)	Bremss. 15-31					Data not clear but probably normalized at 30 MeV.

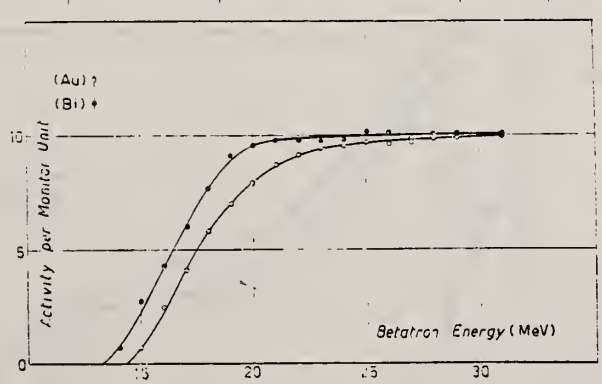

Fig. 8.

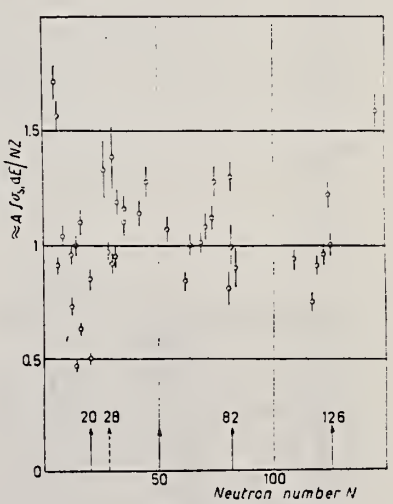

Fig. 9.

Ref. W. Bertozzi, F.R. Paolini, C.P. Sargent
Phys. Rev. 110, 790 (1958)

Elem. Sym.	A	Z
Au	197	79

Method
MIT linear accelerator; time of flight

Ref. No. 58 Be 2 EH

Reaction	E or ΔE	E_o	Γ	$\int \sigma dE$	Jπ	Notes
$Au^{197}(\gamma,n)$	Bremss. ~ 14.3 ~ 15.8					Detector at 120°

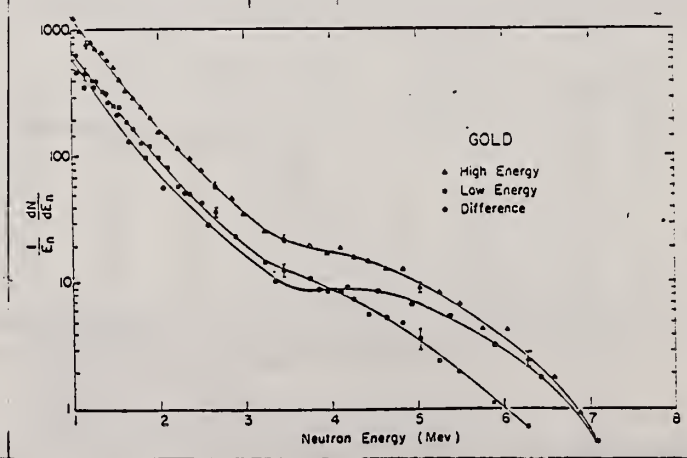

Fig. 2. Energy spectra $(1/E_n)(dN/dE_n)$ of photoneutrons from Au for bremsstrahlung of maximum energies ~14.3 Mev and ~15.8 Mev, and difference spectrum.

Ref. S. Cavallaro, V. Emma, C. Milone, A. Rubbino
Nuovo Cimento 9, 736 (1958)

Elem. Sym.	A	Z
Au	197	79

Method 30 MeV betatron; emulsions; neutron spectrum

Ref. No. 58 Ca 2 EH

Reaction	E or ΔE	E_o	Γ	$\int \sigma dE$	Jπ	Notes
$Au^{197}(\gamma,n)$	Bremss. 30					$E_{th(\gamma,n)} = 7.9$ $\sim 90^\circ$ spectra.

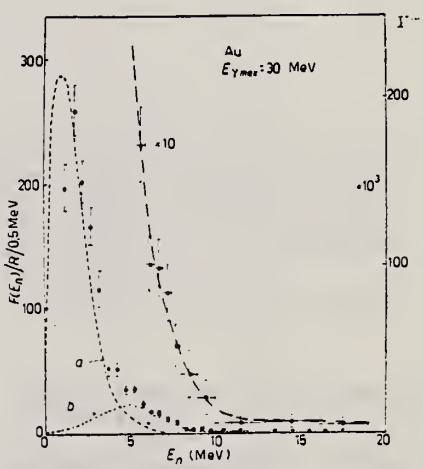

Fig. 1. – Energy spectrum of the photoneutrons from Au emitted at ~90° with the γ-ray beam. ⊕ = Experimental figures. For the high energy tail figures are multiplied by 10. The curve (*a*) is the evaporation spectrum calculated under the assumption indicated in the text. Curve (*b*) is a spectrum calculated for direct emission under the hypothesis that the residual nucleus after the neutron emission is left in the ground state. $Y^{\pm}$ – neutrons/*R*/0.5 MeV/mole/ΔΩ.

Ref. B. Ziegler
Z. Physik 152, 566 (1958)

Elem. Sym.	A	Z
Au	197	79

Method 32 MeV betatron; pair spectrometer; absorption measurement; ionization chamber

Ref. No. 58 Zi 1 EH

Reaction	E or ΔE	E_o	Γ	$\int \sigma dE$	Jπ	Notes
Au(μ_t)	Bremss. 30			2800±500 MeV-mb		

[7] MONTALBETTI, R., L. KATZ u. J. GOLDEMBERG: Phys. Rev. 91, 659 (1953).
[8] NATHANS, R., u. J. HALPERN: Phys. Rev. 93, 437 (1954).
[9] GAVRILOV, B.L., u. L.E. LAZAREWA: Sov. Phys. J.E.T.P. 3, 871 (1957).
[10] BERMAN, A.I., u. K.L. BROWN: Phys. Rev. 96, 83 (1954).
[11] DANOS, M.: Nuclear Phys. 5, 23 (1958).

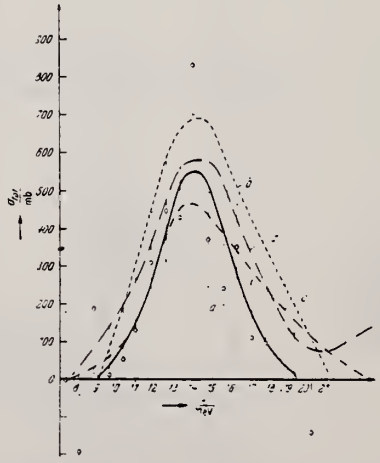

Fig. 3. a Gemessener Kernabsorptionswirkungsquerschnitt σ_{int} (mb) für Au; b $\sigma_{\gamma,n}$ nach [7]; c $\sigma_{\gamma,n}$ nach [8]; d $\sigma_{\gamma,n}$ nach [9]

Ref. L.B. Aull, G.C. Reinhardt, W.D. Whitehead
Nuclear Phys. 13, 292 (1959)

Elem. Sym.	A	Z
Au	197	79

Method: Si detectors

Ref. No.: 59 Au 1 EGF/EH

Reaction	E or ΔE	E_0	Γ	$\int \sigma dE$	Jπ	Notes
$Au^{197}(\gamma,n!)$	Bremss. 18-65			$\int_{}^{65} \sim 700$ MeV-mb		Yield measured relative to $Cu^{63}(\gamma,n)$.

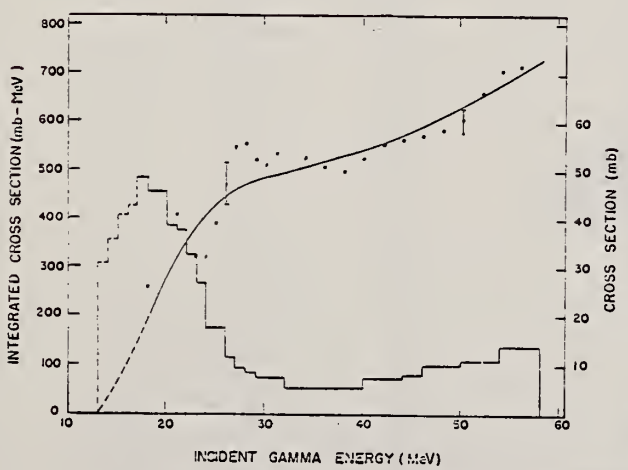

Fig. 4. Gold (γ, fast n) smoothed integrated cross section and cross section, as described under fig. 3.

Fig. 3. Tantalum (γ, fast n) smoothed integrated cross section and cross section. The points and the smooth curve represent the smoothed integrated fast neutron cross section (see text) as defined by

$$\int_0^E \sigma_{(\gamma,\text{fast n})}\, dE$$

where $\sigma_{(\gamma,\text{fast n})}$ is the cross section for photoproduction of neutrons with energies above the $Si^{28}(n,p)Al^{28}$ threshold and E is the incident gamma ray energy. The errors indicated were obtained by propagating the counting uncertainties in the yield data through the integral cross section matrix. The histogram represents the first differences of the integrated cross section curve.

TABLE 1

Ratio of fast neutron integrated cross section to total neutron integrated cross section

	24 MeV	30 MeV	60 MeV
Tantalum	10.3±2.4 % [a]	7.3±1.7 % [b]	10.6±2.2 [b]
Gold	10.9±2.7 % [a]		17.4±4.3 [c]

[a]) Compared to (γ, n) cross section of Fuller and Weiss [17]);
[b]) Compared to (γ, xn) of Terwilliger and Jones [18]);
[c]) Compared to (γ, n) of Edwards and MacMillan (data taken at 70 MeV) [19]).

Ref 17: Fuller & Weiss - Phys. Rev. 112, 560 (1958)

Ref 18: Jones & Terwillinger - Phys. Rev. 91, 699 (1953)

Ref 19: Edwards & MacMillan - Phys. Rev. 87, 377 (1952)

REF.

E. D. Makhnovskii
J. Exptl. Theoret. Phys. (USSR) 36, 739 (1959)
Soviet Phys. JETP 36 (9) 519 (1959)

ELEM. SYM.	A	Z
Au	197	79

METHOD

REF. NO. 59 Ma 1 EGF

REACTION	RESULT	EXCITATION ENERGY	SOURCE		DETECTOR		ANGLE
			TYPE	RANGE	TYPE	RANGE	
G,P	RLY	THR - 70	C	70	EMU-D	5 - 11	90
G,D	RLY	THR - 70	C	70	EMU-D	7 - 14	90

REL D TO P YLD

$Y(\gamma,d)/Y(\gamma,p) = 0.14 \pm 0.07$

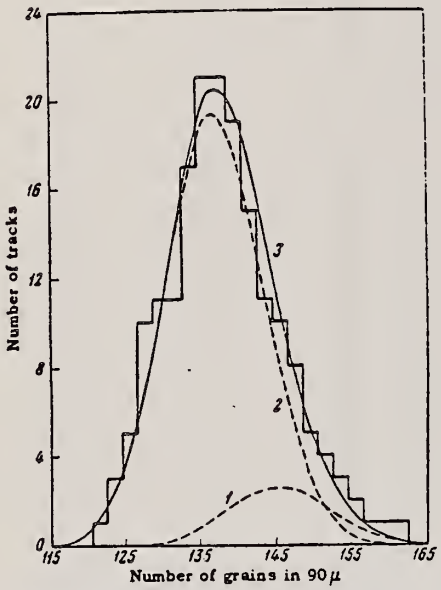

FIG. 4. Distribution of the tracks of photoparticles as a function of the number of grains in the last 90μ of the track. 1 – normal distribution of photodeuterons, 2 – normal distribution of photoprotons, 3 – sum of both.

Ref. R.F. Askew, A.P. Batson
Nuclear Phys. 20, 408 (1960)

Elem. Sym.	A	Z
Au	197	79

Method Electron synchrotron; emulsions

Ref. No. 60 As 1 JHH

Reaction	E or ΔE	E_o	Γ	$\int \sigma dE$	Jπ	Notes
$Au^{197}(\gamma, n)$	Bremss. 55					Peaks observed in neutron spectrum at E_n = 1.25 MeV and 5.5 MeV. Detector at 90°.

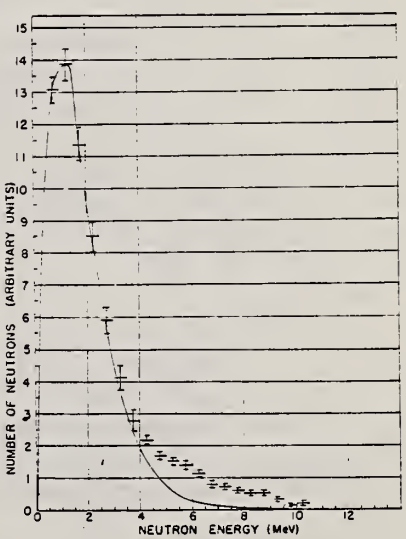

Figure 1: Relative photoneutron energy spectrum. The solid curve is the statistical theory prediction.

Ref. W.C. Barber, T. Wiedling
Nuclear Phys. 18, 575 (1960)

Elem. Sym.	A	Z
Au	197	79

Method 45 MeV linac; three-foil stack (electrodisintegration target, bremss. tradiator, electro- and photo-disintegration target); activation

Ref. No. 60 Ba 2 JHH

Reaction	E or ΔE	E_o	Γ	$\int \sigma dE$	Jπ	Notes
(γ,n)						to Au^{196} (5.6 days)
(γ,2n)						to Au^{195} (30 sec.) (180 days)
(e,e'n) (e,e'2n)						Ratios of electro- to photodisintegration in Figure 7.

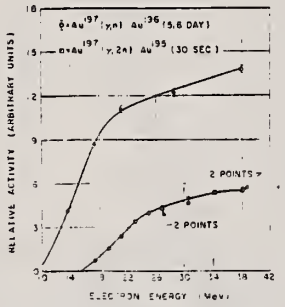

Fig. 2 Yield of Au radioactivities resulting from the real bremsstrahlung of electrons as a function of the electron energy

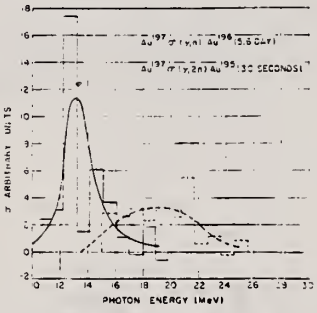

Fig. 4 Cross sections for Au derived from the yield curves of fig. 2. The relative magnitudes of the cross sections for the two reactions were drawn arbitrarily

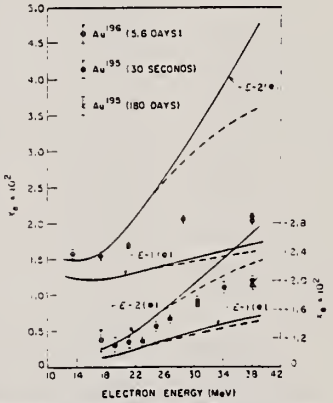

Fig. 7. The radiation length equivalent of the electrodisintegration yields of Au^{196} (ordinate scale on the left margin) and Au^{194} (ordinate scale on the right margin) produced from Au^{197} as a function of electron energy. The circles are the experimental results. Theoretical results for a point nucleus are shown as solid curves. The dashed curves indicate an approximate correction for the nuclear size.

Ref. W.C. Barber, V.J. Vanhuyse
Nuclear Phys. 16, 381 (1960)

Elem. Sym.	A	Z
Au	197	79

Method: Stanford Mark II accelerator; virtual and real photon spectrum from electrons; magnetic spectrum; KI scintillator crystals.

Ref. No.: 60 Ba 5 JHH

Reaction	E or ΔE	E_o	Γ	$\int \sigma dE$	Jπ	Notes
$Au^{197}(\gamma,p)$	$E_{e^-} = \leq 40$			$\int_0^{40} = 75 \pm 25\%$ MeVmb		$\int \sigma dE$ from calculated real and virtual photon spectrum.

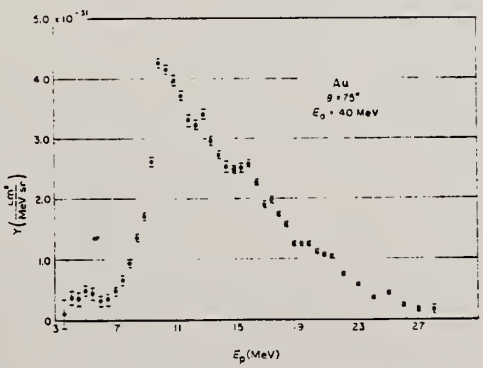

Fig. 8. Energy distribution of protons from Au.

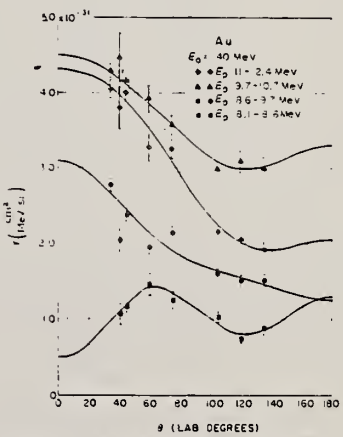

Fig. 13. Angular distribution of protons from Au. The curves represent the following least-squares fit to the data:

diamonds: $(3.2 + 1.15\cos\theta - 0.58\sin^2\theta + 0.51\cos\theta\sin^2\theta) \times 10^{-31}$;
triangles: $(3.9 - 0.62\cos\theta - 0.62\sin^2\theta + 0.39\cos\theta\sin^2\theta) \times 10^{-31}$;
circles: $(2.17 + 0.91\cos\theta - 0.43\sin^2\theta + 0.43\cos\theta\sin^2\theta) \times 10^{-31}$;
squares: $(0.91 + 0.41\cos\theta + 0.26\sin^2\theta - 1.28\cos\theta\sin^2\theta) \times 10^{-31}$.

REF.

M. A. Bak, K. A. Petrzhak, Tei-Mei Chen
Izv. Akad. Nauk SSSR 24, 818 (1960)

ELEM. SYM.	A	Z
Au	197	79

METHOD

REF. NO.	
60 Ba 8	EGF

REACTION	RESULT	EXCITATION ENERGY	SOURCE		DETECTOR		ANGLE
			TYPE	RANGE	TYPE	RANGE	
G,N	ABX	14,18	D	14,18	ACT-I		4PI

σ at 17.5 MeV 460±50 mb

REF.

K. N. Geller, J. Halpern, and E. G. McIrhead
Phys. Rev. 118, 1302-12 (1960)

ELEM. SYM.	A	Z
Au	197	79

METHOD

Betatron; neutron threshold; ion chamber

REF. NO.	
60 Ge 3	NVB

REACTION	RESULT	EXCITATION ENERGY	SOURCE		DETECTOR		ANGLE
			TYPE	RANGE	TYPE	RANGE	
G,N	NØX	THR	C THR		BF3-I		4 PI

THRESHØLD

TABLE I. Summary and comparison of neutron separation energies inferred from present threshold measurements with values predicted from mass data and reaction energies. All energies are expressed in the center-of-mass system in Mev.

Reaction	No. runs	Present results	Other results	Method	Reference
$Au^{197}(\gamma,n)Au^{196}$	3	8.057±0.022	7.96 ±0.07	threshold	f

Ref. V.P. Chizhov
Zhur. Eksp. i Teoret. Fiz. 38, 809 (1960)
Soviet Phys. JETP 11, 587 (1960)

Elem. Sym.	A	Z
Au	197	79

Method: 90 MeV Bremsstrahlung; scintillator counter telescope

Ref. No.: 60 Ch 1 JHH

Reaction	E or ΔE	E_o	Γ	$\int \sigma dE$	Jπ	Notes
$Au^{197}(\gamma,d)$						Energy Range of particles detected:
$Au^{197}(\gamma,p)$						E_d - 15.5-30 MeV
$Au^{197}(\gamma,t)$						E_p - 15.5-30 MeV
						E_t - 17-30 MeV
						Ratios:
						$\sigma(\gamma,d)/\sigma(\gamma,p)$ } at $\vartheta = 90°$
						$\sigma(\gamma,t)/\sigma(\gamma,d)$

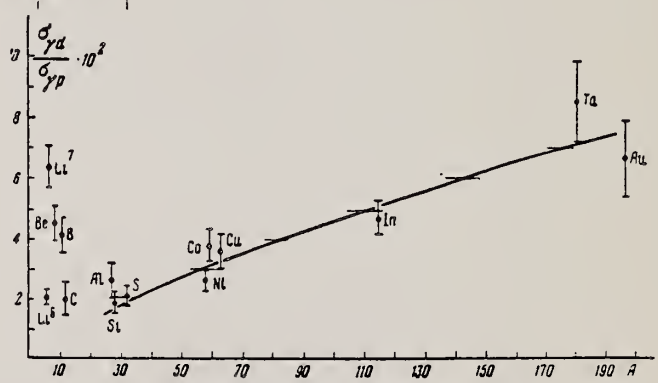

FIG. 3. Ratio of (γ, d) to (γ, p) cross sections for protons and deuterons of energies 15.5–30 Mev as function of atomic weight A. The solid curve shows the dependence given by Eq. (2), arbitrarily normalized.

TABLE I

Element	$100N_t/N_d$	Element	$100N_t/N_d$	Element	$100N_t/N_d$	Element	$100N_t/N_d$
Li^6	30±3	B	39±8	Ni	10±4	In	5±2.5
Li^7	22.5±2.5	Si	10±4	Co	2.5±2	Ta	10±4
Be	13±2.6	S	8±4	Cu	2.2±2	Au	3±3

Ref. E.D. Makhmovskii
Zhur. Eksp. i Teoret. Fiz. 38, 95 (1960)
Soviet Phys. JETP 11, 70 (1960)

Elem. Sym.	A	Z
Au	197	79

Method
Bremss. from Sycnchrotron, 23 MeV max.; emulsions

Ref. No.
60 Ma 1 JH

Reaction	E or ΔE	E_o	Γ	$\int \sigma dE$	J π	Notes
(γ,p)	$E_{\gamma max.}$=22.5	E_p=10.9				Angular distribution, energy distribution, and yield all consistent with Wilkinson calculations. Absolute yeild (1.6 ± 0.9)X10^{-5} proton/mole - MeV. Wilkinson absolute yeild agrees with this.

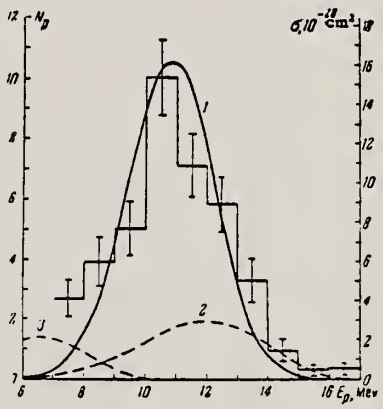

FIG. 1. Proton energy distribution. 1 – energy spectrum from the theory of direct resonance emission of nucleons; 2 – energy spectrum from Courant's theory of a direct photoeffect; 3 – energy spectrum from statistical theory.

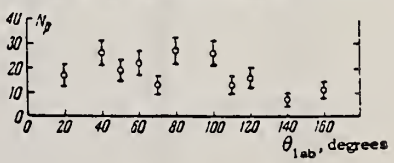

FIG. 2. Proton angular distribution.

Ref. K. Reibel, A.K. Mann
Phys. Rev. 118, 701 (1960)

Elem. Sym.	A	Z
Au	197	79

Method: γ's from $F^{19}(p,\alpha\gamma)$ reaction; protons from Vande Graaff; NaI.

Ref. No.: 60 Re 1 JHH

Reaction	E or ΔE	E_o	Γ	$\int \sigma dE$	Jπ	Notes
$Au^{197}(\gamma,\gamma)$	~ 7					$\langle\bar{\sigma}\rangle$ (E_p = 2.05 MeV) = < 2.7 mb

REF.

J. Miller, C. Schuhl, C. Tzara
J. Phys. Radium 22, 529 (1961)

ELEM. SYM.	A	Z
Au	197	79

METHOD

Positron annihilation; neutron cross section, BF_3 counter; ion chamber

REF. NO. 61 Mi 1 NVB

REACTION	RESULT	EXCITATION ENERGY	SOURCE		DETECTOR		ANGLE
			TYPE	RANGE	TYPE	RANGE	
G,XN	ABX	8-20	D	8-20	BF3-I		4PI

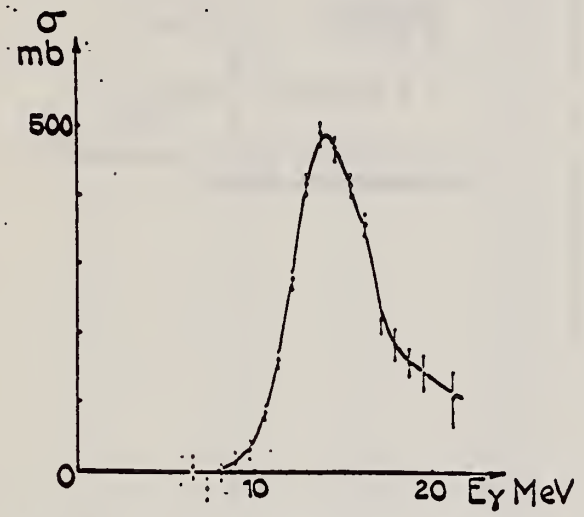

FIG. 3a. — Or, $\sigma(\gamma, n) + 2\sigma(\gamma, 2n) + \sigma(\gamma, np) + \ldots$

Ref. I.C. Nascimento, G. Moscati, J. Goldemberg
Nuclear Phys. 22, 484 (1961)

Elem. Sym.	A	Z
Au	197	79

Method: Betatron; BF_3 neutron counters; NaI for activation method.

Ref. No.: 61 Na 1 JHH

Reaction	E or ΔE	E_o	Γ	$\int \sigma dE$	Jπ	Notes
(γ,n) (γ,2n)	Bremss. 10-22	(581) (582)				581+

Cross sections in Figure 6 derived from data in Figure 1 using Katz and Cameron [Can. J. Phys. 29, 518 (1951)] spectrum tables.

Assumed:

$$\frac{\sigma(\gamma, sn)}{\sigma \text{ abs.}} = 1 - e^{-x}(1+x)$$

$$x = (a/E-E_n)^{3/2} (E-E_{2n})$$

a = 0.035 (A-12) as given by Heidmann and Bethe.

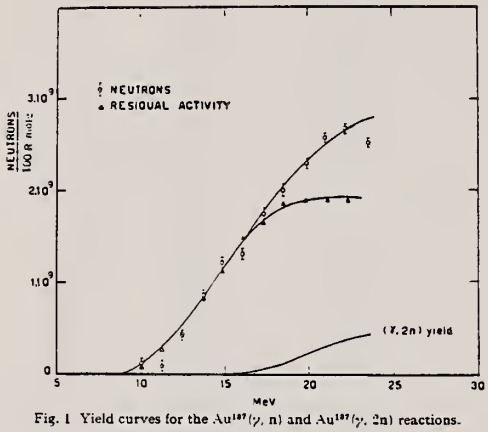

Fig. 1 Yield curves for the $Au^{197}(\gamma, n)$ and $Au^{197}(\gamma, 2n)$ reactions.

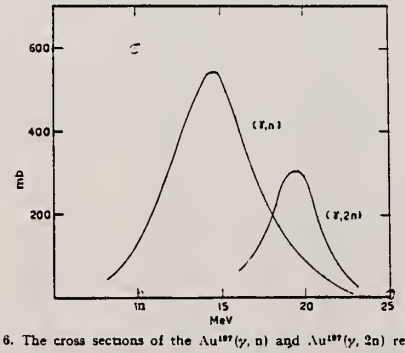

Fig. 6. The cross sections of the $Au^{197}(\gamma, n)$ and $Au^{197}(\gamma, 2n)$ reactions

TABLE I
Comparison of experimental data with evaporation theory

Element	Y_{2n} (semi-empirical) neutrons per 100 R per mole	Y_t Experimental	$\frac{Y_{2n}}{Y_t}$ (semi-empirical)	$\frac{Y_{2n}}{Y_t}$ (experimental)	Refs.
V^{51}	$5.0 \cdot 10^6$	$2.1 \cdot 10^6$	$2.4 \cdot 10^{-3}$		1)
Co^{59}	$3.2 \cdot 10^8$	2.6×10^6	$1.2 \cdot 10^{-2}$		2)
Cu^{63}	$3.8 \cdot 10^8$	$3.0 \cdot 10^6$	$1.2 \cdot 10^{-2}$	1.2×10^{-2}	3)
As^{75}	$1.2 \cdot 10^7$	$3.4 \cdot 10^6$	$3.5 \cdot 10^{-2}$		4)
Nb^{93}	5.2×10^7	$7.1 \cdot 10^6$	7.3×10^{-2}	1.9×10^{-1}	5, 4)
I^{127}	2.7×10^8	$1.4 \cdot 10^6$	$1.9 \cdot 10^{-1}$	1.8×10^{-1}	4), this work
Pr^{141}	$1.8 \cdot 10^8$	$1.4 \cdot 10^6$	1.3×10^{-1}	$1.4 \cdot 10^{-1}$	4)
Er^{167}	3.6×10^8	$1.8 \cdot 10^6$	$2.0 \cdot 10^{-1}$		13)
Ta^{181}	5.1×10^8	1.9×10^6	$2.7 \cdot 10^{-1}$	3.4×10^{-1}	4)
Au^{197}	6.8×10^8	$2.6 \cdot 10^6$	2.6×10^{-1}	$2.7 \cdot 10^{-1}$	4), this work
Bi^{209}	$7.0 \cdot 10^6$	$3.3 \cdot 10^6$	$2.1 \cdot 10^{-1}$		

References

1) J. M. Blatt and V. F. Weisskopf, Theoretical Nuclear Physics (John Wiley and Sons, New York 1952)
2) E. A. Whalin and A. O. Hanson, Phys. Rev. 89 (1953) 324L
3) A. I. Berman and K. L. Brown, Phys. Rev. 96 (1954) 83
4) E. Silva, J. Goldemberg and P. B. Smith, Nuovo Cim. 9 (1958) 17
5) F. Ferrero, R. Malvano, E. Silva, G. Moscati and J. Goldemberg, Nuclear Physics, 10 (1959) 423
6) J. O'Connell, P. Dyal and J. Goldemberg, Phys. Rev. 116 (1959) 173
7) R. Nathans and J. Halpern, Phys. Rev. 93 (1954) 437
8) G. Moscati and J. Goldemberg, Anais da Academia Brasileira de Ciências (to be published)
9) R. Montalbetti, L. Katz and J. Goldemberg, Phys. Rev. 91 (1953) 659
10) D. Strominger, J. M. Hollander and G. T. Seaborg, Rev. Mod. Phys. 30 (1958) 585
11) L. Katz and A. G. W. Cameron, Can. J. Phys. 29 (1951) 518
12) J. Heidmann and H. A. Bethe, Phys. Rev. 84 (1951) 1274
13) E. G. Fuller, B. Petree and M. S. Weiss, NBS Report No. 5686
14) P. C. Gugelot, Phys. Rev. 81 (1950) 51
15) B. M. Spicer, Phys. Rev. 100 (1955) 791

Ref. F. Tagliabue, J. Goldemberg
Nuclear Phys. 23, 144 (1961)

Elem. Sym.	A	Z
Au	197	79

Method 22 MeV betatron; $Si^{28}(n,p)Al^{28}$ threshold detector.

Ref. No. 61 Ta 1 JHH

Reaction	E or ΔE	E_o	Γ	$\int \sigma dE$	Jπ	Notes
$Au^{197}(\gamma,n)$	Bremss. 22					$E_n > 6$ MeV. $W(\theta_n) = A + B \sin^2\theta$ where B/A = 0.66±0.14

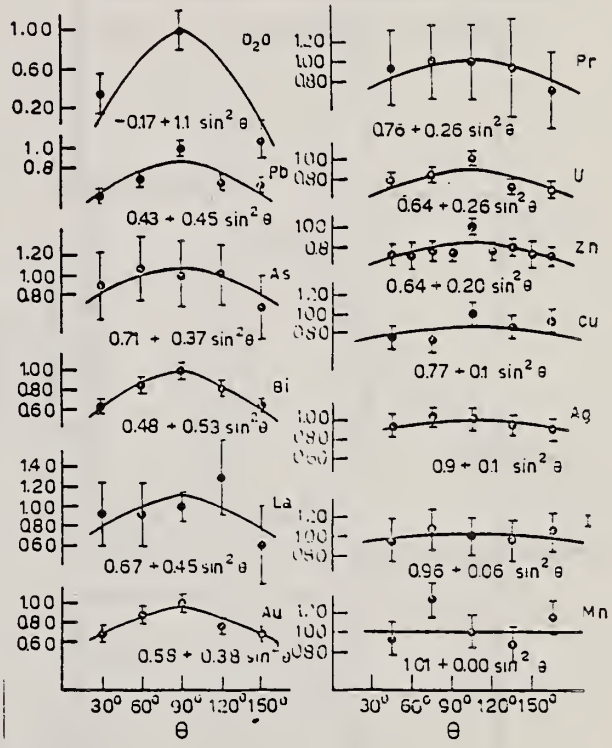

Figure 4: Angular distributions of fast photoneutrons as observed with the $Si^{28}(n,p)Al^{28}$ detector. Data normalized at 90° in each case.

Ref. R. E. Walsh, D.J. Donahue
Phys. Rev. 121, 880 (1961)

Elem. Sym.	A	Z
Au	197	79

Method: Monoergic γ's from thermal n-capture; activation

Ref. No.: 61 We 1 JHH

Reaction	E or ΔE	E_o	Γ	$\int \sigma dE$	Jπ	Notes
(γ,n)	7.91-9.72					Measurement of 65 kev x-ray from K-capture in Au^{196}. Data in Table II (millibarns); compares with Fuller and Weiss in Figure 4. $E_{\gamma\ thresh.}$ = 7.91 - 8.4 MeV.

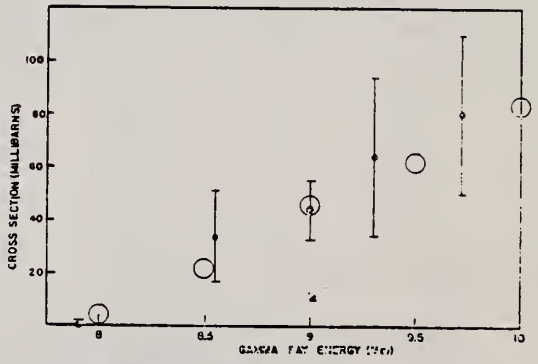

FIG. 4. Cross section vs energy for the $Au^{197}(\gamma,n)Au^{196}$(5.6 day) reaction. The circles are the data of Fuller and Weiss.[4]

TABLE II. Summary of measured cross sections.

γ-ray source / Energy (Mev) / Reaction	Co 7.49	Fe 7.64	Al 7.73	Cu 7.91	Cl 8.56	Ni 8.997	Fe 9.30	Cr 9.72	Fe 10.16	N 10.83
$Ta^{181}(\gamma,n)Ta^{180m}$	0±0.05	0.5±1	4.8±1.6	14±5	32±16	44±15	...	83±33	...	120±48
$Au^{197}(\gamma,n)Au^{196}$	...	...	...	0±2	34±17	44±11	64±30	80±30	...	...
$Ho^{165}(\gamma,n)Ho^{164}$	...	...	...	0±0.1	29±15	30±18	46±21	86±51	...	260±93
$Nb^{93}(\gamma,n)Nb^{92}$	...	...	...	...	...	0.008±0.005	1.0±0.4	2.4±0.7	...	...
$Ag^{107}(\gamma,n)Ag^{106}$	...	...	...	...	...	0±0.1	...	4.4±1.5	22±16	23±7.5

Ref. S.C.Fultz, R.L.Bramblett, J.T.Caldwell, N.A.Kerr

Phys.Rev. 127, 1273 (1962)

Elem. Sym.	A	Z
Au	197	79

Method
Positron annihilation - NaI(Tl), BF_3

Ref. No. 62Fu2 BG

Reaction	E or ΔE	E_o	Γ	$\int \sigma dE$	Jπ	Notes
(γ,n)+(γ,np)	7-25			2.14±0.15) $^{25}_{0}$		$\sigma_{-2} = \int_0^\infty \sigma E^{-2} dE = 15.3\pm1.5$mb/MeV level density parameter a:= $17.1\pm0.5 MeV^{-1}$
(γ,2n)	(358)			0.83±0.16) $^{25}_{0}$		
(γ,n)+(γ,2n) +(γ,np)	(357)	13.90	4.2			Lorentz line fitted to formation cross section (Fig.9). Experimental value of integrated cross section agrees with simple dipole - absorption sum rule.

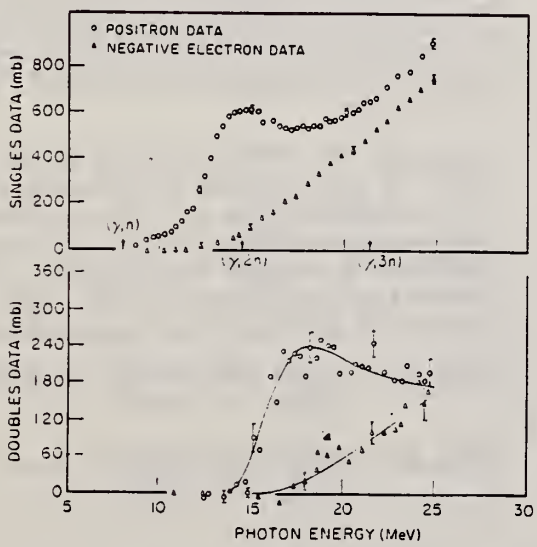

FIG. 6. Partially reduced neutron yield curves for Au. The top set was obtained from counting single neutrons per beam pulse. the lower set from counting two neutrons per beam pulse. For each set of curves, the top curve was obtained by use of positrons while the lower curve was obtained by use of negative electrons.

FIG. 7. Cross section obtained from neutron yield data. The top curve (A) consists of $\sigma(\gamma,n)+2\sigma(\gamma,2n)+\sigma(\gamma,np)+3\sigma(\gamma,3n)$ and was obtained from single-neutron counting data. The lower curve (B) was obtained from double-neutron counting data and consists of $2\sigma(\gamma,2n)+6\sigma(\gamma,3n)$.

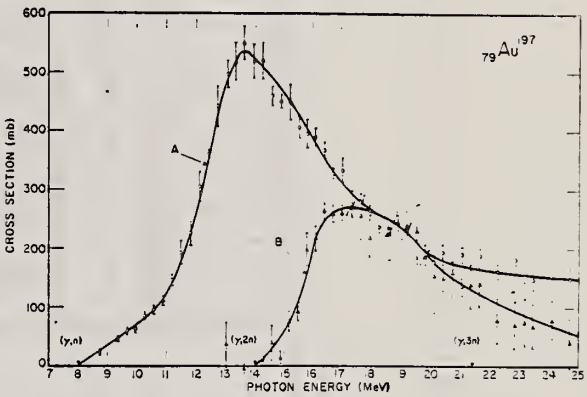

FIG. 9. The nuclear formation cross section for gold, consisting of $\sigma(\gamma,n)+\sigma(\gamma,2n)+\sigma(\gamma,np)$. The solid line is a Lorentz curve with a peak cross section of 335 mb at 13.90 MeV, and a width of 4.2 MeV.

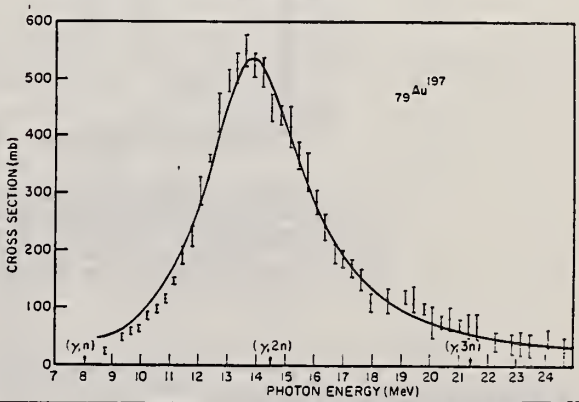

Ref. J.S. O'Connell, P.A. Tipler, P. Axel
Phys. Rev. 126, 228 (1962)

Elem. Sym.	A	Z
Au	197	79

Method
25 MeV betatron; monoergic photons by coincidence with analyzed electrons from Bremss. target; NaI

Ref. No. 62 Oc 1 JHH

Reaction	E or ΔE	E_o	Γ	$\int \sigma dE$	Jπ	Notes
(γ,γ') (γ,γ)	11.48 - 17.72	~ 13.5				Data taken at θ = 135°. Fitted to a "two Lorentz line fit": σ_1= 0.255 barn, E_{o1}= 13.15 MeV, Γ_1= 2.9 MeV. σ_2= 0.365 barn, E_{o2}=13.90 MeV, Γ_2 =4.0 MeV. suggested by Fuller and Weiss [Phys. Rev. 112, 560 (1958)].

TABLE I. Experimental results.

E_γ Mev	E_β Mev	$N_{\gamma\alpha}$ $10^2\times$	Total Counts	Chance Counts	$d\sigma/d\Omega$ 10^{-28} cm²/sr Individual	Average
11.48		2.06	20	12.0	0.80±0.45	
11.66	18.03	1.64	21	9.7	1.41±0.58	1.07±0.30
11.84		1.61	15	7.1	1.00±0.50	
Chance		1.70	9	7.5		
12.50		2.66	72	33.2	3.02±0.66	
12.64	18.03	1.95	55	27.3	2.94±0.79	3.18±0.43
12.78		2.15	57	19.9	3.57±0.73	
Chance		2.15	23	24.5		
13.30		1.39	53	12.2	6.14±1.1	
13.45	19.83	1.11	40	9.0	5.83±1.2	6.73±0.71
13.62		1.15	53	7.8	8.21±1.4	
Chance		1.10	8	8.6		
14.30		3.07	134	29.2	7.20±0.80	
14.44	19.83	2.27	107	19.2	8.18±0.97	7.12±0.52
14.58		2.28	87	22.3	5.99±0.87	
Chance		2.06	18	23.0		
15.29		1.94	104	48.0	6.11±1.1	
15.41	19.83	1.44	66	26.6	5.80±1.2	5.45±0.66
15.53		1.48	61	29.9	4.45±1.1	
Chance		1.34	32	28.8		
16.55		0.820	22	5.6	4.30±1.3	
16.69	22.02	0.564	14	4.6	3.59±1.5	3.83±0.78
16.83		0.623	15	4.6	3.59±1.4	
Chance		0.668	7	4.8		
17.48		0.882	17	12.6	1.08±1.05	
17.60	22.02	0.631	16	5.5	3.59±1.35	3.48±0.80
17.72		0.622	24	7.4	5.78±1.7	
Chance		0.666	7	5.6		

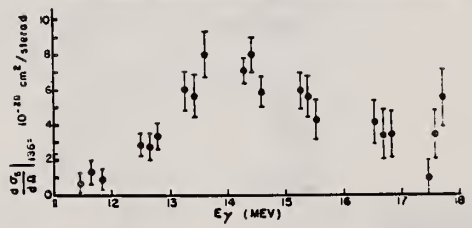

FIG. 6. Differential Scattering Cross Section of Au^{197} at 135°. The cross section includes both elastic scattering and high energy inelastic scattering. The ordinate is the differential cross section in units of 10^{-28} cm²/sr; the abscissa is the gamma ray energy in Mev. The energy resolution varied from point to point but was about 150 kev±30 kev.

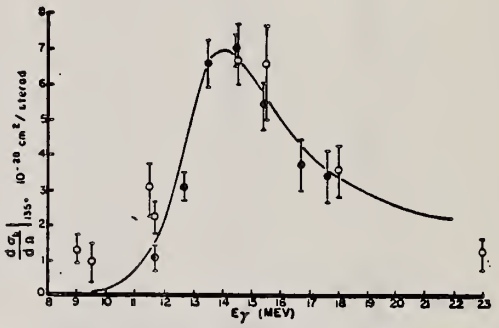

FIG. 7. Differential Scattering Cross Section for Au^{197} at 135°. The experimental dots (this experiment) and open circles (0.82 times the adjusted value obtained from references 23 and 24) may include high energy inelastic scattering; the solid curve is 0.82 times the prediction for only elastic scattering obtained by using published value of measured absorption cross section (reference 21). The energy resolution varies from point to point but is about 350 kev.

Ref. 24: The cross sections given in ref. 23 were reduced by a factor 0.866 in accordance with ref. 15 and they were converted from 120° to 135° by assuming a 1-$Cos^2\theta$ distribution. The normalization factor of 0.82, mentioned in the text was also applied.

Ref. 21: Fuller and Weiss, Phys. Rev. 112, 560 (1958).

Ref: 23: Fuller and Hayward, Phys. Rev 101, 692 (1956).

Ref. J. Miller, C. Schuhl, C. Tzara
Nuclear Phys. 32. 236 (1962)

Elem. Sym.	A	Z
Au	197	79

Method: Linac; monoergic photons by e^+ annihilation in flight; NaI

Ref. No.: 62 Mi 3 | JHH

Reaction	E or ΔE	E_o	Γ	$\int \sigma dE$	Jπ	Notes
Au 197 (γ,xn)	6.5-22	14.2±0.5		$\int_0^{22}$ = 3.00±0.05 MeV-b		

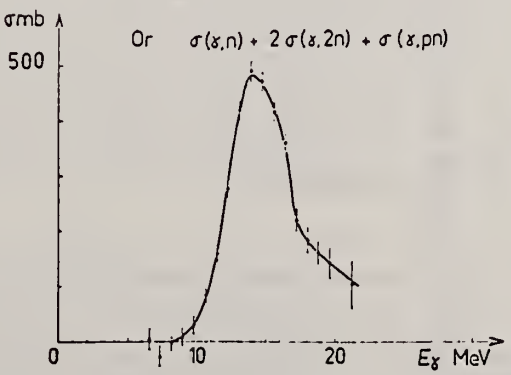

Fig. 10. Section efficace
$\sigma = \sigma(\gamma, n) + \sigma(\gamma, np) + 2\sigma(\gamma, 2n) + \ldots$ pour l'or.

TABLEAU 5

Résultats expérimentaux

Éléments	Fig. No	E_m (MeV)	σ_{int} (MeV · b) [a]	$\frac{\sigma_{int}}{0.06NZ/A}$	Seuils γ, n	γ, p	γ, 2n	γ, np
Cu	6	17 ±0.5	0.45±0.015	0.47±0.015				
La	7	15.6±0.5	1.91±0.03	0.94±0.015	8.80 [13]		14.25 [13]	14.90 [13]
Ce 140	8	15.6±0.5	1.88±0.03	0.92±0.015	9.05 [14]	8.50 [14]	14.1 [14]	
Ce 142					7.15 [14]	9.50 [14]	14.3 [14]	
Ta 181	9	13 ±0.5 16.5±0.5	2.97±0.05	1.13±0.02	7.55 [13]		13.84 [13]	13.47 [13]
Au 197	10	14.2±0.5	3.00±0.05	1.06±0.02	7.90 [13]		13.71 [13]	12.94 [13]
Pb 206	11	13.8±0.5	4.10±0.06	1.38±0.02	10.6 [12]	7.1 [12]	14.3 [12]	14.5 [12]
Pb 207					7.2 [12]	8.2 [12]	14.3 [12]	17.9 [12]
Pb 208					6.9 [12]	8.4 [12]	15.0 [12]	14.2 [12]
Bi 209	12	14.0±0.5	3.73±0.06	1.24±0.02	7.44 [14]	3.76 [14]	10.4 [14]	

[a] L'intégrale $\int_0^{\infty} \sigma dE$ est prise jusqu'à ∞ égal à 19.6 MeV pour Cu, à 21.2 MeV pour La et Ce et à 22 MeV pour Ta, Au, Pb et Bi. D'autre part, les erreurs indiquées sont les erreurs statistiques.

FORM NBS-418
(8-1-63)
USCOMM-DC 18556-P63

U.S. DEPARTMENT OF COMMERCE
NATIONAL BUREAU OF STANDARDS

Ref. G.C. Reinhardt, W.D. Whitehead
Nuclear Phys. 30, 201 (1962)

Elem. Sym.	A	Z
Au	197	79

Method 55 MeV betatron; synchrotron; $Si^{28}(n,p)Al^{28}$ activity; $Cu^{63}(\gamma,n)Cu^{62}$ monitor.

Ref. No. 62 Re 1 | EGF

Reaction	E or ΔE	E_o	Γ	$\int \sigma dE$	Jπ	Notes
$Au^{197}(\gamma,n)$	Bremss. 55					Figure 7: Dotted curve is of form $a_o + a_1\cos\theta + a_2\cos^2\theta + a_2\cos^2\theta - a_1\cos^2\theta$; solid curve is of form $a_o + a_1\cos\theta + a_2\cos^2\theta$; errors on points are statistical errors in counting only.

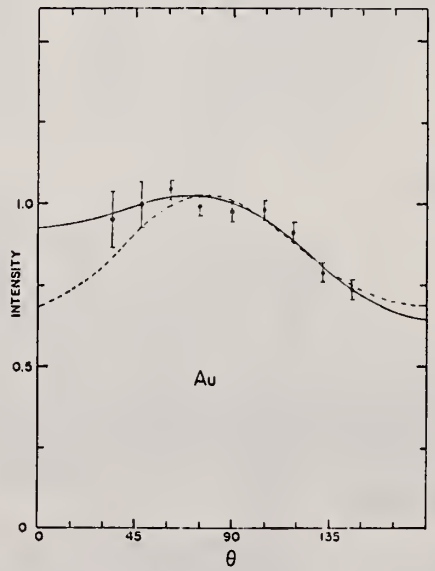

Fig. 7. Angular distribution of fast neutrons from gold
See fig. 5.

TABLE 2

Parameters of the fit (1) for the expressions $a_0 - a_1\cos\theta - a_2\cos^2\theta$, $a - b\sin^2\theta - c\cos\theta$ and $A_0 - A_1P_1 - A_2P_2$

	Bi(1)	Bi(2)	Pr	Au	Y	Ho	La
a_0	1.00±0.02	1.00±0.02	1.00±0.02	1.00±0.02	1.00±0.03	1.00±0.02	1.00±0.01
a_1	0.15±0.03	0.18±0.04	0.17±0.04	0.14±0.03	0.17±0.06	0.12±0.03	0.14±0.03
$-a_2$	0.47±0.06	0.40±0.08	0.41±0.09	0.21±0.07	0.15±0.11	0.34±0.06	0.39±0.06
A_1*)	0.18±0.04	0.21±0.05	0.20±0.05	0.15±0.04	0.18±0.06	0.14±0.04	0.16±0.03
$-A_2$*)	0.37±0.05	0.31±0.06	0.32±0.07	0.15±0.05	0.11±0.08	0.26±0.05	0.30±0.04
a	0.53±0.06	0.60±0.08	0.59±0.09	0.79±0.07	0.85±0.11	0.66±0.06	0.61±0.06
b	0.47±0.06	0.40±0.08	0.41±0.09	0.21±0.07	0.15±0.11	0.34±0.06	0.39±0.06
c	0.15±0.03	0.18±0.04	0.17±0.04	0.14±0.03	0.17±0.06	0.12±0.03	0.14±0.03

*) Renormalized so that $A_0 = 1$

TABLE 4

Parameters of the fit (3) for the expressions $a_0 + a_1\cos\theta + a_2\cos^2\theta + a_3\cos^3\theta$, $1 - A_1P_1 + A_2P_2 - A_3P_3$

	Bi(1)	Bi(2)	Pr	Au	Y	Ho	La
a_0	1.01±0.02	1.00±0.02	1.01±0.03	0.98±0.02	1.00±0.03	1.00±0.02	1.01±0.02
a_1	0.19±0.05	0.17±0.07	0.21±0.07	0.07±0.06	0.16±0.09	0.12±0.05	0.17±0.05
$-a_2$	0.56±0.11	0.37±0.15	0.50±0.16	0.05±0.12	0.13±0.20	0.33±0.12	0.47±0.11
a_3	−0.17±0.18	0.05±0.24	−0.17±0.25	0.31±0.19	0.05±0.32	0.03±0.19	−0.17±0.17
A_1*)	0.11±0.15	0.23±0.18	0.13±0.20	0.27±0.13	0.20±0.22	0.15±0.14	0.09±0.13
$-A_2$*)	0.45±0.09	0.28±0.11	0.39±0.12	0.03±0.08	0.09±0.14	0.24±0.09	0.37±0.09
A_3*)	−0.08±0.09	0.02±0.11	−0.08±0.12	0.13±0.08	0.02±0.13	0.01±0.08	−0.08±0.08

*) Renormalized so that $A_0 = 1$

T. Kaminishi, C. Kojima
Jap. J. Appl. Phys. 2, 399 (1963)

Au	197	79

METHOD: Linac; isomer yield; activity

REF. NO.: 63 Ka 2 | NVB

REACTION	RESULT	EXCITATION ENERGY	SOURCE TYPE	SOURCE RANGE	DETECTOR TYPE	DETECTOR RANGE	ANGLE
G,G/	RLY	1	C 4		ACT-I		4PI
		(0.10, 0.27,					
		0.40)					

Table II. The isomers observed

Isomer	Observed value		Referenced value[11][13]	
	Half-life	Energy (MeV)	Half-life	Energy (MeV)
Se-77m	17.5 sec	0.160	17.5 sec	0.161
Br-79m	4.80 sec	0.209	4.8 sec	0.208
Sr-87m	2.3 hr	0.390	2.8 hr	0.388
Y-89m	15.0 sec	0.920	14 sec	0.915
Rh-103m	58 min	*	57 min	0.040
Ag-107m	42 sec	0.95	44 sec	0.094
Ag-109m			40 sec	0.088
Cd-111m	47 min	0.150,0.255	49 min	0.150,0.247
In-115m	4.5 hr	0.335	4.5 hr	0.335
Sn-117m	17 day	0.160	14 day	0.159,0.161
Ba-137m	2.6 min	0.660	2.6 min	0.662
Er-167m	2.10 sec	0.209	2.5 sec	0.208
Hf-179m	18.5 sec	0.157,0.215	19 sec	0.161,0.217
W-183m	5.4 sec	0.200,0.170,0.115	5.5 sec	0.1025,0.2915 others
Ir-191m	4.90 sac	0.129, <0.07	4.9 sec	0.042-0.129
Pt-195m	4.5 day	0.065**	4.1 day	0.031-0.130
Au-197m	7.0 sec	0.10,0.27,0.40	7.2 sec	0.130,0.270,0.407
Hg-199m	43 min	0.160,0.370	42 min	0.158,0.368

* This isomer was measured with a G-M flow counter.
** This value corresponds to Pt-K X-ray energy.

Table III. Induced activation rate

Element	Beam energy (MeV)	Counting rate (×10000 cpm,	Sample form
Se	5	1300	metallic pellet
Br	4	1600	NaBr grain
Sr	6	0.3	$SrCO_3$ powder
Y	5	80	metallic grain
Rh	5	0.2*	$RhCl_3$ grain
Ag	5	180	metallic plate
Cd	6	0.5	$CdCl_2$ grain
In	6	3	metallic plate
Sn	6	0.0005	metallic plate
Ba	5	0.6	BaS powder
Er	4	4900	Er_2O_3 powder
Hf	5	1600	metallic plate
W	5	120	metallic powder
Ir	5	2100	metallic powder
Pt	5	0.3	metallic plate
Au	4	4300	metallic plate
Hg	6	0.09	metallic liquid

* The value measured with a G-M flow counter

REF.

M. Langevin, J.M. Loiseaux
J. de Physique 24, 1027 (1963)

ELEM. SYM.	A	Z
Au	197	79

METHOD: Betatron; photon scattering

REF. NO.: 63 La 1 NVB

REACTION	RESULT	EXCITATION ENERGY	SOURCE		DETECTOR		ANGLE
			TYPE	RANGE	TYPE	RANGE	
G,G	ABX	9-26	C	32	NAI-D		DST

Angular Distribution:

$$W(\theta) = 1 + a \cos^2\theta$$

for $11 < E < 20$ MeV, find $a = 0.9 \pm 0.1$

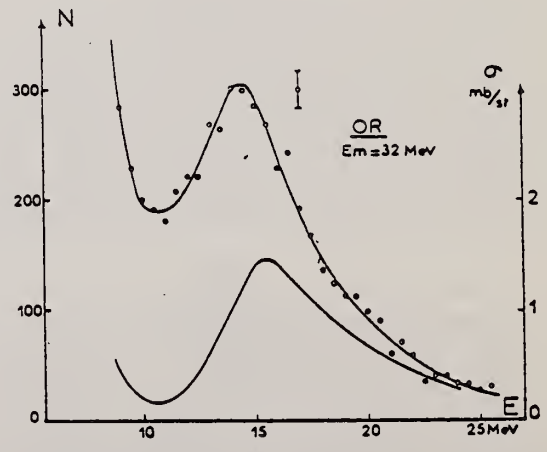

FIG. 1.

REF.

A. Veres
Acta Phys. Acad. Sci.Hung. 16, 261-73 (1963)

ELEM. SYM.	A	Z
Au	197	79

METHOD

Radioactive source

REF. NO.: 63 Ve 2 | NVB

REACTION	RESULT	EXCITATION ENERGY	SOURCE TYPE	SOURCE RANGE	DETECTOR TYPE	DETECTOR RANGE	ANGLE
G,G/	ABX	0-1	D	0-1	NAI-D		

ISØMERS

Таблица II

Измеренные значения после облучения, сравниваемые с другими литературными данными

Элемент	Активность облучения после первого измерения (имп/мин.)	Активи. экстрп. в конце облуч. (имп/мин.)	Лутературные данные $T_{1/2}$	Лутературные данные E (кэв)	Данные измерений $T_{1/2}$	Данные измерений E (кэв)	σ_m (10^{-28} см^2)	$\Gamma_{\gamma m}$ (10^{-4} эв)
Se-77m	3842±96	5400	17,5 сек.	160	18,1±1 сек.	160±10	9,5	1,75
Sr-87m	191±5	200	2,8 ч.	390	2,9±0,1 ч.	365±25	0,85	0,2
У-89m	96±20	170	16 сек.	910	16,7±5 сек.		0,08	0,02
Rh-103m	28±5	31	57 мин.	40	58±2 мин.	20,5±0,5	0,08	0,01
Ag-107m	220±14	250	44 сек.	93	43,8±0,6 сек	91±10	0,8	0,2
Ag-109m			39 сек.	88				
Hf-179m	80±18	155	19 сек.	160; 215	19±2 сек.		1	0,2
Ir-191m	90±20	250	4,9 сек.	42; 130	5±2 сек.		5,6	1
Pt-195m	90±9	100	3,5 д.	31; 100; 130;	3,5±0,2 д.	32±3 67,5±5 96±5 130±10	0,2	0,04
Au-197m	240±16	520	7,2 сек.	130; 277; 407	7,2±1 сек.	68:130: 280±20 390±20	0,07	0,01
Hg-199m	9,6±3,2		42 мин.	160; 370			0,005	0,001

Ref. G.N. Zatsepina, V.V. Igonin, L.E. Lazareva, A.I. Lepestkin
Zhur. Eksp. i Teoret. Fiz. 44, 1787 (1963)
Soviet Phys. JETP 17, 1200 (1963)

Elem. Sym.	A	Z
Au	197	79

Method Synchrotron; neutron spectra, angular distribution data; emulsions; ion chamber monitor

Ref. No. 63 Za 1 JHH

Reaction	E or ΔE	E_0	Γ	$\int \sigma dE$	Jπ	Notes
$Au^{197}(\gamma,n)$	Bremss. 14 19					

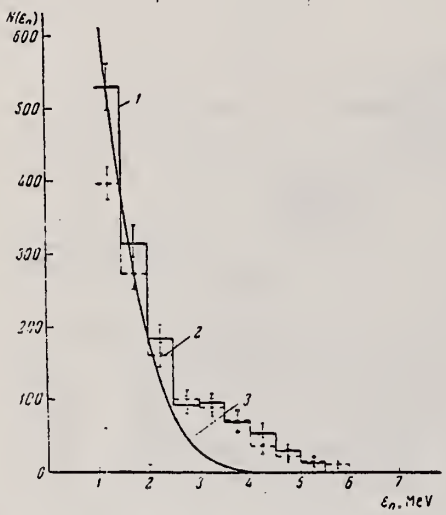

FIG. 5. Energy distribution of photoneutrons from gold at $(h\nu)_{max}$ = 14 MeV; histogram 1 – $N_{90°} + N_{270°}$; histogram 2 – $N_{30°} + N_{150°}$; curve 3 – neutron spectrum calculated in accordance with the evaporation model.

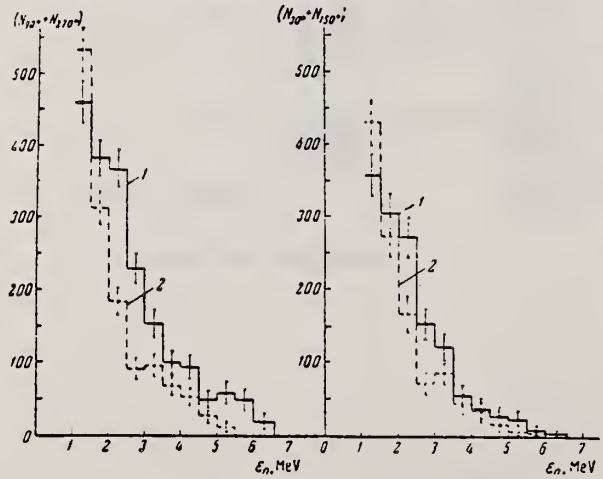

FIG. 6. Comparison of the spectra of photoneutrons from bismuth (1) and gold (2) for different emission angles at $(h\nu)_{max}$ = 14 MeV.

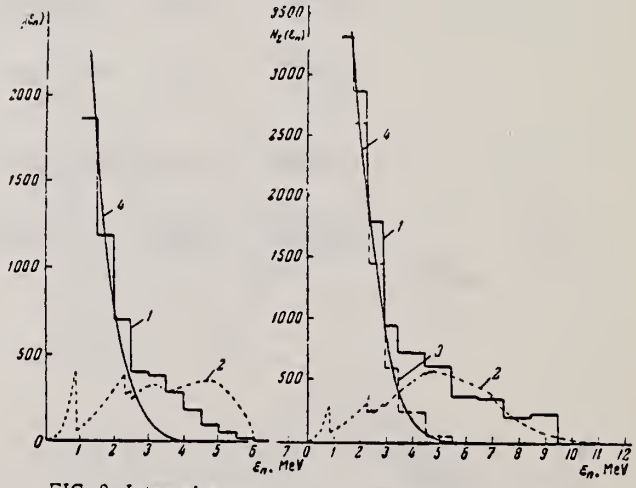

FIG. 8. Integral spectra of photoneutrons from gold at $(h\nu)_{max}$ = 14 MeV (a) and 19 MeV (b);; histogram 1 – summary neutron spectrum $N_\Sigma(\epsilon_n)$ for 30, 90, 150, and 270°; curve 2 – calculated spectrum $N_d(\epsilon_n)$ of the "direct" neutrons; histogram 3 – difference $N_\Sigma(\epsilon_n) - N_d(\epsilon_n)$; curve 4 – calculated spectrum of evaporation neutrons.

FORM NBS-418
(8-1-63)
USCOMM-DC 18556-P63

U.S. DEPARTMENT OF COMMERCE
NATIONAL BUREAU OF STANDARDS

REF.

M. Langevin, J. M. Loiseaux et J. M. Maison
Nucl. Phys. 54, 114-124 (1964)

ELEM. SYM.	A	Z
Au	197	79

METHOD

Bremsstrahlung scattering

REF. NO. 64 La 1 JOC

REACTION	RESULT	EXCITATION ENERGY	SOURCE TYPE	SOURCE RANGE	DETECTOR TYPE	DETECTOR RANGE	ANGLE
G,G	ABX	10-25	C		NAI-D		DST

TABLEAU I

Le paramètre $a(E)$ de la distribution angulaire

Noyau	11.5-14. MeV			14-17.5 MeV			17.5-20 MeV			20-30 MeV	
	Exp.	Ellipsoidal	Triax.	Exp.	Ellips.	Triax.	Exp.	Ellips.	Triax.	Exp.	Ellips.
							Contribution Quadrupolaire %				
Tb	$0.5^{+0.15}_{-0.1}$	0.41	0.39	$0.54^{+0.15}_{-0.1}$	0.70	0.50	25	0.97	0.85		1
Ho	$0.27^{+0.15}_{-0.1}$	0.44	0.407	$0.43^{+0.10}_{-0.05}$	0.71	0.53	25	0.95	0.9	0.4 ± 0.1	1
Er	$0.27^{+0.15}_{-0.1}$	0.44	0.407	$0.8^{+0.15}_{-0.1}$	0.71	0.53	25	0.95	0.9		1
Ta	$0.6^{+0.15}_{-0.1}$	0.58		$0.68^{+0.15}_{-0.1}$	0.81		20	0.96			
Au	a_{exp}(11-20 MeV) = 0.9									0.7 ± 0.1	1
	a_{th} (11-20 MeV) ≈ 1										

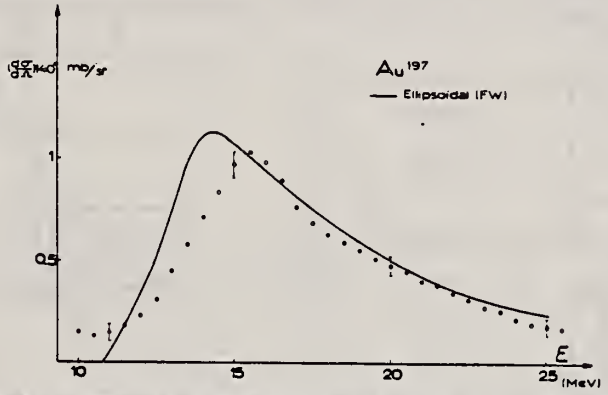

Fig. 6. Sections efficaces différentielles de diffusion obtenues pour l'or. La courbe tracée correspond à l'application des relations de dispersion aux sections efficaces d'absorption de Fuller et Weiss[16]) (F.W.)

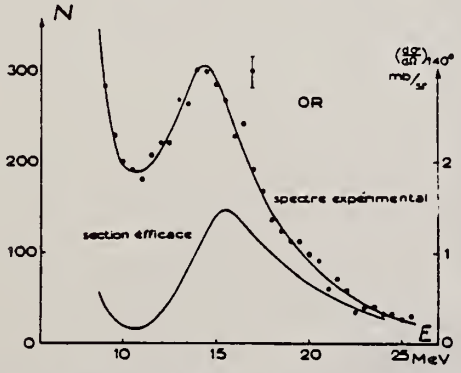

Fig. 2. Résultats expérimentaux et sections efficaces de diffusion déduites pour l'or, E_m = 32 MeV.

REF.

F. I. Havliček and M. Modesto
Energ. Nucl. 12, 77 (1965)

ELEM. SYM.	A	Z
Au	197	79

METHOD

REF. NO.	
65 Ha 2	JOC

REACTION	RESULT	EXCITATION ENERGY	SOURCE		DETECTOR		ANGLE
			TYPE	RANGE	TYPE	RANGE	
G,A	SPC	THR-31	C	31	EMU-D	5-20	DST

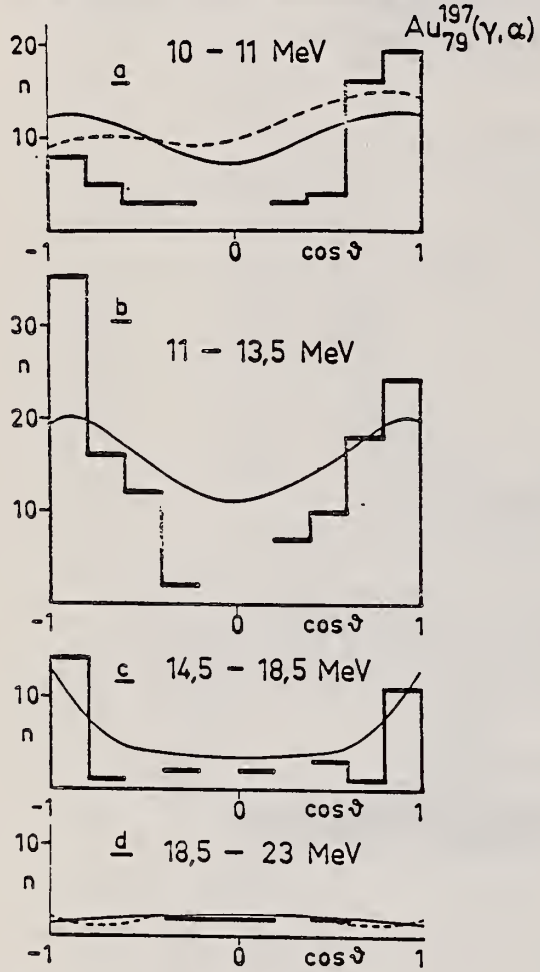

Fig. 11.

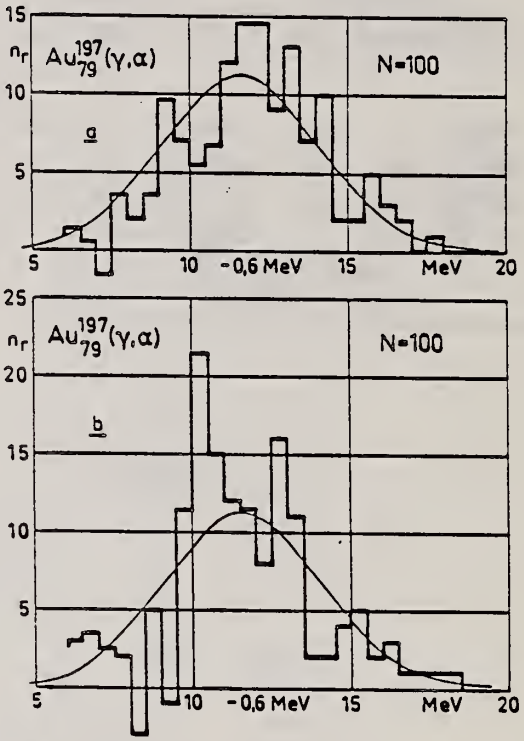

Fig. 10.

REF.
B. MacDonald, J. A. Diaz, S. N. Kaplan, and R. V. Pyle
Phys. Rev. 139, B1253 (1965)

ELEM. SYM.	A	Z
Au	197	79

METHOD
Cyclotron; μ^- capture

REF. NO.
65 Ma 2 NVB

REACTION	RESULT	EXCITATION ENERGY	SOURCE TYPE	SOURCE RANGE	DETECTOR TYPE	DETECTOR RANGE	ANGLE
MU-,XN	NØX	10 - 20	D	0	SCI-I		4PI
		[DO NOT PUT IN DATA INDEX]					

Tries to fit data with Fermi gas and Gaussian momentum distributions.

NEUT MULTIPLICITY

TABLE IV. Corrected experimental results.

Target	Average multiplicity, $\langle n \rangle$	Multiplicity distribution (adjusted to 0.545 efficiency) F_0	F_1	F_2	F_3	F_4	F_5	F_6	F_7
Al	1.262 ±0.059	0.449 ±0.027	0.464 ±0.028	0.052 ±0.013	0.036 ±0.007	−0.0023 ±0.004	−0.001 ±0.004	0.003 ±0.004	
Si	0.864 ±0.072	0.611 ±0.042	0.338 ±0.042	0.045 ±0.018	−0.002 ±0.008	0.003 ±0.005	0.002 ±0.003	0.003 ±0.006	
Ca	0.746 ±0.032	0.633 ±0.021	0.335 ±0.022	0.025 ±0.009	0.004 ±0.006	0.003 ±0.003			
Fe	1.125 ±0.041	0.495 ±0.018	0.416 ±0.019	0.074 ±0.011	0.014 ±0.005	−0.0001 ±0.003	0.002 ±0.003		
Ag	1.615 ±0.060	0.360 ±0.021	0.456 ±0.023	0.144 ±0.017	0.031 ±0.009	0.007 ±0.003	0.002 ±0.004	0.001 ±0.003	
I	1.436 ±0.056	0.396 ±0.021	0.474 ±0.023	0.087 ±0.015	0.035 ±0.009	0.007 ±0.005	0.0002 ±0.004		
Au	1.662 ±0.044	0.370 ±0.015	0.425 ±0.016	0.156 ±0.012	0.032 ±0.006	0.014 ±0.004	0.003 ±0.003	0.0003 ±0.003	
Pb	1.709 ±0.066	0.324 ±0.022	0.483 ±0.025	0.137 ±0.018	0.045 ±0.010	0.011 ±0.006			
Ag*	1.60 ±0.18	0.389 ±0.100	0.455 ±0.075	0.120 ±0.035	0.030 ±0.015	0.001 ±0.003	0.009 ±0.006	0.000 ±0.007	0.010 ±0.007
Pb*	1.64 ±0.16	0.348 ±0.100	0.479 ±0.057	0.137 ±0.027	0.018 ±0.012	0.010 ±0.005	0.005 ±0.004	0.003 ±0.002	0.002 ±0.002

* Results of Kaplan, Moyer, and Pyle (Ref. 1).

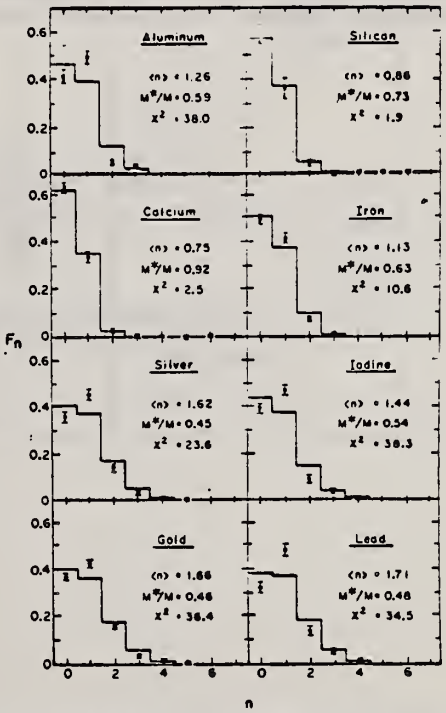

FIG. 11. Comparison of the observed neutron multiplicities with histograms calculated by using the Gaussian momentum distribution, $\alpha^2/2M = 20$ MeV.

REF.

L. Meneghetti and S. Vitale
Nuclear Phys. 61, 316 (1965)

ELEM. SYM.	A	Z
Au	197	79

METHOD

REF. NO.	
65 Me 2	EGF

REACTION	RESULT	EXCITATION ENERGY	SOURCE		DETECTOR		ANGLE
			TYPE	RANGE	TYPE	RANGE	
G,A	SPC	THR - 35	C	35	SCD-D	5-26	90

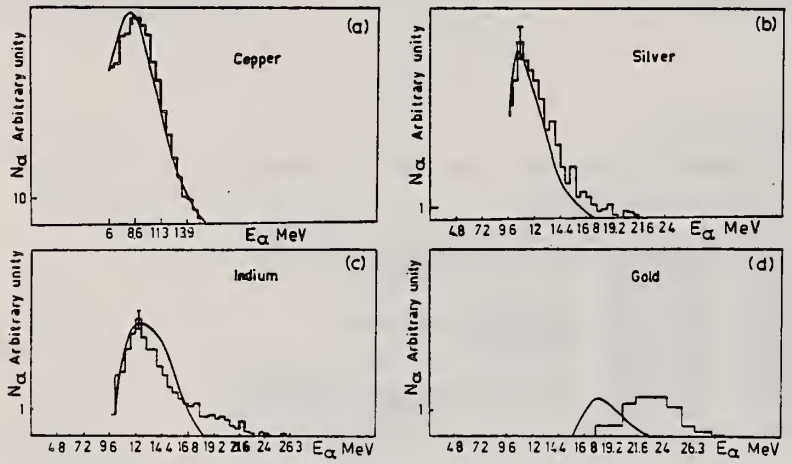

Fig. 2. The histograms show the experimental α-spectra. The solid lines are the calculated evaporative spectra corrected for target self-absorption and normalized to the maximum of the experimental spectra.

TABLE 1
α yields from the 90° data. Yield (per mole R)

Elements	Experimental	Calculated evaporative
Cu	$(1 \pm 0.1)10^{5}$	$3.1\ 10^{4}$
Ag	$(2.8 \pm 0.3)10^{4}$	$3.4\ 10^{3}$
In	$(1.05 \pm 0.1)10^{4}$	$3.05\ 10^{3}$
Au	$(1.7 \pm 0.2)10^{3}$	8.7

Errors in experimental yields are compounded of statistical errors and errors in the absolute calibration of the beam.

REF. H. M. Gerstenberg and E. G. Fuller
NBS Tech. Note 416, June 1967

ELEM. SYM.	A	Z
Au	197	79

METHOD

REF. NO. 67 Ge 2 HMG

REACTION	RESULT	EXCITATION ENERGY	SOURCE		DETECTOR		ANGLE
			TYPE	RANGE	TYPE	RANGE	
G,N	ABY	THR-27	C	22,27	BF3-I		4PI

Table 7. Comparison of neutron yields. Yields are given in units of (neutron cm²/MeV nucleus)x10⁻²⁸. The estimated uncertainties in Y and Y_c are of the order of 6% and 10%, respectively.

Element	E_o	$Y(E_o)$	Y_c				Y_c/Y				Ref.
			UCRL	Saclay	Va.	NBS(Old)	UCRL Exp	Saclay Exp	Va. Exp	NBS(Old) Exp	
Pb	27	103	86				0.83				26,30
	22	111	92	116			0.83	1.05			
Au	27	89	97				1.09				24,30.
	22	92	98	88		115	1.07	0.96		1.25	38
Ta	27	81	82	77			1.01	0.95			27,30,
	22	85	79	80		113	0.93	0.94		1.33	38
Ho	27	67	75				1.12				27,31,
	22	69	77	82		103	1.12	1.19		1.49	39
Ag	27	36									
	22	34.8									
Cu	27	14.4	13.2				0.92				28,30
	22	12.6	11.5	12.4			0.91	0.98			
Co	27	12.7	12.1				0.95				29,34
	22	10.6	9.9		13.5		0.94		1.27		
Ca	27	1.69		1.13	1.01			0.67	0.60		32,35
P	27	2.35			1.76				0.75		36
Al	27	1.92	1.62		1.38		0.84		0.72		25,37
O^{16}	27	0.54	0.42	0.48	0.42		0.78	0.89			16,32, 37
C	27	0.50	0.35	0.33	0.46		0.70	0.66			25,32, 33

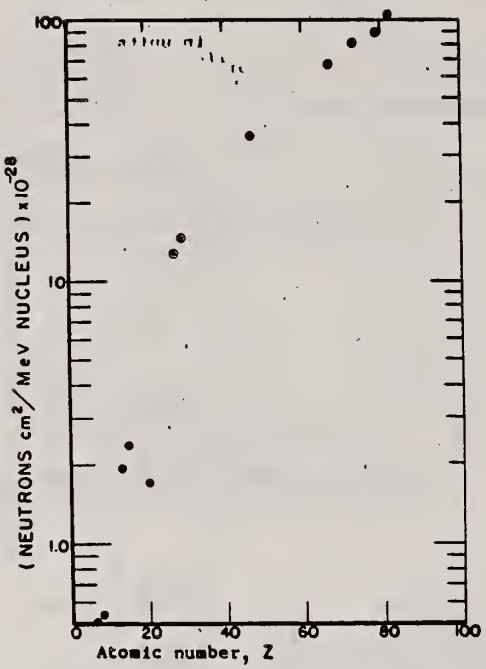

Fig. 31. Absolute neutron yield as a function of atomic number. The neutron yield from calcium (Z = 20) is particularly low in comparison with the other elements because its (γ,n) threshold is high compared to the mean energy of the giant resonance.

REF. R. R. Hurst and D. J. Donahue
Nucl. Phys. A91, 365 (1967)

ELEM. SYM.	A	Z
Au	197	79

METHOD
Neutron capture gamma rays

REF. NO. 67 Hu 1 EGF

REACTION	RESULT	EXCITATION ENERGY	SOURCE		DETECTOR		ANGLE
			TYPE	RANGE	TYPE	RANGE	
G,N	ABX	9-11	D	9-11	BF3-I		4PI

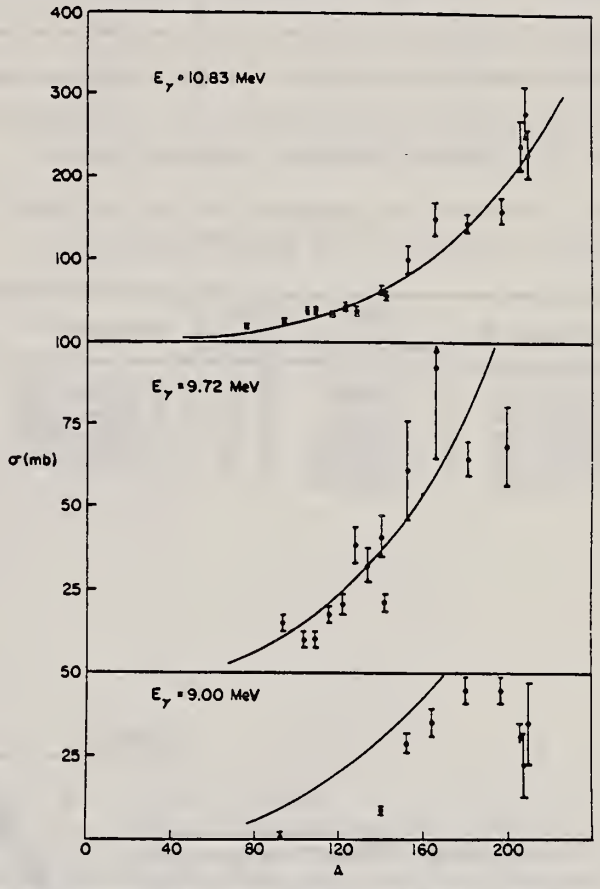

Fig. 1. Cross section (in mb) versus mass number of the target for gamma-ray energies of 9.00, 9.72 and 10.83 MeV. The solid lines are plots of eq. (1) in the text.

TABLE 1
Photoneutron cross sections (mb)

Target	7.72 MeV	9.00 MeV	9.72 MeV	10.83 MeV
^{59}Co				9.0± 0.8
^{75}As				20.4± 1.7
^{93}Nb		0.53± 0.10	14.6± 2.2	25.8± 2.1
^{103}Rh			10.6± 1.7	38.8± 3.1
^{107}Ag, ^{109}Ag			10.0± 1.5	37.6± 2.9
^{115}In			17.1± 2.6	33.3± 2.7
^{121}Sb, ^{123}Sb			20.7± 3.1	42.5± 3.6
^{127}I			38.7± 5.8	38.8± 3.1
^{133}Cs			31.7± 4.8	52.5± 3.8
^{139}La		8.61± 0.86	40.8± 6.5	63.0± 5.0
^{141}Pr			21.5± 3.2	58.3± 4.1
^{151}Eu, ^{153}Eu		28.9 ± 3.2	61.3±14.7	102 ±18
^{165}Ho		35.6 ± 4.3	92.2±27.6	150 ±20
^{181}Ta	4.14±0.36	45.4 ± 3.7	65.0± 5.5	146 ±12
^{197}Au		44.5 ± 3.6	68.4±13.5	160 ±15
^{206}Pb		<34.3		238 ±29
^{208}Pb		22.6 ±11.3		280 ±31
^{209}Bi		36.1 ±12.0		226 ±27

REF. A. V. Mitrofanova, Yu. N. Ranyuk, and P. V. Sorokin
J. Nucl. Phys. (USSR) 6, 703 (1967)
Sov. J. Nucl. Phys. 6, 512 (1968)

ELEM. SYM.	A	Z
Au	197	79

METHOD

REF. NO.	
67 Mi 1	HMG

REACTION	RESULT	EXCITATION ENERGY	SOURCE		DETECTOR		ANGLE
			TYPE	RANGE	TYPE	RANGE	
G,F	ABX	300-999		300-999	TRK-I		

Detector: Fission fragment tracks in glass.

999 = 1600 MEV

Angular distribution measured for Pb was found isotropic; for other elements it was assumed isotropic.

Nucleus	Fissionability D	Cross section σ_K, $\mu\beta$	Nucleus	Fissionability D	Cross section σ_K, $\mu\beta$
Bi	0.11±0.01	7.8±0.6	Os	0.0058±0.0005	0.37±0.04
Pb	0.050±0.004	3.4±0.3	Re	0.0056±0.0006	0.35±0.04
Tl	0.031±0.003	2.1±0.2	Ta	0.0045±0.0005	0.27±0.03
Au	0.019±0.002	1.25±0.10	Hf	0.0042±0.0004	0.25±0.03
Pt	0.012±0.002	0.80±0.08			

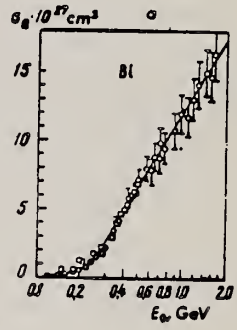

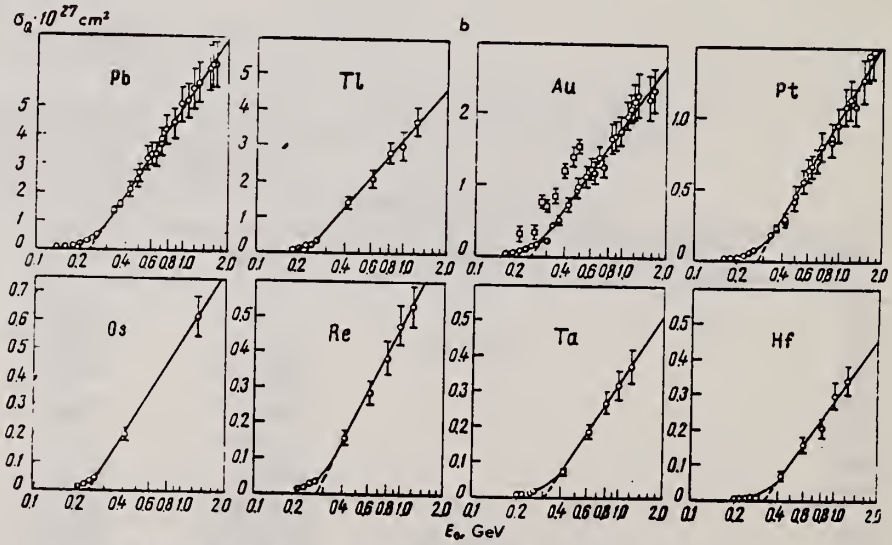

Fig. 1. Photofission fragment yields. ○-present work; □-Jungerman and Steiner.[1] The curves were plotted through the experimental points.

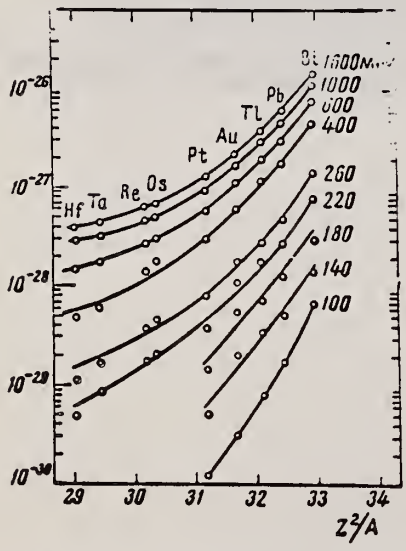

Fig. 2. Photofission fragment yields as a function of Z^2/A. The ordinates are values of σ_Q in units of cm².

REF. Yu. N. Ranyuk and P. V. Sorokin
J. Nucl. Phys. (USSR) 5, 37 (1967)
Sov. J. Nucl. Phys. 5, 26 (1967)

EL EM. SYM.	A	Z
Au	197	79

METHOD

REF. NO. 67 Ra 2 HG

REACTION	RESULT	EXCITATION ENERGY	SOURCE		DETECTOR		ANGLE
			TYPE	RANGE	TYPE	RANGE	
G,F	ABX	THR-260	C	100-260	EMU-I		DST

Angular distribution isotropic to 5%.

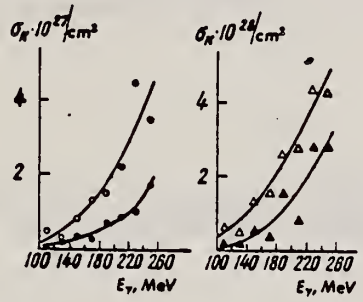

Fig. 3. Photofission cross sections. ○ – Bi, ● – Pb, △ – Au, ▲ – Pt. The curves were calculated from smoothed yield curves.

Table II

$E_{\gamma\,max}$, MeV	Cross section per equivalent γ quantum, 10^{-27} cm²			
	Bi	Pb	Au	Pt
100	0.07±0.005	0.017±0.002	0.003±0.0005	0.0012±0.0002
120	0.15±0.01	0.032±0.003	0.014±0.001	0.0035±0.0003
140	0.20±0.01	0.054±0.004	0.020±0.001	0.0053±0.0006
150 *	0.61±0.12	—	—	—
160	0.31±0.01	0.096±0.005	0.037±0.001	0.012±0.0005
180	0.46±0.02	0.13±0.01	0.055±0.001	0.015±0.001
180 *	0.68±0.09	—	—	—
200	0.62±0.02	0.20±0.01	0.082±0.002	0.031±0.001
200 *	1.3 ±0.24	—	0.31±0.09	—
200 **	0.7	—	—	—
220	0.83±0.03	0.28±0.01	0.108±0.003	0.039±0.001
240	1.22±0.03	0.36±0.01	0.146±0.003	0.063±0.001
240 **	1.5	—	—	—
250 *	1.78±0.22	—	0.33 ±0.07	—
260	1.50±0.04	0.50±0.02	0.180±0.004	0.085±0.002

* From [3].
** From [1].

REF. H. G. De Carvalho, V. Di Napoli, D. Margadonna and F. Salvetti and K. Tesch
Nucl. Phys. A126, 505 (1969)

ELEM. SYM.	A	Z
Au	197	79

METHOD

REF. NO. 69 De 1 egf

REACTION	RESULT	EXCITATION ENERGY	SOURCE		DETECTOR		ANGLE
			TYPE	RANGE	TYPE	RANGE	
G,N	ABY	THR-999	C	1-6	ACT-I		4PI
				(1.0-5.5)			

Yield per equivalent quantum. 999 = 5.5 GEV

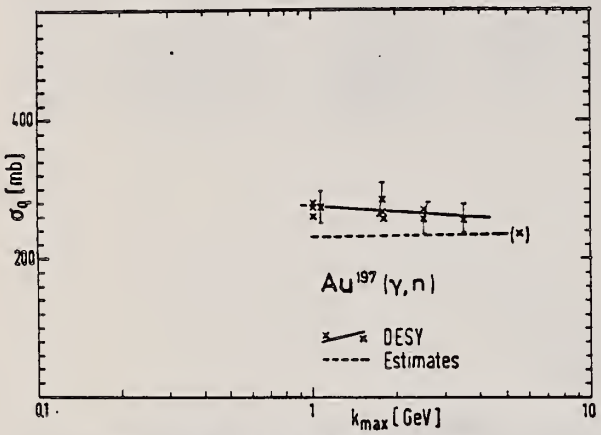

Fig. 4. See caption to fig. 1.

Cross sections per equivalent quantum for (γ, n) reactions as a function of the maximum bremsstrahlung energy. A straight line is adjusted to the experimental points by means of a least-squares fit. The indicated errors are due to the γ-ray spectroscopy. The dashed line gives the result of simple estimates.

REF. V. Di Napoli, D. Margadonna, F. Salvetti, H. G. De Carvalho and J. B. Martins
Lettere al Nuovo Cimento 1, 121 (1969)

ELEM. SYM.	A	Z
Au	197	79

METHOD

REF. NO.	
69 Di 1	egf

REACTION	RESULT	EXCITATION ENERGY	SOURCE		DETECTOR		ANGLE
			TYPE	RANGE	TYPE	RANGE	
G,N	ABY	THR-900	C	400-900	ACT-I		4PI

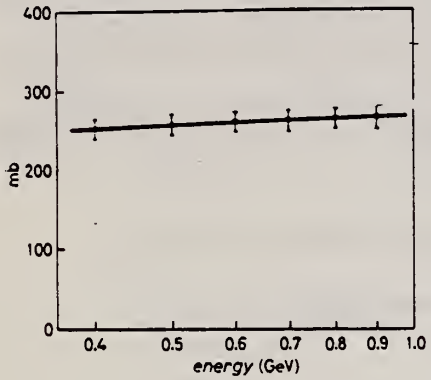

Fig. 1. – The cross-sections per equivalent quantum, σ_Q, are plotted *vs.* the natural logarithm of the peak energy of the bremsstrahlung. The straight line is a least-square fit of the experimental points.

TABLE I.

Peak energy of the bremsstrahlung (GeV)	cross-section per equivalent quantum (mb)
0.4	253 ± 12
0.5	256 ± 13
0.6	260 ± 13
0.7	262 ± 13
0.8	263 ± 13
0.9	265 ± 14

REF. A. P. Komar, B. A. Bochagov, A. A. Kotov, Yu. N. Ranyuk, G. G. Semenchuk, G. E. Solyakin, and P. V. Sorokin
Yad. Fiz. 10, 51 (1969)
Sov. J. Nucl. Phys. 10, 30 (1970)

ELEM. SYM.	A	Z
Au	197	79

METHOD

REF. NO. 69 Ko 2 egf

REACTION	RESULT	EXCITATION ENERGY	SOURCE		DETECTOR		ANGLE
			TYPE	RANGE	TYPE	RANGE	
G,F	SPC	THR-999	C	250-999	SCD-D		DST
		(1000)		(1000)			

999 = 1000 MEV

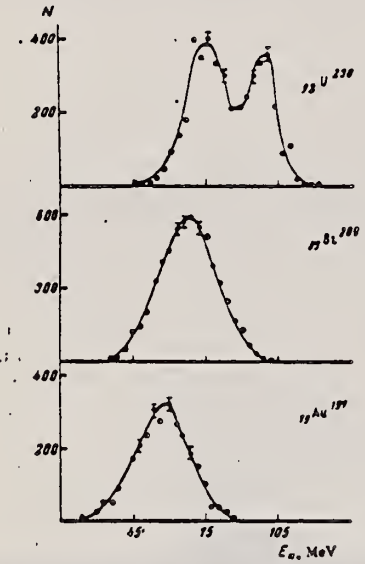

FIG. 2. Single-ended energy spectra of fragments from photofission of $_{92}U^{238}$, $_{83}Bi^{209}$, and $_{79}Au^{197}$.

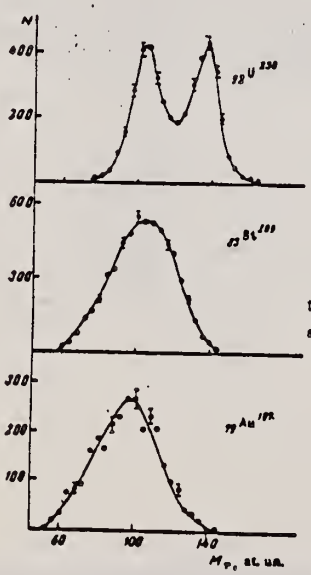

FIG. 3. Fragment mass distributions from photofission of $_{92}U^{238}$, $_{83}Bi^{209}$, and $_{79}Au^{197}$.

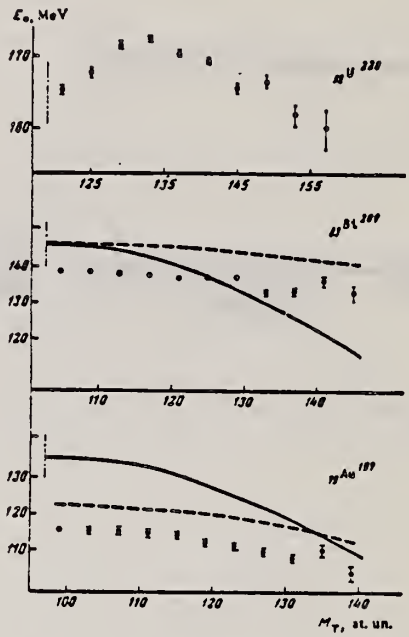

FIG. 4. Average total kinetic energies $\bar{E}_k$ of fragments from photofission of $_{92}U^{238}$, $_{83}Bi^{209}$, and $_{79}Au^{197}$, as a function of the heavy fragment mass. Points—experiment; solid curves—theory; dashed curves—experiment with inclusion of a correction for neutron emission from the fragments.

REF.

Yu. N. Ranyuk, V.M. Sanin, and P.V. Sorokin
Ukr. Fiz. Zhur. 14, 408 (1969)

ELEM. SYM.	A	Z
Au	197	79

METHOD

REF. NO.: 69 Ra 4 egf

REACTION	RESULT	EXCITATION ENERGY	SOURCE		DETECTOR		ANGLE
			TYPE	RANGE	TYPE	RANGE	
G,F	ABX	35-140	C	40-140	TRK-I		4PI

Yields of nuclear fission reaction for Bi, Au and Pt by bremsstrahlung were measured by means of solid state track detectors in the energy range from 40 to 140 MeV. The fission threshold for these nuclei is higher than the giant resonance energy which allowed total photofission cross-sections to be calculated by the yield curves.

A rapid increase of the cross-sections with the photon energy testifies to the preference of the statistical model within which the fission thresholds of target nuclei were calculated.

The results of the present experiment may be used to obtain information on the photon interaction mechanism in the energy region between the giant resonance and the threshold of meson production where this problem is still obscure.

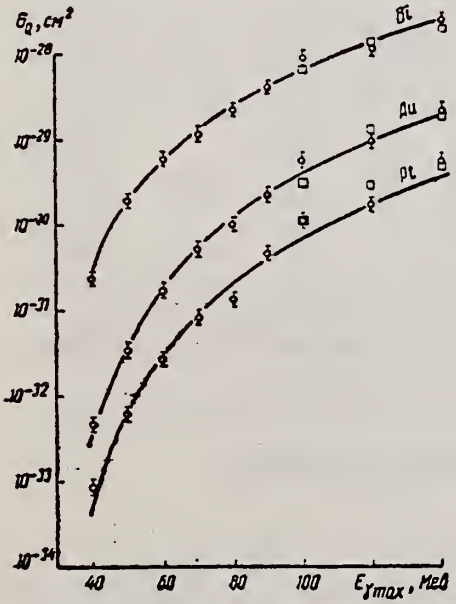

Рис. 2. Виходи уламків поділу: O — дані даної роботи, □ — дані роботи [3]. Суцільні крнві одержані підгонкою за формулою (4).

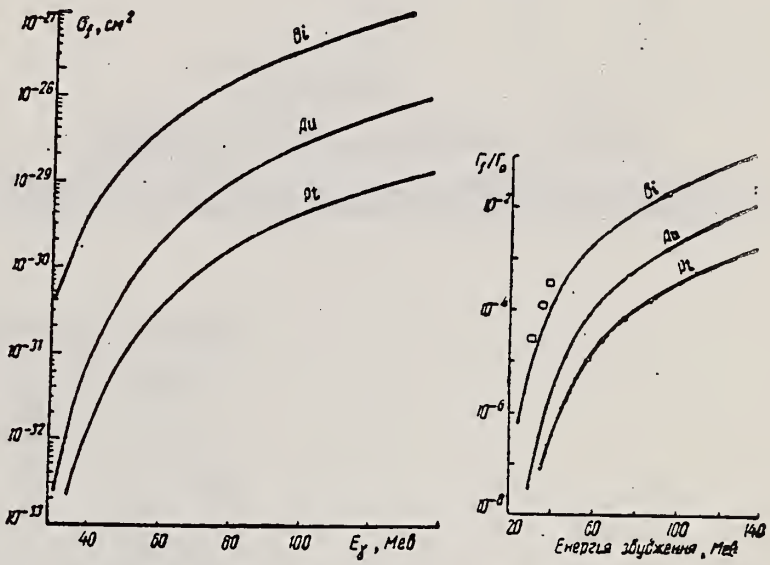

Рис. 3. Перерізи фотоподілу, розраховані на один реальний γ-квант підгонкою за формулою (4).

Рис. 4. Відношення ділильної і нейтронної ширин: □ — дані роботи [5] для суміші ізотопів Bi^{207} і Bi^{209}.

REF. A. Veyssiere, H. Beil, R. Bergere, P. Carlos, A. Lepretre
Nucl. Phys. A159, 561 (1970)

ELEM. SYM.	A	Z
Au	197	79

METHOD

REF. NO. 70 Ve 1 egf

REACTION	RESULT	EXCITATION ENERGY	SOURCE TYPE	SOURCE RANGE	DETECTOR TYPE	DETECTOR RANGE	ANGLE
G,N 334	ABX	8-26	D	7-36	BF3-I		4PI
G,2N 335	ABX	14-27	D	7-36	BF3-I		4PI
G,3N 336	ABX	24-27	D	7-36	BF3-I		4PI

334 +

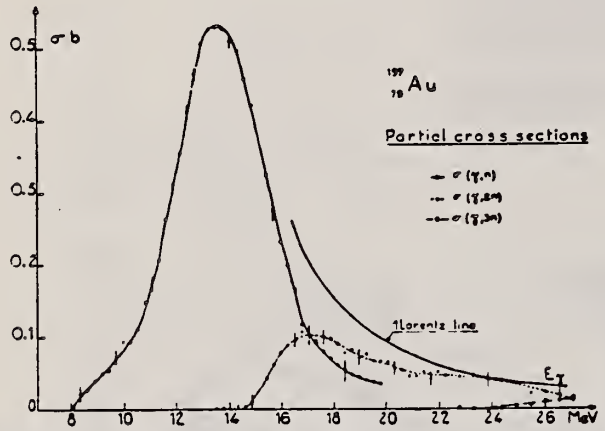

Fig. 2. Partial photoneutron cross sections $\sigma_{\gamma,1n}$, $\sigma_{\gamma,2n}$ and $\sigma_{\gamma,3n}$ of ^{197}Au. We also show the descending part of the unique Lorentz line corresponding to parameters given in table 3.

TABLE 5

Integrated cross sections and sum rule values of ^{208}Pb and ^{197}Au. The notation used is defined in the text

	Refs.	E_M (MeV)	σ_0 (MeV · b)	σ_0' (MeV · b)	$\frac{\sigma_0 A}{0.06\,NZ}$	$\frac{\sigma_0' A}{0.06\,NZ}$	σ_{-1} (mb)	σ_{-2} (mb · MeV^{-1})
^{208}Pb	[1]	22	4.10 ± 0.06	5.10	1.37	1.71	280	20.5
	[8]	28	2.91 ± 0.29	2.94	0.98	0.99		14.1 ± 1.4
	[23]	23	3.91 ± 0.59	5.18	1.31	1.74		18.6 ± 2.4
	present work	25	3.48 ± 0.23	4.00	1.17	1.34	251 ± 20	19.1 ± 2
^{197}Au	[1]	22	3.00 ± 0.05	3.99	1.06	1.40	200	14
	[9]	25	2.97 ± 0.3	3.53	1.05	1.24		15.3 ± 1.5
	present work	25	3.48 ± 0.2	4.07	1.23	1.42	238 ± 20	17.2 ± 2

[1] J.Miller, C.Schuhl and C.Tzara, Nucl.Phys. 32 (1962) 236.
[8] R.R.Harvey, J.T. Caldwell, R.L. Bramblett and S.C. Fultz, Phys. Rev. 136 (1964) B126.
[9] S.C.Fultz, R.L. Bramblett, J.T. Caldwell and N.A. Kerr, Phys.Rev. 127, (1962) 1273.
[23] T.Tomimasu, J. Phys. Soc. Jap. 25 (1968) 655.

[over]

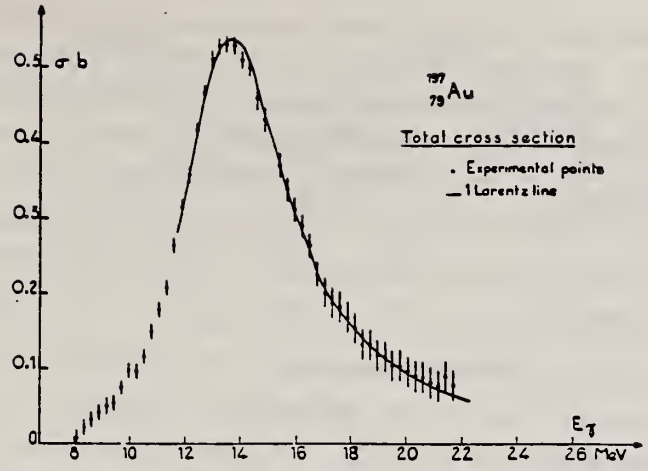

Fig. 4. Total photonuclear cross section $\sigma_{\gamma,T}(E)$ of ^{197}Au and best Lorentz line fit corresponding to parameters given in table 3.

REF. V. Di Napoli, A.M. Lacerenza, D. Margadonna, F. Salvetti, H.G. De Carvalho, J. Benuzzi Martins
Lettere al Nuovo Cimento 1, 65 (1971)

ELEM. SYM.	A	Z
Au	197	79

METHOD

REF. NO.	
71 Di 1	egf

REACTION	RESULT	EXCITATION ENERGY	SOURCE		DETECTOR		ANGLE
			TYPE	RANGE	TYPE	RANGE	
G,N	ABY	8-999	C	300-999	ACT-I		4PI
G,2N	ABY	15-999	C	300-999	ACT-I		4PI

Note: Text says Fig. 2 gives (γ,2n) yield.

999 = 1 GEV

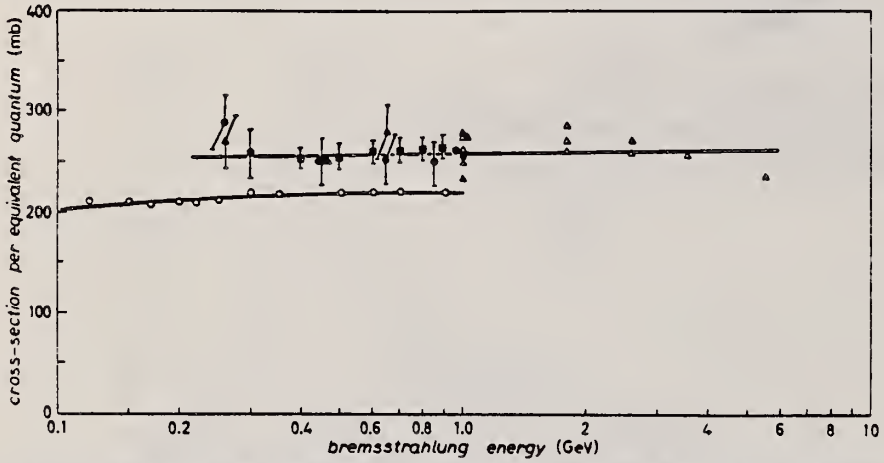

Fig. 1. – ^{197}Au(γ, n)^{196}Au reaction cross-sections per equivalent quantum are plotted *vs.* the natural logarithm of the bremsstrahlung maximum energy. *a)* • present work, collimated beam (8 mm collimator); *b)* ▲ present work, uncollimated beam; *c)* ■ Orsay (¹); *d)* △ DESY (²); *e)* ○ LINDGREN and JONSSON, Lund (³).

(3) K. Lindgren and G. Jonsson: Annual Report 1969, University of Lund, Lund Institute of Technology, Sect. 5A: 2b (Lund, 1970).

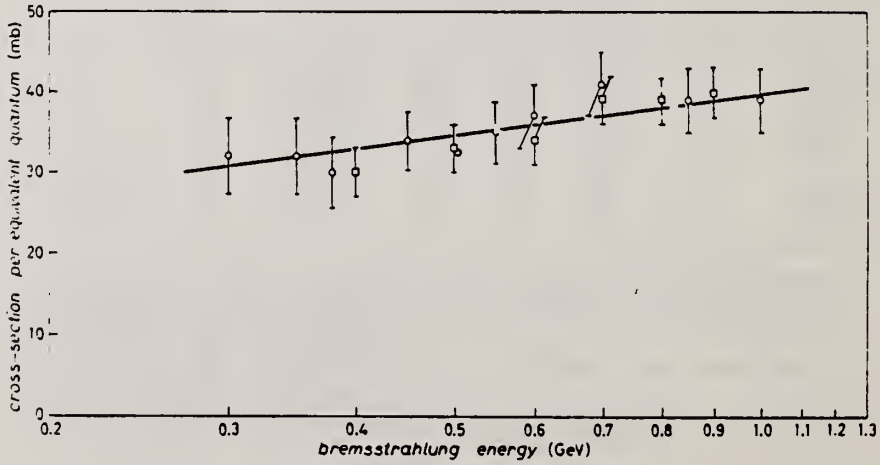

Fig. 2. – ^{197}Au(γ, n)^{196}Au reaction cross-sections per equivalent quantum are plotted *vs.* the natural logarithm of the bremsstrahlung maximum energy. *a)* ○ Frascati data, uncollimated beam; *b)* □ Orsay data, uncollimated beam.

REF. V. Di Napoli, D. Margadonna, F. Salvetti, H.G. De Carvalho, J.B. Martins
Nucl. Inst. Meth. 93, 77 (1971)

ELEM. SYM.	A	Z
Au	197	79

METHOD

REF. NO. 71 Di 5 hg

REACTION	RESULT	EXCITATION ENERGY	SOURCE TYPE	SOURCE RANGE	DETECTOR TYPE	DETECTOR RANGE	ANGLE
G,N	ABY	8-999	C	300-999	ACT-I		4PI

999 = 1 GEV

The use of the $^{19}F(\gamma,n)^{18}F$, $^{27}Al(\gamma,x)^{24}Na$, $^{197}Au(\gamma,n)^{196}Au$, and $^{12}C(\gamma,x)^{7}Be$ reactions as absolute monitors for high-energy, high-intensity bremsstrahlung beams is discussed. The cross sections per equivalent quantum and the absolute cross sections, in the energy range 300-1000 MeV, are reported for these reactions. $^{19}F(\gamma,n)^{18}F$, $^{27}Al(\gamma,x)^{24}Na$, and $^{12}C(\gamma,x)^{7}Be$ reactions are proposed as very simple and suitable systems for monitoring purposes.

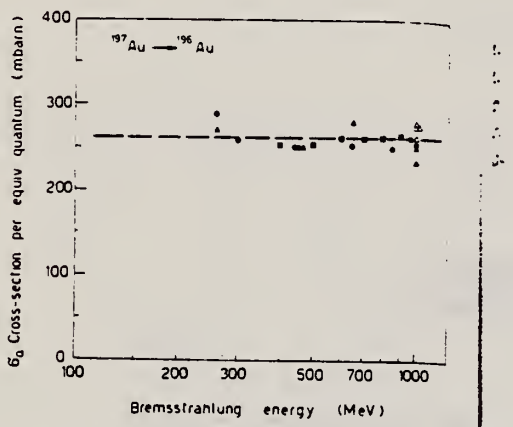

Fig. 3. $^{197}Au \rightarrow ^{196}Au$ reaction cross sections per e.q. Full triangles: present work, uncollimated beam; circles: present work, collimated beam; squares: Orsay[3]; open triangles: DESY[11]). The dashed line represents a constant value of 260 m

TABLE 2

Energy (MeV)	σ_Q(mb) $^{19}F \rightarrow ^{18}F$	$^{27}Al \rightarrow ^{24}Na$	$^{197}Au \rightarrow ^{196}Au$[a]	$^{12}C \rightarrow ^{7}Be$[a]
260			270±14	
300	5.90±0.20	0.37±0.01	258±13	0.37±0.01
320		0.39±0.01		
350	5.90±0.20	0.39±0.01		0.38±0.01
380	5.95±0.20	0.41±0.01		
400				0.42±0.01
420		0.45±0.01		
450	5.95±0.20	0.48±0.01	249±12	0.44±0.02
500	6.65±0.20	0.49±0.01		
550	6.65±0.20	0.50±0.02		0.47±0.02
600	6.80±0.20	0.52±0.02		
650		0.52±0.02	266±13	0.47±0.02
700	7.20±0.30	0.56±0.02		
750		0.55±0.02		
850	7.60±0.30	0.60±0.02	246±12	0.49±0.03
900		0.59±0.02		
1000	7.10±0.30	0.66±0.02	249±12	0.51±0.03

[a] The values given in the last two columns are, in most cases, an average of two or more measurements (see figs. 3 and 4).

REF.

V. Emma, S. Lo Nigro and C. Milone
Lettere al Nuovo Cimento 2, 271 (1971)

ELEM. SYM.	A	Z
Au	197	79

METHOD

REF. NO. 71 Em 2 egf

REACTION	RESULT	EXCITATION ENERGY	SOURCE		DETECTOR		ANGLE
			TYPE	RANGE	TYPE	RANGE	
G,F	ABY	THR-999	C	300-999	FRAG-I		4PI

999 = 1000 MEV

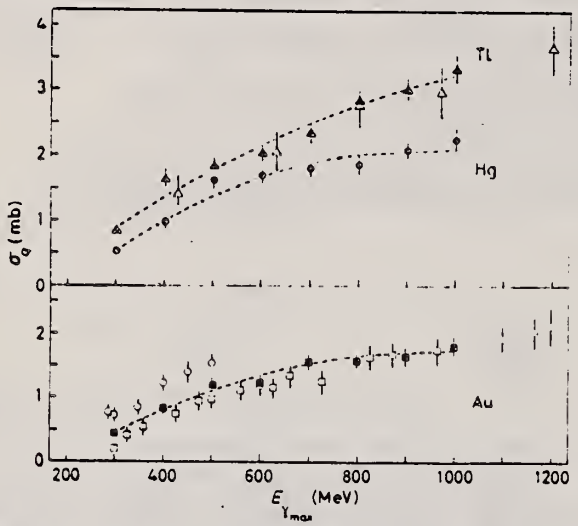

Fig. 1. – Photofission cross-sections per equivalent quantum σ_Q against the maximum energy of photons. Au: ○ ref. (¹), □ ref. (⁴), ■ our results; Hg: ● our results; Tl: △ ref. (⁴), ▲ our results. The dashed curves represent the fits calculated by the least-squares method taking into account our results only.

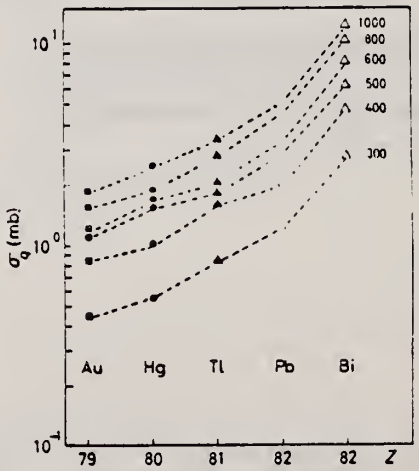

Fig. 2. – σ_Q-values, deduced in our present and previous (¹) experiments, reported *vs.* the atomic number Z of the elements for only some energy values.

(over)

TABLE I. — *Fission cross-sections per photon between 300 and 1000 MeV.*

	σ_f (mb)		
	Our results	Previous results	
Bi	7.6 ± 0.2	7.8 ± 0.6 (a)	7.8 ± 0.8 (c)
Pb	3.3 ± 0.1	3.4 ± 0.3 (a)	
Tl	1.9 ± 0.1	2.1 ± 0.2 (a)	
Hg	1.5 ± 0.1		
Au	1.19 ± 0.06	1.25 ± 0.1 (a)	

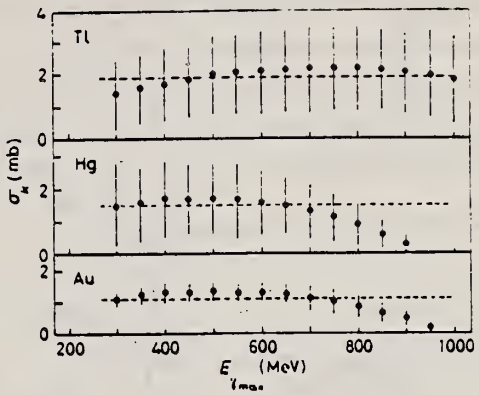

Fig. 3. – Fission cross-section per photon σ_γ of Tl, Hg and Au against $E\gamma_{max}$. The dashed straight lines represent the values $\sigma_\gamma = \text{const}$, calculated as suggested in ref. (c).

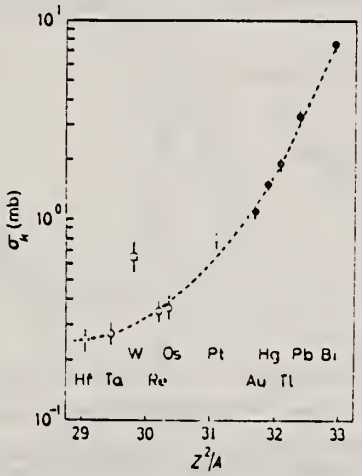

Fig. 4. – σ_γ-values *vs.* Z^2/A for the elements with atomic number in the range from 72 to 83: • our results, □ ref. (b), ○ ref. (c). The dashed curves is drawn by eye.

(a) V. EMMA, S. Lo Nigro and C. MILONE: *Boll. S.I.F.*, No. 70, 119 (1970).
(b) V. EMMA, S. Lo Nigro and C. MILONE: *Lett. Nuovo Cimento*, 3, 512 (1970).
(c) V. EMMA, S. Lo Nigro and C. MILONE: *Lett. Nuovo Cimento*, 2, 117 (1971).
(d) J. JUNGERMAN and H. M. STEINER: *Phys. Rev.*, **106**, 585 (1957).
(e) H. G. DE CARVALHO, G. COSTINI, E. DEL GIUDICE, G. PUPPENA and R. RINZIVILLO: *Nuovo Cimento*, **32**, 293 (1964).
(f) A. V. MITHOFANOVA, YU. N. RANYUK and P. V. SOROKIN: *Sov. Journ. Nucl. Phys.*, **6**, 512 (1968).

REF. K. Lindgren and G. G. Jonsson
Nucl. Phys. A166, 643 (1971)

ELEM. SYM.	A	Z
Au	197	79

METHOD

REF. NO. 71 Li 2 egf

REACTION	RESULT	EXCITATION ENERGY	SOURCE TYPE	SOURCE RANGE	DETECTOR TYPE	DETECTOR RANGE	ANGLE
G,YN	ABY	THR-900	C	75-900	ACT-I		4PI

Y = 1,2,3,4,5,7,9,11,13,15.

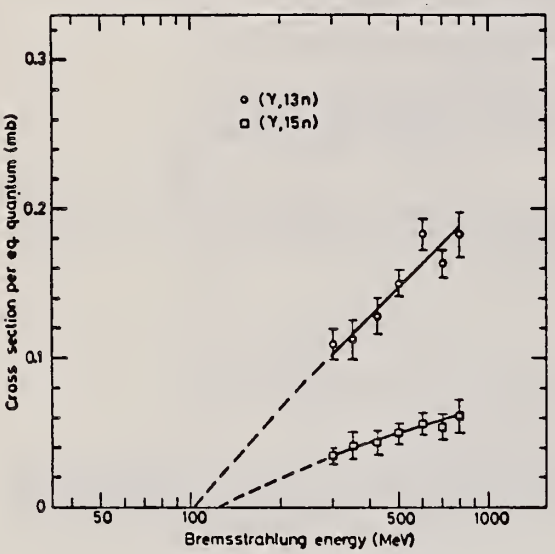

Fig. 5. Yield curves for the reactions (γ, 13n) and (γ, 15n).

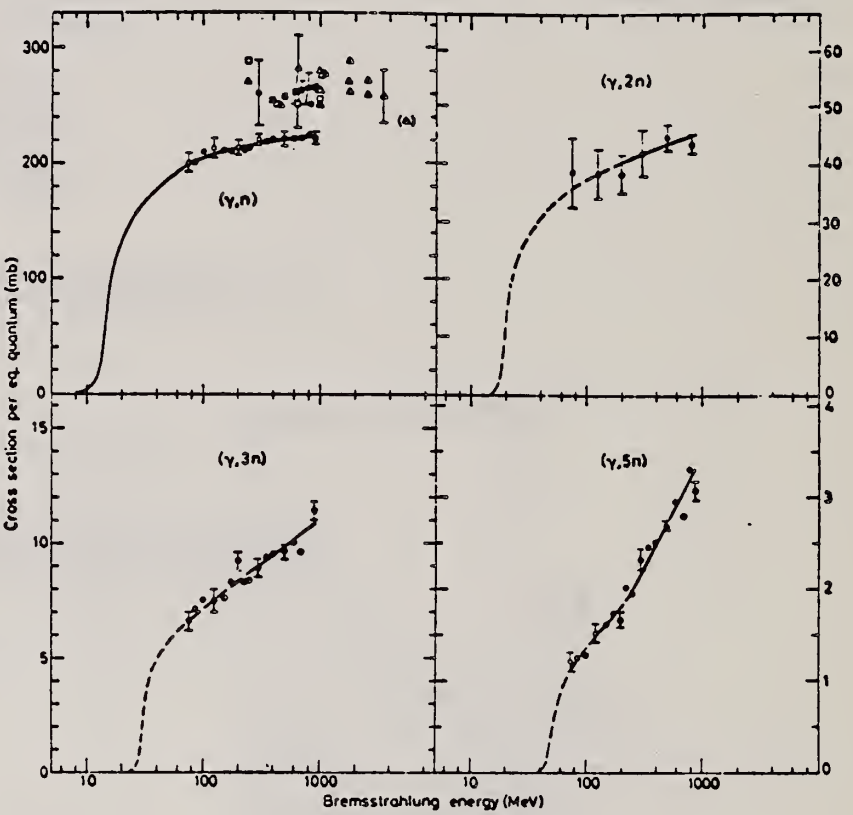

Fig. 3. Yield curves for the reactions (γ, n), (γ, 2n), (γ, 3n) and (γ, 5n). ○ this work, □ ● Frascati collimated beam, ▲ Frascati uncollimated beam, ◘ Orsay uncollimated beam, △ DESY collimated beam.

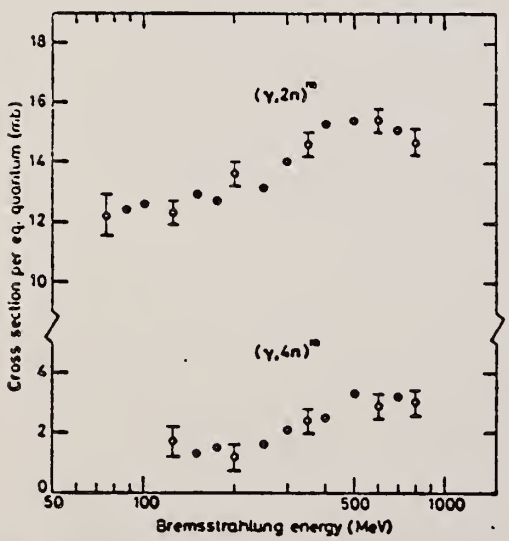

Fig. 6. Yield curves for the reactions (γ, 2n)^m and (γ, 4n)^m

[over]

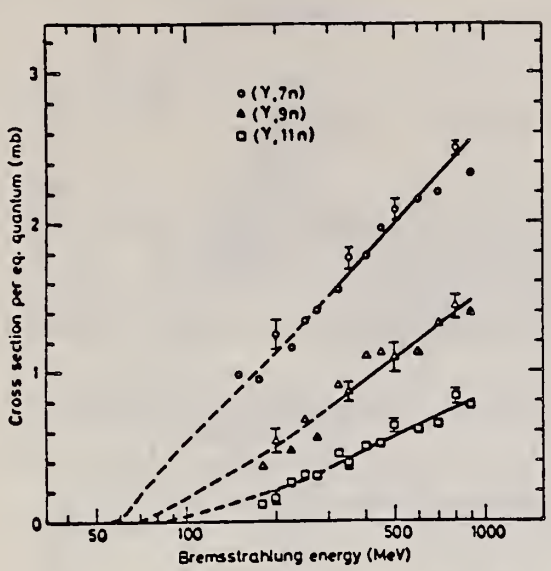

Fig. 4. Yield curves for the reactions (γ, 7n), (γ, 9n) and (γ, 11n).

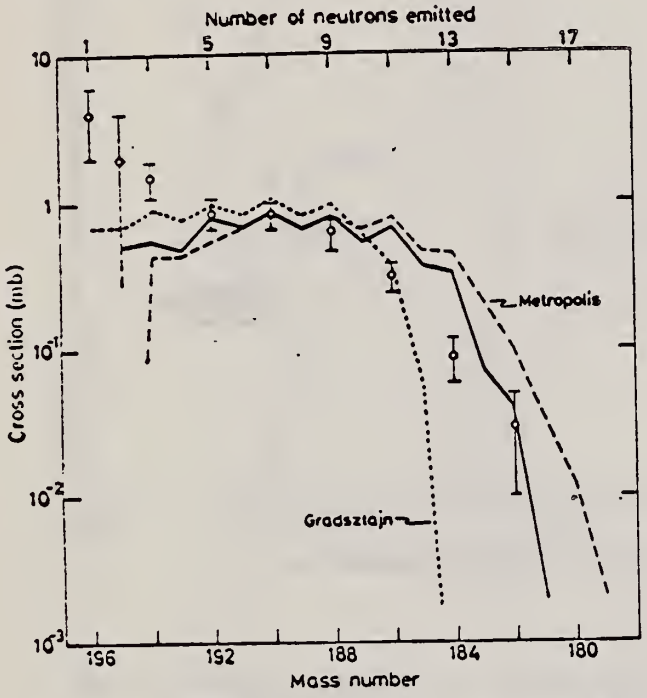

Fig. 7. The mean cross section as a function of mass number, E_γ = 300–900 MeV. The circles are experimental results. The curves give the calculated cross sections from different cascade data.

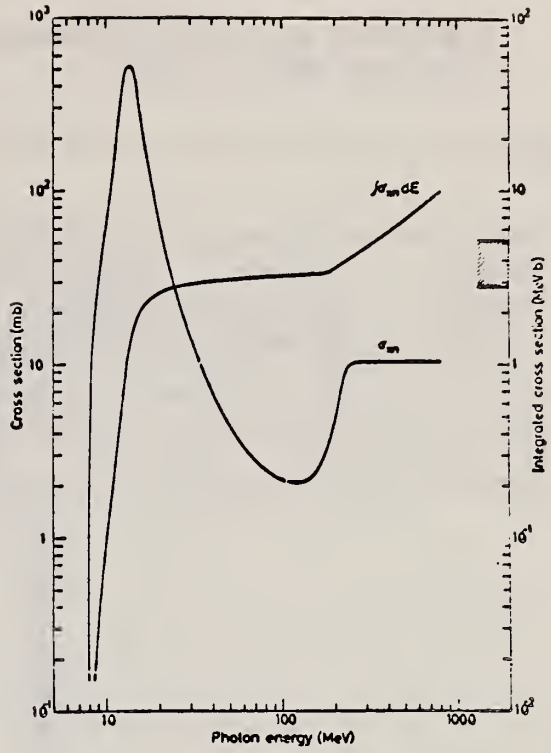

Fig. 8. The total cross section and the total integrated cross section for all the (γ, xn) reactions studied. The dashed region shows the integrated cross section at the pion threshold given by the Gell-Mann sum rule.

TABLE 2

Experimental high-energy (γ, xn) mean cross sections in the energy region 300–900 MeV together with calculated cross sections and the partial fission cross sections obtained

Isotope	$\bar{\sigma}_{exp}$(mb)	$\bar{\sigma}_{calc}$(mb)	$\bar{\sigma}_f$(mb)
^{196}Au	4 ±2		
	(1.8 ±0.8)		
^{195}Au	2 ±2	0.51	
^{194}Au	1.5 ±0.4	0.56	
^{192}Au	0.87±0.20	0.80	
^{190}Au	0.84±0.17	0.87	0.03
^{188}Au	0.63±0.15	0.82	0.19
^{186}Au	0.32±0.07	0.69	0.37
^{184}Au	0.09±0.03	0.34	0.25
^{182}Au	0.03±0.02	0.04	0.01

REF. T. Methasiri and S. A. E. Johansson
Nucl. Phys. A167, 97 (1971)

ELEM. SYM.	A	Z
Au	197	79

METHOD

REF. NO. 71 Me 1 egf

REACTION	RESULT	EXCITATION ENERGY	SOURCE		DETECTOR		ANGLE
			TYPE	RANGE	TYPE	RANGE	
G,F	ABY	THR-900	C	300-900	FRG-I		4PI

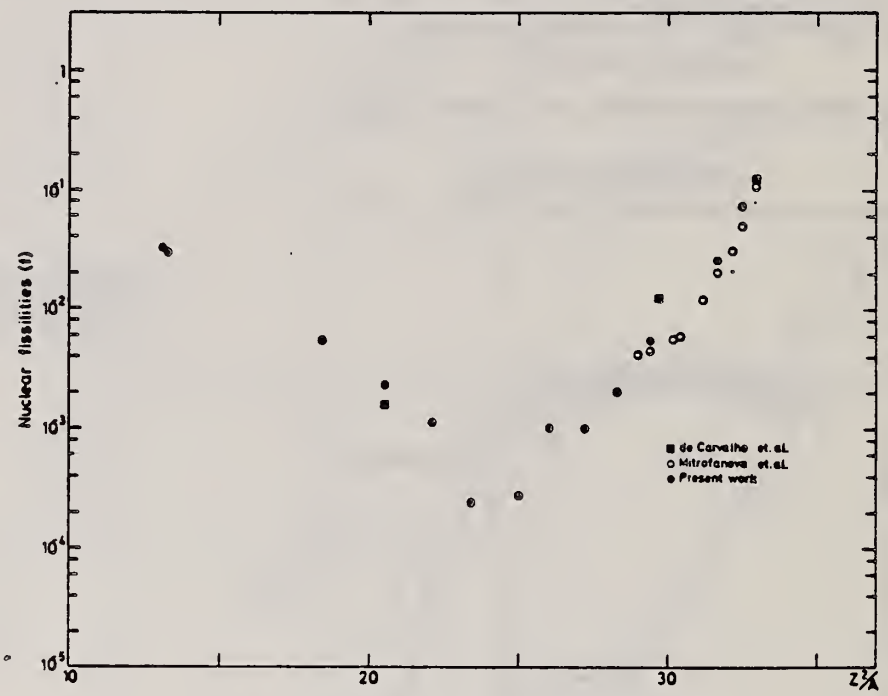

Fig. 2. Nuclear fissilities as a function of Z^2/A.

TABLE 1

The constant fission cross sections above the threshold

Element	σ_f (cm^2)	Element	σ_f (cm^2)
Pb	$(5.0\pm0.2)\times10^{-27}$	La	$(1.1\pm0.1)\times10^{-29}$
Au	$(1.7\pm0.1)\times10^{-27}$	Sn	$(4.3\pm1.1)\times10^{-29}$
Ta	$(3.3\pm0.2)\times10^{-28}$	Ag	$(8.4\pm2.0)\times10^{-29}$
Yb	$(1.2\pm0.2)\times10^{-28}$	Mo	$(1.7\pm0.4)\times10^{-28}$
Ho	$(5.5\pm0.3)\times10^{-29}$	Cu	$(6.6\pm1.2)\times10^{-28}$
Gd	$(5.3\pm0.8)\times10^{-29}$	Ni	$(5.8\pm0.1)\times10^{-28}$
Nd	$(1.3\pm0.2)\times10^{-29}$		

[over]

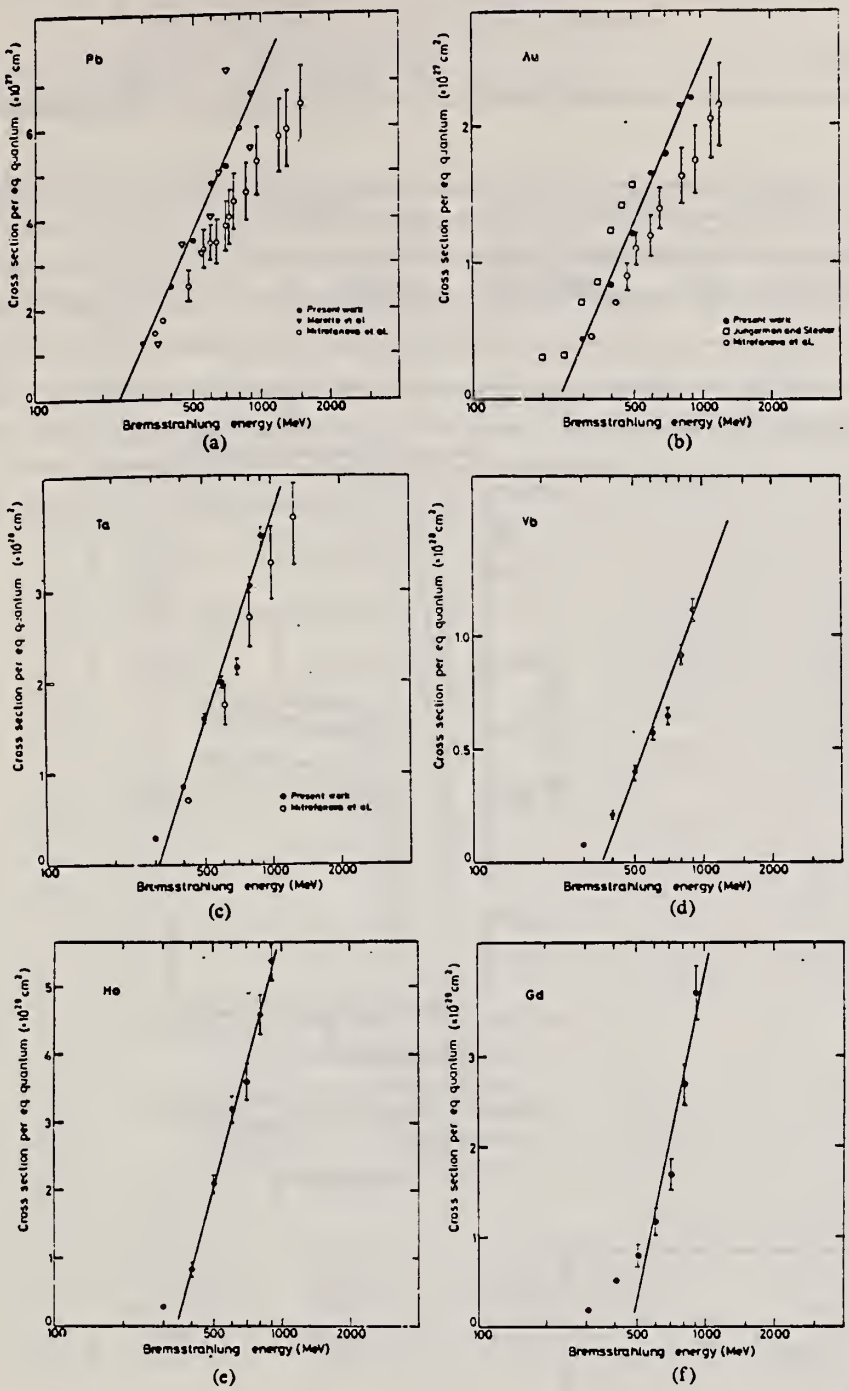

Fig. 1. Cross sections per equivalent quantum $\sigma_q(E)$ as a function of log E.

REF.

Tatsuya Saito
Nippon Kagaku Zasshi 92, 164 (1971)

ELEM. SYM.	A	Z
Au	197	79

METHOD

REF. NO. 71 Sa 1 egf

REACTION	RESULT	EXCITATION ENERGY	SOURCE		DETECTOR		ANGLE
			TYPE	RANGE	TYPE	RANGE	
G,N	ABY	8-68	C	10-68	ACT-I		4PI

Nippon Kagaku Zasshi, 92, 164~168(1971)

The Yields of Radioactivities Induced by (γ, n) Reactions with Bremsstrahlung up to 68 MeV

by Tatsuya SAITO

The (γ, n) yields of 12 target nuclides have been measured at 10, 13, 16, 30, 45 and 68 MeV bremsstrahlung by observing the induced activities.

The energy dependence of the yields has been investigated extensively in the same way as in the previous work at 20 MeV bremsstrahlung.

In the case of heavy nuclides, the yields rise greatly as a function of maximum bombarding energy up to 20 MeV, and rise gradually from 20 MeV up to 68 MeV. However, in the case of light nuclides, the yields rise greatly up to 30 MeV, because the neutron separation energies of light ones are larger than those of heavy ones, and the bremsstrahlung spectrum covers the giant resonance and so the yields rise gradually from 30 MeV up to 68 MeV.

The yields have approximately been estimated from the parameter of the giant resonance, that is the peak cross section and the half width, in order to compare with the experimental data. As a result, the experimental data of light nuclides and heavy ones are nearly in agreement with the estimated data of Nathans et al., Johns et al. and Montalbetti et al., but those of medium weight ones are relatively lower values.

Department of Chemistry, Faculty of Science, Tohoku University; Katahira-cho, Sendai-shi, Japan

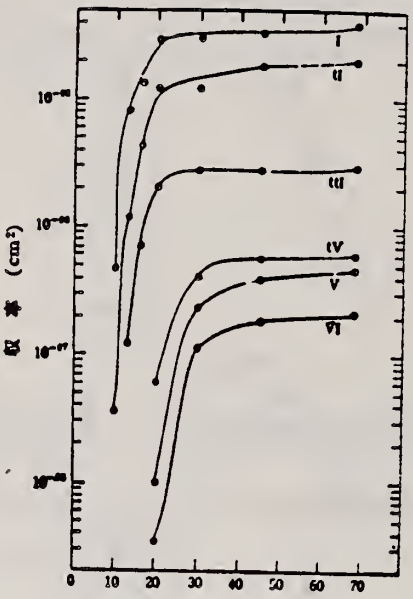

制動輻射最大エネルギー

I : $^{197}Au(\gamma, n)^{196}Au$, II : $^{127}I(\gamma, n)^{126}I$
III : $^{55}Mn(\gamma, n)^{54}Mn$, IV : $^{23}Na(\gamma, n)^{22}Na$
V : $^{16}O(\gamma, n)^{15}O$, VI : $^{12}C(\gamma, n)^{11}C$

図 3 (γ, n)反応の収率

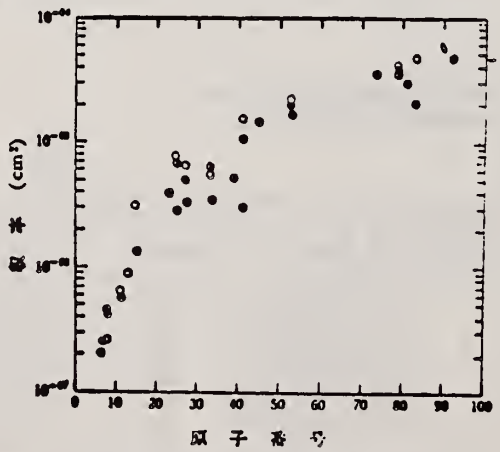

原子番号

●: 実験値, ⊕: Johns ら,
◑: Nathans ら, ○: Monlalbetti ら

図 4 (γ, n)反応の収率の比較

REF.

G.A. Vartapetyan, N.A. Demekhina, V.I. Kasilov, Yu. N. Ranyuk, P.V. Sorokin and A.G. Khudaverdyan
Yad. Fiz. 14, 65 (1971)
Sov. J. Nucl. Phys. 14, 37 (1972)

ELEM. SYM.	A	Z
Au	197	79

METHOD

REF. NO.	
71 Va 4	egf

REACTION	RESULT	EXCITATION ENERGY	SOURCE		DETECTOR		ANGLE
			TYPE	RANGE	TYPE	RANGE	
G,F	ABX	100-999	C	100-999	TRK-I		4PI

999 = 5 GEV

$E_{\gamma max}$, MeV	Photofission yields per cm³ per equivalent photon					
	U^{238}	U^{235}	Th^{232}	Bi^{209}	Au^{197}	Ta^{181}
120	$(226 \pm 20) \cdot 10^{-27}$	$(120 \pm 12) \cdot 10^{-27}$	$(50 \pm 5) \cdot 10^{-27}$	$(0.70 \pm 0.08) \cdot 10^{-25}$	$(3.0 \pm 0.4) \cdot 10^{-25}$	
130				$(1.5 \pm 0.2) \cdot 10^{-25}$	$(1.4 \pm 0.2) \cdot 10^{-25}$	
140				$(2.9 \pm 0.2) \cdot 10^{-25}$	$(2.0 \pm 0.2) \cdot 10^{-25}$	
150	$(240 \pm 20) \cdot 10^{-27}$		$(63 \pm 7) \cdot 10^{-27}$			
160				$(3.1 \pm 0.3) \cdot 10^{-25}$	$(3.7 \pm 0.4) \cdot 10^{-25}$	
180				$(4.6 \pm 0.5) \cdot 10^{-25}$	$(5.5 \pm 0.6) \cdot 10^{-25}$	
200	$(265 \pm 30) \cdot 10^{-27}$	$(150 \pm 15) \cdot 10^{-27}$	$(72 \pm 7) \cdot 10^{-27}$	$(6.1 \pm 0.6) \cdot 10^{-25}$	$(8.2 \pm 0.8) \cdot 10^{-25}$	$(4.9 \pm 0.5) \cdot 10^{-25}$
220				$(8.3 \pm 0.8) \cdot 10^{-25}$	$(1.1 \pm 0.1) \cdot 10^{-24}$	$(8.2 \pm 0.8) \cdot 10^{-25}$
240				$(1.2 \pm 0.1) \cdot 10^{-24}$	$(1.5 \pm 0.2) \cdot 10^{-24}$	$(1.2 \pm 0.1) \cdot 10^{-24}$
245		$(156 \pm 16) \cdot 10^{-27}$				
260				$(1.5 \pm 0.2) \cdot 10^{-24}$	$(1.8 \pm 0.2) \cdot 10^{-24}$	$(1.6 \pm 0.2) \cdot 10^{-24}$
280		$(160 \pm 16) \cdot 10^{-27}$	$(85 \pm 9) \cdot 10^{-27}$			
300				$(2.2 \pm 0.2) \cdot 10^{-24}$	$(2.3 \pm 0.2) \cdot 10^{-24}$	
320				$(3.5 \pm 0.4) \cdot 10^{-24}$	$(4.4 \pm 0.4) \cdot 10^{-24}$	
340				$(4.2 \pm 0.4) \cdot 10^{-24}$	$(5.0 \pm 0.5) \cdot 10^{-24}$	
350	$(318 \pm 30) \cdot 10^{-27}$	$(175 \pm 20) \cdot 10^{-27}$				
360			$(106 \pm 11) \cdot 10^{-27}$			$(7.0 \pm 0.7) \cdot 10^{-24}$
400				$(5.4 \pm 0.5) \cdot 10^{-24}$	$(6.9 \pm 0.7) \cdot 10^{-24}$	
420				$(6.7 \pm 0.7) \cdot 10^{-24}$	$(9.1 \pm 0.9) \cdot 10^{-24}$	
440		$(195 \pm 20) \cdot 10^{-27}$	$(115 \pm 12) \cdot 10^{-27}$	$(8.9 \pm 0.9) \cdot 10^{-24}$	$(9.6 \pm 1) \cdot 10^{-24}$	
460				$(7.9 \pm 0.8) \cdot 10^{-24}$	$(1.0 \pm 0.1) \cdot 10^{-23}$	
480	$(346 \pm 35) \cdot 10^{-27}$					
500				$(9.4 \pm 0.9) \cdot 10^{-24}$	$(1.2 \pm 0.1) \cdot 10^{-23}$	$(1.7 \pm 0.2) \cdot 10^{-24}$
525				$(9.5 \pm 0.9) \cdot 10^{-24}$	$(1.2 \pm 0.1) \cdot 10^{-23}$	
550		$(200 \pm 20) \cdot 10^{-27}$	$(120 \pm 12) \cdot 10^{-27}$	$(9.5 \pm 0.9) \cdot 10^{-24}$	$(1.2 \pm 0.1) \cdot 10^{-23}$	
560				$(9.2 \pm 0.9) \cdot 10^{-24}$	$(1.2 \pm 0.1) \cdot 10^{-23}$	
580						$(2.4 \pm 0.2) \cdot 10^{-23}$
600				$(10.4 \pm 1) \cdot 10^{-24}$	$(1.3 \pm 0.2) \cdot 10^{-23}$	
620	$(386 \pm 40) \cdot 10^{-27}$	$(220 \pm 22) \cdot 10^{-27}$	$(135 \pm 14) \cdot 10^{-27}$			
640		$(224 \pm 23) \cdot 10^{-27}$	$(140 \pm 14) \cdot 10^{-27}$			
660						$(2.9 \pm 0.3) \cdot 10^{-23}$
680				$(11.3 \pm 1.1) \cdot 10^{-24}$	$(1.9 \pm 0.2) \cdot 10^{-23}$	
700	$(418 \pm 40) \cdot 10^{-27}$					
720	$(390 \pm 40) \cdot 10^{-27}$	$(217 \pm 23) \cdot 10^{-27}$	$(136 \pm 14) \cdot 10^{-27}$			
740				$(12.5 \pm 1.3) \cdot 10^{-24}$	$(1.9 \pm 0.2) \cdot 10^{-23}$	
760						$(3.3 \pm 0.3) \cdot 10^{-23}$
780				$(13.5 \pm 1.4) \cdot 10^{-24}$	$(2.1 \pm 0.2) \cdot 10^{-23}$	
800				$(14.3 \pm 1.4) \cdot 10^{-24}$	$(2.0 \pm 0.2) \cdot 10^{-23}$	
820	$(470 \pm 40) \cdot 10^{-27}$	$(193 \pm 20) \cdot 10^{-27}$	$(152 \pm 15) \cdot 10^{-27}$			
840	$(445 \pm 45) \cdot 10^{-27}$	$(238 \pm 24) \cdot 10^{-27}$	$(155 \pm 15) \cdot 10^{-27}$			
860				$(13.9 \pm 1.4) \cdot 10^{-24}$	$(2.1 \pm 0.2) \cdot 10^{-23}$	
880				$(13.5 \pm 1.6) \cdot 10^{-24}$	$(2.2 \pm 0.2) \cdot 10^{-23}$	
900	$(440 \pm 45) \cdot 10^{-27}$	$(207 \pm 21) \cdot 10^{-27}$	$(140 \pm 14) \cdot 10^{-27}$			
920	$(415 \pm 45) \cdot 10^{-27}$	$(242 \pm 24) \cdot 10^{-27}$	$(155 \pm 16) \cdot 10^{-27}$			
940	$(391 \pm 50) \cdot 10^{-27}$	$(245 \pm 25) \cdot 10^{-27}$	$(152 \pm 15) \cdot 10^{-27}$			
960	$(355 \pm 45) \cdot 10^{-27}$	$(256 \pm 23) \cdot 10^{-27}$	$(146 \pm 15) \cdot 10^{-27}$			
980	$(340 \pm 50) \cdot 10^{-27}$	$(251 \pm 25) \cdot 10^{-27}$	$(148 \pm 15) \cdot 10^{-27}$			
1000				$(15.6 \pm 1.6) \cdot 10^{-24}$	$(3.0 \pm 0.3) \cdot 10^{-23}$	$(6.4 \pm 0.6) \cdot 10^{-24}$
1020	$(370 \pm 50) \cdot 10^{-27}$	$(264 \pm 27) \cdot 10^{-27}$	$(183 \pm 18) \cdot 10^{-27}$		$(3.0 \pm 0.3) \cdot 10^{-23}$	$(6.6 \pm 0.7) \cdot 10^{-24}$
1040	$(427 \pm 50) \cdot 10^{-27}$	$(280 \pm 28) \cdot 10^{-27}$		$(20.2 \pm 2) \cdot 10^{-24}$	$(2.8 \pm 0.3) \cdot 10^{-23}$	$(6.8 \pm 0.7) \cdot 10^{-24}$
1060	$(395 \pm 50) \cdot 10^{-27}$	$(274 \pm 28) \cdot 10^{-27}$	$(206 \pm 21) \cdot 10^{-27}$	$(20.2 \pm 2) \cdot 10^{-24}$	$(2.8 \pm 0.3) \cdot 10^{-23}$	$(6.3 \pm 0.6) \cdot 10^{-24}$

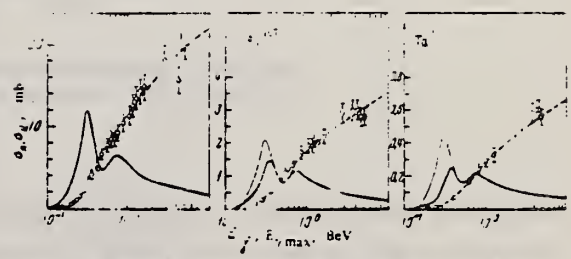

FIG. 3. Solid heavy curve—photofission cross section of Bi^{209}, Au^{197}, Ta^{181}. Dashed curve—the same cross section, integrated over the Schiff bremsstrahlung spectrum (yield per equivalent photon as a function of bremsstrahlung maximum energy). Thin line—cross section for γp interaction, multiplied by the number of nucleons in the nucleus and by the fissility.

REF. G. Andersson, I. Blomqvist, B. Forkman, G. G. Jonsson, A. Jarund, I. Kroon, K. Lindgren and B. Schroder
Nucl. Phys. A197, 44 (1972)

ELEM. SYM.	A	Z
Au	197	79

METHOD

REF. NO. 72 An 8 egf

REACTION	RESULT	EXCITATION ENERGY	SOURCE TYPE	SOURCE RANGE	DETECTOR TYPE	DETECTOR RANGE	ANGLE
G,XN	ABX	1- 7	C	1- 7	ACT-I		4PI
G,F	ABX	1- 7	C	1- 7	ACT-I		4PI

ENERGIES GEV X=1-11

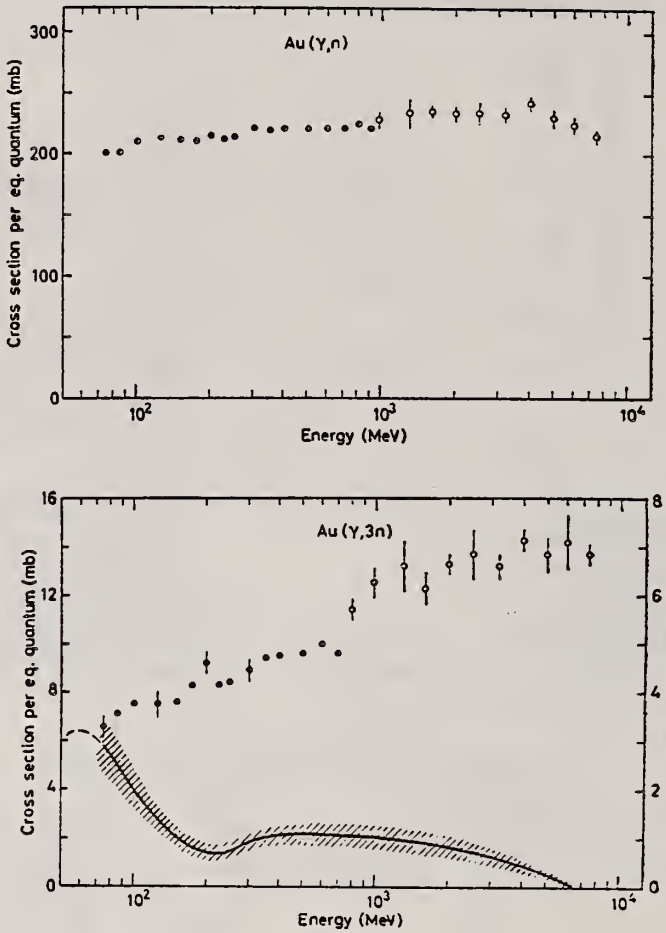

Figs. 12–14. Yields and cross sections for the $^{197}Au(\gamma, xn)$ reactions studied. Open circles from this work and filled circles from ref. [15]). The solid curves show the cross sections and the hatched areas indicate the errors.

TABLE 3

Experimental mean photofission cross sections $\bar{\sigma}_f$ (mb) from refs. [8,18,31]) compared to the results of the present work

	Present work 0.3–7.4 GeV	Ref. [18]) 0.3–0.9 GeV	Ref. [31]) 0.3–1.0 GeV	Ref. [8]) 0.3–1.6 GeV
Au	1.44±0.10	1.7±0.1	1.19±0.06	1.25±0.1
Pb	3.8 ±0.3	5.0±0.2	3.3 ±0.1	3.4 ±0.3

8 A.V. Mitrofanova et al., Sov. J. Nucl. Phys. 6 (1968) 512.
15 K. Lindgren et al., Nucl. Phys. A166 (1971) 193.
18 T. Methasira et al. Nucl. Phys. A167 (1971) 97.
19 I. Kroon, Nucl. Phys. A179 (1972)141
31 V. Emma et al., Nuovo Cim. Lett. 2 (1971) 117, 271

(over)

TABLE 6

Partial reaction cross sections relative to the total photoabsorption cross section, σ/σ_{tot} (in %)

Reaction	0.3 GeV	1.0 GeV	5.0 GeV
$^{12}C(\gamma, n)$	10 ± 5	6.8 ± 3.4	0 ± 5
$^{27}Al(\gamma, \pi^+)$	0.2 ± 0.1	0.1 ± 0.1	0.04 ± 0.02
$(\gamma, 2pn)$	1.7 ± 0.9	1.5 ± 0.8	1.7 ± 0.6
$^{127}I(\gamma, 3n)$	1.6 ± 0.8	0 ± 3	5.5 ± 2.8
$(\gamma, 6n)$	0.9 ± 0.5	1.2 ± 0.6	1.5 ± 0.8
$(\gamma, 7n)$	0.9 ± 0.5	0.5 ± 0.3	0.1 ± 0.1
$(\gamma, 8n)$	0.7 ± 0.4	0.6 ± 0.3	0.4 ± 0.2
$(\gamma, 9n)$	0.3 ± 0.2	0.2 ± 0.1	0.5 ± 0.3
$\Sigma(\gamma, xn)$	4.4 ± 2.2	2.6 ± 1.3	7.8 ± 3.9
$(\gamma, p5n)$	1.7 ± 0.9	1.7 ± 0.9	0.9 ± 0.5
$(\gamma, p7n)$	1.9 ± 1.0	2.1 ± 1.1	0.9 ± 0.5
$(\gamma, p9n)$	1.6 ± 0.8	1.6 ± 0.8	1.3 ± 0.7
$\Sigma(\gamma, pxn)$	5.2 ± 2.6	5.4 ± 2.7	3.1 ± 1.6
$(\gamma, 2p3n)$	0.6 ± 0.3	0.3 ± 0.2	0.3 ± 0.2
$(\gamma, 2p5n)$	0.5 ± 0.3	0.6 ± 0.3	0.8 ± 0.4
$(\gamma, 2p7n)$	1.3 ± 0.7	1.0 ± 0.5	0.4 ± 0.2
$(\gamma, 2p9n)$	1.1 ± 0.6	1.7 ± 0.9	2.4 ± 1.2
$(\gamma, 2p10n)$	2.7 ± 1.4	1.9 ± 1.0	5.0 ± 2.5
$\Sigma(\gamma, 2pxn)$	6.3 ± 3.2	5.6 ± 2.8	8.8 ± 4.4
$(\gamma, 4p12n)$	1.5 ± 0.8	2.4 ± 1.2	2.0 ± 1.0
$(\gamma, 4p14n)$	0.8 ± 0.4	1.9 ± 1.0	2.5 ± 1.3
$(\gamma, 4p15n)$	0.4 ± 0.2	0.6 ± 0.3	1.5 ± 0.8
$\Sigma(\gamma, 4pxn)$	2.7 ± 1.4	4.9 ± 2.5	6.0 ± 3.0
$(\gamma, 6p17n)$		0.5 ± 0.3	1.5 ± 0.8
$(\gamma, 6p18n)$	0.1 ± 0.1	0.2 ± 0.1	0.1 ± 0.1
$\Sigma(\gamma, 6pxn)$	0.1 ± 0.1	0.7 ± 0.4	1.6 ± 0.8
$(\gamma, 8p18n)$		0.8 ± 0.4	2.5 ± 1.3
$\Sigma(\gamma, ypxn)$	19 ±10	20 ±10	30 ±15
$^{197}Au(\gamma, 3n)$	0.9 ± 0.5	2.2 ± 1.1	1.5 ± 0.8
$(\gamma, 7n)$	0.8 ± 0.4	1.3 ± 0.7	2.4 ± 1.2
$(\gamma, 9n)$	0.8 ± 0.4	0.6 ± 0.3	0.3 ± 0.2
$(\gamma, 11n)$	0.4 ± 0.2	0.9 ± 0.5	0.5 ± 0.3
$\Sigma(\gamma, xn)$	2.9 ± 1.5	5.1 ± 2.6	4.6 ± 2.3
$Au(\gamma, f)$	1.5 ± 0.4	2.7 ± 0.7	6.9 ± 2.0
$Pb(\gamma, f)$	3.1 ± 0.8	6.9 ± 1.7	17 ± 5

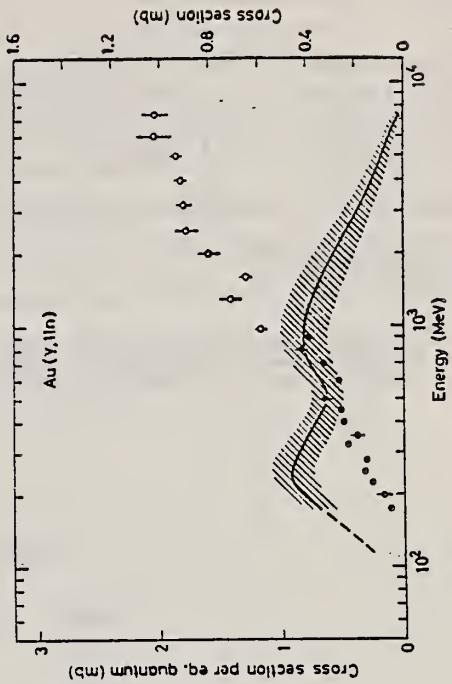

Fig. 14. See caption to fig. 12.

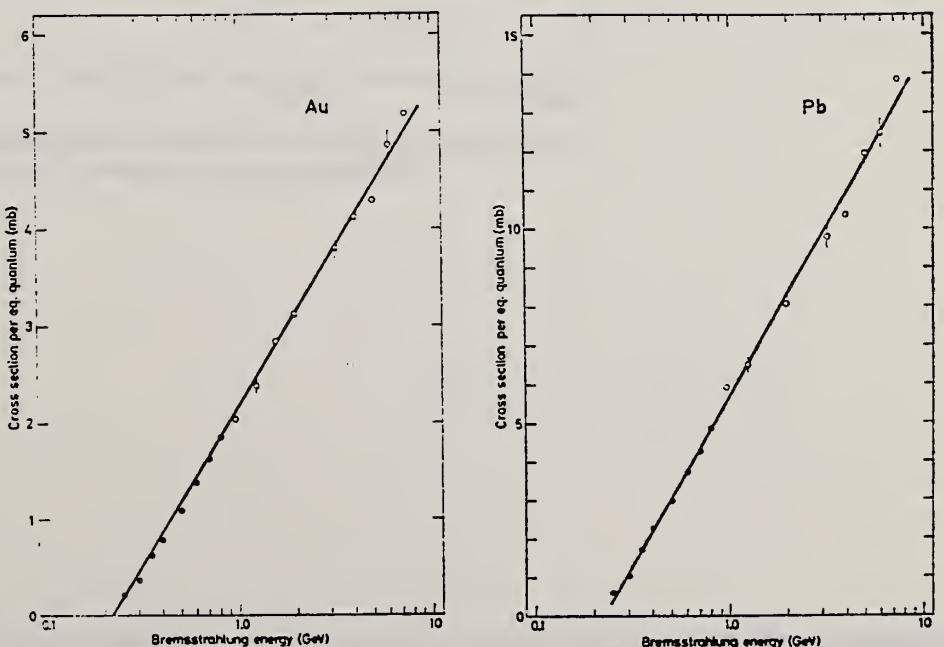

Fig. 17. The gold and lead photofission cross sections per equivalent quantum σ_q as a function of bremsstrahlung peak energy E_{max}. The filled points are taken from our earlier experiment [19]).

REF. W. C. Barber, E. Hayward, J. Sazama
PICNS-72, p. 313 Sendai

ELEM. SYM.	A	Z
Au	197	79

METHOD

REF. NO. 72 Ba 16 hvm

REACTION	RESULT	EXCITATION ENERGY	SOURCE		DETECTOR		ANGLE
			TYPE	RANGE	TYPE	RANGE	
$ G,G	RLX	15.1	D	15.1	NAI-D		90

POL G; ALSO G/

$$\eta = \frac{(d\sigma/d\Omega)_{\parallel} \text{ to polarization vector}}{(d\sigma/d\Omega)_{\perp} \text{ to polarization vector}}$$

Table 1. Results and Comparison with Theory

Target	$\frac{d\sigma}{d\Omega})_{\perp}$ (Arbitrary Units)	η(exp)	η(DCM)	η(HD)
Cd	0.39±0.05	0.09±0.08	0.19	0
Sn	0.65±0.06	0.11±0.06	0.067	0
Ta	1.74±0.14	0.14±0.07	0.180	0.155
Au	2.08±0.15	0.17±0.06	0.067	0
Bi	2.65±0.26	0.02±0.06	0	0

REF.

P. David, J. Debrus, U. Kim, G. Kumbartzki, H. Mommsen, W. Soyez, K. H. Speidel and G. Stein
Nucl. Phys. A197, 163 (1972)

ELEM. SYM.	A	Z
Au	197	79

METHOD

REF. NO.	
72 Da 6	egf

REACTION	RESULT	EXCITATION ENERGY	SOURCE		DETECTOR		ANGLE
			TYPE	RANGE	TYPE	RANGE	
G,F	ABY	THR-999	C	800-999	TRK-I		DST

999=2.2 GEV

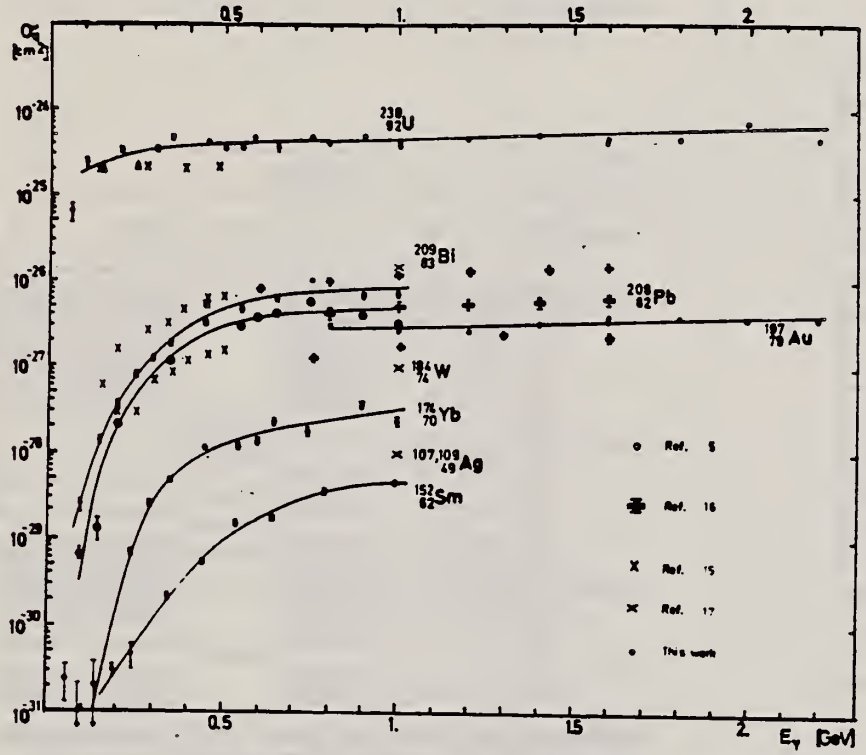

Fig. 3. The bremsstrahlung induced total fission cross section per number of equivalent quanta for uranium and gold in comparison to previous measurements.

REF.

N.A. Demekhina, V.I. Kasilov, A.V. Mitrofanova, Yu. N. Ranyuk, and P.V. Sorokin
Yad. Fiz. 16, 911 (1972)
Sov. J. Nucl. Phys. 16, 502 (1973)

ELEM. SYM.	A	Z
Au	197	79

METHOD

REF. NO. 72 De 12 hmg

REACTION	RESULT	EXCITATION ENERGY	SOURCE TYPE	SOURCE RANGE	DETECTOR TYPE	DETECTOR RANGE	ANGLE
G,F	NOX	THR* 4	C	0* 4	TRK-I		DST

$d\sigma/d\Omega \sim 1+2\ v/V \cos\theta - P \sin^2\theta$

*ENERGIES IN GEV

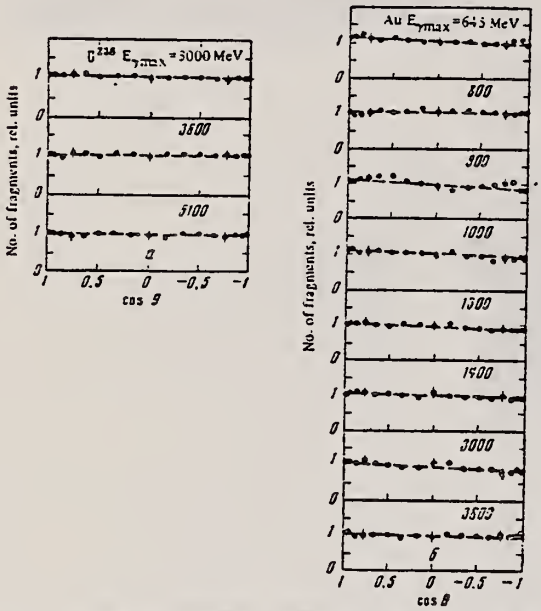

FIG. 2. Angular distributions of fragments from fission of U (a) and Au (b).

Table II

Element	$E_{\gamma\,max}$, MeV	χ^2	$w(\chi^2-\chi^2_0)$	$a = 2v/V$	$a = 2v/V$ [16]	v, (MeV/nucleon)$^{1/2}$	ϵ, MeV
U^{238}	3000	0.16	0.99	−0.031±0.025		0.042±0.005	0.160±0.020
	3800	0.55	0.85	0.013±0.017		0.018±0.002	0.043±0.005
	5100	0.59	0.85	0.040±0.017		0.054±0.006	0.306±0.031
Bi^{209}	700	0.93	0.45	0.155±0.017		0.091±0.009	0.651±0.052
	1000	1.14	0.3	0.085±0.017		0.047±0.005	0.220±0.023
	1200	0.76	0.6	0.094±0.020		0.055±0.006	0.314±0.030
	1300	0.91	0.4	0.093±0.018		0.053±0.006	0.314±0.029
	1480	0.62	0.85	0.034±0.018		0.020±0.002	0.040±0.004
Au^{197}	350				0.097±0.010		
	450				0.105±0.010		
	600				0.090±0.010		
	645	0.87	0.55	0.034±0.018		0.044±0.004	0.187±0.018
	700				0.116±0.010		
	800	0.45	0.95	0.008±0.020		0.005±0.001	0.020±0.002
	850				0.121±0.010		
	900	4.50	0.001	0.124±0.018		0.064±0.005	0.460±0.040
	1000	0.95	0.4	0.101±0.017	0.090±0.010	0.052±0.005	0.262±0.025
	1200	0.87	0.4	0.094±0.017		0.049±0.005	0.234±0.024
	1400	0.90	0.5	0.075±0.018		0.039±0.004	0.147±0.015
	3000	1.34	0.15	0.122±0.017		0.063±0.006	0.410±0.040
	3800	0.7	0.65	0.093±0.17		0.048±0.005	0.223±0.022
Ta^{181}	600	0.8	0.5	0.087±0.018		0.044±0.004	0.176±0.018
	700				0.147±0.010		
	1145	5.2	0.001	0.144±0.018		0.072±0.007	0.468±0.047
	1480	1.25	0.15	0.127±0.018		0.064±0.006	0.370±0.037
	5100	2.02	0.001	0.200±0.020		0.100±0.010	0.900±0.090

Note. χ^2 is the value of χ^2 per degree of freedom, $w(\chi^2-\chi^2_0)$ is the probability of the value of χ^2, $a = 2v/V$ is the anisotropy coefficient, ϵ is the fissioning-nucleus kinetic energy, v is the fissioning-nucleus velocity.

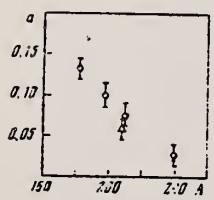

FIG. 3. Anisotropy coefficent as a function of target-nucleus atomic number. Points: O—results of the present work, Δ—results of Kroon and Forkman [16].

$$a = 2\frac{v}{V}$$

REF.

I. Kroon and B. Forkman
Nucl. Phys. A179, 141 (1972)

ELEM. SYM.	A	Z
Au	197	79

METHOD

REF. NO.: 72 Kr 3 egf

REACTION	RESULT	EXCITATION ENERGY	SOURCE		DETECTOR		ANGLE
			TYPE	RANGE	TYPE	RANGE	
G,F	ABY	THR-999	C	350-999	TRK-I		DST

999 = 1 GEV

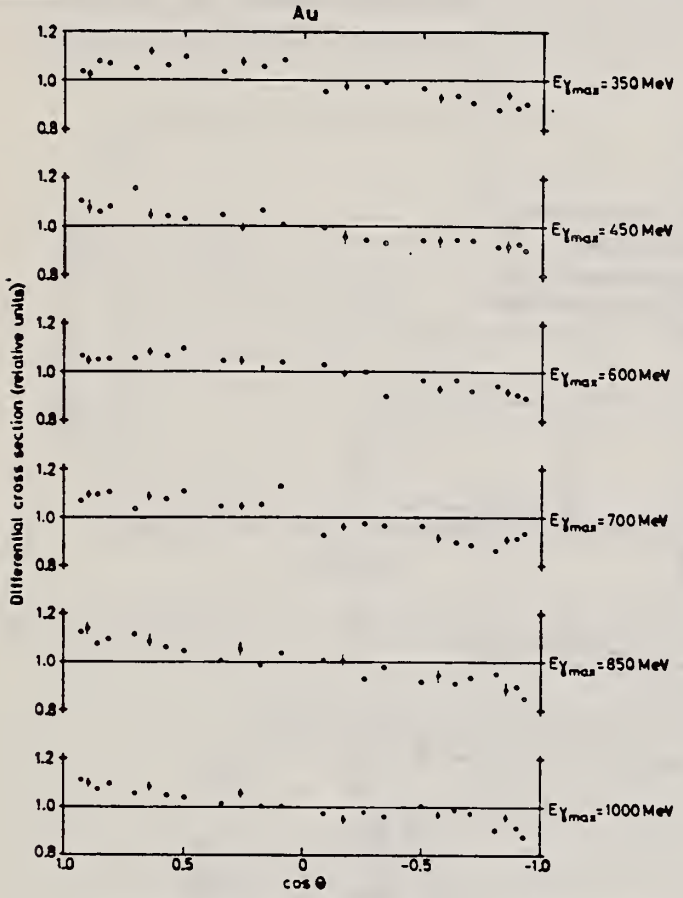

Fig. 3. Angular distributions for gold analogous to those given in fig. 2 for lead.

TABLE 1

Ratios between the number of fragments in the forward and backward directions recorded in glass detectors, N_f/N_b

Element	Present work		Proton sandwich experiment[c])
	from angular distribution[a])	sandwich experiment[b])	
Ta		1.29 ± 0.04	
Re			1.42 ± 0.08
Au	1.19 ± 0.02	1.20 ± 0.01	1.45 ± 0.07
Pb	1.11 ± 0.02	1.13 ± 0.01	1.61 ± 0.15
^{238}U			1.26 ± 0.05

[a]) Ratios calculated from the angular distributions at 700 MeV.
[b]) Ratios obtained with the sandwich technique, 700 MeV for Au and Pb, 800 MeV for Ta.
[c]) From ref. [8]). Proton induced fission at proton energy 660 MeV.

(over)

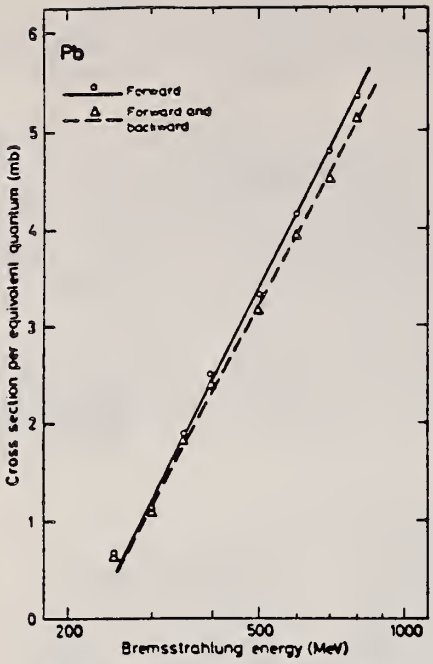

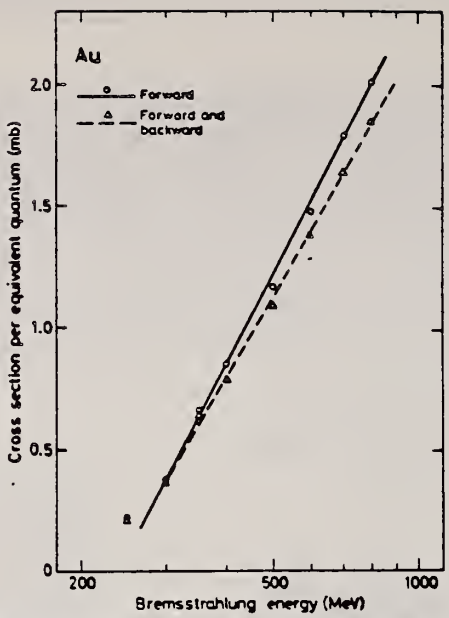

Figs. 5 and 6. The lead and gold photofission cross section per equivalent quantum as a function of bremsstrahlung energy calculated from the number of fission fragment tracks in the forward glass plate (full curve). The corrected cross sections are also shown (dashed curve).

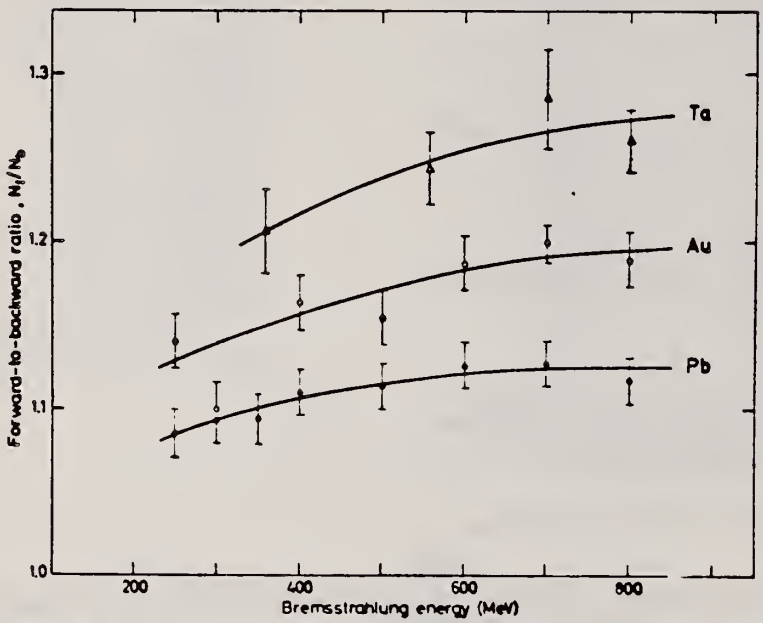

Fig. 4. The tantalum, gold and lead forward-to-backward ratios as a function of bremsstrahlung energy.

9
V.A. Kon'shin, E.S. Matusevich, V.I. Regushevskii, Sov. J. Nucl. Phys. 2, 489 (1966).

REF. J. O. Adler, G. Andersson and H. A. Gustafsson
PICNS-73, Vol.II, p.993 (1973) Asilomar

ELEM. SYM.	A	Z
Au	197	79

METHOD

REF. NO. 73 Ad 3 egf

REACTION	RESULT	EXCITATION ENERGY	SOURCE		DETECTOR		ANGLE
			TYPE	RANGE	TYPE	RANGE	
G,A	SPC	0-500	C	500	TEL-D		DST

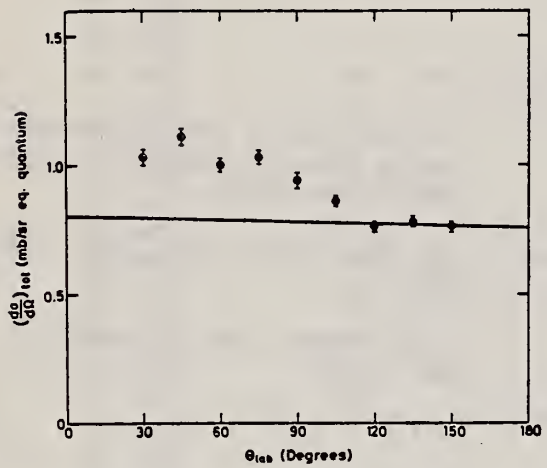

Fig 2 shows the experimental angular distribution together with the results from cascade-evaporation calculations (solid curve). The calculated curve has been fitted to the experimental points between 120 and 150°.

Both fig 1 and fig 2 seem to indicate that there is a small contribution of directly-emitted α-particles in the yield. From fig 1 we estimate this contribution at (13 ± 1)% and from fig 2 at (15 ± 2)%.

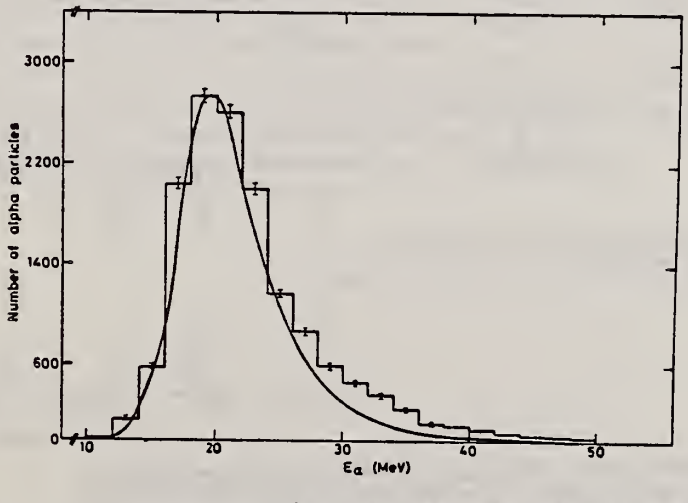

Fig 1 shows the α-energy spectrum resulting when all the nine measurements are added together.

REF.

R.F. Barrett, J.R. Birkelund, B.J. Thomas, K.S. Lam, and H.H. Thies
Nucl. Phys. A210, 355 (1973)

ELEM. SYM.	A	Z
Au	197	79

METHOD

REF. NO. 73 Ba 20 egf

REACTION	RESULT	EXCITATION ENERGY	SOURCE		DETECTOR		ANGLE
			TYPE	RANGE	TYPE	RANGE	
G,N	NOX	THR- 27	C	10- 27	BF3-I		4PI

MEAN NEUT ENERGY

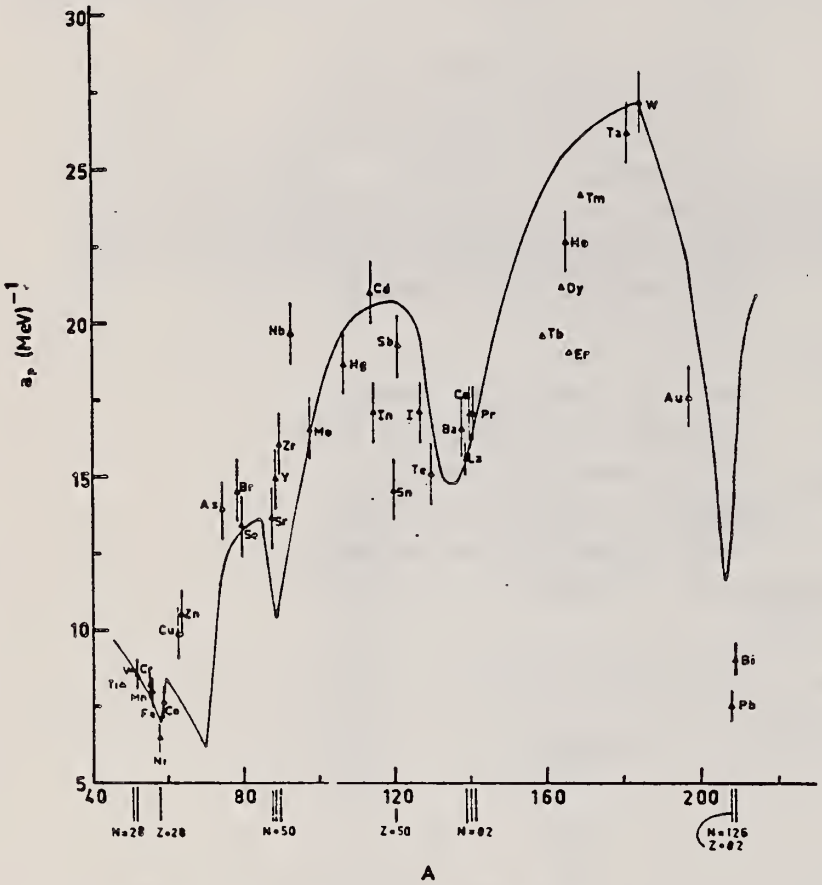

Fig. 12. Experimental values of the level density parameter a_p (Fermi gas formula plus pairing correction) versus atomic number A. The continuous curve is a least-squares fit to the data of a theoretical calculation from Newton [15].

1
H. Baba and S. Baba, Japan Atomic Energy Research Institute report JAERI-1183 (1969).
2
H. Baba, Nucl. Phys. A159, 625 (1970).
15
T.D. Newton, Can. J. Phys. 34, 804 (1956).

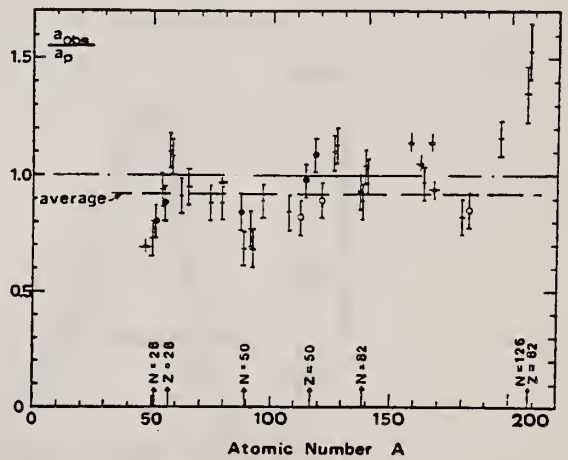

Fig. 15. Ratio a_{obs}/a_p versus atomic number A. Here a_{obs} is the level density parameter taken from the neutron resonance work of refs. [1,2]), and a_p is the level density parameter derived from the present (γ, n) work. Filled circles represent points where nuclei in the neutron resonance and in the (γ, n) experiment were the same. Open circles represent points where the respective nuclei were approximately matched. Triangles represent points which are based on measurement of neutron mean energies at two bremsstrahlung energies only.

(over)

TABLE 3 (continued)

Target	N (residual nucleus) [a]		Goodness of fit [b]		$\hat{E}_n(24)$ (MeV) [c]	T (MeV) [d]	a_p (MeV^{-1}) [e]	a_{obs} (MeV^{-1}) [f]	a_{obs}/a_p
			no p.c.	with p.c.					
Ba	75	1%		F	1.16		16.5–^{136}Ba	15.39–^{136}Ba	0.93
	77	2%							
	78	7%							
	79	8%							
	80	11%							
	81	71%							
La	80	100%	F	F	1.25	0.72	15.5–^{138}La	13.76–^{139}La	0.89
Ce	81	89%	F	G	1.24	0.70	17.0–^{139}Ce	17.8 –^{141}Ce	1.04
	83	11%							
Pr	81	100%	G	G	1.17	0.65	17.0–^{140}Pr	17.05–^{142}Pr	1.00
Tb [g]	93	100%			1.15		19.3–^{158}Tb	21.85–^{160}Tb	1.14
Dy [g]	93	2%			1.06		20.9–$^{161.5}$Dy	21.9 –^{162}Dy	1.05
	94	19%							
	95	25%							
	96	25%							
	97	28%							
Ho	97	100%	P	G	1.06	0.56	21.4–^{164}Ho	20.66–^{166}Ho	0.97
Er [g]	95	2%			1.11		19.2–^{166}Er	21.9 –^{166}Er	1.14
	97	33%							
	98	23%							
	99	27%							
	101	15%							
Tm [g]	99	100%			1.03		24.0–^{168}Tm	22.58–^{170}Tm	0.94
Ta	107	100%		G	1.00	0.49	26.0–^{180}Ta	21.2 –^{181}Ta	0.82
W	107	26%	G	F	0.98	0.50	27.0–^{183}W	23.0 –^{183}W	0.85
	108	14%							
	109	31%							
	111	28%							
Au	117	100%		G	1.19		17.5–^{196}Au	20.24–^{198}Au	1.16
Pb ($Z = 82$)	123	24%		V.P.	1.87	1.20	7.5–^{206}Pb	10.1 –^{207}Pb	1.35
	124	23%							
	125	52%							
Bi	125	100%		F	1.65	1.03	9.0–^{208}Bi	13.8 –^{210}Bi	1.53

[a] Neutron numbers and abundances of respective residual nuclei in (γ, n) experiments.
[b] These give an assessment of the goodness of fit of a calculated $\hat{E}_n$ versus E_0 curve to the observed data, using the Fermi gas level density formula both without and with pairing corrections.
[c] Bremsstrahlung photoneutron mean energies $\hat{E}_n$ for peak bremsstrahlung energy $E_0 = 24$ MeV.
[d] Nuclear temperature from fit with constant-temperature formula.
[e] Level density parameter a_p derived from the present (γ, n) experiment, using a Fermi gas formula plus pairing correction, and corresponding residual nucleus (the atomic weight shown is the weighted average of atomic weights of the respective isotopes present).
[f] As column 7, but using data on n-resonance absorption from refs. [1, 2]).
[g] Measurements of $\hat{E}_n(E_0)$ for these nuclei were made only for $E_0 = 21$, 23 and 24 MeV.

REF. F.R. Buskirk, H.D. Graf, R. Pitthan, H. Theissen, O. Titze, and Th. Walcher
PICNS-73, Vol.I, p.703 Asilomar

ELEM. SYM.	A	Z
Au	197	79

METHOD .

REF. NO. 73 Bu 14 hmg

REACTION	RESULT	EXCITATION ENERGY	SOURCE TYPE	SOURCE RANGE	DETECTOR TYPE	DETECTOR RANGE	ANGLE
E,E/	SPC	2- 20	C	50, 65	MAG-D		DST

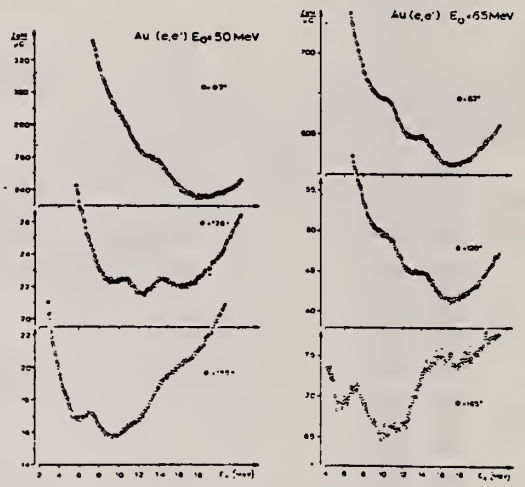

Fig. 1

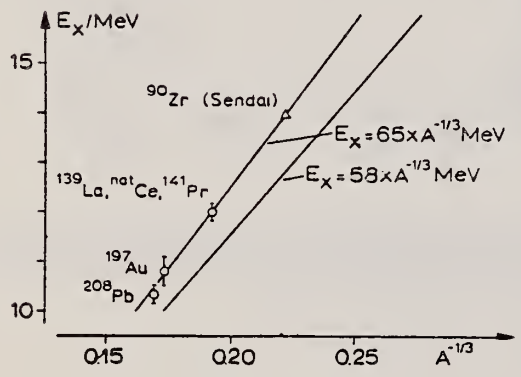

Fig. 2

The E2 resonance which is clearly visible at 10.8 ± 0.2 MeV exhausts more than 50 % of the sum rule. Fig. 2 shows the excitation energy of this resonance as a function of $A^{-1/3}$ for the nuclei measured at Darmstadt and the Sendai result for ^{90}Zr [5]. Bohr and Mottelson [9] predicted a collective E2 resonance whose isoscalar part should depend on A through $E_x = 58\ A^{-1/3}$ MeV. The data of Fig. 2 are consistent with $E_x = 65\ A^{-1/3}$ MeV suggesting to identify the observed resonances with this type of E2 excitation.

REF. P. David, J. Debrus, F. Lubke, H. Mommsen, R. Schoenmackers and G. Stein
PICNS-73, Vol.II, p.985 (1973) Asilomar

ELEM. SYM.	A	Z
Au	197	79

METHOD

REF. NO. 73 Da 6 egf

REACTION	RESULT	EXCITATION ENERGY	SOURCE		DETECTOR		ANGLE
			TYPE	RANGE	TYPE	RANGE	
G,F	ABY	THR- 22	C	1- 2	TRK-I		4PI
G,P	SPC	2-450	C	450	TEL-D		90
G,T	SPC	11-450	C	450	TEL-D		90
G,HE	SPC	14-450	C	450	TEL-D		90
G,A	SPC	0-450	C	450	TEL-D		90

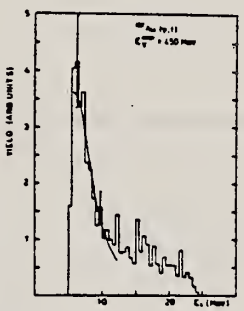

Fig.4: Triton spectrum

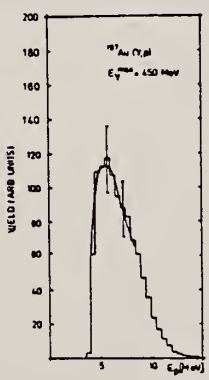

Fig.3: Proton spectrum

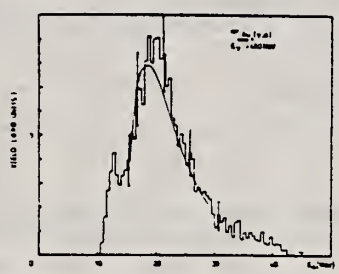

Fig.6: ^{4}He - spectrum

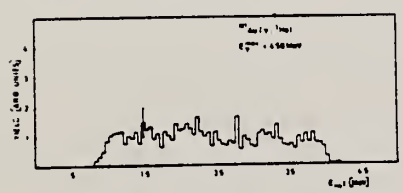

Fig.5: ^{3}He - spectrum

The total photofission cross sections of ^{197}Au and ^{238}U were measured for E_{γ}^{max} = 0.8 to 2.2 GeV (fig. 1). The fission cross sections and the fissionabilities are σ_f^{Au} = 1.4 ± 0.1 mb, f^{Au} = (2.1 ± 0.3) 10^{-2}; σ_f^{U} = 43.2 ± 4.4 mb, f^{U} = 1.04 ± 0.1. 431

REF. P. Dougan and W. Stiefler
Z. Physik 265, 1 (1973)

ELEM. SYM.	A	Z
Au	197	79

METHOD

REF. NO. 73 Do 9 egf

REACTION	RESULT	EXCITATION ENERGY	SOURCE		DETECTOR		ANGLE
			TYPE	RANGE	TYPE	RANGE	
G,XP	ABY	86-400	C	400	TEL-D		DST

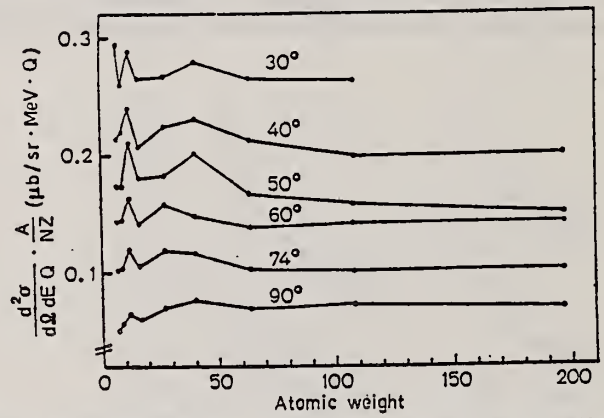

Fig. 8. Experimental cross-sections at various angles for $E_p = 150$ MeV divided by NZ/A plotted as a function of atomic weight

Table 10. Gold. Bremsstrahlung endpoint energy: 400 MeV. Differential cross-sections in microbarns/sterrad · MeV · eq. quantum. Quoted errors: statistical in percent

Energy	Angle							
	30	40	50	60	74	90	110	130
79.5	38.8 2.4	33.3 2.2	28.3 2.0	23.3 2.0	19.4 2.1	13.6 2.2	11.3 2.4	10.0 4.0
97.7	33.2 2.9	25.8 2.7	19.6 2.7	17.6 2.5	13.8 2.7	9.87 2.8	7.03 3.3	6.48 5.4
104.6		22.6 2.8	17.5 2.7	16.0 3.1	12.0 2.7	9.07 2.7	7.07 3.5	
114.9	28.1 3.1	17.1 3.3	13.1 3.3	11.3 3.1	9.65 3.2	6.01 3.6	4.54 4.1	4.21 6.7
127.4		14.8 3.7	12.1 3.6	9.39 4.4	7.92 3.6	5.52 3.8	3.74 5.3	
148.7		9.85 4.6	6.92 4.8	7.05 5.2	4.93 4.6	3.29 5.0	2.12 7.2	
168.2		6.52 3.8	5.01 4.0	4.63 3.2	3.09 4.6	2.05 5.0		
185.3		4.63 4.8	3.68 4.9	3.15 4.2	1.95 6.1	1.07 7.3		
202.3		2.81 6.1	2.46 6.0	1.88 5.3	1.29 7.5	0.596 9.7		
221.1	3.51 7.2	2.14 8.2	1.89 6.2	1.31 9.5				
237.5	1.95 10.1	1.31 11.0	1.20 8.1	0.698 13.5				
253.9	1.18 12.8	0.680 15.1	0.728 10.3	0.222 23.6				

(over)

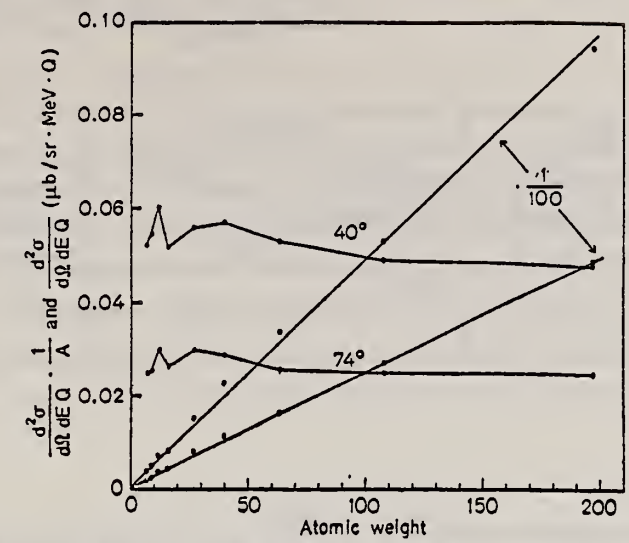

Fig. 9. In this figure, the straight lines show the experimental cross-sections at 40° and 74° for $E_p = 150$ MeV. The other curves are the same cross-sections divided by atomic weight

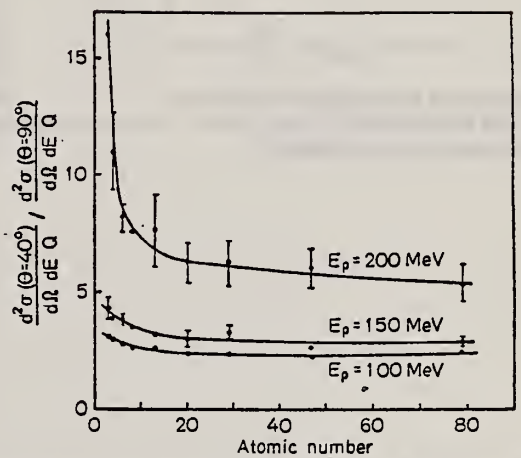

Fig. 6. The ratios of the experimental cross-sections at 40 and 90 degrees for selected proton energies as a function of atomic number

REF.

P. Dougan, T. Kivikas, K. Lugner, V. Ramsay, and W. Stiefler
Phys. Letters 46B, 359 (1973)

ELEM. SYM.	A	Z
Au	197	79

METHOD

REF. NO.: 73 Do 11 | egf

REACTION	RESULT	EXCITATION ENERGY	SOURCE		OETECTOR		ANGLE
			TYPE	RANGE	TYPE	RANGE	
G,XP	ABY	90-400	C	400	TEL-D		DST

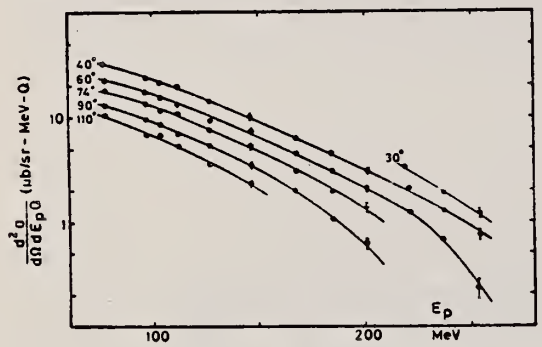

Fig. 1. Energy distributions of high-energy photo-protons at several angles from gold irradiated with 400 MeV bremsstrahlung. The errors shown are purely statistical.

REF. E. Hayward, W. C. Barber, and Jed Sazama
Phys. Rev. C8, 1065 (1973)

ELEM. SYM.	A	Z
Au	197	79

METHOD

REF. NO. 73 Ha 3 hmg

REACTION	RESULT	EXCITATION ENERGY	SOURCE		DETECTOR		ANGLE
			TYPE	RANGE	TYPE	RANGE	
$ G,G	RLY	15	D	15	NAI-D		90
		(15.1)		(15.1)			

POLARIZED PHOTONS

TABLE II. Results.

Target	$d\sigma^{\parallel}/d\Omega_F$ Arbitrary units	$d\sigma^{\perp}/d\Omega_F$ Arbitrary units	η_F	η	$\eta(DCM)$
Cd	0.042 ± 0.028	0.39 ± 0.05	0.11 ± 0.07	0.09 ± 0.07	0.19
Sn	0.084 ± 0.036	0.65 ± 0.06	0.13 ± 0.06	0.11 ± 0.06	0.07
Ta	0.24 ± 0.10	1.47 ± 0.14	0.16 ± 0.07	0.14 ± 0.07	0.20
W	0.52 ± 0.10	1.66 ± 0.12	0.31 ± 0.07	0.29 ± 0.07	0.20
Pt	0.23 ± 0.08	1.94 ± 0.13	0.12 ± 0.04	0.10 ± 0.04	0.08
Au	0.39 ± 0.11	2.08 ± 0.15	0.19 ± 0.06	0.17 ± 0.06	0.07
Bi	0.10 ± 0.15	2.65 ± 0.26	0.04 ± 0.06	0.02 ± 0.06	0

REF. K. Lindgren, G. G. Jonsson and B. Forkman
PICNS-73, Vol.II, p.991 (1973) Asilomar

ELEM. SYM.	A	Z
Au	197	79

METHOD

REF. NO. 73 Li 3 egf

REACTION	RESULT	EXCITATION ENERGY	SOURCE		DETECTOR		ANGLE
			TYPE	RANGE	TYPE	RANGE	
G,G/	ABX	0-800	C	100-800	ACT-I		4PI

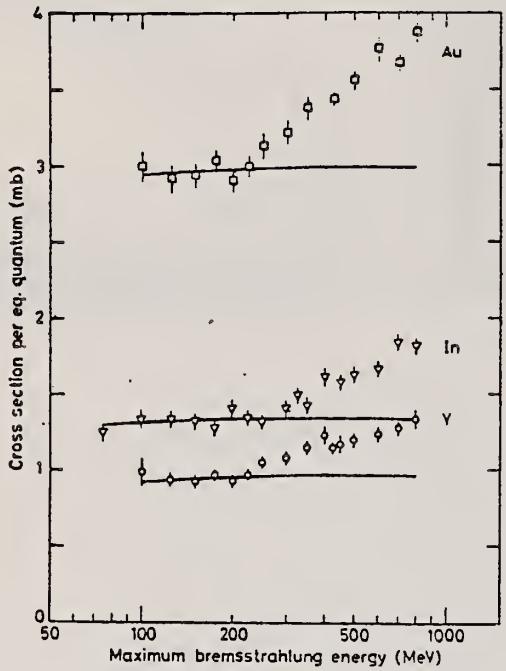

Fig. 1

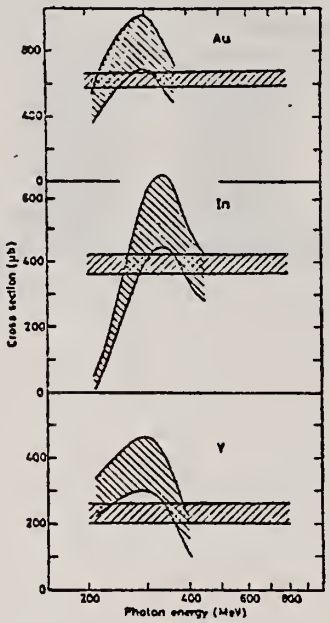

Fig. 2

REF.

Yu.I. Sorokin, V.A. Khrushchev, and B.A. Yur'ev
Izv. Akad. Nauk SSSR Ser. Fiz. 37, 1891 (1973)
Bull. Acad. Sci. USSR Phys. Ser. 37, 80 (1973)

COMPOUND SYM.	A	Z
Au	197	79

METHOD

REF. NO.	
73 So 19	hmg

REACTION	RESULT	EXCITATION ENERGY	SOURCE		DETECTOR		ANGLE
			TYPE	RANGE	TYPE	RANGE	
G,XN	ABX	8- 28	C	8- 28	BF3-I		4PI

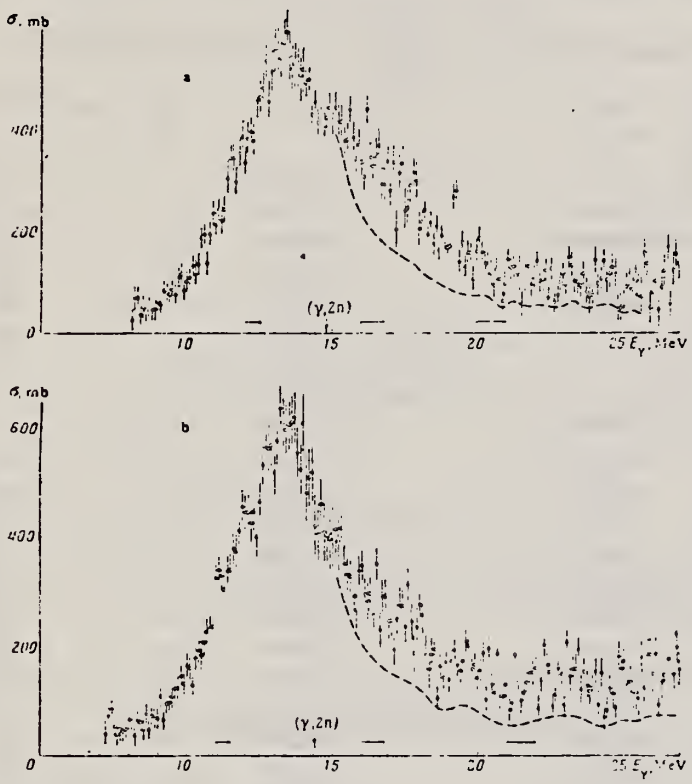

Photoneutron cross section $\sigma(\gamma,Tn)$ for ^{197}Au (a) and ^{209}Bi (b). The dashed curves gives the photoabsorption cross section σ_γ.

Photoneutron Cross-Section Parameter Values for ^{197}Au and ^{209}Bi

	^{197}Au	^{209}Bi
$\sigma(\gamma, Tn)$ [$E_\gamma < 27$ MeV], MeV·b	4.06	4.59
$\sigma(\gamma, Tn)$ [$E_\gamma < 20$ MeV], MeV·b	3.37	3.58
$\sigma(\gamma, Tn)$ [$E_\gamma = 20-27$ MeV], MeV·b	0.69	1.01
σ_γ [$E_\gamma < 20$ MeV], MeV·b	2.81	2.96
σ_γ [$E_\gamma < 27$ MeV], MeV·b	3.15	3.47
σ_γ [E_γ 20 ÷ 27 MeV], MeV·b	0.34	0.51
$\sigma(E1) = \frac{0.06\,NZ}{A}$ MeV·b	2.84	3.00
$\sigma(E2)$, MeV·b	0.48	0.5
σ_m, mb	580	610
E_m, MeV	13.3	13.2
G, MeV	4.3	4.0

REF.

J.O. Adler, G. Andersson, and H.A. Gustafsson
Nucl. Phys. A223, 145 (1974)

ELEM. SYM.	A	Z
Au	197	79

METHOD

REF. NO.: 74 Ad 2 — egf

REACTION	RESULT	EXCITATION ENERGY	SOURCE		DETECTOR		ANGLE
			TYPE	RANGE	TYPE	RANGE	
G,A	ABY	10-500	C	500	TEL-D		DST

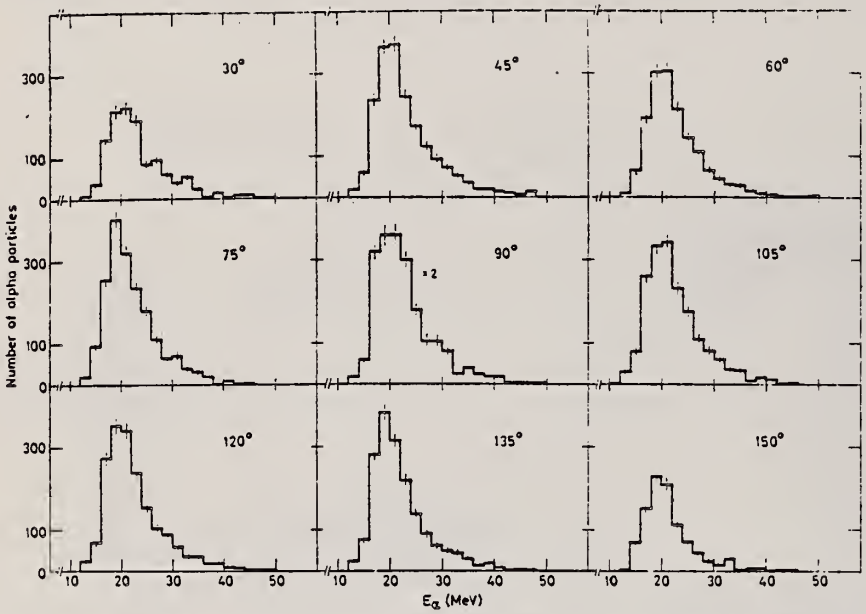

Fig. 3. Experimental energy distributions at the different angles corrected for energy losses in the target.

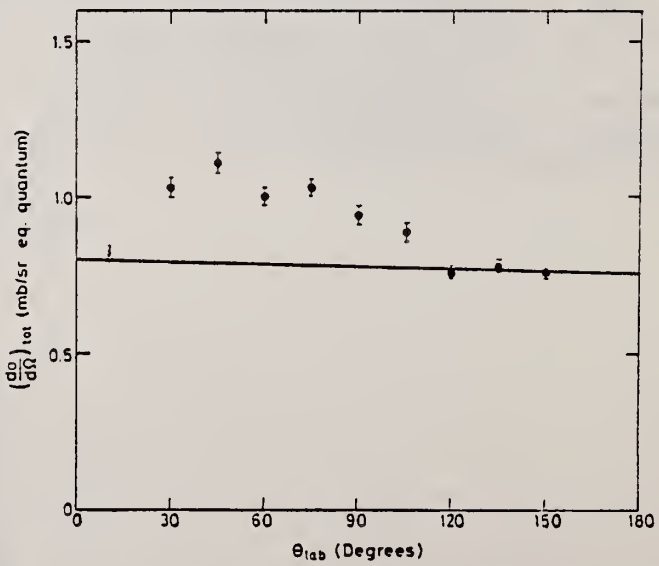

Fig. 4. Total α-particle angular distribution (circles) compared with the angular distribution obtained from cascade-evaporation calculations (solid line).

REF.

M. Areskoug, B. Schroder, K. Lindgren, G. Andersson, B. Forkman
Nucl. Phys. A226, 93 (1974)

Au	197	79

METHOD

REF. NO. 74 Ar 3 egf

REACTION	RESULT	EXCITATION ENERGY	SOURCE		DETECTOR		ANGLE
			TYPE	RANGE	TYPE	RANGE	
G,F	NOX	THR-600	C	600	ACT-I		4PI

REL FRAG YLDS

TABLE I

Formation modes (C = cumulative, I = independent) and decay data [18] for the fission products studied

Nuclide	Type	$T_{\frac{1}{2}}$ (d)	E_γ (branching ratio) (keV)	Y^{exp} (rel. units)	Y^{calc} (rel. units)	Z_p^{calc}
$^{59}_{26}$Fe	C	45	1099(56.5 %), 1291(43.2 %)	1.75±0.05		25.91
$^{69m}_{30}$Zn	C	0.575	439(95 %)	2.23±0.09		30.12
$^{72}_{30}$Zn	C	1.94	145(100 %)	0.69±0.02	0.86	31.38
$^{74}_{33}$As	I	17.9	596(59.5 %)	2.50±0.05	2.06	32.23
$^{75}_{34}$Se	C	120.4	136(58 %)	1.18±0.06	1.26	32.65
$^{82}_{35}$Br			554(72.6 %), 619(37.4 %)	4.56±0.07	4.65	35.59
	I	1.48	698(28.2 %), 1317(26.5 %)			
$^{83}_{37}$Rb			520(47 %), 530(30.4 %)	3.74±0.04	4.09	36.01
	C	83	553(16.6 %)			
$^{84}_{37}$Rb	I	33	882(73.4 %)	5.40±0.07	5.29	36.44
$^{86}_{37}$Rb	I	18.66	1079(8.8 %)	8.48±0.19	6.64	37.28
$^{87}_{39}$Y	C	3.33	388(80 %), 485(92 %)	2.97±0.04	3.03	37.70
$^{88}_{39}$Y	I	108	898(92 %)	5.12±0.11	4.72	38.12
$^{88}_{40}$Zr	C	85	393(97 %), 898 [a])	1.10±0.04	1.01	38.12
$^{89}_{40}$Zr	C	3.27	909(100 %)	2.47±0.03	2.43	38.54
$^{91}_{38}$Sr	C	0.403	1024(33 %)	3.9 ±1.0	2.88	39.38
$^{92m}_{41}$Nb	I	10.16	935(97.5 %)	0.33±0.02		39.80
$^{95}_{40}$Zr	C	65	724(43%), 757(54.6%), 766[a])	5.04±0.04	4.69	41.07
$^{95}_{41}$Nb	I	35	766(99 %)	5.63±0.10	7.71	41.07
$^{95g}_{43}$Tc	C	0.83	766(100 %)	0.69±0.06	0.93	41.07
$^{95m}_{43}$Tc	I	61	582(55.1 %)	0.45±0.04		
$^{97}_{40}$Zr	C	0.71	743(94 %)	0.94±0.05	0.96	41.91
$^{97}_{44}$Ru	C	2.9	215(91 %)	0.62±0.01	0.61	41.91
$^{99}_{42}$Mo	C	2.8	740(14 %), 140 [a])	6.34±0.33	6.32	42.75
$^{99m}_{43}$Tc	I	0.252	140(90 %)	2.20±0.12		42.75
$^{103}_{44}$Ru	C	39.6	497(90 %)	6.61±0.08	7.11	44.43
$^{105}_{45}$Rh	C	1.50	319(19.6 %)	5.61±0.28	7.06	45.27
$^{105}_{47}$Ag	C	40	280(32 %)	1.12±0.04	0.96	45.27
$^{106m}_{47}$Ag	I	8.4	451(31%), 717(32%), 1046(28%)	0.95±0.03		45.70
$^{110m}_{47}$Ag	I	253	658(94.4%), 885 [b]) (75.1%)	1.76±0.03		47.38
$^{111}_{49}$In	C	2.8	171(89 %), 245(94 %)	1.59±0.03	1.47	47.80

Y^{exp} are experimental yields given with statistical errors. The systematic errors are of the order of 5–15 %. Underlined nuclides indicate that the yields in all three samples were measured. Y^{calc} and Z_p^{calc} are yields and peak positions of the charge dispersions calculated from eq. (2).

The following nuclides were detected but not used in the analysis (either because of very poor statistics or because only Y_F or Y_B was measured): ^{69}Ge, ^{86}Zr, ^{90m}Y, ^{96}Nb, ^{96}Tc, ^{112}Pd and ^{112}Ag.

[a]) Gamma radiation from daughter nucleus.

[b]) E_γ = 889 keV was obtained in this work.

[18] M.A. Wakat, Nucl. Data Tables 8 (1971) 445; C.M. Lederer et al, Tables of isotopes (Wiley, N.Y. 1967).

REF.

G. Bologna, V. Emma, A.S. Figuera, S. Lo Nigro, C. Milone
Phys. Lett. 52B, 192 (1974)

ELEM. SYM.	A	Z
Au	197	79

METHOD

REF. NO. 74 Bo 10 egf

REACTION	RESULT	EXCITATION ENERGY	SOURCE		DETECTOR		ANGLE
			TYPE	RANGE	TYPE	RANGE	
G,F	RLX	200-500	D	200-500	TRK-I		4PI

COH BREMS

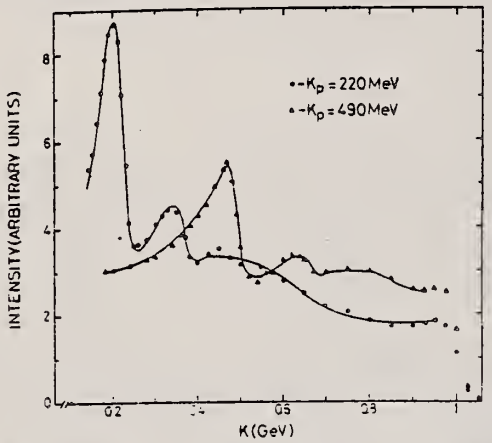

Fig. 1. Coherent bremsstrahlung intensity of E_0 = 1 GeV electrons in a diamond single crystal versus the photon energy K. The solid curves are the best fits.

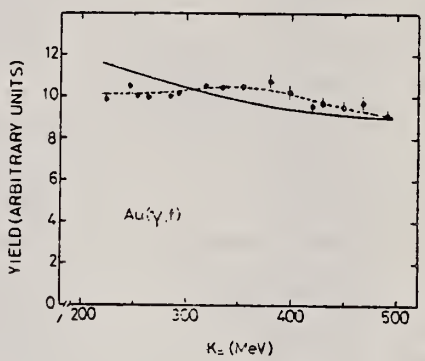

Fig. 2. Yields per equivalent quantum of the Au photofission as a function of the first peak energy K_p of photons. The dots are the experimental data.

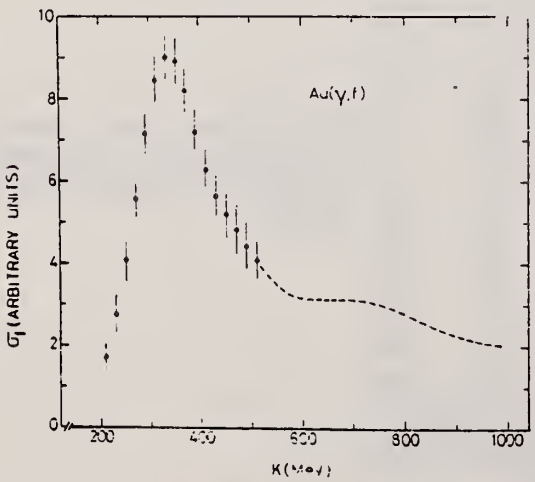

Fig. 3. Photofission cross section σ_f of Au deduced from the experimental yields.

REF. P. David, J. Debrus, F. Lubke, H. Mommsen, R. Schoenmackers, and G. Stein
Nucl. Phys. A221, 145 (1974)

ELEM. SYM.	A	Z
Au	197	79

METHOD

REF. NO. 74 Da 2 egf

REACTION	RESULT	EXCITATION ENERGY	SOURCE		DETECTOR		ANGLE
			TYPE	RANGE	TYPE	RANGE	
G,P	ABY	9-450	C	450	TEL-D		90
G,T	ABY	16-450	C	450	TEL-D		90
G,HE*	ABY	24-450	C	450	TEL-D		90
G,A	ABY	10-450	C	450	TEL-D		90

*HE=HE3

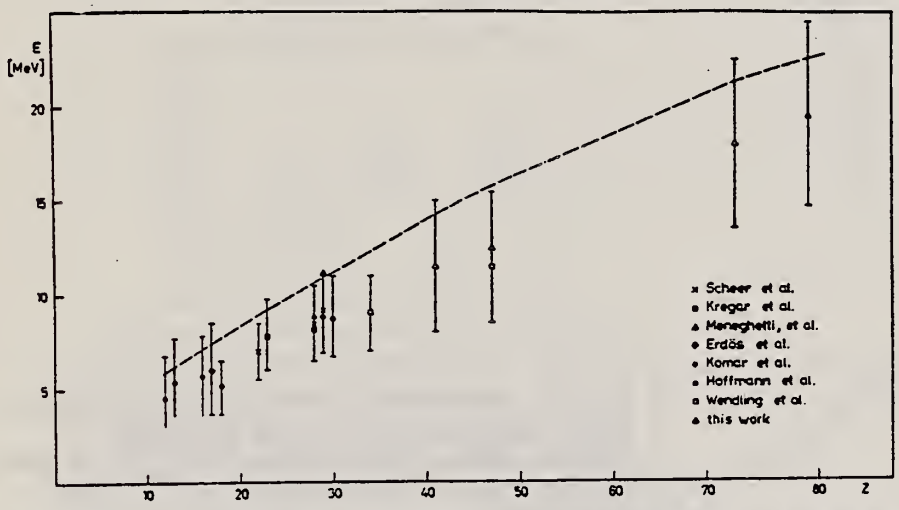

Fig. 8. The position of maxima of the (γ, α) spectra and the width of the spectra at half height. The broken line gives the height of the Coulomb barrier.

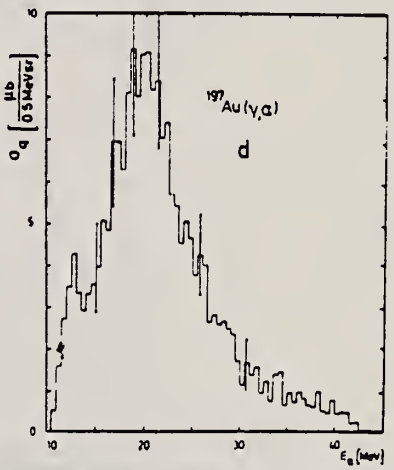

Fig. 4. Characteristic measured spectra of p, t, ^{3}He and ^{4}He from the target nuclei ^{27}Al, ^{40,44}Ca, ^{nat}Ag, ^{197}Au.

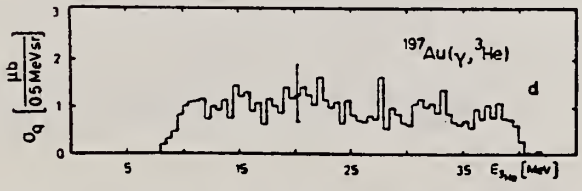

Fig. 3. Characteristic measured spectra of p, t, ^{3}He and ^{4}He from the target nuclei ^{27}Al, ^{40,44}Ca, ^{nat}Ag, ^{197}Au.

(over)

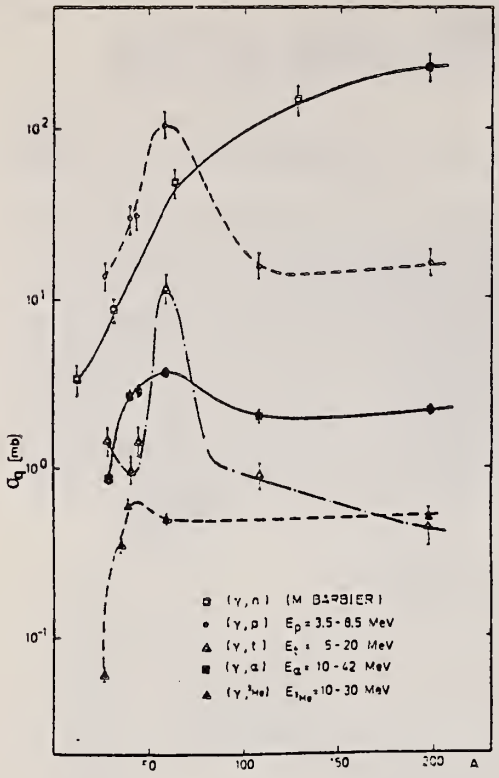

[23] M. Barbier, Induced Radioactivity (North-Holland, Amsterdam, 1969).

Fig. 5. Yield of protons, tritons, ^{3}He and ^{4}He depending on mass number A[ref. [23])]. The lines through the points are to guide the eye.

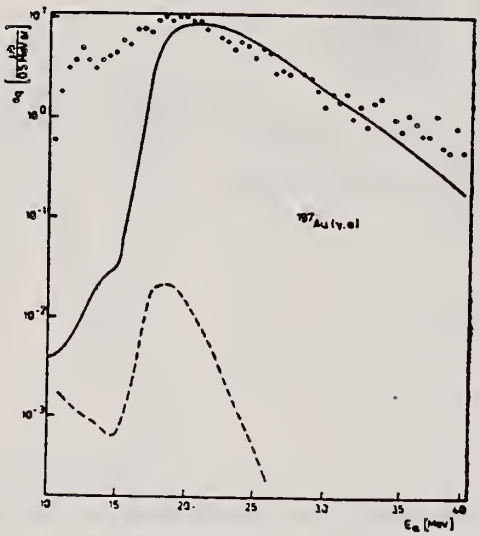

Fig. 7. Experimental data with statistical model calculations for the reaction ^{197}Au(γ,^{3}He). Broken line for E_γ^{max} = 50 MeV (calculation). Full line for E_γ^{max} = 450 MeV (fit).

REF.

L.E. Lazareva, A.I. Lepestkin, and V.I. Sidorov
Yad. Fiz. 20, 242 (1974)
Sov. J. Nucl. Phys. 20, 128 (1975)

ELEM. SYM.	A	Z
Au	197	79

METHOD

REF. NO. 74 La 5 hmg

REACTION	RESULT	EXCITATION ENERGY	SOURCE		DETECTOR		ANGLE
			TYPE	RANGE	TYPE	RANGE	
G,XN	SPC	8- 29	C	29 (28.5)	EMI-D		DST

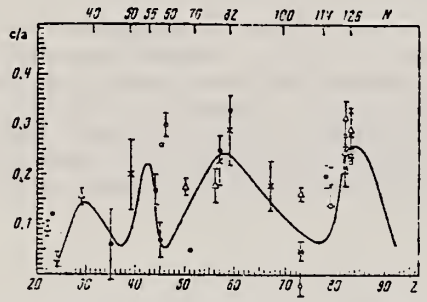

FIG. 2. Assymetry coefficients c/a obtained for nuclei with various Z in the following studies: ref. 10–$E_{\gamma\,max}$ = 25.5 MeV, $E_n > 7.4$ MeV (*); ref. 11–$E_{\gamma\,max}$ = 27–32 MeV, $E_n > \sim 5$ MeV (●); ref. 12–$E_{\gamma\,max}$ = 34 MeV, $E_n > \sim 8$ MeV (○); ref. 13–$E_{\gamma\,max}$ = 55 MeV, $E_n > \sim 5$ MeV (×); present work–$E_{\gamma\,max}$ = 28.5 MeV, $E_n > 5$ MeV (○). The smooth curve shows the coefficient b/a characterizing the photoneutron angular distribution anisotropy as a function of atomic number Z. (This has been converted from the curve given in ref. 11 and and is for the distribution $I(\vartheta) = a + b \sin^2\vartheta + c \cos\vartheta$, normalized at the points Z = 82 -83.)

[11] J.W. Jury, J.S. Hewitt, K.G. McNeill, Can. J. Phys. 46, 1823 (1968).

[12] F.R. Allum, T.W. Quirk, B.M. Spicer, Nucl. Phys. 53, 545 (1964).

[13] G.C. Reinhardt and W.D. Whitehead, Nucl. Phys. 30, 201 (1962).

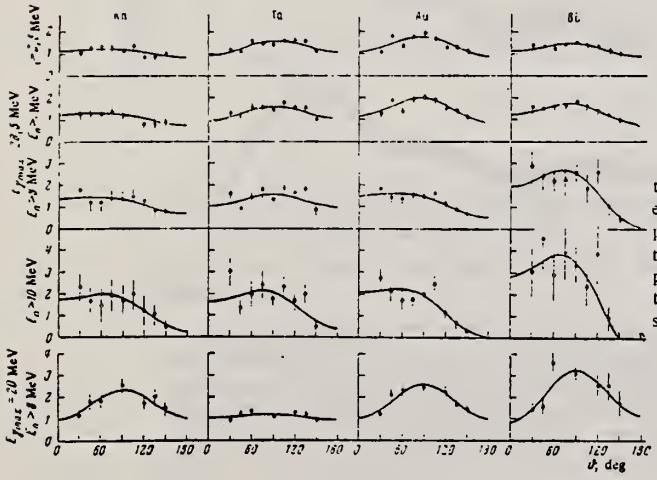

FIG. 1. Angular distributions of photoneutrons obtained in irradiation of Rh, Ta, Au, and Bi samples by bremsstrahlung with maximum energy $E_{\gamma\,max}$ = 28.5 MeV. The curves were calculated from the experimental points by the method of least squares for a distribution of the form $I(\vartheta) = a + b \sin^2\vartheta + c \cos\vartheta$ and normalized (a = 1). For comparison we have shown below the angular distributions of photoneutrons with energy $E_n > 8$ MeV obtained in irradiation of the same samples by bremsstrahlung with $E_{\gamma\,max}$ = 20 MeV.

(over)

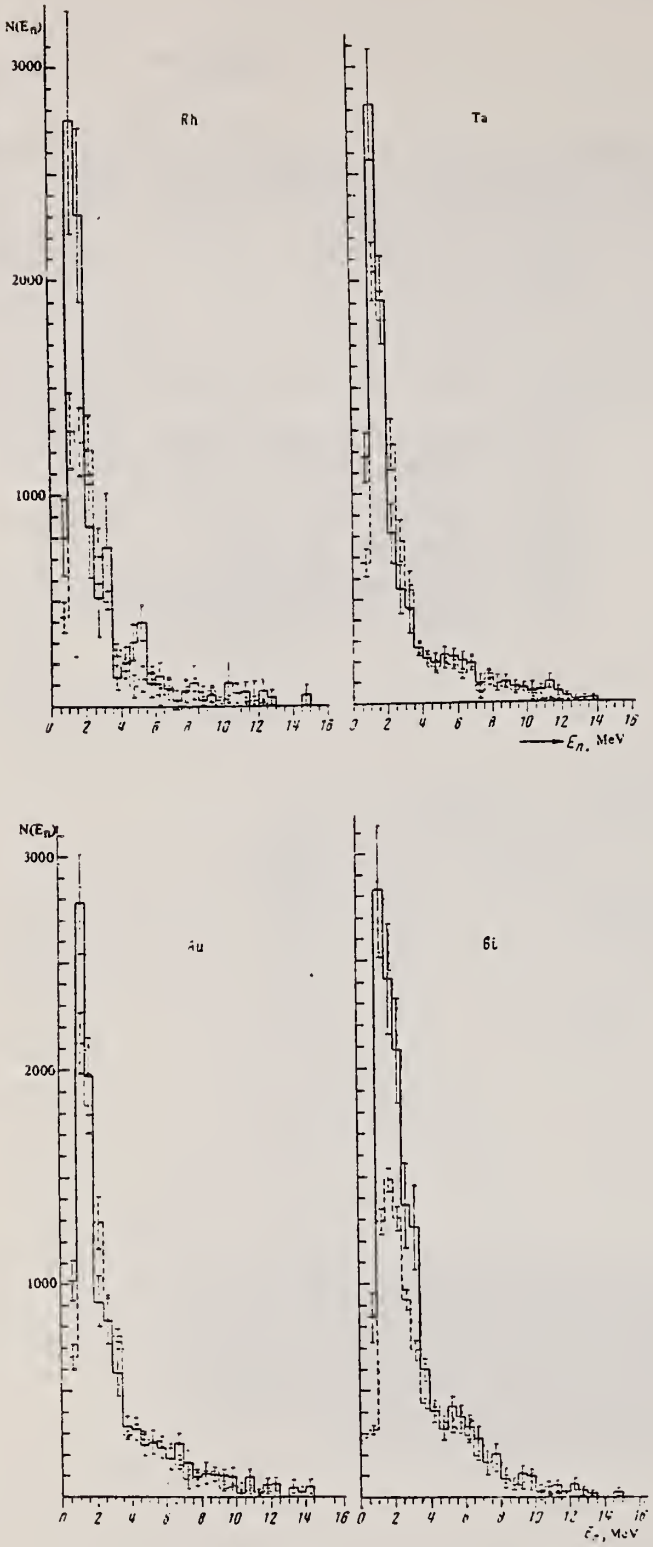

FIG. 3. Photoneutron energy spectra from Rh, Ta, Au, and Bi for irradiation of the samples by bremsstrahlung with maximum energy $E_{\gamma\,max}$ = 20 (dashed line) and 28.5 (solid line) MeV for angles θ with maximum neutron yield. For each nucleus the histograms given for $E_{\gamma\,max}$ = 20 and 28.5 MeV have been combined in the interval E_n = 4–4.5 MeV.

REF. R. Pitthan, F.R. Buskirk, E.B. Dally, J.N. Dyer, and X.K. Maruyama
Phys. Rev. Lett. 33, 849 (1974)

(See Erratum: Phys. Rev. Lett. 34, 848 (1975)

ELEM. SYM.	A	Z
Au	197	79

METHOD

REF. NO. 74 P1 2 hmg

REACTION	RESULT	EXCITATION ENERGY	SOURCE		DETECTOR		ANGLE
			TYPE	RANGE	TYPE	RANGE	
E,E/	FMF	3- 40	D	90	MAG-D		DST

Inelastic electron scattering with 90-MeV electrons shows previously observed giant resonances at excitation energies of $63A^{-1/3}$ ($E2$), $81A^{-1/3}$ ($E1$), $105A^{-1/3}$ ($E3$), and $130A^{-1/3}$ MeV ($E2$). Distorted-wave-Born-approximation analysis of additional structure at $53A^{-1/3}$ and $195A^{-1/3}$ MeV suggests a monopole assignment. Transverse contributions to the $E1$ matrix element are compatible with an electric spin-flip. Differing widths of the respective resonances in the two nuclei are explained through dynamic deformation of Au. The reduced electric transition strengths $B(EL)$ are given.

B(EL)

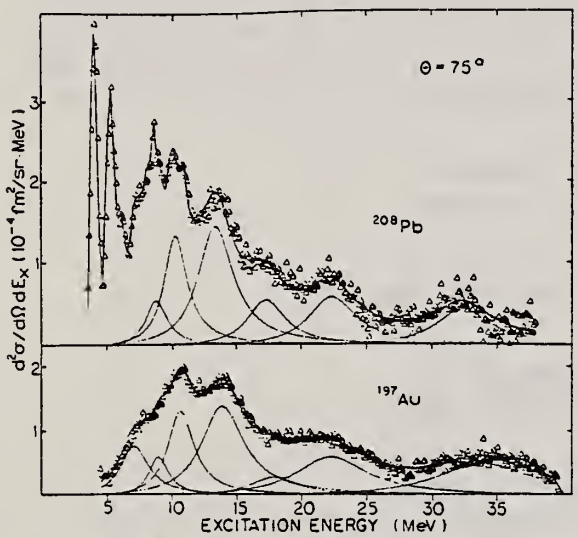

FIG. 2. Same as Fig. 1, after subtraction of the fitted background.

FIG. 1. Spectrum of 90-MeV electrons, scattered inelastically from Pb and Au. The fitted background which consists of the radiation tail and the machine background is shown. The counting rate is corrected for the constant momentum dispersion of the spectrometer. Thus the error increases with the excitation energy.

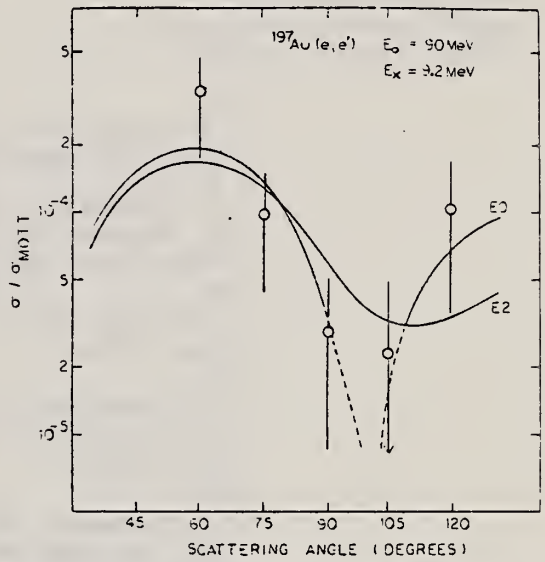

FIG. 3. Ratio of the inelastic cross section of the resonance at 9.2 MeV to the Mott cross section as a function of scattering angle. The curves show the results of DWBA calculations assuming an $E2$ or an $E0$ assignment. At 105° we did not see a resonance. The open circle corresponds to a resonance with a height of 1 standard deviation in the count rate and is, therefore, regarded as an upper limit. The error at 105° represents 1 additional standard deviation.

(over)

TABLE I. Comparison of results for Au and Pb as extracted from the 75° measurements. Columns 2 and 3 show multipolarity and isospin assignments assumed.

			^{197}Au						^{208}Pb					
E_x [$A^{-1/3}$ MeV]	EL	ΔT	E_x [MeV]	B(EL) [fm^{2L}] [a]	Γ_{nat} [MeV]	EWSR [b] [%]	SPU [c]	Others B(EL)	E_x [MeV]	B(EL) [fm^{2L}] [a]	Γ_{nat} [MeV]	EWSR [b] [%]	SPU [c]	Others B(EL)
53	E0	0	9.2	$(3.6\pm1.8)10^3$	2.2 ± 0.5	35	--	--	8.9	$(5\pm3)10^3$	1.8 ± 0.5	50	--	--
63	E2	0	13.8	$(5.2\pm1.2)10^3$	2.9 ± 0.2	77	15.5	$(8.4\pm1.6)10^3$ [h]	10.5	$(6.7\pm2.5)10^3$	2.8 ± 0.3	95	21.5	$(2.6\pm0.9)10^3$ [f][k] $(2.6\pm0.3)10^3$ [g][k]
81	E1	1	14.0	100 ± 20 [d] 50 ± 10 [e]	4.5 ± 0.2	200 100	15.0 7.5	82 ± 11 [d][h] 74 ± 5 [i]	13.6	103 ± 20 53 ± 10	3.9 ± 0.1	205 105	16 8	64 ± 8 [d][f] 71 ± 5 [i]
105	E3	0 1	18.0	$(1.7\pm.8)10^5$	5.2 ± 0.7	45 30	10.0	--	17.5	$(3.2\pm1.5)10^5$	4.2 ± 0.7	90 60	17	$(1.8^{+0.6}_{-1.6})10^5$ [g]
133	E2	1	23.0	$(4.6\pm1.5)10^3$	7 ± 1	95	13.5	$(6.5\pm1.4)10^3$ [h]	22.5	$(4.2\pm1.4)10^3$	5 ± 1	85	14	$(3.4^{+1}_{-2})10^3$ [g]
195	E0	1	33.5	$(10^{+3}_{-7})10^3$	10.5 ± 2	250	--	--	33.0	$(6.5^{+2}_{-3})10^3$	6 ± 1	150	--	--

[a] For the monopole $|M_{if}|^2$ (fm^4).
[b] Energy-weighted sum rule Ref. 19.
[c] Single particle units Ref. 20.
[d] Surface oscillation $\rho_{tr}(r) \sim d\rho_0(r)/dr$.
[e] Volume oscillation $\rho_{tr}(r) \sim \rho_0(r)$.
[f] Ref. 9.
[g] Ref. 8.
[h] Ref. 15.
[i] Ref. 14.
[k] Extracted from a 2-MeV-wide range only.

8 M. Nagao and Y. Torizuka, Phys. Rev. Lett. 30, 1068 (1973).

9 F.R. Buskirk, H.D. Graf, R. Pitthan, H. Theissen, O. Titze, and Th. Walcher, Phys. Lett. 42B, 194 (1972).

14 M. Danos and W. Greiner, Phys. Rev. 134, B284 (1964).

15 A. Veyssiere, H. Beil, R. Bergere, P. Carlos, and A. Lepretre, Nucl.Phys. A159, 561 (1970).

19 N.I. Kassis, Technical Report, Institut fur Kerphysik der Universitat Mainz, 1969, unpublished.

20 R.A. Ferrell, Phys. Rev. 107, 1631 (1957); J. Weneser and E.K. Warburton, in The Role of Isospin in Electromagnetic Transitions, ed. D.H. Wilkinson, (North-Holland, Amsterdam, 1969).

REF.

Yu. I. Sorokin and B. A. Yur'ev
Izv. Akad. Nauk SSSR. Ser. Fiz. 39 114 (1975)
Bull. Acad. Sci. (USSR) Phys. Ser. 39, 98 (1975)

ELEM. SYM.	A	Z
Au	197	79

METHOD

REF. NO.: 75 So 12 hmg

REACTION	RESULT	EXCITATION ENERGY	SOURCE		DETECTOR		ANGLE
			TYPE	RANGE	TYPE	RANGE	
G,XN	ABI	8- 27	C	8- 27	BF3-I		4PI

SEE 73SO19

Table 1

Element	A	σ_0, (γ, Tn) MeV · b: to 27 MeV	$\sigma_{0\gamma n}$ MeV · b: to 20 MeV	$\sigma_{0\gamma n}$ MeV · b: 20–27 MeV	σ_{-1}, mb	σ_{-2}, mb × MeV^{-1}	E_m, MeV	K, MeV	$\alpha(A-1)$ MeV^{-1}	Threshold (γ,2n), MeV	σ_0 (E1), MeV × b
Sn	112	2,23	1,80	1,49	0,41	112	6,7	15,8	20,1	10,2	19,2	1,66
	114	2,26	1,86	1,39	0,47	108	6,5	15,7	21,5	10,2	18,1	1,68
	116	2,40	1,85	1,40	0,45	110	6,6	15,6	21,7	8,1	17,1	1,71
	117	2,52	1,86	1,39	0,47	110	6,7	15,4	21,6	7,3	16,5	1,72
	118	2,45	1,92	1,53	0,39	115	7,1	15,5	20,7	5,6	16,3	1,71
	119	2,63	1,86	1,42	0,44	111	6,8	15,4	22,0	13,2	15,8	1,74
	120	2,69	2,07	1,69	0,38	127	7,9	15,3	19,1	3,6	15,6	1,75
	122	2,94	2,03	1,51	0,52	119	7,1	15,6	21,8	4,5	15,0	1,77
	124	2,90	2,93	1,44	0,49	114	6,9	15,5	23,2	5,4	14,4	1,79
W	182	3,68	2,78	2,32	0,46	184	12,5	—	24,2	5,2	14,9	2,63
	184	4,88	2,95	2,33	0,72	196	13,0	—	23,7	5,2	13,6	2,65
Au	197	4,06	3,15	2,81	0,34	226	15,5	13,3	20,9	17,1	14,8	2,84
Pb	206	3,93	3,21	2,80	0,41	225	16,1	13,5	23,1	6,5	14,8	2,96
	208	4,32	3,28	2,81	0,47	231	16,7	13,3	22,6	9,6	14,1	2,98
Bi	209	4,59	3,47	2,96	0,51	216	17,9	13,2	21,3	10,2	14,3	3,00

REF. G. Bologna, V. Bellini, V. Emma, A.S. Figuera, S. Lo Nigro, C. Milone and G.S. Pappalardo
Il Nuovo Cimento 35A, 91 (1976)

ELEM. SYM.	A	Z
Au	197	79

METHOD

REF. NO. 76 Bo 15 egf

REACTION	RESULT	EXCITATION ENERGY	SOURCE		DETECTOR		ANGLE
			TYPE	RANGE	TYPE	RANGE	
G,F	RLX	220-500	D	220-500	TRK-I		4PI

COHERENT BREMS

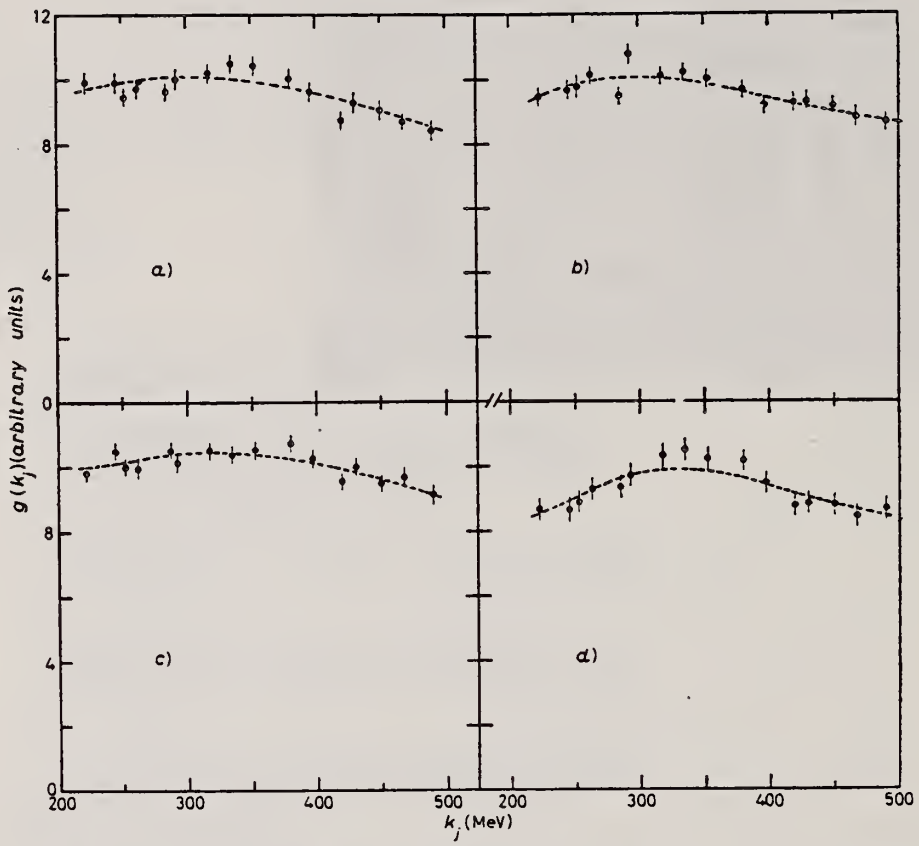

Fig. 6. – Photofission yields per equivalent quantum of Bi, Pb, Au and Pt as a function of the first peak energy k_j of photons. The dots are the experimental data; the dashed curves represent the yield functions estimated as described in sect. 5. *a*) Bi (γ, f), *b*) Pb (γ, f), *c*) Au (γ, f), *d*) Pt (γ, f).

over

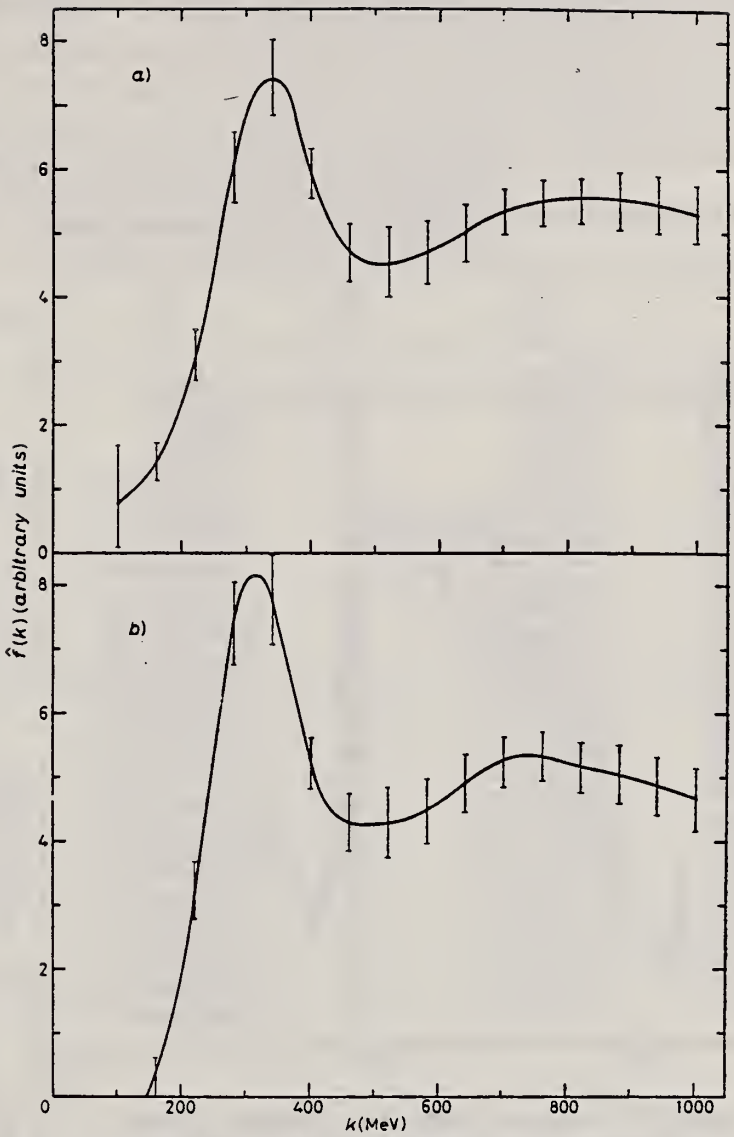

Fig. 8. – See caption to fig. 7. *a*) Au (γ, f), *b*) Pt (γ, f).

REF.

V. Emma, S. Lo Nigro, C. Milone
Nucl. Phys. A257, 438 (1976)

ELEM. SYM.	A	Z
Au	197	79

METHOD

REF. NO. 76 Em 2 egf

REACTION	RESULT	EXCITATION ENERGY	SOURCE		DETECTOR		ANGLE
			TYPE	RANGE	TYPE	RANGE	
G,F	ABY	THR-999	C	999	TRK-I		4PI

999 = 1 GEV

TABLE 1
Measured values of σ_q at $E = 1000$ MeV and deduced values of σ_t assumed constant from E_0 to 1000 MeV

Element	Z^2/A	σ_q (mb)	E_0 (MeV)	σ_t (mb)
Bi	32.96	12.3 ± 0.6	200	7.6 ± 0.6
Pb	32.45	5.4 ± 0.4	220	3.6 ± 0.3
Tl	32.10	4.1 ± 0.3	230	2.8 ± 0.3
Au	31.68	2.0 ± 0.15	240	1.4 ± 0.2
Pt	31.18	1.1 ± 0.08	255	$(8 \pm 0.7) \times 10^{-1}$
Re	30.21	$(3.7 \pm 0.3) \times 10^{-1}$	280	$(2.9 \pm 0.3) \times 10^{-1}$
W	29.78	$(3.5 \pm 0.3) \times 10^{-1}$	290	$(2.8 \pm 0.3) \times 10^{-1}$
Ta	29.45	$(3.3 \pm 0.3) \times 10^{-1}$	300	$(2.7 \pm 0.3) \times 10^{-1}$
Hf	29.04	$(1.7 \pm 0.2) \times 10^{-1}$	310	$(1.4 \pm 0.2) \times 10^{-1}$
Yb	28.31	$(1.3 \pm 0.1) \times 10^{-1}$	330	$(1.2 \pm 0.1) \times 10^{-1}$
Tm	28.18	$(7.5 \pm 0.8) \times 10^{-2}$	335	$(6.8 \pm 0.8) \times 10^{-2}$
Ho	27.21	$(3.6 \pm 0.4) \times 10^{-2}$	355	$(3.5 \pm 0.4) \times 10^{-2}$
Dy	26.80	$(2.6 \pm 0.3) \times 10^{-2}$	360	$(2.5 \pm 0.3) \times 10^{-2}$
Tb	26.58	$(2.5 \pm 0.3) \times 10^{-2}$	370	$(2.5 \pm 0.3) \times 10^{-2}$
Gd	26.04	$(1.6 \pm 0.2) \times 10^{-2}$	380	$(1.7 \pm 0.2) \times 10^{-2}$
Sm	25.56	$(1.3 \pm 0.2) \times 10^{-2}$	390	$(1.4 \pm 0.2) \times 10^{-2}$
Nd	24.96	$(9.2 \pm 0.9) \times 10^{-3}$	405	$(1 \pm 0.1) \times 10^{-2}$
Ce	24.00	$(8 \pm 0.9) \times 10^{-3}$	420	$(9 \pm 1) \times 10^{-3}$
La	23.39	$(8.4 \pm 0.9) \times 10^{-3}$	430	$(1 \pm 0.1) \times 10^{-3}$
Sb	21.36	$(1.2 \pm 0.2) \times 10^{-2}$	460	$(1.5 \pm 0.3) \times 10^{-2}$
Te	21.19	$(8.8 \pm 1) \times 10^{-3}$	465	$(1.2 \pm 0.2) \times 10^{-2}$
Sn	21.06	$(1.3 \pm 0.2) \times 10^{-2}$	465	$(1.7 \pm 0.3) \times 10^{-2}$
Cd	20.49	$(1.7 \pm 0.3) \times 10^{-2}$	470	$(2.2 \pm 0.4) \times 10^{-2}$
Ag	20.47	$(2 \pm 0.3) \times 10^{-2}$	470	$(2.6 \pm 0.4) \times 10^{-2}$
Zn	13.76	$(2 \pm 0.4) \times 10^{-1}$	515	$(3 \pm 0.6) \times 10^{-1}$
Cu	13.44	$(2.4 \pm 0.5) \times 10^{-1}$	515	$(3.6 \pm 0.8) \times 10^{-1}$
Ni	13.35	$(2.4 \pm 0.5) \times 10^{-1}$	510	$(3.6 \pm 0.8) \times 10^{-1}$
Fe	12.10	$(3 \pm 0.6) \times 10^{-1}$	510	$(4.4 \pm 0.9) \times 10^{-1}$

[4] A.V. Mitrofanova et al. Sov. J. Nucl. Phys. 6, 512 (1968).

[7] T. Methasiri et al., Nucl. Phys. A167, 97 (1971).

[12] J.R. Nix et al., Nucl. Phys. 81, 61 (1966).

[20] N.A. Perifilov et al., JETP (Sov. Phys.) 14, 623 (1962); Proc. Symp. on the physics & chemistry of fission, Salzburg 1965, vol. 2 (IAEA) Vienna, 1965, p.283.

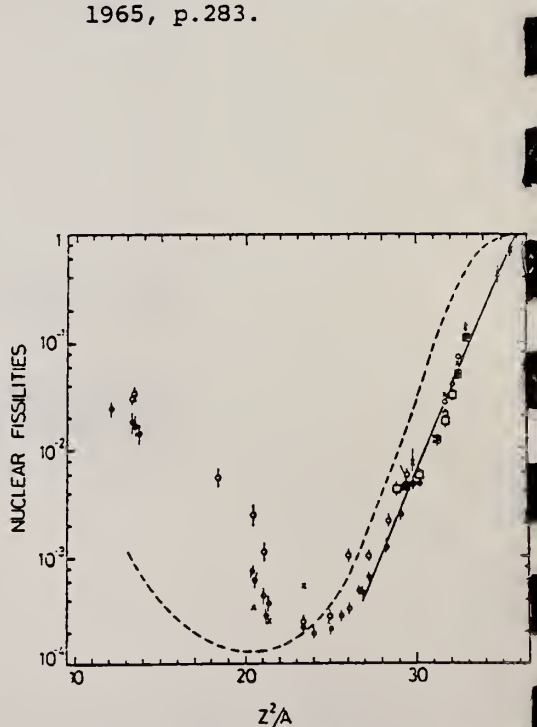

Fig. 2. Nuclear fissilities as a function of Z^2/A. Experimental points: solid circles represent our data; squares, the data from ref. [4]); open circles, the data from ref. [7]); and crosses, the data from (p,f) experiments[20]). The straight line is the best fit calculated from our data for $Z^2/A > 26$. The dashed curve is the curve VI calculated by Nix and Sassi[12]).

REF. G. M. Gurevich, L. E. Lazareva, V. M. Mazur and G. B. Solodukhov
JETP Lett. 23, 370 (1976)
Pis'ma Zh. Eksp. Teor. Fiz. 23, 411 (1976)

ELEM. SYM.	A	Z
Au	197	79

METHOD

REF. NO. 76 Gu 5 hmg

REACTION	RESULT	EXCITATION ENERGY	SOURCE TYPE	SOURCE RANGE	DETECTOR TYPE	DETECTOR RANGE	ANGLE
G,MU-T	ABX	8- 21	C	35	NAI-D		4PI

We measured the total cross section for the absorption of rays in the region of $E1$ resonance for the nuclei ^{165}Ho, ^{178}Hf, ^{180}Hf, ^{181}Ta, ^{182}W, ^{197}Au, and ^{209}Bi. The singularity in the behavior of the resonance widths, observed in the region $160 < A < 185$, is apparently due to the influence of the neutron subshell $N = 108$.

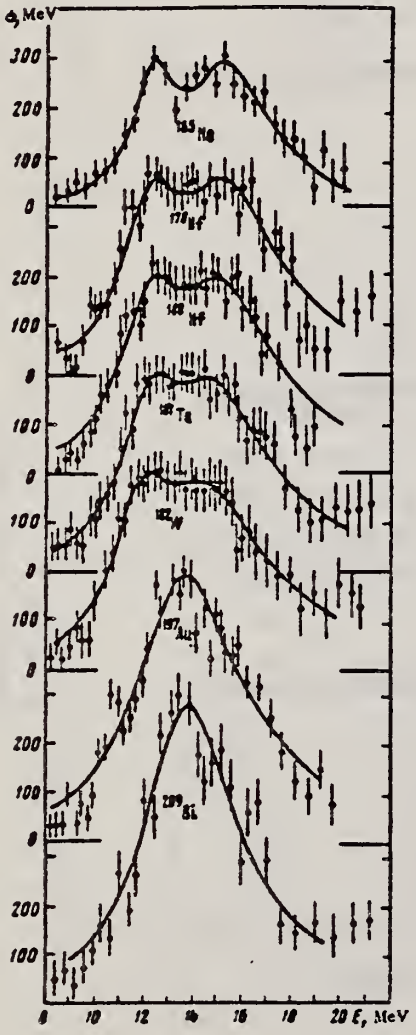

FIG. 1. Total photoabsorption cross sections for the nuclei ^{165}Ho, ^{178}Hf, ^{180}Hf, ^{181}Ta, ^{182}W, ^{197}Au, ^{209}Bi.

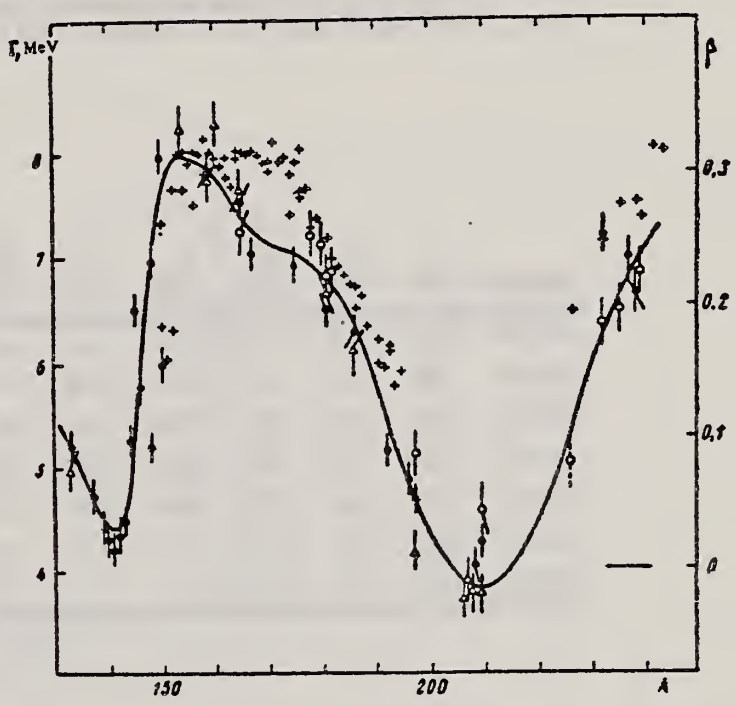

FIG. 2. Widths Γ of $E1$ giant resonance in the region of nuclei with $A > 150$ according to the data of Saclay (●), Livermore (Δ), and the Institute of Nuclear Research of the USSR Academy of Sciences (○). The crosses mark the deformation parameters β.

over

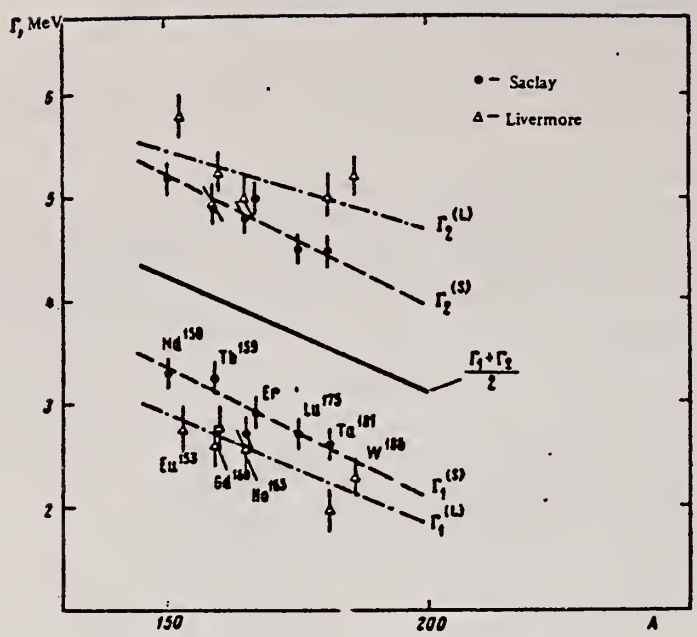

FIG. 3. Width of Lorentz lines approximating the photoabsorption cross sections, for deformed nuclei in the region $150 < A < 185$.

Nucleus	σ_1, mb	Γ_1 MeV	E_1 MeV	σ_2 mb	Γ_2 MeV	E_2 MeV	$\frac{\sigma_2\Gamma_2}{\sigma_1\Gamma_1}$	Q_0 b	β
Ho-165	235	2.0	12.2	272	4.0	15.5	2.3	6.8±0.8	0.29
Hf-178	291	3.1	12.2	334	4.9	15.5	1.8	7.5±0.8	0.28
Hf-180	286	3.2	12.2	324	5.1	15.3	1.8	7.2±0.8	0.27
Ta-181	272	3.0	12.1	316	5.1	15.0	2.0	6.8±0.8	0.26
W-182	267	3.2	11.9	303	5.6	14.8	2.0	7.2±0.8	0.26
Au-197	535	5.2	13.7	...	...	...	...	...	...
Bi-209	600	4.6	13.8	...	...	...	...	...	...

REF.

F.M. Kiely, B.D. Pate, F. Hanappe, and J. Péter
Z. Physik A279, 331 (1976)

ELEM SYM	A	Z
Au	197	79

METHOD

REF. NO.	
76 Ki 6	egf

REACTION	RESULT	EXCITATION ENERGY	SOURCE		DETECTOR		ANGLE
			TYPE	RANGE	TYPE	RANGE	
G,F	ABY	THR - 580	C	580	TRK-D		4PI

Table 3. Fission cross sections and nuclear fissilities (calculated using several formalisms for $\sigma_{\gamma,\mathrm{fiss}}$) obtained from coincident track pairs

Element	Z^2/A	σ, (mb eq. quantum)	$\Pi = \sigma/1.69A^{2/3}$)	σ, 0.33 A
U	35.6	~1.5	$\sim 2.10^{-1}$	$\sim 1.8 \times 10^{-1}$
Au	31.7	6.50	1.13×10^{-1}	9.8×10^{-2}
Te	21.1	2.54×10^{-3}	5.92×10^{-5}	5.8×10^{-5}
Ag	20.5	9.09×10^{-4}	2.37×10^{-5}	2.5×10^{-5}

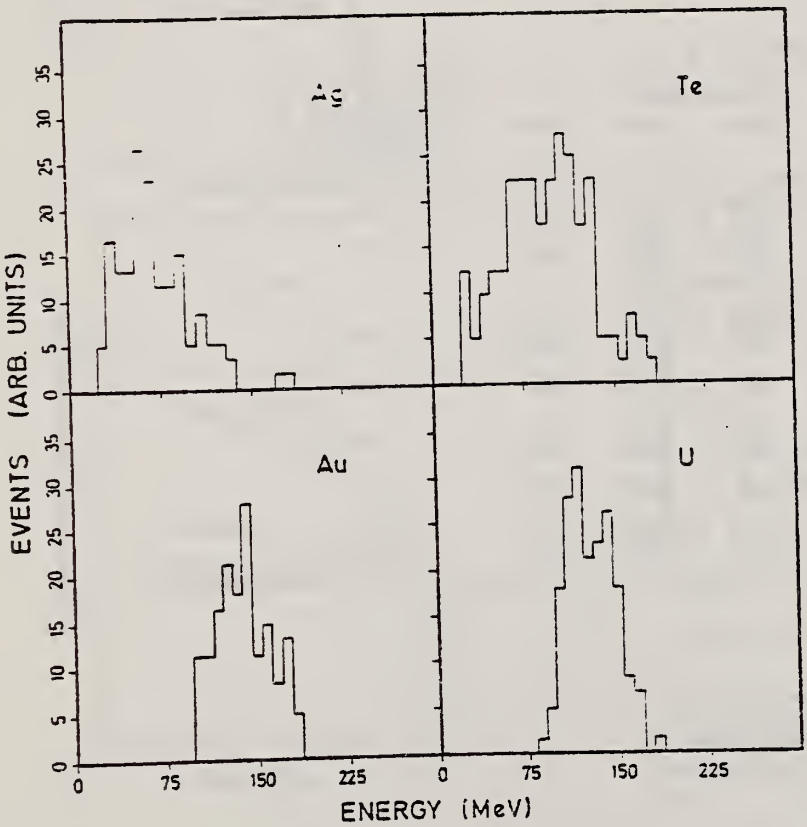

Fig. 3. Fission energy distributions extracted from the present measurements assuming zero centre-of-mass motion for the fissioning systems indicated

REF. H. Hirayama and T. Nakamura
Nucl. Inst. Meth. 147, 563 (1977)

ELEM. SYM.	A	Z
197	Au	79

METHOD

REF. NO. 77 Hi 5 hmg

REACTION	RESULT	EXCITATION ENERGY	SOURCE		DETECTOR		ANGLE
			TYPE	RANGE	TYPE	RANGE	
G,N	ABI	8-30	C	18-30	ACT-I		4PI
		(8.1)					

THICK BREMS TARGET

The integral experiment for a sensitivity check of photonuclear cross section data of C, Mn, Fe, In and Au was performed by using the bremsstrahlung produced in a thick iron target by 18, 22, 26 and 30 MeV electrons from a linear accelerator. The cross section data measured by the activation method showed better results for all incident electron energies than those by the photoneutron method, because the latter include the competing (γ, np) reaction above its threshold energy. It is necessary to obtain the cross section data of (γ, n), (γ, np), $(\gamma, 2n)$, $(\gamma, p2n)$ reactions etc., separately by the activation method.

The effective energy range and effective cross section in the giant resonance region were determined for C, Mn, Fe and Au. By using these quantities, the gross structure of the bremsstrahlung spectrum was obtained in good agreement with the theoretical calculation.

TABLE 3

Ratio of measured and calculated saturated activities at 9°, $R_i = A_i^{exp}/A_i^{cal}$.

Reaction	Reference	Detector	Electron energy 18 MeV	22 MeV	26 MeV	30 MeV	Threshold energy of competing (γ, np) reaction (MeV)
$^{12}C(\gamma, n)^{11}C$	6	ACT[a]	–	1.205	1.09	0.824	27.4
	7	BF3[b]	–	0.757	0.931	–	
	8	BF3	–	1.492	1.189	0.914	
	9	BF3	–	1.418	1.159	–	
$^{55}Mn(\gamma, n)^{54}Mn$	10	BF3	0.575	0.810	0.598	–	17.8
	11		0.595	0.875	0.654	0.609	
$^{54}Fe(\gamma, n)^{53}Fe$	12	ACT	0.542	0.783	0.722	1.12	20.9
$^{115}In(\gamma, n)^{114m}In$	13	BF3	0.448	0.511	–	–	15.9
	14	BF3	0.603	0.672	0.586	1.00	
$^{115}In(\gamma, \gamma')^{115m}In$	15	ACT	0.829	1.00	0.852	0.995	
$^{197}Au(\gamma, n)^{196}Au$	16	BF3	0.743	0.553	0.529		13.7
	17	BF3	0.842	0.628	0.608	0.476	

[a] ACT: measurement of radioactivity of the target.
[b] BF3: BF_3 neutron counter with moderator.

[over]

TABLE 4

Effective cross section and effective energy range.

Reaction	Effective energy range (MeV)	Effective cross section (mb) Electron energy 22 MeV	26 MeV	30 MeV	Average
$^{12}C(\gamma, n)^{11}C$	20.5–24.5	–	5.98	5.28	5.63±0.35
$^{55}Mn(\gamma, n)^{54}Mn$	15.0–20.5	–	56.2	52.7	54.5±1.7
$^{54}Fe(\gamma, n)^{53}Fe$	17.0–24.0	–	33.6	47.9	40.8±7.2
$^{197}Au(\gamma, n)^{196}Au$	12.5–15.0	553.5	532.5	415.0	500±85

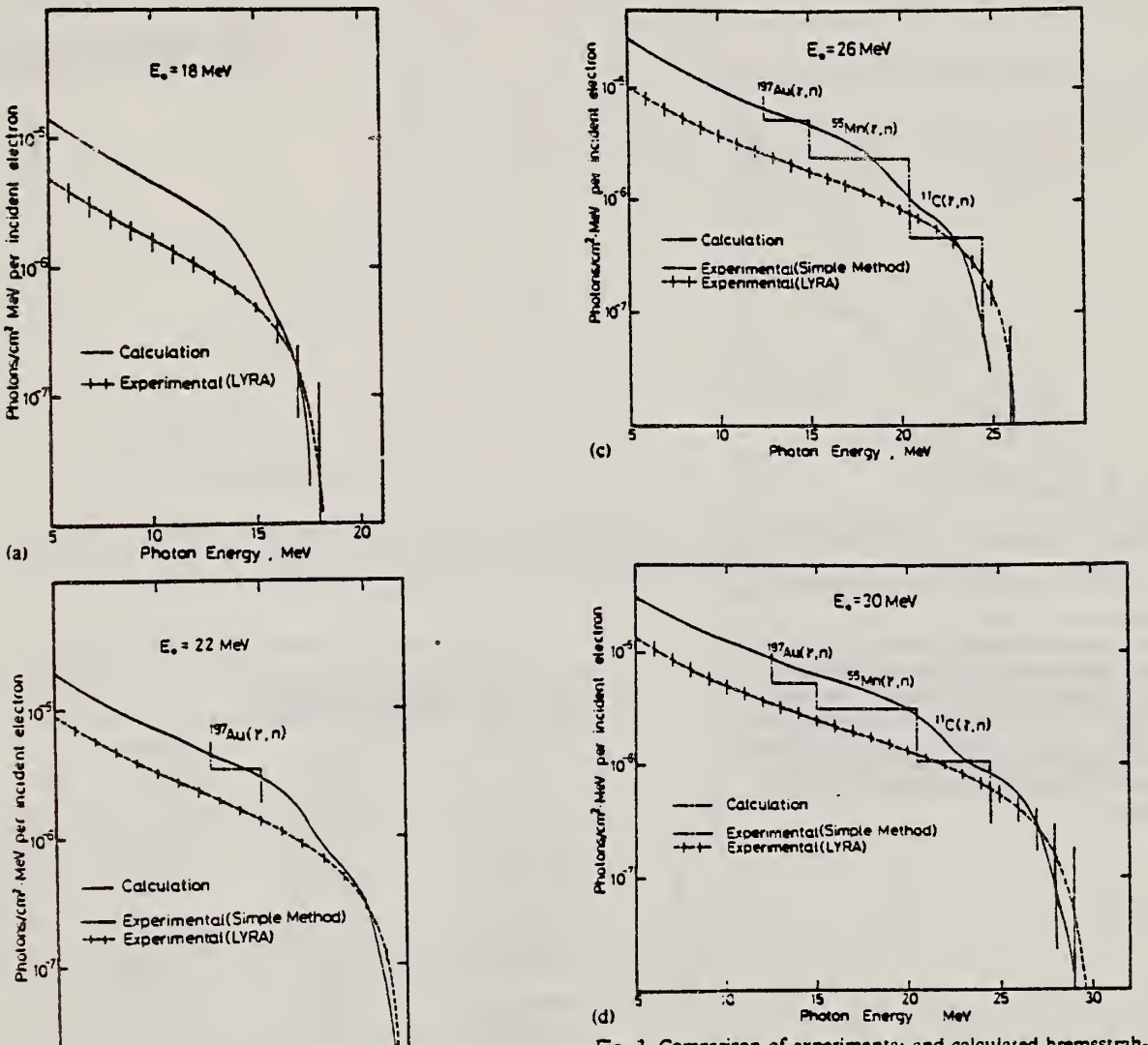

Fig. 3. Comparison of experimental and calculated bremsstrahlung spectra emitted from an iron target in the 9° direction by (a) 18 MeV electrons, (b) 22 MeV electrons, (c) 26 MeV electrons, (d) 30 MeV electrons.

A. Järund and B. Forkman
Z. Physik A281, 47 (1977)

Au	197	79
REF. NO.		
77 Ja 1		egf

METHOD

REACTION	RESULT	EXCITATION ENERGY	SOURCE TYPE	SOURCE RANGE	DETECTOR TYPE	DETECTOR RANGE	ANGLE
G,NA24	NOX	THR - 800	C	800	ACT-I		DST

MEAN FRAGMENT RANGES

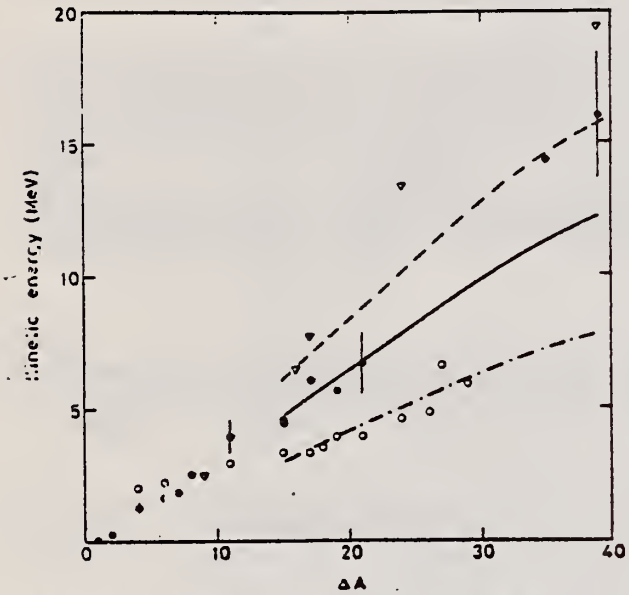

Fig. 1. The kinetic energies of fragments produced in Cu as a function of the mass number difference ΔA between fragments and target: • denotes the measured mean energies, o the energies calculated with Monte Carlo program [10], ▽ the energies from fission calculation [11], –·–·–, ——— and – – – – are the energies calculated from the semiempirical formula of [9] multiplied by factors of 1., 1.56 and 2.02 respectively. The random error is given by bars in some points

Table 1. Mean ranges and mean kinetic energies in three directions for ^{24}Na produced in different targets

	Range mg cm^{-2}	Kinetic energy MeV
Cu forward	3.64 ± 0.55	21.0 ± 3.8
Cu backward	2.17 ± 0.33	10.2 ± 1.8
Cu perpendic.	3.09 ± 0.46	16.7 ± 3.0
Ag forward	7.61 ± 1.14	37.1 ± 6.7
Ag backward	6.65 ± 1.00	31.8 ± 5.7
Ag perpendic.	7.20 ± 1.08	35.0 ± 6.3
Au forward	17.4 ± 2.6	69.5 ± 12.5
Au backward	16.0 ± 2.4	64.0 ± 11.5
Au perpendic.[a]	12.6 ± 8.4	49.2 ± 33.4

[a] The statistical uncertainty in the yield was specially large

A. Järund and B. Forkman
Z. Physik A281, 39 (1977)

Au	197	79	
REF. NO.			
77 Ja 2		egf	

REACTION	RESULT	EXCITATION ENERGY	SOURCE TYPE	SOURCE RANGE	DETECTOR TYPE	DETECTOR RANGE	ANGLE
G,NA24	ABY	THR-999	C	400-999	ACT-I		4PI

999=1 GEV

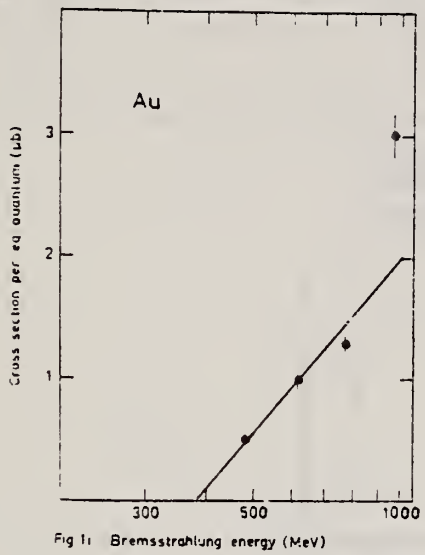

Fig 1: Bremsstrahlung energy (MeV)

Fig. 1a–j. The measured yield as a function of bremsstrahlung end point energy. The error bars give the statistical errors in the numbers of γ-quanta detected. The solid lines are fitted to the yield points with the least-squares method. The yield from Cu (Fig. 1a) is measured in [1] and has been recalculated using the monitor curve of [5]

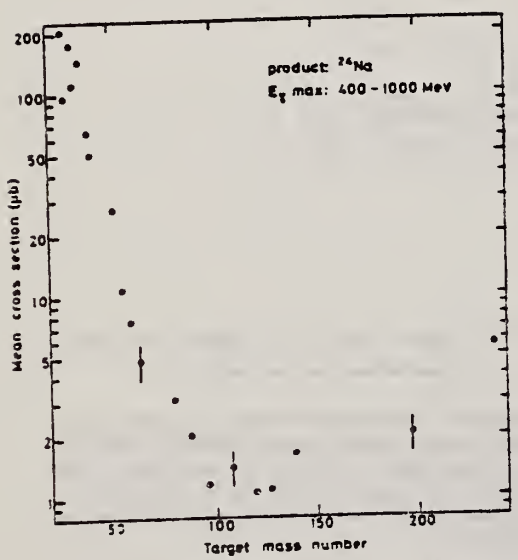

Fig. 2. The mean cross section in the energy range 400 to 1000 MeV [illegible] from the yields of Figure 1 in this work and of Figures 1 to [illegible]. The error is given by bars in some points

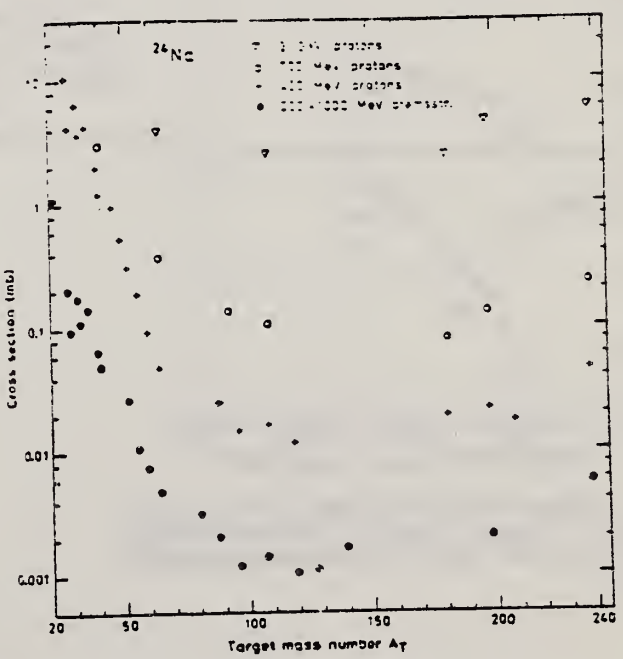

Fig. 4. Mean cross sections of the present work and of [1] (●) compared with the cross sections in proton irradiations: + 400 MeV from [4], ○ 700 MeV from [16] and an extrapolated value from [17], ▽ 3 GeV from [18]

REF. I. Blomqvist, B. Bulow, A. Fredrikson, B. Johnsson, G.G. Jonsson, K. Lindgren, M. Nilsson, R. Petersson, O. Glomset, N. Freed, and W. Rhodes
Z. Physik A288, 313 (1978)

ELEM. SYM.	A	Z
Au	197	79

METHOD

REF. NO. 78 Bl 7 rs

REACTION	RESULT	EXCITATION ENERGY	SOURCE		DETECTOR		ANGLE
			TYPE	RANGE	TYPE	RANGE	
G,PI-	ABY	100-750	C	100-750	ACT-I		UNK

The cross sections for the photoproduction of π^- on ^{197}Au leading to the $1/2^-$ ground and $13/2^+$ isomeric states in ^{197}Hg have been measured from threshold to 750 MeV by use of the activation method. A suitable chemical separation technique was developed and applied in this experiment. The individual cross sections and the isomeric ratio are compared to calculations based on the impulse approximation.

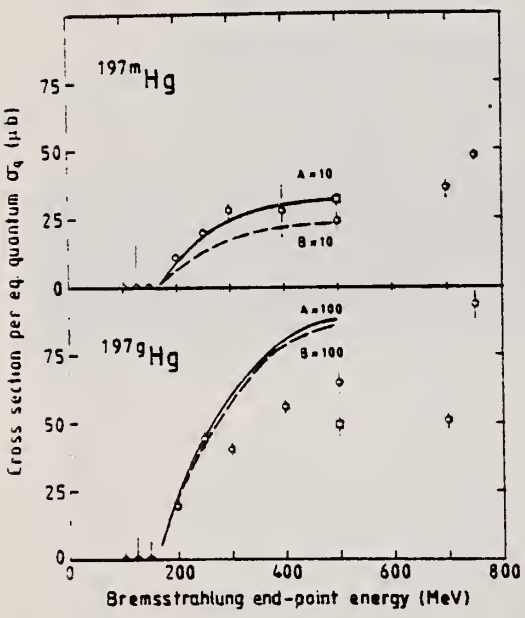

Fig. 1. Experimental und calculated yields, σ_q, for the reactions ^{197}Au(γ, π^-)^{197m}Hg and ^{197}Au(γ, π^-)^{197g}Hg versus bremsstrahlung end-point energy. The solid and dashed curves are described in the text

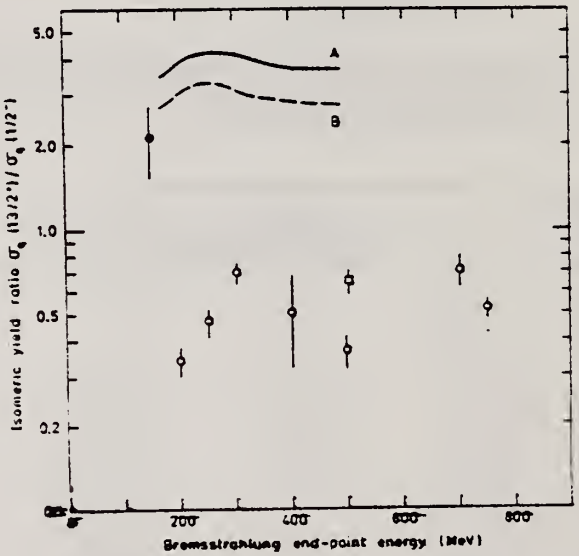

Fig. 2. Experimental and calculated isomeric yield ratios versus bremsstrahlung end-point energy. The open circles are the present results with the new separation method. The open square is our result using the "cold finger" method. The filled circle is the experimental result of Reference 5. The curves *A* and *B* are described in the text

[5] Medicus, H., Smalley, R.: Proc. 6th Int. Conf. on High-Energy Physics and Nucl. Structure, Los Alamos 1975, p. 287.

over

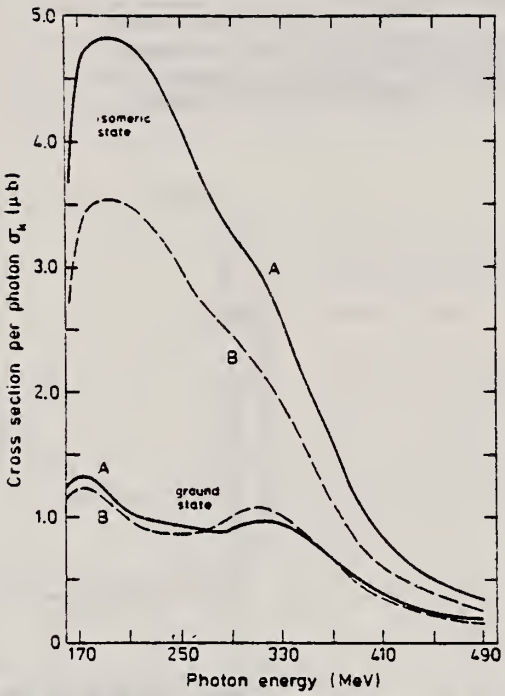

Fig. 3. Theoretically calculated cross sections, σ_k, for the models A and B as a function of photon energy

REF.

J.J. Murphy, II, D.M. Skopik, J. Asai, and J. Uegaki
Phys. Rev. C 18, 736 (1978)

ELEM. SYM.	A	Z
Au	197	79

METHOD

REF. NO. 78 Mu 9 Hg

REACTION	RESULT	EXCITATION ENERGY	SOURCE		DETECTOR		ANGLE
			TYPE	RANGE	TYPE	RANGE	
E,A	ABX	6-100	D	100	MAG-D		50

α particles from the electrodisintegration of seven nuclei with Z between 29 and 79 have been observed. Energy spectra at 50° in the laboratory for six nuclei and angular distributions for five nuclei are reported. The cross sections exhibit a broad peak whose magnitude decreases with increasing Z; the energy of the peak increases as Z increases. Angular distributions at the highest energies measured become increasingly forward peaked suggesting a direct-reaction process.

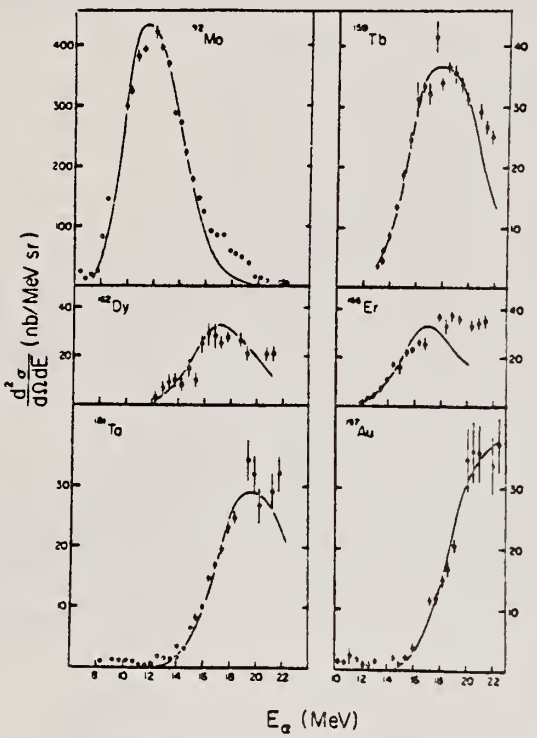

FIG. 2. The α-particle energy spectra at 50° in the laboratory for the four new nuclei studied as well as for two nuclei in which additional data have been obtained. The solid curves are the evaporation model fits described in text.

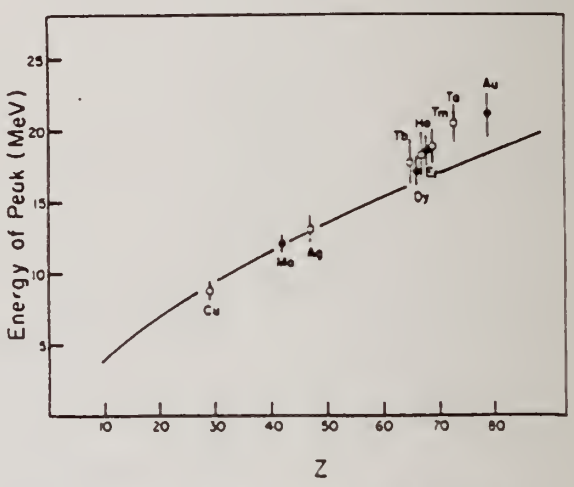

FIG. 3. Energy of the cross section peak as a function of Z. The solid line is the energy of the classical Coulomb barrier. The closed circles are the current work; the open circles are from Ref. 1.

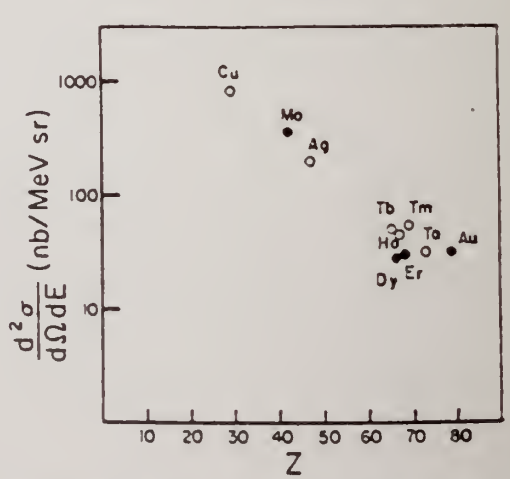

FIG. 4. Magnitude of cross section peak as a function of Z. The closed circles are the current work; the open circles are from Ref. 1.

[1] J.J. Murphy, II, H.J. Gehrhardt, and D.M. Skopik, Nucl. Phys. A277, 69 (1977)

REF. B. Bulow, B. Johnsson, G.G. Jonsson, K. Lindgren, M. Nilsson, R. Petersson
Z. Phys. A290, 393 (1979)

ELEM. SYM.	A	Z
Au	197	79

METHOD

REF. NO. 79 Bu 9 hg

REACTION	RESULT	EXCITATION ENERGY	SOURCE		DETECTOR		ANGLE
			TYPE	RANGE	TYPE	RANGE	
A - G,PI2N	ABY	THR-750	C	100-750	ACT-I		4PI
A - G,PI4N	ABY	THR-750	C	100-750	ACT-I		4PI
B - G,PI5N	ABY	THR-750	C	100-750	ACT-I		4PI

(A) PI IS PI-, ISOMER YLD
(B) PI IS PI-

The yields for some $(\gamma,\pi^- xn)$-reactions on ^{197}Au have been measured from threshold to 750 MeV by use of the activation method. The experimental mean cross sections are compared to results obtained from other experiments on similar reactions and to cascade-evaporation calculations.

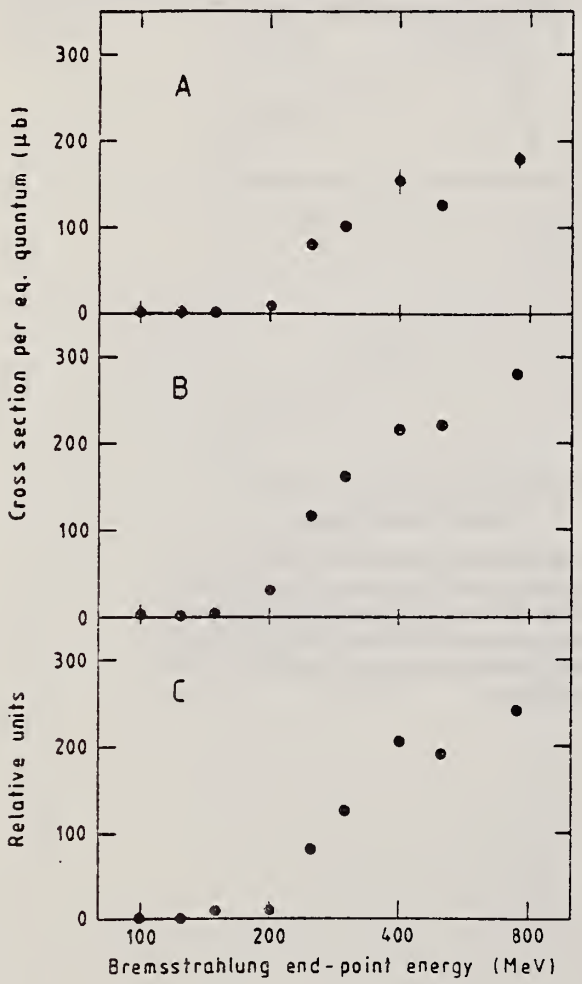

Fig. 1A–C. Measured yields as a function of the bremsstrahlung end-point energy for the following reactions: A ^{197}Au$(\gamma,\pi^- 2n)^{195m}$Hg. B ^{197}Au$(\gamma,\pi^- 4n)^{193m}$Hg. C ^{197}Au$(\gamma,\pi^- 5n)^{192}$Hg

Table 1. Experimental and calculated cross sections and calculated isomeric ratios for the $(\gamma,\pi^- 2n)$ and $(\gamma,\pi^- 4n)$ reactions

Product nucleus	Spin $m;g$	$\frac{\sigma_H}{\sigma_L}$ calc	σ_{calc} (μb) (400 MeV)	$\bar{\sigma}_{exp}$ (μb) (200–750 MeV)
^{195m}Hg	$+13/2;$ $-1/2$	2.0 ± 0.5	87 ± 15	99 ± 16
^{193m}Hg	$+13/2;$ $-3/2$	2.0 ± 0.5	157 ± 22	160 ± 16

REF. A. G. Flowers, D. Brnaford, J. C. McGeorge, A. C. Shotter, P. Thorley, C. H. Zimmerman, R. O. Owens, J. S. Pringle
Phys. Rev. Lett. 43, 323 (1979)

ELEM. SYM.	A	Z
Au	197	79

METHOD

REF. NO. 79F12 hg

REACTION	RESULT	EXCITATION ENERGY	SOURCE		DETECTOR		ANGLE
			TYPE	RANGE	TYPE	RANGE	
E,A	SPC	UKN	D	120	MAG-D		DST

This paper presents energy spectra of α particles emitted following the bombardment of ^{27}Al, ^{nat}Ni, ^{92}Mo, ^{94}Mo, and ^{197}Au with 120-MeV electrons, together with α-particle angular distributions from ^{197}Au and ^{nat}Ni for E_α = 30 and 50 MeV. The data are compared with preequilibrium exciton-model and statistical-model calculations. It is concluded that few-step processes are dominant in the production of α particles with energies above 20 MeV.

PREEQUILIB A EMISS

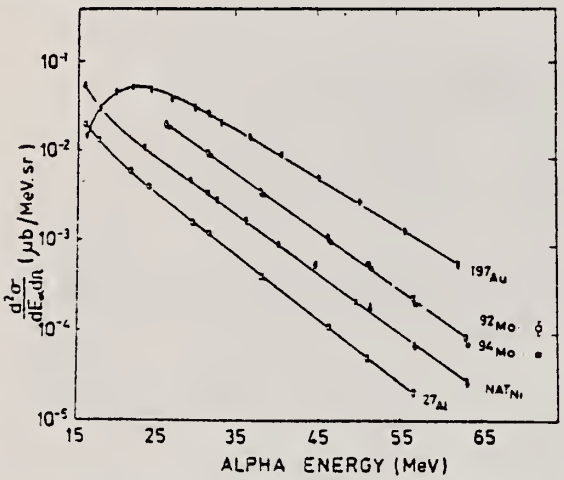

FIG. 1. α-particle energy spectra at $\theta_\alpha = 30°$, for E_e = 120 MeV. Errors shown are the sum of statistical and systematic contributions. The solid lines are a guide to the eye.

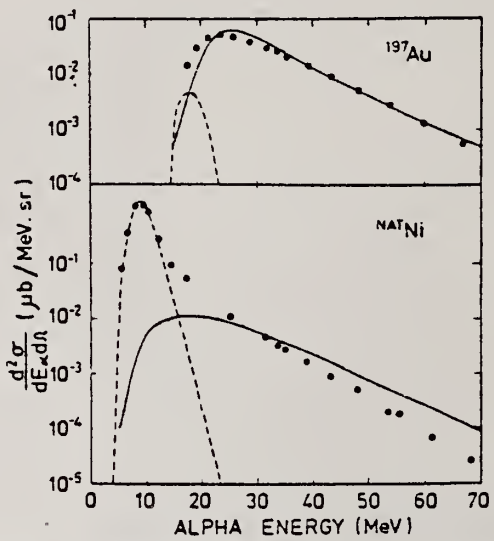

FIG. 2. α-particle energy spectra at $\theta_\alpha = 30°$, for E_e = 120 MeV. The solid circles are experimental points. The solid lines are the results of preequilibrium exciton-model calculations and the dashed lines are the results of statistical calculations neglecting photon absorption above E_γ = 33 MeV.

TABLE I. Temperatures corresponding to the preequilibrium component of the (e,α) reaction, derived from energy spectra at $\theta_\alpha = 30°$ for E_e = 120 MeV.

Target	Temperature[a] (MeV)
^{27}Al	5.3
^{nat}Ni	5.5
^{68}Zn	5.4
^{92}Mo	5.6
^{94}Mo	5.4
^{197}Au	6.1

[a]Error is ± 0.2 MeV.

[over]

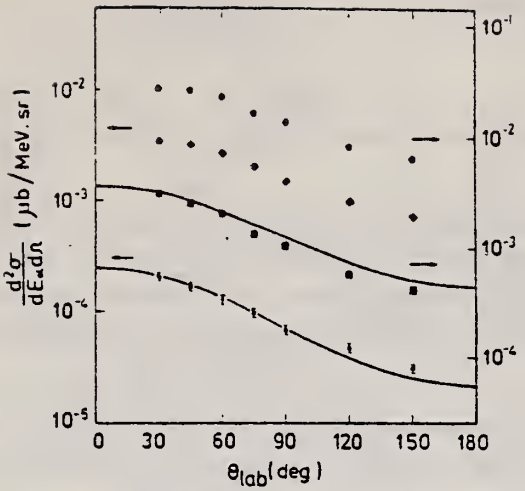

FIG. 3. α-particle angular distributions at $E_\alpha = 120$ MeV for ^{197}Au (shown as circles for $E_\alpha = 30$ MeV and squares for $E_\alpha = 50$ MeV) and ^{nat}Ni (shown as diamonds for $E_\alpha = 30$ MeV and stars for $E_\alpha = 50$ MeV). The solid lines are the result of simple kinematic calculations described in the text. The sum of statistical and systematic errors is shown where it exceeds the size of the points.

J.S. Pringle

REF. A. G. Flowers, D. Branford, J. C. McGeorge, C. H. Zimmerman
Nucl. Phys. A325, 63 (1979)

ELEM. SYM.	A	Z
Au	197	79

METHOD

REF. NO. 79Pr7 hg

REACTION	RESULT	EXCITATION ENERGY	SOURCE		DETECTOR		ANGLE
			TYPE	RANGE	TYPE	RANGE	
E,JN	ABX	THR-147	D	37,147	ACT-I		4PI

Abstract: Cross sections for the (e, xn) reaction on ^{197}Au have been measured for $1 \leqq x \leqq 12$ at 37, 72, 124 and 147 MeV bombarding energies using activation methods. Data for $x \leqq 2$ are compared with cross sections estimated from published (γ, n) and (γ, 2n) data integrated over the virtual photon spectrum. Theoretical cross sections for $x \geqq 4$ were calculated by means of an intranuclear cascade model. Good agreement is found for $x \leqq 7$. The increasing discrepancy between experimental and theoretical cross sections for $x \geqq 7$ is discussed. No evidence is found for giant resonances in regions above the giant dipole resonance.

J=1 TO 12, VIR P ANAL

E NUCLEAR REACTIONS ^{197}Au(e, xn), E = 37, 147 MeV; measured and calculated cross sections: Ge(Li) detector.

TABLE I

Experimental cross sections and decay data used

Isotope	γ-energy (keV)	Half-life	Transition probability P	Refs.	Cross sections (mb) at given bombarding energies (MeV)			
					37	72	124	147
^{196}Au	333	6.18 d	2.38E−1	6)	4.89	6.24	5.08	5.83
^{196}Au	356	6.18 d	8.8E−1	6)	5.48	7.32	4.45	5.45
^{196}Au	426	6.18 d	6.5E−2	6)	4.89	6.30	6.69	5.78
^{195}Au	99	183 d	1.2E−1	6)	0.744	1.040	0.930	1.086
^{194}Au	329	39.5 h	5.913E−1	6)	0.112	0.325	0.303	0.319
^{194}Au	365	39.5 h	1.43E−2	6)		0.312	0.311	
^{194}Au	529	39.5 h	2.21E−2	6)		0.312	0.392	
^{194}Au	1469	39.5 h	6.27E−2	6)	0.115	0.304	0.335	0.635
^{193}Au	268	17.65 h	3.88E−2	6, 7)		0.108	0.139	0.163
^{193}Au	439	17.65 h	1.91E−2	6, 7)		0.105	0.117	
^{192}Au	308	5.0 h	4.69E−2	4, 6)		0.0385	0.0546	
^{192}Au	316	5.0 h	7.9E−1	4, 6)		0.0329	0.0544	0.0562
^{192}Au	613	5.0 h	5.91E−2	4, 6)		0.0292	0.0582	0.0741
^{191}Au	479	3.2 h	(4.0E−2) a)	6)		0.0192		0.0753
^{191}Au	586	3.2 h	(1.0E−1) a)	6)		0.0199	0.0464	0.0614
^{190}Au	296	42.8 min	8.6E−1	4, 6)		0.00728	0.0172	0.0178
^{190}Au	302	42.8 min	2.84E−1	4, 6)			0.0092	0.0117
^{190}Au	598	42.8 min	1.07E−1	4, 6)			0.0204	0.0221
^{189m}Au	167	4.6 min	(1) b)	7)			0.00832	0.00849
^{188}Au	266	8.8 min	(1.0) a)	6, 7)			0.00215	0.00466
^{188}Au	340	8.8 min	(2.27E−1) a)	6, 7)			0.00303	0.00564
^{188}Au	606	8.8 min	(1.15E−1) a)	6, 7)			0.00365	0.00590
^{186}Au	192	10.7 min	(1.0) a)	6, 7)			0.000261	0.001055
^{185}Au	311	4.2 min	(1) b)	7)				0.000455

a) Relative transition probabilities.
b) Assumed probability.

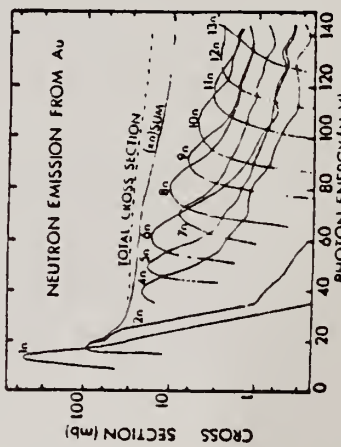

Fig. 1. Plot of cross sections for the ^{197}Au(γ, xn) reactions versus E_γ. The total cross section curve includes all photonuclear reaction channels.

[over]

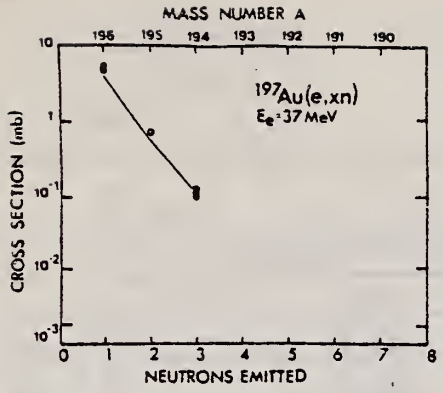

Fig. 2. Comparison of calculated cross sections (solid line) with the measured cross sections for the production of Au isotopes (circles) versus A at E_e = 37 MeV.

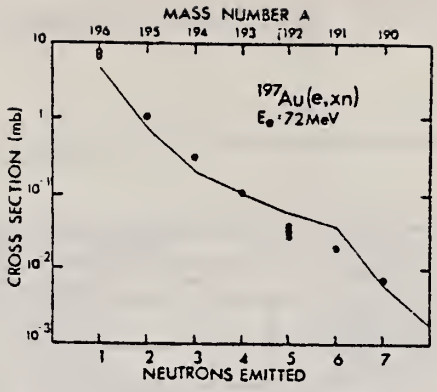

Fig. 3. Comparison of calculated cross sections (solid line) with the measured cross sections for the production of Au isotopes (circles) versus A at E_e = 72 MeV.

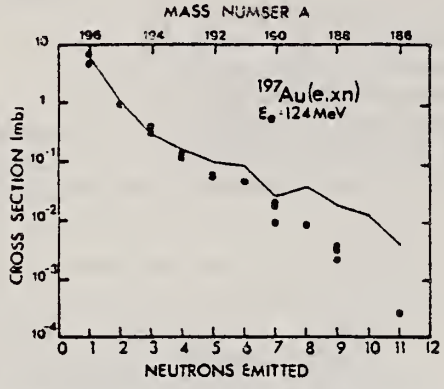

Fig. 4. Comparison of calculated cross sections (solid line) with the measured cross sections for the production of Au isotopes (circles) versus A at E_e = 124 MeV.

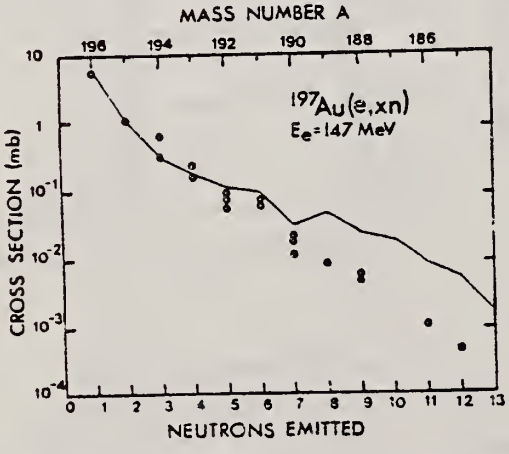

Fig. 5. Comparison of calculated cross sections (solid line) with the measured cross sections for the production of Au isotopes (circles) versus A at E_e = 147 MeV.

REF. J.-O. Adler, G. Andersson, H.-A. Gustafsson, K. Hansen
Z. Phys. A295, 65 (1980)

ELEM. SYM.	A	Z
Au	197	79

METHOD

REF. NO. 80 Ad 10 hg.

REACTION	RESULT	EXCITATION ENERGY	SOURCE		DETECTOR		ANGLE
			TYPE	RANGE	TYPE	RANGE	
G,P	ABY	5-500	C	500	TEL-D		DST
G,D	ABY	11-500	C	500	TEL-D		DST
G,T	ABY	11-500	C	500	TEL-D		DST
G,HE3	RLY	13-500	C	500	TEL-D		DST
G,A	ABY	0-500	C	500	TEL-D		DST

The energy and angular distributions of p, d, t, ^{3}He and ^{4}He from the three targets Cu, Ag and Au were measured at five different angles for bremsstrahlung with peak energy 500 MeV. The measurements were made using a telescope consisting of four surface-barrier detectors. The experimental data are compared with cascade-evaporation calculations. For the ^{4}He-distributions the calculations were extended to include the contribution from knock-out of surface alphas by the cascade nucleons. The comparison shows that the main contribution comes from evaporation but that there is a direct component of the order of 10%.

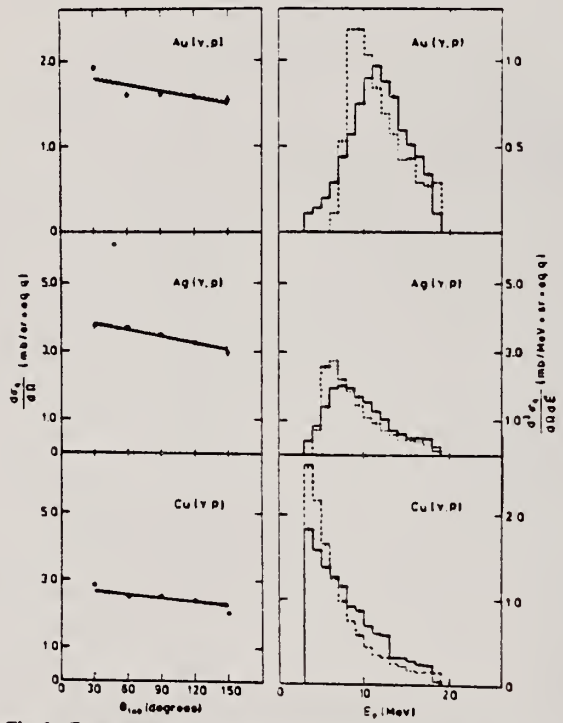

Fig. 2. Experimental proton angular (filled circles) and energy (solid histogram) distributions from the three targets Au, Ag and Cu compared with angular (solid line) and energy (dashed histogram) distributions obtained from cascade-evaporation calculations

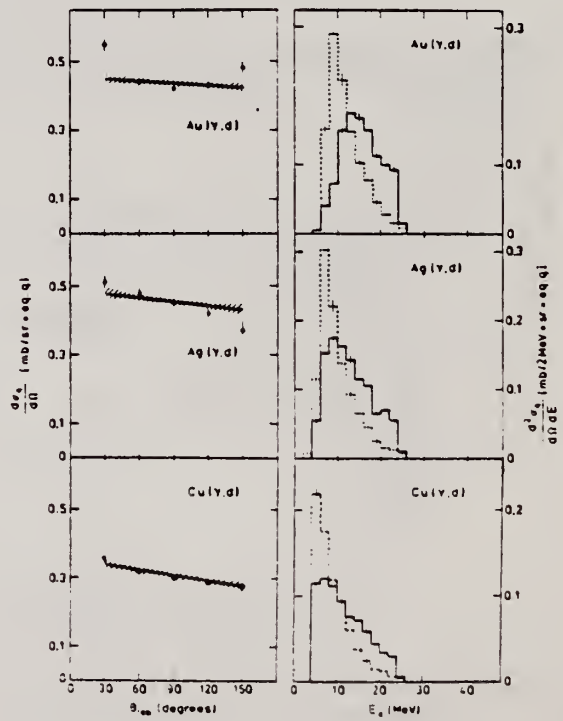

Fig. 3. Deuteron distributions. See caption of Fig. 2

(OVER)

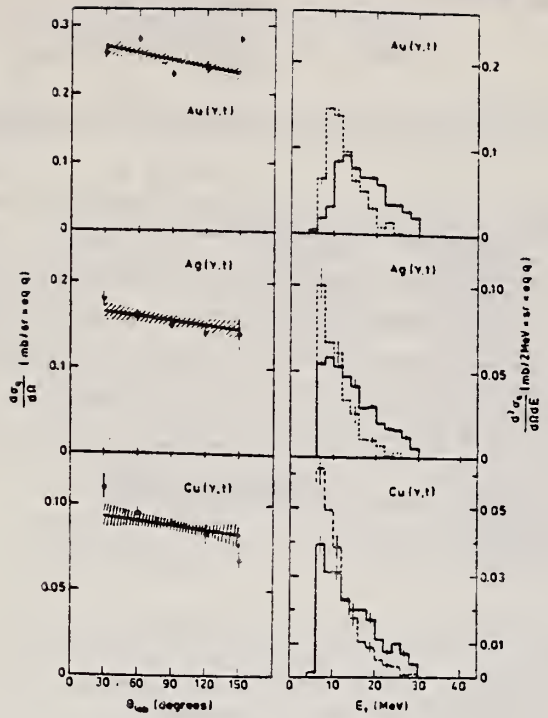

Fig. 4. Triton distributions. See caption of Fig. 2

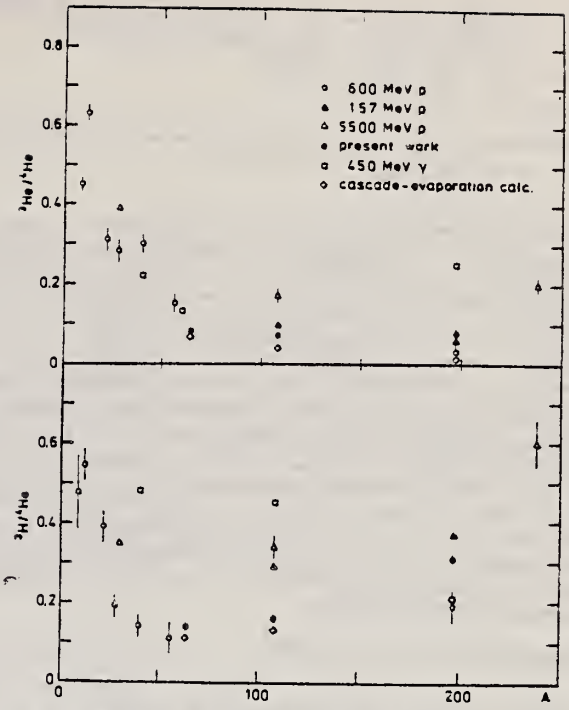

Fig. 6. Comparison between different measurements of the yield ratios $^3He/^4He$ and $^3H/^4He$ as a function of massnumber

Table 2. Integrated yields, normalization factors and calculated direct contributions

Target	Reaction	Y_{int}^{exp} (mb·eq. q)	Normalization factors	Calculated direct contribution in percent	GDR-contribution in percent
Au	(γ, p)	21	0.42	9	–
	(γ, d)	6	0.34	–	–
	(γ, t)	3	0.48	–	–
	(γ, α)	10	0.66	8	–
Ag	(γ, p)	44	0.86	11	5 (Ref. 21)
	(γ, d)	6	0.86	–	–
	(γ, t)	2	1.52	–	–
	(γ, α)	12	1.32	8	–
Cu	(γ, p)	44	0.54	7	28 (Ref. 22)
	(γ, d)	4	0.96	–	–
	(γ, t)	1	2.10	–	–
	(γ, α)	8	1.22	9	10 (Ref. 23)

REF. L.Z. Dzhilavyan, L.E. Lazareva, V.N. Ponomarev, A.A. Sorokin
Sov. J. Nucl. Phys. 33, 308 (1981)
Yad. Fiz. 33, 591 (1981)

ELEM. SYM.	A	Z
Au	197	79

METHOD

REF. NO. 81 Dz 5 hg

REACTION	RESULT	EXCITATION ENERGY	SOURCE TYPE	SOURCE RANGE	DETECTOR TYPE	DETECTOR RANGE	ANGLE
G,N	RLY	8-90	C	10-90	ACT-I		4PI
E,N	RLY	8-90	C	10-90	ACT-I		4PI

Isomeric ratios of the yields of the (γ,n) and $(e,e'n)$ reactions have been measured by an activation method in the nuclei ^{197}Au with formation of high-spin states ($J^{\pi} = 12^{-}$) of ^{196}Au. The dependence obtained for the isomeric ratio for (γ,n) reactions $\bar{x}_{\gamma}$ on $E_{\gamma max}$ has the form of a saturation curve. In the saturation region the value is $\bar{x}_{\gamma} = (6.1 \pm 0.4) \times 10^{-4}$. Analysis of the dependence $\bar{x}_{\gamma}(E_{\gamma max})$ permits the hypothesis that for the (γ,n) reaction the formation of this state has a threshold ~ 12 MeV. The isomeric ratios $\bar{x}_{e}$ for the $(e,e'n)$ reaction exceed the values of $\bar{x}_{\gamma}$. This fact enabled us to conclude that there is an appreciable contribution to excitation of the high-spin state from the isovector quadrupole $E2$ resonance, which is in good agreement with estimates based on a simple model. However, the principal role in population of the isomeric state apparently belongs to cascade γ transitions.

PACS numbers: 25.20. + y, 27.70. + q, 25.30.Cg

ISOMERIC YIELDS

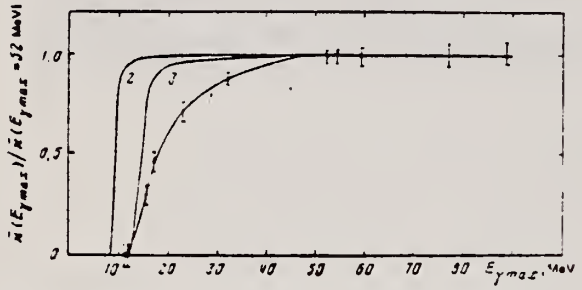

FIG. 3. Relative values of isomeric ratios $\bar{x}$ obtained in bombardment of samples by bremsstrahlung with various maximun energies $E_{\gamma max}$ (curve 1). Curves 2 and 3 were calculated on the assumption $\bar{x}$ const for E_m = 9.7 and 12 MeV, respectively.

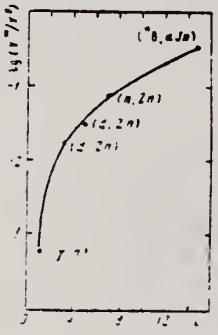

FIG. 5. Experimental values of isomeric ratios of the yields Y^m/Y^g for ^{196}Au nuclei obtained in various reactions with various angular momenta introduced to the nucleus. Points: •—data of Ref. 1, ×—our data.

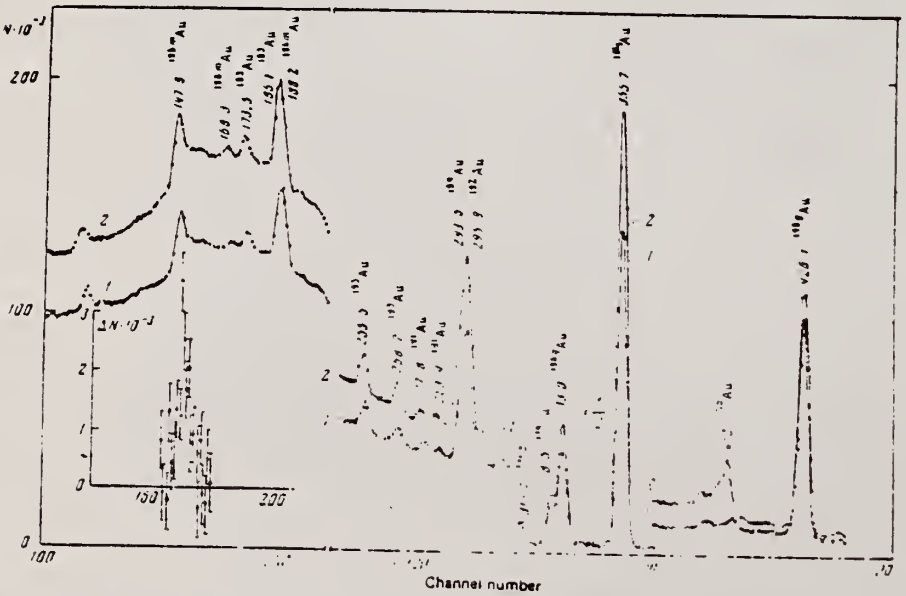

FIG. 6. γ spectra obtained in bombardment of ^{197}Au samples by electrons—spectrum 1, and by bremsstrahlung—spectrum 2 (E_0 = 59 MeV). The insert is the result of subtraction of the spectra 1 and 2 in the region of the 147.8-keV peak after normalization of spectra 1 and 2 on the basis of the 355.7-keV lines.

REF. G.M. Gurevich, L.E. Lazareva, V.M. Mazur, S.Yu. Merkulov, G.V. Solodukhov, V.A. Tyutin
Nucl. Phys. A351, 257 (1981)

ELEM. SYM.	A	Z
Au	197	79

METHOD

REF. NO. 81 Gu 2 hg

REACTION	RESULT	EXCITATION ENERGY	SOURCE		DETECTOR		ANGLE
			TYPE	RANGE	TYPE	RANGE	
G,MU-T	ABX	THR-20	C	27	NAI-D		4PI

Abstract: The curves of the total gamma-absorption cross sections (σ_{tot}) in the E1 giant resonance energy range for the nuclei ^{154}Sm, ^{156}Gd, ^{165}Ho, ^{168}Er, ^{174}Yb, ^{178}Hf, ^{180}Hf, ^{181}Ta, ^{182}W, ^{184}W, ^{186}W and ^{197}Au have been measured using the absorption method. Parameters of the Lorentz curves fitting the measured cross sections σ_{tot} are given. Quadrupole moments (Q_0) and nuclear deformation parameters (β) were obtained.

For deformed nuclei in the $\sim 155 < A < \sim 180$ region a violation of the correlation between giant resonance widths (Γ) and nuclear deformation parameters was found. Γ_1 and Γ_2, the widths of the resonances corresponding to vibrations of nucleons along and across the nuclear deformation axis, were observed to decrease with the increase of A which could be accounted for by the presence of an $N = 108$ subshell.

E NUCLEAR REACTIONS ^{154}Sm, ^{156}Gd, ^{165}Ho, ^{168}Er, ^{174}Yb, ^{178,180}Hf, ^{181}Ta, ^{182,184,186}W, ^{197}Au (γ, X), E = 7-20 MeV; measured total $\sigma(E)$; deduced integrated σ, Lorentz line parameters. ^{154}Sm, ^{156}Gd, ^{165}Ho, ^{168}Er, ^{174}Yb, ^{178,180}Hf, ^{181}Ta, ^{182,184,186}W, ^{197}Au deduced β, Q_0, Γ, giant resonance evolution. Enriched, natural targets.

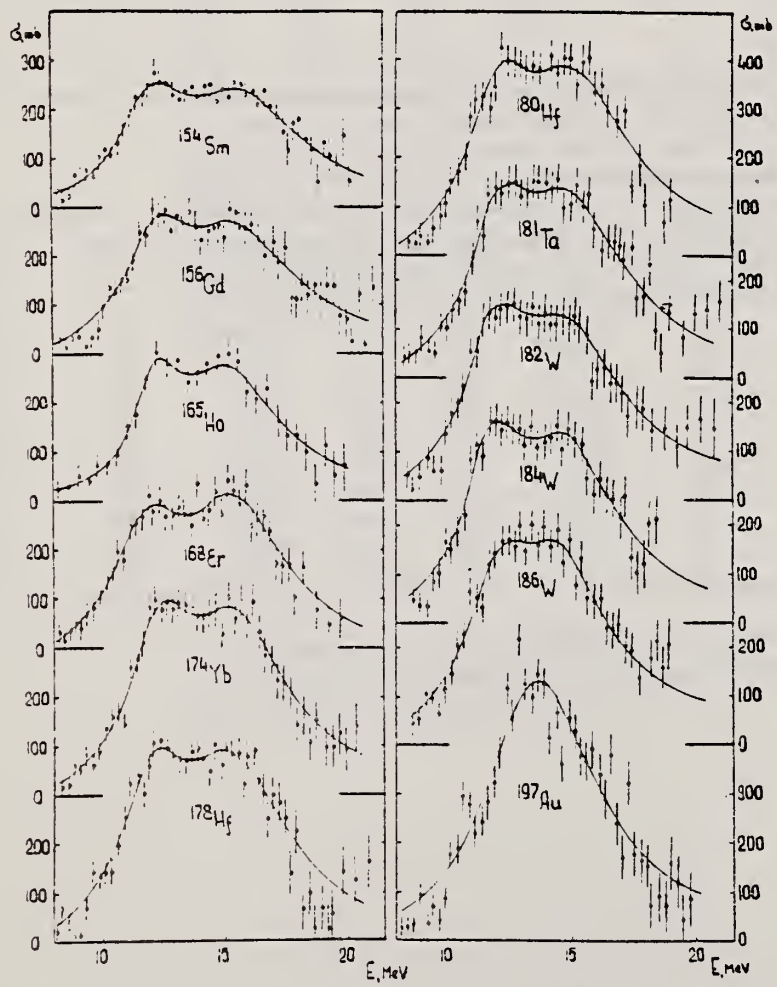

Fig. 2. Total nuclear γ-absorption cross sections (σ_{tot}) measured by the absorption method for ^{154}Sm, ^{156}Gd, ^{165}Ho, ^{168}Er, ^{174}Yb, ^{178}Hf, ^{180}Hf, ^{181}Ta, ^{182}W, ^{184}W, ^{186}W and ^{197}Au. Rms error bars are shown

(OVER)

TABLE 2

Parameters of Lorentz curves fitting the experimental data on σ_{tot}

Nucleus	E_1 (MeV)	σ_1 (mb)	Γ_1 (MeV)	E_2 (MeV)	σ_2 (mb)	Γ_2 (MeV)	$\frac{\sigma_2\Gamma_2}{\sigma_1\Gamma_1}$	Γ (MeV)
^{154}Sm	12.2	188	3.4	15.7	207	5.7	1.85	8.1
^{156}Gd	12.3	206	3.2	15.7	220	5.5	1.81	7.7
^{165}Ho	12.3	202	2.3	15.2	239	4.8	2.47	7.0
^{168}Er	11.9	222	3.2	15.5	275	4.5	1.73	7.4
^{174}Yb	12.3	297	2.9	15.5	320	4.9	1.80	7.1
^{178}Hf	12.2	291	3.1	15.5	334	4.9	1.80	7.2
^{180}Hf	12.2	286	3.2	15.3	324	5.1	1.81	7.1
^{181}Ta	12.1	272	3.0	15.0	316	5.1	1.97	6.8
^{182}W	11.9	267	3.2	14.8	303	5.6	2.01	6.8
^{184}W	11.9	315	2.9	14.8	321	4.7	1.65	6.8
^{186}W	12.0	246	3.3	14.5	332	5.1	2.07	6.4
^{197}Au	13.7	535	5.2					
Average error	1.4 %	11.2 %	9.3 %	1.5 %	9.7 %	4.6 %	0.22	0.2 MeV

TABLE 3

Ratios of nuclear ellipsoid axes (k), deformation parameters (β) and intrinsic quadrupole moments (Q_0), calculated from E_2, E_1

Nucleus	^{154}Sm	^{156}Gd	^{165}Ho	^{168}Er	^{174}Yb	^{178}Hf	^{180}Hf	^{181}Ta	^{182}W	^{184}W	^{186}W
k	1.320	1.302	1.259	1.327	1.289	1.296	1.281	1.263	1.271	1.268	1.229
β	0.326 ±0.017	0.309 ±0.016	0.266 ±0.036	0.334 ±0.032	0.296 ±0.024	0.303 ±0.032	0.288 ±0.036	0.270 ±0.026	0.278 ±0.030	0.274 ±0.032	0.235 ±0.033
Q_0	6.3 ±0.3	6.2 ±0.3	5.8 ±0.8	7.5 ±0.7	7.0 ±0.6	7.5 ±0.8	7.2 ±0.9	6.9 ±0.7	7.2 ±0.8	7.1 ±0.8	6.2 ±0.9

TABLE 4

Integral characteristics of E1 giant resonance

Nucleus	$\sigma_{0\,exp}$ (MeV · b)	$\sigma_{0\,exp}$ $0.06NZ/A$	σ_{0L} (MeV · b)	σ_{0T} $0.06NZ/A$	σ_1 (mb)	σ_{1L} (mb)	$\sigma_{1L}A^{-4/3}$ (mb)	σ_2 (mb · MeV^{-1})	σ_{2L} (mb · MeV^{-1})	$\sigma_{2L}A^{-5/3}$ (μb · MeV^{-1})
^{154}Sm	1.94 ± 0.06	0.87	2.86	1.29	117 ± 3.5	156	0.189	9.1 ± 0.3	14.3	3.23
^{156}Gd	2.07 ± 0.07	0.91	2.95	1.30	143 ± 4.6	163	0.194	10.5 ± 0.4	14.9	3.30
^{165}Ho	1.86 ± 0.06	0.78	2.53	1.06	155 ± 4.4	160	0.177	10.1 ± 0.3	12.6	2.54
^{168}Er	2.24 ± 0.06	0.92	3.07	1.26	161 ± 4.3	197	0.212	12.0 ± 0.3	16.0	3.13
^{174}Yb	2.69 ± 0.05	1.07	3.82	1.52	195 ± 3.4	240	0.247	14.5 ± 0.3	19.2	3.54
^{178}Hf	2.85 ± 0.07	1.11	3.99	1.55	208 ± 4.9	247	0.247	15.3 ± 0.4	20.2	3.59
^{180}Hf	2.72 ± 0.06	1.05	4.03	1.56	200 ± 4.4	250	0.246	15.1 ± 0.3	20.7	3.61
^{181}Ta	2.84 ± 0.07	1.09	3.81	1.46	210 ± 5.3	245	0.239	16.0 ± 0.4	20.0	3.45
^{182}W	2.86 ± 0.07	1.09	4.01	1.52	211 ± 5.3	256	0.248	16.2 ± 0.4	21.6	3.70
^{184}W	2.78 ± 0.07	1.05	3.80	1.43	207 ± 5.3	251	0.240	15.9 ± 0.4	20.9	3.51
^{186}W	2.90 ± 0.07	1.08	3.95	1.48	214 ± 5.3	256	0.241	16.2 ± 0.4	21.6	3.56
^{197}Au	3.12 ± 0.06	1.10	4.37	1.54	229 ± 4.2	276	0.241	18.6 ± 0.4	23.3	3.49

MERCURY
Z=80

"It is a fluid but does not moisten, and runs about, though it has no feet"[1]

A well known metallic element and the only common metal that is liquid at room temperature. The ancient Chinese and Hindus knew of this metal and it has been found in Egyptian tombs of 1500 B. C. The term *mercurius* was first used by alchemists in the 6th century. They used the symbol for the planet Mercury to represent the metal which, because of its mobil form and color, was called quicksilver. The symbol Hg is derived from the Latin *hydrargyrum*, meaning liquid silver.

Hg

1) Waite, A. E., "The Hermetic and Alchemical Writings of ... Paracelsus the Great," James Elliott and Co., London, 1894, Vol.1, pp. 136, 254-5, 314.

Hg

REF.

K. G. McNeill
Phil. Mag. 46, 321 (1955)

ELEM. SYM.	A	Z
Hg		80

METHOD

REF. NO.	
55 Mc 1	EGF

REACTION	RESULT	EXCITATION ENERGY	SOURCE		DETECTOR		ANGLE
			TYPE	RANGE	TYPE	RANGE	
G,XN	RLY	THR - 22	C	22	NAI-I		90

Target element	Counts in 30 minutes per 1000 monitor counts	22 mev yield mol/r relative to copper	Yield mol/r $\times 10^{-6}$
Cu	288 ± 15	1·0	3·2
Cd	647 ± 28	4·1 ± 0·3	13
Hg	661 ± 26	9·5 ± 0·9	30
Pb	470 ± 17	8·4 ± 0·5	27

Ref. W.H. Hartley, W.E. Stephens, E.J. Winhold
Phys. Rev. 104, 178 (1956)

Elem. Sym.	A	Z
Hg		80

Method: Li (p,γ) source, 480 kev protons.

Ref. No.: 56 Ha 1 | EGF

Reaction	E or ΔE	E_o	Γ	$\int \sigma dE$	Jπ	Notes
(γ,xn)						Average Li cross section is 365 mb; cross section with detector response weighted for low energy neutrons, 340 mb. Assumed ratio 17.6/14.8 = 1.7. Calculated cross section at 14.8 and 17.6 MeV assuming cross section curves measured at Pennsylvania and Saskatchewan (refer Table I).

TABLE I. Cross sections for photoneutron emission induced by the lithium gamma rays. The results are compared with previous data.

Element	Present cross-section data: Counter Group A	Present cross-section data: Counter Group B	Data of McDaniel [a]	Betatron data: Pennsylvania $\sigma_{14.8}$	Pennsylvania $\sigma_{14.8}/\sigma_{17.6}$	Saskatchewan $\sigma_{14.8}$	Saskatchewan $\sigma_{14.8}/\sigma_{17.6}$	$\sigma_{14.8}$ [b]	$\sigma_{17.6}$ [b]
$_{26}$Fe	38 mb	33 mb	37 mb			(40)[f] mb	0.5	23 mb	47 mb
$_{27}$Co	49	49	47	60[c] mb	0.5	95[f]	0.5	30	60
$_{28}$Ni	28	25	23			40[e]	0.7	22	32
$_{29}$Cu	64	61	55±12			95[f]	0.6	45	75
$_{45}$Rh	48	45	48			90[f]	0.7	38	54
$_{47}$Ag	175	170	135			240[f]	1.0	175	175
$_{50}$Sn	200	190	180					420[f]	320[f]
$_{73}$Ta	355	360	260	350[d]	1.3	420[e]	2.3	550[f]	240[f]
$_{74}$W	365	355	325						
$_{79}$Au	330	295		315[e]	1.7	480[f]	1.9	460	255
$_{80}$Hg	365	340	290					400[f]	250[f]
$_{82}$Pb	310	295	250	320[e]	1.6	440[f]	2.5	500[g]	200[g]
$_{83}$Bi	305	280	250	270[d]	2.6	550[f]	2.4	490	195

[a] See reference 3.
[b] Average of 14.8- and 17.6-Mev cross sections weighted with relative intensities of the lithium gamma-ray lines.
[c] See reference 14.
[d] R. Nathans, Ph.D. thesis, University of Pennsylvania, 1954 (unpublished).
[e] J. Halpern (private communication).
[f] See reference 13.
[g] See reference 12.
[h] Separate cross sections at 14.8 and 17.6 Mev as obtained from Group A data and 14.8/17.6 betatron cross-section ratios.
[i] Obtained using 14.8/17.6 cross-section ratio from Pennsylvania betatron data.
[j] Obtained using 14.8/17.6 cross-section ratio from Saskatchewan betatron data.

Ref. K. Reibel, A.K. Mann
Phys. Rev. 118, 701 (1960)

Elem. Sym.	A	Z
Hg		80

Method
γ's from $F^{19}(p,\alpha\gamma)$ reaction; protons from VandeGraaff; NaI

Ref. No. 60 Re 1 JHH

Reaction	E or ΔE	E_o	Γ	$\int \sigma dE$	Jπ	Notes
(γ,γ)	E_p = 2.05	~ 7			1	$\langle\bar{\sigma}\rangle$ = 3.5 ± 0.4 mb D (Average level spacing based on J): 0.94 ± 0.62 kev $\bar{\Gamma}_{\gamma o}/\bar{\Gamma}_{\gamma}$ = 0.07 ± 0.03 $\bar{\Gamma}_{\gamma}$ = 3.0 ± 1.5 eV $\bar{\Gamma}_{\gamma o}$ = 0.2 ± 0.1 eV

R.G. Baker, K.G. McNeill
Can. J. Phys. 39, 1158 (1961)

ELEM. SYM.	A	Z
Hg		80

METHOD: Betatron; fast neutron yield, angular distribution; Si threshold detector; ion chamber

REF. NO.: 61 Ba 2 | NVB

REACTION	RESULT	EXCITATION ENERGY	SOURCE		DETECTOR		ANGLE
			TYPE	RANGE	TYPE	RANGE	
G,XN	ABY	THR-22	C	22	THR-I	5-+	DST

In Table 4:

$\bar{\sigma}$ = average cross section of detector weighted with neutron spectrum

Φ = neutrons/100 roentgen/mole

$$W(\theta) = a_o \sum_{n=1}^{\infty} [1 + A_n P_n (\cos \theta)]$$

TABLE IV

I Element	II a_0	III a_1	IV a_2	V $(\bar{\sigma}\Phi)\times10^{26}$	VI Φ_{total}(22 Mev)$\times10^{9}$	VII Φ_{fast}/Φ_{total}
Vanadium	245(1±0.06)	0.01±0.08	−0.00±0.10	6.05	0.21	0.12
Chromium	164(1±0.03)	0.04±0.04	−0.05±0.05	4.05	0.17	0.10
Manganese	308(1±0.02)	0.07±0.03	−0.09±0.04	7.61	0.25	0.12
Iron	200(1±0.03)	0.05±0.04	−0.17±0.05	4.94	0.18	0.11
Cobalt	390(1±0.02)	0.08±0.03	−0.22±0.04	9.63	0.26	0.15
Nickel	145(1±0.05)	0.07±0.07	−0.23±0.09	3.58	0.12	0.12
Copper	347(1±0.02)	0.05±0.03	−0.29±0.04	8.57	0.30	0.12
Arsenic	482(1±0.03)	0.11±0.04	−0.24±0.05	11.91	0.33	0.15
Rubidium	638(1±0.05)	0.13±0.06	−0.14±0.08	15.76		
Strontium	409(1±0.05)	0.10±0.06	−0.17±0.08	10.10		
Yttrium	290(1±0.10)	0.08±0.12	−0.12±0.15	7.16		
Silver	590(1±0.04)	0.10±0.06	−0.22±0.08	14.57	0.87	0.07
Cadmium	905(1±0.02)	0.02±0.02	−0.26±0.03	22.35		
Iodine	1133(1±0.03)	0.04±0.04	−0.29±0.05	27.99	1.42	0.08
Barium	1048(1±0.04)	0.10±0.06	−0.38±0.08	25.89		
Lanthanum	1595(1±0.02)	0.02±0.03	−0.42±0.04	39.40	1.04	0.15
Cerium	1316(1±0.05)	0.05±0.06	−0.39±0.08	32.50		
Dysprosium	1652(1±0.08)	0.04±0.10	−0.34±0.13	40.80		
Tantalum	1558(1±0.02)	0.04±0.03	−0.22±0.04	38.48	2.50	0.06
Tungsten	1365(1±0.02)	−0.07±0.03	−0.24±0.04	33.71		
Mercury	1345(1±0.02)	0.04±0.03	−0.31±0.04	33.22		
Lead	2274(1±0.01)	0.02±0.02	−0.42±0.03	56.17	2.72	0.08
Bismuth	2162(1±0.02)	0.05±0.03	−0.45±0.04	53.40	3.36	0.06
Thorium	3031(1±0.04)	0.06±0.05	−0.32±0.07	74.87		
Uranium	4630(1±0.02)	0.05±0.03	−0.17±0.04	114.36		

*$(\bar{\sigma}\Phi)$ = 2.47×10⁹ a_0 millibarn-neutron. Errors are standard errors due to counting statistics only.

Ref. G. Ben-David (Davis); B. Huebschmann
Phys. Letters 3, 87 (1962)

Elem. Sym.	A	Z
Hg		80

Method
(n,γ) reaction; NaI(Tℓ)

Ref. No. 62 Be 2 | BG

Reaction	E or ΔE	E_o	Γ	$\int \sigma dE$	Jπ	Notes
Hg(γ,γ)	5.44 - 8.997	5.44				σ_t: 55 mb; γ source: Hg Detector at 135°. This is not self resonance; no connection between the nuclear levels responsible for γ emission and level causing resonance.

REF.

H.H. Fleischmann
Ann. Physik 12, 133 (1963)

ELEM. SYM.	A	Z
Hg		80

METHOD

Radioactive source; photon scattering; NaI spectrometer

REF. NO.	
63 Fl 1	NVB

REACTION	RESULT	EXCITATION ENERGY	SOURCE		DETECTOR		ANGLE
			TYPE	RANGE	TYPE	RANGE	
G,G	LFT	2-6	D	2-6	NAI-D		

Peak at 5.4 MeV

G-WDTH

Γ_o = 0.15±0.03 eV

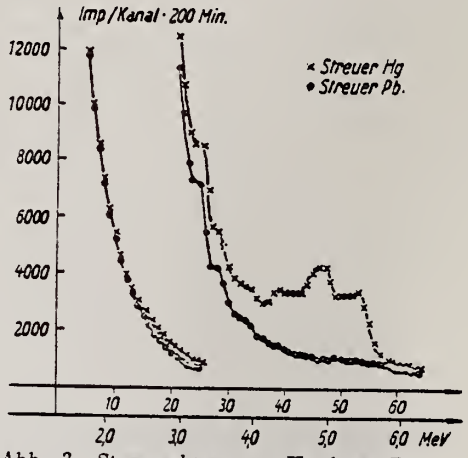

Abb. 3. Streuspektren an Hg bzw. Pb mit Hg-Quelle (Absorber 27,3 g/cm² PbO)

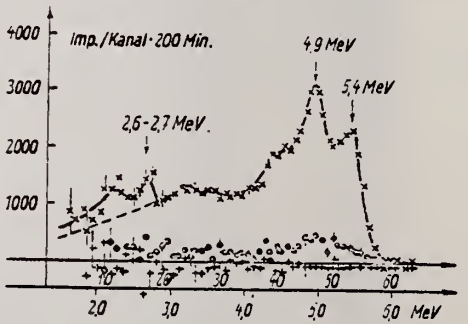

Abb. 4. Differenz der Impulsspektren. —×— bei verschiedenen Streuern HgO bzw. PbO (gemittelt über HgO- und PbO-Absorber von je 27,3 g—cm²), — o — Streuer Hg, Differenz bei verschiedenen Absorbern (wieder je 27,3 g/cm² HgO bzw. PbO), — + — Streuer Pb, Differenz bei verschiedenen Absorbern (wieder je 27,3 g/cm² HgO bzw. PbO)

T. Kaminishi, C. Kojima
Jap. J. Appl. Phys. 2, 399 (1963)

ELEM.		
Hg		80

METHOD
Linac; isomer yield; activity

REF. NO.
63 Ka 2 NVB

REACTION	RESULT	EXCITATION ENERGY	SOURCE		DETECTOR		ANGLE
			TYPE	RANGE	TYPE	RANGE	
G,G/	RLY	1	C 6		ACT-I		4PI
		(0.16, 0.37)					

Table II. The isomers observed

Isomer	Observed value		Referenced value[1][13]	
	Half-life	Energy (MeV)	Half-life	Energy (MeV)
Se-77m	17.5 sec	0.160	17.5 sec	0.161
Br-79m	4.80 sec	0.209	4.8 sec	0.208
Sr-87m	2.3 hr	0.390	2.8 hr	0.388
Y-89m	15.0 sec	0.920	14 sec	0.915
Rh-103m	53 min	*	57 min	0.040
Ag-107m	42 sec	0.95	44 sec	0.094
Ag-109m			40 sec	0.088
Cd-111m	47 min	0.150,0.255	49 min	0.150,0.247
In-115m	4.5 hr	0.335	4.5 hr	0.335
Sn-117m	17 day	0.160	14 day	0.159,0.161
Ba-137m	2.6 min	0.660	2.6 min	0.662
Er-167m	2.10 sec	0.209	2.5 sec	0.208
Hf-179m	18.5 sec	0.157,0.215	19 sec	0.161,0.217
W-183m	5.4 sec	0.200,0.170,0.115	5.5 sec	0.1025,0.2915 others
Ir-191m	4.90 sac	0.129, <0.07	4.9 sec	0.042-0.129
Pt-195m	4.5 day	0.065**	4.1 day	0.031-0.130
Au-197m	7.0 sec	0.10,0.27,0.40	7.2 sec	0.130,0.270,0.407
Hg-199m	43 min	0.160,0.370	42 min	0.158,0.368

* This isomer was measured with a G-M flow counter.
** This value corresponds to Pt-K X-ray energy.

Table III. Induced activation data

Element	Beam energy (MeV)	Counting rate (×10000 cpm)	Sample form
Se	5	1300	metallic [illegible]
Br	4	1600	NaBr grain
Sr	6	0.3	$SrCO_3$ powder
Y	5	90	metallic grain
Rh	5	(0.2*	$RhCl_3$ grain
Ag	5	180	metallic plate
Cd	6	0.5	$CdCl_2$ grain
In	6	8	metallic plate
Sn	5	0.0005	metallic plate
Ba	5	0.6	BaS powder
Er	4	4900	Er_2O_3 powder
Hf	5	1600	metallic plate
W	5	120	metallic powder
Ir	5	2100	metallic powder
Pt	5	0.3	metallic plate
Au	4	4300	metallic plate
Hg	6	0.09	metallic liquid

* The value measured with a G-M flow counter.

REF.

A. Veres
Acta Phys. Acad. Sci.Hung. 16, 261-73 (1963)

ELEM. SYM.	A	Z
Hg		80

METHOD

Radioactive source

REF. NO. 63 Ve 2 NVB

REACTION	RESULT	EXCITATION ENERGY	SOURCE		DETECTOR		ANGLE
			TYPE	RANGE	TYPE	RANGE	
G,G/	ABX	0-1	D	0-1	NAI-D		

ISØMERS

Таблица II

Измеренные значения после облучения, сравниваемые с другими литературными данными

Элемент	Активность облучения после первого измерения (имп/мин.)	Активн. экстрп. в конце облуч. (имп/мин.)	Лутературные данные		Данные измерений		σ_m (10^{-28} см^2)	Γ_{ym} (10^{-4} эв)
			$T_{1/2}$	E (кэв)	$T_{1/2}$	E (кэв)		
Se-77m	3842±96	5400	17,5 сек.	160	18,1±1 сек.	160±10	9,5	1,75
Sr-87m	191±5	200	2,8 ч.	390	2,9±0,1 ч.	365±25	0,85	0,2
У-89m	96±20	170	16 сек.	910	16,7±5 сек.		0,08	0,02
Rh-103m	28±5	31	57 мин.	40	58±2 мин.	20,5±0,5	0,08	0,01
Ag-107m	220±14	250	44 сек.	93	43,8±0,6 сек	91±10	0,8	0,2
Ag-109m			39 сек.	88				
Hf-179m	80±18	155	19 сек.	160; 215	19±2 сек.		1	0,2
Ir-191m	90±20	250	4,9 сек.	42; 130	5±2 сек.		5,6	1
Pt-195m	90±9	100	3,5 д.	31; 100; 130;	3,5±0,2 д.	32±3 67,5±5 96±5 130±10	0,2	0,04
Au-197m	240±16	520	7,2 сек.	130; 277; 407	7,2±1 сек.	68:130: 280±20 390±20	0,07	0,01
Hg-199m	9,6±3,2		42 мин.	160; 370			0,005	0,001

Acta Phys. Hung. Tom. XVI. Fasc. 3.

Ref. C.S. Young, D.J. Donahue
Phys. Rev. 132, 1724 (1963)

Elem. Sym.	A	Z
Hg		80

Method: 200 kW pool reactor; monoergic γ's from (n,γ) in Mn, Fe and Cu; NaI.

Ref. No.: 63 Yo 1 JHH

Reaction	E or ΔE	E_o	Γ	$\int \sigma dE$	Jπ	Notes
(γ,γ)	6.0-8.2					Measured σ (elastic scattering) values in Table II; interpolated to 7 MeV in Table V. In Figure 5, $W(\theta) = 1 + (0.9\pm0.1)\cos^2\theta$

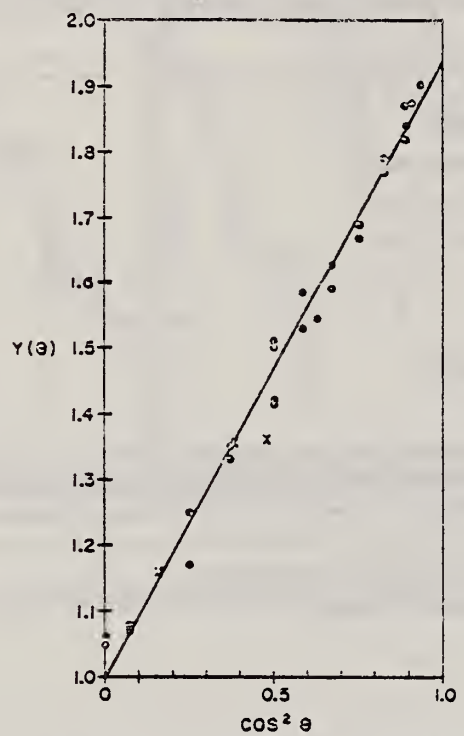

FIG. 5. Relative yield of 7.285-MeV γ rays versus $\cos^2\theta$, where θ is the angle between the incident beam and the scattered γ rays. The points are for angles greater than 90°, the ×'s are for angles less than 90°.

TABLE II. Total elastic scattering cross sections (mb).

Source element	Energy interval (MeV)	Source energy (MeV)	Target (thickness in cm) Ta(1.3)	Hg(3)	Pb(0.6)	Bi(1.3)
Ti	5.0–7.0	6.41 6.75			0.6 ± 0.4	
Mn	6.0–7.5	7.26 7.15 7.05	<0.3	0.5 ±0.3	0.9 ± 0.5	0.8 ±0.4
Fe	6.0–7.6	7.64 7.28	0.7 ±0.4	2.4 ±1.3	125 ±20[a]	2.0 ±1.1
Cu	7.6–8.2	7.91	<0.2	<0.4	<0.2	<0.2

[a] Calculated using the intensity of 7.64-MeV γ rays produced by neutron capture in iron.

TABLE IV. Survey of scattering experiments.

Source element	Target Ta	Hg	Pb	Bi
Chromium	5	6	9	4
Manganese	5	12	10	5
Iron	1	...	2	1
Copper	4	10	11	4
Zinc	3	5	6	3
Silver	...	...	10	...
Lead	...	...	3	1
Titanium	...	...	15	6
Total-each target	18	33	66	24
Total		141		

[1] E. G. Fuller and Evans Hayward, Phys. Rev. 101, 692 (1956); Nucl. Phys. 33, 431 (1962).
[2] K. Riebal and A. K. Mann, Phys. Rev. 118, 701 (1960).
[3] Tsutomu Tohei, Masumi Sugawara, Shigeki Mori, and Motohara Kimara, J. Phys. Soc. Japan 16, 1657 (1961).
[4] P. Axel, K. Min, N. Stein, and D. C. Sutton, Phys. Rev. Letters 10, 299 (1963).

REF.

REF. B. Arad (Huebschmann), G. Ben-David (Davis), I. Pelah, Y. Schlesinger
Phys. Rev. 133, B684-700 (1964)

ELEM. SYM.	A	Z
Hg		80

METHOD: Reactor, (n,γ) reactions source

REF. NO.: 64 Ar 1 NVB

REACTION	RESULT	EXCITATION ENERGY	SOURCE TYPE	SOURCE RANGE	DETECTOR TYPE	DETECTOR RANGE	ANGLE
G,G	ABX	5	D	5	NAI-D		135
		(5.44)		(5.44)			

TABLE III. Effective cross sections.

γ source	Energy (MeV)	Element	Scatterer Protons	Scatterer Neutrons	$\langle\sigma_{\gamma\gamma}\rangle$ (mb)	Notes
Hg	5.44	Hg	80	116, 118, 119, 120, 121, 122, 124	128	
Cl	6.12	Pr^{141}	59	*82*	103	a
V	6.308	Sn	*50*	62, 64–70, 72	14	
Co	6.690	Pr^{141}	59	*82*	2.7	a
Co	6.867	Nd	60	82, 83, 84, 85, 86, 88	22	
Al	6.98	Pb^{208}	*82*	*126*	2900	b
Cl	6.98	Pb	*82*	124, 125, *126*	346	a
Ti	6.996	Bi^{209}	83	*126*	1560	b
Cu	7.01	Sn	*50*	62, 64–70, 72	1000	b
Ti	7.149	Pb^{208}	*82*	*126*	1000	b
Co	7.201	Pb^{208}	*82*	*126*	25	
Mn	7.261	Pb^{208}	*82*	*126*	25	a
Fe	7.285	Pb^{208}	*82*	*126*	4100	a
V	7.305	Pb^{208}	*82*	*126*	12.5	
Hg	7.32	Pb	*82*	124, 125, *126*	5500	c
Fe	7.639	Ni	*28*	30, 32, 34, 36	10.5	d
Fe	7.639	Pr^{141}	59	*82*	10	d
Cr	8.499	Cu	29	34, 36	24.4	
Cr	8.881	Pr^{141}	59	*82*	9.3	
Ni	8.997	Sm	62	*82*, 85–88, 90, 92	2.8	

[a] A large error could be introduced in the cross-section values because of large differences in line intensities quoted by Bartholomew and Higgs and by Groshev *et al.* (Ref. 6).
[b] Because of the low counting rate, thick scatterers were used, which will introduce a systematic error in estimating $(\sigma_{\gamma\gamma})$ for resonances having a high nuclear cross section.
[c] The cross section was evaluated assuming the gamma intensity to be 0.02 photons per 100 captured neutrons (see text).
[d] Reference 6 gives the 7.639 line of iron capture gamma rays as a single line. However, a recent paper by Fiebiger, Kand, and Segel [Phys. Rev. 125, 2031 (1962)] reports two different lines of equal intensities having energies of 7.647 and 7.633 MeV. The present experiment cannot resolve an energy difference of 14 keV, therefore, there is no possibility of deciding which line is responsible for the scattering.

REF. G. Ben-David, B. Arad, J. Balderman, and Y. Schlesinger
Phys. Rev. 146, B852 (1966)

ELEM. SYM.	A	Z
Hg		80

METHOD

Nuclear Resonance Scattering using N,G reactions.

REF. NO. 66 Be 3 JDM

REACTION	RESULT	EXCITATION ENERGY	SOURCE TYPE	SOURCE RANGE	DETECTOR TYPE	DETECTOR RANGE	ANGLE
G,G	RLX	5 - 10	D	5 - 10	NAI-D	5 - 10	135

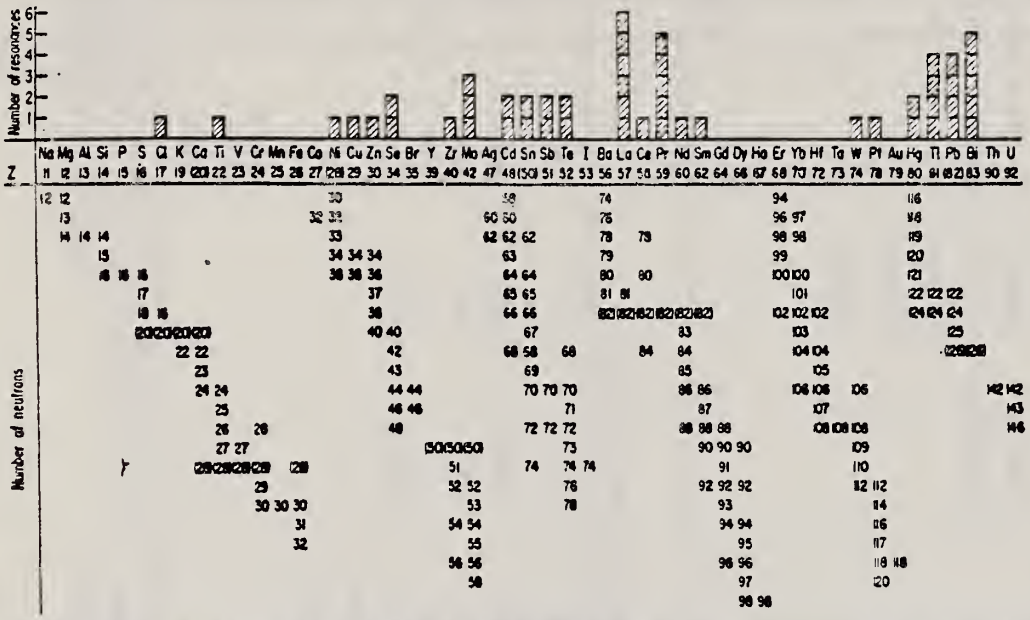

FIG. 3. Histogram of distribution of observed resonances among the different targets. The atomic number is given directly beneath the chemical symbol followed by the neutron numbers of the naturally occurring isotopes. Magic numbers are shown in brackets.

TABLE III. List of effective cross sections.

Scatterer	Energy (MeV)	Gamma source	δ (mb)	Scatterer	Energy (MeV)	Gamma source	δ (mb)
Sm^{144}	8.997	Ni	100	Sn	7.01	Cu	110
Pr^{141}	8.881	Cr	9	Nd	6.867	Co	30
La	8.532	Ni	6	Pr^{141}	6.867	Co	3
Te	8.532	Ni	3[a]	Te	6.7	Ni	...
Cu	8.499	Cr	24	La	6.54	Ag	12
Zr	8.496	Se	3050	Cd	6.474	Co	110
Zn	8.119	Ni	13	Mo	6.44	Hg	25[g]
Se	7.817	Ni	50	La	6.413	Ti	72
Se	7.76	K	90	Mo	6.413	Ti	10
Sb	7.67	V	...[b]	Tl	6.413	Ti	25
Cd	7.64	Fe	40[c]	W	~6.3	Ti	...[b]
Ni	7.64	Fe	7[a]	Sb	6.31	Hg	6[e]
Pr^{141}	7.64	Fe	12[e]	Ti	6.31	Hg	2[e]
Tl	7.64	Fe	370[e]	Sn	6.27	Ag	75
La	7.634	Cu	7	Pb^{208}	6.15	Gd	...[c]
Mo	7.634	Cu	11	Te	5.8	Ni	...[f]
Bi^{209}	7.634	Cu	4	La	6.12	Cl	35
Te	7.528	Ni	66[d]	Pr^{141}	6.12	Cl	110
Bi^{209}	7.416	Se	100	Pt	5.99	Hg	40[a,g]
Bi^{209}	7.300	As	80[e]	Tl	5.99	Hg	5[g]
Pb^{208}	7.285	Fe	4100	Pb^{208}	5.9	Sr	...[b]
Cl	7.285	Fe	34	Ce	5.646	Co	17
Pr^{141}	7.185	Se	80	Bi^{209}	5.646	Co	55
Tl	7.16	Cu	120	Pb^{208}	5.53	Ag	70
La	7.15	Mn	50	Hg	5.44	Hg	75[g]
Bi^{209}	7.149	Ti	2000	Hg	4.903	Co	385

[a] High-energy component of a complex spectrum.
[b] A broad scattered spectrum with no observable peak structure.
[c] There are actually two lines of energies 7.647 and 7.633 MeV having equal intensities in the iron capture gamma spectrum. The cross section has therefore been corrected, although there is no possibility at present of deciding which line is responsible for each resonance.
[d] Is probably an independent level in the complex spectrum of Ni γ rays on Te.
[e] Rough estimate.
[f] May be inelastic component from 7.528 level in Te.
[g] The relative line intensities in this case are due to Groshev and co-workers.
[h] No line is known for the source at this energy.
[i] Difficult to resolve among the many source lines present at this energy.

REF.

S. Ramchandran and J. A. McIntyre
Phys. Rev. 179, 1153 (1969)

Hg		80

METHOD

REF. NO.	
69 Ra 1	hmg

REACTION	RESULT	EXCITATION ENERGY	SOURCE		DETECTOR		ANGLE
			TYPE	RANGE	TYPE	RANGE	
G,G	NOX	5	D	5	NAI		DST

$W(\theta) \sim [1 + \alpha P_2(\cos\theta)]$

5 = 4.906 MEV

[over]

TABLE II. Experiment compared to theory assuming a pure dipole transition.

$\alpha\pm\Delta\alpha$ (Experimental)										
^{90}Zr	Cd	Sn	Hg	^{205}Tl	^{206}Pb	^{209}Bi (7.416 MeV)	^{209}Bi (7.149 MeV)	$A_1^3(J_0, J_1, L=1)$ (Theoretical)	J_0	J_1
0.489±0.027	0.488±0.034	0.490±0.095	0.48±0.11		0.485±0.026			0.500	0	1
	0.488±0.034	0.490±0.095	0.48±0.11	0.0017±0.0110				0.000	1/2	1/2
	0.488±0.034	0.490±0.095	0.48±0.11	0.0017±0.0110				0.250	1/2	3/2
			0.48±0.11					0.000	3/2	1/2
			0.48±0.11					0.160	3/2	3/2
			0.48±0.11					0.140	3/2	5/2
						0.195±0.033	0.184±0.074	0.024	9/2	7/2
						0.195±0.033	0.184±0.074	0.194	9/2	9/2
						0.195±0.033	0.184±0.074	0.083	9/2	11/2

TABLE V. Summary of energy-level parameters.

Element	^{90}Zr	Cd	Sn	Hg	^{205}Tl	^{206}Pb	^{209}Bi	^{209}Bi
Level energy (MeV)	8.496[a]	6.485[b]	6.988[c]	4.906[b]	7.647[d]	7.277[e]	7.416[a]	7.149[a]
γ ray source	Se	Co	Cu	Co	Fe	Fe	Se	Ti
	0→1	0→1	0→1	0→1	1/2→1/2	0→1	9/2→7/2	9/2→7/2
		(1/2→3/2)	(1/2→3/2)	3/2→5/2	(1/2→3/2)		9/2→9/2	9/2→9/2
$J_0\rightarrow J_1$				(1/2→3/2)			9/2→11/2	9/2→11/2
				(3/2→3/2)				
Γ_0/Γ	0.8±0.2				0.85±0.17[f]	$0.95_{-0.17}^{+0.05}$	0.6±0.2	
Γ_0 (eV)	1.68±0.02				1.0[f]	0.68±0.03	0.14±0.09	
ϵ (eV)	5.60±0.15				11.5±0.2[f]	8.00±0.14	3.4±1.6	

[a] L. V. Groshev, V. N. Lutsenko, A. M. Demidov, and V. I. Polekov, *Atlas of Gamma Spectra from Radiative Capture of Thermal Neutrons* (Pergamon Press, Inc., New York, 1959).
[b] E. B. Shera and D. W. Hafemeister, Phys. Rev. 150, 894 (1966).
[c] H. H. Bolotin (private communication from L. M. Bollinger).
[d] R. Moreh and G. Ben-Yaacov, Nuclear Research Center—Negev Report, NRCN-180, 1967, (unpublished).
[e] L. V. Groshev, A. M. Demidov, G. A. Kotelnikov, and V. N. Lutsenko, Nucl. Phys. 58, 465 (1964); G. T. Ewan and A. J. Tavendale, Nucl. Instr. Methods 26, 183 (1964).
[f] See Ref. 24a.

REF.

V. Emma, S. Lo Nigro and C. Milone
Lettere al Nuovo Cimento 2, 271 (1971)

ELEM. SYM.	A	Z
Hg		80

METHOD

REF. NO.	
71 Em 2	egf

REACTION	RESULT	EXCITATION ENERGY	SOURCE		DETECTOR		ANGLE
			TYPE	RANGE	TYPE	RANGE	
G,F	ABY,	THR-999	C	300-999	FRAG-I		4PI

999 = 1000 MEV

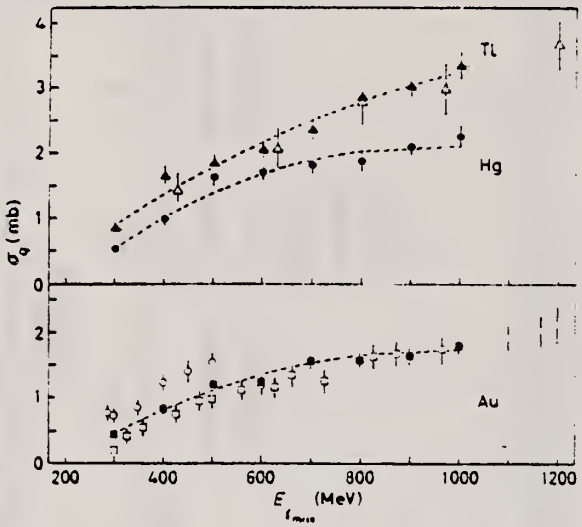

Fig. 1. – Photofission cross-sections per equivalent quantum σ_q against the maximum energy of photons. Au: ○ ref. (4), □ ref. (5), ■ our results; Hg: ● our results; Tl: △ ref. (5), ▲ our results. The dashed curves represent the fits calculated by the least-squares method taking into account our results only.

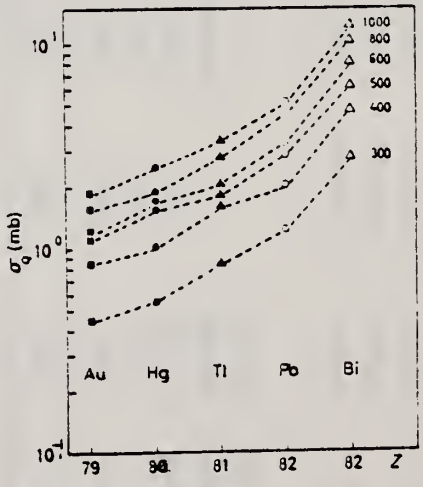

Fig. 2. – σ_q-values, deduced in our present and previous (4) experiments, reported vs. the atomic number Z of the elements for only some energy values.

(over)

TABLE I. – *Fission cross-sections per photon between 300 and 1000 MeV.*

	σ_f(mb)		
	Our results	Previous results	
Bi	7.6 ± 0.2	7.8 ± 0.6 (5)	7.8 ± 0.8 (7)
Pb	3.3 ± 0.1	3.4 ± 0.3 (5)	
Tl	1.9 ± 0.1	2.1 ± 0.2 (5)	
Hg	1.5 ± 0.1		
Au	1.19 ± 0.06	1.25 ± 0.1 (6)	

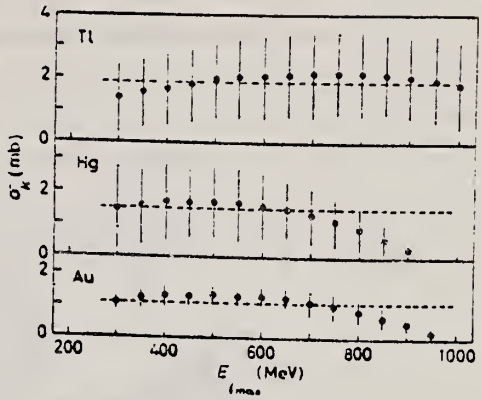

FIG. 3. – Fission cross-section per photon σ_f of Tl, Hg and Au against E_{max}. The dashed straight lines represent the values σ_f = const, calculated as suggested in ref. (5).

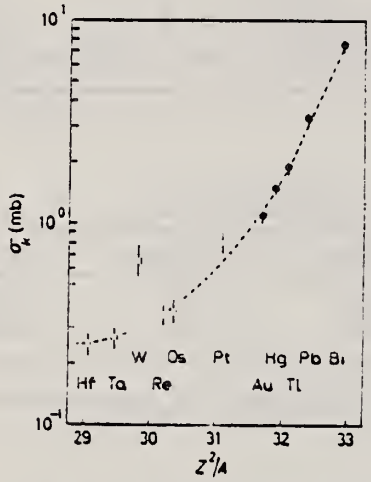

FIG. 4. – σ_f-values *vs.* Z^2/A for the elements with atomic number in the range from 72 to 83: • our results, □ ref. (5), ○ ref. (6). The dashed curves is drawn by eye.

(5) V. EMMA, S. LO NIGRO and C. MILONE: *Boll. S.I.F.*, No. 70, 119 (1970).
(6) V. EMMA, S. LO NIGRO and C. MILONE: *Lett. Nuovo Cimento*, 3, 512 (1970).
(7) V. EMMA, S. LO NIGRO and C. MILONE: *Lett. Nuovo Cimento*, 2, 117 (1971).
(8) J. JUNGERMAN and H. M. STEINER: *Phys. Rev.*, 106, 585 (1957).
(9) H. G. DE CARVALHO, G. COCCINI, E. DEL GIUDICE, G. FURENZA and R. RENZIVILLO: *Nuovo Cimento*, 32, 293 (1964).
(10) A. V. MITROFANOVA, YU. N. RANYUK and P. V. SOROKIN: *Sov. Journ. Nucl. Phys.*, 6, 512 (1968).

REF. S. J. Mecca and J.R. Rothamel
Nucl. Phys. A201, 570 (1973)

ELEM. SYM.	A	Z
Hg		80

METHOD

REF. NO. 73 Me 1 egf

REACTION	RESULT	EXCITATION ENERGY	SOURCE TYPE	SOURCE RANGE	DETECTOR TYPE	DETECTOR RANGE	ANGLE
G,G	NOX	5	D	5	SCD-D		135

5 = 4.924

TABLE 1
Resonant energy results

E_γ [a] (MeV)	I_γ [a]	E_γ [b] (MeV)	I_γ [b]	E'_γ (present work) (MeV)	E'_γ [c] (MeV)
5.646±0.006	8	5.608±0.005	1.3	5.609±0.005	5.646
		5.643±0.005	1.0		
		5.663±0.005	5.4		
4.903±0.008	3	4.890±0.005	0.9		4.903
		4.908±0.005	1.1		
		4.924±0.005	0.65	4.924±0.005	

[a]) Co(n,γ) from ref. [3]).
[b]) Co(n,γ) from ref. [4]).
[c]) Ref. [1]).

TABLE 2
Effective cross-section results

Target	$\langle\sigma_{\gamma\gamma'}\rangle$ [a]) (mb)	$\langle\sigma_{\gamma\gamma'}\rangle$ [b]) (mb)	$\langle\sigma_{\gamma\gamma'}\rangle$ [c]) (mb)
^{209}Bi	55±20%	338	348±20%
^{nat}Hg	385±20%	1777	not measured

[a]) Ref. [1]).
[b]) Value from ref. [1]) adjusted using the intensity from ref. [4]), consistent with the resonance energy from the present work.
[c]) Present work.

[1] G. Ben-David, B. Arad, J. Balderman & Y. Schlesinger, Phys. Rev. 146, 852 (1966).
[4] Nucl. Data Tables A3, (1967). 1966 data.

REF.

E. Hayward, W.C. Barber, and J.J. McCarthy
Phys. Rev. C10, 2652 (1974)

ELEM. SYM.	A	Z
Hg		80

METHOD

REF. NO. 74 Ha 4 hmg

REACTION	RESULT	EXCITATION ENERGY	SOURCE TYPE	SOURCE RANGE	DETECTOR TYPE	DETECTOR RANGE	ANGLE
$ G,G	ABX	15	D	15	NAI-D		90
		(15.1)		(15.1)			

POL PHOTONS

TABLE I. Results.

Target	$d\sigma^{\parallel}/d\Omega_F$ (Arbitrary units)	$d\sigma^{\perp}/d\Omega_F$ (Arbitrary units)	η_F	η	η(DCM)
Cd	0.042 ± 0.028	0.39 ± 0.05	0.11 ± 0.07	0.09 ± 0.07	0.19
In [a]	0.026 ± 0.020	0.54 ± 0.04	0.05 ± 0.04	0.03 ± 0.04	0.19
Sn	0.084 ± 0.036	0.65 ± 0.06	0.13 ± 0.06	0.11 ± 0.06	0.07
Sb [a]	0.14 ± 0.030	0.77 ± 0.05	0.18 ± 0.05	0.16 ± 0.05	
Nd [a]	0.14 ± 0.07	1.03 ± 0.10	0.14 ± 0.07	0.12 ± 0.07	
Ta	0.24 ± 0.10	1.47 ± 0.14	0.16 ± 0.07	0.14 ± 0.07	0.20
W	0.52 ± 0.10	1.66 ± 0.12	0.31 ± 0.07	0.29 ± 0.07	0.20
Pt	0.23 ± 0.08	1.94 ± 0.13	0.12 ± 0.04	0.10 ± 0.04	0.08
Au	0.39 ± 0.11	2.08 ± 0.15	0.19 ± 0.06	0.17 ± 0.06	0.07
Hg [a]	0.33 ± 0.09	2.16 ± 0.15	0.15 ± 0.04	0.13 ± 0.04	0.03
Pb [a]	0.19 ± 0.14	2.42 ± 0.19	0.08 ± 0.06	0.06 ± 0.06	0
Bi	0.10 ± 0.15	2.65 ± 0.26	0.04 ± 0.06	0.02 ± 0.06	0
Th [a]	0.31 ± 0.12	2.26 ± 0.19	0.14 ± 0.05	0.12 ± 0.05	0.07
U [a]	0.21 ± 0.11	2.38 ± 0.19	0.09 ± 0.05	0.07 ± 0.05	0.08

[a] Data not previously reported.

TABLE II. Comparison with Saclay data.

Target	$\lvert A_0\rvert^2$ This experiment (Arbitrary units)	$\lvert A_0\rvert^2$ Saclay (mb)	Ratio
Cd	0.337 ± 0.058	0.508	0.663 ± 0.114
In [a]	0.507 ± 0.046	0.591	0.859 ± 0.078
Sn	0.550 ± 0.072	0.822	0.669 ± 0.096
Sb [a]	0.590 ± 0.061	0.794	0.743 ± 0.077
Nd [a]	0.837 ± 0.100	1.170	0.715 ± 0.086
Ta	1.19 ± 0.18	1.88	0.633 ± 0.096
W	1.05 ± 0.17	2.05	0.512 ± 0.083
Pt	1.67 ± 0.16	2.70	0.619 ± 0.059
Au	1.62 ± 0.20	2.92	0.555 ± 0.068
Hg [a]	2.16 ± 0.20	3.29	0.540 ± 0.060
Pb [a]	2.20 ± 0.27	3.43	0.641 ± 0.078
Bi	2.53 ± 0.31	3.43	0.737 ± 0.090
Th [a]	1.89 ± 0.22	2.73	0.692 ± 0.080
U [a]	2.13 ± 0.22	2.83	0.754 ± 0.077
			0.656 ± 0.021

[a] Data not previously reported.

REF. A. Veyssiere, H. Beil, R. Bergere, P. Carlos, A. Lepretre, A. De Miniac
J. Phys. Lett. 36, L267 (1975)

ELEM. SYM.	A	Z
Hg		80

METHOD

REF. NO. 75 Ve 5 egf

REACTION	RESULT	EXCITATION ENERGY	SOURCE TYPE	SOURCE RANGE	DETECTOR TYPE	DETECTOR RANGE	ANGLE
G,N*	ABX	8- 22	D	8- 22	MOD-I		4PI
G,2N**	ABX	13- 22	D	8- 22	MOD-I		4PI

Abstract. — Partial photoneutron cross-sections $[\sigma(\gamma, n) + \sigma(\gamma, pn)]$, and $\sigma(\gamma, 2n)$ of W, Re, Ir, Pt and Hg were measured by means of monochromatic photons of 8 MeV $\leqslant E \leqslant$ 22 MeV so as to study the giant resonance. The experimentally observed evolution of the shape of the GDR, as one proceeds from permanently deformed prolate nuclei (W and Re) towards oblate or even triaxial gamma unstable nuclei (Pt), corresponds to the theoretical predictions of the dynamic collective model.

*1032+
**1033

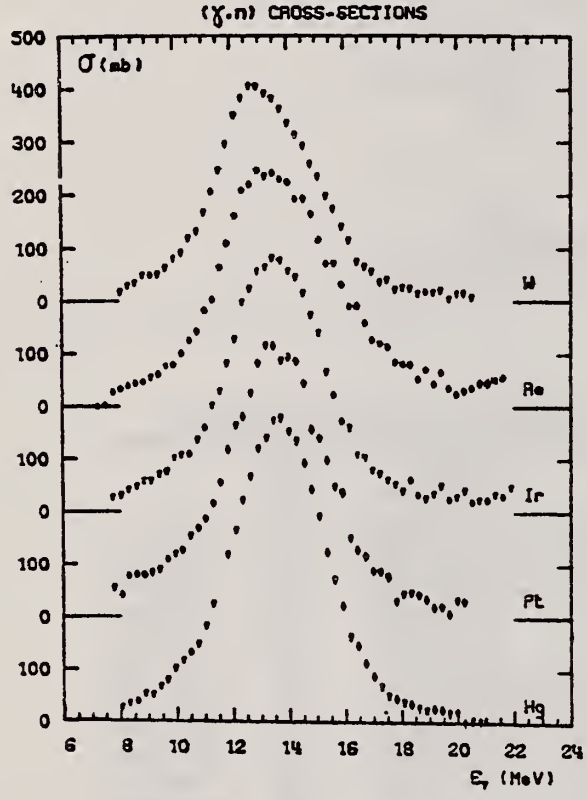

FIG. 1. — Sections efficaces partielles $\sigma(\gamma, n) + \sigma(\gamma, pn)$ des noyaux W, Re, Ir, Pt, Hg.

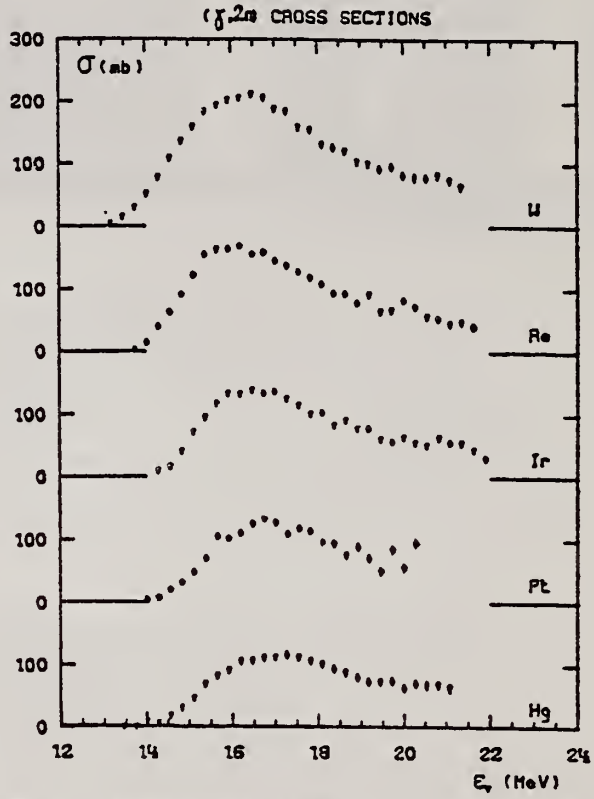

FIG. 2. — Sections efficaces partielles $\sigma(\gamma, 2n)$ des noyaux W, Re, Ir, Pt, Hg.

(over)

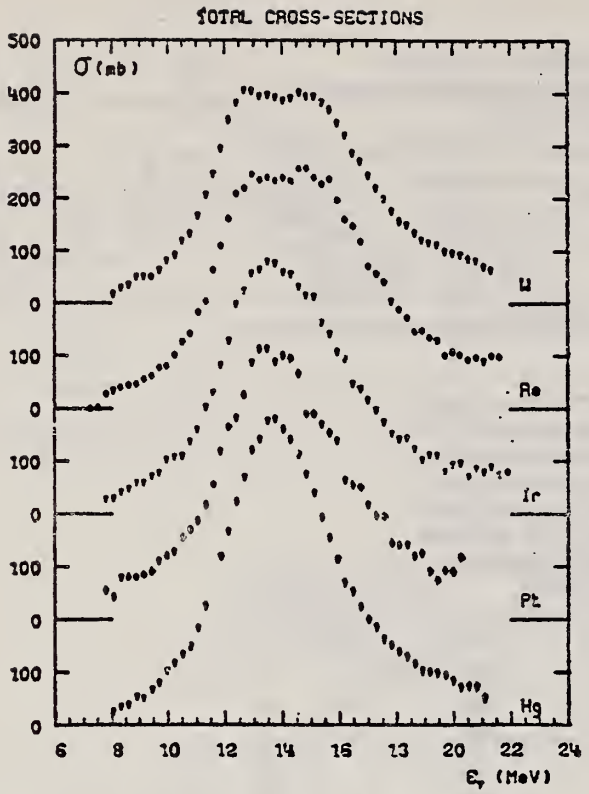

FIG. 3. — Sections efficaces totales $\sigma_T(E)$ des noyaux W, Re, Ir, Pt, Hg.

REF. R.M. Laszewski and P. Axel
Phys. Rev. C 19, 342 (1979)

ELEM. SYM.	A	Z
Hg		80

METHOD

REF. NO. 79 La 1 hg

REACTION	RESULT	EXCITATION ENERGY	SOURCE TYPE	SOURCE RANGE	DETECTOR TYPE	DETECTOR RANGE	ANGLE
G,G	ABX	4- 7	D	4-7	NAI-D		135
		(4.5-6.2)		4.6-6.8			

Average elastic photon scattering cross sections were measured for ^{209}Bi, ^{208}Pb, ^{207}Pb, ^{206}Pb, Tl and Hg at excitation energies between 4.5 MeV and the neutron emission threshold, with an energy resolution in the range between 50 and 150 keV. This resolution was sufficient to determine the strengths of most of the strong levels in this energy region for ^{208}Pb; there are concentrations of strength in a few levels near 5.5 and 7 MeV with the sum of $B(E1)\uparrow$ values equal to about 0.84 and 0.65 e^2 fm^2, respectively; each of these two groups of levels corresponds to only about 0.63% of the electric dipole sum rule. In the neighboring isotopes, approximately the same amount of strength is distributed among many more energy levels; although this strength is spread in energy more than it is in ^{208}Pb, it remains relatively localized.

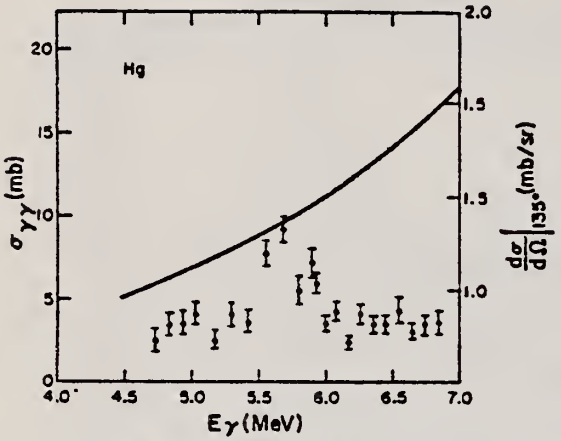

FIG. 8. Natural Hg: See caption of Fig. 4.

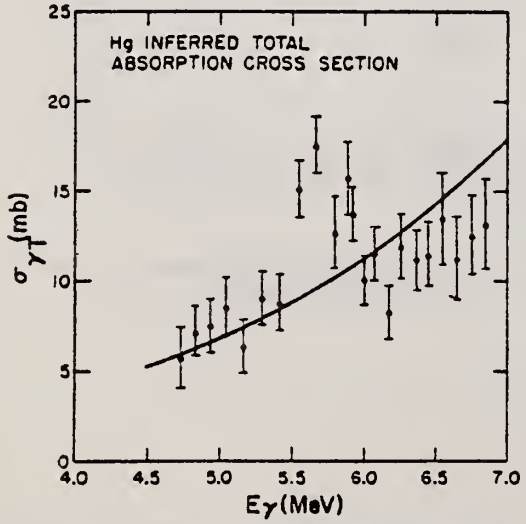

FIG. 10. Hg: inferred total photon absorption cross section.

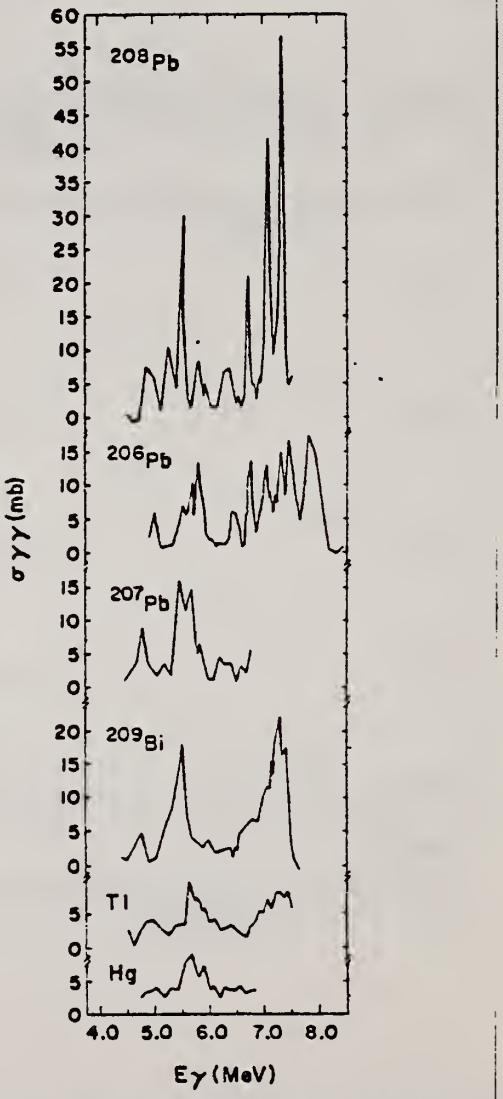

FIG. 12. Comparison of the measured cross sections of, respectively, from the top, ^{208}Pb, ^{206}Pb, ^{207}Pb, ^{209}Bi, Tl, and Hg.

over

TABLE VI. Transition strength comparison at 5.5 and 7 MeV.

Nucleus	5.0–6.0 MeV $\int\sigma_{\gamma\gamma}dE$ (MeV mb)	5.0–6.0 MeV % ^{208}Pb strength	6.5–7.5 MeV $\int\sigma_{\gamma\gamma}dE$ (MeV mb)	6.5–7.5 MeV % ^{208}Pb strength
Bi	10.4	68%	10.7	44%
^{208}Pb	15.2	100%	24.4	100%
^{207}Pb	12.6	83%	...	...
^{206}Pb	15.8	104%	20.2	83%
Tl	8.3	55%	7.8	32%
Hg	11.6	76%	...	...

TABLE IV. Parameters used in inferring $\bar{\sigma}_{\gamma\gamma}$ from $\bar{\sigma}_{\gamma n}$. (Level spacing is assumed to be of the form $D \propto e^{-E/T}$.)

Nucleus	D_0 (eV)	E_0 (MeV)	T (MeV)	Γ_γ (eV)	Ref.
Hg	83	8.03	0.86	0.12	15,22,23
Tl	430	6.54	0.90	0.12	15,22,23

[15] G.A. Bartholomew, E.D. Earle, A.J. Ferguson, J.W. Knowles, and M.A. Lone, in *Advances in Nuclear Physics*, edited by M. Baranger and E. Vogt (Plenum, New York, 1973), Vol. 7, p. 229.

[22] J.E. Lynn, *The Theory of Neutron Resonance Reactions* (Clarendon, Oxford, 1968)

[23] H. Molecky, Sov. J. Nucl. Phys. 13, 133 (1971).

REF. M. Schumacher, F. Smend, W. Mückenheim, P. Rullhusen, H.G. Börner
Z. Phys. A300, 193 (1981)

ELEM. SYM.	A	Z
Hg		80

METHOD

REF. NO. 81 Sc 6 egf

REACTION	RESULT	EXCITATION ENERGY	SOURCE TYPE	SOURCE RANGE	DETECTOR TYPE	DETECTOR RANGE	ANGLE
G,G	ABX	2-7		2-7	SCD-D		90

2.60-6.76 MEV

Elastic scattering by nuclei in the range of mass numbers between 64 and 238 has been studied with monochromatic photons in the energy range between 2 and 8 MeV. These photons were provided either by a Ti(n,γ) source installed in the tangential through channel of the Grenoble high flux reactor, or by ^{24}Na and ^{56}Co sources produced by deuteron bombardment of Al or Fe at the Göttingen cyclotron. The photoexcitation of 23 nuclear levels has been observed and the decay properties and groundstate widths of the majority of these levels have been determined. For the lead scattering target the coherent elastic differential cross section has been studied in detail. There is evidence that below the photo-neutron threshold the elastic scattering via virtual photoexcitation of the nucleus can be approximated by extrapolating the real part of the Giant Dipole Resonance amplitude along a Lorentzian curve. Coulomb corrections to Delbrück scattering seem to play a small role at 6.5 MeV.

Table I. Differential cross sections for elastic scattering $(d\sigma/d\Omega)^{exp}$ of photons from ^{56}Co and ^{24}Na sources by different scattering targets, in units of μb/sr. Errors in the last digits are given in parentheses.

Θ deg	Scattering targets	2.599[a] (MeV)	2.754[b] (MeV)	3.010[a] (MeV)	3.202[a] (MeV)	3.254[a] (MeV)	3.273[a] (MeV)	3.452[a] (MeV)
90	^{238}U	52.7(25)	57.5(25)[c]	56(16)	47(4)	456 (10)[c]	34(6)	49(14)
	^{209}Bi	33.1(30)	32 (2)	33(11)	32(4)	25.6(20)	29(6)	33(15)
	^{nat}Pb	31.5(23)	31.0(16)	35 (8)	27(3)	26.6(22)	25(4)	23 (8)
	^{nat}Tl	31.5(33)	-	27(12)	32(5)	24 (3)	22(7)	34(15)
	^{nat}Hg	30.0(27)	-	24(10)	28(5)	25.5(18)	26(8)	20 (8)
	^{nat}W	22.5(11)	-	17 (7)	19(3)	18.4(15)	18(5)	21 (6)
	^{181}Ta	20.0(15)	19.2 (6)	193(20)[c]	20(4)	17.3(21)	18(5)	21 (8)
	^{165}Ho	15.9(13)	-	17(10)	13(6)	15.6(20)	18(8)	-
	^{nat}Nd	11.4 (7)	14.2 (5)[d]	15 (7)	14(3)	24.2(12)[d]	13(3)	9 (6)
	^{nat}Ce	11.1 (9)	11.0 (5)	-	11(3)	9.5(13)	8(4)	-
	^{127}J	8.4(10)	8.6 (5)	-	9(2)	7 (1)	5(3)	-
	^{nat}Sb	8.0(11)	-	-	10(4)	6.8(19)	-	1,270(50)[c]
	^{nat}Sn	6.5 (7)	7.0 (5)	-	5(2)	7.6 (8)	6(3)	-
	^{nat}Cd	6.2 (5)	-	-	6(2)	6.6 (8)	7(3)	-
120	^{238}U	55.1(25)	64 (4)[c]	43(15)	55(5)	574 (10)[c]	48(5)	48(11)
	^{181}Ta	27.5(15)	25.0 (9)	227(20)[c]	22(5)	21 (2)	22(8)	-
	^{nat}Nd	17.9(30)	17.0 (9)[d]	-	-	29.8(47)[d]	-	-

[a] ^{56}Co source in Fe lattice [b] ^{24}Na source in Al lattice (part of data have been published elsewhere)
[c] Transitions to excited states observed in addition to the ground-state transition
[d] Photoexcitation of nuclear level identified from the size of the differential cross section

(OVER)

Table 2. Elastic differential cross sections $d\sigma/d\Omega(\Theta=90°)$ in μb/sr measured with the Ti(n,γ) source and compared with theoretical predictions. n: predicted number of levels in a $\Delta E=25$ eV interval at 6.5 MeV. Errors in the last digits are given in parentheses

Scattering target	6.418 MeV		6.555 MeV		6.759 MeV		7.168 MeV		n
	exp.	th.	exp.	th.	exp.	th.	exp.	th.	
^{238}U	23 (12)	10.3	-	-	-	-	-	-	45
^{209}Bi	-	-	219(39)[b,c]	8.0	12 (4)	7.4	$1.5(3)\cdot10^{3}$[b,c]	5.7	0.1
^{nat}Pb	7.0(15)	8.6	-	-	6.5(11)	7.4	-	-	0.05
^{nat}Tl	2,586 (92)[a,c]	7.5	-	-	13 (3)[b]	6.0	-	-	0.4
^{nat}Hg	12 (3)	7.8	74(17)[b]	6.5	6.7(15)	6.4	-	-	3.4
^{nat}W	159 (10)[a,c]	6.6	306(33)[a,c]	6.3	20 (2)[a,c]	5.6	-	-	13
^{181}Ta	68 (4)[a,c]	6.3	-	-	10.1(12)[b,c]	5.3	-	-	28
^{165}Ho	15 (3)[b]	4.7	-	-	9.5(14)[b]	3.9	-	-	18
^{nat}Ce	4.1(21)	4.1	-	-	17 (1)[b,c]	3.6	-	-	0.04
^{nat}Sn	4.2(13)	3.0	-	-	2.5 (5)	2.7	-	-	1.9
^{nat}Mo	1,474 (44)[a,c]	2.5	407(39)[a,c]	2.5	8.5(15)[b,c]	2.3	817(258)[b,c]	2.0	0.5
^{nat}Zn	2.4 (8)	1.6	-	-	1.8 (5)	1.5	-	-	0.3

[a] Transitions to excited states observed [b] Photoexcitation identified from size of differential cross section
[c] Photoexcitation reported in [11]

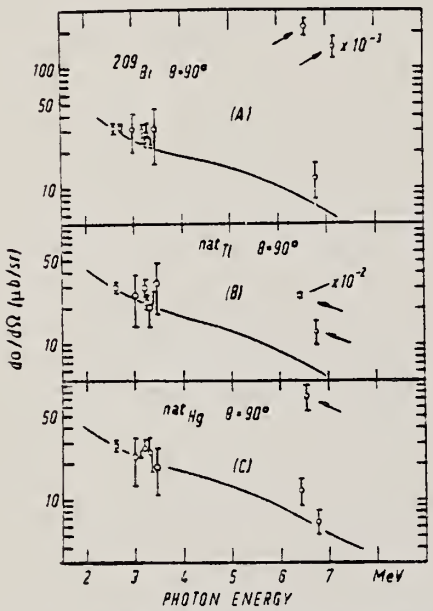

Fig. 9. Differential cross sections for elastic scattering of photons by (A) ^{209}Bi, (B) ^{nat}Tl and (C) ^{nat}Hg through $\Theta=90°$. Solid lines: calculated including R, T, lowest-order D, and N (Lorentzian shape) scattering

HG
A=198

HG
A=198

J.H. Carver, G.E. Coote, T.R. Sherwood
Nuclear Phys. 37, 449 (1962)

Elem. Sym.	A	Z
Hg	198	80

Method: 30 MeV electron synchrotron; activation; NaI

Ref. No.: 62 Ca 1 JHH

Reaction	E or ΔE	E_0	Γ	$\int \sigma dE$	$J\pi$	Notes
$Hg^{198}(\gamma,n)$	Bremss. 30					

TABLE I

Isomeric ratios from (γ, n) reactions

Target nucleus	J_0	Residual nucleus: Ground state			Residual nucleus: Metastable state			Intermediate state	Isomer ratio $Y_1/(Y_1+Y_0)$	σ
			Spin	Half-life	Spin	Half-life		Spin		
Co^{59}	$\frac{7}{2}^-$	Co^{58}	2^+	71.3 d	5^-	9.2 h			0.44 ± 0.02	3.2
Ge^{74}	0^+	Ge^{73}	$\frac{9}{2}^+$	82 min	$\frac{1}{2}^-$	49 s			0.48 ± 0.07	2.8
Br^{81}	$\frac{3}{2}^-$	Br^{80}	1^+	18 min	5^-	4.4 h		2^-	0.32 ± 0.02	6.5
Sr^{88}	0^+	Sr^{85}	$\frac{9}{2}^+$	64 d	$\frac{1}{2}^-$	70 min		$\frac{1}{2}^-$	0.36 ± 0.07	2.2
Zr^{90}	0^+	Zr^{89}	$\frac{9}{2}^+$	79 h	$\frac{1}{2}^-$	4.4 min			0.33 ± 0.10	2.8
Mo^{92}	0	Mo^{91}	$\frac{9}{2}^+$	15.7 min	$\frac{1}{2}^-$	66 s			0.46 ± 0.04	
Ag^{107}	$\frac{1}{2}^-$	Ag^{106}	1^+	24 min	6	8.3 d			0.04 ± 0.02	2.0
In^{113}	$\frac{9}{2}^+$	In^{112}	1^+	14.5 min	4^+	20.7 min		7^-	0.8 ± 0.1	3.1
Cd^{116}	0^+	Cd^{115}	$\frac{1}{2}^+$	53 h	$\frac{11}{2}^-$	43 d			≤ 0.2	
Ce^{140}	0^+	Ce^{139}	$\frac{3}{2}^-$	140 d	$\frac{11}{2}^-$	55 s			0.08 ± 0.01	2.7
Hg^{198}	0^+	Hg^{197}	$\frac{1}{2}^-$	65 h	$\frac{13}{2}^+$	24 h		$\frac{5}{2}^-$ $\frac{1}{2}^-$	0.03 ± 0.01	3.0

	Ref.	Previous work							
Br^{81}	19)	$\frac{3}{2}^-$	Br^{80}	1^-	18 min	5^-	4.4 h	2^-	0.33
Se^{82}	13)	0^+	Se^{81}	$\frac{1}{2}^-$	18 min	$\frac{7}{2}^-$	57 min		0.5
Zr^{90}	13)	0^+	Zr^{89}	$\frac{9}{2}^+$	79 h	$\frac{1}{2}^-$	4.3 min		0.44 ± 0.06
In^{113}	23)	$\frac{9}{2}^+$	In^{114}	1^+	72 s	5^-	50 d	8 ($T_{\frac{1}{2}}$ = 2.5 s)	0.85

The yields Y_1 and Y_2 are for (γ, n) reactions ending in the isomeric- or ground-state. Y_1 + Y_0 is for the higher-spin state

References

1) J. R. Huizenga and R. Vandenbosch, Phys. Rev. **120** (1960) 1305
2) T. Ericson, Advances in Physics **9** (1960) 425
3) D. L. Allan, Nuclear Physics **24** (1961) 274
4) C. T. Hibdon, Phys. Rev. **114** (1959) 179
5) C. T. Hibdon, Phys. Rev. **122** (1961) 1235
6) T. Ericson, Nuclear Physics **11** (1959) 481
7) J. H. Carver, and G. A. Jones, Nuclear Physics **19** (1960) 184
8) A. C. Douglas and N. MacDonald, Nuclear Physics **13** (1959) 382
9) T. Ericson and V. M. Strutinski, Nuclear Physics **8** (1958) 284
10) L. Katz, L. Pease and H. Moody, Can. J. Phys. **30** (1952) 476
11) L. Katz, R. G. Baker and R. Montalbetti, Can. J. Phys. **31** (1953) 250
12) E. Silva and J. Goldemberg, An. Acad. Brasil Cience **28** (1956) 275
13) J. H. Carver and D. C. Peaslee, Phys. Rev. **120** (1960) 2155
14) J. M. Blatt and V. F. Weisskopf, Theoretical nuclear physics (John Wiley, New York, 19
15) S. H. Vegors, L. L. Marsden and R. L. Heath, U. S. Atomic Energy Commission Rep. IDO-16370 (1958)
16) Nuclear Data Sheets (National Research Council, Washington, 1960) sets 1-5 inclusive
17) R. Vandenbosch and J. R. Huizenga, Phys. Rev. **120** (1960) 1313
18) E. Wergold and R. N. Glover, Nuclear Physics **32** (1962) 106
19) K. J. Le Couteur and D. W. Lang, Nuclear Physics **13** (1959) 32
20) T. D. Newton, Can. J. Phys. **34** (1956) 804
21) D. W. Lang, Nuclear Physics **26** (1961) 434
22) M. E. Rose, Internal conversion coefficients (North Holland Publ. Co., Amsterdam, 1
23) J. Goldemberg and L. Katz, Phys. Rev. **90** (1953) 308

REF.

E. Friedland, H.R. Lemmer
Z. Physik 174, 507 (1963)

ELEM. SYM.	A	Z
Hg	198	80

METHOD

Radioactive source; photon scattering; NaI spectrometer

REF. NO. 63 Fr 2

NVB

REACTION	RESULT	EXCITATION ENERGY	SOURCE		DETECTOR		ANGLE
			TYPE	RANGE	TYPE	RANGE	
G,G	ABX	1	D	1	NAI-D	1	DST
		(412 keV)		(412 keV)		(412 keV)	

LFT

$\frac{W(120^\circ)}{W(160^\circ)}$ = 0.37±0.05, consistent with 0 - 2 - 0 transition.

Tabelle 1

Streuwinkel	Zunahme der elastischen Streuung
120°	3.80 ± 0.26 %
160°	9.97 ± 1.04 %

Tabelle 2

Streuwinkel	$\frac{\partial\sigma}{\partial\Omega}$ in mb/sterad	σ in mb	$\tau_\gamma \cdot 10^{11}$ sec
120°	(3.10 ± 0.21)	65.1 ± 4.5	5.11 ± 0.35
160°	8.35 ± 0.87	59.6 ± 6.1	5.58 ± 0.58

REF. K. Masumoto, T. Kato, N. Suzuki
Nucl. Inst. Meth. 157, 567 (1978)

ELEM. SYM.	A	Z
Hg	198	80

METHOD

REF. NO. 78 Ma 10 hg

REACTION	RESULT	EXCITATION ENERGY	SOURCE		DETECTOR		ANGLE
			TYPE	RANGE	TYPE	RANGE	
G,N	ABY	8-68	C	30-68	ACT - /		4PI

Analysis is made of reactions interfering with photon activation analysis procedures.

TO HG-197M

The activation yield curves have been presented for a number of photonuclear reactions in the energy range from 30 to 68 MeV, in order to evaluate quantitatively the interferences due to competing reactions in multielement photon activation analysis. The general features of the yields as functions of both target mass number and excitation energy were elucidated from the data obtained, discussion being given on the results in terms of the reaction mechanism.

Simultaneous neutron activation due to appreciable neutron production from the converter and surrounding materials has also been studied, and, finally, the magnitudes of interferences in real multielement analysis were given in the form of their energy dependences.

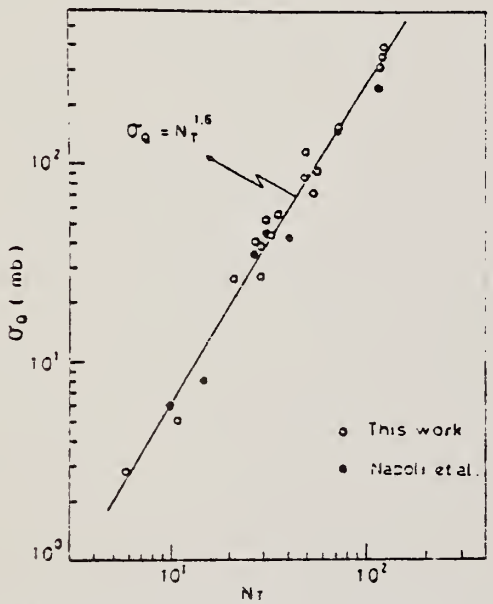

Fig. 2. Yield per equivalent quanta versus target neutron number.

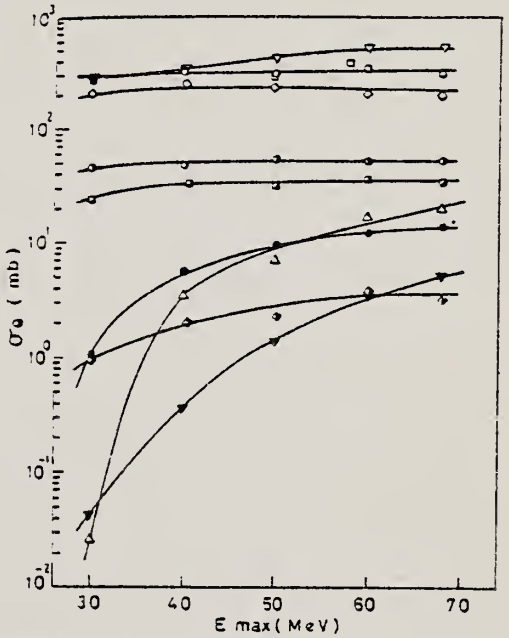

Fig. 8. Activation yield curves for the reactions on Pb, Tl and Hg.

□ $^{204}Hg(\gamma, n)^{203}Hg$, ◇ $^{198}Hg(\gamma, n)^{197g}Hg$,
◪ $^{198}Hg(\gamma, n)^{197m}Hg$, ◁▶ $^{199}Hg(\gamma, p)^{198}Au$,
▽ $^{204}Pb(\gamma, n)^{203}Pb$, ▼ $^{204}Pb(\gamma, 2n)^{202m}Pb$,
△ $^{204}Pb(\gamma, 3n)^{201}Pb$, ○ $^{203}Tl(\gamma, n)^{202}Tl$,
◗ $^{203}Tl(\gamma, 2n)^{201}Tl$, ● $^{203}Tl(\gamma, 3n)^{200}Tl$.

(over)

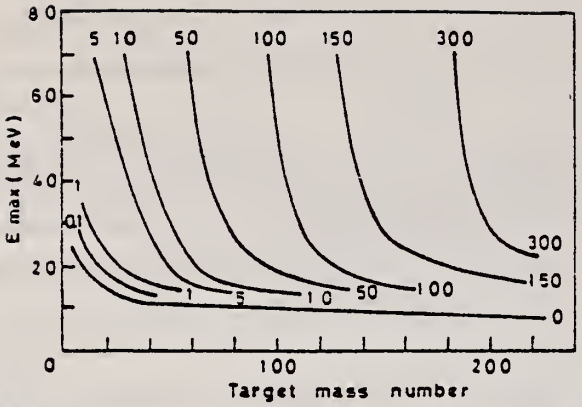

Fig. 9. Yields of the (γ, n) reactions as a function of bremsstrahlung maximum energy and target mass number. The numerical values in the figure are yields per equivalent quanta in mb.

HG
A=199

HG
A=199

REF.

V. Knapp
Proc. Phys. Soc. (London) A70, 142 (1957)

ELEM. SYM.	-	-
Hg	199	80

METHOD

REF. NO.	
57 Kn 1	EGF

REACTION	RESULT	EXCITATION ENERGY	SOURCE		DETECTOR		ANGLE
			TYPE	RANGE	TYPE	RANGE	
G,G	LFT	1	D	1	SCI-D	0-1	90
		209 keV					

High speed rotor technique

Lifetime of 209 keV state $(7.3 \pm 1.2) \times 10^{-11}$ second

K. N. Geller, J. Halpern, and E. G. Muirhead
Phys. Rev. 118, 1302-12 (1960)

ELEM. SYM.	A	Z
Hg	199	80

METHOD
Betatron; neutron threshold; ion chamber

REF. NO. 60 Ge 3 NVB

REACTION	RESULT	EXCITATION ENERGY	SOURCE TYPE	SOURCE RANGE	DETECTOR TYPE	DETECTOR RANGE	ANGLE
G,N	NØX	THR	C THR		BF3-I		4 PI

THRESHØLD

TABLE I. Summary and comparison of neutron separation energies inferred from present threshold measurements with values predicted from mass data and reaction energies. All energies are expressed in the center-of-mass system in Mev.

Reaction	No. runs	Present results	Other results	Method	Reference
$Hg^{199}(\gamma,n)Hg^{198}$	1	6.59 ±0.09	6.680±0.011	mass data	r
			6.68 ±0.06	mass data	q

[q] W. H. Johnson, Jr., and V. B. Bhanot, Phys. Rev. 107, 6 (1957).
[r] J. L. Benson, R. A. Damerow, and R. R. Ries, Phys. Rev. 113, 1103 (1959).

REF.

Y. Oka, T. Kato, K. Nomura, T. Saito, Hui-Tuh Tsai
Bull. Chem. Soc. Japan 41, 380 (1968)

ELEM. SYM.	A	Z
Hg	199	80

METHOD

REF. NO. 68 Ok 3 egf

REACTION	RESULT	EXCITATION ENERGY	SOURCE		DETECTOR		ANGLE
			TYPE	RANGE	TYPE	RANGE	
G,P	ABY	THR-20	C	20	ACT-I		4PI

TABLE 1. SUMMARY OF DATA ON (γ, p) REACTIONS WITH 20 MeV BREMSSTRAHLUNG

Nuclide: Parent (Natural abundance, %)	Nuclide: Residual (Half-life)	S_p (MeV)	Observed γ-ray: Energy (MeV)	Observed γ-ray: Branching ratio (%)	Observed γ-ray: Type of multipole transition	Yield determined: μCi/mg[a]	Yield determined: Yield/mol·R
^{25}Mg (10.11)	^{24}Na (15 hr)	12.06	1.37	100	$E2$	1.48×10^{-1}	1.7×10^{5}
^{29}Si (4.71)	^{28}Al (2.27 min)	12.33	1.78	100	$E2$	1.91	2.8×10^{5}
^{30}Si (3.12)	^{29}Al (6.56 min)	13.59	1.28	93.8	$E2+M1$	6.51×10^{-1}	1.5×10^{5}
^{44}Ca (2.06)	^{43}K (22.4 hr)	12.17	0.374	85	$E2+M1$	7.86×10^{-3}	1.3×10^{5}
^{47}Ti (7.32)	^{46}Sc (84.1 d)	10.47	0.887	100	$E2$	7.11×10^{-4}	3.1×10^{5}
^{48}Ti (73.99)	^{47}Sc (3.4 d)	11.44	0.160	100	$E2+M1$	6.83×10^{-2}	1.2×10^{5}
^{49}Ti (5.46)	^{48}Sc (1.8 d)	11.35	1.31	100	$E2$	4.40×10^{-3}	5.8×10^{4}
^{53}Cr (9.55)	^{52}V (3.8 min)	11.15	1.43	100	$E2$	5.01×10^{-1}	6.6×10^{4}
^{57}Fe (2.17)	^{56}Mn (2.58 hr)	10.57	1.81	23.5	$E2+M1$	8.10×10^{-2}	2.1×10^{5}
^{74}Ge (36.74)	^{73}Ga (4.8 hr)	10.92	0.295	97	$(E2)$	3.70×10^{-1}	1.3×10^{5}
^{77}Se (7.58)	^{76}As (26.5 hr)	9.61	0.559	41	$E2$	1.48×10^{-2}	1.3×10^{5}
^{87}Sr (7.02)	^{86}Rb (19 d)	9.41	1.08	9	$E2$	5.15×10^{-4}	9.9×10^{4}
^{113}Cd (12.26)	^{112}Ag (3.2 hr)	9.74	1.39	35	$E2$	1.91×10^{-2}	2.1×10^{4}
^{117}Sn (7.57)	^{116m}In (54 min)	9.58	1.27	84	$E2$	9.80×10^{-3}	6.9×10^{5}
^{137}Ba (11.32)	^{136}Cs (13 d)	8.67	0.830	100	$E2$	1.68×10^{-4}	2.2×10^{4}
^{199}Hg (16.84)	^{199}Au (2.7 d)	7.27	0.412	100	$E2$	8.43×10^{-4}	2.2×10^{4}

a) The value corrected at the end of 1 hr irradiation (9.4×10^{6} R/min).

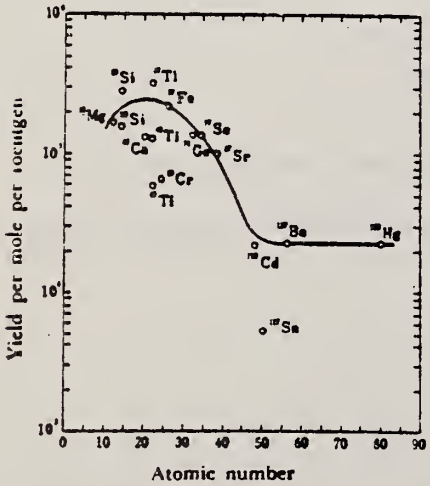

Fig. 2. The yield curve for the (γ, p) reaction with 20 MeV bremsstrahlung.

M. Boivin, Y. Cauchois and Y. Heno
Nucl. Phys. A137, 520 (1969)

Hg	199	80

METHOD

REF. NO.: 69 Bo 3 | egf

REACTION	RESULT	EXCITATION ENERGY	SOURCE TYPE	SOURCE RANGE	DETECTOR TYPE	DETECTOR RANGE	ANGLE
G,G	ABX	0-2	C	0-2	ACT-I		4PI

6 LEVELS

TABLEAU 5

Energie des niveaux excités, sections efficaces intégrées et $u = g\Gamma_s\Gamma_m/\Gamma$ pour ^{199}Hg

E (keV)	$\sigma(\mu b \cdot MeV)$	u(eV)
1000 ± 20	$1.1^{+2}_{-0.4} \times 10^{-5}$	$2.7^{+5}_{-1} \times 10^{-9}$
1340 ± 10	$5.1^{+10}_{-2} \times 10^{-4}$	$2.3^{+4.5}_{-0.9} \times 10^{-7}$
1380 ± 10	$2.2^{+3.8}_{-0.7} \times 10^{-3}$	$1.1^{+1.9}_{-0.3} \times 10^{-6}$
1420 ± 10	$7.9^{+13.6}_{-2.8} \times 10^{-3}$	$4.3^{+7.5}_{-1.5} \times 10^{-6}$
1530^{+20}_{-10}	$1.2^{+2.1}_{-0.3} \times 10^{-1}$	$7.7^{+13}_{-2.1} \times 10^{-5}$
1700 ± 20	$2^{+4.9}_{-1.2} \times 10^{-1}$	$1.6^{+3.3}_{-1} \times 10^{-4}$

Indirect Activation of 43m 534 keV level by .5-2.0 MeV bremsstrahlung.

REF. K. Masumoto, T. Kato, N. Suzuki
Nucl. Inst. Meth. 157, 567 (1978)

ELEM. SYM.	A	Z
Hg	199	80

METHOD

REF. NO.	
78 Ma 10	hg

REACTION	RESULT	EXCITATION ENERGY	SOURCE		DETECTOR		ANGLE
			TYPE	RANGE	TYPE	RANGE	
G,P	ABY	7-68	C	30-68	ACT - I		4PI

Analysis is made of reactions interfering with photon activation analysis procedures.

The activation yield curves have been presented for a number of photonuclear reactions in the energy range from 30 to 68 MeV, in order to evaluate quantitatively the interferences due to competing reactions in multielement photon activation analysis. The general features of the yields as functions of both target mass number and excitation energy were elucidated from the data obtained, discussion being given on the results in terms of the reaction mechanism.

Simultaneous neutron activation due to appreciable neutron production from the converter and surrounding materials has also been studied, and, finally, the magnitudes of interferences in real multielement analysis were given in the form of their energy dependences.

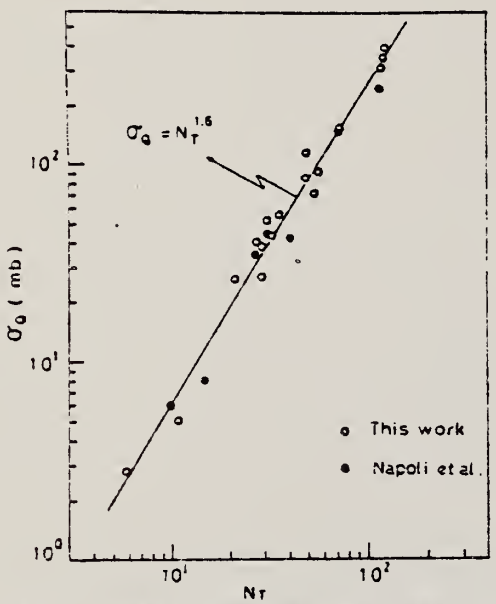

Fig. 2. Yield per equivalent quanta versus target neutron number.

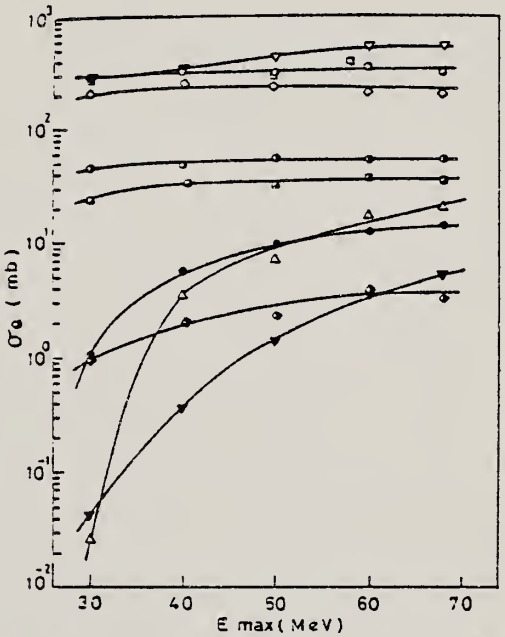

Fig. 8. Activation yield curves for the reactions on Pb, Tl and Hg.
□ $^{204}Hg(\gamma, n)^{203}Hg$, ◇ $^{198}Hg(\gamma, n)^{197g}Hg$,
◪ $^{198}Hg(\gamma, n)^{197m}Hg$, ◈ $^{199}Hg(\gamma, p)^{198}Au$,
▽ $^{204}Pb(\gamma, n)^{203}Pb$, ▼ $^{204}Pb(\gamma, 2n)^{202m}Pb$,
△ $^{204}Pb(\gamma, 3n)^{201}Pb$, ○ $^{203}Tl(\gamma, n)^{202}Tl$,
◑ $^{203}Tl(\gamma, 2n)^{201}Tl$, ● $^{203}Tl(\gamma, 3n)^{200}Tl$.

(over)

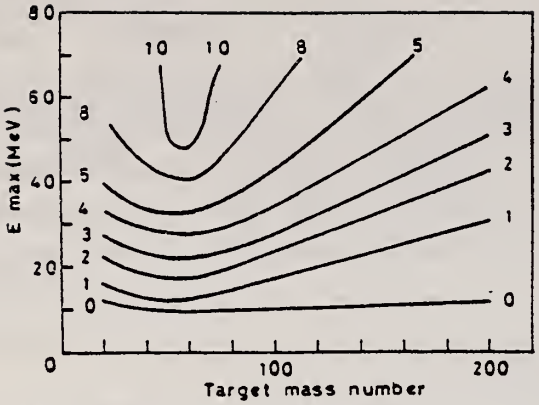

Fig. 10. Yields of the (γ, p) reactions as a function of bremsstrahlung maximum energy and target mass number. The numerical values in the figure are yields per equivalent quanta in mb.

Hg
A=201

Hg
A=201

K. N. Geller, J. Halpern, and E. G. Muirhead
Phys. Rev. 118, 1302-12 (1960)

Hg	201	80

METHOD

Betatron; neutron threshold; ion chamber

REF. NO. 60 Ge 3 NVB

REACTION	RESULT	EXCITATION ENERGY	SOURCE TYPE	SOURCE RANGE	DETECTOR TYPE	DETECTOR RANGE	ANGLE
G,N	NØX	THR	C THR		BF3-I		4 PI

THRESHØLD

TABLE I. Summary and comparison of neutron separation energies inferred from present threshold measurements with values predicted from mass data and reaction energies. All energies are expressed in the center-of-mass system in Mev.

Reaction	No. runs	Present results	Other results	Method	Reference
$Hg^{201}(\gamma,n)Hg^{200}$	1	6.21 ±0.07	6.234±0.011	mass data	r
			6.27 ±0.06	mass data	q

[q] W. H. Johnson, Jr., and V. B. Bhanot, Phys. Rev. 107, 6 (1957).
[r] J. L. Benson, R. A. Damerow, and R. R. Ries, Phys. Rev. 113, 1105 (1959).

Ref. J.H. Carver, D.C. Peaslee, R.B. Taylor
Phys. Rev. 127, 2198 (1962)

Elem. Sym.	A	
Hg	201	80

Method: 33 MeV electron synchrotron; activation; NaI

Ref. No.: 62 Ca 2 JHH

Reaction	E or ΔE	E_o	Γ	$\int \sigma dE$	Jπ	Notes
(γ,p)	Bremss. 16-32	25		$40\int_0^{32}$ MeV-mb		Absolute yields by comparison with $Ta^{181}(\gamma,n)$, $Cu^{63}(\gamma,n)Cu^{62}$ and results of Berman and Brown [Phys. Rev. 96, 83 (1954)].

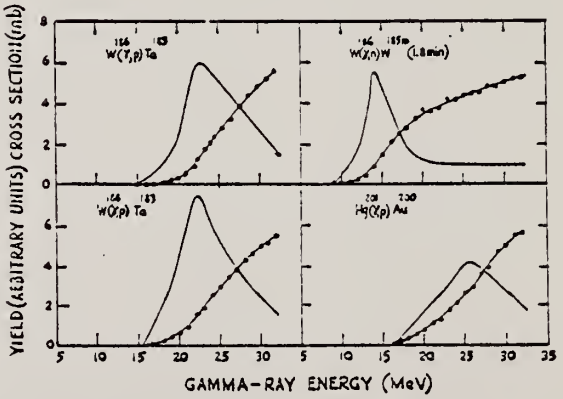

FIG. 7. Excitation functions and derived cross sections for the photodisintegration of tungsten and mercury.

D. E. Carlson and A. A. Temperley
Phys. Letters 30B, 322 (1969)

ELEM. SYM.	A	Z
Hg	201	80

METHOD

REF. NO.	
69 Ca 2	egf

REACTION	RESULT	EXCITATION ENERGY	SOURCE		DETECTOR		ANGLE
			TYPE	RANGE	TYPE	RANGE	
G,MU-T	ABX	0	D	0	SCI-D	0	

Spin parity assignment $1/2^-$

0=32.2 KEV,J-PI

HG
A=202

HG
A=202

Ref. F.R. Metzger
Phys. Rev. 98, 200 (1955)

Elem. Sym.	A	Z
Hg	202	80

Method: Radioactive source; photon scattering

Ref. No.: 55 Me 1 cs | NVB

Reaction	E or ΔE	E_o	Γ	$\int \sigma dE$	Jπ	Notes
$Hg^{202}(\gamma,\gamma)$	439 kev	439 kev			2	Lifetime of 439 keV transition: $\tau_\gamma = (3.4 \pm 0.7)\ 10^{-11}$ sec.

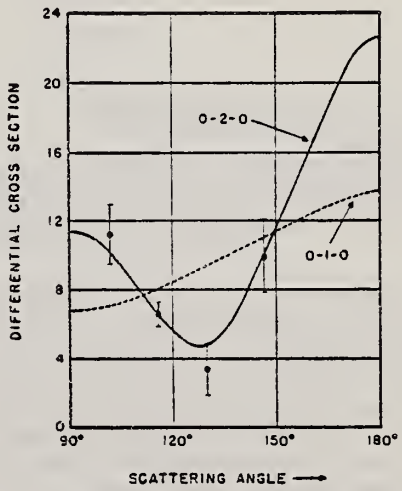

FIG. 1. Angular distribution of the resonance radiation from the 439-kev level of Hg^{202}. The solid line represents the theoretical angular distribution for an excited state with spin 2 and a ground state with spin 0. The dashed line represents the theoretical distribution for an excited state with spin 1. The differential cross section in arbitrary units is plotted as the ordinate.

REF.

K. N. Geller, J. Halpern, and E. G. Muirhead
Phys. Rev. 118, 1302-12 (1960)

ELEM. SYM.	A	Z
Hg	202	80

METHOD

Betatron; neutron threshold; ion chamber

REF. NO. 60 Ge 3 NVB

REACTION	RESULT	EXCITATION ENERGY	SOURCE		DETECTOR		ANGLE
			TYPE	RANGE	TYPE	RANGE	
G,N	NØX	THR	C THR		BF3-I		4 PI

THRESHØLD

TABLE I. Summary and comparison of neutron separation energies inferred from present threshold measurements with values predicted from mass data and reaction energies. All energies are expressed in the center-of-mass system in Mev.

Reaction	No. runs	Present results	Other results	Method	Reference
$Hg^{202}(\gamma,n)Hg^{201}$	1	7.60 ±0.13	7.760±0.011	mass data	r
			7.77 ±0.06	mass data	q

[q] W. H. Johnson, Jr., and V. B. Bhanot, Phys. Rev. 107, 6 (1957).
[r] J. L. Benson, R. A. Damerow, and R. R. Ries, Phys. Rev. 113, 1105 (1959)

Ref. P.Euthymiou, P.Axel

Phys.Rev. 128, 274 (1962)

Elem. Sym.	A	Z
Hg	202	80

Method

25 MeV Betatron - NaI

Ref. No. 62Eu1 BG

Reaction	E or ΔE	E_o	Γ	$\int \sigma dE$	Jπ	Notes
(γ,n)	9.35 - 23.20			33±10% $)_{9.35}^{23.9}$		* 100±6μsec isomer from natural Hg target. Produced mainly by (γ,n) process. Assumed parent is 30% isotope Hg^{202}. (γ.n) apparent threshold 11.3±0.3MeV

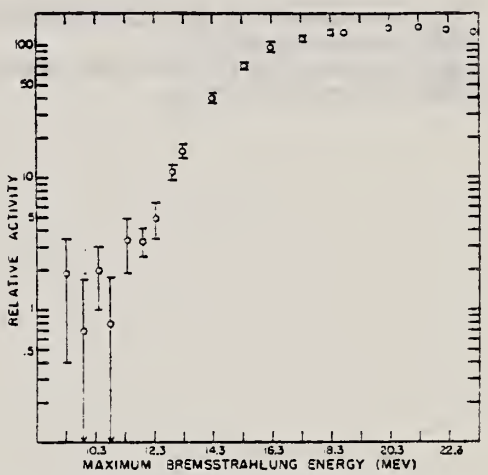

FIG. 1. Activation curve of 100-μsec Hg isomer. The ordinate gives the relative amount of 100-μsec isomer per unit ionization produced in the ionization chamber monitor. If the isomer is in Hg^{201}, the ordinate is approximately 4.1 times the energy-integrated cross section in MeV-mb.

19 different values of the peak energy of the bremsstrahlung spectrum. At each energy, a complete pulse height distribution was obtained for the gamma rays which reached the detector between 40 and 180 μsec after each yield pulse. In addition, the long-lived background was measured after each run, and an estimate was made of contributions due to slow neutrons. The activity assigned to the 100-μsec isomer was obtained by summing the counts above background in the region of the 533-keV photopeak. The energy dependence of the relative activity produced per unit monitor reading is shown in Table I and plotted in Fig. 1. The data

REF.

J. Tenenbaum, R. Moreh, and A. Nof
Nucl. Phys. A218, 95 (1974)

EL EM. SYM.	A	Z
Hg	202	80

METHOD

REF. NO. 74 Te 1 egf

REACTION	RESULT	EXCITATION ENERGY	SOURCE TYPE	SOURCE RANGE	DETECTOR TYPE	DETECTOR RANGE	ANGLE
G,G	LFT	4	D	4- 8	SCD-D		DST

4=4.922

TABLE 4

Values of Γ, Γ_0 and the energy separation δ (between the incident γ-line and the resonance level) as obtained from the analysis of the various experiments

Scatterer	E_γ (keV)	Γ (meV)	Γ_0 (meV)	δ (eV)	D (eV)	K_{E1} (10^{-9} MeV^{-3})	K_{M1} (10^{-9} MeV^{-3})
^{55}Mn	7491	450±250	80± 40	17 ±1			
^{140}Ce [a])	5660	13± 3	12± 2	4.7±0.3	6800	0.33	
^{141}Pr [a])	6877	85± 35	17± 9	6.7±1.5	450		116
^{142}Nd [a])	6877	340± 40	270± 20	12.4±0.3	1200	26	
^{202}Hg	4922	300± 50	260± 20	4.2±0.5	19000	3.4	
^{209}Bi [a])	5603	950±200	950±200	13 ±1	34000		160

The radiative strengths K_{E1} and K_{M1} are also given. The level spacing D refers to the excitation energy of the resonance level E_γ.

[a]) These values are slightly different from those of ref. [8]) and were obtained from a renewed analysis of the experimental results.

TABLE 2

Measured angular distribution coefficients A_2, the ratios $N_{||}/N_\perp$, the spins and parities of the ground and the resonance levels, J_0^π and J_r^π, and the character of the ground state transition

Scatterer	E_γ (keV)	A_2	$N_{||}/N_\perp$	J_0^π	J_r^π	Transition
^{55}Mn	7491	0.01±0.02	1.00±0.02	$\frac{1}{2}^-$	$\frac{3}{2}$	
^{140}Ce	5660	0.51±0.02	1.14±0.04	0^+	1^-	E1
^{141}Pr	6877	0.11±0.02	0.95±0.03	$\frac{5}{2}^+$	$\frac{7}{2}^+$	M1
^{142}Nd	6877	0.51±0.03	1.10±0.04	0^+	1^-	E1
^{202}Hg	4922	0.51±0.02	1.18±0.03	0^+	1^-	E1
^{209}Bi	5603	0.06±0.02	0.97±0.02	$\frac{9}{2}^-$	$\frac{11}{2}^-$	M1

[8] A. Wolf, R. Moreh, A. Nof, O. Shahal, J. Tenenbaum, Phys. Rev. C6, 2276 (1972).

HG
A=204

HG
A=204

REF. K. Masumoto, T. Kato, N. Suzuki
Nucl. Inst. Meth. 157, 567 (1978)

ELEM. SYM.	A	Z
Hg	204	80

METHOD

REF. NO. 78 Ma 10 hg

REACTION	RESULT	EXCITATION ENERGY	SOURCE		DETECTOR		ANGLE
			TYPE	RANGE	TYPE	RANGE	
G,N	ABY	8-68	C	30-68	ACT I		4PI

Analysis is made of reactions interfering with photon activation analysis procedures.

The activation yield curves have been presented for a number of photonuclear reactions in the energy range from 30 to 68 MeV, in order to evaluate quantitatively the interferences due to competing reactions in multielement photon activation analysis. The general features of the yields as functions of both target mass number and excitation energy were elucidated from the data obtained, discussion being given on the results in terms of the reaction mechanism.

Simultaneous neutron activation due to appreciable neutron production from the converter and surrounding materials has also been studied, and, finally, the magnitudes of interferences in real multielement analysis were given in the form of their energy dependences.

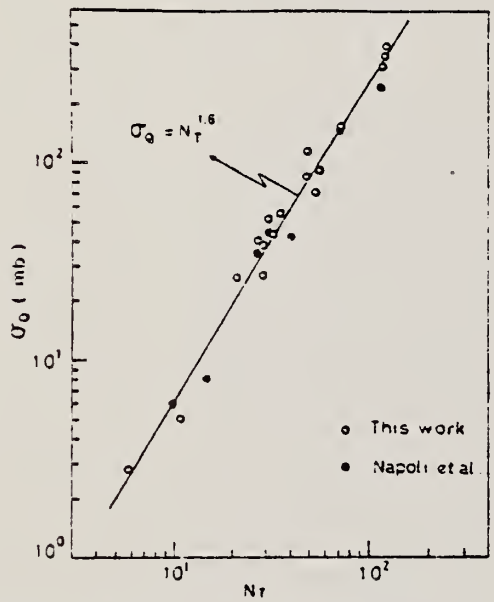

Fig. 2. Yield per equivalent quanta versus target neutron number.

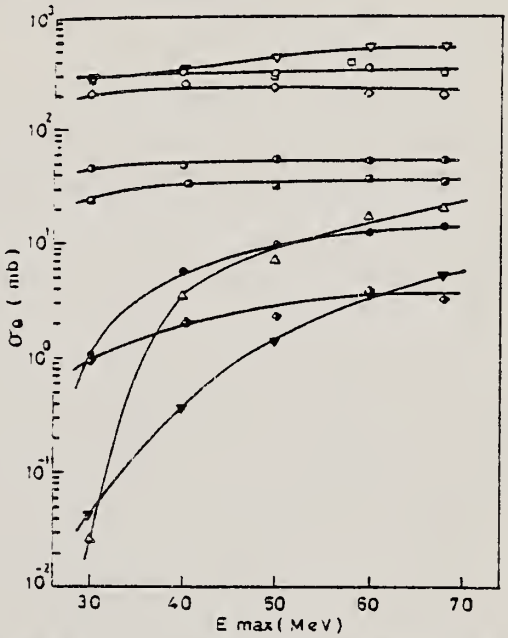

Fig. 8. Activation yield curves for the reactions on Pb, Tl and Hg.
□ $^{204}Hg(\gamma, n)^{203}Hg$, ◇ $^{198}Hg(\gamma, n)^{197g}Hg$,
◪ $^{198}Hg(\gamma, n)^{197m}Hg$, ◈ $^{199}Hg(\gamma, p)^{198}Au$,
▽ $^{204}Pb(\gamma, n)^{203}Pb$, ▼ $^{204}Pb(\gamma, 2n)^{202m}Pb$,
△ $^{204}Pb(\gamma, 3n)^{201}Pb$, ○ $^{203}Tl(\gamma, n)^{202}Tl$,
◑ $^{203}Tl(\gamma, 2n)^{201}Tl$, ● $^{203}Tl(\gamma, 3n)^{200}Tl$.

(over)

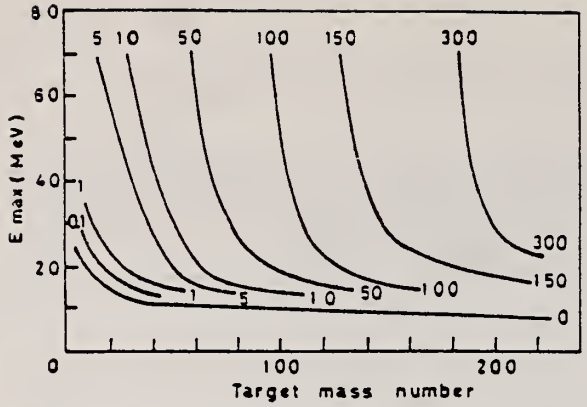

Fig. 9. Yields of the (γ, n) reactions as a function of bremsstrahlung maximum energy and target mass number. The numerical values in the figure are yields per equivalent quanta in mb.

Tl

THALLIUM
Z=81

Thallium is a bluish-white metal that is malleable, very soft and has a low tensile strength. It was discovered in 1861 by Sir William Crookes, using a spectroscope, while searching for tellurium in the residues from a sulfuric acid plant. He observed an unaccountable green line in the spectroscope and concluded it was from a new element. Because the bright green color reminded him of the tint of new vegetation in the spring, he called the element thallium from the Latin word *Thallus* —— a budding twig.

Tl

Tl

B.I. Gavrilov, L.E. Lazareva
Zhur. Eksp. i Teoret. Fiz. 30, 855 (1956);
Soviet Phys. JETP 3, 871 (1957)

Elem. Sym.	A	Z
Tl		81

Method: γ-Bremsstrahlung; synchrotron; BF_3 counter

Ref. No.: 56 Ga 1 EGF

Reaction	E or ΔE	E_0	Γ	$\int \sigma dE$	Jπ	Notes
(γ,xn)	~ 7-27	14.6	5.4	4.99 MeV-b		
(μ_t)	~ 7-27	14.0	4.6	3.77 MeV-b		

TABLE I. Fundamental characteristics of photoneutron cross sections.

Element	$E_{\sigma_n \max}$ in mev	$\sigma_{n\max}$ in barns	Half width in mev	$\int_{E_\gamma}^{E_0} \sigma_n(E)\,dE$ in mev-barns	$\int_{E_n}^{E_0} \sigma_n(E)\,dE / \sigma_{n\max}$
Copper	17.2	0.126	4.3	0.93	7.4
Zinc	16.3	0.132	6.3	0.66	8.1
Cadmium	15.0	0.270	6.4	2.28	8.4
Iodine	15.5	0.288	6.0	2.65	9.2
Tantalum	14.5	0.452	6.8	3.87	8.6
Gold	14.2	0.571	6.6	4.37	7.6
Thallium	14.6	0.655	5.4	4.99	7.6
Bismuth	13.9	0.537	5.9	3.96	7.4
Thorium	14.5	0.736	5.6	6.33	8.0
Uranium	13.9	1.18	6.8	12.5	10.6

TABLE II. Threshold of photoneutron reactions (mev).

Element	(γ, n)	$(\gamma, 2n)$	$(\gamma, 3n)$	(γ, xn)
Cadmium	8.7	14.6	23.0	>30
Iodine	9.4	16.2	26.0	32.0
Tantalum	7.6	13.9	21.6	28.2
Gold	8.1	14.9	23.0	>30
Thallium	7.5	14.6	22	29.8
Bismuth	7.4	14.2	22.6	29.6

TABLE III. Characteristics of the cross section of absorption of γ-quanta by nuclei.

Element	E_{res} in mev	$\sigma_\gamma(E=E_{res})$ in barns	Half width in mev	$\int_{E_\gamma}^{E_0} \sigma_\gamma dE$ in mev-barns	$\int_{E_n}^{E_0} \sigma_\gamma dE / 0.60 \times (2NA)$	$\int_{E_n}^{E_0} \sigma_\gamma(E)\,dE / E_n$	$\int_{E_n}^{E_0} \sigma_\gamma(E)\,dE / E_n$	$r_0 \times 10^3$ in cm
Cadmium	15.0	0.268	5.1	1.76	1.06	0.111	0.00715	1.26
Iodine	15.5	0.258	5.2	1.80	1.00	0.117	0.00758	1.16
Tantalum	13.9	0.428	5.1	2.74	1.65	0.190	0.0139	1.15
Gold	14.2	0.571	5.0	3.69	1.23	0.244	0.0182	1.23
Thallium	14.0	0.648	5.7	3.77	1.28	0.266	0.0200	1.25
Bismuth	13.8	0.537	4.5	3.12	1.04	0.220	0.0178	1.96

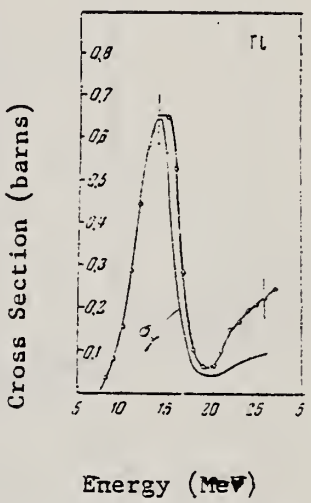

Figure 2: Photoneutron cross section σ_n, computed from the yield curves by the "photon difference method." Curve is presented for the cross section of γ-quanta, computed from the statistical theory of neuclei.

Ref.

K.Reibel, A.K. Mann
Phys. Rev. 118, 701 (1960)

Elem. Sym.	A	Z
Tl		81

Method

γ's from $F^{19}(p,a\gamma)$ reaction; protons from VandeGraaff; NaI.

Ref. No. 60 Re 1 JHH

Reaction	E or ΔE	E_o	Γ	$\int \sigma dE$	Jπ	Notes
(γ,γ)	E_p=2.05					$\langle\bar{\sigma}\rangle$ = 3.9 ± 0.6 mb
	E_p=2.40					$\langle\bar{\sigma}\rangle$ = 2.1 ± 0.3 mb
	E_γ= 6.9					$\langle\bar{\sigma}\rangle$ = 1.6 ± 0.4 mb
	E_γ= 7.1					$\langle\bar{\sigma}\rangle$ = 4.4 ± 1.0 mb

REF.

J. Moffatt and D. Reitmann
Nuclear Phys. 65, 130 (1965)

ELEM. SYM.	A	Z
Tl		81

METHOD

[Page 1of 2]

REF. NO.	
65 Mo 2	EGF

REACTION	RESULT	EXCITATION ENERGY	SOURCE		DETECTOR		ANGLE
			TYPE	RANGE	TYPE	RANGE	
G,XN	ABX	10 - 110	C	16 - 110	ACT-I		4PI

Measured yields of $Tl^{202,201,200}$ by activation technique.

Targets natural thallium (Tl^{203} 29.5%, Tl^{205} 70.5%) NBS chamber.

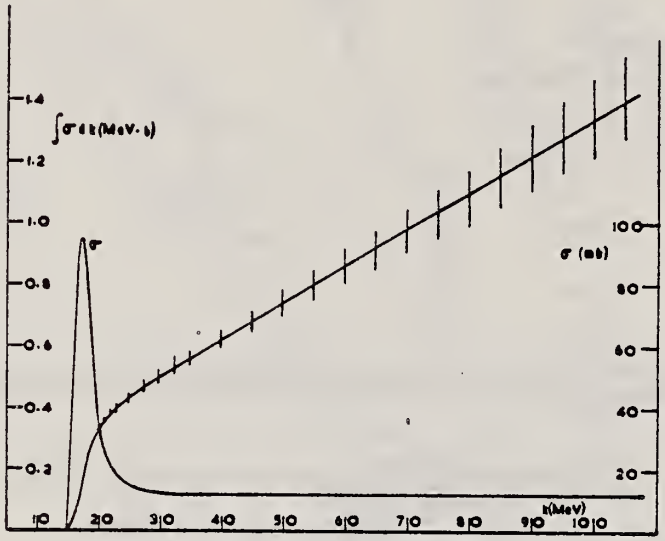

Fig. 2. Cross-section for production of Tl^{202}.

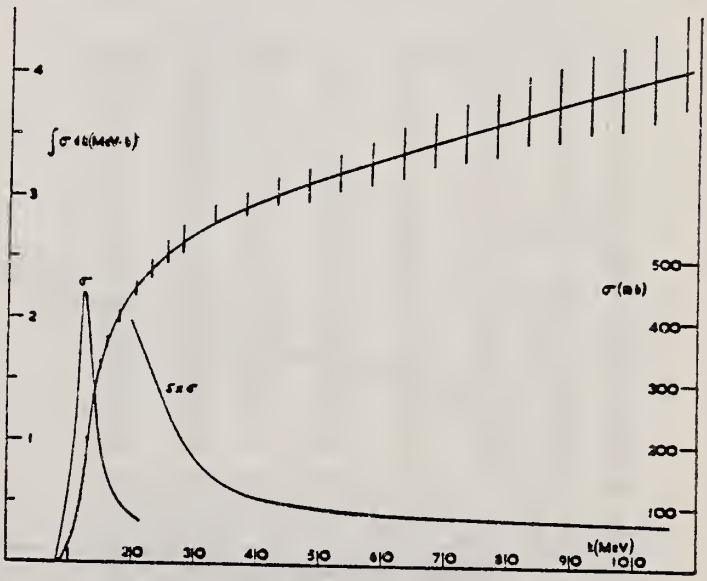

Fig. 3. Cross-section for production of Tl^{201}.

REACTION	RESULT	EXCITATION ENERGY	SOURCE TYPE	SOURCE RANGE	DETECTOR TYPE	DETECTOR RANGE	ANGLE

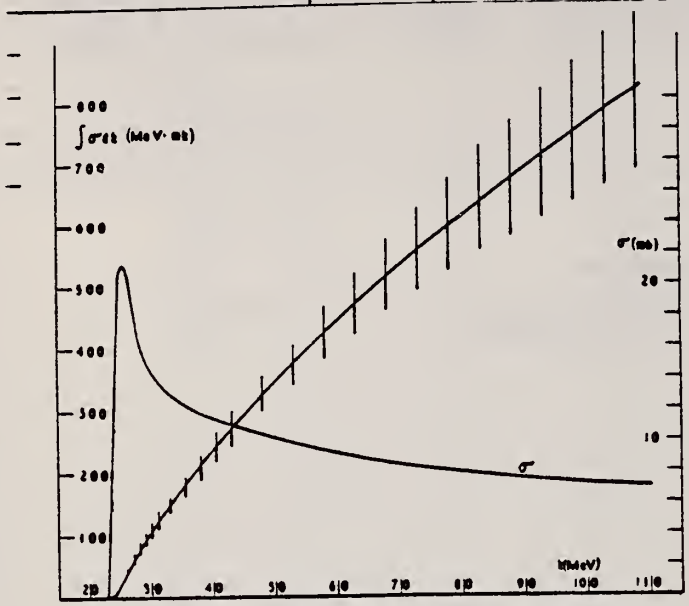

Fig. 4. Cross-section for production of Tl^{200}.

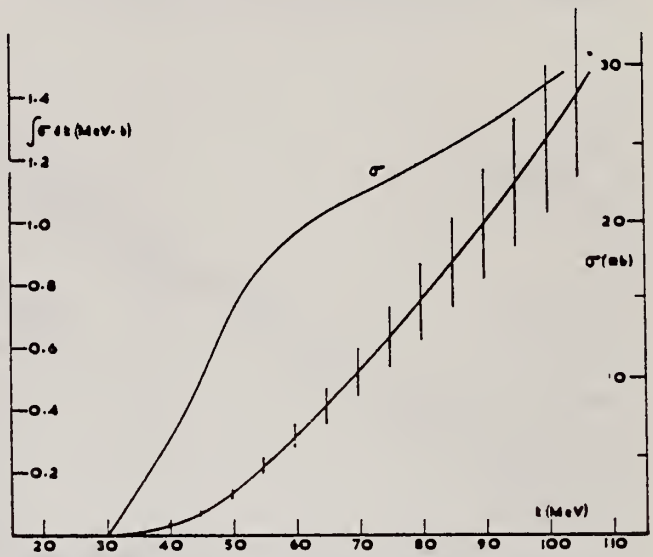

Fig. 5. Cross-section for production of $Tl^{<200}$.

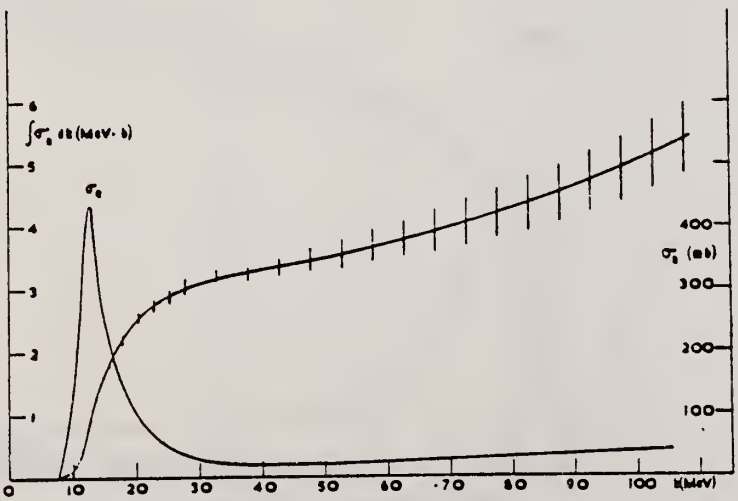

Fig. 6. Total cross-section for all neutron-producing reactions in Tl^{202}.

REF. G. Ben-David, B. Arad, J. Balderman, and Y. Schlesinger
Phys. Rev. 146, B852 (1966)

ELEM. SYM.	A	Z
Tl		81

METHOD

Nuclear Resonance Scattering using N,G reactions.

REF. NO. 66 Be 3 JDM

REACTION	RESULT	EXCITATION ENERGY	SOURCE TYPE	SOURCE RANGE	DETECTOR TYPE	DETECTOR RANGE	ANGLE
G,G	RLX	5 - 10	D	5 - 10	NAI-D	5 - 10	135

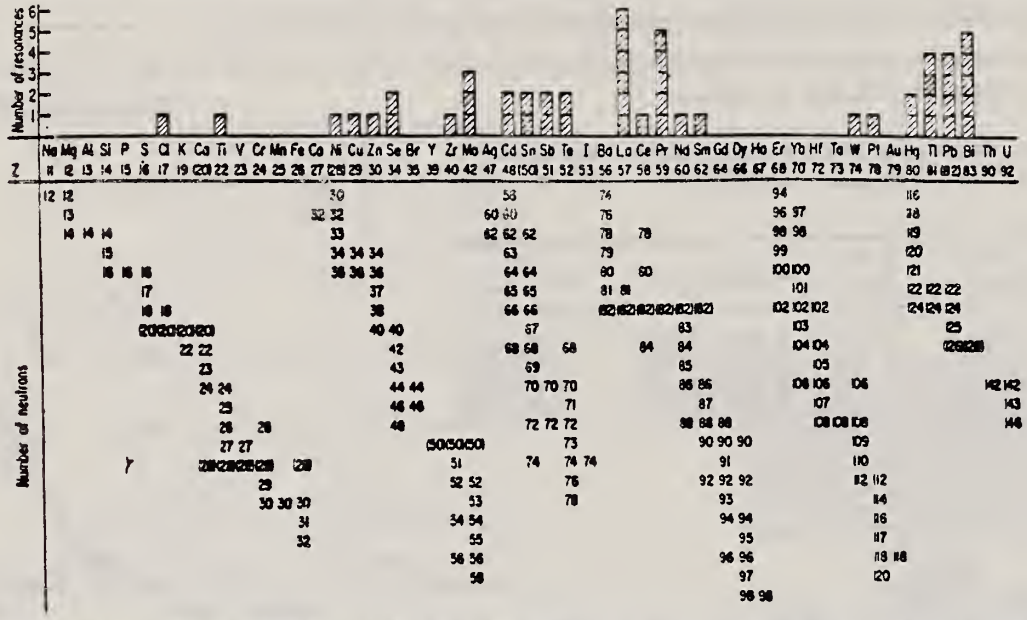

FIG. 3. Histogram of distribution of observed resonances among the different targets. The atomic number is given directly beneath the chemical symbol followed by the neutron numbers of the naturally occurring isotopes. Magic numbers are shown in brackets.

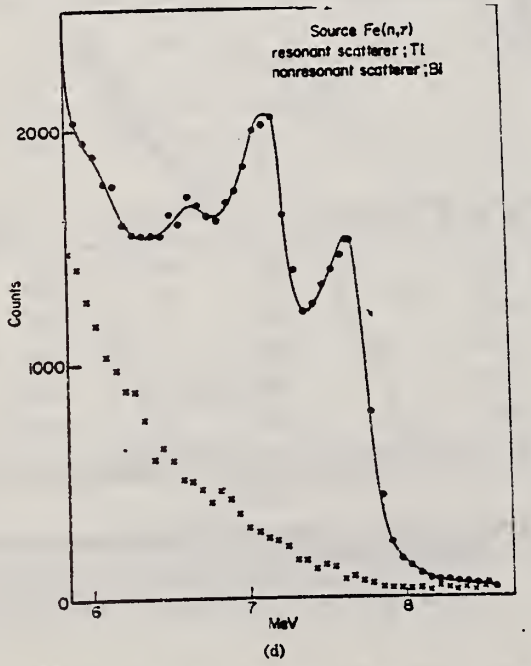

Fig.1.(d) Simple scattered spectrum from Tl excited by Fe capture gamma rays (with Bi background).

TABLE III. List of effective cross sections.

Scatterer	Energy (MeV)	Gamma source	δ (mb)	Scatterer	Energy (MeV)	Gamma source	δ (mb)
Sm^{144}	8.997	Ni	100	Sn	7.01	Cu	110
Pr^{141}	8.881	Cr	9	Nd	6.867	Co	30
La	8.532	Ni	6	Pr^{141}	6.867	Co	3
Te	8.532	Ni	3[a]	Te	6.7	Ni	...
Cu	8.499	Cr	24	La	6.54	Ag	12
Zr	8.496	Se	3050	Cd	6.474	Co	110
Zn	8.119	Ni	13	Mo	6.44	Hg	25[e]
Se	7.817	Ni	50	La	6.413	Ti	72
Se	7.76	K	90	Mo	6.413	Ti	10
Sb	7.67	V	...[b]	Tl	6.413	Ti	25
Cd	7.64	Fe	40[c]	W	~6.3	Ti	...[b]
Ni	7.64	Fe	7[c]	Sb	6.31	Hg	6[e]
Pr^{141}	7.64	Fe	12[c]	Ti	6.31	Hg	2[e]
Tl	7.64	Fe	370[c]	Sn	6.27	Ag	75
La	7.634	Cu	7	Pb^{206}	6.15	Gd	...[g]
Mo	7.634	Cu	11	Te	5.8	Ni	...[f]
Bi^{209}	7.634	Cu	4	La	6.12	Cl	35
Te	7.528	Ni	66[d]	Pr^{141}	6.12	Cl	110
Bi^{209}	7.416	Se	100	Pt	5.99	Hg	40[e,g]
Bi^{209}	7.300	As	80[c]	Tl	5.99	Hg	5[e]
Pb^{206}	7.285	Fe	4100	Pb^{206}	5.9	Sr	...[h]
Cl	7.285	Fe	34	Ce	5.646	Co	17
Pr^{141}	7.185	Se	80	Bi^{209}	5.646	Co	55
Tl	7.16	Cu	120	Pb^{206}	5.53	Ag	70
La	7.15	Mn	50	Hg	5.44	Hg	75[e]
Bi^{209}	7.149	Ti	2000	Hg	4.903	Co	385

[a] High-energy component of a complex spectrum.
[b] A broad scattered spectrum with no observable peak structure.
[c] There are actually two lines of energies 7.647 and 7.633 MeV having equal intensities in the iron capture gamma spectrum. The cross section has therefore been corrected, although there is no possibility at present of deciding which line is responsible for each resonance.
[d] Is probably an independent level in the complex spectrum of Ni γ rays on Te.
[e] Rough estimate.
[f] May be inelastic component from 7.528 level in Te.
[g] The relative line intensities in this case are due to Groshev and co-workers.
[h] No line is known for the source at this energy.
[i] Difficult to resolve among the many source lines present at this energy.

REF. A. V. Mitrofanova, Yu. N. Ranyuk, and P. V. Sorokin
J. Nucl. Phys. (USSR) 6, 703 (1967)
Sov. J. Nucl. Phys. 6, 512 (1968)

ELEM. SYM.	A	Z
Tl		81

METHOD

REF. NO.	
67 Mi 1	HMG

REACTION	RESULT	EXCITATION ENERGY	SOURCE		DETECTOR		ANGLE
			TYPE	RANGE	TYPE	RANGE	
G,F	ABX	300-999		300-999	TRK-I		

Detector: Fission fragment tracks in glass.

999 = 1600 MEV

Angular distribution measured for Pb was found isotropic; for other elements it was assumed isotropic.

Nucleus	Fissionability D	Cross section σ_{-}, $\mu\beta$	Nucleus	Fissionability D	Cross section σ_{K}, $\mu\beta$
Bi	0.11±0.01	7.8±0.6	Os	0.0058±0.0005	0.37±0.04
Pb	0.050±0.004	3.4±0.3	Re	0.0056±0.0006	0.35±0.04
Tl	0.031±0.003	2.1±0.2	Ta	0.0045±0.0005	0.27±0.03
Au	0.019±0.002	1.25±0.10	Hf	0.0042±0.0004	0.25±0.03
Pt	0.012±0.002	0.80±0.08			

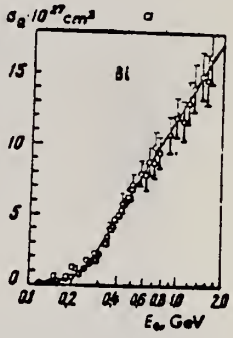

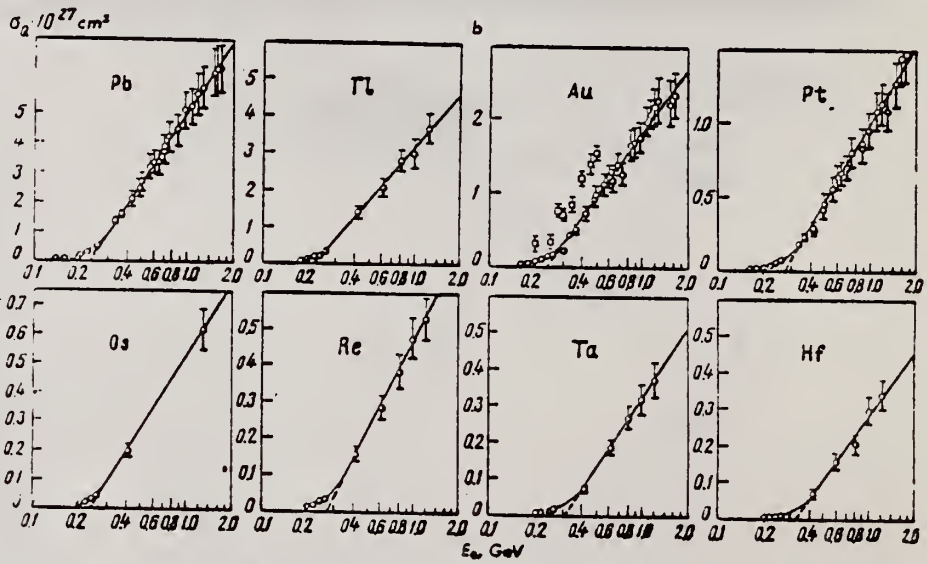

Fig. 1. Photofission fragment yields. ○-present work; □-Jungerman and Steiner.[1] The curves were plotted through the experimental points.

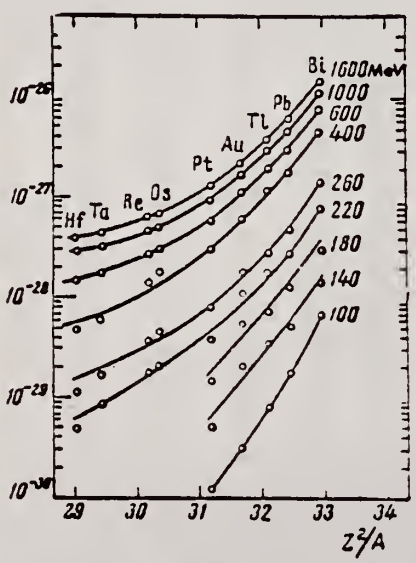

Fig. 2. Photofission fragment yields as a function of Z^2/A. The ordinates are values of σ_Q in units of cm².

REF. N. N. Kaushal, E. J. Winhold, P. F. Yergin, H. A. Medicus and R. H. Augustson
Phys. Rev. 175, 1330 (1968)

ELEM. SYM.	A	Z
Tl		81

METHOD

REF. NO. 68 Ka 1 HMG

REACTION	RESULT	EXCITATION ENERGY	SOURCE TYPE	SOURCE RANGE	DETECTOR TYPE	DETECTOR RANGE	ANGLE
G,N	ABX	50-85	C	55,85	TOF-D	10-85	67
							(67.5)

NEUT ENGY SPEC

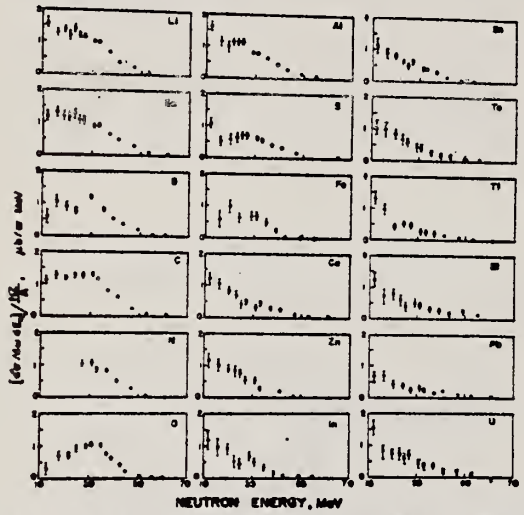

FIG. 6. Observed neutron spectra due to 55–85-MeV difference photon spectra. The effective cross sections have been divided by NZ/A.

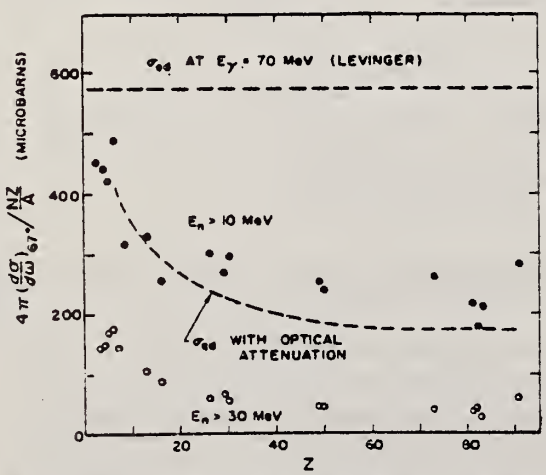

FIG. 7. Effective cross sections for production of fast neutrons with energies greater than 10 MeV (solid circles) and 30 MeV (open circles) by the 55–85-MeV photon difference spectrum. The dashed curves are modified quasideuteron model predictions as discussed in the text.

TABLE I. Comparison of present cross-section values in mb for production of high-energy photoneutrons by 55–85-MeV photons with measured cross sections $\sigma(\gamma,Tn)$, also in mb, for total photoneutron production. The present cross-section values are uncertain by 8 to 10% because of counting statistics and normalization errors; in addition all values depend on an absolute normalization in terms of the deuteron photodisintegration cross section, which is known to about 10% at these energies.

Target	$4\pi(d\sigma/d\omega)_{90°}$ (E_n>10 MeV) [Present experiment]	$\sigma(\gamma,Tn)$ Jones and Terwilliger[a]	Costa *et al.*[b]	Other results
Li	0.75		1.0	
Be	1.0	2.7	2.3	2.3[c]
B	1.0		1.4	
C	1.5	1.3	1.4	2.4[d]
O	1.3		1.6	
Al	2.8	5.5	4.6	8[d]
S	2.1		4.4	6.5[d]
Fe	4.2	16	12	
Cu	4.3	20	19	
Zn	4.4		15	
In	7.4			
Sn	7.0			
Ta	10.7	95		
Tl	10.7			
Pb	8.3	100		
Bi	13			
U	16	65		

[a] Average cross sections between 55 and 85 MeV, as read from Figs. 4 and 5 of Ref. 4.
[b] $\int_{\epsilon_0}^{E_{max}}\sigma dE - \int_{\epsilon_0}^{E_{max}}\sigma dE/50$, as taken from Fig. 4 of Ref. 5 and Table I of Ref. 6.
[c] S. Costa, L. Pasqualini, G. Piragino, and L. Roasio, Nuovo Cimento 42, 306 (1966).
[d] G. Bishop, S. Costa, S. Ferroni, R. Malvano, and G. Ricco, Nuovo Cimento 42, 148 (1966).

REF.

V. Emma, S. Lo Nigro and C. Milone
Lettere al Nuovo Cimento 2, 271 (1971)

ELEM. SYM.	A	Z
Tl		81

METHOD

REF. NO.	
71 Em 2	egf

REACTION	RESULT	EXCITATION ENERGY	SOURCE		DETECTOR		ANGLE
			TYPE	RANGE	TYPE	RANGE	
G,F	ABY	THR-999	C	300-999	FRAG-I		4PI

999 = 1000 MEV

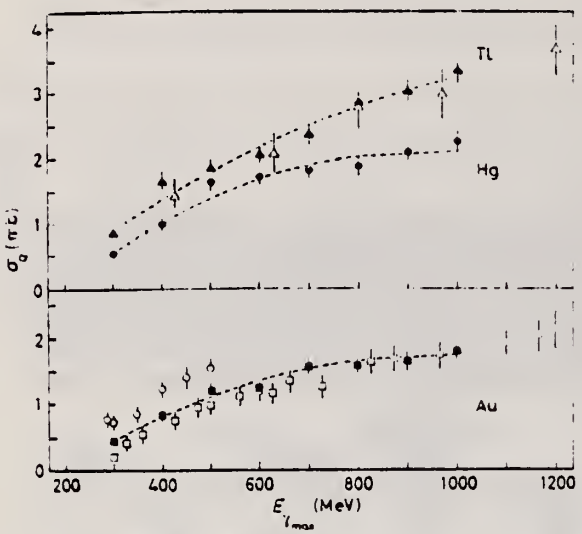

Fig. 1. – Photofissinn cross-sections per equivalent quantum σ_q against the maximum energy nf photons. Au: ○ ref. (*), □ ref. (*), ■ our results; Hg: • our results; Tl: ▲ ref. (*), ▲ our results. The dashed curves represent tho fits calculated by tho least-squares method taking into account our results only.

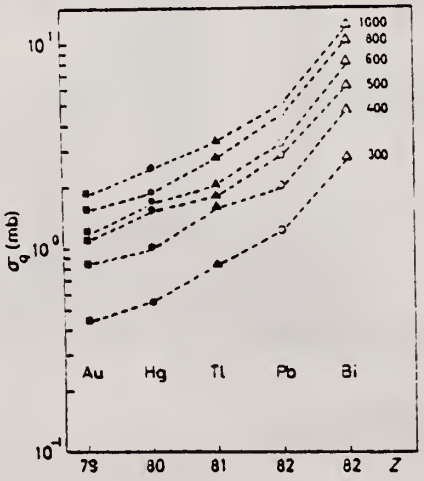

Fig. 2. – σ_q-values, deduced in nur present and previous (*) experiments, reported *vs.* the atomic number Z of the elements for only some energy values.

(over)

TABLE I. – *Fission cross-sections per photon between 300 and 1000 MeV.*

	σ_f(mb)		
	Our results	Previous results	
Bi	7.6 ± 0.2	7.8 ± 0.6 [5]	7.8 ± 0.8 [5]
Pb	3.3 ± 0.1	3.4 ± 0.3 [5]	
Tl	1.9 ± 0.1	2.1 ± 0.2 [5]	
Hg	1.5 ± 0.1		
Au	1.19 ± 0.06	1.25 ± 0.1 [6]	

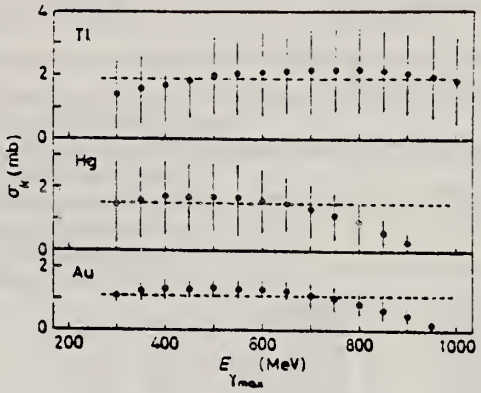

Fig. 3. – Fission cross-section per photon σ_f of Tl, Hg and Au against $E_{\gamma_{max}}$. The dashed straight lines represent the values $\sigma_f = \text{const}$, calculated as suggested in ref. (6).

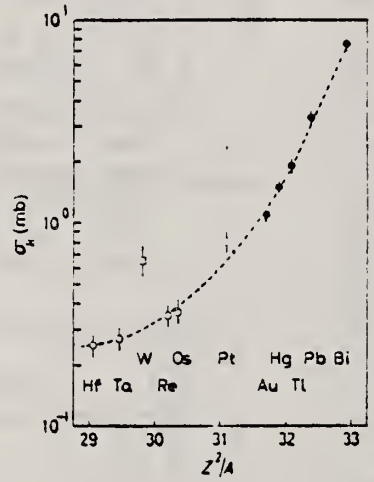

Fig. 4. – σ_f-values *vs.* Z^2/A for the elements with atomic number in the range from 72 to 83: • our results, ▫ ref. (5), ○ ref. (6). The dashed curves is drawn by eye.

(5) V. EMMA, S. LO NIGRO and C. MILONE: *Boll. S.I.F.*, No. 70, 119 (1970).
(6) V. EMMA, S. LO NIGRO and C. MILONE: *Lett. Nuovo Cimento*, 3, 512 (1970).
(7) V. EMMA, S. LO NIGRO and C. MILONE: *Lett. Nuovo Cimento*, 2, 117 (1971).
(8) J. JUNGERMAN and H. M. STEINERT: *Phys. Rev.*, 106, 583 (1957).
(9) H. H. DE CARVALHO, G. CORTINI, E. DEL GIUDICE, G. PATRICOLA and R. RINZIVILLO: *Nuovo Cimento*, 32, 293 (1964).
(10) A. V. MITROFANOVA, YU. N. RANYUK and P. V. SOKOLOV: *Sov. Journ. Nucl. Phys.*, 6, 512 (1968).

REF.

V. Emma, S. Lo Nigro, C. Milone
Nucl. Phys. A257, 438 (1976)

ELEM. SYM.	A	Z
Tl		81

METHOD

REF. NO. 76 Em 2 egf

REACTION	RESULT	EXCITATION ENERGY	SOURCE TYPE	SOURCE RANGE	DETECTOR TYPE	DETECTOR RANGE	ANGLE
G,F	ABY	THR-999	C	999	TRK-I		4PI

999 = 1 GEV

TABLE 1

Measured values of σ_q at $E = 1000$ MeV and deduced values of σ_t assumed constant from E_0 to 1000 MeV

Element	Z^2/A	σ_q (mb)	E_0 (MeV)	σ_t (mb)
Bi	32.96	12.3±0.6	200	7.6±0.6
Pb	32.45	5.4±0.4	220	3.6±0.3
Tl	32.10	4.1±0.3	230	2.8±0.3
Au	31.68	2.0±0.15	240	1.4±0.2
Pt	31.18	1.1±0.08	255	(8 ±0.7)×10^{-1}
Re	30.21	(3.7±0.3)×10^{-1}	280	(2.9±0.3)×10^{-1}
W	29.78	(3.5±0.3)×10^{-1}	290	(2.8±0.3)×10^{-1}
Ta	29.45	(3.3±0.3)×10^{-1}	300	(2.7±0.3)×10^{-1}
Hf	29.04	(1.7±0.2)×10^{-1}	310	(1.4±0.2)×10^{-1}
Yb	28.31	(1.3±0.1)×10^{-1}	330	(1.2±0.1)×10^{-1}
Tm	28.18	(7.5±0.8)×10^{-2}	335	(6.8±0.8)×10^{-2}
Ho	27.21	(3.6±0.4)×10^{-2}	355	(3.5±0.4)×10^{-2}
Dy	26.80	(2.6±0.3)×10^{-2}	360	(2.5±0.3)×10^{-2}
Tb	26.58	(2.5±0.3)×10^{-2}	370	(2.5±0.3)×10^{-2}
Gd	26.04	(1.6±0.2)×10^{-2}	380	(1.7±0.2)×10^{-2}
Sm	25.56	(1.3±0.2)×10^{-2}	390	(1.4±0.2)×10^{-2}
Nd	24.96	(9.2±0.9)×10^{-3}	405	(1 ±0.1)×10^{-2}
Ce	24.00	(8 ±0.9)×10^{-3}	420	(9 ±1)×10^{-3}
La	23.39	(8.4±0.9)×10^{-3}	430	(1 ±0.1)×10^{-3}
Sb	21.36	(1.2±0.2)×10^{-2}	460	(1.5±0.3)×10^{-2}
Te	21.19	(8.8±1)×10^{-3}	465	(1.2±0.2)×10^{-2}
Sn	21.06	(1.3±0.2)×10^{-2}	465	(1.7±0.3)×10^{-2}
Cd	20.49	(1.7±0.3)×10^{-2}	470	(2.2±0.4)×10^{-2}
Ag	20.47	(2 ±0.3)×10^{-2}	470	(2.6±0.4)×10^{-2}
Zn	13.76	(2 ±0.4)×10^{-1}	515	(3 ±0.6)×10^{-1}
Cu	13.44	(2.4±0.5)×10^{-1}	515	(3.6±0.8)×10^{-1}
Ni	13.35	(2.4±0.5)×10^{-1}	510	(3.6±0.8)×10^{-1}
Fe	12.10	(3 ±0.6)×10^{-1}	510	(4.4±0.9)×10^{-1}

[4] A.V. Mitrofanova et al. Sov. J. Nucl. Phys. 6, 512 (1968).

[7] T. Methasiri et al., Nucl. Phys. A167, 97 (1971).

[12] J.R. Nix et al., Nucl. Phys. 81, 61 (1966).

[20] N.A. Perifilov et al., JETP (Sov. Phys.) 14, 623 (1962); Proc. Symp. on the physics & chemistry of fission, Salzburg 1965, vol. 2 (IAEA) Vienna, 1965, p.283.

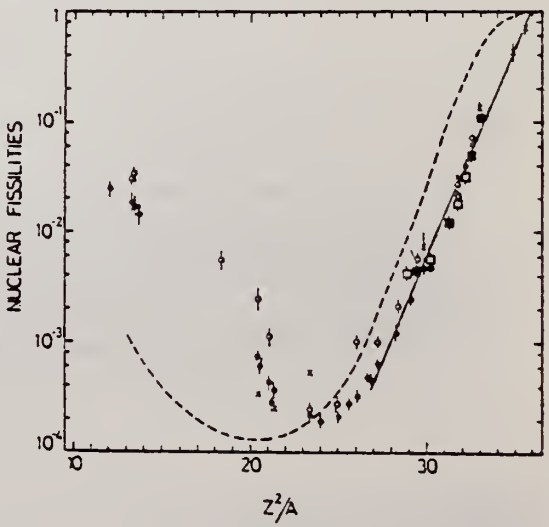

Fig. 2. Nuclear fissilities as a function of Z^2/A. Experimental points: solid circles represent our data; squares, the data from ref. [4]); open circles, the data from ref. [7]); and crosses, the data from (p,f) experiments[20]). The straight line is the best fit calculated from our data for $Z^2/A > 26$. The dashed curve is the curve VI calculated by Nix and Sassi[12]).

REF.

R.M. Laszewski and P. Axel
Phys. Rev. C 19, 342 (1979)

ELEM. SYM.	A	Z
Tl		81

METHOD

REF. NO.
79 La 1 hg

REACTION	RESULT	EXCITATION ENERGY	SOURCE		DETECTOR		ANGLE
			TYPE	RANGE	TYPE	RANGE	
G,G	ABX	4- 7	D	4-8	NAI-D		135
		(4.5-6.6)		4.5-7.5			

Average elastic photon scattering cross sections were measured for ^{209}Bi, ^{208}Pb, ^{207}Pb, ^{206}Pb, Tl and Hg at excitation energies between 4.5 MeV and the neutron emission threshold, with an energy resolution in the range between 50 and 150 keV. This resolution was sufficient to determine the strengths of most of the strong levels in this energy region for ^{208}Pb; there are concentrations of strength in a few levels near 5.5 and 7 MeV with the sum of $B(E1)\uparrow$ values equal to about 0.84 and 0.65 e^2 fm^2, respectively; each of these two groups of levels corresponds to only about 0.63% of the electric dipole sum rule. In the neighboring isotopes, approximately the same amount of strength is distributed among many more energy levels; although this strength is spread in energy more than it is in ^{208}Pb, it remains relatively localized.

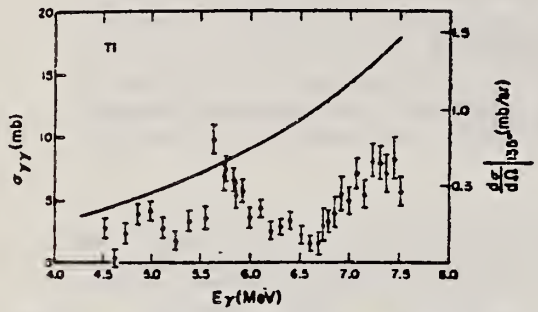

FIG. 7. Natural Tl (71% 205 isotope, 29% 203 isotope): See caption of Fig. 4.

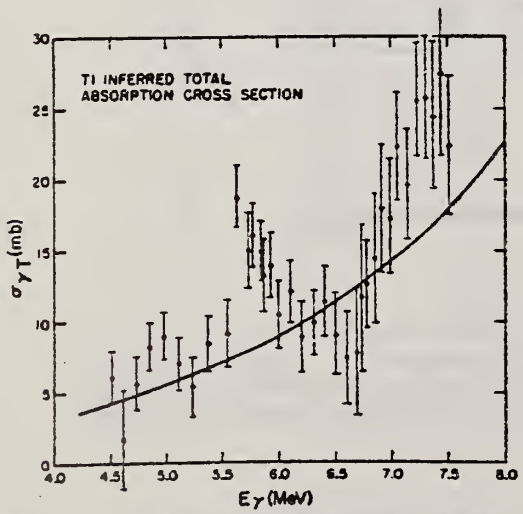

FIG. 9. Tl: inferred total photon absorption cross section.

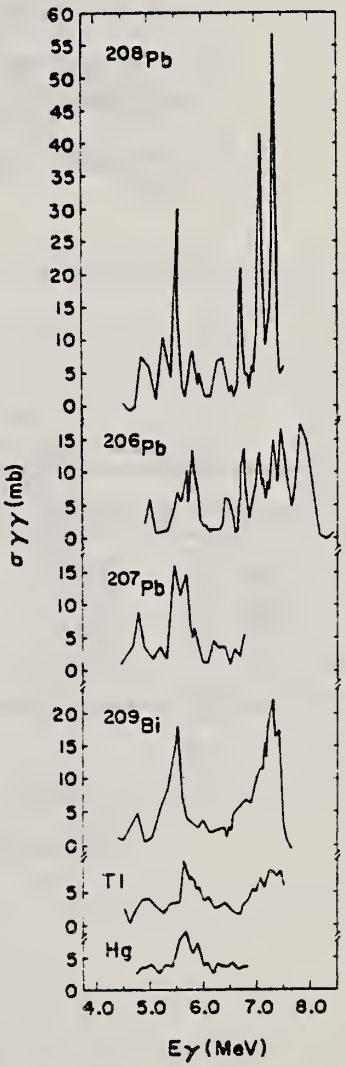

FIG. 12. Comparison of the measured cross sections of, respectively, from the top, ^{208}Pb, ^{206}Pb, ^{207}Pb, ^{209}Bi, Tl, and Hg.

over

TABLE IV. Parameters used in inferring $\sigma_{\gamma\Gamma}$ from $\bar{\sigma}_{\gamma\gamma}$. (Level spacing is assumed to be of the form $D \propto e^{-E/T}$.)

Nucleus	D_0 (eV)	E_0 (MeV)	T (MeV)	Γ_c (eV)	Ref.
Hg	83	8.03	0.86	0.12	15,22,23
Tl	430	6.54	0.90	0.12	15,22,23

[15] G.A. Bartholomew, E.D. Earle, A.J. Ferguson, J.W. Knowles, and M.A. Lone, in *Advances in Nuclear Physics*, edited by M. Baranger and E. Vogt (Plenum, New York, 1973), Vol. 7, p. 229.

[22] J.E. Lynn, *The Theory of Neutron Resonance Reactions* (Clarendon, Oxford, 1968)

[23] H. Molecky, Sov. J. Nucl. Phys. 13, 133 (1971).

TABLE VI. Transition strength comparison at 5.5 and 7 MeV.

Nucleus	5.0–6.0 MeV $\int\sigma_{\gamma\gamma}dE$ (MeV mb)	5.0–6.0 MeV % ^{208}Pb strength	6.5–7.5 MeV $\int\sigma_{\gamma\gamma}dE$ (MeV mb)	6.5–7.5 MeV % ^{208}Pb strength
Bi	10.4	68%	10.7	44%
^{208}Pb	15.2	100%	24.4	100%
^{207}Pb	12.6	83%	...	...
^{206}Pb	15.8	104%	20.2	83%
Tl	8.3	55%	7.8	32%
Hg	11.6	76%	...	...

REF. M. Schumacher, F. Smend, W. Mückenheim, P. Rullhusen, H.G. Börner
Z. Phys. A300, 193 (1981)

ELEM. SYM.	A	Z
Tl		81

METHOD

REF. NO. 81 Sc 6 egf

REACTION	RESULT	EXCITATION ENERGY	SOURCE		DETECTOR		ANGLE
			TYPE	RANGE	TYPE	RANGE	
G,G	ABX	2-7		2-7	SCD-D		90

2.60-6.76 MEV

Elastic scattering by nuclei in the range of mass numbers between 64 and 238 has been studied with monochromatic photons in the energy range between 2 and 8 MeV. These photons were provided either by a Ti(n,γ) source installed in the tangential through channel of the Grenoble high flux reactor, or by ^{24}Na and ^{56}Co sources produced by deuteron bombardment of Al or Fe at the Göttingen cyclotron. The photoexcitation of 23 nuclear levels has been observed and the decay properties and groundstate widths of the majority of these levels have been determined. For the lead scattering target the coherent elastic differential cross section has been studied in detail. There is evidence that below the photo-neutron threshold the elastic scattering via virtual photoexcitation of the nucleus can be approximated by extrapolating the real part of the Giant Dipole Resonance amplitude along a Lorentzian curve. Coulomb corrections to Delbrück scattering seem to play a small role at 6.5 MeV.

Table 1. Differential cross sections for elastic scattering $(d\sigma/d\Omega)^{exp}$ of photons from ^{56}Co and ^{24}Na sources by different scattering targets, in units of μb/sr. Errors in the last digits are given in parentheses.

Θ deg	Scattering targets	2.599[a] (MeV)	2.754[b] (MeV)	3.010[a] (MeV)	3.202[a] (MeV)	3.254[a] (MeV)	3.273[a] (MeV)	3.452[a] (MeV)
90	^{238}U	52.7(25)	57.5(25)[c]	56(16)	47(4)	456 (10)[c]	34(6)	49(14)
	^{209}Bi	33.1(30)	32 (2)	33(11)	32(4)	25.6(20)	29(6)	33(15)
	^{nat}Pb	31.5(23)	31.0(16)	35 (8)	27(3)	26.6(22)	25(4)	23 (8)
	^{nat}Tl	31.5(33)	-	27(12)	32(5)	24 (3)	22(7)	34(15)
	^{nat}Hg	30.0(27)	-	24(10)	28(5)	25.5(18)	26(8)	20 (8)
	^{nat}W	22.5(11)	-	17 (7)	19(3)	18.4(15)	18(5)	21 (6)
	^{181}Ta	20.0(15)	19.2 (6)	193(20)[c]	20(4)	17.3(21)	18(5)	21 (8)
	^{165}Ho	15.9(13)	-	17(10)	13(6)	15.6(20)	18(8)	-
	^{nat}Nd	11.4 (7)	14.2 (5)[d]	15 (7)	14(3)	24.2(12)[d]	13(3)	9 (6)
	^{nat}Ce	11.1 (9)	11.0 (5)	-	11(3)	9.5(13)	8(4)	-
	^{127}J	8.4(10)	8.6 (5)	-	9(2)	7 (1)	5(3)	-
	^{nat}Sb	8.0(11)	-	-	10(4)	6.8(19)	-	1,270(50)[c]
	^{nat}Sn	6.5 (7)	7.0 (5)	-	5(2)	7.6 (8)	6(3)	-
	^{nat}Cd	6.2 (5)	-	-	6(2)	6.6 (8)	7(3)	-
120	^{238}U	55.1(25)	64 (4)[c]	43(15)	55(5)	574 (10)[c]	48(5)	48(11)
	^{181}Ta	27.5(15)	25.0 (9)	227(20)[c]	22(5)	21 (2)	22(8)	-
	^{nat}Nd	17.9(30)	17.0 (9)[d]	-	-	29.8(47)[d]	-	-

[a] ^{56}Co source in Fe lattice [b] ^{24}Na source in Al lattice (part of data have been published elsewhere)
[c] Transitions to excited states observed in addition to the ground-state transition
[d] Photoexcitation of nuclear level identified from the size of the differential cross section

(OVER)

Table 2. Elastic differential cross sections $d\sigma/d\Omega(\Theta=90°)$ in μb/sr measured with the Ti(n,γ) source and compared with theoretical predictions. n: predicted number of levels in a $\Delta E=25$ eV interval at 6.5 MeV. Errors in the last digits are given in parentheses

Scattering target	6.418 MeV		6.555 MeV		6.759 MeV		7.168 MeV		n
	exp.	th.	exp.	th.	exp.	th.	exp.	th.	
^{238}U	23 (12)	10.3	-	-	-	-	-	-	45
^{209}Bi	-	-	219(39)[b,c]	8.0	12 (4)	7.4	1.5(3)·10^5[b,c]	5.7	0.1
^{nat}Pb	7.0(15)	8.6	-	-	6.5(11)	7.4	-	-	0.05
^{nat}Tl	2,586 (92)[a,c]	7.5	-	-	13 (3)[b]	6.0	-	-	0.4
^{nat}Hg	12 (3)	7.8	74(17)[b]	6.5	6.7(15)	6.4	-	-	3.4
^{nat}W	159 (10)[a,c]	6.6	306(33)[a,c]	6.3	20 (2)[a,c]	5.6	-	-	13
^{181}Ta	68 (4)[a,c]	6.3	-	-	10.1(12)[b,c]	5.3	-	-	28
^{165}Ho	15 (3)[b]	4.7	-	-	9.5(14)[b]	3.9	-	-	18
^{nat}Ce	4.1(21)	4.1	-	-	17 (1)[b,c]	3.6	-	-	0.04
^{nat}Sn	4.2(13)	3.0	-	-	2.5 (5)	2.7	-	-	1.9
^{nat}Mo	1,474 (44)[a,c]	2.5	407(39)[a,c]	2.5	8.5(15)[b,c]	2.3	817(258)[b,c]	2.0	0.5
^{nat}Zn	2.4 (8)	1.6	-	-	1.8 (5)	1.5	-	-	0.3

[a] Transitions to excited states observed
[b] Photoexcitation identified from size of differential cross section
[c] Photoexcitation reported in [11]

Table 4. Properties of levels observed by photoexcitation. $(d\sigma_0/d\Omega)^{Nat}$: experimental differential cross section per identified isotope or element for resonance scattering through $\Theta=90°$. I^π: spin-parity of excited level; $W(\Theta)$: angular correlation function; $g=(2I_{ex}+1)/(2I_g+1)$; Γ_0: radiative groundstate transition width, Γ: total level width. Errors in the last digits are given in parentheses

Isotope	E_r (MeV)	$(d\sigma_0/d\Omega)^{Nat}$ (μb/sr)	I^π	Γ_0/Γ[c]	$W(\Theta)g\Gamma_0^2/\Gamma$ (meV)	Γ_0^1 (meV)	Γ_0[e] (meV)
^{238}U	2.754	13 (4)	(1)	0.77	0.145	0.084	-
^{238}U	3.254	421 (5)	1$^-$	0.24	0.83	1.5	0.52(15)[d]
^{209}Bi	6.555	2.1 (4)·10^2	-	-	0.74	0.74[b]	-
^{209}Bi	7.168	1.7 (3)·10^3	9/2^{+}[a]	1.00	710	786	820 (40)[a]
^{203}Tl	6.418	8.75(30)·10^3	1/2[a]	0.28	30	102	82 (15)[a]
Tl	6.759	7 (3)	-	-	-	-	-
Hg	6.555	68 (17)	-	-	-	-	-
^{186}W	6.418	5.2 (3)·10^2	1$^-$[a]	0.32	1.75	2.4	-
^{184}W	6.555	9.8 (10)·10^2	(1)	0.52	3.44	2.9	-
^{184}W	6.759	46 (10)	(1)	0.58	0.17	0.13	-
^{181}Ta	3.010	174 (17)	-	0.72	0.42	0.59	-
^{181}Ta	6.418	62 (4)	-	0.73	0.2	0.27[c]	-
^{181}Ta	6.759	4.8 (12)	-	-	0.018	0.018[b]	-
^{165}Ho	6.418	10.3 (30)	-	-	0.035	0.035[b]	-
^{165}Ho	6.759	5.6 (14)	-	-	0.021	0.021[b]	-
Nd	2.754	2.6 (5)	-	-	-	-	-
Nd	3.254	14.0 (10)	-	-	-	-	-
Ce	6.759	13.4 (10)	-	-	-	-	-
^{121}Sb	3.452	2.20 (5)·10^3	-	0.60	2.9	4.9[b]	-
^{100}Mo	6.418	1.53 (4)·10^4	1$^-$[a]	0.88	52	26	25 (8)[a]
^{94}Mo	6.555	4.4 (4)·10^3	(1)	0.33	15	21	-
Mo	6.759	6.2 (15)	-	-	-	-	-
Mo	7.168	8.2 (26)·10^2	-	?	-	-	-

[a] [11]
[b] $W(\Theta)g\Gamma_0/\Gamma=1$ assumed
[c] $W(\Theta)g=1$ assumed
[d] [28] (a small correction has been applied to the data of [28])
[e] Upper limits in case not all the transitions to lower levels were observed
[f] Present work
[g] Previous work

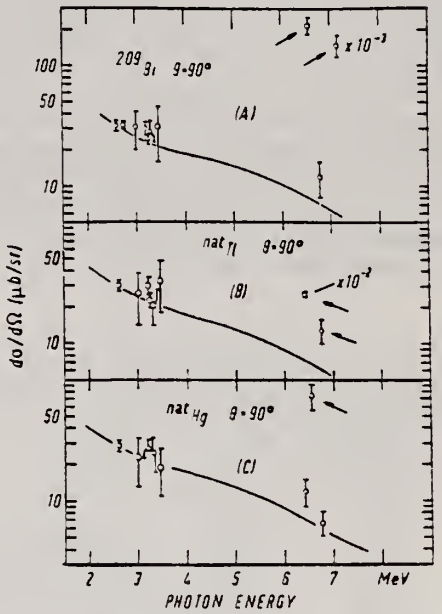

Fig. 9. Differential cross sections for elastic scattering of photons by (A) ^{209}Bi, (B) ^{nat}Tl and (C) ^{nat}Hg through $\Theta=90°$. Solid lines: calculated including R, T, lowest-order D, and N (Lorentzian shape) scattering

Tl
A=203

Tl
A=203

REF.

F. Heinrich, H. Wäffler, and M. Walter
Helv. Phys. Acta 29, 3 (1956)

ELEM. SYM.	A	Z
Tl	203	81

METHOD

REF. NO.	
56 He 2	EGF

REACTION	RESULT	EXCITATION ENERGY	SOURCE		DETECTOR		ANGLE
			TYPE	RANGE	TYPE	RANGE	
G,A	RLY	THR - 31	C	31	ACT-I		4PI

REL NEUTRONS

Yield measured relative to (γ,n) yield in ^{63}Cu.

31 MeV bremsstrahlung yields

$$\frac{^{203}Tl(\gamma,a)}{^{203}Tl(\gamma,n)} = 2.3 \times 10^{-5}$$

$$\frac{^{203}Tl(\gamma,a)}{^{63}Cu(\gamma,n)} = 1.4 \times 10^{-4}$$

Ref. P. Erdos, P. Scherrer, P. Stoll
Helva. Phys. Acta 30, 639 (1957)

Elem. Sym.	A	Z
Tl	203	81

Method: Betatron; α yield; radioactivity; $Cu^{65}(\gamma,n)$ reaction.

Ref. No.: 57 Er 1 EGF

Reaction	E or ΔE	E_o	Γ	$\int \sigma dE$	$J\pi$	Notes
$Tl(\gamma,\alpha)$ + $(\gamma,n\alpha)$	Bremss. 32			0.13±0.03 MeV-mb		Based on yield measurement.

B.I. Deutch, F.R. Metzger
Phys. Rev. 122, 848 (1961)

ELEM. SYM.	A	Z
Tl	203	81

METHOD: Radioactive source; photon scattering; NaI

REF. NO.: 61 De 3 | NVB

REACTION	RESULT	EXCITATION ENERGY	SOURCE TYPE	SOURCE RANGE	DETECTOR TYPE	DETECTOR RANGE	ANGLE
G,G	RLX	0	D	0	NAI-D		DST
		(279 keV)		(279 keV)			

LIFETIME

Mixing ratio $\delta = \pm\sqrt{\frac{E2}{M1}}$

$\delta = +1.20^{+0.20}_{-0.12}$

TABLE IV. Experimental values of the coefficient A_2 in the angular distribution $W(\theta) = 1 + A_2 P_2(\cos\theta)$ of the resonance radiation from the 279-kev level.

Run No.	A_2
1	0.83±0.08
2	1.02±0.08
3	0.76±0.07
Average	0.87±0.08

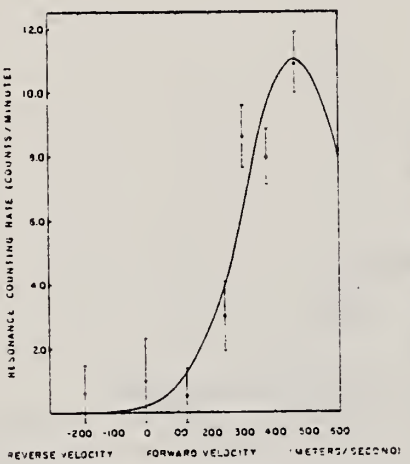

FIG. 3. The resonance scattering effect as a function of the velocity of the source. The heavy line represents the theoretical counting rate for $\tau_\gamma = 5.00\times10^{-10}$ sec. The experimental points from the first (weak) source are shown for comparison purposes.

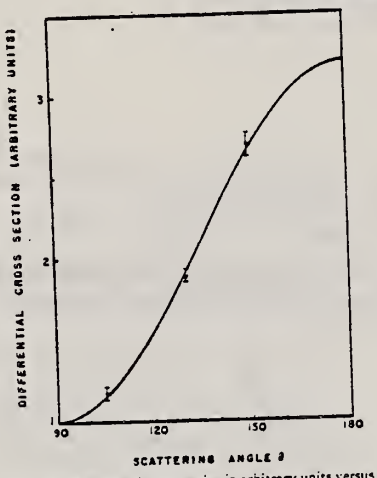

FIG. 4. The differential cross section in arbitrary units versus the scattering angle. The heavy curve is the mean square fit to the angular distribution data uncorrected for the finite size of the detector.

TABLE V. Recent experimental values of the mean gamma-ray lifetime of the 279-kev transition in Tl^{203}.

τ_γ (10^{-10} sec)	Method	Author(s)
4.7 ±0.8	Resonance fluorescence	Metzger[a]
5.1 ±0.5	Delayed coincidences	Berlovich and Dubinkin[b]
5.2 ±0.6	Coulomb excitation[c]	McGowan and Stelson[c]
5.0 ±0.5	High-frequency deflection[d]	Johansson and Alvager[d]
5.1 ±0.4	Delayed coincidences[e]	Basnandv *et al.*[e]
5.10 ±0.30	Delayed coincidences[f]	Gorodetzsky *et al.*[f]
4.26 ±0.18	Delayed coincidences[g]	Pederson and Bell[g]
4.95 ±0.10	Delayed coincidences[h]	Schwarzschild and Kane[h]
4.83 ±0.05	Average delayed coincidences	
5.00 ±0.24	Resonance fluorescence	Present work (1960)

[a] Corrected for the average $\delta' = +1.43 \pm 0.07$ computed from the three independent determinations of the mixing amplitude: the polarization of the Coulomb excitation (1.30 ± 0.08), Coulomb excitation and resonance fluorescence lifetimes (1.31 ± 0.09), and the angular distribution of the resonance fluorescence radiation (1.20 ± 0.09).
[b] For the cases in which $T_\frac{1}{2}$, the half-life of the 279-kev level, was listed, the value was corrected by a factor $(1+\alpha)/0.693$, where $\alpha = 0.223$ is the total conversion coefficient.
[c] See reference 17.
[d] E. E. Berlovich and G. V. Dubinkin, J. Exptl. Theoret. Phys. (U.S.S.R.) 32, 223 (1957) [translation: Soviet. Phys. JETP 5, 164 (1957)].
[e] See reference 3.
[f] See reference 13.
[g] See reference 11.
[h] See reference 12.
[i] See reference 15.
[j] See reference 14.

TABLE III. Experimental values for τ_γ, the mean gamma lifetime of the 279-kev level in Tl^{203}.

Source	τ_γ (sec)
1	$(5.10\pm0.28)\times10^{-10}$
2	$(4.78\pm0.47)\times10^{-10}$
2	$(4.97\pm0.38)\times10^{-10}$
2	$(5.00\pm0.58)\times10^{-10}$
Average 2	$(4.92\pm0.26)\times10^{-10}$
Average 1+2	$(5.00\pm0.19)\times10^{-10}$

[2] F. R. Metzger, *Proceedings of the 1954 Glasgow Conference on Nuclear and Meson Physics* (Pergamon Press, New York, 1955), p. 201.
[3] F. K. McGowan and P. H. Stelson, Phys. Rev. 109, 901 (1958).
[10] V. Knapp, Proc. Phys. Soc. (London) A71, 194 (1958).
[11] E. Basnandv, T. R. Gerholm and J. Lindskog, Arkiv Fysik 17, 421 (1960).
[12] S. Gorodetzsky, R. Manquenouille, R. Richert, and A. Knipper, Compt. rend. 251, 65 (1960).
[13] B. Johansson and T. Alvager, Arkiv Fysik 17, 163 (1960).
[14] A. Schwarzschild and J. Kane, following paper [Phys. Rev. 122, 854 (1961)].
[15] E. C. B. Pederson and R. E. Bell, Nuclear Phys. 21, 393 (1960).
[16] F. R. Metzger in *Progress in Nuclear Physics*, edited by O. R. Frisch (Pergamon Press, New York, 1959), Vol. 7.
[17] F. R. Metzger, J. Franklin Inst. 261, 219 (1956).

REF.

J. C. Palathingal and M. L. Wiedenbeck
Nucl. Phys. A101, 193 (1967)

ELEM. SYM.	A	Z
Tl	203	81

METHOD

REF. NO.	
67 Pa 1	EGF

REACTION	RESULT	EXCITATION ENERGY	SOURCE		DETECTOR		ANGLE
			TYPE	RANGE	TYPE	RANGE	
G,G	LFT	1	D	1	NAI-D	1	110
		279 MeV					

Used β recoil to supply Doppler shift
Compared Rayleigh and resonance scattering

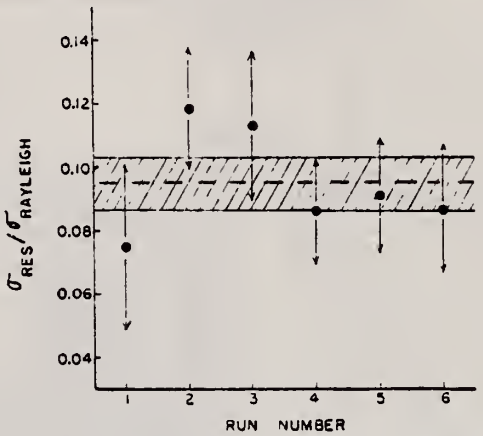

Fig. 5. Values of $\sigma_{res}/\sigma_{Rayleigh}$ obtained from the various runs and their weighted mean. The shaded area represents one standard deviation to either side of the mean value (the dashed line).

TABLE 1

Values of τ obtained by various observers

τ (nsec)	Method of measurement	Ref.
0.28 ±0.04	beta decay recoil (resonance fluorescence)	present work
0.408 ±0.010	delayed coincidence	[18])
0.402 ±0.003	delayed coincidence	[19])
0.410 ±0.020	centrifuge (resonance fluorescence)	[1])
0.405 ±0.008	delayed coincidence	[20])
0.348 ±0.014	delayed coincidence	[21])
0.408 ±0.025	delayed coincidence	[22])
0.41 ±0.03	delayed coincidence	[23])
0.32 ±0.04	high-frequency deflection	[24])
0.43 ±0.05	Coulomb excitation	[25])
0.42 ±0.04	delayed coincidence	[26])
0.38 ±0.07	thermal Doppler effect (resonance fluorescence)	[2])
0.41 ±0.12	Coulomb excitation	[27])
0.18 ±0.05	delayed coincidence	[28])
0.3 ±0.1	delayed coincidence	[29])
0.36 ±0.10	delayed coincidence	[30, 9])

Wherever a parameter other than τ, but one directly related to it has been quoted as the result, τ is computed from this parameter.

REF.

G.P. Antropov, I.E. Mitrofanov, A.I. Prokof'ev & V.S. Russkikh
Izv. Akad. Nauk. Fiz. 34, 116 (1969)
Bull. Acad. Sci. USSR-Phys. 34, 108 (1970)

ELEM. SYM.	A	Z
Tl	203	81

METHOD

REF. NO.	
69 An 10	hmg

REACTION	RESULT	EXCITATION ENERGY	SOURCE		DETECTOR		ANGLE
			TYPE	RANGE	TYPE	RANGE	
G,XN	ABX	7-20	C	7-30	BF3-I		4PI

451

Isotope	$\sigma_0 = \int_0^{20\,MeV} \sigma(E)\,dE$, b MeV(exp)	$\sigma_0 = 0.06\frac{NZ}{A}$, b MeV	$\sigma_{-1} = \int_0^{20\,MeV} \sigma(E)/E\,dE$, b/MeV(exp)	$\sigma_{-1} = 0.00225A^{5/3}$, b/MeV
^{203}Tl	2,61	2,92	15,1	16,0
^{205}Tl	2,78	2,94	15,2	16,0

451

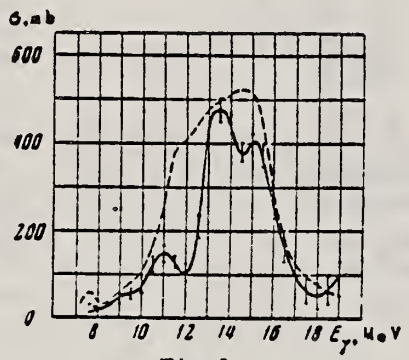

Fig.1

Fig.1. $\sigma\gamma n + \sigma\gamma,2n$ versus $E\gamma$ for ^{203}Tl (full curve and ^{209}Bi (dashed curve (Ref. 3)).

REF. R. Moreh, A. Nof, and A. Wolf
Phys. Rev. C2, 249 (1970)

ELEM. SYM.	A	Z
Tl	203	81

METHOD

REF. NO. 70 Mo 1 hmg

REACTION	RESULT	EXCITATION ENERGY	SOURCE		DETECTOR		ANGLE
			TYPE	RANGE	TYPE	RANGE	
G,G	LFT	6	D	6	SCD-D	0-7	DST
		(6.418)		(6.418)			

J=1/2; E=6.418 MEV

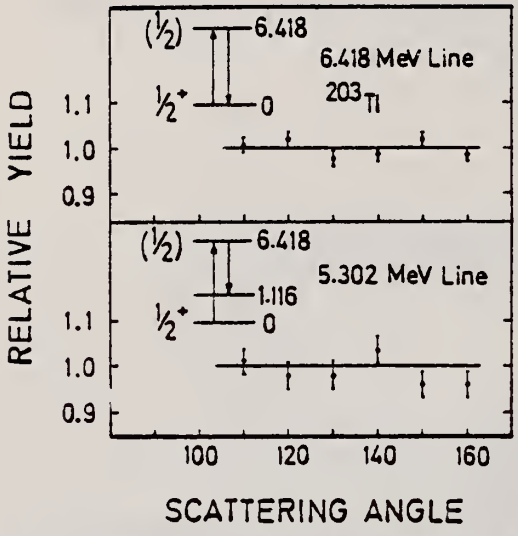

FIG. 4. Angular distribution of the elastic and one inelastic scattered line as measured using a 20-cc Ge(Li) detector.

TABLE II. Partial radiation widths Γ_i and $E1$, $M1$ radiation strengths of intense transitions from the 6.418-MeV resonance state in ^{203}Tl; the level spacing D was taken 1.0 keV.

γ energy (MeV)	Γ_i (10^{-3} eV)	k_{E1} (10^{-8} MeV^{-3})	k_{M1} (10^{-8} MeV^{-3})
6.418	90	9.8	338
6.139	35	4.4	145
5.302	58	11.3	390
5.132	10	2.0	67
5.008	51	11.8	384
4.966	26	6.2	212
4.777	8	2.1	73
4.577	9	2.7	94
4.533	8	2.5	86
4.483	6	1.9	67
3.546	10	6.3	216

Elastic and inelastic nuclear resonant scattering of monochromatic photons from ^{203}Tl has been studied using a 20-cc Ge(Li) detector. The γ source was obtained from thermal-neutron capture in titanium. The scattering isotope was identified by using an isotopically enriched thallium target. The energy of the resonance level in ^{203}Tl was found to be 6.418 MeV. Assuming the high-energy lines to be primary transitions deexciting the resonance level, some 14 energy levels were found from the ground state up to 2.9 MeV, 4 of which may be identified with recently reported levels.

By measuring the angular distribution of the scattered radiation, the spin of the 6.418-MeV level was determined to be $\frac{1}{2}$, and thus, based on the assumption of dipole transitions, the spins of several low-lying levels were found to be either $\frac{1}{2}$ or $\frac{3}{2}$. The total radiative width of the resonance level was determined and found to be $\Gamma_\gamma = 0.32 \pm 0.06$ eV and $\Gamma_0/\Gamma_\gamma = 0.026$. The spectral shape of scattered radiation was found to have a strong intensity bump at about 5 MeV; this is discussed in the light of similar bumps obtained in (n,γ) and $(d,p\gamma)$ reactions on nuclei in the same mass region.

REF.

Tatsuya Saito
Nippon Kagaku Zasshi 92, 164 (1971)

ELEM. SYM.	A	Z
Tl	203	81

METHOD

REF. NO.: 71 Sa 1 egf

REACTION	RESULT	EXCITATION ENERGY	SOURCE		DETECTOR		ANGLE
			TYPE	RANGE	TYPE	RANGE	
G,N	ABY	7-68	C	10-68	ACT-I		4PI

Nippon Kagaku Zasshi, 92, 164~168(1971)

The Yields of Radioactivities Induced by (γ, n) Reactions with Bremsstrahlung up to 68 MeV

by Tatsuya SAITO

The (γ, n) yields of 12 target nuclides have been measured at 10, 13, 16, 30, 45 and 68 MeV bremsstrahlung by observing the induced activities.

The energy dependence of the yields has been investigated extensively in the same way as in the previous work at 20 MeV bremsstrahlung.

In the case of heavy nuclides, the yields rise greatly as a function of maximum bombarding energy up to 20 MeV, and rise gradually from 20 MeV up to 68 MeV. However, in the case of light nuclides, the yields rise greatly up to 30 MeV, because the neutron separation energies of light ones are larger than those of heavy ones, and the bremsstrahlung spectrum covers the giant resonance and so the yields rise gradually from 30 MeV up to 68 MeV.

The yields have approximately been estimated from the parameter of the giant resonance, that is the peak cross section and the half width, in order to compare with the experimental data. As a result, the experimental data of light nuclides and heavy ones are nearly in agreement with the estimated data of Nathans et al., Johns et al. and Montalbetti et al., but those of medium weight ones are relatively lower values.

Department of Chemistry, Faculty of Science, Tohoku University; Katahira-cho, Sendai-shi, Japan

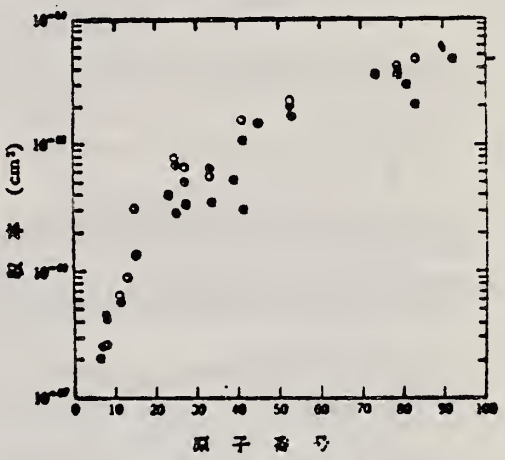

●: 実験値, ⊕: Johns ら,
◑: Nathans ら, ○: Monlalbetti ら

図 4 (γ, n)反応の収率の比較

REF. R. Alberini, P. R. Oliva and D. Prosperi
Nuovo Cimento Lett. 10, 726 (1974)

ELEM. SYM.	A	Z
Tl	203	81

METHOD

REF. NO.	
74 Al 10	egf

REACTION	RESULT	EXCITATION ENERGY	SOURCE		DETECTOR		ANGLE
			TYPE	RANGE	TYPE	RANGE	
G,G	RLY	6	D	6	SCD-D		135

6 = 6.419 MEV

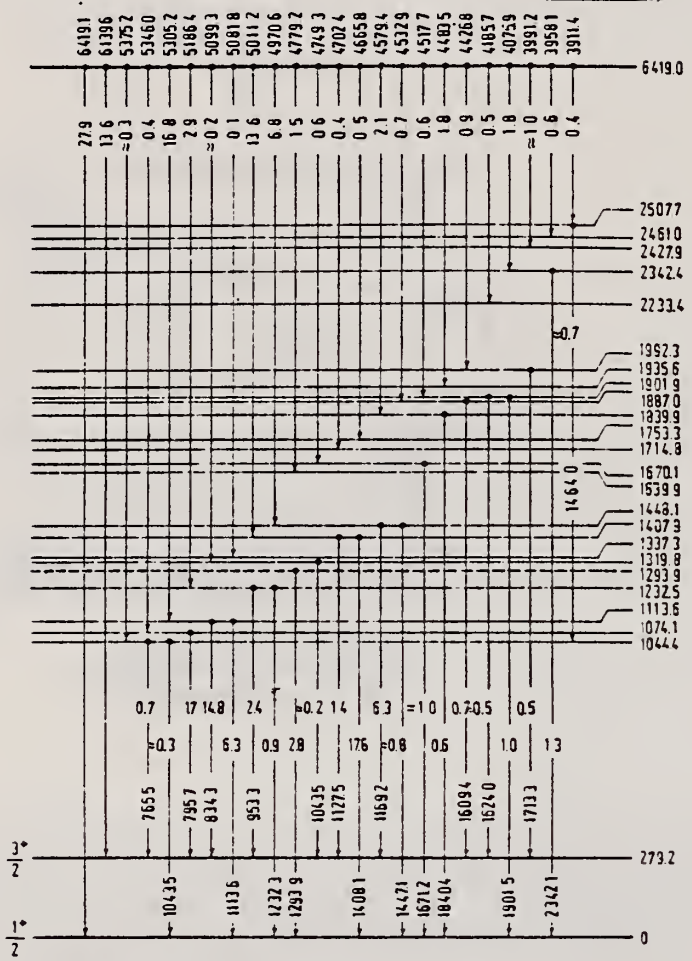

Fig. 2. – Decay scheme of the 6419.0 keV level in ^{203}Tl.

REF. K. Masumoto, T. Kato, N. Suzuki
Nucl. Inst. Meth. 157, 567 (1978)

ELEM. SYM.	A	Z
Tl	203	81

METHOD

REF. NO. 78 Ma 10 hg

REACTION	RESULT	EXCITATION ENERGY	SOURCE		DETECTOR		ANGLE
			TYPE	RANGE	TYPE	RANGE	
G,N	ABY	8-68	C	30-68	ACT - I		4PI
G,2N	ABY	15-68	C	30-68	ACT - I		4PI
G,3N	ABY	23-68	C	30-68	ACT - I		4PI

Analysis is made of reactions interfering with photon activation analysis procedures.

The activation yield curves have been presented for a number of photonuclear reactions in the energy range from 30 to 68 MeV, in order to evaluate quantitatively the interferences due to competing reactions in multielement photon activation analysis. The general features of the yields as functions of both target mass number and excitation energy were elucidated from the data obtained, discussion being given on the results in terms of the reaction mechanism.

Simultaneous neutron activation due to appreciable neutron production from the converter and surrounding materials has also been studied, and, finally, the magnitudes of interferences in real multielement analysis were given in the form of their energy dependences.

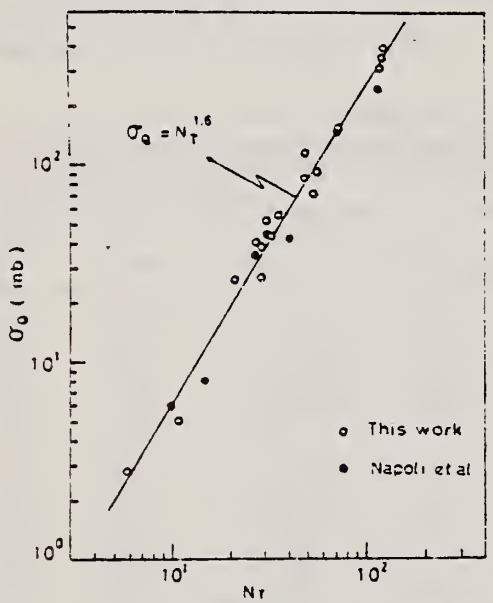

Fig. 2. Yield per equivalent quanta versus target neutron number.

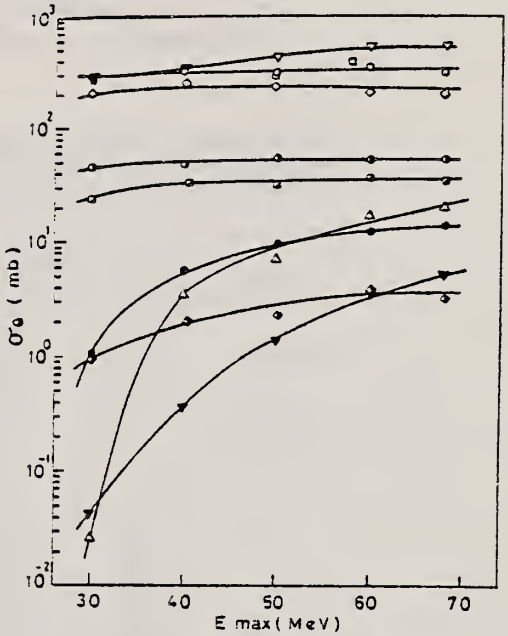

Fig. 8. Activation yield curves for the reactions on Pb, Tl and Hg.

□ $^{204}Hg(\gamma, n)^{203}Hg$, ◇ $^{198}Hg(\gamma, n)^{197g}Hg$,
◪ $^{198}Hg(\gamma, n)^{197m}Hg$, ◈ $^{199}Hg(\gamma, p)^{198}Au$,
▽ $^{204}Pb(\gamma, n)^{203}Pb$, ▼ $^{204}Pb(\gamma, 2n)^{202m}Pb$,
△ $^{204}Pb(\gamma, 3n)^{201}Pb$, ○ $^{203}Tl(\gamma, n)^{202}Tl$,
◗ $^{203}Tl(\gamma, 2n)^{201}Tl$. ● $^{203}Tl(\gamma, 3n)^{200}Tl$.

(over)

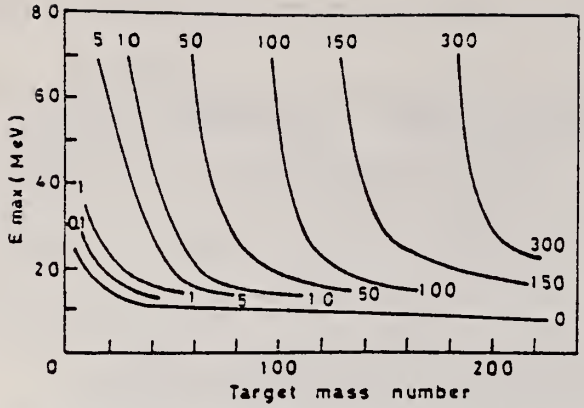

Fig. 9. Yields of the (γ, n) reactions as a function of bremsstrahlung maximum energy and target mass number. The numerical values in the figure are yields per equivalent quanta in mb.

REF. M. Schumacher, F. Smend, W. Mückenheim, P. Rullhusen, H.G. Börner
Z. Phys. A300, 193 (1981)

ELEM. SYM.	A	Z
Tl	203	81

METHOD

REF. NO. 81 Sc 6 egf

REACTION	RESULT	EXCITATION ENERGY	SOURCE TYPE	SOURCE RANGE	DETECTOR TYPE	DETECTOR RANGE	ANGLE
G,G	ABX	6		6	SCD-D		90

6.418 MEV

Elastic scattering by nuclei in the range of mass numbers between 64 and 238 has been studied with monochromatic photons in the energy range between 2 and 8 MeV. These photons were provided either by a Ti(n,γ) source installed in the tangential through channel of the Grenoble high flux reactor, or by ^{24}Na and ^{56}Co sources produced by deuteron bombardment of Al or Fe at the Göttingen cyclotron. The photoexcitation of 23 nuclear levels has been observed and the decay properties and groundstate widths of the majority of these levels have been determined. For the lead scattering target the coherent elastic differential cross section has been studied in detail. There is evidence that below the photo-neutron threshold the elastic scattering via virtual photoexcitation of the nucleus can be approximated by extrapolating the real part of the Giant Dipole Resonance amplitude along a Lorentzian curve. Coulomb corrections to Delbrück scattering seem to play a small role at 6.5 MeV.

Table 4. Properties of levels observed by photoexcitation. $(d\sigma/d\Omega)^{NRF}$: experimental differential cross section per identified isotope or element for resonance scattering through $\Theta = 90°$. I^π: spin-parity of excited level; $W(\Theta)$: angular correlation function; $g = (2I_{ex}+1)/(2I_g+1)$; Γ_0: radiative groundstate transition width, Γ: total level width. Errors in the last digits are given in parentheses

Isotope	E_γ (MeV)	$(d\sigma/d\Omega)^{NRF}$ (μb/sr)	I^π	Γ_0/Γ [c]	$W(\Theta)\,g\,\Gamma_0^2/\Gamma$ (meV)	Γ_0 [f] (meV)	Γ_0 [g] (meV)
^{238}U	2.754	13 (4)	(1)	0.77	0.145	0.084	-
^{238}U	3.254	421 (5)	1^-	0.24	0.83	1.5	0.52(15)[d]
^{209}Bi	6.555	2.1 (4)·10^2	-	-	0.74	0.74[b]	-
^{209}Bi	7.168	1.7 (3)·10^5	$9/2^{-a}$	1.00	710	786	820 (40)[a]
^{203}Tl	6.418	8.75(30)·10^3	$1/2^a$	0.28	30	102	82 (15)[a]
Tl	6.759	7 (3)	-	-	-	-	-
Hg	6.555	68 (17)	-	-	-	-	-
^{186}W	6.418	5.2 (3)·10^2	1^{-a}	0.32	1.75	2.4	-
^{184}W	6.555	9.8 (10)·10^2	(1)	0.52	3.44	2.9	-
^{184}W	6.759	46 (10)	(1)	0.58	0.17	0.13	-
^{181}Ta	3.010	174 (17)	-	0.72	0.42	0.59	-
^{181}Ta	6.418	62 (4)	-	0.73	0.2	0.27[c]	-
^{181}Ta	6.759	4.8 (12)	-	-	0.018	0.018[b]	-
^{165}Ho	6.418	10.3 (30)	-	-	0.035	0.035[b]	-
^{165}Ho	6.759	5.6 (14)	-	-	0.021	0.021[b]	-
Nd	2.754	2.6 (5)	-	-	-	-	-
Nd	3.254	14.0 (10)	-	-	-	-	-
Ce	6.759	13.4 (10)	-	-	-	-	-
^{121}Sb	3.452	2.20 (5)·10^3	-	0.60	2.9	4.9[b]	-
^{100}Mo	6.418	1.53 (4)·10^4	1^{-a}	0.88	52	26	25 (8)[a]
^{94}Mo	6.555	4.4 (4)·10^3	(1)	0.33	15	21	-
Mo	6.759	6.2 (15)	-	-	-	-	-
Mo	7.168	8.2 (26)·10^2	-	-	-	-	-

[a] [11] [b] $W(\Theta)\,g\,\Gamma_0/\Gamma = 1$ assumed [c] $W(\Theta)\,g = 1$ assumed
[d] [28] (a small correction has been applied to the data of [28])
[e] Upper limits in case not all the transitions to lower levels were observed
[f] Present work [g] Previous work

(OVER)

Table 2. Elastic differential cross sections $d\sigma/d\Omega(\Theta=90°)$ in μb/sr measured with the Ti(n,γ) source and compared with theoretical predictions. n: predicted number of levels in a $\Delta E=25$ eV interval at 6.5 MeV. Errors in the last digits are given in parentheses

Scattering target	6.418 MeV		6.555 MeV		6.759 MeV		7.168 MeV		n
	exp.	th.	exp.	th.	exp.	th.	exp.	th.	
^{238}U	23 (12)	10.3	-	-	-	-	-	-	45
^{209}Bi	-	-	219(39)[b,c]	8.0	12 (4)	7.4	1.5(3)·10^5[b,c]	5.7	0.1
^{nat}Pb	7.0(15)	8.6	-	-	6.5(11)	7.4	-	-	0.05
^{nat}Tl	2,586 (92)[a,c]	7.5	-	-	13 (3)[b]	6.0	-	-	0.4
^{nat}Hg	12 (3)	7.8	74(17)[b]	6.5	6.7(15)	6.4	-	-	3.4
^{nat}W	159 (10)[a,c]	6.6	306(33)[a,c]	6.3	20 (2)[a,c]	5.6	-	-	13
^{181}Ta	68 (4)[a,c]	6.3	-	-	10.1(12)[b,c]	5.3	-	-	28
^{165}Ho	15 (3)[b]	4.7	-	-	9.5(14)[b]	3.9	-	-	18
^{nat}Ce	4.1(21)	4.1	-	-	17 (1)[b,c]	3.6	-	-	0.04
^{nat}Sn	4.2(13)	3.0	-	-	2.5 (5)	2.7	-	-	1.9
^{nat}Mo	1,474 (44)[a,c]	2.5	407(39)[a,c]	2.5	8.5(15)[b,c]	2.3	817(258)[b,c]	2.0	0.5
^{nat}Zn	2.4 (8)	1.6	-	-	1.8 (5)	1.5	-	-	0.3

[a] Transitions to excited states observed
[b] Photoexcitation identified from size of differential cross section
[c] Photoexcitation reported in [11]

Tl
A=205

Tl
A=205

REF.

A. El Sioufi, P. Erdos and P. Stoll
Helv. Phys. Acta 30, 266 (1957)

ELEM. SYM.	A	Z
Tl	205	81

METHOD

REF. NO.	
57 El 2	JOC

REACTION	RESULT	EXCITATION ENERGY	SOURCE		DETECTOR		ANGLE
			TYPE	RANGE	TYPE	RANGE	
G,A	ABX	THR-32	C	32	ACT-I		4PI

Tabelle 1.
Charakteristische Daten bekannter (γ,α)-Anregungskurven.
E_0: Einsatzenergie. E_{max}: Gammaenergie beim Wirkungsquerschnittsmaximum in MeV. σ_{max}: Maximaler Wirkungsquerschnitt in Mikrobarns.

	E_0 MeV	E_{max} MeV	σ_{max} μb
Cu^{65}	13	21	1500
Rb^{87}	15	22	100
Tl^{205}	20	26	100

Ref. P. Erdos, P. Scherrer, P. Stoll
Helva. Phys. Acta 30, 639 (1957)

Elem. Sym.	A	Z
Tl	205	81

Method: Betatron; α yield; radioactivity; $Cu^{65}(\gamma,n)$ reaction.

Ref. No.: 57 Er 1 EGF

Reaction	E or ΔE	E_o	Γ	$\int \sigma dE$	Jπ	Notes
$Tl^{205}(\gamma,\alpha)$	Bremss. 18-32	25.0±1.0		0.35±0.07 MeV-mb		σ_{max} = 95±20 μb.
$Tl^{205}(\gamma,n\alpha)$				0.16 MeV-mb		Integral to 32 MeV.

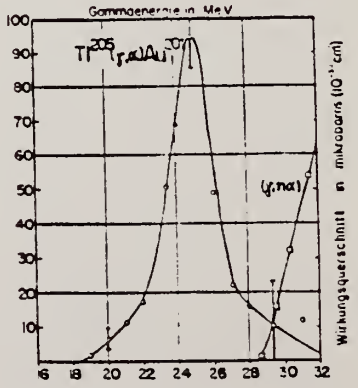

Fig. 13.
Wirkungsquerschnittsverlauf der Reaktionen $Tl^{205}(\gamma,x)Au^{201}$ und $Tl^{205}(\gamma,nx)Au^{200}$.

REF.

K. N. Geller. J. Halpern, and E. G. Muirhead
Phys. Rev. 118, 1302-12 (1960)

ELEM. SYM.	A	Z
Tl	205	81

METHOD

Betatron; neutron threshold; ion chamber

REF. NO.	
60 Ge 3	NVB

REACTION	RESULT	EXCITATION ENERGY	SOURCE		DETECTOR		ANGLE
			TYPE	RANGE	TYPE	RANGE	
G,N	NØX	THR	C THR		BF3-I		4 PI

THRESHØLD

TABLE I. Summary and comparison of neutron separation energies inferred from present threshold measurements with values predicted from mass data and reaction energies. All energies are expressed in the center-of-mass system in Mev.

Reaction	No. runs	Present results	Other results	Method	Refcrence
$Tl^{205}(\gamma,n)Tl^{204}$	1	7.515±0.029	7.62 ±0.17	LSA	[5]

[5] J. R. Huizenga, Physica 21, 410 (1955).

REF.

G. P. Antropov, I. E. Mitrofanov, A. I. Prokof'ev & V. S. Russkikh
Izv. Akad. Nauk. Fiz. 34, 116 (1969)
Bull. Acad. Sci. USSR-Phys. 34, 108 (1970)

ELEM. SYM.	A	Z
Tl	205	81

METHOD

REF. NO.	
69 An 10	hmg

REACTION	RESULT	EXCITATION ENERGY	SOURCE		DETECTOR		ANGLE
			TYPE	RANGE	TYPE	RANGE	
G,XN	ABX	7-20	C	7-30	BF3-I		4PI

452

Isotope	$a_0 = \int_0^{20\,MeV} \sigma(E)\,dE$, b MeV (exp)	$a_0 = 0{,}06\,\frac{NZ}{A}$, b MeV	$\sigma_{-1} = \int_0^{20\,MeV} \sigma(E)/E\,dE$, b/MeV (exp)	$\sigma_{-1} = 0{,}0225\,A^{5/3}$, b/MeV
^{205}Tl	2,61	2,92	15,1	16,0
^{208}Tl	2,78	2,94	15,2	16,0

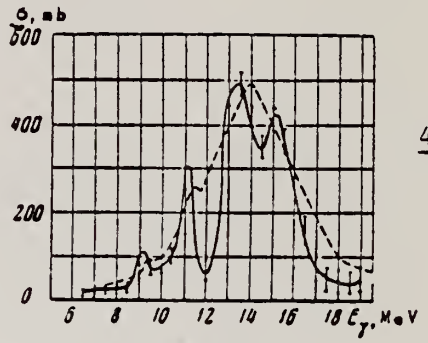

452

Fig.2

Fig.2. $\sigma_{\gamma n} + \sigma_{\gamma,2n}$ versus E_γ for ^{205}Tl (full curve) and ^{208}Pb (dashed curve (Ref. 1)).

REF.

R. Moreh and A. Wolf
Phys. Rev. 182, 1236 (1969)

ELEM. SYM.	A	Z
Tl	205	81

METHOD

REF. NO.	
69 Mo 2	HMG

REACTION	RESULT	EXCITATION ENERGY	SOURCE		DETECTOR		ANGLE
			TYPE	RANGE	TYPE	RANGE	
G,G	LFT	7	D	7	SCD-D	0-9	DST
		(7.646)		(7.646)			

Ground state radiation width of the 7.646 MeV level is $\Gamma_o = 0.57 \pm 0.06$ eV.

7=7.646

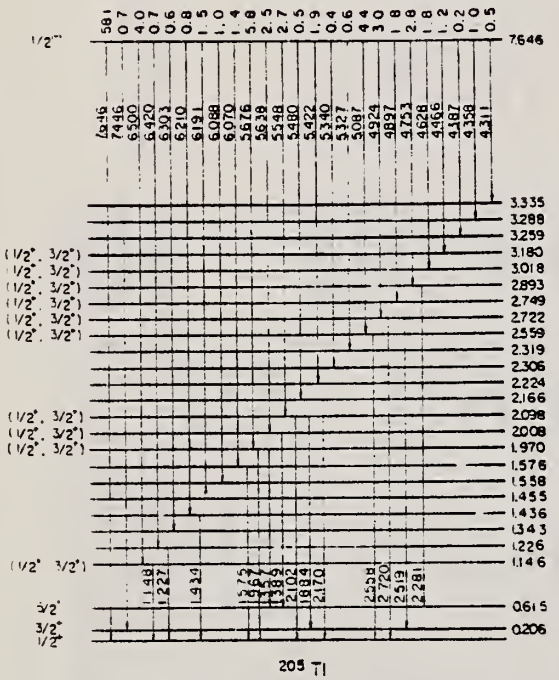

FIG. 6. Decay scheme of 7.646-MeV level of ^{206}Tl showing level energies and corresponding branching ratios as constructed by assuming that all high-energy γ lines in the scattered-radiation spectrum are emitted in primary transitions. Most probable spin values of some levels assigned in the present work are shown. The parity of the scattering level shown in parentheses is uncertain.

TABLE III. Partial radiation widths Γ_i and $E1$ radiation strengths k_{E1} of intense transitions from the 7.646-MeV resonance state in ^{206}Tl. The level spacing D was taken to be 1.0 keV.

Transition energy (MeV)	Level energy (MeV)	Γ_i (eV)	k_{E1} (10^{-9} MeV^{-2})
7.646	0	0.569	36.7
6.500	1.146	0.040	4.2
6.191	1.455	0.015	1.8
5.676	1.970	0.058	9.1
5.638	2.008	0.025	4.0
5.548	2.098	0.027	4.5
5.422	2.224	0.019	3.4
5.087	2.559	0.044	9.6
4.924	2.722	0.030	7.2
4.897	2.749	0.018	4.4
4.753	2.893	0.028	7.5
4.628	3.018	0.018	5.2
4.466	3.180	0.012	3.9
4.358	3.288	0.010	3.5

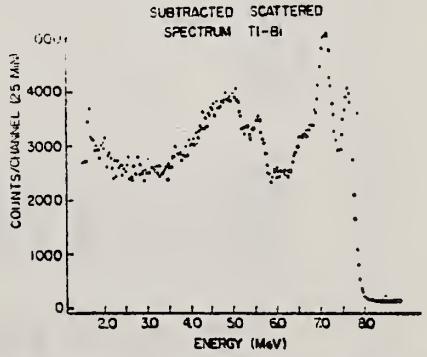

FIG. 4. Scattered γ-ray spectrum from a Tl target after substracting the contribution of a comparative Bi nonresonant scatterer of Fig. 3. The bump of strong intensity γ-rays around 5 MeV is clear.

REF.

S. Ramchandran and J. A. McIntyre
Phys. Rev. 179, 1153 (1969)

CLASS.		
T1	205	81

METHOD

REF. NO.	
69 Ra 1	hmg

REACTION	RESULT	EXCITATION ENERGY	SOURCE		DETECTOR		ANGLE
			TYPE	RANGE	TYPE	RANGE	
G,G	LFT	8	D	8	NAI		DST

$W(\theta) \sim [1 + a\ P_2(\cos\theta)]$

8 = 7.647 MEV

[over]

TABLE II. Experiment compared to theory assuming a pure dipole transition.

$\alpha\pm\Delta\alpha$ (Experimental)										
^{90}Zr	Cd	Sn	Hg	^{205}Tl	^{208}Pb	^{209}Bi (7.416 MeV)	^{209}Bi (7.149 MeV)	$A_2^3(J_0, J_1, L=1)$ (Theoretical)	J_0	J_1
0.489±0.027	0.488±0.034	0.490±0.095	0.48±0.11		0.485±0.026			0.500	0	1
	0.488±0.034	0.490±0.095	0.48±0.11	0.0017±0.0110				0.000	1/2	1/2
	0.488±0.034	0.490±0.095	0.48±0.11	0.0017±0.0110				0.250	1/2	3/2
			0.48±0.11					0.000	3/2	1/2
			0.48±0.11					0.160	3/2	3/2
			0.48±0.11					0.140	3/2	5/2
						0.195±0.033	0.184±0.074	0.024	9/2	7/2
						0.195±0.033	0.184±0.074	0.194	9/2	9/2
						0.195±0.033	0.184±0.074	0.083	9/2	11/2

TABLE V. Summary of energy-level parameters.

Element	^{90}Zr	Cd	Sn	Hg	^{205}Tl	^{208}Pb	^{209}Bi	^{209}Bi
Level energy (MeV)	8.496[a]	6.485[b]	6.988[c]	4.906[b]	7.647[d]	7.277[e]	7.416[a]	7.149[a]
γ ray source	Se	Co	Cu	Co	Fe	Fe	Se	Ti
	0→1	0→1	0→1	0→1	1/2→1/2	0→1	9/2→7/2	9/2→7/2
		(1/2→3/2)	(1/2→3/2)	3/2→5/2	(1/2→3/2)		9/2→9/2	9/2→9/2
$J_0\rightarrow J_1$				(1/2→3/2)			9/2→11/2	9/2→11/2
				(3/2→3/2)				
Γ_0/Γ	0.8±0.2				0.85±0.17[f]	$0.95_{-0.17}^{+0.05}$	0.6±0.2	
Γ_0 (eV)	1.68±0.02				1.0[f]	0.68±0.03	0.14±0.09	
ϵ (eV)	5.60±0.15				11.5±0.2[f]	8.00±0.14	3.4±1.6	

[a] L. V. Groshev, V. N. Lutsenko, A. M. Demidov, and V. I. Polekov, *Atlas of Gamma Spectra from Radiative Capture of Thermal Neutrons* (Pergamon Press, Inc., New York, 1959).
[b] E. B. Shera and D. W. Hafemeister, Phys. Rev. 150, 894 (1966).
[c] H. H. Bolotin (private communication from L. M. Bollinger).
[d] R. Moreh and G. Ben-Yaacov, Nuclear Research Center—Negev Report, NRCN-180, 1967, (unpublished).
[e] L. V. Groshev, A. M. Demidov, G. A. Kotelnikov, and V. N. Lutsenko, Nucl. Phys. 58, 465 (1964); G. T. Ewan and A. J. Tavendale, Nucl. Instr. Methods 26, 183 (1964).
[f] See Ref. 24a.

R. Cesareo, M. Giannini, P. R. Oliva, D. Prosperi, M. C. Ramorino
Nucl. Phys. A141, 561 (1970)

ELEM. SYM.	A	Z
Tl	205	81

METHOD

REF. NO.	
70 Ce 1	egf

REACTION	RESULT	EXCITATION ENERGY	SOURCE		DETECTOR		ANGLE
			TYPE	RANGE	TYPE	RANGE	
G,G	SPC	8	D	8	SCD-D	0-8	145
		(7.646)		(7.646)			

8 = 7.646 MEV

TABLE 1
Energies and intensities of elastic and inelastic γ-rays scattered from a Tl target

E_γ (keV)	I_γ (rel) %	Energy levels: pres. work (keV)	a) (MeV)	b) (MeV)	c) (keV)
7646	61.7 ±9.2	0	0	0	0
		211±5			205±2
		623±6			615±5
6505±3	3.60±0.55	1141±3	1.14		
			1.21		
6309±3	0.80±0.15	1337±3	1.34		
6213±3	1.75±0.30	1433±3	1.43		
			1.48		
6089±3	1.25±0.20	1557±3	1.58		
6071±5 d)	0.75±0.15	1575±5			
5772±4 d)	0.50±0.15	1874±4	1.86		
5681±2	7.7 ±1.2	1965±2	1.96		
5645±3	3.35±0.50	2001±3			
			2.04		
5556±3	2.90±0.45	2090±3			
			2.12		
5483±3	1.00±0.20	2163±3			
5436±5 d)	0.45±0.15	2210±5			
5424±3	2.00±0.30	2222±3			
5346±3	0.65±0.15	2300±3			
5331±3	0.75±0.15	2315±3			
			2.43		
			2.49		
5088±3	3.4 ±0.5	2558±3			
				2.61	
4977±4	0.30±0.10	2669±4			
				2.69	
4941±5	0.25±0.10	2705±5			
4923±3	2.05±0.30	2723±3			
4895±3	1.05±0.20	2751±3	2.74		
4750±3	1.75±0.30	2896±3			
4625±3	0.85±0.15	3021±3			
4470±5	0.50±0.15	3176±5			
4357±3	0.65±0.15	3289±3			

a) $^{206}Pb(t,\alpha)^{205}Tl$ reaction. The errors are ±20 keV. Ref. [10]).
b) Ref. [11]). No error is given.
c) Ref. [12]).
d) The evidence for this γ-transition is regarded as uncertain.

10) S. Hinds, R. Middleton, J. H. Bjerregard, O. Hansen and O. Nathan, Nucl. Phys. 83 (1966) 17
11) J. P. Wurm and E. Grosse, Phys. Lett. 28B (1969) 413
12) C. Lederer, J. M. Hollander and J. Perlman, Table of isotopes (J. Wiley and Sons Inc., New York, 1967) p. 394

[over]

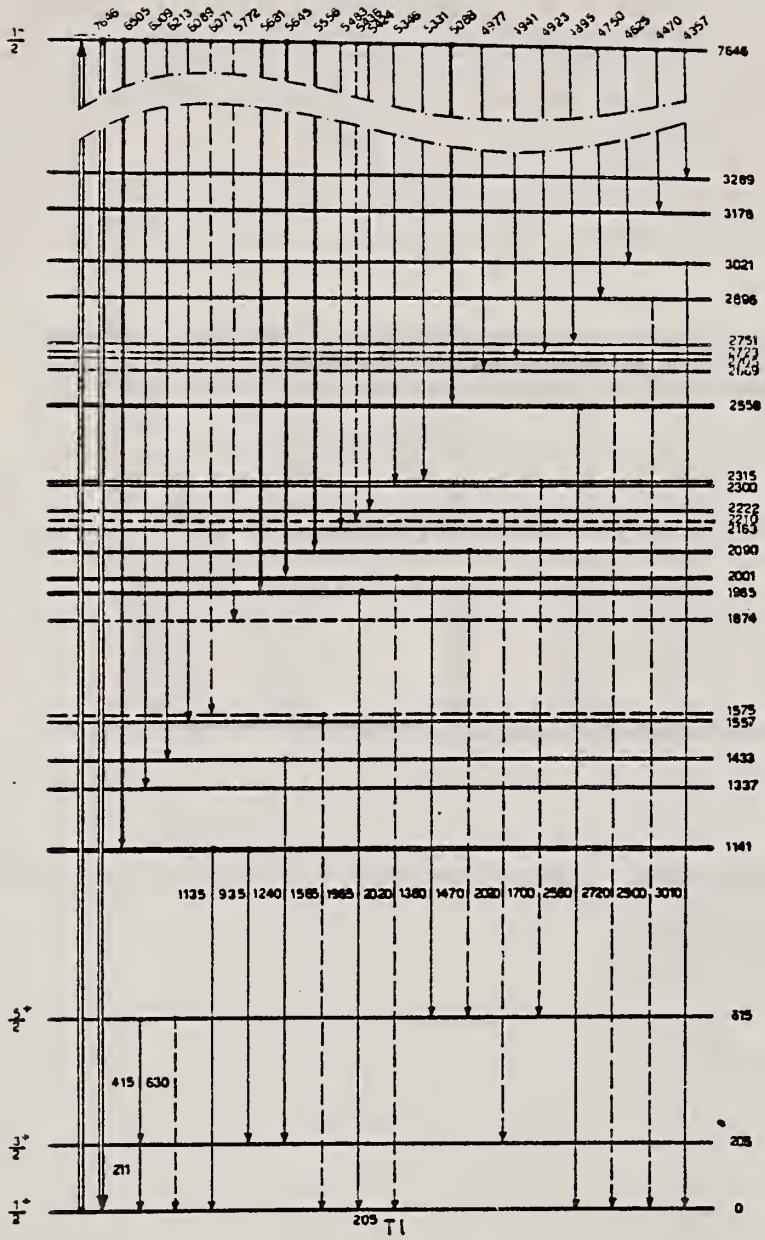

Fig. 5. The energy levels of ^{205}Tl as observed in the present work. The dashed lines indicate that the existence of that level or transition is questionable.

REF. R. Moreh, S. Shlomo, and A. Wolf
Phys. Rev. C2, 1144 (1970)

ELEM. SYM.	A	Z
Tl	205	81

METHOD

REF. NO. 70 Mo 2 hmg

REACTION	RESULT	EXCITATION ENERGY	SOURCE TYPE	SOURCE RANGE	DETECTOR TYPE	DETECTOR RANGE	ANGLE
G,G	ABX	8	D	8	SCD-D		DST
		(7.646)		(7.646)			

8 = 7.646, LFT

TABLE III. Summary of the results of spins, parities, and total widths of resonance levels excited by γ rays obtained from neutron capture in iron. Parities in parantheses are uncertain.

Isotope	Energy (MeV)	$\delta = \lvert E_r - E_e \rvert$ (eV)	J^π_0	J^π_r	Transition	Γ_0/Γ_γ (=8%)	Γ_γ (10^{-3} eV)
^{50}Cr	8.388	18 ±1	0^+	1	···	0.90	750 ± 200
^{62}Ni	7.646	14 ±1	0^+	1^-	$E1$	0.64	480 ± 50
^{74}Ge	6.018	4.5 ± 0.5	0^+	1^-	$E1$	0.19	120 ± 15
^{75}As	7.646	7.4 ± 0.3	$3/2^-$	$1/2^{(+)}$	···	0.11	360 ± 100
^{109}Ag	7.632	9 ±1	$1/2^-$	3/2	···	0.7	2 ± 1
^{112}Cd	7.632	4.8 ± 0.4	0^+	1^-	$E1$	0.55	86 ± 15
^{139}La	6.018	8.2 ± 0.6	$7/2^+$	$7/2^-$	$E1$	0.50	51^{+14}_{-9}
^{141}Pr	7.632	$11.4^{-0.3}_{-0.9}$	$5/2^+$	$5/2^+$	$M1$	0.46	72^{+24}_{-9}
^{205}Tl	7.646	9.3 ± 0.3	$1/2^+$	$1/2^{(-)}$	···	0.58	980 ± 90
^{203}Pb	7.279	7.1 ± 0.3	0^+	1^+	$M1$	1.00	780 ± 60

TABLE IV. Effective elastic scattering cross section $\langle\sigma_r\rangle = \sigma_0^m(\Gamma_0/\Gamma_\gamma)\Psi(x_0,t_0)$, where δ, J, Γ_0, Γ_γ were taken from Table III. The temperature of the scatterer was 300°K, while that of the iron γ source was 640°K.

Target	Resonance energy (MeV)	$\langle\sigma_r\rangle$ (mb)
^{50}Cr	8.388	905
^{62}Ni	7.646	569
^{74}Ge	6.018	61
^{75}As	7.646	4.4
^{109}Ag	7.632	3.5
^{112}Cd	7.632	198
^{139}La	6.018	39
^{141}Pr	7.632	20
^{205}Tl	7.646	574
^{208}Pb	7.279	5560

REF.

E. D. Earle, J. W. Knowles, M. A. Lone, G. A. Bartholomew
Nucl. Phys. A257, 365 (1976)

ELEM. SYM.	A	Z
Tl	205	81

METHOD

REF. NO.	
76 Ea 1	egf

REACTION	RESULT	EXCITATION ENERGY	SOURCE		DETECTOR		ANGLE
			TYPE	RANGE	TYPE	RANGE	
G,G	ABX	3- 8	D	3- 8	NAI-D		90

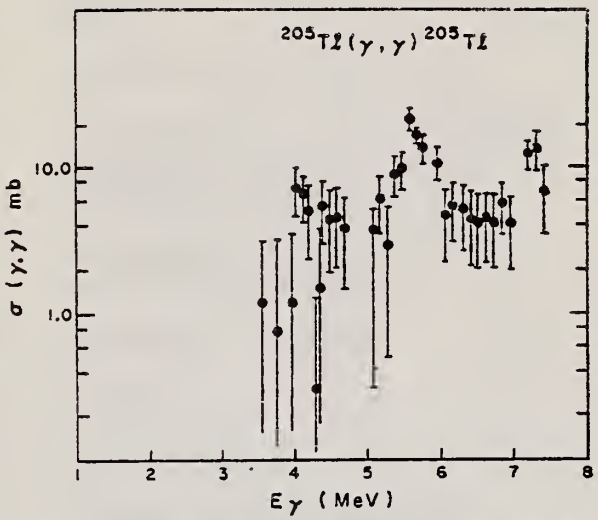

Fig. 4. The γ-ray quasielastic scattering cross section for ^{205}Tl as a function of γ-ray energy.

DEFINITIONS OF ABBREVIATIONS AND SYMBOLS

Note: In this list definitions are given for various photoneutron reactions in which the following symbols are used: N, NL, nN, SN and XN. Corresponding definitions apply for reactions involving other nuclear particles where the symbols N (neutron) is replaced by, e.g. P, D, T, HE, A etc. Where unknown reactions result in the production of a specific radionuclide, the chemical symbol and mass number is listed as the reaction product, e.g. a G,NA22 reaction in ^{59}Co.

A	alpha particle
ANAL	analysis
ABI	absolute integrated cross-section data
ABX	absolute cross-section data
ABY	absolute yield data. Often means cross-section per equivalent quantum is listed.
ACT	measurement of induced radioactivity of the target
ASM	asymmetric, asymmetry
AVG	average
BBL	bubble chamber
BEL B(EL)	reduced electric radiative transition probability
BF3	BF_3 neutron counter with moderator e.g., Halpern detector, long counter
BML	reduced magnetic radiative transition probability, B(ML)
BREAKS	levels located by "breaks" in the yield curve
BRKUP	breakup
BRMS	bremsstrahlung
BTW	between
C	continuous. Used to describe a photon source or a detector response function. Contrast with D = discrete.
CCH	cloud chamber
CF	compared with
CHRGD	charged
CMPT	Compton
COIN COINC	coincidence, coincide
COH	coherent
CK	Cerenkov
D	deuteron or discrete. When discrete, it is used to describe a photon source or a detector response function. Contrast with C = continuous.
DLTE	energy loss
DLTQ	momentum transfer
DST	distribution
DT BAL	detailed balance
E	electron
E/	inelastically scattered electron
E+	positron
EDST	energy distribution or spectrum
E/N	used only to indicate a coincidence experiment as in (E,E/N).

	N stands for any outgoing particle measured in coincidence with an inelastically scattered electron. Distinguish from eg., (E,N) which is used to represent an electron induced reaction when only the outgoing particle N is detected.
EMU	emulsions (photographic plates)
EXCIT	excited
F	fission
FMF	form factor
FM-1	inverse femtometers
FRAG	fragment
G	photon
G/	inelastically scattered photon
G-WIDTH	gamma-ray transition width
HAD	hadrons, hadron production
HE He3	^{3}He particle
INT	interaction, integral, intensity
INC	includes
ION	ionization chamber
ISOB	isobaric
ISM	isomer
J	multiplicity of particle defined by following symbol e.g. (G,PJN) with remark J = 2,3,5,7
JPI J-PI	spin and parity of a nuclear state
K	second multiplicity index, e.g. (G,JPKN) with both J & K positive integers greater than 1
KE	kinetic energy
L	may be an integer or zero that always follows a reaction product symbol. This is used to indicate transitions to specific states in the residual nuclide. When the letter is used as in (G,NL) the cross section given is that for the sum of transitions to two or more specific final states.
LFT	excited state lifetime
LIM	limit
LV,LVS	level, levels
LQD	liquid
MAG	magnetic spectrometer
MEAS	measurement(s)
MGC	magnetic Compton spectrometer
MGP	magnetic pair spectrometer
MOD	moderated neutron detector not employing a BF_3 counter, e.g. rhodium foil, Szilard-Chalmers reaction, ^{3}He, ^{6}Li reactions, GD loaded liquid scintillator, etc.
MSP	mass spectrometer
MULT	multiple, multipole, multiplicity
MU-T	used only in combination with G to indicate a total photon absorption cross section measurement, i.e. (G,MU-T)
N	neutron (see also XN and SN). The notation (G,N) is used to indicate a reaction in which only a single neutron is emitted, i.e. the reaction that can, in many cases, be measured by observing the radioactive decay of the residual nuclide.

nN	where n is any integer. (G,nN) indicates the sum over all reaction cross sections in which n neutrons are emitted.
NAI	NaI(Tl) spectrometer
NEUT	neutron(s)
NOX	no cross-section data
P	proton (see also XP)
PART	particle(s)
PHOT	photon(s)
PI	pion, usually written as PI+, PI-, PIO to indicate charge
POL	polarized or polarization
Q-SQUAR	momentum transfer squared (q^2)
RCL	recoil
REL	relative
RLI	relative integrated cross-section data
RLX	relative cross-section data
RSP	reaction spectrometer
RLY	relative yield data
SCTD	scattered
SCD	semiconductor (solid state) detector
SCI	scintillator detector other than NaI, e.g., CsI, KI, organic (liquid or solid), stilbene, He
SEP	separation
SEP ISOTP	separated isotope used
SIG	SIGMA (cross section)
SN	sum of neutron producing reactions, $\sigma(\gamma,SN)=\sigma(\gamma,N) + \sigma(\gamma,NP) + \sigma(\gamma,2N) + \sigma(\gamma,3N)$ + etc.
SPC	photon or particle energy spectrum
SPK	spark chamber
SPL	spallation
STAT	statistical
SYM	symetric, symmetry
T	triton
TEL	counter telescope
THR	threshold for reaction or threshold detector, e.g., $^{29}Si(n,p)^{29}Al$.
TOF	time-of-flight detector
TRK	tracks of particles or fragments observed in solid materials (glass, mylar, etc.)
TRNS	transition
UKN UNK	unknown
VIB	vibrational
VIR PHOT	virtual photon(s)
XN	all neutrons, total neutron yield, $\sigma(\gamma,XN) = \sigma(\gamma,N) + 2\sigma(\gamma,2N) + 3\sigma(\gamma,3N) + \sigma(\gamma,NP)$ + etc.
XP	all protons, total proton yield $\sigma(\gamma,XP) = \sigma(\gamma,P) + \sigma(\gamma,NP) + 2\sigma(\gamma,2P)$ + etc.
XX XXX	reaction products defined in REMARKS
YLD	yield

4PI	a 4π geometry was used or a method like radioactivity or a total absorption measurement
999	energy defined in REMARKS
S	indicates the measurement involved beams or targets that were either polarized or aligned, or that the polarization of the reaction products was determined. The polarized particle is indicated in REMARKS.
* or @	symbols used to indicate that the units associated with the numerals on one or both sides of the symbol in a specific column are not MeV. The units are defined in REMARKS.

NBS-114A (REV. 2-8C)

U.S. DEPT. OF COMM. BIBLIOGRAPHIC DATA SHEET (See instructions)	1. PUBLICATION OR REPORT NO.	2. Performing Organ. Report No.	3. Publication Date

4. TITLE AND SUBTITLE

Photonuclear Data-Abstract Sheets
1955-1982

5. AUTHOR(S)

E.G. Fuller and Henry Gerstenberg

6. PERFORMING ORGANIZATION (If joint or other than NBS, see instructions)

NATIONAL BUREAU OF STANDARDS
DEPARTMENT OF COMMERCE
WASHINGTON, D.C. 20234

7. Contract/Grant No.

8. Type of Report & Period Covered

9. SPONSORING ORGANIZATION NAME AND COMPLETE ADDRESS (Street, City, State, ZIP)

10. SUPPLEMENTARY NOTES

☐ Document describes a comouter program; SF-185, FIPS Software Summary, is attached.

11. ABSTRACT (A 200-word or less factual summary of most significant information. If document includes a significant bibliography or literature survey, mention it here)

These abstract sheets cover most classes of experimental photonuclear data leading to information of the electromagnetic matrix element between the ground and excited states of a given nucleus. This fifteen volume work contains nearly 7200 abstract sheets and covers 89 chemical elements from hydrogen through americium. It represents a twenty-seven year history of the study of electromagnetic interactions. The sheets are ordered by target element, target isotope, and by an assigned bibliographic reference code. Information is given on the type of measurement, excitation energies studied, source type and energies, detector type, and angular ranges covered in the measurement. For a given reference, the relevant figures and tables are mounted on a separate sheet for each nuclide studied.

12. KEY WORDS (Six to twelve entries; alphabetical order; capitalize only proper names; and separate key words by semicolons)

data-abstract sheets, elements, experimental, isotopes, nuclear physics, photonuclear reactions

13. AVAILABILITY

☐ Unlimited

☒ For Official Distribution. Do Not Release to NTIS

☐ Order From Superintendent of Documents, U.S. Government Printing Office, Washington, D.C. 20402.

☐ Order From National Technical Information Service (NTIS), Springfield, VA. 22161

14. NO. OF PRINTED PAGES

15. Price

USCOMM-DC 6043-P80